# On High-Altitude and High-Latitude Frost Environments

A thesis submitted in fulfilment of the requirements for the degree of

DOCTOR OF PHILOSOPHY (PhD)

OF

RHODES UNIVERSITY

BY

CHRISTEL DOROTHEE HANSEN

8 MARCH 2018

SUPERVISOR

PROFESSOR K.I. MEIKLEJOHN (GEOGRAPHY DEPARTMENT, RHODES UNIVERSITY)

CO-SUPERVISOR

ASSOCIATE PROFESSOR W. NEL (DEPARTMENT OF GEOGRAPHY AND ENVIRONMENTAL SCIENCE, UNIVERSITY OF FORT HARE)

*The assistance of the National Research Foundation (NRF) and the German Academic Exchange Service (DAAD) is hereby acknowledged. Opinions expressed, and conclusions arrived at are that of the author and are not necessarily attributed to the NRF or DAAD or any affiliated entities.*

# Plagiarism Declaration

I, CHRISTEL DOROTHEE HANSEN, hereby declare that this thesis is my own original work, that all assistance and sources of information have been properly acknowledged, and that this work has not been presented to any other University for a higher degree.

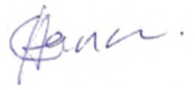

Christel D Hansen

# Abstract

Frost environments occur throughout the world, with associated processes occurring across climatic zones. Climatic geomorphology proposes that climatic zones, largely derived from annual average air temperature and precipitation values, have specific landforms and processes active within that zone. This study offers unique insights into the frost environments of three locations in the Southern Hemisphere, namely the Eastern Cape Drakensberg of South Africa, sub-Antarctic Marion Island, and Dronning Maud Land of Antarctica. The Drakensberg ranges from temperate to alpine, Marion Island is hyper-maritime, and Dronning Maud Land a polar desert. Drivers and forcings on the ground frost regime are identified, as are future climatic scenarios. Altitude and latitude were identified as the most important locational drivers, while air temperature showed highest correlation with freezing events. The initiation of a freeze event correlated strongly with maximum ground temperatures. Vegetation cover was found to ameliorate frost cycles, thereby increasing ground temperatures. Dronning Maud Land of Antarctica is characterised by annual frost (permafrost), with limited seasonal thaw in summer. Thawing cycles reflected the depth of the active layer, which ranged from just under 60 cm for Robertskollen (at lowest altitude) to less than 15 cm on Slettfjell (at greatest altitude). Marion Island had the most active frost environment, exhibiting both seasonal frost, and ubiquitous shallow diurnal frost cycles. The Drakensberg were largely frost-free, with limited seasonal frost and few diurnal freeze-thaw events.

Diurnal frost processes were found to be azonal, and present at all three study locations. Evidence of landforms derived from diurnal frost processes were evident in each zone. Equifinality/convergence of form was present to a degree. The presence of patterned ground, which was not wholly derived from frost processes, suggests a measure of equifinality. Furthermore, openwork block deposits, of which not all are either blockstreams nor blockfields, are not necessarily the result of frost processes. The periglacial environment is poorly defined and methods to delineate this environment, as well as other climatic zones, should include additional parameters. Delineating zones on annual (and limited) monthly averages based on predominantly temperature, is not sufficient. While concepts of climatic geomorphology may be applied in a general sense, this framework is not suited to working at smaller scales. Specifically, periglacial environments should be delineated using ground moisture, as well as air temperature. Furthermore, vegetation and snow cover are important, as are soil textural properties.



*Keywords*: Climatic geomorphology, frost environments, equifinality/convergence of form, zonality/azonality, Eastern Cape, Elandsberg, High Drakensberg, Marion Island, Dronning Maud Land

# Acknowledgements

The author would like to express her gratitude and sincere appreciation to Professor Ian Meiklejohn of Rhodes University, as well as Professor Werner Nel of the University of Fort Hare, for their guidance and support throughout the years of study undertaken to complete the thesis.

The work conducted here would not have been possible without funding by the National Research Foundation of South Africa (NRF) and the German Academic Exchange Service (DAAD). John Gillam and Liezel Strydom are thanked for their continuous and unwavering support through the Rhodes University Postgraduate Financial Aid office. Without the financial support of these institutions, as well as the support received by Rhodes University, the PhD studies would not have been possible.

The Department of Environmental Affairs (DEA), the South African National Antarctic Programme (SANAP), and the Norwegian Polar Institute (NPI) are thanked for providing logistical support during the fieldwork seasons conducted in Dronning Maud Land and the Prince Edward Islands.

The South African Weather Service (SAWS), National Geo-Spatial Information (NGI), and Council for Geoscience (CGS) are thanked for the provision of digital data. The University of Pretoria is thanked for the provision of laboratory space and equipment. Lew Campbell and Peter Pilz of Tiffindell (Pty) Ltd, and the staff of Tiffindell Ski & Alpine Resort are thanked for granting access to the slopes of Ben MacDhui and for always being accommodating during field visits. A special thank-you goes out to Mark and Linda Anderson, who not only granted access to the Elandsberg but also opened their home to me. Finally, fieldwork and site visits were made possible by the support of numerous field assistants who greatly assisted in the data collection process and provided great laughs and company along the way. These are:

- Calle Borg for his assistance during numerous visits to the Drakensberg and on Marion Island;
- Rosie Dwight for assisting on several occasions in the data collection process on the Elandsberg;
- Jamie Lodge for helping in the data collection process on the Elandsberg and for providing insightful information on the geological formations found there;
- Abuyiselwe Nguna for his assistance in data collection on Marion Island;
- Jessica Rosenfels for her assistance in the Drakensberg, on Marion Island, as well as Dronning Maud Land;
- Liezel Rudolph for her assistance in Dronning Maud Land and the Drakensberg; and
- All those members (too numerous to list) of the 2012/13, 2013/14, and 2014/15 summer relief voyage teams to the South African National Antarctic Expedition (SANAE IV) for assisting during the fieldwork data collection process.

# Table of Content

# Table of Figures

# Table of Tables

# Table of Equations

# Table of Abbreviations

ADD – Antarctic Digital Database

ALT – Active Layer Thickness

ANTPAS – Antarctic Permafrost, Periglacial Environments and Soils

CALM – Circumpolar Active Layer Monitoring

CGS – Council for Geoscience

CPZ – Continuous Permafrost Zone

CSDA – Confirmatory Spatial Data Analysis

DD – Degree Days

DEM – Digital Elevation Model

DJF – December, January, February (summer months)

DPZ – Discontinuous Permafrost Zone

EC – Eastern Cape

ECVs – Essential Climate Variables

ELA – Equilibrium Line Altitude

ESDA – Exploratory Spatial Data Analysis

Esri – Environmental Systems Research Institute

FD – Freezing Depth

FEF – Fine Earth Fraction

FI – Winter Freezing Index

FTC – Freeze-Thaw Cycles

GCOS – Global Climate Observing System

GFI – Ground Freezing Index

GLUE – Generalised Likelihood Uncertainty Estimation

GLZ – Generalised Linear Model

GMT – Greenwich Mean Time

GST – Ground Surface Temperatures

GTN-P – Global Terrestrial Network for Permafrost

GTOS – Global Terrestrial Observing Network

GWC – Gravimetric Water Content

IDW – Inverse Distance Weighted

IPA – International Permafrost Association

ITDZ – Inter-Tropical Convergence Zone

JJA – June, July, August (winter months)

K-S – Kolmogorov-Smirnov Test

LGM – Last Glacial Maximum

LOI – Loss on Ignition

m a.s.l. – Meters above sea level

Ma – Mega-annum

MAAT – Mean Annual Air Temperature

MAGT – Mean Annual Ground Surface Temperature (temperature recorded at ± 2 cm within the ground)

MAM – March, April May (autumn months)

MAST – Median Annual Near Surface Temperature (temperature recorded at ± 1 cm within the ground)

MODIS – Moderate Resolution Imaging Spectroradiometer

MSAT – Mean Seasonal Air Temperature

Nasa – National Aeronautics and Space Agency

NGI – National Geo-Information

NST – Near Surface Temperatures

PC – Principal Component

PCA – Principal Component Analyses

PFTE – Potential Freeze-Thaw Events

Prec – Precipitation

PSA – Particle Size Analysis

QQ plot – Quantile-Quantile plot

**R** – R Project for Statistical Computing

**RH** – Relative Humidity

**Sansa** – South African National Space Agency

**SAR** – Simultaneous Autoregressive Model

**SAWS** – South African Weather Service

**SCAR** – Scientific Committee on Antarctic Research

**SM** – Soil/Sediment Moisture

**SMAP** – Soil Moisture Active Passive

**SO** – Surface (Thermal) Offset

**SON** – September, October, November (spring months)

**S-W** – Shapiro-Wilk Test

**TI** – Summer Thawing Index

**TOC** – Total Organic Carbon

**TSI** – thermal Stress Index

**TSP** – Thermal State of the Permafrost

**Tukey HSD** – Tukey Honestly Significance Difference

**VWC** – Volumetric Water Content

**WD** – Wind direction

**WMO** – World Meteorological Organisation

**WS** – Wind Speed

**XR5** – PACE Scientific XR5 data logger

# Table of Symbols

$C_u$ – Uniformity coefficient

$\theta_v$ – VWC

$\theta_w$ – Field weight

$d$ – Expected rate of penetration of a freezing cycle ($d$

$d_{10}$ – Grain size for which 10% of the sediment is finer by weight

$d_{60}$ – Grain size for which 60% of the sediment is finer by weight

$d_b$ – Bulk density

$d_p$ – Porosity

$M_c$ – GWC expressed as a percentage

$O_p$ – Organic proportion of soil/sediment

$q$ – Studentised range distribution

$r$ – Pearson's product-moment coefficient of linear correlation

S – Sorting index

$s$ – Standard deviation

$s_d$ – soil solid density

$S_y$ – Specific yield

$T_{10}$: temperatures at 10-cm depth

$T_{100}$: temperatures at 100-cm depth

$T_{15}$: temperatures at 15-cm depth

$T_{150}$: temperatures at 150-cm depth

$T_{20}$: temperatures at 20-cm depth

$T_{200}$: temperatures at 200-cm depth

$T_{30}$: temperatures at 30-cm depth

$T_{45}$: temperatures at 45-cm depth

$T_5$: temperatures at 5-cm depth

$T_{50}$: temperatures at 50-cm depth

$T_{60}$: temperatures at 60-cm depth

$T_{AIR}$ – Air temperatures

$T_{AM}$ – Annual mean

$T_{D:max}$ – Daily maximum temperature

$T_{D:min}$ – Daily minimum temperature

$T_{DM}$ – Diurnal mean

$T_{DR}$ – Diurnal range

$T_{MM}$ – Monthly mean

$T_{MM:Jan}$ – Mean monthly temperature recorded in January

$T_{MM:July}$ – Mean monthly temperature recorded in July

$T_{MM:Max}$ – Maximum monthly mean temperature

$T_{MM:Min}$ – Minimum monthly mean temperature

$T_{SM}$ – Seasonal mean

$T_{sp}$ – Annual mean permafrost surface temperature

$T_{SR}$ – Seasonal range

V – Volume of sample

$\boldsymbol{\theta_g}$ – GWC

# CHAPTER 1: Introduction

Geomorphology, as an integral component to geography and physical geography, concerns itself with the study of the earth's surface, processes and landforms. It is the study of earth systems (Rhoads and Thorn, 1996), as well as complex and dynamic earth surface dynamics (Murray *et al.*, 2009). This multidisciplinary and interdisciplinary field (Sack and Orme, 2013) is driven by scientific exploration and is empirical in nature (Goudie, 2004b). Furthermore, geomorphology is concerned with achieving a greater understanding of the surface features of our planet and how these relate to humans within this geomorphic system (Sack and Orme, 2013). Throughout its history geomorphology has been applied within various frameworks and paradigms. Schools of thought have varied from the mobilistic/morphological view based on the works of Penck and Grenoble (1920s), to the eustatic view (1890-1950) that concerns itself with altitudinal grading and forcing, and finally to the climatic approach of the climatic geomorphologist (1940's onwards) (King, 1966). As such, descriptive studies have alternated with systematic and process-driven research. Six major developmental phases in the discipline can be identified and these have ranged from the *historic* phase of Davis to the *reconciliation* and *unification* phase of the 21$^{st}$ century (Goudie, 2004b). Contemporary geomorphology generally makes use of holistic approaches based on first order system theory, where steady state systems and linear relations between components are the focus of study (von Elverfeldt, 2012).

Geomorphology can be divided into several specialised domains, such as fluvial, aeolian, glacial or periglacial geomorphology, amongst others. Within these sub-fields a focus on specific agents or processes acting on the landscape is made. Periglacial geomorphology, as a sub-field of geomorphology, consists of the examination of diurnal, seasonal and perennial ground ice (permafrost) and their impact on landform and landscape development (Thorn, 1992) in cold, polar (high-latitude) and high-altitude environments (Barsch, 1993). By dividing the study of geomorphology into sub-domains based on processes and landforms the landscape is simultaneously divided into sub-domains. While processes may be active on a global scale, their effects may also be localised. Climate is argued to have a definitive impact on the distribution and development of processes and landforms, forming the basis of climatic geomorphology. This forms the basis of climatic geomorphology, whose proponents argue that climatic zones influence geomorphological processes and features. Zonality is a core concept within climatic geomorphology, where climatic zones control mechanical and chemical weathering (Sumner *et al.*, 2004b). Within these zones climate is proposed to exert a direct or indirect influence on geomorphic processes. Proponents of this sub-field of geomorphology propose that each climate zone (tropical, subtropical, continental, glacial and arid) determines landforms characteristic to each specific zone (Goudie, 2004a; Huggett, 2007), resulting in morphogenetic regions (Bremer, 2004). The work on the periglacial cycle by Peltier contributed to the determination and usage of morphogenetic regions (King, 1966). As such, climate geomorphologists believe that geomorphic processes inherent to each climatic zone will engender regional patterns and landforms characteristic of that zone (Priesnitz, 1988; Goudie, 2004a); *i.e.* landforms develop because of one overriding process or specific climatic factor. Equifinality, or self-organisation, applies when a given end state may be achieved by multiple means, *i.e.* a convergence of form occurs due to the same or different processes and agents. As such, equifinality does not only imply convergence of form but can also be ascribed to convergence of any physical characteristics, such as sediment yield or drainage densities (Phillips, 1999;

Odoni, 2007). While self-organisation is generally shown through convergence of form, various uses and descriptions of self-organisation are present in the literature (Phillips, 1999). The multiple working hypotheses approach allows for the critical evaluation, and subsequent acceptance or rejection, of various theories or processes within a system and has been described as early as 1987 (Chamberlin, 1987). This contrasts with the equifinality approach whose proponents argue that different processes may act on different time scales, at dissimilar intensities and from dissimilar initial conditions to achieve the same result (Culling, 1957; von Bertalanffy, 1968; Phillips, 1997; Beven, 2000; Beven and Freer, 2001; Beven, 2006). Others, such as Cooke and Reeves (1976), have suggested that the two approaches complement each other, while *e.g.* Haines-Young and Petch (1983) have argued against the broad application of the equifinality thesis. Instead, they propose that equifinality only truly exists when a landform is shown to form from various initial conditions but the same process, essentially limiting the presence of equifinality. Culling (1987) and Phillips (1997), in turn, suggest that equifinality becomes applicable at various scale levels and Beven (2006) argues for increasing complexity of models yielding equifinality. Phillips (1999), in turn, proposes that increased complexity generally yields divergence of form and spatial patterns. This is due to conditionality within geomorphic systems, where landscapes and landforms may develop differently due to thresholds either exceeded or not. An example of this would be the development of patterned ground associated with permafrost, or that associated with the active layer. In the active layer water may be found in its unfrozen state, allowing frost heave and thrust to occur, yielding sorted patterned ground. In a permafrost environment, in the case of no liquid water inherent to the system, patterned ground will more likely be of the non-sorted variety. Here patterned ground would develop due to the thermal expansion and contraction of frozen ground in the absence of liquid water. Phillips (2007), furthermore, argues that the 'perfect landscape' is unique and that the combination of many factors may lead to a singular outcome. However, as divergence of form may be ascribed to increasing complexity and more processes, a cohort of multiple processes may also lead to similar landforms. Equifinality and the multiple working hypotheses approach, therefore, have associated advantages and system equifinality should be evaluated using equifinality models (Beven, 1996), not only considering why something occurs, but also how it comes about and in which manner (Gerrard, 1984). This study falls within the discipline of physical geography and the sub-field of geomorphology and makes use of the theoretical framework of climatic geomorphology. Within this framework, the method of equifinality within systems (if such equifinality in the presence of convergence of form applies to the environments of the selected study regions) is employed. Furthermore, the focus of the study is the frost environment and its presence across selected climatic geomorphological zones.

Cold climate zones are found throughout the globe, generally at high-altitudes or -latitudes, and characterised by glacial, paleoglacial and periglacial landforms (Goudie, 2004b). Although no quantitative parameters used to define the periglacial environment have gained universal acceptance within geomorphology, the periglacial zone may, nevertheless, be delineated by using the presence of permafrost, or the presence of freeze-thaw processes and deep seasonal freezing (van Everdingen, 1998; Goudie, 2004b). The periglacial environment is one in which frost-action dominates and permafrost-related processes occur (French, 1996) and indications of such environments include specific features, such as patterned ground (Grab *et al.*, 2012). Permafrost describes perennially frozen ground that remains continually below 0 °C for more than two years *(e.g.* Thorn, 1992; van Everdingen, 1998; Goudie, 2004b; Skinner, 2004; Hedding, 2008; Adlam *et al.*, 2009), and its depth and extent varies

across the globe. Permafrost, whose definition is based solely on the ground temperature regime, does not require the presence of frozen water. Nevertheless, water constitutes an integral component of the freeze-thaw process. Mean annual soil surface temperatures of below -5 °C and mean annual air temperatures (MAAT) of below -8 °C are required for a continuous permafrost zone (CPZ). In the CPZ ± 90% of the area is underlain by permafrost. In discontinuous permafrost zones (DPZ) 50-90% of the ground is underlain by permafrost (Harris, 1981; Osterkamp and Burn, 2003). The active layer that overlies permafrost, is subject to annual freeze-thaw cycles and potential freeze-thaw events. Both cycles and their depths are determined by the intersection of the 0 °C isotherm with the annual maximum soil temperature profile (Burn, 1998; Adlam *et al.*, 2009; Christiansen, 2013). Freeze-thaw weathering and freeze-thaw cycles, while not fundamental, are important components to the periglacial environment, as are frost wedging, heaving, sorting and similar processes (Washburn, 1979). A potential freeze-thaw event is the cycle where temperatures fluctuate above and below zero degrees Celsius (Goudie, 2004a), with freeze-thaw cycles defined by temperatures fluctuating above and below 0 °C in the presence of moisture (Holden, 2007), *i.e.* where temperature fluctuations cause the freezing and concomitant thawing of water/ice (van Everdingen, 1985). Potential freeze-thaw events generally yield less freeze-thaw cycles, since a greater energy input is required for a temperature change to occur when moisture is present within the ground (Brady and Weil, 2016). This increased energy requirement is related to the specific heat of soils and changes in the presence of moisture. Dry mineral soils have a specific heat of about 0.20 on average; an increase of 20 % of moisture content raises the specific heat to 0.33; and an increase of 30 % of moisture content raises the specific heat to ± 0.38 (Brady and Weil, 2016). Another consideration is that evaporation translates into a drop in observed temperatures, whereas freezing translates into a release of latent heat (Brady and Weil, 2016). Such temperature dynamics may be recorded and used to analyse the freeze-thaw environment of a specific site.

Freeze-thaw action is one of the main geomorphic agents in periglacial environments (Fahey, 1973; Sumner *et al.*, 2004b). These cycles may yield frost heave, vertical, lateral or mechanical frost sorting and/or frost creep (needle ice/diurnal/annual). Furthermore, patterned ground occurs due to, amongst others, freeze-thaw processes (Boelhouwers, 1995; Grab, 1997a; Easterbrook, 1999). While such cycles generally only affect the upper surface of the ground (0-5 cm) (van Everdingen, 1998; Goudie, 2004a), their impact can be significant; especially since freeze-thaw cycles have a wide geographic distribution, are azonal in nature and occur across climatic zones. While the highest number of freeze-thaw cycles occur in regions with low annual temperature ranges, the least number of cycles are observed for high latitudes and continental climates (Goudie, 2004a). Where permafrost occurs, freeze-thaw cycles occur only within the active layer. Furthermore, the depth of the active layer determines the depth of freeze-thaw cycles. In non-permafrost zones these cycles increase in depth with increasing latitude (Goudie, 2004a).

This study aims to evaluate the frost environment found at various altitudes and latitudes. These areas (high- and mid-latitudes; high altitudes) are sensitive to climatic changes (Barsch, 1993; Lewis, 2008a), warranting scientific investigation and exploration. In the milder zones of the mid latitudes patterned ground, because of frost heave (cryoturbation) and freeze-thaw processes, become less frequent when air and surface temperatures increase. A warming of a few degrees would have serious implications for

CPZ, DPZ and especially SPZ. Warmer temperatures affect surface temperatures of permafrost and effectively deepen the active layer. In areas where permafrost is within a few degrees of thawing, such as in DPZ and SPZ, warmer temperatures initiate thawing and in worst case scenarios, an altogether disappearance of permafrost (Osterkamp and Burn, 2003). In the presence of a warming global climate, patterned ground may, therefore, increase in the colder areas of the high latitudes due to an increase in active layer dynamics (Guglielmin, 2012). For systems that exhibit non-linearity, climate change may have two main effects. These are either a phase change, where the system changes 'phase' from one attractor to another, or when the attractor changes due to the changing climate (Murray *et al.*, 2009). In cold regions, which have lower thresholds and are sensitive to small changes in climate, this phase change can occur rapidly. However, if the change occurs gradually, non-linear feedbacks may be introduced into the system (Murray *et al.*, 2009). When comparing the effect of latitude to altitude, a rise in altitude is generally equivalent to an increase in latitude (Strahler, 1974; Adlam *et al.*, 2009). A notable difference is in the range of temperatures observed, as mid- to low latitudes receive greater direct insolation, yielding higher temperatures. In comparison, high-latitudes receive less direct insolation and temperatures are, therefore, lower (Strahler, 1974). For this study, a summative assessment of the frost environment of selected sites representing high-altitude and -latitude environments is made, as well as an inter-site comparison regarding frost processes and resultant landforms. Questions of zonality/azonality of landforms regarding frost processes within the three climatic zones exhibited by the three chosen study areas are addressed. To allow for inter-site comparisons, locations were selected based on how many external factors were similar. As such, high altitudinal settings are predominantly considered, although a few sites are located at lower altitudes or near sea level.

The study focuses on three study areas. These are western and central Dronning Maud Land (DML) of Antarctica, Marion Island in the sub-Antarctic, as well as the High Drakensberg and Elandsberg of the Eastern Cape of South Africa. The varying altitudes, latitudes and climates found in these regions allow for an investigation into zonality/azonality of processes and landforms within climatic zones. Types of patterned ground, such as circles, steps and stripes, are found at all sites. Patterned ground, periglacial or non-periglacial, which is representative of a model for self-organisation (Phillips, 1999), suggest a measure of equifinality. Yet not all landforms are found within each zone, even if the same process exists. Continental DML is a polar desert and ice dominated. Marion Island is hyper-maritime, receives a high degree of annual rainfall, and dominated by the ocean (Boelhouwers *et al.*, 2003; Nel *et al.*, 2009). The oceanic climate of the Elandsberg in the Eastern Cape is mild and temperate, whereas the High Drakensberg has an alpine environment (Guetter and Kutzbach, 1990). Within these climatic zones a further subdivision may be made in terms of the periglacial or frost-driven environment. Using the presence of freeze-thaw processes and seasonal freezing as the delineating factor for the periglacial environment (Goudie, 2004b), one may argue that the subtropical zone (High Drakensberg) has periglacial zones where MAAT ranges from < 3 °C-6 °C, the mid-latitude zones have periglacial zones where MAAT is less than 5 °C, and in sub polar zones periglacial zones exist where MAAT is less than -2 °C (Karte, 1983). Washburn (1979) assigns periglacial zones to the polar lowlands (mean temperature of the coldest month less than -3 °C), subpolar lowlands (mean temperature of the coldest month less than -3 °C and of the warmest month greater than 10 °C), mid-latitude lowlands (mean temperature of the coldest month less than -3 °C and of the four warmest months greater than 10 °C), as well as highlands (the influence of aspect becomes dominant; large diurnal ranges).

In general, deep seasonal frost cycles or permafrost require MAAT of between -0.5 °C to -6 °C (French and Demitroff, 2001) and Bockheim (1995) uses MAAT of -1 °C to delineate the northern extent of permafrost in the Southern Circumpolar Region (< 50°S). Permafrost is, therefore, expected to occur at some of the chosen study sites and diurnal frost environments are common for all three sites. The azonal nature of these frost processes and concomitant dynamics are, as such, the focus of the study. The study makes use of climatic geomorphology as a theoretical framework and its limitations and benefits critiqued and applied where appropriate. Applying this framework to the three study sites based on the presence of diurnal frost cycles, one can assume that characteristic geomorphological features should be found for each site. Furthermore, unless otherwise indicated, diurnal refers to a 24-hour cycle, *i.e.* the diurnal cycle spanning a full 24-hour period.

Patterned ground, as an example of self-organisation (Phillips, 1999), is not unique to the periglacial environment and does not occur only due to cold-climate processes (Goudie, 2004b). For example, patterned ground found in the tropics is the result of the swelling of clay particles; desiccation polygons occur due to contraction of the ground following desiccation events; and, in dry regions patterns, such as the Namibian faery circles (Tschinkel, 2015), may result due to vegetation banding of faunal influences (Goudie, 2004b). Characteristic features found in cold environments, such as angular clasts, are also found in hot environments, suggesting azonality of landforms and/or processes. Such features, therefore, don't necessarily indicate frost weathering and may instead be attributed to salt weathering, thermal stress, hydration, dilatation and fire-induced spalling (Boelhouwers *et al.*, 2002). Furthermore, mechanical weathering due to wetting and drying is present in cold regions (Hall, 2002) and frost-weathered debris does not necessarily have to have one specific form (Hall and Thorn, 2011). However, cold environments with sensitive threshold levels – required to effect change within the present geomorphic system – as those found in the Antarctic and sub-Antarctic, are more sensitive to small changes than those where threshold levels are higher (Barsch, 1993; Boelhouwers, 2003a; Boelhouwers *et al.*, 2003; Nel, 2012). Further evidence of azonality of landforms occurs for features such as tafoni, which are found across a range of climatic zones (Bourke *et al.*, 2007). Tafoni, furthermore, are argued to exhibit attributes of self-organisation in form development (Viles, 2005). For the current study, it is apparent that convergence of form, or equifinality, exits, with landform and -features common to all three. Furthermore, frost cycles, common in cold environments, are also known to occur in hot-desert environments (Sumner *et al.*, 2004b) and their presence for all three sites, as mentioned above, suggests an azonality of processes. As such, the azonal nature of processes acting over a long period of time (Meiklejohn and Hall, 1997; André, 2003; Boelhouwers, 2004), and non-linear weathering rates (Sumner *et al.*, 2009), should be considered when investigating frost cycles across the various study sites.

Permafrost and periglacial studies, as well as diurnal frost environments in sub-Antarctic and Antarctic environments are less well understood than their Northern Hemisphere counterparts (Boelhouwers and Meiklejohn, 2002). However, environmental and locational conditions within which frost cycles occur may be different to the Northern Hemisphere and any investigation into diurnal frost environments in the Southern Hemisphere will improve our understanding of these systems. In addition, there exists a need to map these environments for both the Northern and Southern

Hemisphere using contemporary global climate, soil and vegetation datasets. When freeze-thaw cycles occur, various processes combine in a single process (cryogenesis) (Kumar, 2011a). In high-altitude and -latitude environments processes such as cryoturbation (Kumar, 2011b), frost wedging, heave and creep (Thorn, 1992; Rempel, 2011), as well as weathering are a fundamental part of soil formation, determining ecological environments (Hefferan and O'Brien, 2010; Vieira *et al.*, 2010; Guglielmin, 2012) and the sorting of the soil and ground (Washburn, 1979; Hjort and Luoto, 2009). The frequent freezing and thawing of the ground results in the mixing of the soil/sediment column and is an important landform shaping process in periglacial and polar regions (Kumar, 2011b). Soil properties such as pore size and grain distribution greatly influence freeze-thaw dynamics. In turn, the thermodynamic properties of frozen soil are largely driven by temperature (Goudie, 2004a). Frost creep in environments where permafrost is either present of absent, as described by Mackay (1981), occurs at varying rates. This study offers the opportunity to investigate frost processes and resultant landforms for three climatically different settings in the Southern Hemisphere. The different study sites allow for the investigation of frost heave in permafrost and non-permafrost settings, where dissimilar circumstances (freezing from below and above the active layer; freezing below the active layer; freeing in the absence of permafrost) yield similar results. The summertime frost heave found in permafrost regions (Thorn, 1992) is of interest, as is autumn- and wintertime freezing of the ground in the mid-latitudinal and high-altitude region.

In cold climates snowmelt in spring allows for deeper thawing of the ground (Vieira *et al.*, 2010), and contributes to soil/sediment moisture (Adlam *et al.*, 2009). Furthermore, melt-out processes are effective erosional agents in periglacial environments (Hedding, 2008). This study provides data for the identification of common processes at work within the three environmental settings. Furthermore, the Elandsberg and Eastern Cape High Drakensberg are impacted by human habitation, altering the environments to a certain degree. In the Lesotho Highlands diurnal frost cycles play an important role in accelerating land degradation, where frost action may structurally weaken the soil (Barsch, 1993), and produce debris, contributing to stream erosion as well as altering carrying capacity of the land (Boelhouwers and Meiklejohn, 2002; Grab, 2002a). The highly seasonal nature of rainfall for the High Drakensberg, with dry winters and the occurrence of needle ice (Borg, 2017), lends itself to desiccation and subsequent deflation of exposed surfaces (Grab, 2002a). Needle ice makes a surface not only more susceptible to deflation, but also to denudation, contributing to debris supply. Particles heaved to the surface become entrained in surface runoff (Strahler, 1974), or deflated by the wind, contributing to the amount of sediment feeding into local fluvial systems. Cryoplanation/nivation within these high mountain environments also warrants further investigation. Hall (1998a) and Thorn and Hall (2002) argue for cryoplanation and nivation to be members of the same process and this outlook is adopted for the study. Marion Island and DML, on the other hand, are regions largely undisturbed by human presence. Marion Island, although some flora and fauna have been introduced *(e.g.* Chown and Smith, 1993; Gremmen *et al.*, 1998; Gremmen and Smith, 1999; Gremmen *et al.*, 2003; Jones *et al.*, 2003; Yeloff *et al.*, 2007; Chown *et al.*, 2008, 2012), remains minimally disturbed by human impacts (Chown and Froneman, 2008), and DML even less so. These regions, due to the potentially simple systems (Boelhouwers and Meiklejohn, 2002), can, therefore, provide information on diurnal frost environments in the absence of human interference. The potential for debris supply and concomitant stream erosion, as suggested by Boelhouwers and Meiklejohn (2002), begs the investigation of the potential of freeze-thaw weathering and frost creep (needle ice creep, diurnal frost creep, annual frost

creep) as a sediment source to local fluvial systems. On sub-Antarctic Marion Island needle ice activity contributes to the sediment movement along slopes at rates of 2.6 $cm.yr^{-1}$ for blocky material to 53.2 $cm.yr^{-1}$ for fine textured material (Holness, 2004). An average of 21.5 $cm.yr^{-1}$ for the Island highlights the importance of diurnal frost events in creating friable surfaces (Boelhouwers *et al.*, 2000). Furthermore, vegetation removal due to freeze-thaw cycles and the disaggregation of sediment within the ground column increases the potential for wind and water erosion, especially on steeper slopes, bare surfaces and poorly drained soils (Brady and Weil, 2016). A wind speed of 5.4 $m.s^{-1}$ is required for deflation to occur, with particles less than 0.1 mm in diameter prone to erosion when not aggregated (Brady and Weil, 2016). Boelhouwers and Meiklejohn (2002) argue for the need for a better understanding of the periglacial processes of the High Drakensberg and this study aims to contribute to the current knowledge of the periglacial environment for the Elandsberg, if it exists, and the Eastern Cape High Drakensberg. Southern Hemispheric research focused on frost cycles may contribute toward our understanding of how climate change impacts landscape dynamics, erosion rates, sediment supply, natural hazards and ecosystem functioning (Boelhouwers and Meiklejohn, 2002). Furthermore, Barsch (1993) proposes intensified research on the relationship between process and landform, as well as the need for modelling such environments and the current project contributes to these issues.

The premise of climatic geomorphology facilitates a top-down approach that lends itself to generalisation and regional studies, decomposing systems into sub-systems using deductive approaches (Thorn, 1992; Bremer, 2004). However, geomorphic processes should be investigated to deduce their role in landscape development, utilising an abductive and bottom-up approach. Assigning specific landforms and overriding geomorphic processes to specific climatic zones introduces potential fallacy of the converse through affirming the consequent. While a specific process may mould specific landforms, the reverse is not necessarily true. As such, the idea of applying specific geomorphic processes to specific climatic regimes has been critiqued *(e.g.* Twidale and Lageat, 1994), and needs to be re-investigated, as local environmental conditions may override regional climatic conditions (Ballantyne and Matthews, 1982), and the division that lies between humid-temperate, semi-arid and arid landscapes, is less than originally argued for *(e.g.* King, 1971). Greater consideration must also be given to moisture regimes (moisture fluctuations, the state of water and the absolute moisture content) within these environments (Boelhouwers and Meiklejohn, 2002; Hall, 2002; Sumner *et al.*, 2004b). Specifically, Thorn and Hall (2002) argue that moisture is the most important factor to weathering and erosional processes within periglacial environments. Surface albedo must also be considered, as higher albedo yields potentially lower ground temperatures, as well as soluble salts (Campbell *et al.*, 1998). Incident solar radiation influences thermal regimes, having implications on freeze-thaw cycles (Doornkamp and King, 1971). In comparison, total annual solar radiation does not significantly affect active layer thickness (Adlam *et al.*, 2009), due to the insulation effects of snow observed during winter months with snow depth of 80-100 cm required to provide the necessary insulation against air temperatures (Schoeneich, 2011). During winter, when snow depth is greatest, ground surface temperatures (GST), which are measured in the uppermost centimetres of the ground, stabilise and reach near-equilibrium values (Schoeneich, 2011). When snow cover decreases from spring to autumn GST is strongly influenced by air temperatures, with an increase in diurnal cycles observed (Ishikawa, 2003; Schoeneich, 2011). This applies to permafrost and active layer senvironment. Furthermore, snowmelt during the warmer months percolates through the soil, resulting in heat transfer, increasing active layer thickness through thermal conductivity and heat transfer via sub-surface flow (Adlam *et al.*,

2009). Ambient air temperatures exert the greatest influence on active layer dynamics, *i.e.* high air temperatures yield deeper active layers, with a time lag of a few hours to ± 24 hours observed between air and ground temperatures. In the absence of permafrost snow presence has other effects on GST. For sub-Antarctic Marion Island, snowfall events yield deeper and longer potential soil frost events (Nel, 2012), with the frequency of freeze-thaw events increasing with the occurrence of cloudless nights (Boelhouwers, 2003a; Boelhouwers *et al.*, 2003; Boelhouwers, 2007; Nel *et al.*, 2009), attributed to a change in the exchange of short- and longwave radiation received and emitted by the surface of the earth (Brady and Weil, 2016). In general, temperature gradients are greatest during cloud-free days (Campbell *et al.*, 1998). Cloud cover, therefore, is a potential driver of frost cycles. Furthermore, the presence of snow in non-permafrost environments leads to longer duration of freeze-thaw cycles, as well as deeper penetration of the freezing front into the ground. The absence of snow, in turn, may translate to high-frequency freeze-thaw cycles (Nel, 2012). Ground temperature dynamics are also influenced by vegetation cover, moisture availability, sediment characteristics, topography, and relief (Ishikawa, 2003; Grab *et al.*, 2012; Bierman, 2014). Vegetation cover acts as a critical boundary to certain periglacial processes (Washburn, 1979). As the percentage of fines ($\phi > 4$: silt and clay) in the soil column increases, reaching a threshold at 16%, the amount of moisture required for frost processes to occur decreases (Meentemeyer and Zippin, 1981). Moisture values as low as 2% (volume per volume) have been shown to be sufficiently high, even in coarse-grained soils, to yield needle ice growth on sub-Antarctic Marion Island (Haussmann *et al.*, 2009a). Mean summer and winter temperatures, as well as total summer radiation (Adlam *et al.*, 2009; Schoeneich, 2011), all affect active layer thickness and freeze-thaw cycles. The amount of sediment displaced through freeze-thaw cycles is in turn controlled by the size of ice formation, soil texture, moisture and surface roughness, as well as the ice mass to atmosphere void ratio (Meentemeyer and Zippin, 1981). Sediment movement rates and mobilisation due to freeze-thaw cycles is also significantly correlated to slope angle, explain 57% of variation, and altitude, explaining 24% of variation (Holness, 2001a, 2004). Strong winds (> 11 $m.s^{-1}$) and mean summer wind speeds influence the ground response to ambient temperatures, having positive correlation to active layer thickness (Adlam *et al.*, 2009; Hansen, 2014). The generalised approach of climatic geomorphology should, therefore, be combined with the specific approach of the process geomorphologist. This facilitates the extrapolation of the large-scale focus of the process geomorphologist to the small-scale arena of climatic geomorphology. This study aims at bridging the gap between the general and specific approach and a refinement of applying climatic geomorphological concepts to geographical zones. Several locations with differing climates are selected and for each location, frost cycles and processes are investigated, as are their resultant landforms and -features. This is of specific interest since many types of patterned ground, such as circles and stripes, occur across the study sites. While the focus is on the diurnal rhythms, frost cycles are also evaluated on a seasonal and annual scale. Site-specific characteristics are analysed in terms of inter-site correlations to identify commonalities and differences between the three climatic settings.

Thorn (1992) stresses the role that ground ice has within periglacial geomorphology and proposes five main objectives inherent to this sub-field. These are the identification of:

1) Chemistry/physics/mechanics of periglacial processes;
2) Periglacial landforms;
3) The occurrence of permafrost;

4) The permafrost-active layer dynamics; and
5) To reconstruct paleoenvironments.

The current project falls partly or wholly within objectives 1 – 4. It is exploratory in nature and falls within the sub-field of geomorphology, which, in turn, forms part of the discipline of physical geography. While the research is not wholly focused on periglacial geomorphology it, nevertheless, falls within the broader context of such. Geomorphology, as a system science, focuses on landform studies, landscape studies and landscape change (Murray *et al.*, 2009; Church, 2010). Periglacial geomorphology in turn, focuses on periglacial systems and geosystems (Thorn, 1992; Barsch, 1993). The project makes use of holistic approaches based on first order system theory, where steady state systems and linear relations between components are the focus of study (von Elverfeldt, 2012). However, non-linearity and self-organisation are present, requiring first order systems theory to be expanded to second order system theory (von Elverfeldt, 2012). Chorley and Kennedy (1971) define four main systems within geomorphological studies. These are, with increasing complexity, 1) the morphological system, 2) cascading system, 3) process-response system, and 4) control system. Complexity refers to a high number of elements and concomitant high degree of relationships found between these (von Elverfeldt, 2012). The current project addresses questions pertaining to landforms resultant of processes, such as the freezing and thawing of the ground, within frost environments. A focus is on the present environment and processes active within it and landforms are evaluated in terms of the processes that form and define them. While no attempt is made to quantify past environments, landforms resultant of such are acknowledged. Furthermore, a holistic approach is employed when investigating the multivariate periglacial environment and associated processes, acknowledging the non-linearity of geomorphic systems. While the Newtonian paradigm, or linear systems theory, and empiricism (Goudie, 2004a; Murray *et al.*, 2009), provide the framework for this study, the non-linear interaction of local deterministic geomorphic processes is considered (Church, 2010). Major themes addressed are those of stress-strength relationships and polygenesis and inheritance of landscapes (Goudie, 2004a). The research is partly hypothesis driven but also uses a strong exploratory and investigative approach and may be assigned to the morphological and process-response system classification of Chorley and Kennedy (1971). While positive and negative feedback loops and their influence on single variables are considered, so are the quality and quantity of input-output relations. Research methods employed include:

1) A theoretical approach with respect to contextualising contemporary diurnal frost environments for the three study sites within the framework of climatic geomorphology;
2) Observation based methods based on a large fieldwork component; and
3) An experiment-based approach conducted in the field in DML, on Marion Island, the Elandsberg, as well as the High Drakensberg of the Eastern Cape of mainland South Africa.

The analytical method is more suited for geomorphological studies due to multiple working hypotheses being considered and not only one (King, 1966). As such, the analytical method, rather than deductive nor inductive analyses methods are employed, and the overall approach is objective and quantitative in nature, making use of a variety of mathematical and statistical methods. Where deemed necessary, methodologies are adapted to local conditions and project requirements.

## 1.1 Problem Statement

Periglacial geomorphology as a sub-field, and climatic geomorphology, as a theoretical framework, overlap in many ways, especially where processes common to the periglacial environment – such as frost cycles – yield specific landforms. However, as discussed above, this is not always the case. Landforms and -features like those resulting of periglacial processes have been observed in settings different to that of the periglacial environment. Periglacial conditions may initiate landforms, influence their development as well as maintenance. However, these (landform initiation/development/ maintenance) are not all necessarily due to periglacial or ice-driven conditions. Depending on site-specific characteristics only one, two or these may be due to periglacial conditions (Thorn, 1992). The challenge lies in identifying which of these (origin/growth/maintenance) is due to periglacial processes. Furthermore, the processes contributing to the various stages of landform development within the periglacial framework need to be identified and if possible, quantified. Identifying the role periglacial conditions and processes have on landform initiation and development allows for an investigation into zonality of climatic zones. As such, this study aims to investigate high-altitude and high-latitude frost environments with a specific focus on the zonality/azonality of landforms and processes.

## 1.2 Aim

The project aim is to improve our knowledge within three specific environments and the cold climate processes common to each. A key focus is why convergence of form/equifinality exists in regions of different climates and local condition and if the concept of zonality should or should not be applied when investigating geomorphic landforms in specific regions. Questions addressed include:

1) Do climatic attributes within climate zones result in landforms characteristic of that zone;
2) Are specific frost processes only found within characteristic climatic zones; and
3) Are specific processes and environments, particularly diurnal frost environments, substantially altered and affected by human interference?

The overall aim is approached in several ways. First, an extensive literature review for the three areas under investigation is utilised to provide an in-depth description of each study area, landforms found for each, as well as known processes active in each. Second, fieldwork comprising of the deployment of temperature and moisture loggers, a variety of markers, ground truthing of data, as well as observational records is used to augment the literature study and to assist in answering the research questions. Third, laboratory and statistical analyses are used to answer questions regarding sediment characteristics and field moisture and temperature dynamics.

## 1.3 Objectives

The research is conducted at three separate areas, namely the Elandsberg and High Drakensberg of the Eastern Cape of mainland South Africa, sub-Antarctic Marion Island, as well as western Dronning Maud Land (WDML) and central Dronning Maud Land (CDML) of Antarctica. For this study five key objectives are identified. These are listed below and apply to all three sites. An in-depth discussion of each follows

under 4.1.1 Objective 1-4.1.5 Objective 5 (pg. 72-77), found in CHAPTER 4: Data Requirements, Collection and Methods. The five key objectives identified are as follows:

1) To investigate the dynamics of frost cycles in the short-term (diurnal), as well as longer term (seasonal and annual) using a variety of methods;
2) To evaluate soil temperature and moisture data regarding snow cover, climate data and other environmental factors to determine trends, forcings and/or correlations;
3) To compile a comprehensive register of landforms in diurnal frost environments at each study site near each data logger;
4) To draw a comparison between the three sites with respect to zonality/azonality and to develop a model for diurnal cycles for each site; and
5) To map all findings and make the content of the landform database available using interactive and accessible resources.

## 1.4 Thesis Structure

This thesis may be divided into seven chapters. The current chapter, CHAPTER 1: Introduction, provides an overview of this study, its aims and objectives. CHAPTER 2: Background and Context (pg. 12) provides additional and more in-depth information on the topic under investigation, whereas CHAPTER 3: Study Area and Site Description (pg. 25) details the specifics of each study site. CHAPTER 4: Data Requirements, Collection and Methods (pg. 72) expands in detail on the various methods employed, as well as data requirements. CHAPTER 5: Results (pg. 113) and CHAPTER 6: Discussion of Findings (pg. 281) are dedicated to representing this study's results and the discussion thereof respectively. The document concludes with CHAPTER 7: Conclusion (pg. 312).

# CHAPTER 2: Background and Context

This chapter provides a background to current theories in climatic geomorphology and how these have developed. Furthermore, a selection of climatic classification systems in use today is described. A detailed discussion of climatic classification systems is available from Essenwanger (2001). Figure 1 of APPENDIX A, provides a graphic description of these systems and their defining parameters. Furthermore, this chapter addresses the question of equifinality and self-organisation within the context of the current study. All appendices form part of the supplementary material to this document.

Classification based on precipitation and temperature provides an efficient way of delineating zones, as well as dominant vegetation type (Guetter and Kutzbach, 1990). Köppen (1936) devised a climate classification system based predominantly on precipitation, but also factored in temperature, particularly near-surface temperature, known vegetation and soil distribution. His classification focused on vegetation zones and once these had been identified, numerical climatic data were extracted from these boundary lines to give rise to his climatic classification system. The soil-moisture balance, as originally proposed by Thornthwaite (1948), considers precipitation, as well as evapotranspiration in its climate classification. Thornthwaite (1948), stressed the importance of a quantitative but also rational classification systems, where natural break points within climatic data should be considered for borders between zones. Using temperature, evaporation or evapotranspiration data requires delineation along continuous datasets, where these natural breaks are difficult to identify. However, if datasets are used in conjunction, applying multi criteria decision analysis, such breaks become apparent. This speaks to multiple controls within climatic zones, which shows similarity to the multiple controls evident in geomorphic systems, as argued by Phillips (2007). Thornthwaite (1948), identified these breaks within climatic zones to be related to heat and moisture, not so much in the simple quantitative values of temperature and moisture but rather in a more general sense of whether a climate is moist and dry or warm and cold. Furthermore, seasonal variations, specifically mean seasonal air temperatures (MSAT) must be considered and not only mean annual air temperature (MAAT).

Köppen's classification is empirically based on fixed values of temperatures and precipitation, making the assignation of classes simple, if the correct data are available. The Köppen climate classification system designates five major climate groups, based on annual and monthly temperature and precipitation averages (Strahler, 1974, 1989). These five groups are based on plants of the tropical rainy or equatorial climate (A), dry or arid climate (B), mild/humid or temperate (mesothermal) climate (C), snowy-forest (microthermal) climate (D) and the polar/ice climate (E) (Kottek *et al.*, 2006). Groups A and C-E are based on temperature averages whereas B is based on the precipitation-evaporation ratio. Each of these five groups may have a subdivision based on the semi-arid (steppe) (*S*), and arid (desert) (*W*) climate. Further subdivisions are based on moist or humid areas (*f*), dry winter season (*w*), dry summer season (*s*) or rainforest or monsoonal conditions (*m*). Combining the various groups and subgroups a total of 11 distinct climates emerge. A summary of these is given in Table 1 in APPENDIX B. Using Köppen's classification system, climate type E (ET and EF) contains the periglacial zone, with the periglacial zone defined by the upper limit of the timber line in high-altitude environments (Barsch,

1993). It is worth mentioning that Köppen devised this classification to aid the study of plant ecology by creating climate-vegetation maps and the assignation of landforms to specific processes was not the desired outcome (Guetter and Kutzbach, 1990). Nevertheless, such climatic delineation may be used to infer process and landform dynamics. The Köppen-Geiger system of climate classification (Köppen-Geiger-Pohl) expands the Köppen classification system to yield a total of 31 potential zones. While the main climate groups (A-E) and types (based on precipitation: *W*, *S*, *f*, *w*, *s*, *m*) are retained, several new ones are added, based mostly on an increased use of temperature ranges. These include hot arid (*h*) and cold arid (*k*) regions, hot (*a*), warm (*b*) and cool (*c*) summers, as well as extreme continental (*d*) temperature ranges. A summary of this classification system is given in Table 2 in APPENDIX B. Based on the Köppen-Geiger classification system, the Elandsberg and High Drakensberg have a warm temperate climate (Climate Group C, subtype *fb*), with mean temperatures of the coldest month as low as -3 °C, sufficient precipitation in all months, with warmest month means less than 22 °C and at least four months with means exceeding 10 °C. Dronning Maud Land (DML) exhibits a polar climate (climate group E) with average temperatures of the warmest month below 10 °C. This region can further be assigned to the polar frost climate (subtype EF), with annual mean monthly temperatures below 0 °C. Marion Island, in comparison, is not generally assigned a climate zone and omitted from most climatic zonation maps. A critique of the Köppen-Geiger system is that zones are drawn at broad scales with macro-scale divisions, representing only a portion of the actual vegetation-climatic diversity (Guetter and Kutzbach, 1990). A further criticism arises from the climatic zones not accurately reflecting soil and vegetation boundaries (Guetter and Kutzbach, 1990).

Walter (1985) devised a climatic classification system on nine climatic-vegetation zonobiomes (ZB), with further subdivisions possible based on precipitation values (as denoting dryness). The nine zones range from the equatorial (I), to tropical (II), subtropical (III), arid (VII), boreal (VIII), and polar (IX) (Table 3, APPENDIX B). Washburn (1979), while not defining a global climatic classification system, did delineate periglacial zones based on temperature (Table 4, APPENDIX B). His delineation yields four distinct zones, three based on latitude and one on altitude. His inclusion of altitude within this classification compares to the classification system of Strahler (1989). Strahler (1989) devised a classification based on thermal regimes and precipitation types that also accounts for highland climates, which are not constrained by latitudinal position (Table 5, APPENDIX B). There are three broad climate groups delineated into areas using precipitation and temperature values. In many ways this classification relates directly to the locations of the Hadley, Ferrell and Polar cells (Strahler, 1989). The three broad climate groups, based on the three climate cells and their associated air masses, consist of the 1) low-latitude, 2) mid-latitude, and 3) high-latitude climates (Strahler, 1974, 1989). Group 1 (low-latitude) is controlled by subtropical high-pressure cells and tropical low-pressure (Strahler, 1989) along the Inter-Tropical Convergence Zone (ITCZ). Group 2 (mid-latitude) is controlled largely by the polar frontal zone, whereas Group 3 (high-latitude) is dominated by polar (Arctic/Antarctic) air masses (Strahler, 1989). The mid-latitude zone stretches from the 35° to the 60° latitudes (Group II). However, this climatic zone is more prevalent in the Northern Hemisphere, due to it having more landmass in these parallels than the Southern Hemisphere. Less land occurs beyond the 40$^{th}$ parallel in the Southern Hemisphere, making these areas more affected by the oceans. Each group consists of various climates, yielding 13 in total, with four distinct climates assigned to Group I, six to Group II, and three to Group III. These climatic zones are assigned using climate subtypes based, predominantly, on precipitation values. Dry climates

are described for areas where evaporation/transpiration exceeds precipitation; in moist climates, the opposite is true. Semi-arid (steppe) (*s*), semi-desert (*sd*) and desert (*d*) climates are all described as dry climate subtypes. In comparison, the sub humid (*sh*), humid (*h*), per humid (*p*) all form part of the moist climate subtypes. The moist-dry climate subtypes exhibit seasonal variations between wet and dry seasons and consist of the wet-dry tropical and Mediterranean climates. The Mediterranean climates, for example, may be divided into 13 climate types consisting of the wet-equatorial, monsoon and trade-wind littoral, wet-dry tropical, dry tropical, dry mid-latitude (all low-latitude climates), moist subtropical, Mediterranean, marine west-coast, dry mid-latitude, moist continental (all mid-latitude climates), boreal forest, tundra, ice sheet highlands (all high-latitude), and dry subtropical (falling into low-latitude and mid-latitude climates). A critique of this system is that not enough parameters are used in its zonation, while the scale at which zones are drawn is too small. The Drakensberg and Marion Island fall within Group II of this system. The mid-latitude climates range from extreme seasonality (Mediterranean) to approximate uniform precipitation throughout the year, as is observed on Marion Island. Marion Island receives high amounts of rainfall and falls within the marine sub-Antarctic climate (Schulze, 1971), characterised by high amounts of annual precipitation and a small annual temperature range (Strahler, 1974). Most of South Africa is assigned to the dry subtropical climate, but the Drakensberg to an undifferentiated highland climate. The inclusion of moist tropical air into the polar front in summer yields high rainfall and a wet climate. For South Africa, the dry subtropical climate (25°-35°S) includes the steppe, semi desert and desert subtype. These three subtypes receive seasonal (summer) rainfall, with annual precipitation less than annual evaporation/transpiration. The influence of cyclones on the western coast of mainland South Africa yields the Mediterranean climate subtype. This region receives predominantly winter rainfall with mild temperatures and summers that are warm to hot and dry. The eastern coast, in comparison, experiences an apparent monsoon and trade wind littoral (narrow coastal zones) influenced climate. This classification, however, is not correct. While moisture-rich Indian Ocean air masses interact with mountains and produce orographic rain throughout most of the year along this coast, this climatic condition cannot be truly classed as monsoonal (Galvin, 2008). Nevertheless, temperatures are warm and humidity high with an annual cycle observed (Strahler, 1974). The climate of Group III consists of high-latitude climates and are characterised by the interaction of maritime and continental polar air (Strahler, 1974). In the Southern Hemisphere, this yields the Antarctic Polar Front, just south of Marion Island. Dronning Maud Land falls within this group and can be ascribed to the tundra or ice sheet climate. This area is dry and cold, with little to no precipitation received annually.

It is apparent that many climatic classification systems may be used, with the different systems yielding varying delineations. While work has been done on finding corresponding zonations for the various systems (Guetter and Kutzbach, 1990), no two systems are the same. Nevertheless, such systems are widely applied and provide an affective framework for delineating climatic zones. The Köppen-Geiger system has widest application (Wang and Overland, 2004; Kottek *et al.*, 2006; Peel *et al.*, 2007; Rubel and Kottek, 2010) and is useful as a basis of predictive climatic modelling (Kalvová *et al.*, 2003). This system has also been updated using current climate figures and its defining parameters fine-tuned to reflect current global zones more accurately (Peel *et al.*, 2007). Therefore, for this study this climatic classification system is used. Climatic geomorphology uses zones derived from such classifications to delineate morphogenetic regions – regions where specific landforms are expected to be found. However, geomorphology is considered a multivariate scientific field (Washburn, 1979), where several

processes may yield similar forms or processes yield specific forms (Thorn, 1992). While processes need to be investigated, it is often challenging to isolate these in geomorphic regimes and the complex interrelationships between processes, drivers and local setting are common in geomorphic systems (Phillips, 1999, 2007; Hjort and Luoto, 2009). While the investigation of landforms allows for identifying processes, many processes yield similar landforms, increasing the complexities of these systems. Therefore, assigning characteristic processes and landforms to climatic zones is not ideal nor suited to the multivariate nature of geomorphology.

Büdel (1951, 1953) describes processes and landforms typical to specific climatic zones. These morphoclimatic zones include the glacial, nival, humid temperate, semi-humid temperate, semi-arid and arid temperate, semi-humid tropical, semi-arid and arid tropical, and humid tropical zones, occurring in broad swathes from pole to equator (Büdel, 1953) (Figure 1). A typical description of morphoclimatic zones for Europe during the last glacial period would be glacial, periglacial, tundra, deciduous forest, forest, steppe, arid steppe, savannah and desert, semi-arid savannah, and savannah and tropical rainforest (Büdel, 1953). Within each zone further subdivisions occur, such as arid, desert and continental savannah. Morphoclimatic zones also have distinct divisions known as morphoclimatic borders (Büdel, 1951). These borders occur due to sudden changes in climate and concomitant processes active within that zone. For example, the well-defined northern boundary of European loess deposits, as described by Büdel (1951), is a morphoclimatic border and came about due to the limiting effect on cryoturbation of tundra and vegetation cover during the last ice age.

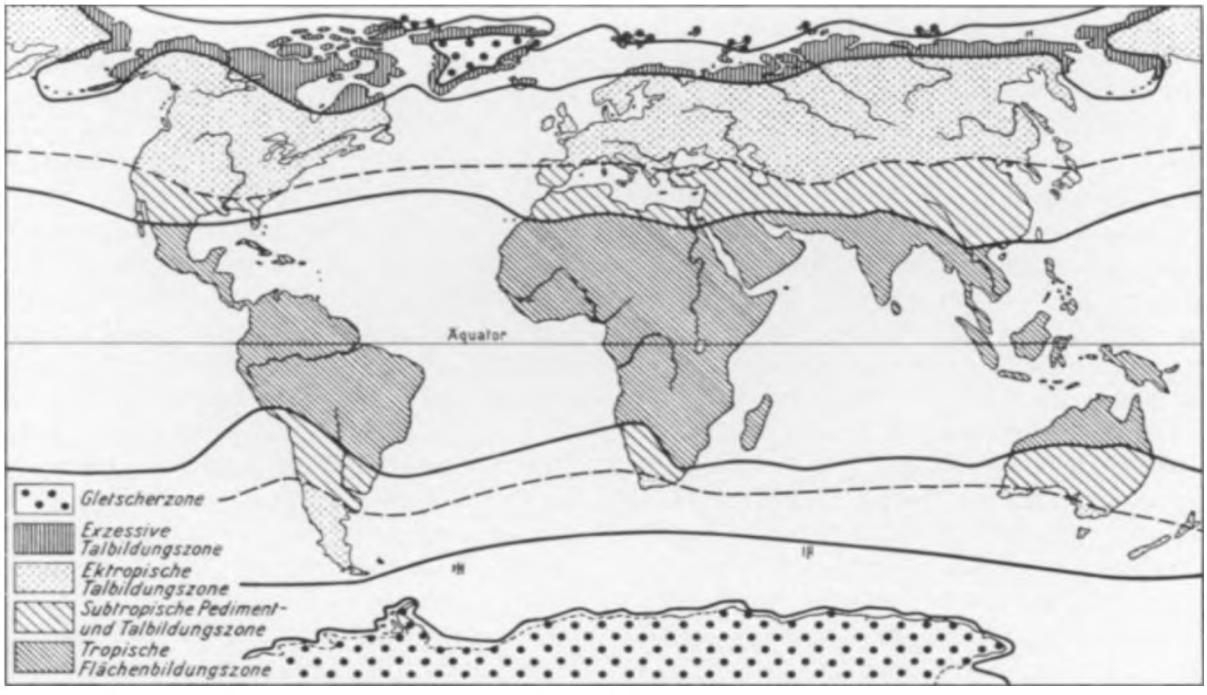


**Figure 1: Broadly-defined morphoclimatic zones (Büdel, 1953).**

Although Büdel focused on regional processes (Mensching, 1984), zonal divisions are essentially limited only by the scale a person is interested in, increasing the overall complexity of the system. As complexity

increases, so equifinality becomes integral to the system (Beven, 2000). Self-organisation, such as observed pattern formation or mutual adjustments, implies that individual landscape parameters and characteristics adjust to the general characteristics of the system (Phillips, 1999). The linear stationary non-equilibrium state of an open system is dependent on time-independent state variables and constant gradients between system and environment and a suitable description of geomorphic systems (King, 1966; von Elverfeldt, 2012). This stationary state is a feature of open systems, where the system achieves a local (or temporary) equilibrium state and is not a reflection of the final equilibrium state of a closed (or isolated) system (von Elverfeldt, 2012). Such systems apply the equilibrium or non-equilibrium worldviews. In the *equilibrium* worldview, the dynamic balance between force and resistance yield steady-states, contemporary processes may override historical states, and landscape evolution is convergent outcome (Phillips, 2007). In the *non-equilibrium* worldview, the non-equilibrium state of a system overrides and is more common than the equilibrium state outcome (Phillips, 2007). Furthermore, this worldview accounts for non-linear, open, and dynamic systems and landscape evolution may be both divergent and/or convergent (Phillips, 2007). The *perfect landscape* approach, as proposed by Phillips (2007), incorporates the non-equilibrium and historical worldview. Historical inheritance in landscapes is acknowledged, while global and local factors are fundamental to any landscape. Global factors, such as temperature and precipitation values used for climatic zone delineation, therefore, force landscape evolution. However, local contingent factors, such as geology, vegetation and aspect, impact landscape evolution, and concomitant landform morphology, as well.

Zonality is a core concept in climatic geomorphology, where climatic zones control mechanical and chemical weathering (Sumner *et al.*, 2004b), driving processes, which in turn form zone-specific landforms and landscapes (Thorn, 1992). The glacial zone, for example, will have characteristic landforms such as glacial valleys, hanging valleys, striations, and moraines. The arid zone will have landforms such as dune fields. As such, climate geomorphologists believe that geomorphic processes inherent to each climatic zone will engender regional patterns and landforms characteristic of that zone (Priesnitz, 1988; Goudie, 2004c), *i.e.* landforms develop because of one overriding process or specific climatic factor (Priesnitz, 1988). At these scales it becomes apparent that this contradicts the concept of equifinality as argued by *e.g.* Culling (1957), where in an open system similar processes yield similar, or specific, landforms, irrespective of the initial condition. Culling (1957), stressed that equifinality, as a concept should not be too broadly applied, when considering a single stable state and the chaotic nature of natural systems. Nevertheless, he argued for ergodic and topologic equifinality (Culling, 1987), referring to the simplexity of systems (Cohen and Stewart, 1994; Phillips, 1997). Although arguments have been made against equifinality as a concept within geomorphology by *e.g.* Haines-Young and Petch (1983), simplexity requires that a measure of equifinality is present. However, this should not be too broadly applied but rather at specific scales (Phillips, 1997), such as those applicable to periglacial environments. Geomorphology, as a system science, requires the consideration of open systems and the inclusion of self-organisation concepts, where individual open systems make up closed systems, dependent on how these systems are delineated (von Elverfeldt, 2012). As introduced in CHAPTER 1: Introduction (pg. 1 onwards) periglacial geomorphology consists of the examination of diurnal, seasonal and perennial ground ice (permafrost) and their impact on landform and landscape development (Thorn, 1992). Periglacial geomorphology concerns itself with past, present and future processes and environments and the integral role that frost action and low temperatures have in these settings (Thorn, 1992; Skinner, 2004). Furthermore, snow packs, fluvial, lacustrine, as well as marine

ice are investigated, and not only glacial ice that older definitions focused on. The definition of the periglacial environment has changed with time, shifting from the mid-latitudinal, pro-glacial and mountainous description used by Lozinski (1909), to one where frost processes and/or permafrost are dominant, with a greater emphasis placed on seasonal freezing and thawing over short-term cycles (French, 2000). The geographical location of such environments within climatic zonations has, therefore, shifted. Nevertheless, the process of assigning periglacial environments to specific climatic zones still applies. In general, periglacial zones are thought to cover ± 25% of the earth's surface, spanning the circumpolar zones and are also found at high altitudes (Skinner, 2004; Lewis, 2008b; Hjort and Luoto, 2009). Depending on the definition of the periglacial environment that percentage ranges from 35% (using the freeze-thaw process as the defining characteristic) to 20%, when using the presence of permafrost as the defining characteristic (Washburn, 1979; Goudie, 2004b). Freeze-thaw processes are fundamental to the periglacial environment (Washburn, 1979). The assumption of climatic geomorphology, therefore, would discern freeze-thaw processes integral to periglacial environments, as already pointed out by Büdel (Mensching, 1984). In his paper *'Die "periglazial"-morphologischen Wirkungen des Eiszeitklimas auf der ganzen Erde'* (The morphological effects of climates outside the glaciated areas during the Ice Age) the glacial and periglacial climatic zones, especially during the Würm period, are discussed, as is the role frost cycles have on weathering and debris-supply of soil and ground (Büdel, 1953).

Glacial and periglacial landforms are associated with cold climatic conditions, and are found globally in high-altitude and -latitude areas, such as Greenland, Antarctica, sub-Antarctic islands and mountains such as the Andes and Himalayas (Lewis, 2008a). They also occur in high regions of the mid-latitudes, such as the Southern Alps of New Zealand. The migration of ground water and concomitant volumetric expansion of water from the liquid to solid phase causes primary and secondary heave (Barsch, 1993), whereas the thawing of water leads to subsidence of the ground (Goudie, 2004a, 2004b). The combined dynamics associated with phase changes of water from liquid to solid stages and *vice versa*, as well as the gaseous phase, yields specific landforms (Goudie, 2004b). Periglacial landforms, or those found in current regions falling under the periglacial description, range from the macro- to the microscale and include solifluction lobes, patterned ground (sorted or unsorted), openwork block deposits, and rock glaciers. For this study, solifluction is used in favour of gelifluction (Barsch, 1993), as it refers to the movement of saturated ground over an impermeable layer and not specifically only a frozen substrate. Specific landforms range from thermal contraction polygons, sorted and non-sorted circles, sorted and non-sorted stripes, nets, autochthonous and allochthonous block deposits, mud boils, and terraces/steps, as well as stone-/vegetation-/mixed-banked lobes *(e.g.* Williams and Smith, 1991; van Everdingen, 1998; Goudie, 2004b; Stewart, 2011; Warburton, 2013). Although freeze-thaw processes are common to periglacial environments, the resultant landforms are not always unique and azonality of landforms has been shown to exist. Not all landforms thought to have developed under periglacial conditions are necessarily formed under these conditions and indicative of previous climatic conditions (André *et al.*, 2008). Angular nature of clasts commonly found in periglacial settings may be as much due to local lithology and geology as due to freeze-thaw cycles (Whalley *et al.*, 2004). Furthermore, the angularity of clasts, previously thought to support periglacial origins, doesn't necessarily prescribe periglacial conditions (Hall *et al.*, 2002). Angular clasts are also found in warm deserts, areas that don't fall within the periglacial environmental. Zonation may also be applied with a focus on parameters such as soil aggregates (Weinert, 1980). An example of such delineation is Weinert's *N*-value, a ratio with

wide application in South Africa (Weinert, 1984; Republic of South Africa, 2007). This ratio makes use of the climatic parameter of annual precipitation and evaporation rates of the warmest month (Weinert, 1984). Here the focus is not on landforms, but rather on determining the type of soil aggregates found for an area using climatic parameters as proxies for the weathering of bedrock (Kleinhans, 2006; Diop *et al.*, 2011). The assignation of climatic zones and the parameters used to delineate these zones are, therefore, driven by the purpose of zonation and the data available for delineation.

Today climatic geomorphology still largely focuses on the dominant and overriding role that climate has on processes and landforms. Like Büdel's (1953) original use of temperature as the defining criteria, based on vegetation zones, delineation of zones is still largely based on annual average air temperature values to the exclusion of ground temperatures. However, annual averages are not suitable to identify zones where seasonal and, specifically, diurnal cycles effect the landscape. Furthermore, Thornthwaite (1948), stresses the importance of evaporation within climatic zonation and critiques the use of average air temperatures as a proxy for the soil-moisture balance. The number of freezing cycles observed in the air does not equate to the same quantity of freezing cycles in the ground and using average air temperatures as a defining parameter is not sufficient. Furthermore, the depth of diurnal freezing in the ground is also less, with cold periods of several days only penetrating the ground by a few centimetres (Williams and Smith, 1991). Using the intensity (absolute temperature minimums reached) of freezing and thawing of the ground as a delineating parameter to the periglacial environment is also highly complex. Barsch (1993) argues that intensity of freeze-thaw cycles can be given on various scales, such as diurnal or seasonal, and may also refer to air or ground temperatures. Furthermore, intensity may also use various thresholds, such as minimums or averages, warranting a re-evaluation of these defining parameters. Although average temperature and moisture values are generally applied, local variations may occur, making the general assignation of climate to an area not necessarily appropriate at several scales. Topographic control on freeze-thaw cycles in high mountain areas, as well as aspect-related climatic controls need to be considered (Barsch, 1993). A greater understanding of radiation budgets, linked to solar radiation, is also required to more appropriately delineate *e.g.* periglacial environment (Barsch, 1993).

A further critique of climatic classification systems, on which climatic zones are based, is that the soil-moisture balance isn't considered for all systems, although Thornthwaite's (1948) classification and the Köppen-Geiger system (1936) do consider moisture in their classification. Moisture is an integral component of the frost environment. Moisture phase change leads to soil heave, as well ground subsidence. The phase change of ground moisture, driven by temperature dynamics, yields periglacial features and excluding ground moisture from climatic zonations leads to the exclusion, or incorrect delineation, of this environment within climatic classification systems. Büdel (1953) highlights the importance that moisture has within each zone, stressing that landforms develop due to the interrelation of many factors (relief, climate, geology, hydrology, weathering *etc.*) and processes active within each zone. Yet additional parameters, such as soil characteristics, geology, and vegetation are often excluded when delineating climatic zones. Lastly, current morphoclimatic zones would have paleolandforms found in each, *i.e.* the relative short period of the Holocene yields morphoclimatic

zones that have inherited paleolandforms resultant of older morphoclimatic zones. Climatic zones are not static and change with time. Guetter and Kutzbach (1990), for example, show that only 30% of the land cover found in current climatic zones is comparable to that of 126 000 Ma, with that proportion increasing to 45% for 18 000 Ma, the time of the last glacial maximum (LGM). Only the Amazon Basin and northern Sahara are calculated to have not undergone land surface change, although Antarctica is excluded in these calculations (Guetter and Kutzbach, 1990). It follows that landforms found within those of the Amazon Basin and northern Sahara are likely to be an indicator of the climate of the last 126 000 years. For other regions on the globe, the same cannot be said. Significantly, the mid- to high-latitudes showed the greatest change (45%) in surface cover from 18 000 Ma to the present. Climatic changes, therefore, may bring about a shift of climatic zones (including periglacial belts), complicating climatic zonal delineation (Barsch, 1993). As climatic zones shift some landforms, due to their often-longer life span and time for development required, may develop into paleolandforms within the new climatic zones. Such landform may also be formed and shaped by the contemporary processes of the new climatic zone, increasing the complexity of these landforms. Inherited landforms, therefore, obfuscate the evaluation of landscapes and often contribute to the appearance of convergence of form (Odoni, 2007). This is particularly noticeable in Europe, where many glaciated areas have been at least partly moulded under periglacial conditions (Goudie, 2004b). In addition, the sensitivity of high- and mid-latitudinal geographical zones to changes in climate yields areas often exhibiting paleoglacial, as well as periglacial landforms (Lewis, 2008a). Periglacial zones are, furthermore, difficult to delineate dependent on which definition of the periglacial environment the individual is applying to the zonation (Barsch, 1993). It is, therefore, apparent that although climatic geomorphology offers a polished approach to landscape studies, shortcomings remain. Climatic zones are not appropriately and consistently identified, and a failure to establish process-form and climate-form links is apparent. Furthermore, there is an uncertainty in determining meteorological/climatic inputs, as well as geomorphic processes on a temporal scale. Finally, the failure to approach the subject in a holistic manner is worrisome (Thorn, 1992). Zones are defined on the macro-scale, with local characteristics and dynamics ignored (Graham and Midgley, 2000). This over-simplification of zones and processes leads to the exclusion of significant processes (Mensching, 1984). Climatic geomorphology does not consider the rate of processes and historically the measurement of processes and forms is inadequate (Goudie, 2004a). Assumptions stemming from climatic geomorphology, such as chemical weathering being absent in cold climates, are incorrect (Hall, 2002). Landforms found in current climates may also constitute relict landforms, indicative of past environments (Goudie, 2004a). In addition, research by *e.g.* Sumner *et al.* (2004b) have indicated that similar geomorphic features occur in different climates and that geomorphic effects may be similar across climate zones. Sumner *et al.* (2004b), show that rock surface thermal regimes are azonal. Furthermore, Birnie and Thom (1982), argue that landforms such as rock glaciers are more likely to be affected by debris supply than a zonal climate.

It is not sufficient nor appropriate to identify linear processes considering many geomorphological processes operating at varying intensities, produce similar landforms. Beyond identifying the appropriate model for estimating a process and its distribution given the data available, it is crucial to know that the 'optimum' model might not always be such (Hornberger and Spear, 1981), and that such models exhibit uncertainty in representation of that system (Beven, 1996; Rhoads and Thorn, 1996; Beven, 2000). This particularly applies to open models (von Bertalanffy, 1968). Furthermore, global parameters are not sufficient to model local parameters, which often have unique characteristics

(Beven, 1996, 2000; Phillips, 2007). Multiple parameters working at various scales and intensities may yield the same result, but also a divergence of form (Phillips, 1999). Therefore, the broad delineation of climatic zones using limited defining parameters is not sufficient. Climatic geomorphology argues for specific processes yielding specific landforms, while equifinality argues for various processes yielding specific landforms. Ascribing landforms to specific processes introduces potential fallacy of the converse (Equation 1).

**Equation 1: Affirming the consequence.**

$$\frac{P \rightarrow Q, Q}{\therefore P}$$

An error in formal logic occurs when the antecedent is said to be true, based on the assumption that the consequent is true (Jevon, 1918). The antecedent of a conditional statement follows the '*if*' portion of the statement, whereas the consequent of a conditional statement follows the '*then*' portion of the statement (Jevon, 1918). In a conditional statement the consequent follows on from the antecedent. However, the antecedent can only be inferred from the consequent if the statement is not conditional, but rather a biconditional proposition (Jevon, 1918). Affirming the consequent can be explained using examples based on a specific landform and mean annual air temperature (MAAT), as given in Table 1.

**Table 1: Affirming the consequence: illustrative examples. MAAT: mean annual air temperature.**

| Logical Expressions | Example 1 | Example 2 |
|---|---|---|
| Antecedent: P | Gelifluction lobes are present. | MAAT is 5 °C. |
| Consequent: Q | This is a cold environment. | This is a periglacial environment |
| Conditional Statement: $P \rightarrow Q$ | If gelifluction lobes are present, then this is a cold environment. | If MAAT is 5 °C, then this is a periglacial environment. |
| Affirming the Consequent: $\frac{P \rightarrow Q, Q}{\therefore P}$ | This is a cold environment. Therefore, gelifluction lobes are present. | This is a periglacial environment. Therefore, MAAT is 5 °C. |

Parameter titles are given in the 1st row. The antecedent is given in the 2nd row, the consequent in the 3rd row. The conditional statement (4th row) requires that, if the antecedent is valid, the consequent is valid too. An error in logic arises when this statement is applied in reverse: assuming the antecedent is valid when the consequent is valid (5th row). Just because gelifluction lobes are commonly found in cold climates does not make every area, in which they occur, a cold climate zone (Example 1). Furthermore, mean annual air temperature does not have to be 5 °C in a periglacial environment (Example 2). The argument of climatic geomorphology, therefore, contains logical fallacy. While climatic conditions may yield specific processes and these processes in turn help form specific landforms, this is not always, nor exclusively, the case. Specific processes will not necessarily produce the same resultant landform, nor

is any landform necessarily the result of specific processes (Hall and Thorn, 2011). As such, climatic geomorphology makes use of a conditional statement, not a biconditional proposition, leading to a logical fallacy.

Beven (2006) argues for increased system complexity, leading to equifinality, while Phillips (1999) argues for such complexity yielding divergence of form. When applying equifinality to current climatic zone delineation, azonality of landforms should be evident. While equifinality should be considered, this must be done at the appropriate scales (Phillips, 1997). Furthermore, excluding the equifinality concept places unnecessary artificial constraints on models (Beven, 2006). While the search for an optimal model and a simplification of environmental systems when running predictive analyses is valid, while also an important concept within scientific inquiry, such an approach should not be done to the exclusion of eliminating other significant parameters. An attempt must be made to move from the optimal model to behavioural models (Beven, 2000). If that is not possible, then perhaps greater focus should be made to identify the various sub-sets of behavioural models within the greater space of the climatic geomorphology model, *i.e.* considering ergodic and topologic equifinality (Culling, 1987). This simplexity is applicable to the frost environment, where small-scale changes, such as soil textural properties, do not change the overall effect of freeze-thaw cycles and the thermal regime of specific landforms. One limitation of behavioural models is that sufficient numbers of samples need to be obtained to provide a robust and repeatable model output (Beven, 2006). As such, the current project has focused on obtaining a wealth of climatic and site-specific data, to allow for some measure of behavioural modelling. Geographical space is not homogeneous, and processes and agents act variable across it. As such, two settings might yield similar characteristics, yet have different underlying parameters. Simultaneously, two settings with mostly-similar parameters might exhibit different characteristics. Furthermore, optimal models of *e.g.* the Köppen-Geiger system do not account for the complexity of true natural models (Beven, 2006). Atmospheric climatic conditions alone are not enough to identify processes (Williams and Smith, 1991). External parameters such as geology and lithology, altitude, latitude, soil characteristics and the local time scale influence processes and landforms alike. Lower latitudes are also associated with higher radiation budgets and continental emissivity budgets differ for climate regimes. Furthermore, radiation budgets in mountainous areas (high-altitudes) are topographically controlled (Washburn, 1979; Barsch, 1993). Vegetation cover has been identified as a limiting factor in frost environments, having a negative feedback on periglacial systems (Hjort and Luoto, 2009), due to vegetation ameliorating ground temperature dynamics (Brady and Weil, 2016). Many forms of patterned ground are either initiated by vegetation, or controlled by it (French, 2000). In sparsely vegetated zones periglacial processes become more dominant, whereas an increase in vegetation cover decreases the effects of processes common to the periglacial environment (Hjort and Luoto, 2009). The removal of vegetation increases freeze-thaw cycles, leading to thawing of the ground in permafrost regions (Jones *et al.*, 2015), and an increase in the depth of thaw cycles (Rocha *et al.*, 2012; Nossov *et al.*, 2013). Similarly, the removal of organic matter may increase freezing events in areas where vegetation provides an insulating layer. This is particularly applicable to the High Drakensberg, where burning and overgrazing may remove vegetation and surface soil organic matter (Liljedahl *et al.*, 2007; Myers-Smith *et al.*, 2008; Nossov *et al.*, 2013; Jones *et al.*, 2015), thereby exposing the ground to greater thermal fluctuations with subsequent increased landscape-scale microtopography (Jones *et al.*, 2015). Moisture availability too, is an important component (Williams and Smith, 1991). Although longer sustained freezing and frequent diurnal freeze-thaw cycles are most

common in mid-latitudes and high altitudes, short cycles of freeze-thaw can occur in many climates. The mid-latitudes exhibit a higher number of diurnal cycles when compared to the high-latitudes, due to longer periods where fluctuations around 0 °C may occur (Williams and Smith, 1991). Snow cover may have both an insulating effect (Williams and Smith, 1991; Ishikawa, 2003; Hedding, 2008), or an enhancing effect (Holness, 2003a; Boelhouwers *et al.*, 2008), and must be considered when investigating periglacial processes and landforms. Finally, the lack of consensus on how to delineate periglacial environments, *i.e.* to base such delineation on 1) the presence/absence of permafrost, and 2) the presence of freeze-thaw cycles and deep seasonal freezing illustrate the difficulty of climatically demarcating geographic areas based on a limited number of factors. This is further complicated by the fact that, depending on which parameter is used, an area might be described as not periglacial under Condition 1 (permafrost presence), but periglacial when using Condition 2 (freeze-thaw cycles) (Goudie, 2004b). This project applies Condition 2 when describing the periglacial environment. While permafrost is present at some of the chosen study sites (those located in DML of Antarctica), it is not present in the Drakensberg, nor on Marion Island. As such, the presence of freeze-thaw cycles is used to delineate the periglacial environment.

Another topic of discussion is the changing climate that the world is experiencing. Simulations by *e.g.* Rubel and Kottek (2010) have shown that the Drakensberg and Elandsberg will shift from the current C*fb* classification to C*wb* and C*fa* respectively. This suggests a generally drier and warmer climate, having implications on freeze-thaw cycles and associated landforms. The high latitudes of the Southern Hemisphere have also shown increasing temperatures over the last 40 years (Bargagli, 2005), potentially shifting climatic and vegetation zones (Chown and Smith, 1993). Holden (2007) discusses how small changes in temperature can have a significant impact on the number of potential freeze-thaw events and freeze-thaw cycles observed for Marion Island. Furthermore, the frost environment on the sub-Antarctic islands is particularly sensitive to climate change (Boelhouwers, 2003a; Boelhouwers *et al.*, 2003) and the ice cap once present on Marion Island in the 1960's has now disappeared (Sumner *et al.*, 2004a; Meiklejohn, 2011). An increasingly drier, windier and warmer climate is observed on sub-Antarctic Marion Island (Smith, 2002). Frost processes contribute to sediment generation and cryoturbation, mainly due to heave and subsidence associated with alternating freezing and thawing of water. Furthermore, such cycles are effective as disintegration and disaggregation agents (Brady and Weil, 2016), and may alter the physical condition of medium and fine textured soils (Brady and Weil, 2016). Slight increases in temperature can have significant effects on environments exhibiting temperatures near the threshold for freeze-thaw cycles to occur. Polar and boreal/tundra zones are projected to decrease in surface coverage under a warming climate (Kalvová *et al.*, 2003; Wang and Overland, 2004), having significant implications on the release of organic carbon and methane from the thawing permafrost (Schuur *et al.*, 2008). Cold climate zones are sensitive to climatic changes and are projected to decrease by ± 30% in surface coverage by 2085 (Barsch, 1993). Subsequently, these climatic zones have the potential to show warming trends faster than areas where no, or limited, frozen water occurs, warranting the need for intensive investigation of processes and landforms found within them. As such, a greater understanding of these cold climate zones is required, especially for the Southern Hemisphere. Associations established to further such understanding include the International Permafrost Association (IPA) and its initiative, the Global Terrestrial Network for Permafrost (GTN-P). GTN-P is an international initiative that concerns itself with the monitoring of permafrost and was initiated in the 1990s by the IPA under the Global Climate Observing System (GCOS)

and the Global Terrestrial Observing Network (GTOS). Such monitoring includes investigating dynamics of the active layer, as well as contributing to our knowledge on the Essential Climate Variables (ECVs) of changes in active layer thickness and permafrost temperatures (Christiansen, 2013). Data collected in DML contributes to our current knowledge and understanding of the Thermal State of the Permafrost (TSP), as well as active layer dynamics and thickness for western DML and central DML. While the monitoring sites within western and central DML do not meet the specifications of the Circumpolar Active Layer Monitoring (CALM) protocols, results obtained here, nevertheless, contribute to a greater understanding of the active layer within the greater area of DML. Further associations established to address the current need for further studies on Southern Hemispheric permafrost and active layer research are the Antarctic Permafrost, Periglacial Environments and Soils (ANTPAS) (a working group of the Scientific Committee on Antarctic Research [SCAR]), as well as initiatives such as the National Aeronautics and Space Agency's (Nasa) Soil Moisture Active Passive (SMAP) sensor. The launch of SMAP on 31 January 2015 was a response to the need for, amongst others, a greater understanding of those zones across the globe where ground is either frozen or thawed. One of SMAPs missions is to aid scientists in more accurate and certain climate predictions and has, thus far, produced the highest-accuracy soil moisture maps ever obtained from space (Nasa, 2015). Unfortunately, SMAP's radar antenna failed in the latter part of 2015, affecting the scientific data output of the mission (Nasa, 2015). Furthermore, while SMAP obtains global soil moisture data, the freeze-thaw product (L3_FT_A) is only available for Northern Hemispheric, and not Southern Hemispheric, regions above 45° (National Aeronautics Space Agency (Nasa), 2014). This presents the opportunity for the current project to contribute towards such a product. Another scientific endeavour worth noting are the 80 SCAR Horizon Scan questions (Kennicutt *et al.*, 2014, 2015). While the Horizon Scan outcomes focus on research on the Antarctic continent, scientific direction for such research is placed within the global scientific environment. Questions that form part of the Horizon Scan focus on the southern polar regions and aim to provide insight into topics and fields, which would be difficult to answer outside of Antarctica (Kennicutt *et al.*, 2014, 2015). Questions relevant to the periglacial environment include questions numbered 10, 20, 22, 23, 48, 49, 50, 53, 59, and 60 (Table 6, APPENDIX C). Horizon Scan questions that the current project contributes toward are Question 39 and Question 42. Both questions fall within the dynamic earth topic. Question 39 deals with dating ancient landscapes that have been, or are currently, covered by ice, allowing for the emergence for new paradigms within the evaluation of surface processes and landscape evolution (Kennicutt *et al.*, 2014, 2015). Question 42 focuses on the state of permafrost and its role within terrestrial hydrological systems and ecosystems, as well as its role as a contributor to climate change (Kennicutt *et al.*, 2014, 2015).

***#39*** *What are and have been the rates of geomorphic change in different Antarctic regions, and what are the ages of preserved landscapes?*

***#42*** *How will permafrost, the active layer and water availability in Antarctic soils and marine sediments change in a warming climate, and what are the effects on ecosystems and biogeochemical cycles?*

By evaluating freeze-thaw processes across several sites together with observed landforms and other relevant geomorphological information at various spatial and temporal scales, this study aims to reconcile and refine our current understanding and delineation of periglacial zones. A summative assessment of the frost environment is presented for three defined study areas within the Southern Hemisphere. This contributes toward an estimation of frozen and thawed ground found in the Southern Hemisphere within the investigated region, while the work conducted in DML of Antarctica and the sub-Antarctic also contributes towards the SCAR Horizon Scan questions. A holistic approach is applied with climate-form and process-form links investigated and presented. The climatic geomorphology paradigm is investigated with reference to freeze-thaw cycles. Furthermore, equifinality is critically evaluated for the given study areas. An intra-site comparison is made to identify site-specific drivers, whereas an inter-site comparison is made to identify the dominant drivers and agents of freeze-thaw processes. Furthermore, an argument is presented based on the identification of these main drivers in terms of delineating climatic zones (regarding processes) with greater applicability.

# CHAPTER 3: Study Area and Site Description

The research is focused on three locations of varying climates ranging from hyper-arid, to areas of high rainfall, differing geology as well as a range of altitudes and latitudes. The different altitudes and latitudes are of interest as both elevation and latitude control active layer thickness with an increase in latitude and altitude resulting in a decrease in active layer thickness (Fahey, 1973; Adlam *et al.*, 2009). Each site is described in terms of climate, vegetation biome, geology, soil and other relevant parameters. Soil classification is based on the World Reference Base for soil resources (IUSS Working Group WRB, 2015). Where necessary the USDA soil taxonomy is provided as well (Soil Survey Staff, 1999). The three study sites are the High Drakensberg and Elandsberg of the Eastern Cape of mainland South Africa, sub-Antarctic Marion Island, and Dronning Maud Land (DML), Antarctica (Figure 2, pg. 26). All appendices mentioned in the text form part of the supplementary material to this document.

The Eastern Cape Drakensberg has an alpine environment, Marion Island is hyper-maritime with high annual rainfall, and DML is a polar desert. On Marion Island and the Eastern Cape Drakensberg two main sites are investigated. In comparison, the larger area of DML necessitates numerous study sites. As such, seven sites are located within western DML (WDML), with two in central DML (CDML). The southernmost study site is Slettfjell (72°08'S) in WDML, with Ben MacDhui (30°38'45"S) in the Eastern Cape the northernmost site. The westernmost site is Flårjuven (03°23'W) in WDML, whereas sub-Antarctic on Marion Island (37°45'E) is the easternmost site. There is a range of 3 000 m in altitude and ± 40 degrees in both latitude and longitude. One study site on Marion Island is located near sea level at 87 meters above sea level (m a.s.l.), while the highest site on Ben MacDhui in the Eastern Cape Drakensberg has an altitude of 2993 m a.s.l.

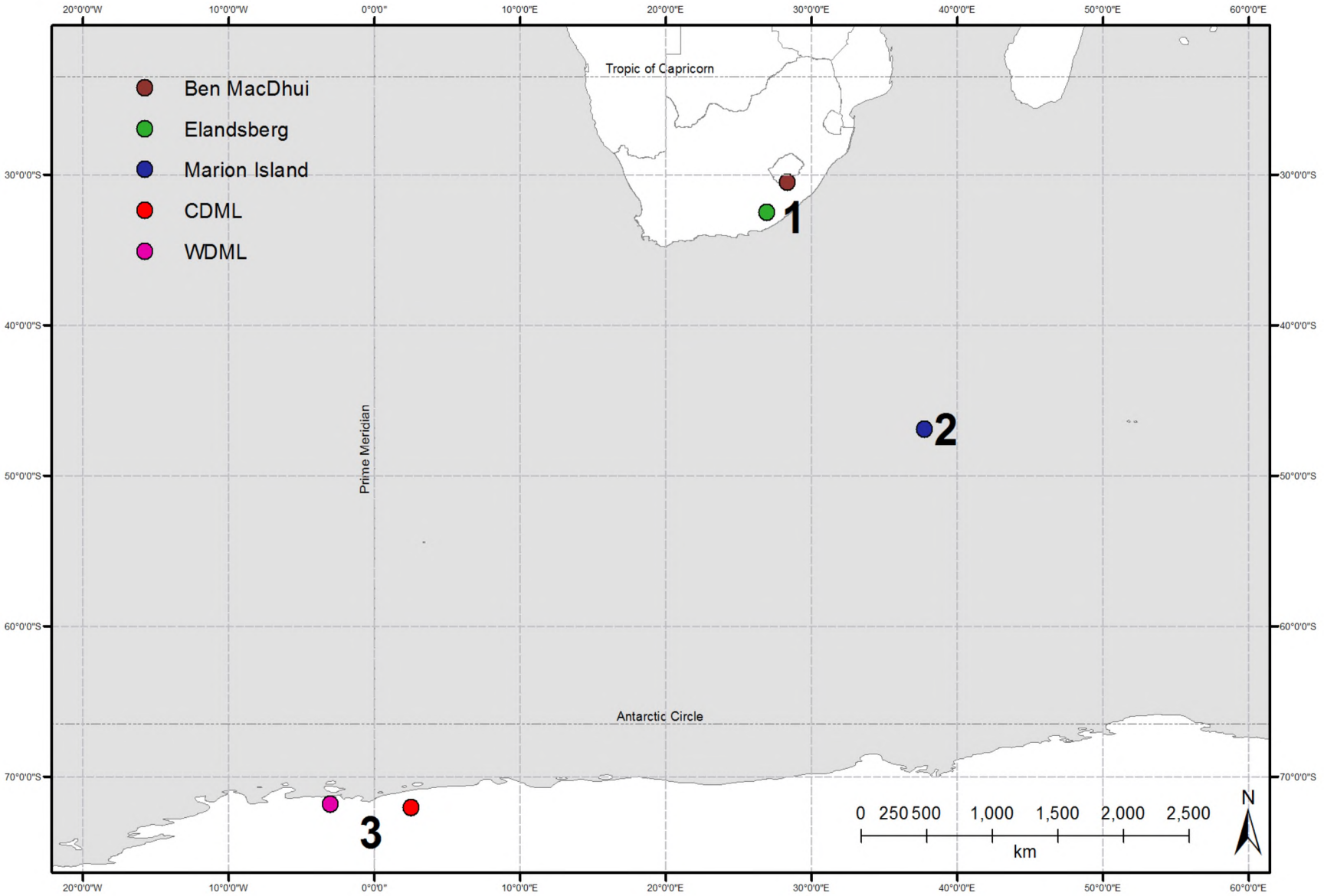


**Figure 2: The location of the three study sites in relation to each other. The Eastern Cape Drakensberg are indicated by '1'; sub-Antarctic Marion Island by '2'; and Dronning Maud Land by '3'. CDML: central Dronning Maud Land. WDML: western Dronning Maud Land.**

## 3.1 Eastern Cape

Two study sites were chosen to represent the Eastern Cape Drakensberg (Figure 3, pg. 28). The area falls within the mid-latitudes and has the lowest latitude for this study. One site is located near the Tiffindell Ski & Alpine Resort (Tiffindell), on the slopes of Ben MacDhui (30°39'S, 27°56'E), which rises to a height of 3001.2 m a.s.l. (Kück, 1997). The second site is the Elandsberg (32°29'S, 26°52'E) near Hogsback in the Eastern Cape.

The Eastern Cape High Drakensberg has a mid-latitude cool alpine environment with a mean annual rainfall of 1 050 mm (Sumner *et al.*, 2004b), compared to the mild temperate climate of the Elandsberg. Both locations fall within the *Cfb* classification of the Köppen-Geiger system (Kottek *et al.*, 2006), where the mean temperature of the coolest month is between 18 °C and -3 °C and precipitation expected throughout the year. Kück (1997), in comparison, appropriately assigns Ben MacDhui to *Cwb*, where precipitation falls predominantly in summer. Mean annual air temperature (MAAT) at altitudes exceeding 2 800 m a.s.l. ranges from 3 °C to 7 °C (Boelhouwers, 1994; Grab, 2002b). Diurnal and seasonal freeze-thaw patterns are well-developed in high-lying mountainous areas of the mid-latitudes, with ranges in MAAT between 15 °C and 22 °C (French, 1996). In the northern, central and southern Drakensberg ground temperatures are generally higher than air temperatures, and seasonal/long-duration ground freezing is absent (Nel, 2008). Active periglacial activity occurs, with increasing altitude, from Barkly East toward Lesotho. Active periglacial landforms consist of sorted and non-sorted features driven largely by needle ice (Boelhouwers and Meiklejohn, 2002). Diurnal freezing has been observed to 2 300 m a.s.l. on Ben MacDhui (Kück, 1997), but freeze-thaw cycles are possible to altitudes as low as 2 000 m a.s.l., as suggested by minimum nocturnal temperatures at Rhodes Village, near Ben MacDhui, recorded to be -22 °C during the 1990s (Lewis *et al.*, 1994). Furthermore, needle ice has been observed for the Elandsberg (*pers. obs.*), as well as Gaika's Kop (Meiklejohn, 2017; *pers. comm.*). Temperatures for Tiffindell between June-August of 1995 and 1996 show ground level oscillations above and below freezing 20% of the time (Kück, 1997), indicating the presence of freeze-thaw cycles and the suitability of the area to diurnal freezing and thawing. At this site 62 and 65 frost days are recorded for the winters of 1995 and 1996 respectively (Kück and Lewis, 2002). Ambient air temperatures show soscillation above/below zero 40% of the time and diurnal ranges of 10 °C are common. Moisture levels are low during winter but increase in spring (Kück, 1997). Thawing towards the end of September results in the ground being saturated with lower levels still frozen, creating suitable conditions for solifluction (Kück, 1997).

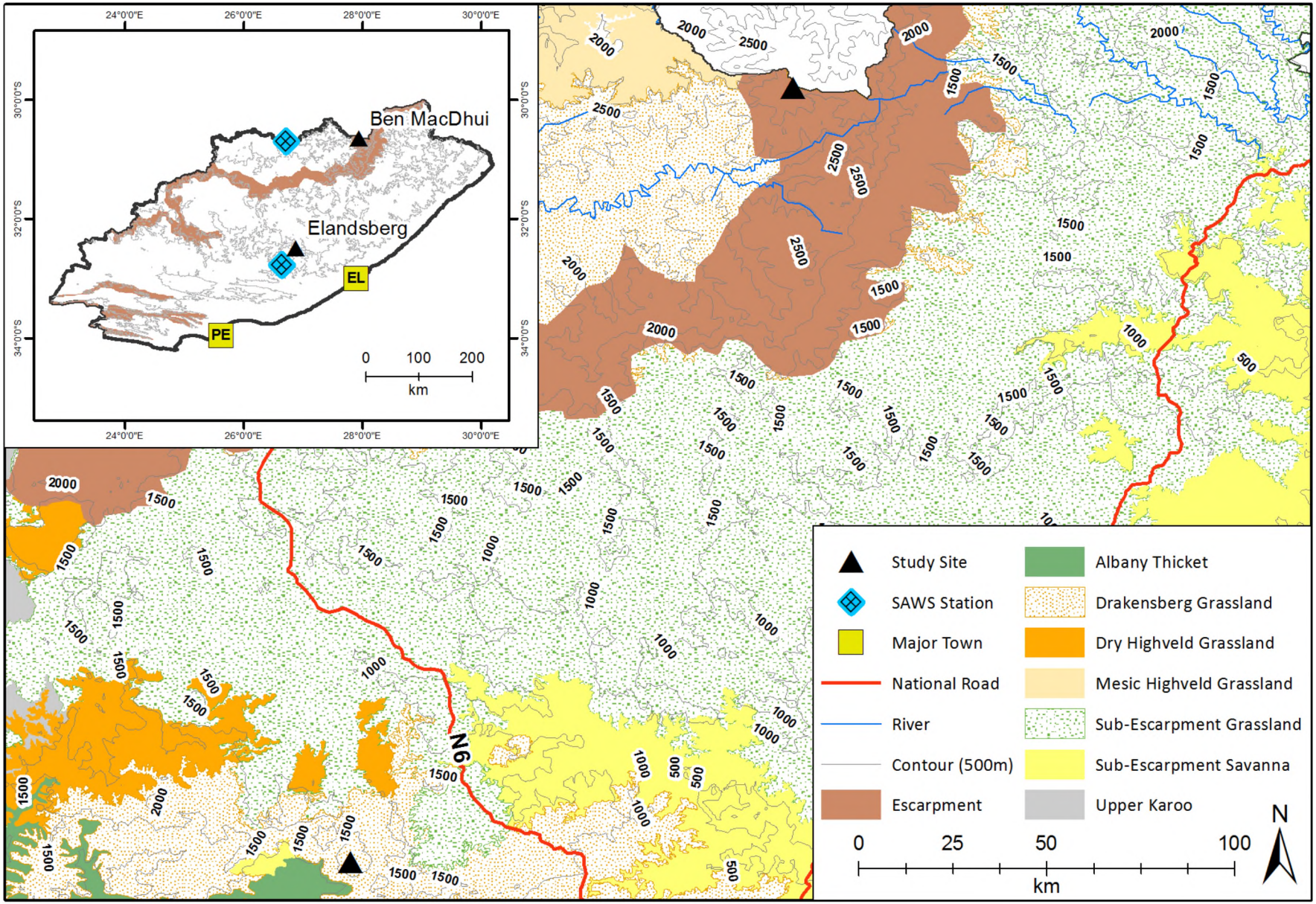


**Figure 3: The Eastern Cape study area. Bioregions are indicated, as is the escarpment. Study sites (n = 2) are indicated by triangles. South African Weather Service (SAWS) stations are indicated by a rectangle on its tip, over a blue background.**

In the Eastern Cape Drakensberg, the area above 2 550 m a.s.l. is classified as an active alpine (montane) periglacial zone, due to many active periglacial features present and MAAT near Tiffindell, at an altitude of 2 750 m a.s.l., between ± 4.8 °C and ± 6.1 ° (Lewis, 2008b). From this altitude down to 1800 m a.s.l., inactive periglacial features exist and are indicative of paleoperiglacial environments (Lewis, 2008b). Occasional snow cover occurs during the winter months in these mountains (Hanvey and Marker, 1992; Boelhouwers and Meiklejohn, 2002), although snow cover can be present in the winter for up to a few months in the High Drakensberg and Lesotho (Hanvey and Marker, 1992). For Ben MacDhui, snow cover is present for less than one month of the year and the blanketing effect of prolonged snow cover on ground thermal dynamics is, thus, minimised (Kück, 1997). The region experiences highly seasonal precipitation, with ± 80% of precipitation falling in the summer months between October and March (Tyson *et al.*, 1976; Hanvey and Marker, 1992). Moisture for freezing events is, thus, limited in winter, unless moisture becomes available through snowfall. Nevertheless, under the present climate diurnal frost cycles have been observed at high altitudes (> 3 000 m a.s.l.) in shaded areas in the Drakensberg outside of winter months (Hanvey and Marker, 1992; Boelhouwers and Meiklejohn, 2002). The mid-latitudinal setting, coupled with clear winter skies and high insolation promote strong diurnal heating and large diurnal temperature ranges (Boelhouwers and Meiklejohn, 2002), and periglacial processes occur here where MAAT is between ± 4 °C and ± 7 °C (Hanvey and Marker, 1992). During winter frost cycles are common at lower altitudes (Boelhouwers, 1991a; Grab, 1997b), especially in frost-susceptible loam-rich soils with a fine fraction ($\phi > 4$: silt and clay) between 7-57% (Boelhouwers and Meiklejohn, 2002). No permafrost is found *(e.g.* Boelhouwers, 1994; Grab, 1997c, 1998; Boelhouwers and Meiklejohn, 2002; Lewis, 2008a), although Lewis and Hanvey (1988) argue for permafrost extending previously down to 1 840 m a.s.l. Nevertheless, arguments against the extent of previous or contemporary cold climates are made as well (Hall and Thorn, 2011).

Vegetation influences cryoturbation with reference to heat regimes and moisture conditions of soils (Hjort and Luoto, 2009). The Eastern Cape study site is the most vegetated of all three locations and vegetation is of interest in terms of frost processes in this region. The Elandsberg falls within the Amatole mistbelt grassland (Mucina and Rutherford, 2006). Ben MacDhui falls within the Lesotho Highland basalt grassland, where the high-montane landscape lacks trees and is characterised by grassland and shrubs (Mucina and Rutherford, 2006). Both the Elandsberg and Ben MacDhui fall within the bioregion of the Drakensberg grassland (Mucina and Rutherford, 2006), with the vegetation of Ben MacDhui consisting mainly of tussock grasses, low shrubs, an absence of trees, and *Helichrysum* herbs (Kück, 1997; Carbutt and Edwards, 2003). The Elandsberg comprises Karoo dolerite, consisting of a network of dolerite sills, sheets and dykes, mainly intrusive into the Beaufort Group of the Karoo Supergroup (Johnson *et al.*, 2006). The lithostratigraphy of Ben MacDhui is of the Drakensberg Group, *i.e.* basaltic lava, with minor sandstone, tuff and agglomerate in place in the lower part of the succession (Johnson *et al.*, 2006). These basalts weather to a loamy regolith (Boelhouwers and Meiklejohn, 2002) that may, depending on local conditions, exhibit a high freeze-thaw potential. The type of soil found within an area is, therefore, important when considering freeze-thaw cycles. The Drakensberg are classified to have alfisols, specifically the suborder of udalfs (Brady and Weil, 2016), reflecting the retisol classification of the World Reference Base for soil resources (IUSS Working Group WRB, 2015). For alfisols, a sub-surface horizon of clay accumulates with a high base status (contains illite), whereas udalfs are predominantly brown in colour. The mountain soils may consist of podzolic soil zones with lithosols and alpine meadow soils at high elevations (Strahler, 1974). The most recent South African soil

classification by Fey (2010) describes Ben MacDhui soils as lithic, with some humic soils in evidence. Ben MacDhui soils are shallow (± 30 cm), with silty-sand containing larger rocks and little cohesion. Organic content is variable, ranging from 4% in non-vegetated areas to 20% on vegetated slopes (Kück, 1997). Elandsberg soils are also mostly lithic, with oxidic, plinthic, and duplex soils also present (Fey, 2010). Where no knowledge on soils is available Weinert's (1980) climatic N-value map may be used to determine weathering predominance, and subsequent soil type for an area (Kleinhans, 2006). Applying such zonation shows all sites of the Eastern Cape to fall within areas of moderate N-values (2-5) (Mndawe *et al.*, 2013), suggesting a chemically driven weathering environment with soils exhibiting significant clay (kaolinite or montmorillonite) proportions (Weinert, 1980). Such substrates lend themselves to frost occurrence and freeze-thaw cycles are known to frequently occur in the top 10 cm of the soil, although depths of 20 cm have been recorded for spring on Ben MacDhui (Kück, 1997). In comparison, more coarse-grained soils with larger clasts show less potential for freeze-thaw cycles (Boelhouwers and Meiklejohn, 2002). When substantial portions of clay and silt are present (loamy soils) frost is more likely to occur due to the soil being able to hold intermediate amounts of water (Osterkamp and Burn, 2003). Clay and silt have finer textures and allow for slower water and air movement (Brady and Weil, 2016). Subsequently soil containing clay and silt particles have greater water-holding capacities, reflecting higher freeze-thaw potential. In addition, loamy soils are also associated with high erodibility indices (Gyamfi *et al.*, 2016). Such a relationship warrants further investigation with a specific focus on freeze-thaw cycles and their role in erosion of such soils. The Eastern Cape study area and the two study sites found within it offer the unique opportunity to draw a comparison of an animal-impacted diurnal frost environment to one not influenced by animal movements, such as that of Dronning Maud Land (DML) of Antarctica. Animals are known to alter landscapes (Boelhouwers and Meiklejohn, 2002), disrupting the natural balance. Furthermore, biogeomorphological effects are noticeable in the alpine (Hall *et al.*, 1999) and permafrost zones (Hall, 1997). Overgrazing and human-made fires lead to erosion and instability, increasing total sediment yield and erosion (Strahler, 1974, 1989). While the soil degradation index for the Elandsberg and Ben MacDhui sites are low (zero and three respectively), the vegetation degradation indices for the sites are much higher at 190 and 96 respectively (Hoffman *et al.*, 1999). Coupled with erodibility values of nine and 12 respectively (Hoffman *et al.*, 1999), it can be argued that the Elandsberg is potentially more degraded than Ben MacDhui. Erodibility is an index of erodibility determined by slope, soil type, rainfall intensity and land use with values approaching zero indicating high erodibility scores (Hoffman *et al.*, 1999). Nevertheless, the sensitive environment of the Drakensberg and that of Ben MacDhui might be more severely affected due to longer recovery periods required. Almost 10% of the Lesotho Highland basalt grassland vegetation type has been transformed, mostly due to cultivation of crops, grazing by domesticated animals and erosion is evident in many areas, especially on steeper slopes and where natural vegetation has been stripped and/or altered, forming small terraces (Mucina and Rutherford, 2006). Grazing has the potential to destroy vegetation cover, seedling establishment and can, therefore, increase the potential for frost activity (Hjort and Luoto, 2009). Increased frost activity can, in turn, reduce existing vegetation cover or prevent re-vegetation of the ground. Work by Borg (2017) on the slopes of Ben MacDhui, however, shows that needle ice activity does not reduce vegetation stability, although vegetation expansion is limited through frost processes. As such, frost processes at Ben MacDhui and the Elandsberg are not expected to have a significant impact on vegetation growth and cover. Furthermore, high levels of grazing under communal systems by domesticated animals, including sheep, goats, cattle and donkeys is mostly noticeable at lower altitudes with high altitudes predominantly grazed during the warmer months of the year (Mucina and Rutherford, 2006).

Nevertheless, private and commercial farming may occur at any altitude and any time, depending on local circumstances. While grazing seldom occurs above 2 500 m a.s.l., Ben MacDhui extends above this altitude and sheep are grazed on the slopes of the mountain during the summer and autumn months (*pers. obs.*). The larger area of the Elandsberg has very low to low erosion levels (Mucina and Rutherford, 2006). Furthermore, fieldwork visits show that the slopes of the Elandsberg have undergone limited alteration by human activities and exhibit low erosion levels. Occurring at an altitude of 1 380-2 082 m a.s.l. and predominantly between 1 500-1 682 m a.s.l., very little of the Amatole mistbelt grassland has been transformed (Mucina and Rutherford, 2006). Although the vegetation type is affected by the invasive alien *Acacia dealbata* only ± 3% of the natural vegetation cover has been transformed by *e.g.* plantations (Mucina and Rutherford, 2006). As such, the Elandsberg study site provides a counterpoint to the Tiffindell site in terms of human and animal impact.

To obtain an altitudinal gradient in terms of ground thermal regimes, five logging stations were erected for Ben MacDhui, with an additional seven erected for the Elandsberg. Logging stations were erected at 100 m altitudinal intervals and given the identifiers T1-T5 for Ben MacDhui, and E1-E7 for the Elandsberg. T1 has the highest elevation, with T5 the lowest elevation for Ben MacDhui. Similarly, E1 has the highest elevation for the Elandsberg, with E7 the lowest. A more detailed description of logging sites in the Eastern Cape follows under the section 4.3.1.1 Eastern Cape on pg. 83. Table 7 and Table 8 in APPENDIX D provide detailed information on the Eastern Cape site parameters.

### 3.1.1 Active and relict periglacial landforms and -features

There is some evidence for glaciations of the Eastern Cape and paleoglaciation features are found here. Lewis *et al.* (1994) and Lewis (2008b), argue for widespread glaciation during the Cenozoic and Quaternary, citing glacial striations in the Eliasdale as evidence of warm-based glaciation. However, this glacial evidence has been disputed by various authors and glacial paleolandforms are not necessarily representative of previous climatic conditions. The dispute regarding the extent and presence/absence of glaciation is mainly based on the lack of consensus regarding the intensity, dominance and spatial distribution of paleoprocesses (de Villiers, 2000). Furthermore, limited information is available on regional climatic data and ground thermal dynamics (Sumner, 2003a). Finally, work by Nel (2008), has shown that mean annual precipitation has been overestimated in paleoclimatic modelling, having implications on paleoperiglacial and -glacial environment. Nevertheless, arguments for glaciation are based on proposed relict periglacial deposits found in the region, including head deposits, cryoturbation, stone-banked lobes/terraces/garlands, blockstreams, protalus ramparts, and rock glaciers. Arguments are made for glacial landforms and sediments from the Quaternary, including end moraines near Elliot (Lewis *et al.*, 1994). The glacier that yielded these features is thought to have occurred at 2 100 m a.s.l. at the equilibrium line altitude (ELA) (Lewis *et al.*, 1994), where net ablation equals net accumulation (Summerfield, 1999). Further evidence put forth for Quaternary glaciation consists of valley glaciation for farms Tantallon and Glen Orchy, where hanging valleys, striations on bedrock, truncated spurs and troughs are argued to occur (> 1 900 m a.s.l.). A late Quaternary glacial moraine (cirque moraine) is proposed near the Bokspruit on Kilmore farm, as are truncated spurs and striations near Rifle Spruit and Eliasdale respectively (Lewis *et al.*, 1994). Glacigenic deposits are thought to occur near Stillorgan (1820 m a.s.l.), at Hendria (1 780 m a.s.l.), where terraces and unconsolidated

material are found, Ravenfell/Chesney Wold (1 820 m a.s.l.), where water-laid deposits on bedrock are found, at Rhodes/Kimnel, and Carlisle's Hoek (Lewis *et al.*, 1994). Near Rhodes Village in the Bell River Valley a terrace up-valley of the village is described as a kame moraine (Lewis *et al.*, 1994). Head deposits (± 40 000-26 250 BP) are proposed for a road cutting at Dynevor Park, on the R58 between Barkly East and Barkly Pass, as well as near Rhodes at 1 980 m a.s.l. on the farm of Buttermead (Lewis, 2008b). A further argument for a head deposit is made along a road cutting in the Bottleneck valley (± 24 000 BP) (Lewis, 2008b). Protalus ramparts have been described for two sites at Kilmore (Lewis, 1994), in a tributary of the Bokspruit Valley east of Barkly East, and on Mount Enterprise Farm between Ugie and Barkly East. A further two ramparts are described on Mount Enterprise farm, one of ± 80 m and one of ± 55 m length and above an altitude of ± 2 160 m a.s.l. Arguments for rock glaciers of talus origin are made for the south-facing slopes of the Bottleneck Valley near Barkley East at an altitude of ± 1 840-2 200 m a.s.l. (Lewis and Hanvey, 1993; Lewis, 2005). The authors argue that these landforms were active from ± 24 000 BP to sometime before 15 000 BP (Lewis, 2008b, 2008c), falling within the Bottleneck Stadial. Down-valley from Rhodes an argument is made of an oblate rock glacier (Lewis *et al.*, 1994), and landslides due to periglacial origin (now relict landforms) are proposed for Howison's Poort (± 22 000-23 000 BP) (Lewis, 2008d). In the upper reaches of Bottleneck Valley (2 000 m a.s.l.), arguments are made for slope deposits of periglacial origin, and at Tushielaw north of the Bell River near Rhodes debris slobe deposits are said to occur (Lewis and Hanvey, 1988; Lewis *et al.*, 1994). Additional solifluction deposits are said to occur at Kilchurn (1 920 m a.s.l.), on the road from Rhodes to Barkly Pass (Lewis *et al.*, 1994).

However, contemporary glaciation has been disputed (Osmaston and Harrison, 2005) and inferences for paleoclimatic and -geomorphic conditions based on landforms identified are contentious (Fitchett *et al.*, 2016). Evidence of the Bottleneck Stadial is lacking and estimations of paleoglacial conditions based on current MAAT, and deviations thereof, are not sufficient for determining the last glacial maximum (LGM) (Boelhouwers and Meiklejohn, 2002). Furthermore, depressions of 5 °C to 6 °C from current MAAT suggest permafrost to be absent or marginally present at best (Grab, 2002b; Boelhouwers, 2003b; Sumner, 2003b, 2004a), and extrapolations of paleoclimatic conditions based on contemporary mean annual precipitation (Nel and Sumner, 2008) favour previous periglacial conditions over glaciation. If permafrost was previously present, it was likely localised and of short duration (Grab, 2002b). Furthermore, evidence of permafrost is contested (Sumner, 2004b). While evidence exists for localised glaciation in the eastern Drakensberg (Mills *et al.*, 2009), with further argument for such glaciation being cold-based (Hall, 2010), glaciation remains a topic of debate (Knight, 2012), with widespread glaciation unlikely (Hall and Meiklejohn, 2011). Landforms ascribed to the periglacial environment of the Eastern Cape Drakensberg may be derived from a host of processes within and outside of the periglacial environment (Boelhouwers and Meiklejohn, 2002), suggesting equifinality. This has led to landforms described, such as rock glaciers, openwork block deposits and protalus ramparts, that are unlikely to be due to permafrost but rather as evidence of deep seasonal freezing (Sumner, 2004a). Furthermore, structural control on landforms must be considered and landforms identified, as those described as relict sorted circles (Grab, 2002b), may have developed due to conditions outside of the periglacial environment (Sumner, 2004c). The presence of angular clasts does not necessarily suggest previous glaciation, nor a periglacial environment where freeze-thaw weathering is present. Furthermore, freeze-thaw weathering does not exclusively yield angular clasts (Hall and Thorn, 2011) and head deposits of the Barkly Pass and the Bottleneck Valley, likely to be debris

deposits, don't necessarily indicate previous glaciation. The landform found on the ridge at Kilmore farm is not likely to be a moraine, pronival rampart, nor rock glacier. Instead, argument is made by Hedding (2014) that the landform developed due to rock-slope failure. Similarly, Hedding (2014) disputes the classification of the pronival rampart on Mount Enterprise farm. As such, arguments for previous glaciation, the extent thereof for the area, and resultant landforms should be used with caution when inferring paleoclimatic conditions in the Eastern Cape.

Irrespective of this, features ascribed to the Permocarboniferous glaciation are evident. These features are from a time when southern Africa lay over the South Pole ± 300 Ma (306-275 Ma) (Lewis, 2008b). Permocarboniferous ice sheets were warm based with melted basal ice, causing erosion of bedrock that became incorporated into the ice sole (Lewis, 2008b). Cold-based glacial ice is frozen to the bedrock and in these circumstances erosion of the bedrock is limited. Glacial landforms that are remnant of the Permocarboniferous glaciations are the erosional landforms of glacial pavements and roches moutonées. Glacial pavements evolve when clasts carried within the glacial ice scratch the surface of the bedrock, yielding bare rock surfaces (Summerfield, 1999). Roches moutonées are glacially moulded outcrops that are asymmetric in cross-section with gentle ascending striated and polished up-flow sides and a steep ice-plucked down-flow side (Summerfield, 1999). In the Eastern Cape glacial landforms of the Permocarboniferous are seen in the in the lithified glacial sediments (tillites), such as those on the surface of the peneplain around Grahamstown (Lewis, 2008b).

The escarpment and summits of the High Drakensberg are considered marginal periglacial/sub-periglacial (Boelhouwers, 1994), with MAAT at Sani Pass 5.8 °C (Nel and Sumner, 2008). Periglacial and active areas are known to exist in the Eastern Cape on the slopes of Ben MacDhui where active solifluction occurs above 2 755 m a.s.l. Kück (1997) describes the area above 2 550 m a.s.l. as an active periglacial zone, although this area is more properly defined as sub-periglacial. Nevertheless, frost action is present and active periglacial features include solifluction terraces, non-sorted and sorted patterned ground, as well as thúfur. Solifluction terraces occur on the slopes (15°-26°) of Ben MacDhui between 2 765-2 755 m a.s.l. (Kück, 1997). These vegetation-banked terraces are crescentic in shape with fronts between 0.4-1.0 m in height and have an average length and tread of 1.7 m and 2.1 m respectively. Terraces occur along linear drainage lines where more moisture becomes available; ice lenses of up to 3.5 cm and interstitial ice have been observed and their rarely vegetated treads are affected by frost heave (< 1.9 cm). Their low liquid limits (24-28%), low clay content, low plasticity and lack of cohesion makes them susceptible to flowage when water exceeds the liquid limits and the terraces move downslope by ± 1.7 $cm.y^{-1}$ with movement restricted to the upper 13 cm of the ground (Kück, 1997). Ephemeral sorted polygons are ± 7 cm wide; occur on slopes less than 3° in vegetation free areas and above 2 900 m a.s.l. (Kück, 1997). They form due to frost action during the winter months and are easily destroyed by wind and/or water once frost cycles are not sufficient to sustain their forms. Non-sorted polygons occur on slopes up to 11°, but predominantly on slopes up to 3 °, from 2 755 m a.s.l. upwards to the summit of Ben MacDhui at 3 001 m a.s.l. (Kück, 1997). These polygons occur in shallow depressions and range from 3-25 cm in width. Ephemeral in nature, they form overnight due to desiccation and frost cycles associated with needle ice, and frost formation of 16 cm in the ground has been observed. In the High Drakensberg, in the presence of sufficient moisture, needle ice forms

daily during May to mid-September (Grab, 2001). Needle ice, measured to 7 cm, is common above 2 300 m a.s.l. on Ben MacDhui, occurs predominantly during winter months, and requires high moisture levels with poorly drained areas, such as solifluction terraces (Kück, 1997).

Stone banked lobes/garlands initiate as stone-fronted solifluction terraces. Larger particles along lobes are deposited due to frost heave displaced sediment that gravitates downslope faster than finer sediment (Kück, 1997). Stone garlands are the result of the outwashing of finer material, leaving larger clasts behind. Such landforms exist on the south-facing slopes of Ben MacDhui between 2 730-2 895 m a.s.l. (Kück, 1997). Garlands are shown to consist of three layers. The first is between 60-90 cm in depths and consists of larger clasts (cobble to boulder size) without fine interstitial material. The second, underlying the first, is a layer of smaller clasts up to 20 cm thick, generally less than 2 mm in length (Kück, 1997). The third, underlying the second, is a basal layer of fine debris consisting of more than 22% silt (Kück, 1997). This layer is frost-susceptible and of interest to the current study. Gravel and sandy soils have a low frost potential, due to high permeability and low capillary forces. Soils comprised mostly of fine sand have a medium frost potential, having lower permeability and higher capillary forces (Brady and Weil, 2016). Silty soils, while highly permeable, also exhibit high capillary forces, making these soils frost-susceptible. Turf exfoliation has also been noted for the High Drakensberg (Grab, 2002a). Found in periglacial areas, turf exfoliation requires the presence of uneven temporal precipitation patterns, restricted snow cover, and is generally formed by the actions of needle ice, desiccation and aeolian erosion (Grab, 2002a). The presence of turf exfoliation on Ben MacDhui is an important consideration in terms of soil erosion and vegetation removal. Needle ice occurs on Ben MacDhui (Kück, 1997; Borg, 2017) and its role in vegetation disruption and concomitant increased erosion of surfaces is noted. At higher altitudes terracettes are more likely found than turf exfoliation, due to terracettes more likely forming on slopes exceeding 10° (Grab, 2002a). Needle ice has also been observed for the Elandsberg (*pers. obs.*), as well as Gaika's Kop (Meiklejohn, 2017; *pers. comm.*).

Thúfur mounds are domed-shaped hummocks that form due to seasonal frost action, heave-sensitive sediments and sufficient moisture (Summerfield, 1999). They require gentle or flat surfaces, sufficient moisture and ground underlain by fine-grained sediment. In addition, MAAT not exceeding ± 6 °C is required (Koaze *et al.*, 1974). Thúfur align themselves downslope and, for slopes exceeding 6°, become elongated into non-sorted stripes (Ballantyne and Harris, 1994). In the High Drakensberg thúfur are influenced by aspect-controlled freezing, where southern and southwestern aspects receive less sunlight and freeze before the northern/northeastern aspects (Grab, 2005). Freezing takes place from late May/early June until September (Grab, 2005). By September the interior of thúfurs, excepting the coldest south/southwestern portions, are no longer frozen (Grab, 2005). Ice lenses, which occupy more space than unfrozen water, lead to frost heave and sediment is displaced in a southwesterly direction. Thúfur for the Eastern Cape Drakensberg occur above 2 550 m a.s.l. on the floor of the Bell River Valley, at Tina Head, above 2 900 m a.s.l., on the Tiffindell summit plateau, and at 2 780 m a.s.l. and 2 650 m a.s.l. in the grounds of Tiffindell (Kück, 1997), as well as in the Lesotho Drakensberg (Grab, 1998, 2005). Ben MacDhui experiences MAAT between ± 4.8 °C and 6.1 °C when weather data from the Barkly East and Rhodes weather stations is extrapolated by reducing observed MAAT by the standard lapse rate of 6.5 °C.km$^{-1}$ (Humlum and Christiansen, 1998). Thúfur on Ben MacDhui occur at their highest extent at

± 2 900 m a.s.l. wetland areas on slopes less than 3° (Kück, 1997). Furthermore, these mounds reach an average 15 cm and 38 cm in height and diameter respectively, with ice lenses observed during winter (Kück, 1997). Quartzite, microgranite, felsite, and porphyrite are particularly susceptible to macrogelivation (Ballantyne and Harris, 1994) and are often constituents of blockstreams. Blockstreams are found at 2 900 m a.s.l. mid-way between Ben MacDhui and the Lesotho border in a northward draining valley. Between 1 859 m a.s.l. and 1 554 m a.s.l. blockstreams, predominantly found in drainage lines, occur near Queenstown and Hogsback, although this has been disputed by Sumner and de Villiers (2002). Several openwork block deposits are located on the southern slopes of the Elandsberg near Hogsback (Sumner and de Villiers, 2002), but there is no evidence to show that these features are currently active. Furthermore, the geographical location and morphology of these landforms must be used with caution when inferring paleoclimatic conditions (Sumner and de Villiers, 2002). Further relict blockstreams are found near Sani Pass at an elevation between 3 000 and 3 200 m a.s.l. (Boelhouwers *et al.*, 2002), as well as the slopes of Thabana-Ntlenyana, Lesotho, (Sumner, 2004a). High-frequency, low-intensity processes take the form of needle ice (Borg, 2017). A summary of periglacial landforms and -features that are found for the area is given in Figure 4 (pg. 36) and in Table 2 (pg. 37). The table is extracted from the literature, as well as adapted from de Villiers (2000). It represents a summary of features discussed in the literature since 1990. However, the table is not a complete list of such features found in the area. For an in-depth discussion on relict and active periglacial landforms found in South Africa (until 2000), please consult Kück (1997) and de Villiers (2000).

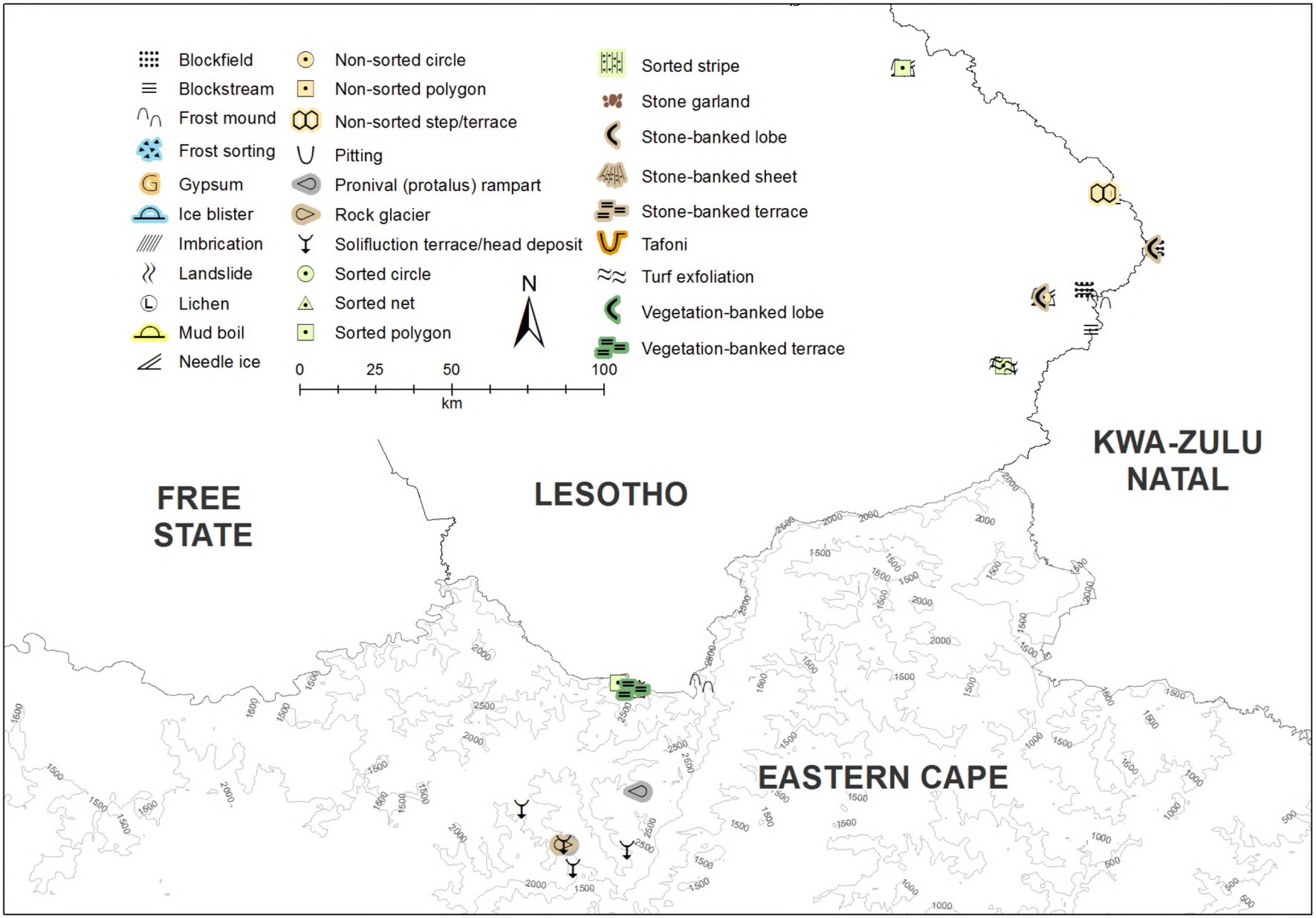


**Figure 4: Landforms observed for the Eastern Cape study area, as per literature review.**

**Table 2: A summary of periglacially derived landforms and -features for the Eastern Cape Drakensberg and vicinity. The active or relict state of the landform is indicated when known. *Includes pingo, palsa, thúfur. § Disputed.**

| Feature | Location | Altitude | Active/Relict | Source |
|---|---|---|---|---|
| Blockfield | Giant's Castle | 3 140-3 300 | Relict | (Boelhouwers, 1991b, 1994) |
| | Thabana-Ntlenyana, Lesotho | 3 482 | Relict | (Sumner, 2004a) |
| Blockstream | Bottleneck Valley, Barkly East § | ± 1 840 | Relict | (Lewis and Hanvey, 1993) |
| | Elandsberg | 1 740 | Relict | (Sumner and de Villiers, 2002) |
| | Giant's Castle | 3 140-3 300 | Relict | (Boelhouwers, 1994) |
| | Njesuthi-Mafadi Summit, Lesotho Drakensberg | 3 400 | Relict | (Grab, 1999) |
| | Sani Pass, Lesotho Drakensberg | 3 000-3 200 | Relict | (Boelhouwers *et al.*, 2002) |
| | Thabana-Ntlenyana, Lesotho | 3 482 | Relict | (Sumner, 2004a) |
| Frost mound * | Bell River Valley & Tina Head | > 2 550 | Active | (Lewis, 2008b) |
| | Ben MacDhui | 2 650; 2 780; > 2 900 | Active | (Kück, 1997) |
| | KwaZulu Natal Drakensberg | ± 3 000 | Active | (Boelhouwers, 1991b) |
| | Mafadi Valley, Lesotho Drakensberg | up to 3 482 | Active | (Grab, 1998) |
| | Mashai Valley, Lesotho Drakensberg | ± 2 950 | Active | (Grab, 1997c, 2005) |
| | Mashai Valley, Lesotho Drakensberg | up to 3 482 | Active | (Grab, 1998) |
| | Mohlesi Valley, Lesotho Drakensberg | 2 750-3 360 | Active | (Grab, 1994) |
| | Tlaeeng Pass, Lesotho Highlands | 3 275 | Active | (Hanvey and Marker, 1992) |
| Landslide | Howison's Poort § | ± 485 | Relict | (Lewis, 2008d) |
| Mud boil | *None observed* | | | |
| Needle ice | Ben MacDhui | > 1 800 | Active | (Kück, 1997) |
| | High Lesotho Drakensberg | > 2 750 | Active | (Grab, 2001) |
| | KwaZulu Natal Drakensberg | up to 3 842 | Active | (Boelhouwers, 1991b) |
| | Tlaeeng Pass, Lesotho Highlands | 3 275 | Active | (Hanvey and Marker, 1992) |
| Non-sorted circle | KwaZulu Natal Drakensberg | up to 3 842 | Active | (Boelhouwers, 1991b, 1994) |
| | Tlaeeng Pass, Lesotho Highlands | 3 275 | Active | (Hanvey and Marker, 1992) |
| Non-sorted polygon | Ben MacDhui | > 2 755 | Active | (Kück, 1997) |
| | Mafadi Summit | 3 400 | Active | (Grab, 1997a) |
| | Tlaeeng Pass, Lesotho Highlands | 3 275 | Active | (Hanvey and Marker, 1992; Grab, 1997a, 2005) |
| Non-sorted step/terrace | Mafadi Valley, Lesotho Drakensberg | 3 400 | Active | (Grab, 1997a, 2005) |
| Pronival (protalus) rampart | Mount Enterprise farm (between Ugie & Barkly East) § | ± 2 160 | Relict | (Lewis, 2008b) |

| Feature | Location | Altitude | Active/Relict | Source |
|---|---|---|---|---|
| | Kilmore § | ± 2 000 | Relict | (Lewis, 1994; Lewis *et al.*, 1994) |
| Rock glacier | Bottleneck Valley, Barkly East § | ± 1 840 | Relict | (Lewis and Hanvey, 1993; Lewis *et al.*, 1994; Lewis, 2005) |
| Solifluction terrace/head deposit/frost creep | Ben MacDhui | 2 755-2 765 | Active | (Kück, 1997) |
| | Bottleneck Valley, Barkly East § | ± 1 840 | Relic | (Lewis, 2008b) |
| | Buttermead farm § | ± 1 800 | Relict | (Lewis, 2008b) |
| | Dynevor Park § | ± 1 980 | Relict | (Lewis, 2008b) |
| | Giant's Castle | 3 140-3 300 | Active | (Boelhouwers, 1991b, 1994) |
| | Kilchurn § | 1 920 | Active | (Lewis *et al.*, 1994) |
| Sorted circle | KwaZulu Natal Drakensberg | 3 140-3 300 | Active | (Boelhouwers, 1991b, 1994) |
| | Mashai Valley, Lesotho Drakensberg § | 2 950 | Relict | (Grab, 1997a) |
| | Tlaeeng Pass, Lesotho Highlands | 3 275 | Active | (Hanvey and Marker, 1992) |
| Sorted polygon | Ben MacDhui | > 2 900 | Active | (Kück, 1997) |
| | Eastern Cape Drakensberg | 2 550 | Active | (Lewis, 1988) |
| | Mashai Valley, Lesotho Drakensberg | 2 420; 2 950 | Active | (Grab, 1997a) |
| | Tlaeeng Pass, Lesotho Highlands | 3 275 | Active | (Hanvey and Marker, 1992) |
| Sorted stripe/net | KwaZulu Natal Drakensberg | up to 3 842 | Active | (Boelhouwers, 1991b, 1994; Grab, 1997a) |
| Stone garland | Ben MacDhui | 2 730-2 895 | Relict | (Kück, 1997) |
| Stone-banked lobe | Giant's Castle | 3 140-3 300 | Active | (Boelhouwers, 1991b, 1994) |
| | High KwaZulu-Natal/Lesotho Drakensberg | > 3 300 | Active | (Grab, 2000) |
| Turf exfoliation | Mashai Valley, Lesotho Drakensberg | 2 900-3 100 | Active | (Grab, 2002a) |

## 3.2 Marion Island

Marion Island (Figure 5, pg. 40), the second study location, is found north of the Antarctic Convergence (Polar Front) at 46°54'S, 37°45'E (Holness, 2003a) in the sub-Antarctic part of the Indian Ocean (Stewart, 2011). It lies in within the influence of the Antarctic Circumpolar Current (Rouault *et al.*, 2005), 300km south of the Southwest Indian Rift on the Marion Rise (Zhou and Dick, 2013). The Island rises to a height of 1 231 m a.s.l. (Sumner *et al.*, 2002; Holness, 2003a), covers an area of 290 $km^2$ (de Villiers, 1976) and is the top of a shield volcano that emerges from a mid-oceanic ridge (Verwoerd, 1971). Eight successional lava outflows have shaped the Island (Verwoerd, 1971; McDougall *et al.*, 2001) and evidence of at least two former sea levels exist (Hall, 1977). The older grey lava has been dated to 450 000 ± 10 000 to 30 000 BP, whereas the younger black lava shows ages of 10 000 to present (Prince Edward Islands Management Plan Working Group, 1996; McDougall *et al.*, 2001; Field *et al.*, 2006). More recently a geological lineament at N26.5°E, influencing fauna and flora distributions, has been recognised (Mortimer *et al.*, 2012). This geological lineament also has implications on climate and geomorphological landform distribution. The Island was glaciated during the Quaternary (Verwoerd, 1971; Hall, 1982; Sumner, 2004d; Boelhouwers *et al.*, 2008; Hedding, 2008; Haussmann *et al.*, 2010a), evidenced by striations found on grey lava deposits at *e.g.* Jan Smuts Peak, Tafelberg, as well as on grey lava in the Central Highland (Verwoerd, 1971; Hall, 1982; Hall, 1990; Sumner *et al.*, 2004a; Boelhouwers *et al.*, 2008; Hedding, 2008; Haussmann *et al.*, 2010a). Black lava shows little evidence of striations (Hall, 1990; Boelhouwers *et al.*, 2008), indicating these lava outflows occurred after glaciation (Hall, 1990; Hedding, 2008). The Island is formed mainly of alkali basalts with some trachybasalts also present (le Roex *et al.*, 2012). Field *et al.* (2006) suggest a deglaciation of 10 000 BP with seven glacial periods (McDougall *et al.*, 2001), whereas work by Haussmann *et al.* (2010a) shows a potential deglaciation age of ± 7 000 BP. Soils for the Marion Island are generally coarse (sandy gravel or gravely sand) (Lubbe, 2010), attributed to slow weathering rates and the young age of the Island (Sumner, 2004d). In comparison to other study areas of this study, Marion Island has a mid-latitudinal location and is an ideal study site for studying frost environments at both low and high altitudes. Like other sub-Antarctic islands, Marion Island is characterised by low-intensity and high-frequency frost cycles with needle ice the most common form of ice segregation observed, and its sub-Antarctic periglacial environment is distinct to those of seasonal and permafrost areas (Boelhouwers *et al.*, 2003). Mean annual temperature is strongly correlated with elevation for the Island (Chown *et al.*, 2012), as such, Marion Island is a suitable location to evaluate freeze-thaw cycles at various altitudes. The Island is also characterised by significant climatic variation across its altitudinal range (Gabriel *et al.*, 2001) and its distinct periglacial environment is sensitive to climate change (Nel, 2012). Furthermore, high number of freeze-thaw cycles occur for climates of low annual temperature ranges (Goudie, 2004a), such as those observed on Marion Island. Research by Boelhouwers (2003a) and Nel and Boelhouwers (2014a) also shows that the Island may be used as a proxy in evaluating regional climatic trends within the Southern Ocean, highlighting the need for a greater understanding of its ground thermal regime.

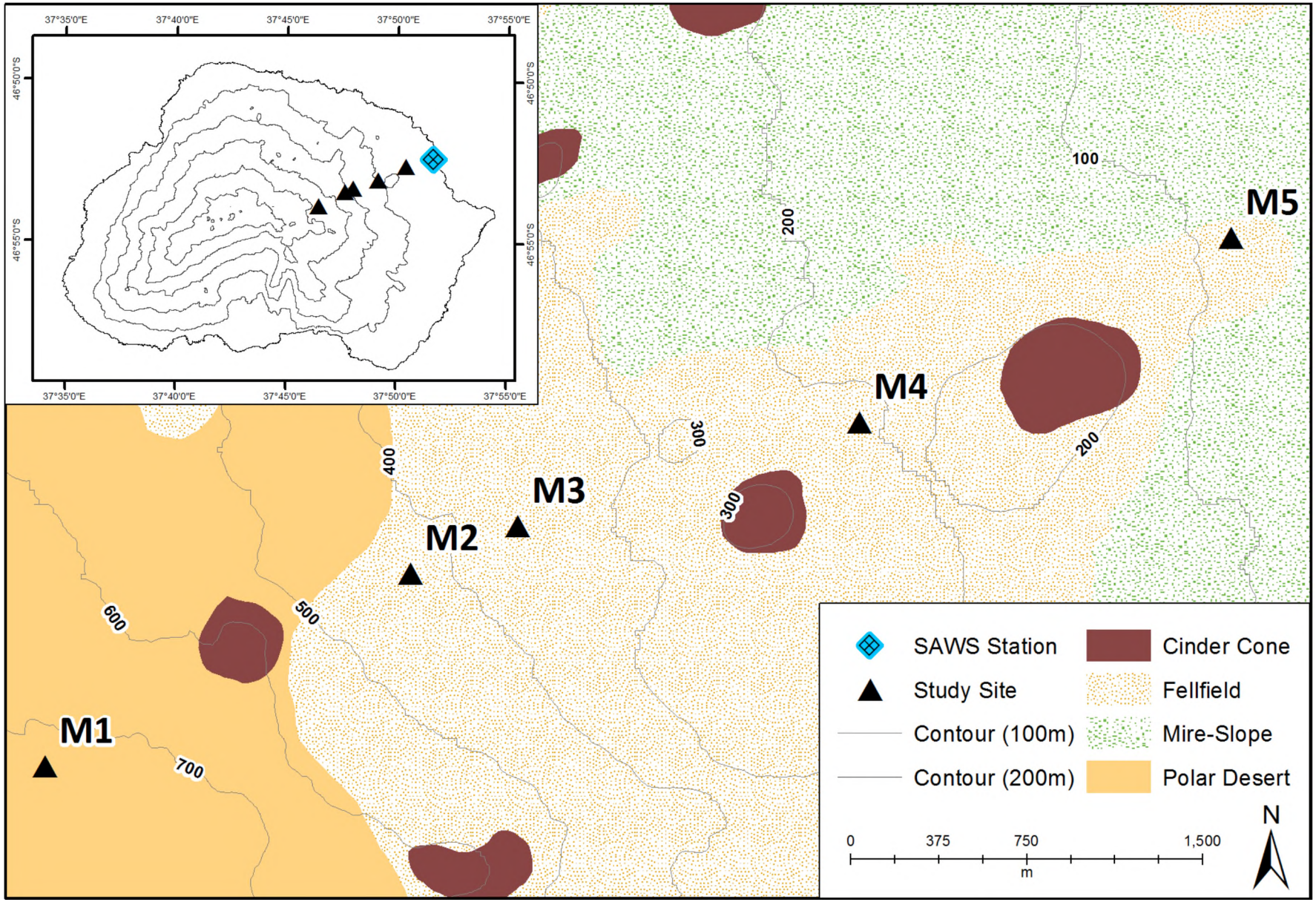


**Figure 5: Marion Island in the Southern Ocean (inset). The various vegetation and surface zones are indicated (Mucina and Rutherford, 2006), as well as the meteorological station at the South African personnel base. A triangle identifies various logging sites from Katedraalkrans (M1) past Tafelberg (M2-M4) down to 87 m a.s.l. (M5).**

Marion Island experiences an exceptionally maritime and thermally stable climate (Boelhouwers *et al.*, 2000), with mean air temperatures exhibiting little variation (Smith, 2002; Le Roux, 2008), a high degree of cloudd cover (Schulze, 1971), strong winds and relatively high (Bate and Smith, 1983) and stable (Schulze, 1971) humidity. Gusts exceeding 290 m.s-1 have been recorded (La Grange, 1954) and gale force winds (17.5-24.2 $m.s^{-1}$) are reached on ± 100 or more days annually (Gremmen *et al.*, 1998). Cloud cover is ubiquitous and near-complete for most days, with precipitation recorded throughout the year (Le Roux, 2008). Diurnal and seasonal freeze-thaw patterns are not well-developed for islands of the sub-Antarctic (French, 1996), due to a lack of seasonality observed at these locations (Boelhouwers *et al.*, 2003). Instead, freezing and thawing events occur throughout the year (in all seasons). The Island is characterised by strong winds and high soil moisture values, yielding between 60 to 200 days on which oscillations around 0 °C occur (Nel *et al.*, 2009). Furthermore, ranges in mean annual air temperature (MAAT) of 8 °C in the vicinity of 0 °C are expected (French, 1996). The Island has three distinct frost zones. The coastal diurnal frost zone, ranging from sea level to 400 m a.s.l., is dominated by needle ice (Nel, 2001). The upper diurnal frost zone is characterised by needle ice and ice lens formation. The high-altitude frost zone, above 750 m a.s.l., is dominated by seasonal freezing (Boelhouwers *et al.*, 2003). This study focuses on all zones with sites ranging from 87 m a.s.l. to 765 m a.s.l.

The biota of Marion Island is impoverished (Gremmen *et al.*, 2003), with only 42 species of vascular plants recorded for the Island (Gremmen and Smith, 1999), although soil bacterial activity is high when compared to other sub-Antarctic islands (Grobler *et al.*, 1987). Small forbs, grasses, ferns and mosses make up the bulk of the vegetation, with woody plants absent (Mucina and Rutherford, 2006). Six major floral community complexes are identified by Gremmen (1981) and have subsequently been adjusted to seven major terrestrial habitats (Smith and Steenkamp, 2001). These include the Coastal Salt-Spray Complex; Fellfield; Slope; Biotic Herbfield; Biotic Grassland; Mire; and Polar Desert. Closed vegetation is uncommon, despite the abundance of cushion-forming *Azorella selago* (Apiaceae) and bryophytes found in lower-altitude Fellfield (Gabriel *et al.*, 2001). As altitude increases, vegetation becomes sparse, with *A. selago* giving way to bryophytes and subsequently to interstitial cryptogarms and lichen (Gremmen, 1981). For an overview of study sites on Marion Island and their respective location within the vegetation biomes found there, please refer to Figure 6 (pg. 42).

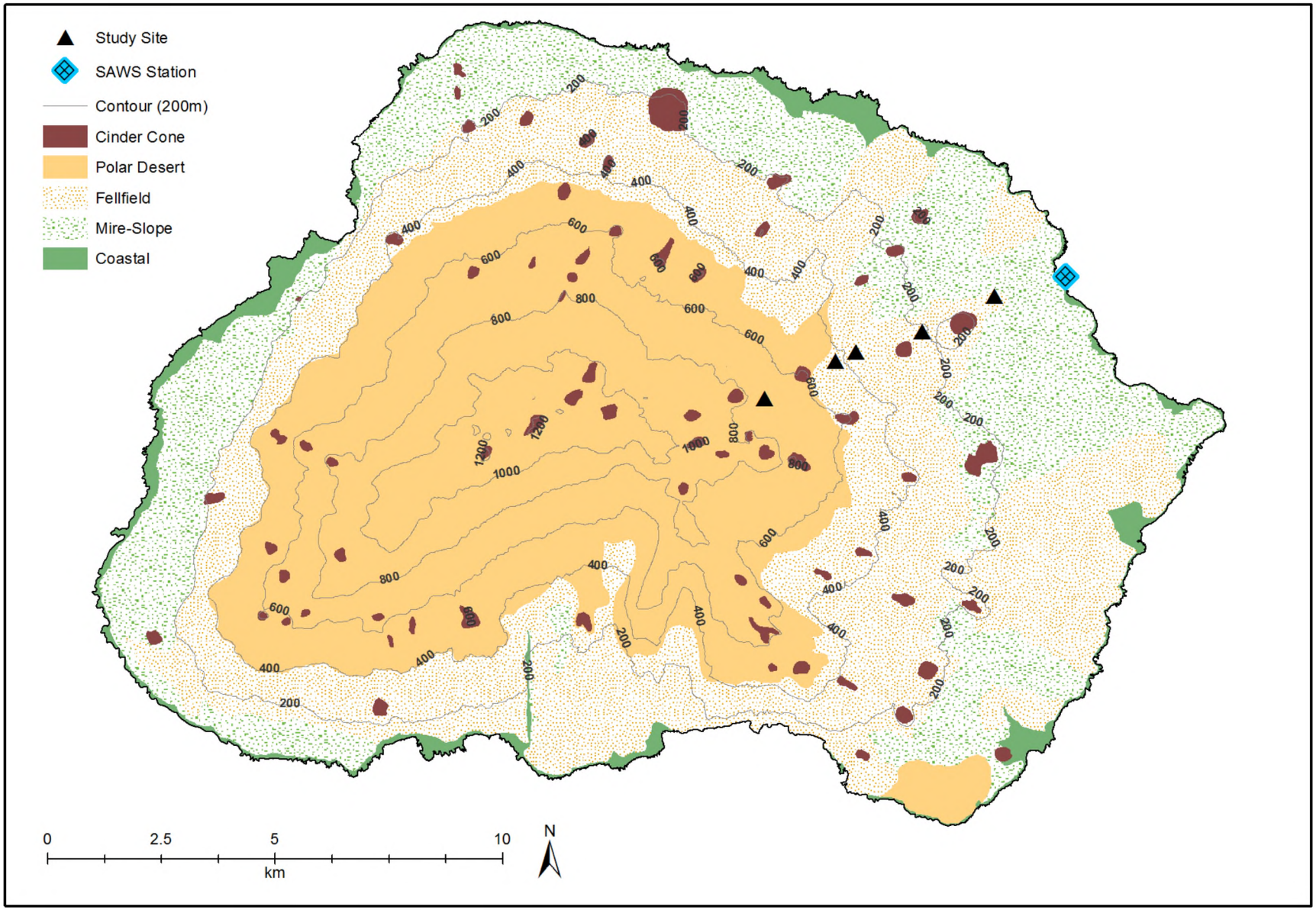


**Figure 6: Study sites and their location within the vegetation biomes of Marion Island. SAWS: South African Weather Service.**

The vegetation near Katedraalkrans is that of the sub-Antarctic Polar Desert Complex and falls within the Polar Desert biome (Mucina and Rutherford, 2006). The sub-Antarctic Polar Desert Complex is common on Marion Island, with 120 $km^2$ of the Island's total area of 290 $km^2$ making up this habitat (Smith and Steenkamp, 2001). Roughly 10% of the area below 300 m a.s.l. is occupied by this vegetation type (Mucina and Rutherford, 2006). Between 100-500 m a.s.l. this proportion rises to 32% and above 500 m a.s.l. ± 98% of all surfaces is covered by the Polar Desert Complex (Mucina and Rutherford, 2006). This vegetation type is characterised by bare rock and scoria, an absence of soils, with limited growth of lichens and mosses, as well as active and relict periglacial features (Smith and Steenkamp, 2001). Although ± 46% of the Island is covered by the Polar Desert Complex, 33% of the area below 100 m a.s.l, 72% of that between 100-500 m a.s.l., and 15% of that above 500 m a.s.l., is occupied by the sub-Antarctic Fellfield Complex (Mucina and Rutherford, 2006). Fellfield (feldmark; fjaeldmark) is common between 200-550 m a.s.l., although it may occur at lower altitudes where the surface is exposed and can also be found up to 800 m a.s.l. (Grobler *et al.*, 1987). Fellfield may be further subdivided into xeric fellfield (drier and less acidic soil; less vegetation cover; dominated by lichens and cushion bryophytes) and mesic fellfield (wetter and more acidic soil; more vegetation cover; dominated by *A. selago*) (Smith and Steenkamp, 2001). This Fellfield Complex is characterised by skeletal mineral soils that contain volcanic ash (Smith and Steenkamp, 2001), as well as scattered compact cushions of *A. selago* (Grobler *et al.*, 1987). Soils of this complex have higher bulk densities, as well as lower moisture values and concentrations of organic and inorganic nitrogen and phosphorus (Smith and Steenkamp, 2001) when compared to other vegetation complexes, excluding the Polar Desert Complex. Bulk densities tend to increase, and moisture values decrease as one moves away from the coast towards the dry volcanic sediment of the interior (Conradie and Smith, 2012). Lubbe (2010) identifies soils of the Fellfield Complex to have average bulk densities of 0.7 $g.cm^{-3}$, characteristic of andosols (bulk densities between 0.6-0.9 $g.cm^{3}$). These surface samples also have average moisture contents approximating 47% and organic proportions of 10% (ranging from 7-28%). The Polar Desert and Fellfield Complex are both classified as andosols with Polar Desert soils poorly formed (if formed at all) with less than 5% (ranging from 1-11%) total organic carbon (TOC) (Lubbe, 2010). The gravelly loams of the Fellfield Complex (Gremmen, 1981) lend themselves to frequent freeze-thaw cycles (Haussmann *et al.*, 2009b) and have a high needle ice potential when the proportion of fines ($\phi > 4$: silt and clay) exceeds 7.9% in saturated soils (Meentemeyer and Zippin, 1981). This stands in contrast to scoria derived surfaces, where the potential for freeze-thaw cycles is less (Hedding, 2008), and back lava sediment, which exhibits no frost potential (Holness, 2001a). Soil moisture values for a site just below First Red Hill at 550 m a.s.l. (Figure 10, pg. 52) show higher moisture values for samples taken under *A. selago* than those taken where no vegetation cover is present (Grobler *et al.*, 1987). Organic content for these sampling sites show a similar pattern, with higher organic content recorded for samples taken from underneath *A. selago*. Haussmann *et al.* (2009a, 2009b) show the influence of these cushion plants on ground temperature and freeze-thaw cycles. A decrease in altitude reflects an increase of organic and moisture content of sediment samples (Grobler *et al.*, 1987). However, with respect to ground moisture, Holness (2001a) shows that moisture availability is not a limiting factor to the frost environment on Marion Island. This is due to the Island receiving a high amount of precipitation throughout the year *(e.g.* Holness, 2003a; Hedding, 2008). For an overview of the five study locations and their location within soil type regions, please consult Figure 7 (pg.44).

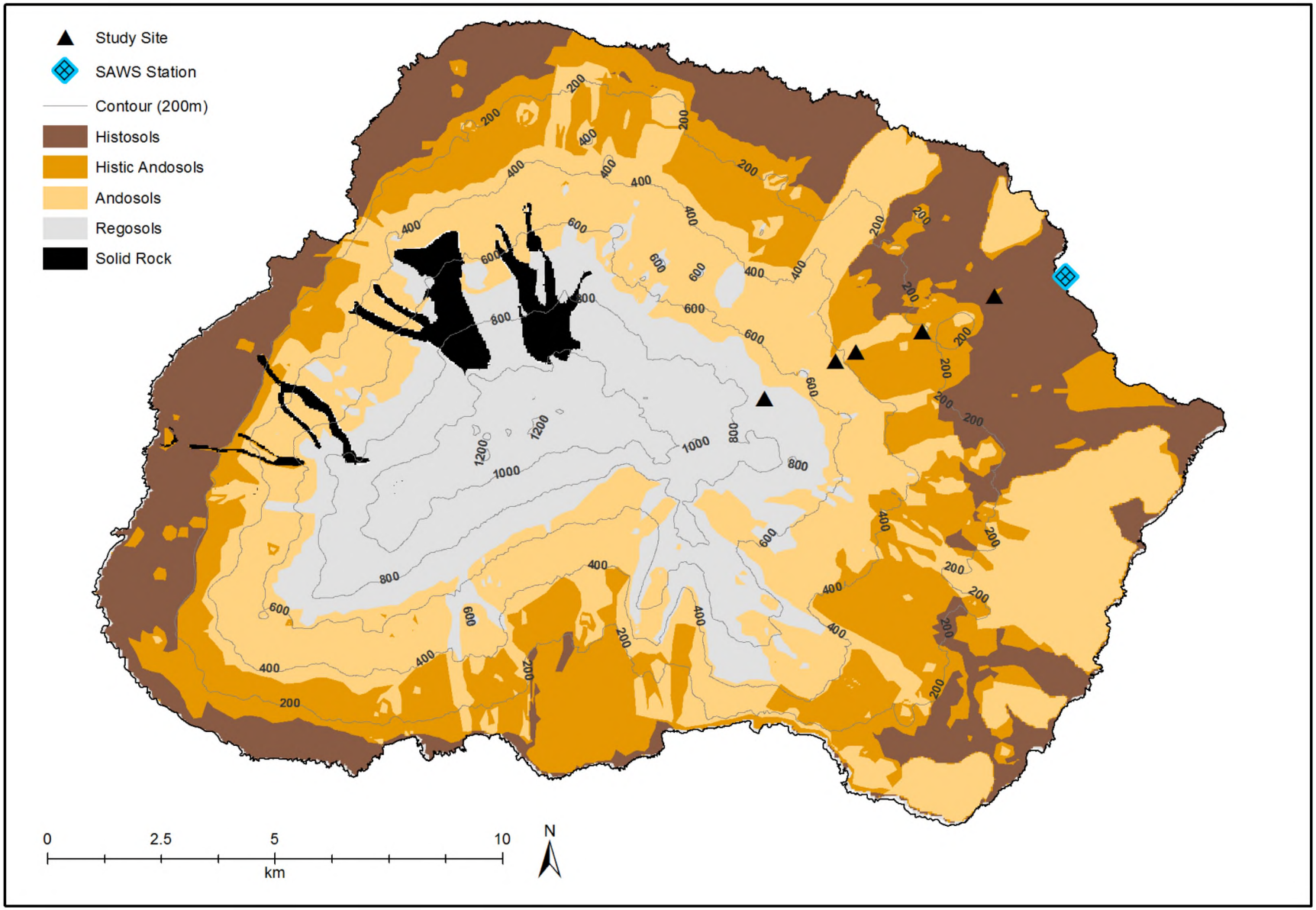


**Figure 7: Study sites and their location regarding soil types found on Marion Island. SAWS: South African Weather Service.**

The low but stable temperatures, with annual mean temperatures of 6 °C (Dartnall and Smith, 2012) yield small diurnal (< 2 °C) and seasonal (< 4 °C) temperature ranges (Smith, 2002; Holness, 2003a; Hedding, 2008), resulting in high-frequency, low-magnitude and short diurnal frost cycles in the coastal regions (Holness, 2003a), as well as in regions above 1 000 m a.s.l. (Boelhouwers *et al.*, 2008). Ground frost occurs throughout the year, with freezing temperatures recorded in any month (Le Roux, 2008). Mean annual air temperatures at elevations exceeding 1 000 m a.s.l. approximate 0.9 °C, with summer and winter environmental lapse rates of 4.5 °C.1km$^{-1}$ and 4 °C.1km$^{-1}$ respectively (Schulze, 1971). This approximates the environmental lapse rate of 5 °C.1km$^{-1}$ determined by Holness (2001a) for ambient air temperature sensors placed 100 cm above the ground. Mean annual air temperatures at Katedraalkrans range from 2 °C-2.6 °C (Blake, 1996; Holness, 2001a). The Island's MAAT differs little from mean sea surface temperatures and the warmest months are January-March, even though the highest solar radiation is received in December (Le Roux, 2008). Frost cycles are ubiquitous and active patterned ground exhibits uniform morphology (Boelhouwers *et al.*, 2008). Most frost cycles have a duration of less than 20 hours, although cycles as long as 100 hours have been recorded (Haussmann *et al.*, 2009a). Work by Hedding (2006) at Delta North (975 m a.s.l.), shows that the greatest maximum and minimum ground temperatures, as well as greatest diurnal ranges of ± 9 °C and oscillations around 0 °C for 236 days of the year, occur at the near surface (± 1 cm within the ground). Furthermore, at this depth no seasonal frost is recorded ( maximum frost duration of four days). At a depth of 25 cm seasonal frost, spanning 71 days, is recorded between August and October. The longest duration of seasonal frost, lasting 113 days from June to October, is recorded at 50 cm within the ground. At 75 cm within the ground seasonal frost occurred on 110 days (June-October). Freeze-thaw cycles and sorting depth vary per location but, in general, an increase in altitude is related to an increase in frost depth. Holness and Boelhouwers (1998) show a sorting depth of 4-7 cm for sediment found on grey lava at Long Ridge (Bill Briggs; 350 m a.s.l.), with freeze-thaw cycles restricted to the upper 5-10 cm of the ground at Tafelberg (350 m a.s.l.) (Boelhouwers *et al.*, 2000). Sorting up to a depth of 10-15 cm has been found in sorted stripes at Long Ridge South (500 m a.s.l.) (Holness and Boelhouwers, 1998) and freeze-thaw cycles are restricted to the upper 10 cm of the ground below 200 m a.s.l. (Holness, 2004). At altitudes above 800 m a.s.l., freeze-thaw cycles reach 25 cm depths with some seasonal freezing and ice lensing observed at altitudes exceeding 800-1 000 m a.s.l. (Holness, 2003b). Above 750 m a.s.l. the ground remains seasonally frozen for ± two months of the year (Holness, 2003a). At lower altitudes, diurnal frost cycles occur for 119 days of the year (Holness, 2001a) with only 47 days of freeze-thaw cycles occurring along the coast at 23 m a.s.l. (Holness, 2003b). Smith and French (1988) estimate frost cycles to take place in the upper 5 cm of the ground for Fellfield below 300 m a.s.l. with frost cycles occurring on 92 days of the year (25%). Haussmann *et al.* (2009b) show that mean ground temperature at 5 cm depth at 300 m a.s.l. is 4.7 °C. At these lower altitudes no zero-curtain effect is observed, in contrast to elevations of 1 000 m a.s.l. and higher where this effect has been recorded (Boelhouwers, 2003a). At altitudes below ± 300-400 m a.s.l. needle ice dominates; at higher elevations deeper frost cycles and ice lensing may occur (Holness, 2001a; Boelhouwers *et al.*, 2003).

Frost cycles, while of low intensity (generally not dropping below -1 °C) and shallow (dominant in the upper 2 cm of the ground but occurring to a depth of 10 cm), translate into significant heave of 80-90 mm per year with needle ice formation (nucleation) at above -2 °C (Haussmann *et al.*, 2009a). (Frost cycle intensity refers the absolute minimum temperature reached during the freeze-thaw event.) Nel and Boelhouwers (2014b) argue for ice nucleation at ± -0.2 °C at 1 cm depths and -1 °C at 2 cm depths,

in contrast to the accepted nucleation temperature of -2 °C (Outcalt, 1971, 1972). It must be noted, however, that the threshold defined by Outcalt (1971) applies to windless and calm nights, conditions that are rarely met on Marion Island. This suggests that high winds and concomitant heat transfer elevate temperatures required for needle ice formation (Nel and Boelhouwers, 2014b). Most potential freeze-thaw events (90%) also occur during the colder period of May to October (Haussmann *et al.*, 2009a), the same time when snow cover is most likely (Hedding, 2008). The longest frost duration has been recorded for August, with significantly shorter freeze-thaw cycles observed in September and October (Haussmann *et al.*, 2009a). At lower altitudes freeze-thaw cycles are also less common, with cycles at 200 m a.s.l. restricted to the months between May and September (Boelhouwers *et al.*, 2008). February is not only the warmest month on the Island (Bate and Smith, 1983), but also registers lower occurrence of gale force winds (Schulze, 1971). In comparison, July to September show a higher occurrence of gale force winds (Schulze, 1971). Potential summer soil frost, occurring generally at night, is impacted by synoptic weather patterns, with the intensity and duration of potential freeze-thaw events affected by post-cyclonic Antarctic air masses (Nel, 2012). These climatic drivers also affect potential freeze-thaw events on an hourly or diurnal scale, rather than on longer seasonal and annual scales (Nel *et al.*, 2009). Diurnal frost cycles and needle ice events are thought to be the most important geomorphic process on the Island (Holness, 2004), resulting in particle displacement within the top 5-15 cm of the soil, and needle ice, ice lensing and micro-patterned ground have all been observed (Hall, 2002; Holness, 2003a).

Mean annual rainfall for Marion Island is 2332 mm (Holness, 2003a; Hedding, 2008) with a strong ($32 km.h^{-1}$ [Hedding *et al.*, 2007]) and predominant westerly wind (Hall, 2002). The Island receives the bulk of its precipitation as rainfall (le Roux and McGeoch, 2008), occurring throughout the year (Dartnall and Smith, 2012) at an average of 25 days per month (Boelhouwers, 2003a). Snow falls in all seasons (Gremmen *et al.*, 1998), but mainly during the winter months of May-October (Hedding, 2008). Snowfall has been recorded on ± 50 days of the year and is more common at altitudes above 600 m a.s.l. (Hedding *et al.*, 2007). On Marion Island snow also causes an extended and deeper freeze event when falling at high altitudes (Holness, 2003a; Boelhouwers *et al.*, 2008). Mean annual precipitation has decreased since the 1960's from almost 3 000 mm per annum to the current amount of just above 2000 mm (le Roux and McGeoch, 2008). During this time, the Island has experienced and average rise of 0.21 °C in temperature per decade (Nel and Boelhouwers, 2014a), a drop of 25 mm of precipitation per year (or 25% drop since the 1950s) (Smith and Steenkamp, 2001) and an increase of ± 3.3 annual sunshine hours (Smith, 2002). Average monthly temperatures, annual and diurnal average maxima and minima temperatures have also increased (Chown and Smith, 1993; le Roux and McGeoch, 2008), while interannual temperature variability has declined (le Roux and McGeoch, 2008). Maximum diurnal temperatures tend to occur around noon, with minimums at 04:00 (Schulze, 1971). Temperature ranges have not significantly changed since the 1960's, since an increase in maximum temperatures is accompanied by increasing minimum temperatures. This is ascribed to the overriding influence of sea surface temperatures on air temperatures (Smith and Steenkamp, 2001). The warmer temperatures are accompanied by warmer growing seasons, facilitating vegetation growth (Chown and Smith, 1993). Fewer and less intense precipitation events are observed, with average precipitation declining by 1.5 mm per rainfall event and the larger precipitation events (> 5 mm) declining consistently (le Roux and McGeoch, 2008). Longer dry spells are also observed (Smith and Steenkamp, 2001), with the number of consecutive dry days almost doubling since the 1960's (le Roux and McGeoch, 2008). Diurnal

evaporation rates have increased, while cloud cover has decreased (le Roux and McGeoch, 2008). Wind speed has also shown a shift since the 1960's. Overall the average diurnal and maximum wind speeds have increased, although the global annual maximums have decreased, as have the number of wind-still days observed per annum (le Roux and McGeoch, 2008). This shows that while maximum recorded wind speeds have decreased, Marion Island is becoming increasingly windier, warmer and drier. The climatic changes are also more pronounced in the summer months (Smith, 2002; Rouault *et al.*, 2005).

Le Roux and McGeoch (2008) argue that longer dry spells and changes recorded for wind speed, temperature maxima and variability affect biota for Marion Island. Similarly, it can be argued that the decrease in precipitation, as well as the increase in temporal variability of precipitation, increase in average temperatures and less temperature variability have implications on freeze-thaw cycles. Longer dry spells and less intense precipitation events have significant impacts on soil moisture, especially where water holding capacity of soils is low, such as observed for Fellfield (le Roux and McGeoch, 2008). Such conditions translate into less freeze-thaw cycles, although not specifically less potential freeze-thaw events. The decline in temperature variability and stable diurnal temperature ranges, as well as the warmer conditions coupled with stronger winds (le Roux and McGeoch, 2008) have further implications on freeze-thaw cycles. Particularly, the increased potential evaporation rates impact needle ice development, altering the frost environment. The warming and drier climate has already translated into less frost days (Huyser *et al.*, 2000). If the prediction of Le Roux and McGeoch (2008) holds true that at higher altitudes Fellfield will replace Polar Desert, freeze-thaw cycles for these areas will concomitantly be affected. A 1 °C increase in temperature is predicted to halve potential freeze-thaw cycles, having potential subsequent effects on nutrient concentrations, cryoturbation and weathering, amongst others (Boelhouwers *et al.*, 2003). Furthermore, freeze-thaw cycles affect biological communities and a change in the frost environment has implications for floral distribution and diversity on the Island. Soil moisture is a driving factor for Marion Island's floral complexes (Smith and Steenkamp, 2001), and a change in freeze-thaw cycles, requiring the presence of moisture, may, as such, be used as a proxy for soil moisture.

Sumner *et al.* (2002) and Holness (2003a) have suggested that historical permafrost presence was not widespread, nor of long duration. The disappearance of permafrost in recent years is attributed to warming temperatures (Boelhouwers *et al.*, 2008), as discussed in CHAPTER 1: Introduction (pg. 1 onwards). Permafrost once existed in the interior, and an Ice Plateau was found in the Central Highland as late as the 1960s with the snow line in the 1950s located at ± 650 m a.s.l. (Hedding, 2008). Nevertheless, no permanent ice cover (Sumner *et al.*, 2004a) nor glaciers are now present. An argument is made for discontinuous permafrost at east- and south-facing slopes above 1 000 m a.s.l. where snow accumulation is possible (Boelhouwers *et al.*, 2003; Holness, 2003a; Sumner *et al.*, 2004a). However, work by Hedding (2008) excludes the likelihood of contemporary permafrost. Buried glacial ice is found for ± 250 m of a large basin in the Central Highland, with additional sporadic pockets of buried ice found above 1 050 m a.s.l. (Hedding, 2008). This stands in contrast to other sub-Antarctic islands, such as South Georgia or Heard Island-McDonald Island, where active glaciers and permafrost are found (Kiernan and McConnell, 1999).

Bierman (2014) argues that a definitive altitudinal gradient is present for air temperatures, with near surface ground temperatures, temperatures recorded at ± 1 cm within the ground, exhibiting a more complex trend with respect to increasing elevation. Synoptic weather patterns drive this complexity, with different atmospheric circulation types yielding variable ground temperatures. As such, data collection from Marion Island occurred for increasing altitudinal ranges from ± 80 m a.s.l. between Marion Base to Tafelberg, and Katedraalkrans at over 750 m a.s.l. The five logging sites closely follow the transect used by Lubbe (2010) and were given the identifier M1-M5 with M1 signifying Katedraalkrans and M5 the lowest altitudinal site (Figure 5, pg. 40). All sites would have been glaciated during the last glacial maximum (LGM) (Hall *et al.*, 2011). The Tafelberg sites (M2-M4) consist of unsorted glacial till that is underlain by pre-glacial basalts of an approximate age of 147 000 ± 14 000 years (Haussmann *et al.*, 2010a), characterised by superficial frost heave and creep (Haussmann *et al.*, 2009a). The dominant vegetation at these sites is sub-Antarctic Fellfield, whereas M1 (Katedraalkrans) forms part of the sub-Antarctic Polar Desert (Figure 6, pg. 42). M1 is comprised of regosols, M2 and M3 are classified as andosols and M4 and M5 are histic andosols (Lubbe, 2010) (Figure 7, pg. 44). All logging stations of Marion Island occur in areas with minimal human and animal presence and minimal vegetation cover. While the Island supports diverse fauna *(e.g.* Condy *et al.*, 1978; Crawford *et al.*, 2003, 2006, 2008; Tosh *et al.*, 2008), these are found along the coast and at distance from all logging stations. All sites are located on grey lava. Katedraalkrans is characterised by scoria and black lava deposits (Nel, 2012), nevertheless M1 is also located on grey lava (Figure 8, pg. 49). Although cushions of *A. selago* occur in near some logging sites (M3 and M4), no loggers were set up near these plants and their influence on ground temperatures (Haussmann *et al.*, 2009a, 2009b, 2010b) is, therefore, eliminated. Instead these loggers were placed on relict solifluction terraces (Haussmann *et al.*, 2009b), at distance from *A. selago*. A more detailed description of logging sites on Marion Island follows from pg. 88 onwards (4.3.1 Ground temperature and moisture data). Table 7 and Table 8 in APPENDIX D provide detailed information on the Marion Island site parameters.

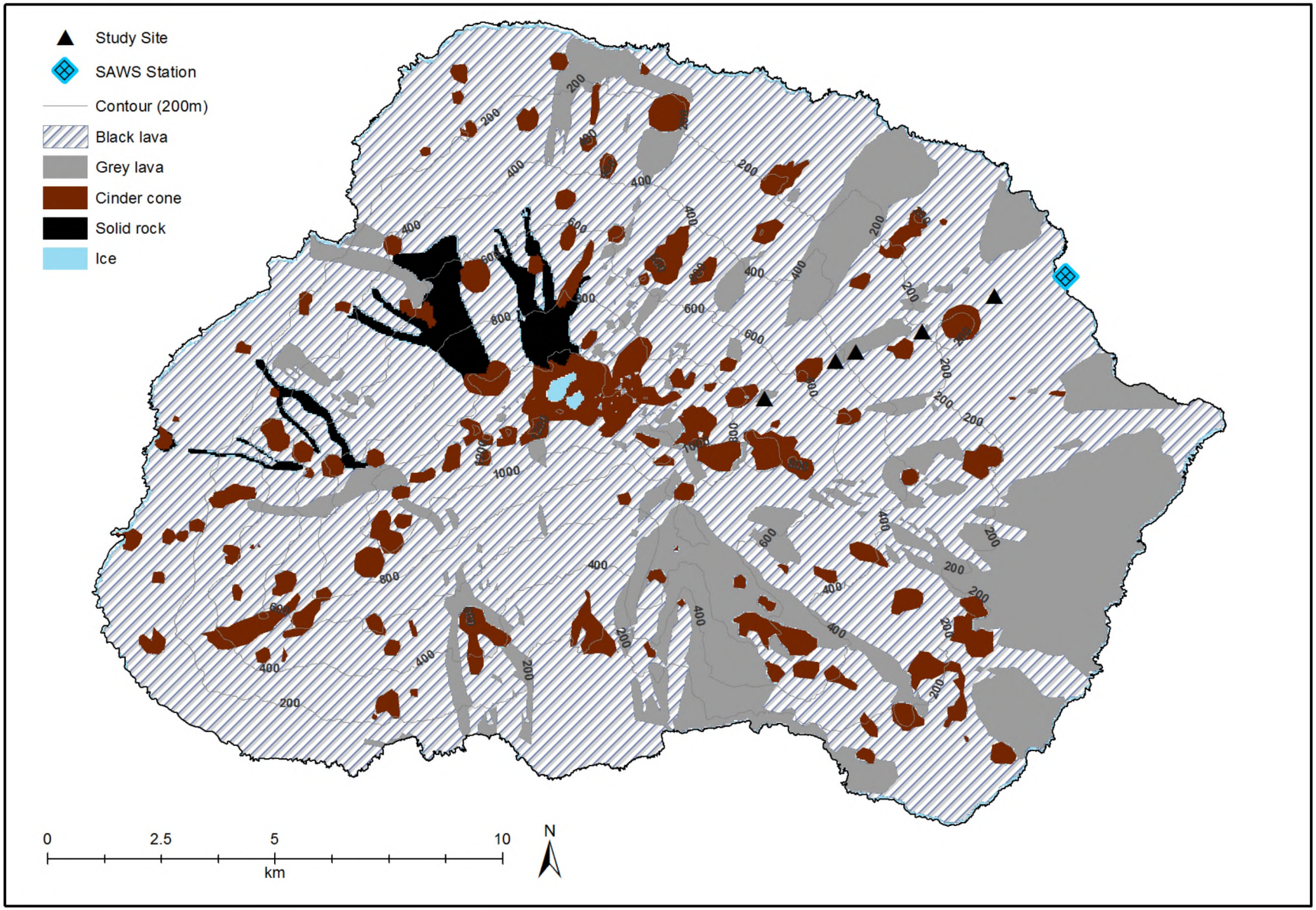


**Figure 8: Study sites and their location regarding geology on Marion Island. SAWS: South African Weather Service.**

### 3.2.1 Active and relict periglacial landforms and -features

Marion Island exhibits glacial, as well as active and relict periglacial features (Holness and Boelhouwers, 1998a, 2002), and its periglacial and glacial landforms are well documented *(e.g.* Hall, 1981, 1979; Holness and Boelhouwers, 1998; Holness, 2001a, 2001b; Hall, 2002; Hedding *et al.*, 2007; Hedding, 2008). Holness (2001a) argues for intense periglacial activity until 7 000 BP, with relict periglacial features including stone-banked lobes, stone-banked terraces, vegetation-banked terraces and blockstreams. An overview of glacial landforms by Boelhouwers *et al.* (2008) can be viewed in Figure 9 (pg. 51). Additional glacial features in the Central Highland comprising striations, polished bedrock, a cirque glacier, relict cirques, and roches moutonées are described by Hedding (2006).

Glacial features, such as moraines and till, exhibit evidence of present day frost processes (Boelhouwers *et al.*, 2008). While the current frost environment yields small examples of patterned ground and solifluction lobes (Boelhouwers *et al.*, 2008), larger examples of such landforms reflect a stronger paleofrost environment and in general, periglacial landforms found below 750-800 m a.s.l. can be considered relict. The Feldmark Plateau (for place names on Marion Island please refer to Figure 10, pg. 52), is characterised by distinct periglacial features that Boelhouwers *et al.* (2008) and Holness (2001a) describe as allochthonous block deposits, stone-banked terraces and lobes. The blockstream located at Beret Hill on the Feldmark plateau extends for more than 160 m with platy clasts that exhibit some preferred orientation (Holness, 2003a). Stone-banked lobes are widely distributed, although these landforms do not occur at the highest elevations. Vegetation-banked lobes are less common and also absent at high elevations (Holness, 2003a). The abundance of stone-banked lobes instead of vegetation-banked lobes suggests frost creep, instead of gelifluction, as the dominant process (Holness, 2003a). Hall (1981) describes relict stone-banked lobes on Tafelberg, Long Ridge (North/South), Kildalkey Bay, Stoney Ridge and Junior's Kop at elevations ranging from 70-450 m a.s.l. Further lobes are described by Sumner *et al.* (2002) at Macaroni Bay and Piew Crags, and by Holness (2003a) for Albatross Lakes, Repettos Hill, Skua Ridge, Greyheaded-Albatross Ridge, Watertunnel, Kerguelen Rise, Fred's Hill, Tate's Hill, Eduard, Beret Hill, Black Haglet Valley, and Delta Extension. Lobate landforms are found on glacial debris and characterised by a non-vegetated to limited vegetated treads, sorting on their surfaces with lobes banked by clasts of varying sizes and imbrication in evidence. Relict stone-banked lobes on Long Ridge at 200-500 m a.s.l. have risers up to 4 m in height (Holness, 2001a), with lobes controlled by bedrock outcrops having higher rises of up to 6 m (Holness and Boelhouwers, 1998; Nel, 2001). Furthermore, these lobes may be up to 20 m in length. Here riser height increases with increasing altitude, with landforms located at 200 m a.s.l. having risers of ± 30 cm and those located at higher elevations (550 m a.s.l.) having riser heights of up to 120 cm (Holness and Boelhouwers, 1998). Only the smallest of these landforms (risers ± 1 m) are considered active under current climatic conditions. Further relict solifluction lobes and terraces are found in the Tafelberg region at 300 m a.s.l. (Holness and Boelhouwers, 1998; Boelhouwers *et al.*, 2008), and in the Central Highland, where lobes have risers of up to 1.2 m (Hedding, 2008). Relict solifluction terraces on the Central Highland have heights of up to 40 cm (Hedding, 2008).

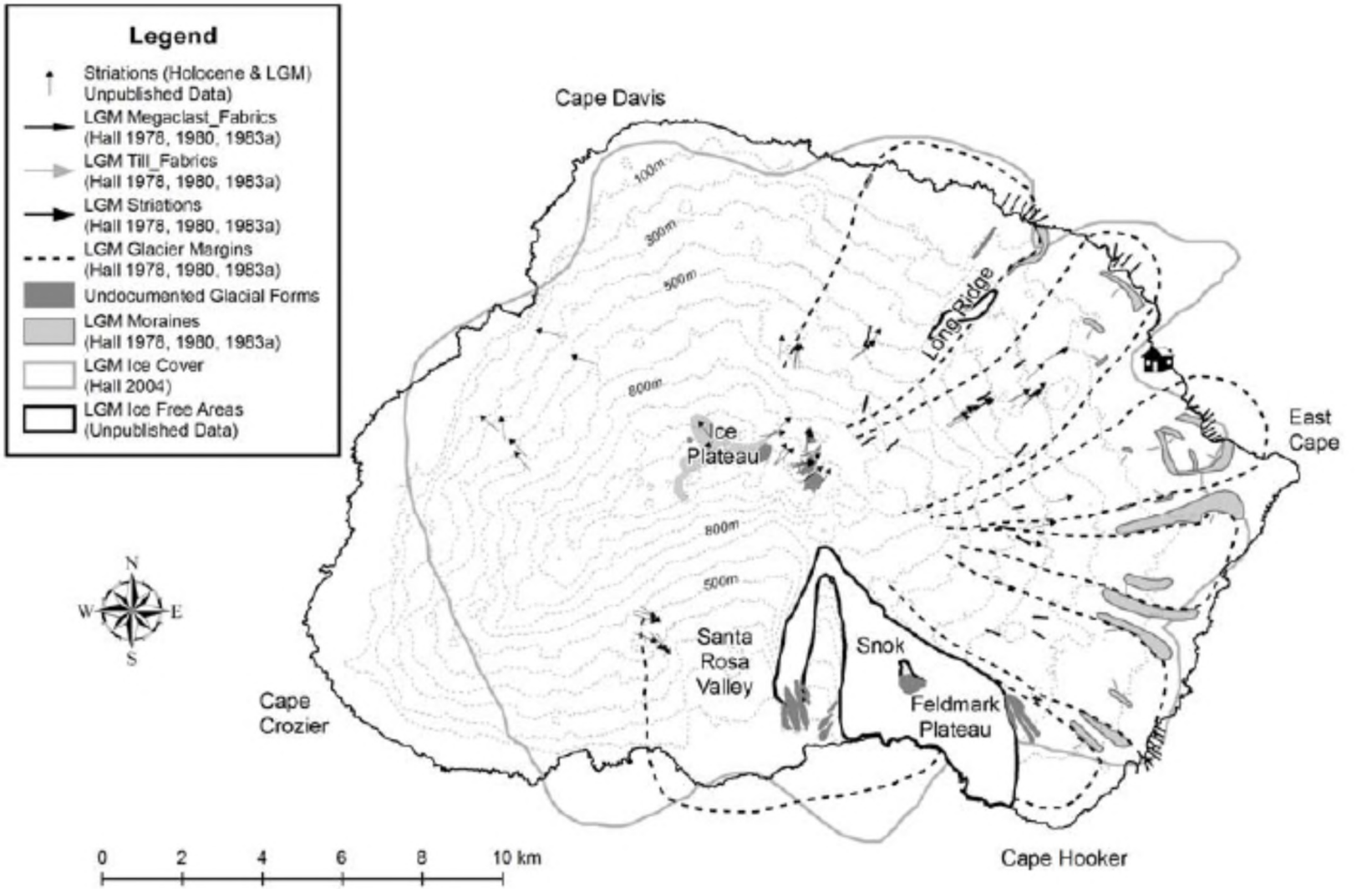


**Figure 9: Glacial landforms on Marion Island (Boelhouwers *et al.*, 2008).**

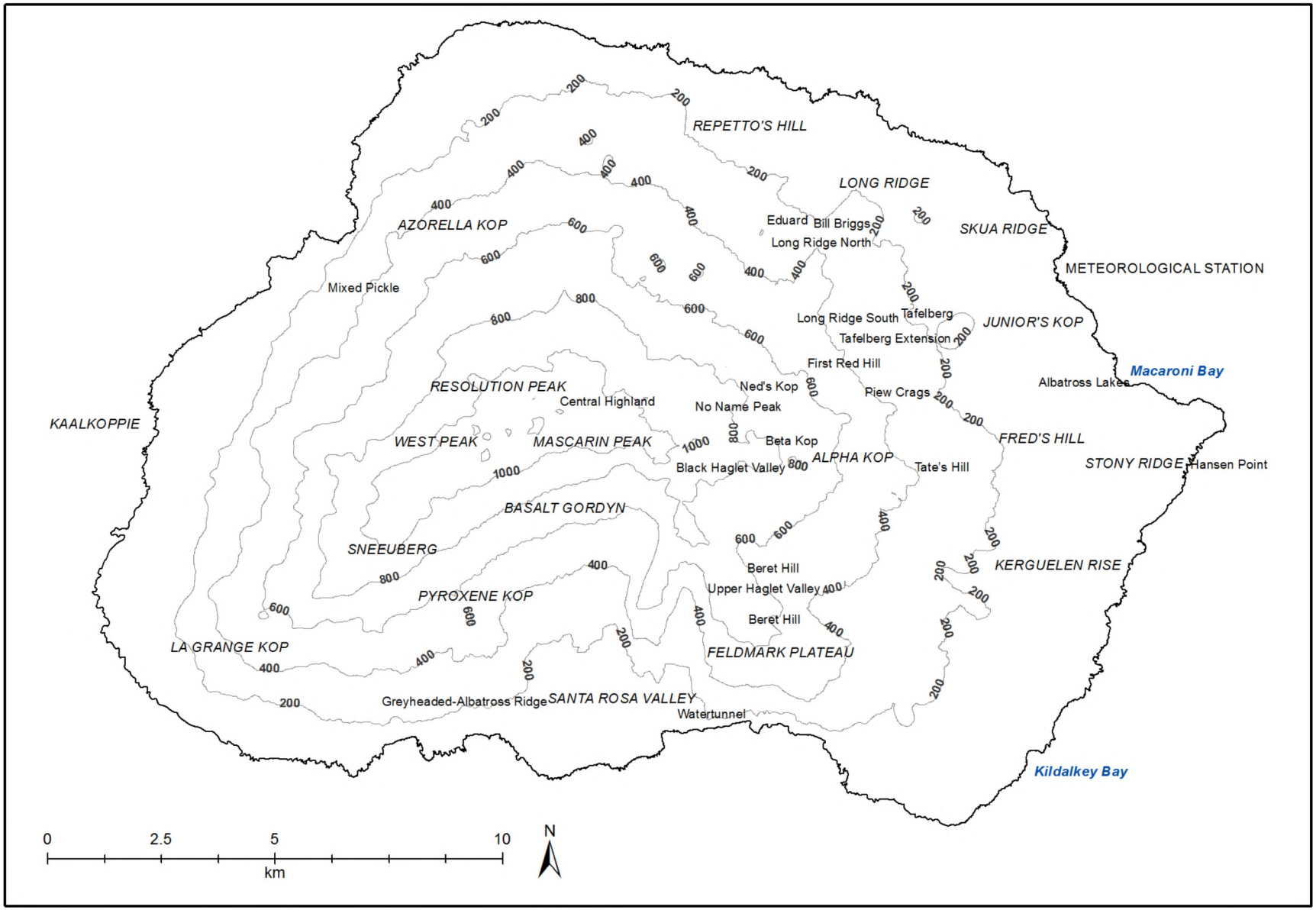


**Figure 10: Points of interest on Marion Island.**

A relict allochthonous block deposit is found on Long Ridge (Holness and Boelhouwers, 1998), with further relict blockfields occurring above 450 m a.s.l. (Boelhouwers, 2003a). The blockstream at Long Ridge covers an approximate area of 5 000 $m^2$ and is characterised by large angular clasts with average a-axes lengths of 2.5 m (Holness and Boelhouwers, 1998). Further poorly developed autochthonous block deposits have been described for Tafelberg, Tate's Hill, Long Ridge and the Central Highland (Sumner and Meiklejohn, 2004). The autochthonous blockfield on Long Ridge is located on grey lava and the most well-developed one described for the Island (Sumner and Meiklejohn, 2004). Relict solifluction terraces are located at Long Ridge South with terraces ranging from tens to hundreds of meters laterally, with riser heights up to 2 m at the higher elevations. At Bill Briggs, where sorted nets are also found, such terraces are smaller, extending for shorter distances and having risers of ± 1 m (Holness and Boelhouwers, 1998). Differences between stone-banked lobes and solifluction terraces lie in smaller clasts found on/in solifluction lobes (Holness and Boelhouwers, 1998). In the Central Highland thermokarst has been reported (Sumner *et al.*, 2004a; Boelhouwers *et al.*, 2008; Hedding, 2008).

Active patterned ground, including sorted stripes/polygons/nets/circles and non-sorted stripes, is present on the Island (Boelhouwers *et al.*, 2003; Holness, 2003a), at all altitudes (Boelhouwers *et al.*, 2008). Diurnal frost cycles occur in coastal and higher inland regions, with shorter cycles of lower intensity present in the coastal areas and the higher inland areas characterised by longer and higher intensity freezing events (Holness, 2003b). Holness (2008) argues that dimensions of sorted circles are positively correlated to altitude on the Island. Further evidence of deep frost cycles and processes is inferred from imbrication patterns (Haussmann *et al.*, 2009b). Debris flows are common, such as those described for Juniors Kop (Boelhouwers *et al.*, 2000), and there is evidence of ice lensing and micro-patterned ground (Hall, 2002; Holness, 2003a). Needle ice is ubiquitous *(e.g.* Holness and Boelhouwers, 1998; Boelhouwers *et al.*, 2003; Holness, 2003a; Haussmann *et al.*, 2009a, 2009b, 2010b; Nel, 2012; Borg, 2017). Where vegetation is present, excluding the coastal areas, turf exfoliation due to needle ice is observed (Boelhouwers *et al.*, 2003). Haussmann *et al.* (2009a) demonstrate that frost cycles and associated needle ice events are more common on the leeward side of *A. selago* and argue for a frost pull mechanism over frost push. *A. selago* also form vegetation-banked terraces (Haussmann *et al.*, 2009b), with active examples of these found at elevations exceeding 200 m a.s.l. (Holness and Boelhouwers, 1998). Needle ice has also been recorded for the Central Highland (Ned's Kop) (Hedding, 2006), as well as Katedraalkrans (Borg, 2017). Sorted stripes, which are generally aligned with the dominant wind direction, are common (Hall, 1979; Holness, 2001b), and have been observed in the Central Highland, on Greyheaded-Albatross Ridge, Long Ridge (Bill Briggs, Long Ridge South), Skua Ridge, Stoney Ridge, Fred's Hill, Tate's Hill, Delta Extension, Hansen Point, Katedraalkrans, Kildalkey Bay, Tafelberg, Tafelberg Extension, and Upper Haglet Valley (Holness and Boelhouwers, 1998; Holness, 2001b; Boelhouwers *et al.*, 2003; Hedding, 2008).

An increase in altitude translates into deeper freeze-thaw cycles and more lateral sorting of stripes. For example, the sorting depth on Bill Briggs (350 m a.s.l.) is 4-7 cm, whereas sorting depth at Long Ridge South (500 m a.s.l.) is 10-15 cm (Holness and Boelhouwers, 1998). Sorted circles and polygons occur in the Central Highland, Greyheaded-Albatross Ridge, Long Ridge (North; South), Repettos Hill, Eduard

Grey, Skua Ridge, Stoney Ridge, Fred's Hill, Tate's Hill, Delta Extension, Hansen Point, Kildalkey Bay, Beret Hill, Tafelberg, Watertunnel, and Upper Haglet Valley (Boelhouwers *et al.*, 2003; Holness, 2003b; Hedding, 2008). These sorted circles consist of domed, finer and roughly circular centres surrounded by a border of coarse material and are common on low angle treads of relict solifluction lobes and terraces (Holness, 2003b). Non-sorted thermal contraction polygons with an approximate diameter of 500 cm have been recorded on black lava in the Central Highland (Hedding, 2008). An active pronival rampart has been described for the head of the Black Haglet valley (Hedding *et al.*, 2007), in the Central Highland (Hedding, 2008), as well as one at the backwall of the cirque at Snok (Boelhouwers *et al.*, 2008). A summary of periglacial landforms and -features found on the Island is given in Figure 11 (pg. 55) and in Table 3 (pg. 56). The information contained within this table has been largely adapted from Boelhouwers *et al.* (2003) and Hedding (2008), and supplemented by additional readings and resources. Field observations made during April and May 2014 have also been added.

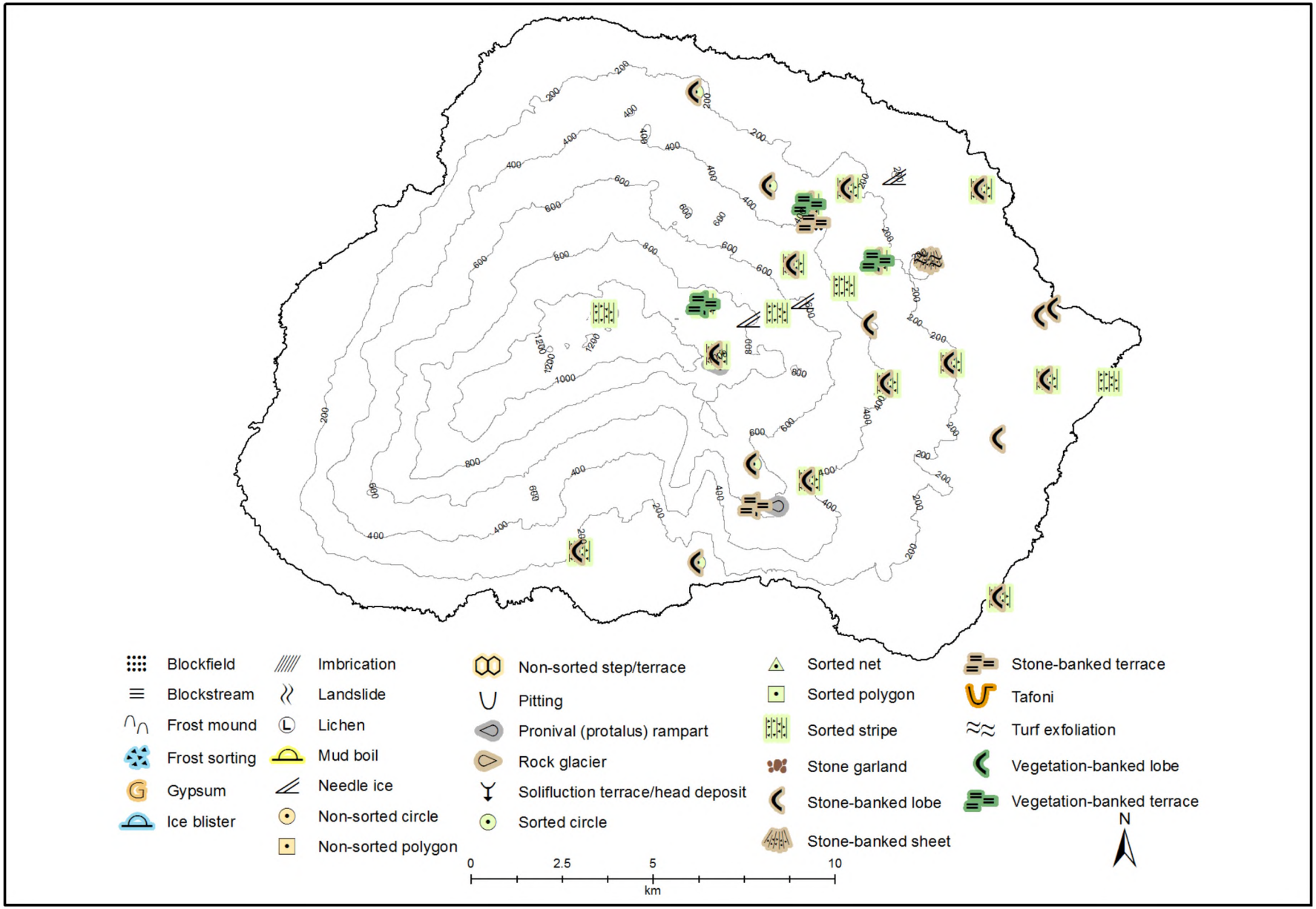


**Figure 11: Landforms observed on Marion Island, as per literature review.**

**Table 3: This table provides a summary of periglacially derived landforms and -features for Marion Island. The active or relict state of the landform is indicated when known. * Includes pingo, palsa, thúfur.**

| Feature | Location | Altitude | Active/Relict | Source |
|---|---|---|---|---|
| Blockfield | Above 450 m a.s.l. and below 750 m a.s.l. | > 450 and < 750 | Relict | (Boelhouwers, 2003a; Sumner and Meiklejohn, 2004) |
| | Long Ridge | 400 | Relict | (Sumner and Meiklejohn, 2004) |
| | Tafelberg | 200 | Relict | (Sumner and Meiklejohn, 2004) |
| | Tate's Hill | 400 | Relict | (Sumner and Meiklejohn, 2004) |
| Blockstream | Feldmark Plateau (Beret Hill) | 750 | Relict | (Holness, 2001a) |
| | Long Ridge South | 500 | Relict | (Holness and Boelhouwers, 1998) |
| Frost mound * | *None observed* | | | |
| Imbrication | Long Ridge South | 500 | Relict | (Holness and Boelhouwers, 1998) |
| | Tafelberg area | 300 | Relict | (Haussmann *et al.*, 2009b) |
| Mud boil | *None observed* | | | |
| Needle ice | First Red Hill (Cinder cone) | 550 | Active | (Holness, 2004) |
| | Junior's Kop | 306 | Active | (Boelhouwers *et al.*, 2000) |
| | Junior's Kop (Cinder cone) | 200 | Active | (Holness, 2004) |
| | Katedraalkrans | ± 750 | Active | (Borg, 2017) |
| | Katedraalkrans Nek (Cinder cone) | 750 | Active | (Holness, 2004) |
| | Ned's Kop | ± 800 | Active | (Hedding, 2006) |
| | Ned's Hill (Cinder cone) | 750 | Active | (Holness, 2004) |
| | Tafelberg | 300 | Active | (Haussmann *et al.*, 2009a) |
| | Twisted Sister (Cinder cone) | 150 | Active | (Holness, 2004) |
| Non-sorted circle | *None observed* | | | |
| Non-sorted polygon | Central Highland | 750 | Active | (Sumner and Meiklejohn, 2004) |
| | Central Highland | 950 | Relict | (Hedding, 2008) |
| Non-sorted step/terrace | *None observed* | | | |
| Pronival (protalus) rampart | Black Haglet Valley | 900 | Active | (Hedding *et al.*, 2007) |
| | Central Highland (Delta Kop) | ± 1 000 | Active | (Hedding, 2006, 2008) |
| | Snok cirque backwall | 550-600 | Relict | (Boelhouwers *et al.*, 2008) |
| Rock glacier | *None observed* | | | |
| Solifluction terrace/head deposit/frost creep | Bill Briggs (Long Ridge) | 350 | Relict | (Holness and Boelhouwers, 1998) |
| | Central Highland; No Name Peak | > 750; ± 950 | Relict | (Hedding, 2006, 2008) |

| Feature | Location | Altitude | Active/Relict | Source |
|---|---|---|---|---|
| | Long Ridge South | 500 | Relict | (Holness and Boelhouwers, 1998) |
| | Tafelberg | 300 | Relict | (Holness and Boelhouwers, 1998; Boelhouwers *et al.*, 2008) |
| Sorted circle | At all altitudes, excluding the coastal area | All altitudes | Active | (Boelhouwers *et al.*, 2003) |
| | Beret Hill | 750 | Active | (Holness, 2003b) |
| | Delta Extension | 1 000 | Active | (Boelhouwers *et al.*, 2003) |
| | Eduard | 350 | Active | (Holness, 2003b) |
| | Fred's Hill | 290 | Active | (Boelhouwers *et al.*, 2003) |
| | Greyheaded-Albatross Ridge | 100 | Active | (Boelhouwers *et al.*, 2003; Holness, 2003b) |
| | Hansen Point | 10 | Active | (Boelhouwers *et al.*, 2003) |
| | Kildalkey Bay | 70 | Active | (Boelhouwers *et al.*, 2003; Holness, 2003b) |
| | Long Ridge North | 200 | Active | (Boelhouwers *et al.*, 2003; Holness, 2003b) |
| | Long Ridge South | 500 | Active | (Boelhouwers *et al.*, 2003; Holness, 2003b) |
| | Repettos Hill | 300 | Active | (Holness, 2003b) |
| | Skua Ridge | 90 | Active | (Boelhouwers *et al.*, 2003; Holness, 2003b) |
| | Stoney Ridge | 150 | Active | (Boelhouwers *et al.*, 2003; Holness, 2003b) |
| | Tafelberg | 450 | Active | (Boelhouwers *et al.*, 2003; Holness, 2003b) |
| | Tate's Hill | 460 | Active | (Boelhouwers *et al.*, 2003; Holness, 2003b) |
| | Upper Haglet Valley | 850 | Active | (Boelhouwers *et al.*, 2003) |
| | Watertunnel | 100 | Active | (Holness, 2003b) |
| Sorted net | Bill Briggs (Long Ridge) | 350 | Relict | (Holness and Boelhouwers, 1998) |
| Sorted polygon | Central Highland | > 750 | Active | (Hedding, 2008) |
| Sorted stripe | At all altitudes, excluding the coastal area | All altitudes | Active | (Boelhouwers *et al.*, 2003) |
| | Bill Briggs (Long Ridge) | 350 | Active (4-7 cm depth) | (Holness and Boelhouwers, 1998) |

| Feature | Location | Altitude | Active/Relict | Source |
|---|---|---|---|---|
| | Central Highland (Delta Kop) | ± 1 000 | Active | (Hedding, 2006, 2008) |
| | Delta Extension | 1 000 | Active | (Boelhouwers *et al.*, 2003) |
| | Fred's Hill | 290 | Active | (Boelhouwers *et al.*, 2003; Holness, 2001b) |
| | Greyheaded-Albatross Ridge | 100 | Active | (Holness, 2001b; Boelhouwers *et al.*, 2003) |
| | Hansen Point | 10 | Active | (Boelhouwers *et al.*, 2003) |
| | Katedraalkrans | 750 | Active | (Boelhouwers *et al.*, 2003) |
| | Kildalkey Bay | 70 | Active | (Boelhouwers *et al.*, 2003; Holness, 2001b) |
| | Long Ridge North | 200 | Active | (Holness, 2001b; Boelhouwers *et al.*, 2003) |
| | Long Ridge South | 500 | Active (10-15 cm depth) | (Holness, 2001b; Boelhouwers *et al.*, 2003) |
| | Skua Ridge | 100 | Active | (Holness, 2001b; Boelhouwers *et al.*, 2003) |
| | Stoney Ridge | 150 | Active | (Holness, 2001b; Boelhouwers *et al.*, 2003) |
| | Tafelberg | 300 | Active (5-10 cm depth) | (Holness, 2001b; Boelhouwers *et al.*, 2003) |
| | Tafelberg Extension | 400 | Active | (Holness, 2001b) |
| | Tate's Hill | 460 | Active | (Holness, 2001b; Boelhouwers *et al.*, 2003) |
| | Upper Haglet Valley | 850 | Active | (Holness, 2001b; Boelhouwers *et al.*, 2003) |
| Stone garland | *None observed* | | | |
| Stone-banked lobe | Albatross Lakes | 50 | Relict | (Holness, 2003a) |
| | Beret Hill | 750 | Relict | (Holness, 2003a) |
| | Bill Briggs | 350 | Relict for risers exceeding ± one meter; active for those below | (Holness and Boelhouwers, 1998) |
| | Black Haglet Valley | 700 | Relict | (Holness, 2003a) |
| | Delta Extension | 1 000 | Relict | (Holness, 2003a) |
| | Eduard | 600 | Relict | (Holness, 2003a) |
| | Feldmark Plateau | 600-750 | Relict (risers of 3 m) | (Holness, 2001a) |
| | Fred's Hill | 290 | Relict | (Holness, 2003a) |

| Feature | Location | Altitude | Active/Relict | Source |
|---|---|---|---|---|
| | Greyheaded-Albatross Ridge | 100 | Relict | (Holness, 2003a) |
| | Junior's Kop | 150 | Relict | (Hall, 1981) |
| | Kerguelen Rise | 250 | Relict | (Holness, 2003a) |
| | Kildalkey Bay | 70 | Relict | (Hall, 1981; Holness, 2003a) |
| | Long Ridge North | 200 | Relict | (Hall, 1981; Holness, 2003a) |
| | Long Ridge South | 500 | Relict for risers exceeding ± one meter; active for those below | (Holness and Boelhouwers, 1998) |
| | Macaroni Bay | 40 | Relict | (Sumner *et al.*, 2002) |
| | Piew Crags | 400 | Relict | (Sumner *et al.*, 2002) |
| | Repettos Hill | 75 | Relict | (Holness, 2003a) |
| | Skua Ridge | 90 | Relict | (Holness, 2003a) |
| | Stoney Ridge | 100 | Relict | (Hall, 1981; Holness, 2003a) |
| | Tafelberg | 450 | Relict | (Hall, 1981; Holness, 2003a) |
| | Tate's Hill | 450 | Relict | (Holness, 2003a) |
| | Watertunnel | 150 | Relict | (Holness, 2003a) |
| Stone-banked sheet | Junior's Kop | 150 | Active | (Boelhouwers *et al.*, 2003) |
| Stone-banked terrace | Feldmark Plateau | 600-750 | Relict (risers of 4 m) | (Holness, 2001a) |
| | Feldmark Plateau | 600-750 | Relict (risers of 6 m) | (Nel, 2001) |
| | Long Ridge | 200-550 | Relict (larger landforms)/Active (smallest landforms) | (Holness and Boelhouwers, 1998) |
| Turf exfoliation | At all altitudes where vegetation is present, excluding the coastal area | All altitudes | Active | (Boelhouwers *et al.*, 2003) |
| | Junior's Kop | 150 | Active | (Boelhouwers *et al.*, 2003) |
| Vegetation-banked lobe | At all altitudes, excluding the highest areas | All altitudes | Active | (Boelhouwers *et al.*, 2003) |
| Vegetation-banked terrace | At all altitudes, excluding the highest areas | All altitudes | Active | (Boelhouwers *et al.*, 2003) |
| | Long Ridge (Long Ridge South; Bill Briggs; Long Ridge North) | 200-550 (500; 350; 200) | Relict (larger landforms)/Active (smallest landforms) | (Holness and Boelhouwers, 1998) |
| | Tafelberg (but common throughout fellfield) | 300 | Active/Relict (state may be identified by surface sediment mobility) | (Haussmann *et al.*, 2009a, 2009b) |

## 3.3 Dronning Maud Land (DML), Antarctica

The third study area, Dronning Maud Land (DML) (**Figure 2**, pg. 26), is located in the Antarctic and individual sites within this region are centred on 72°S, 3°W. Dronning Maud Land, one of the major identified regions in East Antarctica, stretches from the Stancomb-Wills Glacier in New Schwabenland at 20°W to Shinnan Glacier in Enderby Land at 44°38'E (Stewart, 2011). In DML mountain peaks generally exceed 1 000 m a.s.l. (Stewart, 2011), rising above the ice sheet as nunataks (Bliss *et al.*, 2013). Wind scoops with floors of blue ice are found around most nunataks (Elvevold and Ohta, 2010). The region may be divided into a western and eastern portion based on the geological and topographical divisions of Fimbulheimen and Maudheimvidda (Stewart, 2011). Fimbulheimen describes the mountain area between the Jutulstraumen inter-continental glacier in the west and the Borchgrevinkisen glacier in the east (Stewart, 2011). Maudheimvidda describes the westernmost part of DML and stretches from 20°W to the Jutulstraumen outlet glacier at 0°30' W (Stewart, 2011). However, definitive geographical delineation of DML into a western, central and eastern portion is not clear and the usage of such divisions not consistent *(e.g.* Isaksson and Karlén, 1994; Golynsky *et al.*, 1997; Bauer, 2009; Thamban *et al.*, 2011; Keskitalo *et al.*, 2013). Western DML (WDML) may also be delineated by the extent of the Grunehogna Craton, necessitating the inclusion of the H. U. Sverdrupfjella area of the Maud Belt as the eastern margin of WDML (at ±5°E), due to this belt arguably being an overprinting of the Archaean craton (Groenewald *et al.*, 1995; Perritt, 2001; Grosch *et al.*, 2007; Marschall *et al.*, 2013). Stewart's (2011) delineation into a western and eastern portion neglects the inclusion of a central part to DML and yields a delineation of DML into a much larger eastern portion. McGibbon (2014), for example, defines WDML as the area extending from 70°S to 75°S and 15°W to 03°E, being made up of the two geologically distinct provinces of the Archean to Mesoproterozoic Grunehogna Province and the Mesoproterozoic to early Palaeozoic Maud Belt. Barton *et al.* (1987), similarly, describe WDML as consisting of two distinct geological terranes on either side of the Penck-Jutulstraumen Trough System. For this study, WDML is shown as the area defined as Maudheimvidda by Stewart (2011), a delineation also followed by *e.g.* Krynauw (1986), Barton *et al.* (1987) and Hunter *et al.* (2013), with the central portion stretching east from the Pencksøkket-Jutulstraumen glaciers to the eastern extent of Fimbulheimen. This delineation is also applied, to some extent, by *e.g.* Marschall *et al.* (2013). Eastern DML (EDML) is defined as the area stretching eastward from the Sør Rondane Mountains toward Enderby Land (Figure 12, pg. 61).

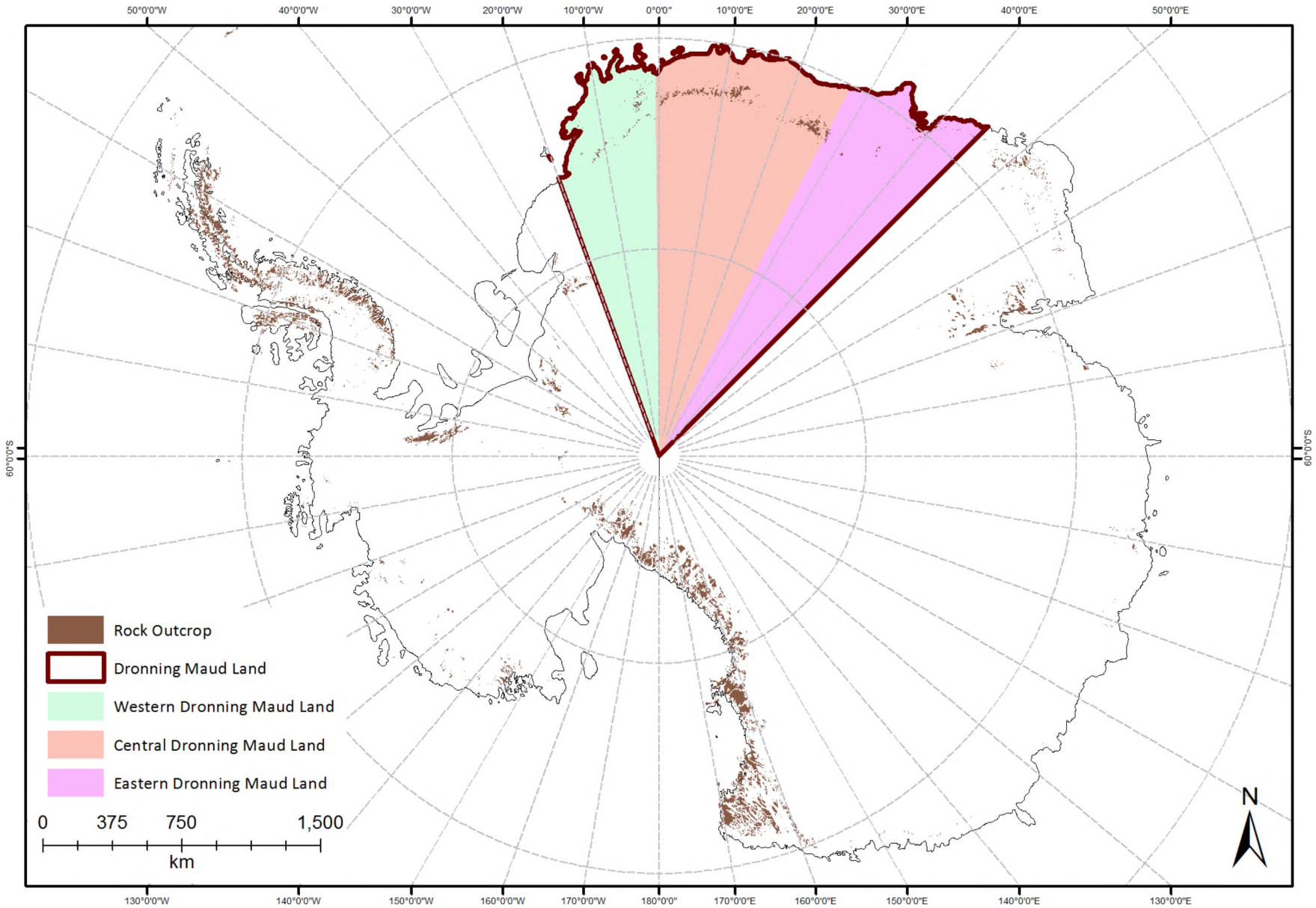


**Figure 12: Delineation of Dronning Maud Land (DML) into western Dronning Maud Land (WDML), central Dronning Maud Land (CDML), and eastern Dronning Maud Land (CDML).**

This study area is both high-altitudinal and -latitudinal. A total of eight study sites were chosen in DML, on seven separate nunataks. Of these seven nunataks, six are in western DML (WDML), and one in central DML (CDML). These include Flårjuven 1 (72°01'S, 03°39'W; 1 239 m a.s.l.), Flårjuven 2 (72°02'S, 03°39'W; 1 234 m a.s.l.), Grunehogna (72°05'S, 2°79'W; 1 291 m a.s.l.), Robertskollen (71°48'S, 03°33'W; 284 m a.s.l.), Schumacherfjellet (71°91'S, 02°97'W; 1 230 m a.s.l.), Slettfjell (72°13'S, 03°27'W; 1 435 m a.s.l.), Valterkulten (71°90'S, 03°23'W; 975 m a.s.l.), and the Vesleskarvet nunataks (71°69'S, 02°84'W; 805 m a.s.l.). The Robertskollen logger is located on the Peaceful Hill nunatak (Ryan *et al.*, 1989; Ryan and Watkins, 1989), with the Vesleskarvet logger located on the Northern Buttress of the Vesleskarvet nunataks (Hansen, 2014). The Southern Buttress of the Vesleskarvet nunataks is also the location of the South African National Antarctic Expedition IV (SANAE IV) research station, located ± 160km inland from the ice shelf (Steele *et al.*, 1994). The Valterkulten logger was placed near a brine pond (Marshall *et al.*, 1995), whereas the Grunehogna logger is located on a scree slope (Krynauw, 1986). A further two loggers are found in the Jutulsessen of CDML. Troll Station 1 (72°01'S, 02°53'E; 1 320 m a.s.l.) and Troll Station 2 (72°01'S, 02°53'E; 1 326 m a.s.l.) are sited on the eastern side of the Jutulstraumen with both loggers located on the slope of Nonshøgda, directly west of Troll station (Hansen *et al.*, 2016b). The ten logging sites were given the identifiers of A1-A10 respectively and a more detailed description of logging sites in DML follows under the section 4.3.1.3 Dronning Maud Land (DML), Antarctica on pg. 90. Please refer to Figure 13 (pg. 63) for an overview of the study sites within DML, as well as Table 7 and Table 8 in APPENDIX D for a detailed description of the logger locations. Due to various naming conventions in use for Antarctic features, the Norwegian naming conventions, as they appear in the Composite Gazetteer of Antarctica, have been applied (Antarctic Data Centre, 2016).

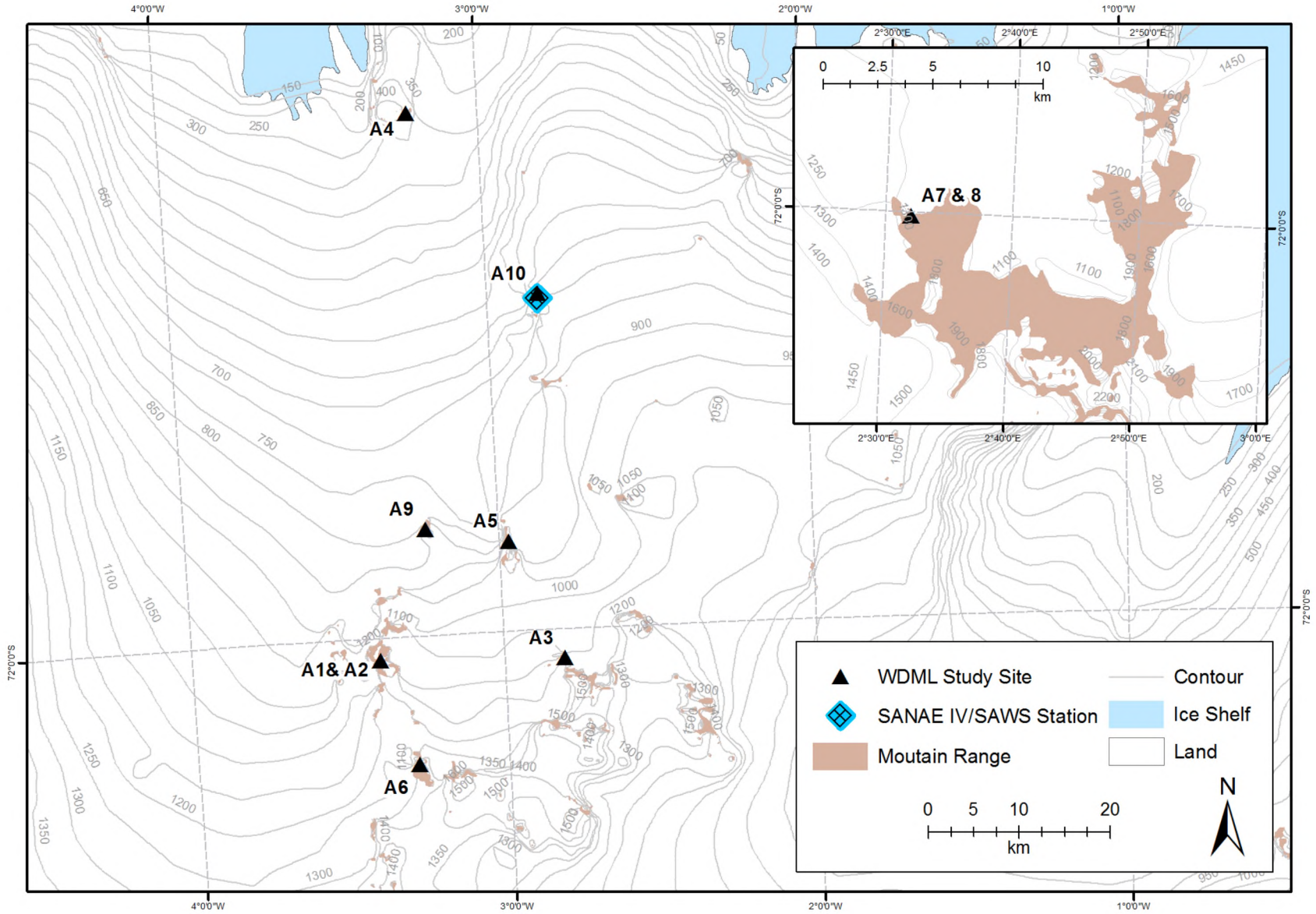


**Figure 13: Study sites within western Dronning Maud Land (WDML) and the Jutulsessen (inset) near Troll Station, Norwegian research base (n = 10).**

Ravindra and Chaturvedi (2011) argue that the Antarctic ice sheet reached its current extent ± 8 000 BP, during the Last Interglacial Transition with Hall (2009) and Hodgson *et al*. (2014) arguing that the ice sheet of Dronning Maud Land (DML) was already receding from the glacial maximum during the Holocene. Work by Ryan *et al.* (1989) on accumulations of oil regurgitations found near snow petrel nesting sites on Robertskollen suggest nest occupation of ± 10 000 BP. This supports a deglaciation sequence for WDML of ± 10 000 BP. Shrivastava *et al.* (2014) argue that the moraines and till deposits of the Jutulsessen were deposited during the last glacial maximum (LGM), with the higher-elevated nunataks remaining ice free during the last glaciation. Nunataks near SANAE IV comprise homogenous mafic doleritic and dioritic Borgmassivet intrusives (Steele *et al.*, 1994) consisting of lherzolite, pyroxenite, norite, gabbro and quartz monzodiorite (Groenewald *et al.*, 1995). The continental tholeiitic Borgmassivet Intrusions are of Mesoproterozoic origin (Republic of South Africa, 1981) and form most of the outcrops (nunataks) of the northern part of the Grunehogna province (Groenewald *et al.*, 1995). The Borgmassivet intruded into the Ritscherflya Supergroup at 1 107 Ma, with mafic dykes intruding and into the northeastern and southwestern part of the Maud Belt at 600 Ma (Moyes *et al.*, 1995; Grosch *et al.*, 2007). Overall, the Maud Belt and its greater area have experienced little surface weathering since exposure (McGibbon, 2014). All logging sites for WDML, excluding CDML, are found on geologies of the Borgmassivet Intrusions and none are located on the sedimentary sequences of the Ritscherflya Supergroup. The two logging sites in CDML, on the Jutulsessen metasupacrustals, are found east of the Jutulstraumen-Pencksøkket Rift Zone, which separates a Proterozoic platform to the west with high-grade metamorphic areas to the east (Ohta *et al.*, 1990). The Jutulsessen, consisting predominantly of granitic gneisses (Moyes, 1993), form part of the Gjelsvikfjella of the Maud Belt, directly east of the H. U. Sverdrupfjella. This region is defined by intensely deformed granulite and amphibolite facies gneisses, specifically hornblende biotite gneisses of intermediate composition, orthogneisses (Dallmann *et al.*, 1990) and felsic gneisses (Ohta *et al.*, 1990) attributed to volcanic rather than intrusive origins of ± 1 100-1 200 Ma (Grantham *et al.*, 1995; Groenewald *et al.*, 1995; Marschall *et al.*, 2013). Intrusions into this high-grade igneous province occurred at 450-500 Ma (Dallmann *et al.*, 1990). The geologies of the two CDML logging sites are distinct to others of WDML, having implications on ground thermal and moisture regimes recorded.

Diurnal and seasonal freeze-thaw patterns are generally, respectively, weak and strongly-developed for continental Antarctica, with ranges in mean annual air temperature (MAAT) of 25-36 °C and MAAT near -8 °C to -14 °C expected (French, 1996). Dronning Maud Land is a hyper-arid and cold region (EF in the Köppen-Geiger climatic classification), receiving precipitation between 55-81 mm annually (Reijmer and Broeke, 2001) and study sites within the area are located near the 50-mm annual water equivalent contour (Noone *et al.*, 1999). Limited recorded ambient air temperature data are available for the region. Average air temperatures at the South African Weather Service (SAWS) station at Vesleskarvet, spanning 2000 to 2012, are -16 °C, with average winter temperatures -22 °C (absolute winter minimums of -29 °C) and average summer temperatures -8 °C (absolute summer maximums of -2 °C) (Hansen, 2014). Average relative humidity is high at 63%, with average wind speeds of 11 $m.s^{-1}$ (Hansen, 2014). Active layer thickness for Vesleskarvet is 16 cm for a six-year period from 2009-2014 (Kotzé and Meiklejohn, 2016). Robertskollen exhibits winter minimum temperatures of -34 °C and summer maximums of 5 °C (Newton, 1994). Data on potential freeze-thaw events are available for Vesleskarvet, with an average of ± 47 potential cycles observed annually from 2010-2014 (Kotzé and Meiklejohn, 2016), with wind speed correlated negatively and air temperatures positively to ground temperatures

(Hansen, 2014; Kotzé and Meiklejohn, 2016). Western DML experiences a dominant easterly to northeasterly wind (Ryan and Watkins, 1989; Hansen, 2014), yielding drift snow accumulations on the leeward side of clasts and landforms. This snow is a water source during warmer months, when temperatures are sufficiently warm to melt these accumulations. At Troll Station in CDML temperatures range from ± -34 °C in mid-spring to ± 5 °C in late spring/early summer (Hansen *et al.*, 2009). Dominant wind direction is northeast during summer and northeast to eastnortheast during winter, with strong winds (> 11 $m.s^{-1}$) originating out of the northeast and gusts of ± 37 $m.s^{-1}$ recorded (Hansen *et al.*, 2009). The Ahlmannryggen of WDML protect the region from continental katabatic winds. In comparison, CDML is at the edge of the plateau and within reach of katabatic winds. Dronning Maud Land shows stable snow and ice net accumulation rates over the last 1 000 years (Rotschky *et al.*, 2007) and surface net accumulation for DML is 0.16-0.10 m water equivalent per year (Elvevold and Ohta, 2010). In comparison, annual net ablation is 10 to 15 $cm.y^{-1}$ (Hagen, 1997), with local ablation highest where katabatic winds and concomitant evaporation rates are strong (Orheim, 1997). While the general flow of ice is northwards towards the Princess Martha Coast (Shrivastava *et al.*, 2014), the surface slope of the blue ice area of the Jutulsessen suggests that local ice flow is south towards the rocks of the glacier cirque of Sætet (Orheim, 1997). Sharp increases in surface slope towards rock margins suggest high ablation rates and lakes are common at rock-ice boundary zones (Orheim and Lucchitta, 1990). Permafrost is present, with a variable active layer (Vieira *et al.*, 2010), and diurnal frost cycles have been observed (Hansen, 2014). In WDML the active layer is shallow with little moisture content, like that observed for continental Antarctica where moisture content is exceptionally low at less than 3% (Bockheim and Hall, 2002). In the coastal areas of the McMurdo Sound ice-cemented permafrost occurs at 0.60 m depth, with active layer water content increasing from the ground surface (½%) down to the bottom of the active layer (10%) (Campbell *et al.*, 1998). For areas where no surface water is present, permafrost has little to no ice content and active layer thicknesses decrease to ± 0.25 m, with moisture contents less than 1%. In the mountainous areas of the McMurdo Sound region the active layer thickness decreases to 0.1 m with active layer moisture contents between ½-3% (Campbell *et al.*, 1998). Active layer thickness also reaches its greatest extent during early February (Turner *et al.*, 2009). In high altitudes of WDML the active layer thickness ranges from 0.1-0.25 m (Vieira *et al.*, 2010), like the McMurdo Sound-Dry Valleys for mountainous and dry areas. Soil moisture is crucial to cryoturbation (Ballantyne and Matthews, 1982). Therefore, frost sorting and -heave is dominant in months when increasing temperatures and concomitant snowmelt allow for deeper thawing of the ground (Vieira *et al.*, 2010). Liquid water is only available during the warmer months and driven by microclimate rather than macroclimate temperatures (Lee *et al.*, 2013). For example, an analysis of moisture values of thermal contraction cracks of polygons found on Mimelia (CDML) show higher mean values than moisture values collected for polygon centres (Lee *et al.*, 2013). Depending on site-specific characteristics, liquid water, therefore, becomes available during the short summer when microclimate ambient temperatures are sufficient to melt snow and ice that has accumulated in *e.g.* depressions. Furthermore, while moisture is a limiting factor to geomorphological and biological systems in the region, summer meltwater streams occur at Robertskollen (Ryan *et al.*, 1989), Vesleskarvet (*pers. obs.*), and Grunehogna (Meiklejohn, 2017; *pers. comm.*).

Soils from continental Antarctica are generally arid and lack organic content (Hall and Walton, 1992) and ground material is generally comprised of weathered regolith. Organic matter, per dry mass, is less than 1% for Vesleskarvet, with mean sediment nutrient concentrations between 0.207-0.383 mg $P.g^{-1}$

dry mass soil (sediment) and 0.125-0.217 mg $N.g^{-1}$ dry mass soil (sediment) (Steele *et al.*, 1994). Sediment from Vesleskarvet comprises mineral constituents (Hansen, 2014), with lithosols described for Robertskollen (Ryan *et al.*, 1989). However, all sites are in a continuous permafrost zone (CPZ). Therefore, the sediment for the region is best classed within the suborders of orthels (anyorthels) and turbels (anhyturbels) of the gelisol order (Soil Survey Staff, 1999; Bockheim and Hall, 2002) or cryosols of the World Reference Base for soil resources classification (IUSS Working Group WRB, 2015). Irrespective of this organic content is low overall and sediment most closely classed as lithosols. Total organic carbon (TOC) for Jutulsessen sediment samples is on average less than ½% and analyses show that sediment is derived from sediment transport in the basal zone of glaciers (Shrivastava *et al.*, 2014). All sediments for WDML sites show a lack of fines ($\phi > 4$: silt and clay), as well as low moisture contents with arid conditions prevailing (Steele *et al.*, 1994). Sediment for the Jutulsessen (CDML) is ice-cemented (Dallmann *et al.*, 1990), suggesting a gravimetric moisture content of at least 5% (Campbell *et al.*, 1998). The ice-cemented nature of the permafrost also indicates coarser, rather than finer-grained material that favours ice segregation (Easterbrook, 1999), as confirmed during numerous field visits. The glacial sediments of the Jutulsessen exhibit lack of sorting and a variable mean particle sizes (Hansen, 2014; Shrivastava *et al.*, 2014; Hansen *et al.*, 2016a). Although Hall (2013) argues that chemical weathering cannot be discounted in cold climates, textural and grain size/shape analyses from the Jutulsessen suggest limited chemical weathering with greater weight given to mechanical weathering processes (Shrivastava *et al.*, 2014). This is supported by the presence of labile minerals *(e.g.* feldspar and ferromagnesian minerals) and angular sediment grains, suggesting an immature state, being predominantly derived from immature and/or mechanical processes (Shrivastava *et al.*, 2014). Mechanical action as a major weathering agent is further supported by the chemical index for alteration being independent of organic content, suggesting no relationship between chemical weathering and biogenic activity for Jutulsessen sediment samples (Shrivastava *et al.*, 2014). Localised meltwater channels remove finer particles, such as silt and clay, yielding sediments with a bi-modal distribution and enriched in coarser (sand-sized) particles (Shrivastava *et al.*, 2014). Fines are an important component when considering frost heave since ice segregation and frost heave generally occur in fine-grained soils. The water-holding capacity of sandy material is low due to large pore spaces present (Brady and Weil, 2016). Furthermore, percolation of water is rapid, and drainage enhanced in sandy soils, as is good air movement (Brady and Weil, 2016). In the Jutulsessen, unfrozen water content is sufficient to allow for migration into the freezing ground. However, due to coarse-grained sediment permeability and the unfrozen water content is low, affecting frost heave (Osterkamp and Burn, 2003). Moisture is important in cold-climate weathering and processes and becomes a limiting factor (Hall *et al.*, 2005) if the ground is not able to entrain sufficient water for freeze-thaw cycles to take place. The Jutulsessen have almost no active-layer related landforms, such as sorted circles, although permafrost-related landforms, such as thermal contraction polygons, are common. Since the area is characterised by sand-sized particle distributions and a concomitant lack of moisture-holding ability of the ground, it is suggested that the particle distribution of the ground becomes and overriding factor when analysing freeze-thaw cycles for this site.

All study sites fall within the Polar Desert biome and while vegetation is mostly absent for this region, lichen and bryophytes occur on rocky outcrops (nunataks) (Ryan *et al.*, 1989; Steele *et al.*, 1994; Lee *et al.*, 2013; Hansen, 2014). Robertskollen has a larger diversity of lichen and bryophytes (Ryan *et al.*, 1989; Steele *et al.*, 1994), compared to the other DML study sites, with 20 species of lichen, 17 algal

taxa and four species of mosses recorded (Ryan *et al.*, 1989). Algae are also found in the Jutulsessen (*pers. obs.*). Lichen is present on other nunataks such as Vesleskarvet, with nine species recoded (Steele *et al.*, 1994). One species of moss has been identified for Grunehogna (Ryan *et al.*, 1989), and lichen recoded on Flårjuven and Slettfjell (*pers. obs.*), as well as Valterkulten (Marshall *et al.*, 1995). However, these colonies are small and not as widely distributed, nor as varied, as those found on Robertskollen (Steele *et al.*, 1994). Bacteria, microalgae, fungi, rotifers and ciliates have been recorded in Vesleskarvet sediment samples, as has one species of mite and three species of tardigrades and nematodes (Steele *et al.*, 1994). One species of tardigrade (*Hypsibius antarcticus*) and two species of rotifer *(Philodina gregaria* and *Adineta grandis*) are described for the brine pond on Valterkulten (Marshall *et al.*, 1995). Mites (*Maudheimia wilsonia, Eupodes angari, Nanorchestes antarcticus*) are common, found on several nunataks in the Ahlmannryggen (Steele *et al.*, 1994), including Robertskollen (Ryan *et al.*, 1989), with the oribatid *Maudheimia wilsonia* found in the Jutulsessen (Lee *et al.*, 2013), and on nunataks near SANAE IV (Ryan *et al.*, 1989).

While animals are present in DML, their impacts are minimal. A bird colony of Antarctic petrels (*Thalassoica antarctica*) and south polar skuas (*Catharacta maccormicki*) exists at Tor in the Jutulsessen (CDML), with some evidence of nesting by snow petrels (*Pagodroma nivea*) and south polar skuas on the lower slopes Nonshøgda, Grjotøyra, Vassdalen, Jutuldalen and Brugdedalen (*pers. obs.*). The only bird-nesting colony near logger sites in WDML is located on the southern nunatak of the Robertskollen nunataks. Limited snow petrel and Wilson's storm petrel (*Oceanites oceanicus*) nests have also been recorded here, with Antarctic petrels also observed (Ryan *et al.*, 1989). However, since the logging site is located further north from this colony, the impact of birds on diurnal frost environments is negligible and it is unlikely these animals have any significant impact on the local frost environment. Human impact, although minimal, is more significant. A vehicle shed was erected near the original PACE Scientific XR5 (XR5) data logger at Troll Station in summer of 2011/12. A comparison of temperatures taken before and after this date from this logging station shows that ground temperature regimes are significantly warmer following shed construction. Similarly, the South African overwintering station of SANAE IV is located on the Southern Buttress of the Vesleskarvet nunataks, with the Northern Buttress the site of the logging station. Unfortunately, no data exist from before the time the base was built. As such, no quantitative assessment of impacts of the base on the Vesleskarvet ground frost environment can be made. However, due to the distance of the base to the logging station it is unlikely that the impacts are great.

### 3.3.1 Active and relict periglacial landforms and - features

Various types of glacial deposits are found in the Jutulsessen, with most slopes covered by loose sediment that is characterised by unconsolidated and unstratified glacial deposits (Shrivastava *et al.*, 2014). A residual ice field from a former glacier cirque is located on the southeastern portion of Grjotlia (Jutulsessen) (Dallmann *et al.*, 1990), extending over the rock glacier of Grjotøyra (Rudolph, 2015). A large cirque, characterised by blue-ice deposits on its lower part, is found by Sætet toward the east of Grjotlia (Dallmann *et al.*, 1990). Other examples of minor cirques, some of them still active, are also found in this area (Dallmann *et al.*, 1990). Rock glaciers are common for the Jutulsessen, specifically Brugdedalen, Grjotlia/Grjotøyra, Jutuldalen and, Vassdalen (Rudolph, 2015). Investigations on Caesium-

137 for Grjotlia/Grjotøyra and Vassdalen show reworking of surface material on the middle and lower extent of these rock glaciers (Rudolph, 2015), suggesting an active environment were frost cycles are concerned. Some evidence of ice lensing exists for the Jutulsessen, although pore ice is more common, as evidenced by ice-cemented permafrost (*pers. obs.*). As previously mentioned, the sediment of the Jutulsessen, characterised by sand-sized particles, is also not suited for ice segregation. Blockfields have been described for the flat-topped ridges of the Jutulsessen, including the ridge above Jutulhogget and their development has been ascribed to deep weathering processes (Dallmann *et al.*, 1990). An autochthonous blockfields is located on the Northern Buttress of the Vesleskarvet nunataks (Hansen *et al.*, 2013; Hansen, 2014). These blockfields exhibit no signs of glacial striations, suggesting cold-based glaciation for the area or an argument for high nunataks not having been glaciated during the LGM (Rea *et al.*, 1996; Whalley *et al.*, 2004; Kleman and Glasser, 2007; Hansen *et al.*, 2013; Hansen, 2014). Further blockfields occur on Flårjuven, Grunehogna, Robertskollen, Schumacherfjellet, Slettfjell, and Valterkulten (*pers. obs.*). An autochthonous block deposit has been described for Basen (Boelhouwers, 2004), and it is assumed that more blockfields are found in this area where nunataks are in evidence. However, data is scarce for the region and further nunataks have yet to be visited.

Pingos were once in evidence on the slopes of Nonshøgda in the Jutulsessen (Dallmann *et al.*, 1990), but have since disappeared (*pers. obs.*). Similar features near the toe of the Vassdalen rock glacier have been described (Hansen *et al.*, 2016a), yet require further study. Thermal contraction polygons (sand wedge polygons) are found in abundance on the Quaternary cover (Verma *et al.*, 2014) and glacial sediments (Shrivastava *et al.*, 2014) of the Jutulsessen. A large 192 Ha field of these landforms, of the non-sorted variety, is found at Mimelia, north of Troll Station (Hansen *et al.*, 2014). Further polygons have been observed on the toes of rock glaciers at Brugdedalen, Grjotlia, and Vassdalen (Rudolph, 2015), as well as on the gentle slopes of talus and lateral moraine material of Nonshøgda (Hansen *et al.*, 2014), directly west of Troll Station. Cyclical freezing of the soil and the flexing / contraction of permafrost following thermal changes yield cracks and subsequent polygonal formations (van Everdingen, 1998; Goudie, 2004a; Lee *et al.*, 2013). Ice-sorted polygons have been described for Valterkulten (Marshall *et al.*, 1995), and ice-wedge-polygons have been noted for Grunehogna (Meiklejohn, 2015; *pers. comm.*). The Valterkulten nunatak is characterised by a biologically-rich meltwater brine pond found in the base of a deep rocky depression (*pers. obs.*). This pond is generally warmer and remains unfrozen for longer than similar water bodies found in the area (Marshall *et al.*, 1995). This is ascribed due to a local site-specific effect where the surrounding rock radiates heat more than ice or snow would, creating a warmer micro-climate in the Valterkulten bowl (*pers. obs.*). The waterbody is thought to freeze completely during winter (Marshall *et al.*, 1995) and is known to thaw and evaporate completely during summer (*pers. obs.*). $Ca^{2+}$ and $Cl^{-}$ ion concentrations provide evidence of cryogenic meromixis (Marshall *et al.*, 1995). An active pronival rampart is described for Grunehogna (Hedding *et al.*, 2010). Active sorted circles, based on Caesium-137 analyses, are described for Robertskollen, Slettfjell and Flårjuven with Robertskollen showing greatest activity and Flårjuven the least (Kotzé, 2016). Needle ice has been observed on the Vesleskarvet nunataks by SANAE IV. However, these landforms are not permanent and are likely more generally distributed than as indicated in Table 4 (pg. 70). A summary of periglacial landforms and -features of the study area shown in Figure 14 (pg. 69) and Table 4 (pg. 70). Literature for this region is scarce and most of the landforms have been observed in the field. However, an attempt was made to draw as much as possible from the available literature.

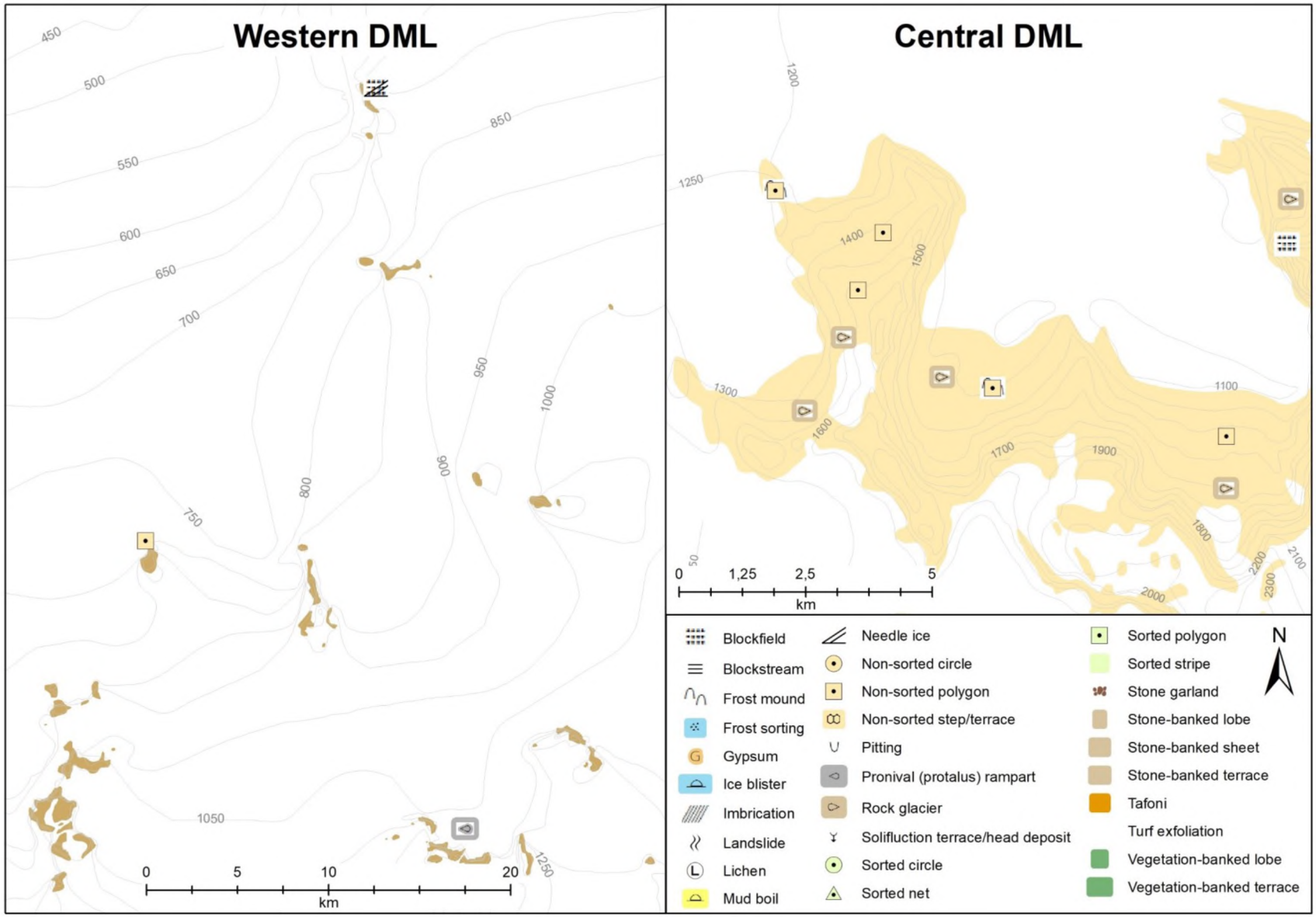


**Figure 14: Landforms observed for western and central Dronning Maud Land (DML), as per literature review.**

**Table 4: A summary of periglacial landforms- and -features found within western Dronning Maud Land (WDML) and the Jutulsessen of central Dronning Maud Land (CDML). The active or relict state of the landform is indicated when known. * Includes pingo, palsa, thúfur.**

| Feature | Location | Altitude | Active/Relict | Source |
|---|---|---|---|---|
| Blockfield | Basen | 443 | Active | (Boelhouwers, 2004) |
| | Jutulsessen (flat-topped ridges) | 1800-2000 | Unknown | (Dallmann *et al.*, 1990) |
| | Northern Buttress, Vesleskarvet | 856 | Active | (Hansen *et al.*, 2013; Hansen, 2014) |
| Blockstream | *None observed* | | | |
| Frost mound * | Nonshøgda | 1331 | No longer in evidence | (Dallmann *et al.*, 1990) |
| | Vassdalen | 1184 | Unknown | (Hansen *et al.*, 2016a) |
| Landslide | *None observed* | | | |
| Mud boil | *None observed* | | | |
| Needle ice | Vesleskarvet nunataks | 856 | Active | (Hedding *et al.*, 2010) |
| Non-sorted circle | *None observed* | | | |
| Non-sorted polygon | Brugdedalen | 1325 | Unknown | (Rudolph, 2015) |
| | Grjotlia | 1602 | Unknown | (Rudolph, 2015) |
| | Mimelia | 1130-1350 | Active | Dallmann *et al.*, 1990; Lee *et al.*, 2013; Hansen *et al.*, 2014) |
| | Nonshøgda | 1331 | Unknown | (Dallmann *et al.*, 1990) |
| | Valterkulten | 1006 | Unknown | (Marshall *et al.*, 1995) |
| | Vassdalen | 1163 | Unknown | (Rudolph, 2015) |
| Non-sorted step/terrace | *None observed* | | | |
| Pronival (protalus) rampart | Grunehogna | 1390 | Active | (Hedding *et al.*, 2010) |
| Rock glacier | Brugdedalen | 1500 | Relict | (Rudolph, 2015) |
| | Grjotlia | 1530 | Relict | (Rudolph, 2015) |

| Feature | Location | Altitude | Active/Relict | Source |
|---|---|---|---|---|
| | Grjotøyra | 1475 | Relict | (Dallmann *et al.*, 1990; Rudolph, 2015) |
| | Jutuldalen | 1340 | Active | (Rudolph, 2015) |
| | Vassdalen | 1260 | Relict | (Rudolph, 2015) |
| Solifluction terrace/head deposit/frost creep | *None observed* | | | |
| Sorted circle | Flårjuven | 1290 | Active | (Kotzé, 2016) |
| | Robertskollen | 463 | Active | (Kotzé, 2016) |
| | Slettfjell | 1507 | Active | (Kotzé, 2016) |
| Sorted polygon | *None observed* | | | |
| Sorted stripe | *None observed* | | | |
| Stone garland | *None observed* | | | |
| Stone-banked lobe | *None observed* | | | |
| Turf exfoliation | *None observed* | | | |

# CHAPTER 4: Data Requirements, Collection and Methods

This chapter details data requirements, data collection methods, as well as analyses methods used throughout the study. The chapter is divided into several subsections. Each of the study's five key objectives introduced in 1.3 Objectives (pg. 10), are discussed in detail (4.1.1 Objective 1-4.1.5 Objective 5 from pg. 72-78), as are methods and sources used in the digital data collection process (4.2 Digital Data Collection and External Data Sources, pg. 78-79), particulars of fieldwork visits (4.3 Fieldwork, pg. 79-95), laboratory analyses (4.4 Laboratory Analyses, pg. 95), as well as statistical analyses (4.5 Statistical Analyses, pg. 99), and geographical and mathematical analyses (4.6 Geographical Statistics and Modelling, pg. 108). Furthermore, logging stations and their geographical setting are described for the Eastern Cape (pg. 83-88), Marion Island (pg. 88-90), and Dronning Maud Land (DML) of Antarctica (pg. 90-91). Data are described in Table 17 of APPENDIX G.

## 4.1 Objectives

An investigation of frost environments requires data on soil temperature and moisture. Additional climate data, such as relative humidity, precipitation, air temperature, wind speed, and wind direction, are needed to draw comparisons to ground temperature data, as well as identifying the number of cloud-free days and their correlation to diurnal frost cycles. For this study air temperature reflects ambient air temperature. Data on particle movement along slopes were collected using painted markers and strings. Snow cover presence was extracted from climatic data, as well as during field visits. Human and animal presence and impact, as well as vegetation cover (if present) were identified for each study site near each logger during field visits, as well as consulting the relevant literature. Furthermore, a comprehensive survey of needle ice, ice lensing, and other evidence of frost heave, frost sorting (patterned ground) and frost (thermal contraction) cracking was conducted near each data logger for each study site. The prevalence of contraction cracks occurring in regions underlain by permafrost (Thorn, 1992), makes these landforms most likely to occur in the Antarctic. Nevertheless, seasonal contraction may occur (Thorn, 1992), and the possibility exists of observing these landforms on both Marion Island as well as the Eastern Cape High Drakensberg. Thermal contraction cracks have been noted on Marion Island (Meiklejohn, 2016; *pers. comm.*). Furthermore, the comparison of large-scale features, focusing on geomorphic characteristics provides valuable information in understanding the distribution, role and characteristics of frost environments. Similarly, soil found at each study site impacts frost cycles and as such, soil samples were collected at each data-logging site. Fieldwork is supplemented by subsequent laboratory analyses, statistical, geostatistical and mathematical analyses.

### 4.1.1 Objective 1

*To investigate the dynamics of frost cycles in the short-term (diurnal), as well as longer term (seasonal and annual) using a variety of methods.*

Water and temperature are crucial to the periglacial process (Goudie, 2004b). Changes in temperature affect the water-ice balance found within the ground. Changes may lead to heave due to the volumetric

expansion of water when freezing, while accompanied by the release of latent heat. Furthermore, subsidence of the ground associated with thawing interstitial ice may occur. Objective 1 focuses on the investigation of soil temperature and moisture dynamics in the short-term (diurnal), as well as longer term (seasonal and annual). This is achieved through ground thermal and moisture monitoring using a variety of sensors, determining moisture contents using laboratory methods, and determining heave/displacement of particles within the soil column using sunken lengths of strings and painted markers. Movement of painted markers within the ground is determined on an annual basis for different depths within the ground. Similarly, lateral movement of particles within the ground is determined using sunken lengths of string and measuring their subsequent displacement. Methods to determine frost heaving and thrusting is detailed in discussions in 4.3.2 Particle displacement on pg. 91. The depth of freeze-thaw cycles within the soil, the number and duration of freeze-thaw cycles for specified time scales, hours the ground is frozen (if applicable), as well as the importance of soil moisture regimes for each study site is determined. Further thermal indices investigated include the summer thawing (TI) and winter freezing (FI) indices. These are described in detail in subsections 4.5.2 Statistical methods (pg. 102) and 4.5.2.1 Freeze-thaw cycle indices and statistical calculations (pg. 104).

### 4.1.2 Objective 2

*To evaluate soil temperature and moisture data regarding snow cover, climate data and other environmental and locational factors to determine trends, forcings and/or correlations.*

Objective 2 aims to statistically compare soil temperature and moisture data to snow and cloud cover, climate data and other environmental factors to determine trends, forcings and/or correlations (Figure 15). To achieve this information on sediment bulk density and porosity, gravimetric and volumetric water content, total organic carbon, and particle size analysis was done (refer to the relevant sections under 4.4 Laboratory Analyses, pg. 95 onwards). Several statistical methods were employed to determine significant trends and/or correlations between the various parameters. Furthermore, Principal Component Analysis (PCA) was used to identify the main contributing parameters to frost cycle dynamics (4.5.2 Statistical methods, pg. 102 onwards).

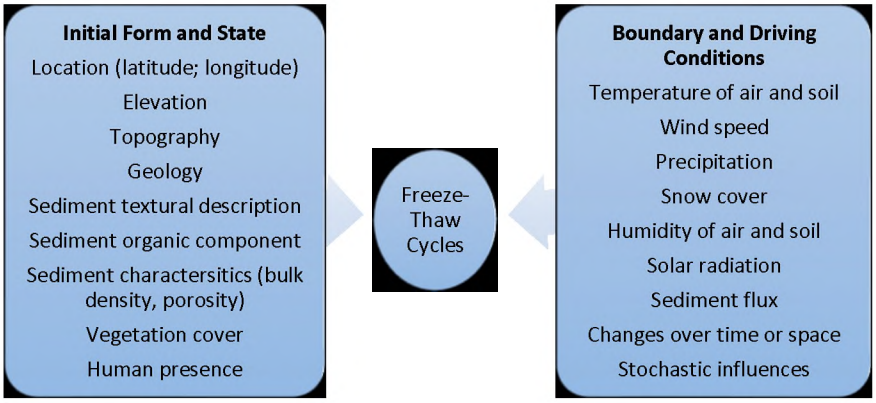


**Figure 15: Conceptual graphic depicting parameters that influence the frost environment.**

Frost effected deflation in periglacial environments, described by Troll (1948) as gelideflation and one of the six periglacial process groups responsible for cold-climate denudation, is the process whereby a surface becomes deflated in periglacial environments following frost action (Seppälä, 2004). Frost heave, through processes such as ice lensing or needle ice, occurs orthogonal to the ground and causes the displacement of particles upward (following ice formation) and outward from the central point (Thorn, 1992). As such, frost heave has the potential to displace a significant amount of sediment. Heave, following the freezing of water, occurs through capillary flow of water to the cooling plane, or due to the volumetric expansion of water upon freezing (Barsch, 1993). As such, moisture content of the soil/sediment column is a crucial component to freeze-thaw cycles. Needle ice, which makes the surface more susceptible to deflation (Clark and Hedges, 1992), also contributes to frost affected deflation (Seppälä, 2004). It yields material for subsequent transport elsewhere, generating a friable surface layer of sediment (Boelhouwers *et al.*, 2000). This is due to material losing bulk density and cohesion following freeze-thaw cycles (Williams and Smith, 1991).

Bulk density is an indicator of soil compaction and represents the dry weight of sediment compared to a known volume (McKenzie *et al.*, 2002), representing the volume of sediment particles, as well as pores amongst particles (Brady and Weil, 2016). Higher densities indicate low sediment porosity and sediment compaction, affecting and restricting the movement of water through sediment (McKenzie *et al.*, 2002), which in turn affects freeze-thaw cycles. Sandy soils often have higher densities due to larger and fewer pores present when compared to silty and clayey soils. Bulk densities exceeding 1.6 $g.cm^{-3}$ also restrict the growth of roots, and bulk densities of less than 1.5$g.cm^{-3}$ are considered preferable in terms of the movement of air and water through the soil/sediment column (McKenzie *et al.*, 2002). Another consideration, when determining bulk density, is the organic component of the soil. Organic matter in soil interacts with clay minerals to bind particles together and improves the water-holding capacity of soils (Schumacher, 2002), having implications on freeze-thaw cycles. As such, humic soils have low bulk density values. Bulk densities also increase with depth due to increased compaction occurring with increasing depth in the ground. In comparison, porosity values tend to decrease with depth (Brady and Weil, 2016). Increased bulk densities may also lead to higher runoff (Natural Heritage Trust (Australia), 2001) as well as influencing the amount of moisture that is available for freeze-thaw cycles. The lack of organic material of sandy soils yields high bulk density values, due to particles lying near each other. In comparison, particles of fine-textured soils do not generally lie close to each other and exhibit low densities (Brady and Weil, 2016). Freeze-thaw cycles and associated heave will yield lower bulk density values due to encouraged granulation and aeration. Due to coarse sediment fragments having densities ranging from 2.2-3.0 $g.cm^{-3}$ these samples will overestimate bulk density values. The typical bulk density of clayey soil is between 1.1-1.3 g $g.cm^{-3}$, that of silt loam soil ± 1.33 $g.cm^{-3}$, and that of sandy soil between 1.5-1.7 $g.cm^{-3}$. Mineral soils have bulk densities of ± 1.25 $g.cm^{-3}$ (1.1-1.5 $g.cm^{-3}$) (Briggs, 1977a), and soils high in organic matter typically have bulk density values in the region of 0.5 $g.cm^{-3}$. Average bulk density values for sediment classes are provided in Table 9 of APPENDIX E. It is worth noting that standard bulk densities are less suited to sediments where the gravel content of the sediment volume exceeds 10% (McKenzie *et al.*, 2002).

Porosity values reflect the maximum possible volumetric water content of a sample. The macro pores

of sandy soils encourage water percolation and air movement, while the micro pores of fine-textured soils restrict water percolation and air movement. Soils with high pore volume (loose and porous) will have low weights per unit volume, while more compact soils will have high weights, *i.e.* high bulk densities generally translate into low porosity values and *vice versa* (Brady and Weil, 2016). Medium-textured soils and soils with high organic content will have high pore volumes, with sandy soils having 35-50% pore space and fine-textured soils a 40-60% pore space (Brady and Weil, 2016). Expected porosity values per sediment classes are provided in Table 10 of APPENDIX E. Permeability, in comparison, reflects how easily water is transmitted through the sediment/soil column. Here clay samples reflect low permeability values, with sandy samples exhibiting high permeability.

Specific yield ($S_y$) indicates the volume of water that drains from a saturated rock or sediment by gravity. Average $S_y$ values for particle sizes are given in Table 11 of APPENDIX E. While porosity affects how much water is retained within a sample, permeability affects how easily the sample loses water content. Both these parameters, as well as specific yield, affect the thermodynamical properties of the sample and, in turn, freeze-thaw cycles. Factors influencing the occurrence of potential freeze-thaw events and freeze-thaw cycles are vegetation, snow and cloud cover (or the lack thereof), textural characteristics of soil and sediment, moisture characterisation of the soil/sediment column, as well as the geographical location in terms of latitude, longitude and altitude of a site (Table 5).

**Table 5: Evaluation of various parameters on potential freeze-thaw events (PFTE) and freeze-thaw cycles (FTC).**

| Parameter | Evaluator | Additional Comment | Effect on FTC |
|---|---|---|---|
| Vegetation cover | Present | Insulating effect: slower rates of heating and cooling | Negative |
| Snow cover | Present | Insulating effect: Slower rates of heating and cooling | Negative<br>*Depth of cycles increased at mid-latitudes* |
| Cloud cover | Present | Insulating effect: Slower rates of heating and cooling | Negative |
| Soil/sediment porosity | High | Enhanced water holding capacity | Positive |
| Soil/sediment permeability | High | High water transfer capability | Negative |
| Soil/sediment bulk density | High | Affecting porosity and compaction | Negative |
| Organic component | Medium | Improvement on porosity and cohesion | Positive |
| Mean annual air temperature | High | Main forcing agent; required to overcome specific heat of soil/sediment | Negative |
| Altitude | High | Increase in altitude associated with a reduction in MAAT | Positive |
| Latitude | High | Increase in latitude associated with a reduction in MAAT | Positive |

### 4.1.3 Objective 3

*To compile a comprehensive register of landforms resultant of diurnal frost environments for each study site near each data logger.*

Objective 3 requires the use of an extensive literature review to compile a register of periglacial landforms found at each study site, accompanied by observations made during field visits. The type and classification of landforms for each site facilitate an investigation into the zonality/azonality of landforms, the aim of Objective 4 (see below). Specific processes yield specific landforms, and landforms associated with periglacial environments are included in this database. Periglacial landforms can be divided into those derived from snow processes, such as pronival ramparts; those derived from permafrost dynamics, such as thermal contraction polygons; and those derived from periglacial sorting phenomena, such as sorted circles and stripes (King, 1966). However, the study focuses on diurnal freeze-thaw cycles. As such, smaller landforms derived of low-intensity and high-frequency cycles, such as needle ice, circles and evidence of frost heave and frost thrust, are predominantly considered. While a focus on morphospaces is not made, the suitability of applying the concept of morphospaces to landform development is acknowledged (Inkpen and Hall, 2016), as such an approach allows for an evaluation of azonality. Contents of the landform database derived from an extensive literature review are shown in Table 2 for the Eastern Cape (pg. 37), Table 3 for Marion Island (pg. 56), and Table 4 for central and western Dronning Maud Land (DML) (pg. 70). Landforms recorded following field visits are shown in Table 21 (pg. 121) for the Eastern Cape, Table 51 (pg. 171) for Marion Island, and Table 80 (pg. 208) for central and western DML. The finalised and integrated database is contained in Table 22 of APPENDIX I.

### 4.1.4 Objective 4

*To draw a comparison between the three sites with respect to zonality/azonality and to develop a model for diurnal cycles for each site.*

If frost processes are indeed present for all study locations, self-regulation implies that specific landforms will be found in the areas (Phillips, 1999). If that is the case, azonality of frost processes compared to climatic zones is suggested to exist and Objective 4 aims to investigate the validity of that question. The evaluation of temperature and moisture regimes per site within the context of each specific location (local geology, lithology, vegetation cover, human and fauna impacts) allows for an evaluation of drivers and processes inherent to the diurnal frost environment. Evaluating the various parameters and their respective forcing on freeze-thaw cycles, an argument for mutual adjustment (Phillips, 1999), in terms of self-organisation and the interaction of non-linear deterministic processes (Church, 2010), can be made. Once each site has been analysed considering the parameters mentioned above, sites are compared to each other to identify the overriding drivers. Furthermore, such comparisons allow for an identification of commonalities, such as specific landforms and/or processes. The strength of using all available significant parameters, as those determined using PCA, when predicting the frost environment extent, the non-linear nature of processes within models is considered (Beven and Freer, 2001; Beven, 2006). Optimum model approaches have intrinsic non-stationary bias, variance, and skewness (Beven and Freer, 2001; Beven, 2006). While the limitations of an optimum model are considered, and the knowledge that even moderate levels of model complexity yield

equifinality (Beven and Freer, 2001), a maximum likelihood model, nevertheless, will assist in predicting the distribution of the frost environment for the investigated study locations across the study area. While an optimal model might be too simple and exclude crucial site-specific parameters, an equifinality model might be too complex and introduce large margins of error. Furthermore, over-parameterisation of models is a concern when using equifinality models (Beven, 1996). Non-linearity and heterogeneity issues may arise when *in situ* measurements are compared to model predictions (Beven, 2006). A further consideration is observation bias, which can be multiplied by model bias (Beven, 2006). Furthermore, a fully reductionist approach to modelling frost environments across the various geographical settings is not yet possible with current methodologies and data available. Nevertheless, to account for shortcomings of both approaches, the project utilises a variety of parameters. These parameters are statistically comparatively evaluated to reduce assumption bias and only then modelled, whose outputs are subsequently compared to *in situ* measurements. While this study does not attempt to employ a true equifinality model, due to its high level of complexity, such a general approach is followed. The strength of this approach lies in using known influences on freeze-thaw cycles, as determined by current literature, and combining and comparing these to a wealth of additional data collected during the study. The general optimum model is expanded to a stochastic identification model, with reference to the equifinality thesis (Beven, 2006). Therefore, Objective 4 is largely achieved using statistical and geostatistical methods, as described under 4.5 Statistical Analyses (pg. 99) and 4.6 Geographical Statistics and Modelling (pg. 108). While an attempt is made to provide a robust quantitative model, an element of qualitative assessment remains, and the model reflects a partially specific representation of the frost environment for the investigated locations. Such a model is provided by Equation 15 (pg. 108).

### 4.1.5 Objective 5

*To map all findings and make the content of the landform database available using interactive and easily accessible resources.*

The aim of this study is not only to investigate frost cycles within the broader framework of climatic geomorphology, but to also make the results and information collected during this study available to fellow researchers and the public at large. Communicating academic research and output has become increasingly relevant, particularly when applied to publicly funded research (ICSU, 2010; SciDev.Net, 2010). Communicating science and scientific concepts to those not involved in scientific fields is a crucial component of any research, not only because the effective communication of science has many benefits to the scientists involved, such as opening doors for collaboration, but also because it is the responsibility of scientists to make their discoveries accessible to the public. This has recently been highlighted as Objective 4 (communicating Antarctic research data) and Objective 5 (facilitating access to Antarctic research data) by the Scientific Committee on Antarctic Research (SCAR) Strategic Plan: 2017-2022 (Scientific Committee on Antarctic Research, 2017). Furthermore, communicating academic discoveries ensures transparency, accountability and accuracy of findings and methods employed (ICSU, 2010). This communication requires a multipronged approach, comprising not only properly managed data accessible in databases and associated metadata, but also publications (both academic and general interest), and interactive digital resources. To achieve this data collected during the study are made available using Environmental Systems Research Institute (ESRI) online resources, specifically

their open-access and free online maps using ArcGIS Online. In addition, data outputs and general information on sites and results are available through a project website, Facebook page, and Twitter account. The database and various online resources contribute to the International Permafrost Association's (IPA) initiative, the Global Terrestrial Network for Permafrost (GTN-P), as well as to the objectives of Antarctic Permafrost, Periglacial Environments and Soils (ANTPAS) (a working group of SCAR). Details to site specific information, data specifics, and logger characteristics applicable to this study are available in Table 7-8, Table 17, and 18 of APPENDIX D, APPENDIX G, and APPENDIX H respectively. Details on the ArcGIS Online map URLs (Table 19), website URL (Table 20), Facebook page URL (Table 20), and Twitter account handle (Table 20) are also available in APPENDIX I. A summary of the landform database (4.1.3 Objective 3, pg. 76) is provided in Table 22 (APPENDIX I).

## 4.2 Digital Data Collection and External Data Sources

Climate data, including precipitation, relative humidity, pressure, air temperature, wind speed, and wind direction were obtained from the South African Weather Service (SAWS). Data are recorded at hourly intervals and obtained from weather stations located at the South African National Antarctic Expedition IV (SANAE IV) on Vesleskarvet in the Antarctic and the research base at Marion Island, as well as the automatic weather stations of Fort Beaufort and Aliwal North in the Eastern Cape of mainland South Africa. Weather station parameters are listed in Table 6. Relative humidity is measured as a percentage (%), air temperature in degrees Celsius ( °C), and pressure in millibar (mb), with one mb (1 mb) equal to one hPa (hecto Pascal). Wind direction and wind speed are observed as degrees clockwise from north and in meters per second ($m.s^{-1}$) respectively. Precipitation is measured in millimetres (mm). Figure 16 gives a description of wind direction and associated bearing, as designated by SAWS.

**Table 6: Weather station description. Number reflects the station number; Lat indicates latitude; Long indicates Longitude and Alt the elevation above sea level in meters.**

| Station | Number | Lat | Long | Alt |
|---|---|---|---|---|
| Aliwal North (Plaatkop) | 0175678A0 | 30.84°S | 26.88°E | 1347 |
| Fort Beaufort | 0078227A3 | 32.79°S | 26.63°E | 455 |
| Marion Island | 00006531 | 46.88°S | 37.87°E | 24 |
| Vesleskarvet | 00000024 | 71.68°S | 2.85°W | 849 |

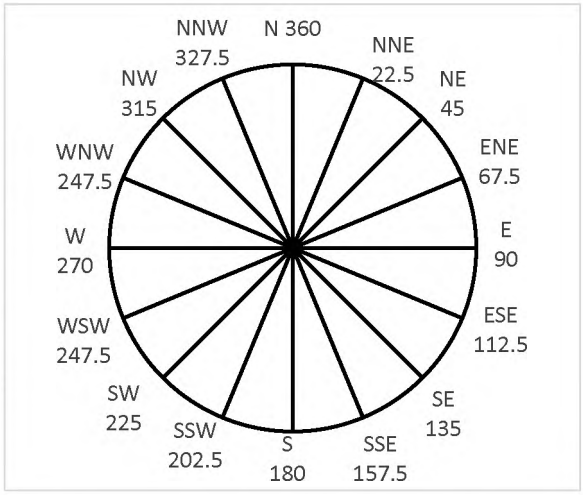


**Figure 16: Orientation and bearing for wind direction, as classified by and adapted from the South African Weather Service (SAWS).**

Moderate Resolution Imaging Spectroradiometer (MODIS) imagery are used to identify overcast days,

as well as surface albedo (National Aeronautics Space Agency (Nasa), 2016a, 2016b). Geology information is provided by the South African Council of Geoscience (CGS), with vegetation data extracted from Mucina and Rutherford (2006). The Scientific Committee on Antarctic Research (SCAR) Antarctic Digital Database (ADD) (British Antarctic Survey, 2016) and Quantarctica (Norwegian Polar Institute, 2016) are used for vector and raster data for the Antarctic. Similarly, National Geo-Information (NGI) provides these data for South African territory. Table 7 below provides an overview of data requirements and sources.

**Table 7: An overview of data sources and accompanying data requirements. DML: Dronning Maud Land.**

| Data Source | Data Type |
|---|---|
| ADD | Topographical and boundary data on western DML |
| CGS | South African geology |
| MODIS | Cloud cover, surface albedo |
| Mucina and Rutherford | South African vegetation |
| NGI | South African topographical and boundary data |
| Quantarctica | Ice extent and movement in DML |
| SAWS | Precipitation (mm), relative humidity (%), pressure (mb), air temperature ( °C), wind speed ($m.s^{-1}$), wind direction (°) |

## 4.3 Fieldwork

Fieldwork for western Dronning Maud Land (WDML) and central Dronning Maud Land (CDML) was conducted during the annual summer voyages to the region. These occurred during the Austral summer of 2012/13, 2013/14 and 2014/15, constituting three field visits. Fieldwork for Marion Island took place during the annual relief voyages to the Island. These took place during April/May 2014 and 2015, constituting two field visits. Fieldwork for the Eastern Cape Drakensberg was done every few months throughout the year for the duration of the study. Seasons referred to apply to Austral seasons, *i.e.* winter (June-August), spring (September-November), summer (December-February), and autumn (March-May).

At each study site loggers were set up to enable ambient air and ground temperature and moisture recording. Soil samples were collected to facilitate bulk density, porosity, fine earth fraction (particles smaller than 2 mm in size), analysis, as well as gravimetric moisture determination. Furthermore, lengths of strings were sunk into the ground for sites located on Marion Island and on Ben MacDhui in the Eastern Cape. Painted markers were buried at various sites for the Eastern Cape and on Marion Island to determine sediment and clast displacement within the ground, as well as displacement down a slope. Finally, within the vicinity of each data logger at each study site a record was made of the presence of vegetation, human and animal influence, as well as landforms/-features characteristic of frost environments. Where possible, data logging and sampling points were selected at each location

to remove spatial bias and to facilitate an investigation into equifinality modelling, as discussed in CHAPTER 1: Introduction and CHAPTER 2: Background and Context (pg. 1 and 12 onwards). Optimum models reflect stationary parameters, or *point in space* predictions (Beven, 2006). Sampling at various locations across study sites provides a greater spread of data, facilitating equifinality modelling (Beven, 2006). Temperature and moisture measurements were predominantly undertaken at pre-existing sites and the selection of these sites was, therefore, not random. Where new sites were determined a systematic selection method was employed. This applies to the altitudinal transects deployed on Ben MacDhui and the Elandsberg in the Eastern Cape, as well as on Marion Island. Figure 17 provides a summary of the various activities carried out at each study site.

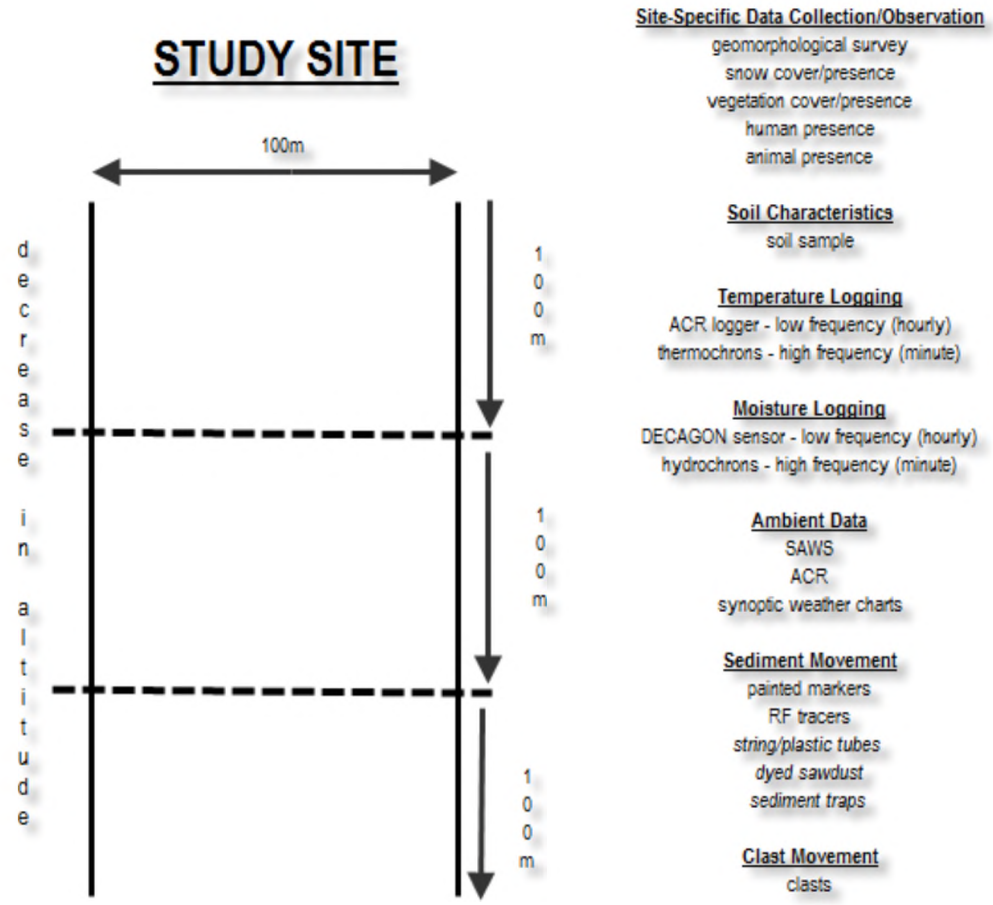


**Figure 17: Schematic of the layout of each study site, with activities employed in each transect block. Activities carried out on Marion Island and the Drakensberg only are italicised.**

### 4.3.1 Ground temperature and moisture data

Temperature and moisture data at the three sites were collected using PACE XR5 (XR5) systems with ACR data loggers used as back-ups in case of XR5 systems' failure. Furthermore, thermochron iButtons were deployed to supplement data collected using XR5 and ACR systems. Logger specifics are provided in Table 18 of APPENDIX H. The set-up for XR5 system loggers is shown in Figure 18 (pg. 82). Loggers at all locations had sensors buried at similar depths to ensure comparison of data across the locations. Loggers for Marion Island were set to record hourly soil temperatures at the near surface (1 cm) (NST), 2 cm (GST), 5 cm ($T_5$), 10 cm ($T_{10}$), 15 cm ($T_{15}$) and 20 cm ($T_{20}$) depths within the ground. Loggers for the

Eastern Cape recorded hourly soil temperatures at the near surface (1 cm) (NST), 2 cm (GST), 5 cm ($T_5$), and 10 cm ($T_{10}$) depths within the ground. Sensors were not placed beyond 20 cm due to freeze-thaw cycles not generally known to occur beyond 10 cm for the Drakensberg (Boelhouwers and Meiklejohn, 2002) and 20 cm for Marion Island (Boelhouwers *et al.*, 2003). Thermistors of XR5 logger set-ups in Dronning Maud Land (DML) of Antarctica extend to depths of 60 cm in the ground (1 cm [NST], 15 cm [$T_{15}$], 30 cm[$T_{30}$], 45 cm[$T_{45}$], 60 cm[$T_{60}$]), as well as to 200 cm (1 cm [NST], 50 cm [$T_{50}$], 100 cm [$T_{100}$], 150 cm [$T_{150}$], 200 cm [$T_{200}$]) for the two Troll sites to adhere to international and Antarctic Permafrost, Periglacial Environments and Soils (ANTPAS) standards for permafrost monitoring. Sites in western Dronning Maud Land (WDML) do not reflect boreholes. Rather, sensors are placed directly into the ground. Even though ground surface temperatures (GST) apply to the upper few centimetres of the ground, for this study sensors buried at 1 cm record near surface temperatures (NST), those buried at 2 cm GST. A Decagon EC5 sensor measured soil moisture at a depth of 1 cm. The World Meteorological Organisation (WMO) specifies the true diurnal mean (or average) temperature to be the calculated from 24 (hourly) observation points (World Meteorological Organisation (WMO), 2011). If hourly observation points are not available the mean can be derived from any combination of observation points, if these depart as little as possible from the mean derived using hourly data. As such, XR5 and iButton loggers were set to record data at a maximum of 1-hourly intervals. Due to instrument memory limitations ACR loggers recorded data every 3 hours. iButton thermo- and hygrochrons from Fairbridge Technologies (Pty) were used to record high-frequency (minute) ground temperature and moisture data respectively. These self-contained data loggers are enclosed within a watertight stainless steel can (Hubbart *et al.*, 2005), and their small size, as well as relatively low cost and durability (Hubbart *et al.*, 2005; Johnson *et al.*, 2005), allow them to be placed in many environments and locations, as well as allowing for large sample sizes. Furthermore, being a wireless stand-alone logger (Johnson *et al.*, 2005), the ease of using these sensors in the field allows for spatial variable sampling (Ashcroft and Gollan, 2012), as sensors do not need to be fixed to permanent structures. Thermo- and hygrochrons were placed at a depth of 2 cm in the soil and securely fastened to a support, as described by Hansen (2014), to ensure that loggers were not heaed out of the ground following frost cycles. Figure 19 (pg. 82) provides an overview of this set-up.

Ambient air temperature was recorded as part of the XR5 logging set-up. Ambient temperature thermistors are located 100 cm above the ground and protected by a radiation shield to ensure measurements are not unduly influenced by the ground micro-climate (Vieira *et al.*, 2010). The combination of ambient temperature monitoring with Decagon EC5 moisture and XR5/ACR ground temperature sensors allows for simultaneous recording of ground-air moisture and temperature dynamics. One logger was installed in the Eastern Cape Drakensberg on the slopes of Ben MacDhui during the winter of 2014, with an additional XR5 logger installed in the Elandsberg towards the end of 2015 (Figure 3, pg. 28). On Marion Island two loggers were installed during the 2014 expedition to the Island, one on Tafelberg, with an additional logger installed at Katedraalkrans (Figure 5, pg. 40). A total of ten XR5/ACR logging locations were used for the Antarctic part of the study (Figure 13, pg. 63). Data of a total of 22 XR5 and/or ACR loggers were used for the completion of this study.

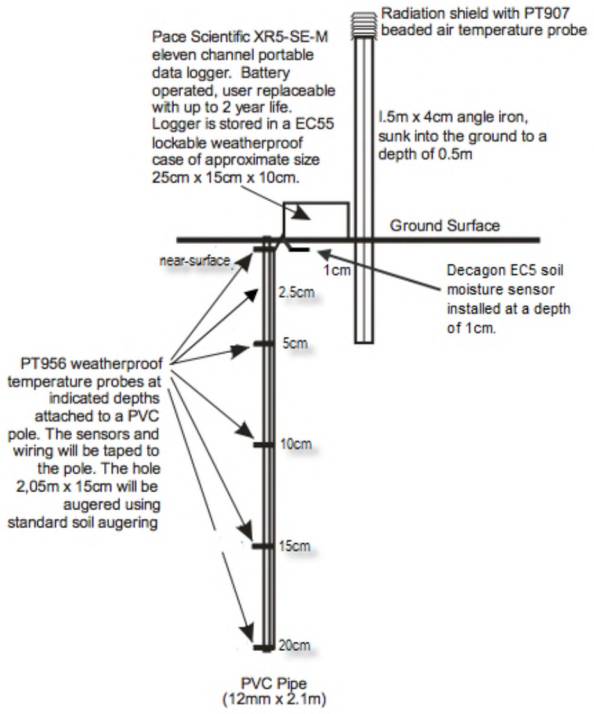


**Figure 18: XR5/ACR logger set-up. Sensor depths are indicated, as is the radiation shield. Adapted from Hansen (2014).**

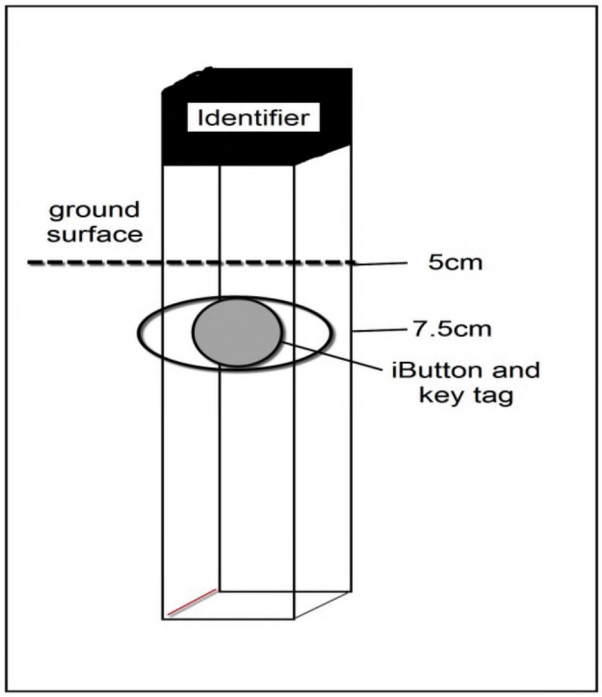


**Figure 19: iButton thermochron set-up. Thermochrons are fastened to a key tag and a support; ensuring loggers do not get heaved out of the ground (Hansen, 2014).**

The lack of soil at DML study sites makes the emplacement of thermo- and hygrochrons problematic. Nevertheless, data were collected during the summers of 2012/13 and 2014/15 for selected locations within DML. Thermo-and hygrochrons were installed for Marion Island during the 2014 expedition to the Island. Similarly, these high-frequency loggers were installed at the Elandsberg in 2013, and at Ben MacDhui during the 2014 winter season. iButtons, although affordable and small, have small storage capacities (Hubbart *et al.*, 2005). Due to this inherent limitation, multiple thermo- and hygrochrons were installed at each emplacement site (Johnson *et al.*, 2005). Loggers were programmed to a delayed start with end and beginning dates of separate loggers overlapping, to record annual data successfully. Thermo-and hygrochrons were also placed in the field near each XR5/ACR loggers, as well as along transects running downslope. When emplaced along a latitudinal gradient, thermochrons were placed at a decreasing altitude of ± 100 m along these transects. Before placing loggers in the field each type of logger (iButton/XR5/ACR/Decagon EC5) and associated sensors were calibrated using manufacturer's instructions. Please refer to Table 7 and Table 8 found in APPENDIX D for an overview of the various logging sites.

#### *4.3.1.1 Eastern Cape*

On Ben MacDhui one XR5 logger was placed at an altitude of 2 987 m a.s.l. This allows for the identification of the height threshold, above which frost cycles occur for the study area. Thermochron iButtons (Fairbridge technology) were placed at ± 100 m changes in elevation at 2 993 m a.s.l., 2 909 m a.s.l., 2 802 m a.s.l., 2 711 m a.s.l., and 2 604 m a.s.l. and given the identifier T1-T5 respectively (Figure 20). iButtons and the XR5 system were set to record at 10-minute intervals, buried on level ground and all sites located on southward-facing slopes (bearing: S) (Figure 3, pg. 28). This aspect is also characterised by expected *in situ* saprolite, due to ineffectiveness of slow mass wasting on southward facing slopes (Boelhouwers, 2003b).

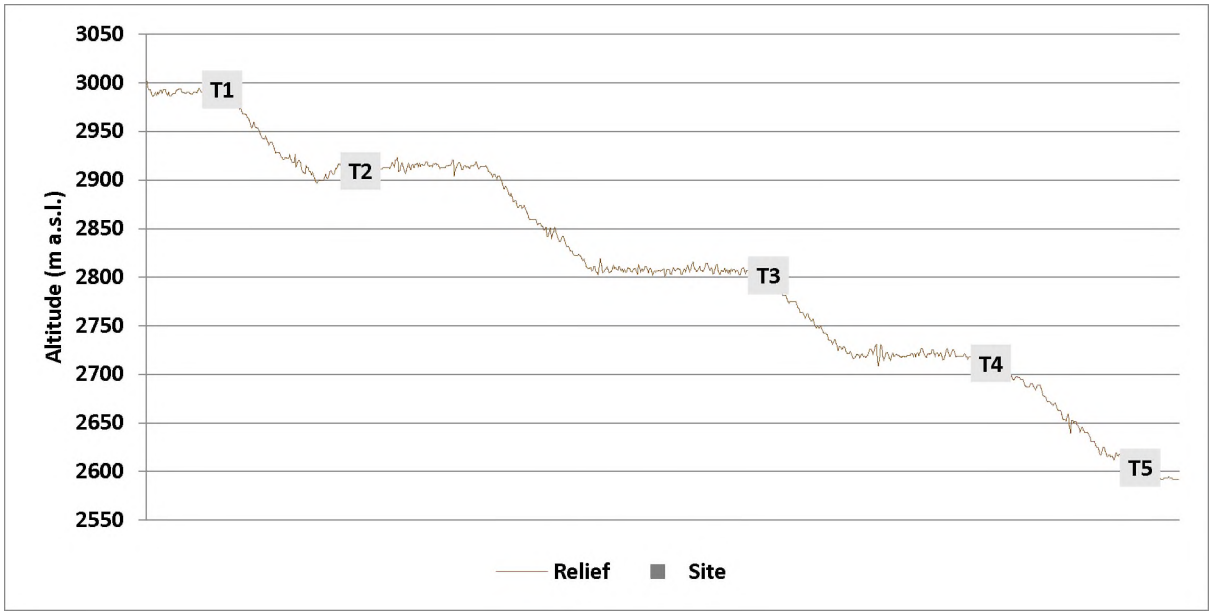


**Figure 20: Location of study sites for Ben MacDhui. Sites are shown along the transect taken in the field during site visits. NOTE: the horizontal axis represents distance along the field transect. Distance from T1 to T5: ~ 1.4 km.**

Lengths of string to measure slope displacement were set up at each site with three placements per site. In addition, two trenches were dug per site, except for the lowest site at 2 604 ma.s.l. At this site soil cover was too shallow to allow for the digging of trenches. More detailed information on the set up and placement of lengths of string and painted markers in trenches is described in 4.3.2 Particle displacement (pg. 91). Detailed information on the Ben MacDhui site parameters is shown in Table 7 and Table 8 in APPENDIX D. Figure 21 on pg. 84 shows the locations of the various instruments, once deployed in the field, for Ben MacDhui.

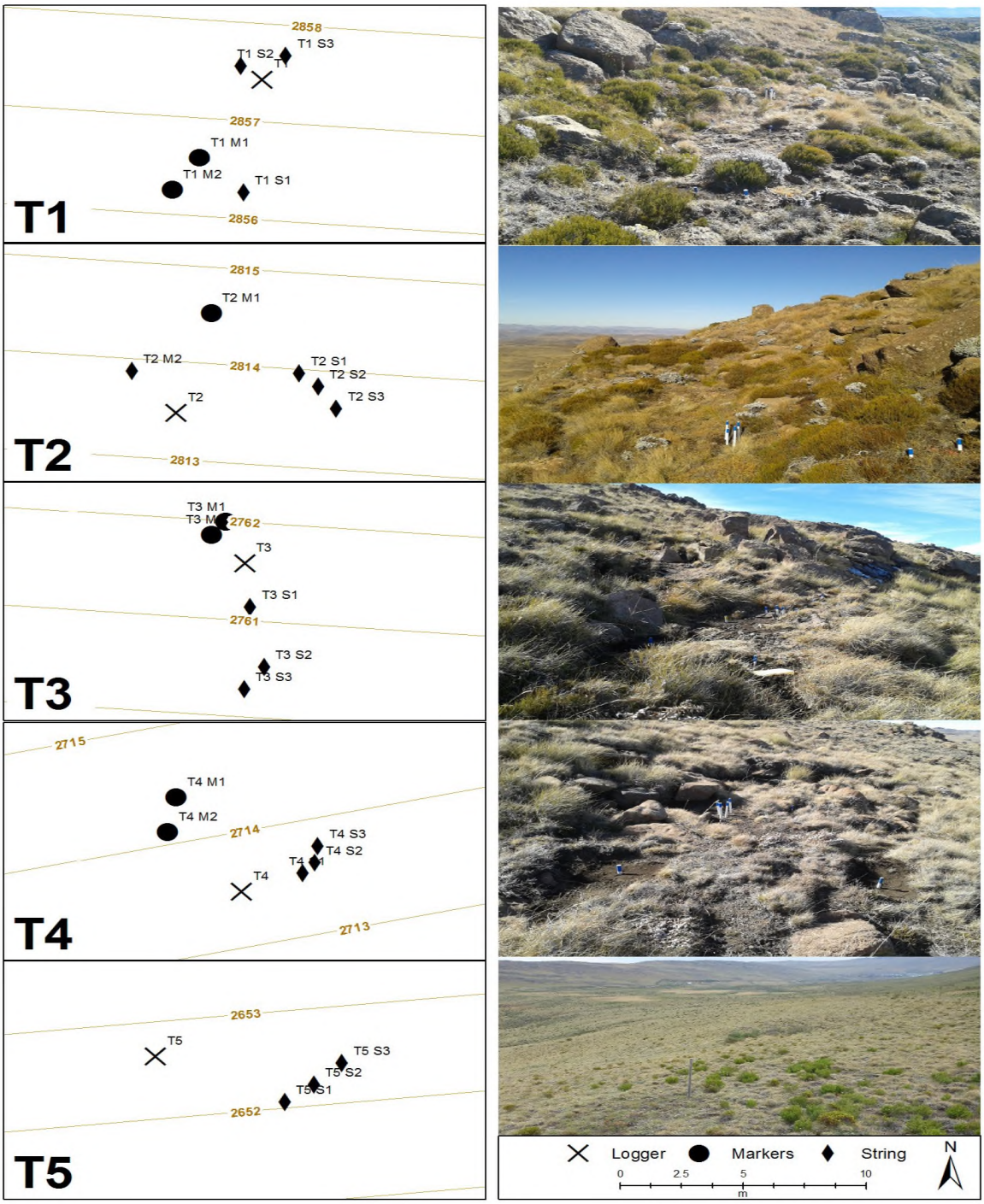


**Figure 21: Logger and experiment locations for the five sites located on the slopes of Ben MacDhui. The column on the left of the graphic shows the experiment locations, whereas the column on the right of the graphic shows a picture of the general site. Scale, as indicated in the figure, is the same for all sites.**

One XR5 logger was placed in the Elandsberg at an altitude of 1 803 m a.s.l. (E3). Thermochron iButtons (Fairbridge technology) were placed at ± 100 m elevation changes, at 1 997 m a.s.l., 1 902 m a.s.l., 1 803 m a.s.l., 1 702 m a.s.l., 1 611 m a.s.l., 1 504 m a.s.l., and 1 397 m a.s.l. (Figure 22, pg. 85). These sites were given the identifier E1-E7 respectively and can be viewed in Figure 23 to Figure 36 (pg. 85-87). iButtons and the XR5 system were set to record at 10-minute intervals, buried on level ground and

all sites located on southward-facing slopes (bearing: S to SE) (Figure 3, pg. 28). Please refer to Table 7 and Table 8 in APPENDIX D for logger site descriptions.

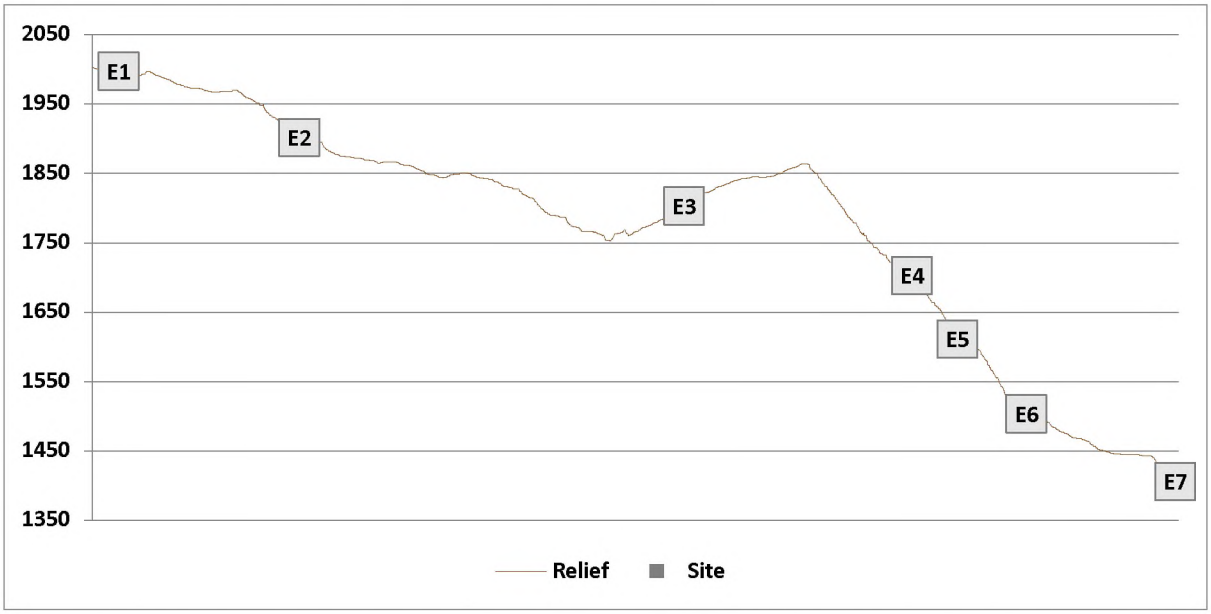


**Figure 22: Location of study sites for the Elandsberg. Sites are shown along the transect taken in the field during site visits. NOTE: the horizontal axis represents distance along the field transect. Distance from E1 to E5: ~ 6.7 km.**

**Figure 23: Logger (iButton) locations of E1. Scale: 40 cm.**


**Figure 24: Broader view of E1.**

Figure 25: Logger (iButton) locations of E2. Scale: 70 cm.

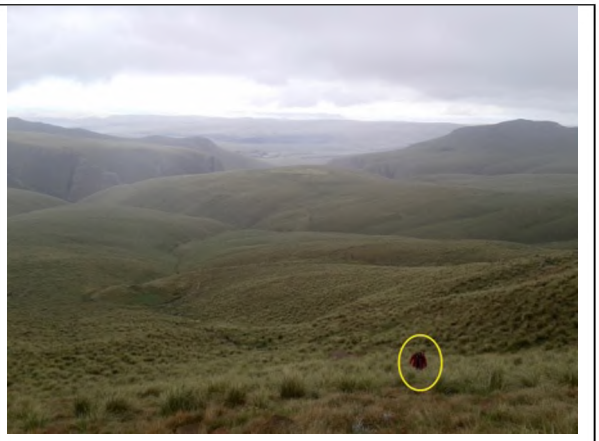

Figure 26: Broader view of E2. Person for scale.

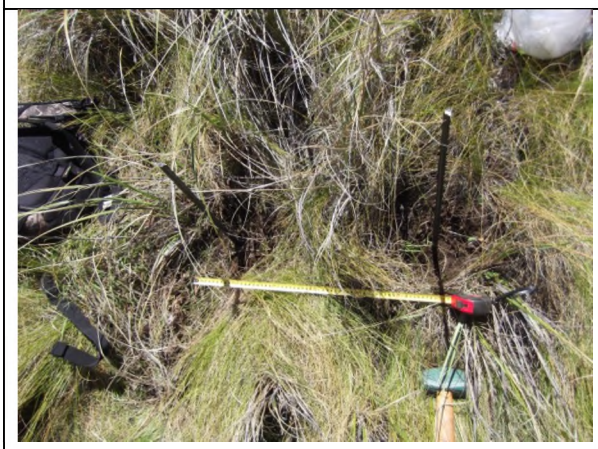

Figure 27: Logger (iButton) locations of E3. Scale: 60 cm.


Figure 28: Broader view of E3.

Figure 29: Logger (iButton) locations of E4. Scale: 80 cm.


Figure 30: Broader view of E4.

Figure 31: Logger (iButton) locations of E5. Scale: 60 cm.


Figure 32: Broader view of E5.

Figure 33: Logger (iButton) locations of E6. Scale: 50 cm.

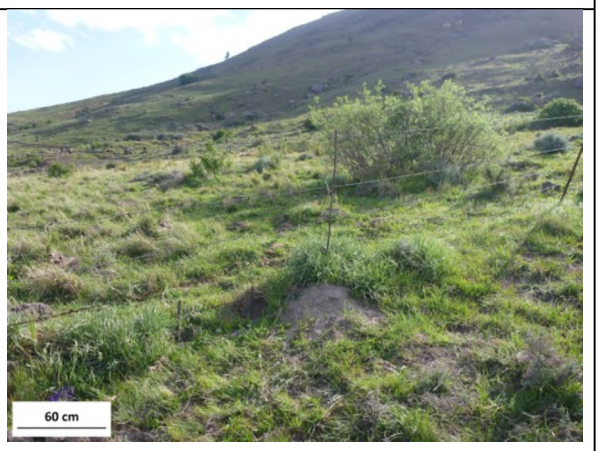


Figure 34: Broader view of E6.


Figure 35: One of the logger (iButton) locations of E7.


Figure 36: Broader view of E7.

#### *4.3.1.2 Marion Island*

Five logging sites were set up along a transect from an elevation of less than 100 m a.s.l. to an elevation of just under 800 m a.s.l. All sites are located on the Island Slope physiographic unit (Verwoerd, 1971). Two XR5 loggers were set up, one at an elevation of 765 m a.s.l. at Katedraalkrans and one at an elevation of 450 m a.s.l. at Tafelberg. These were given the identifiers M1 and M2 respectively. Thermochron iButtons (Fairbridge Technology) were placed at ± 100 m changes in elevation at M2, 363 m a.s.l., 228 m a.s.l., and 87 m a.s.l. These additional locations were given the identifiers M3-M5 respectively (Figure 37). The highest logging site (M1) exceeds the altitude that defines the lower limit of seasonally frozen ground on Marion Island (Boelhouwers *et al.*, 2001). Loggers were deployed on level areas and do not face in any general direction (Figure 5, pg. 40). Please refer to Table 7 and Table 8 in APPENDIX D for logger site descriptions. Lengths of string, to identify slope displacement were set up for each site with three string placements per site. In addition, two trenches were dug per site. More detailed information on the set up and placement of strings and painted markers within trenches is provided in 4.3.2 Particle displacement ( pg. 91). Detailed information on Marion Island site parameters is described in Table 6 and Table 7 in APENDIX D. Figure 38 on pg. 89 shows the locations of the various instruments, once deployed in the field, on Marion Island.

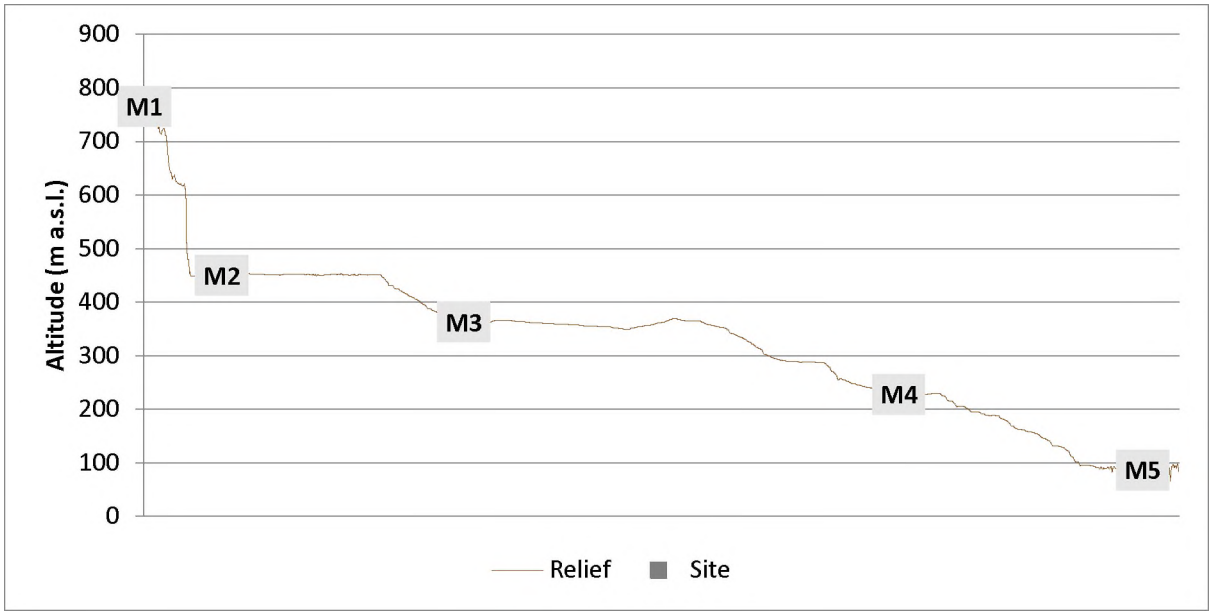


**Figure 37: Location of study sites for Marion Island. Sites are shown along the transect taken in the field during site visits. NOTE: the horizontal axis represents distance along the field transect. Distance from M1 to M5: ~ 5.6 km.**

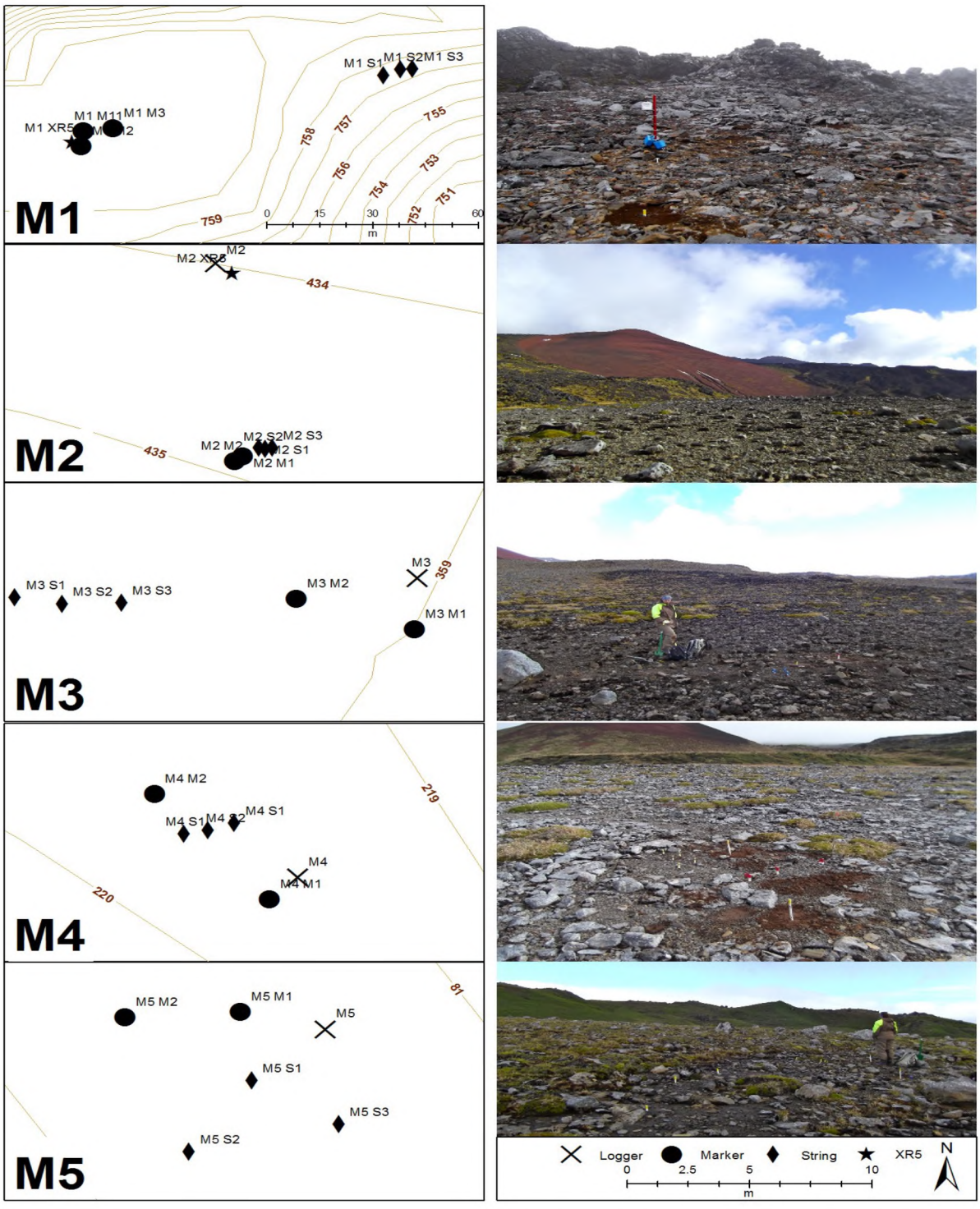


**Figure 38: Logger and experiment locations for the five sites located on Marion Island. The column on the left of the graphic shows the experiment locations, whereas the column on the right of the graphic shows a picture of the general site. The scale on the bottom right is applicable to M2-M5. The scale for M1 is shown in its own frame.**

#### *4.3.1.3 Dronning Maud Land (DML), Antarctica*

Eight logging sites were selected for Dronning Maud Land (DML) of the Antarctic, with two logger set-ups each at Flårjuven and Troll research station. One logging site is present for each of Grunehogna, Robertskollen, Schumacherfjellet, Slettfjell, Valterkulten, and the Northern Buttress of the Vesleskarvet nunataks. Temperature and moisture are recorded at 1-hour intervals. However, higher-frequency data are also available. Data, recorded at ten-minute intervals, were collected for Vesleskarvet during the 2011/12, 2013/14, and 2014/15 summer seasons using thermochron iButtons (Fairbridge technology). One-minute data are available for December 2013 and 2014, and January 2014 and 2015 using ACR systems. Similarly, one-minute data are available for XR5 systems for January 2011 and December 2015. At Robertskollen one-minute data are available, using an ACR system, for January 2015. One-minute data are available for Troll for January 2013 and December 2014 (ACR system).

Flårjuven 1, Flårjuven 2, Grunehogna Peaks, Robertskollen, Schumacherfjellet, Slettfjell, Troll Station 1, Troll Station 2, Valterkulten, and Vesleskarvet were given the identifier A1-A10 respectively. Each of the ten sites has an XR5 logger, with A1 and A3-A9 also having an ACR as back-up. Loggers are located on level areas and do not face in any general direction. The exception to this, are the loggers located at Grunehogna, Schumacherfjellet and Troll, which face in a northnortheast (bearing: N-NE), north (bearing: N) and southeastern direction (bearing: S-SE) respectively. Please refer to Figure 13 (pg. 63) for an overview of the study sites within DML. Flårjuven 2 (A2) is located furthest to the west, with Troll Station 1 (A7) located furthest to the east. Slettfjell (A6) is located furthest to the south, with Robertskollen (A4) closest to the ice shelf and, therefore, furthest north. Locations A1-A10 have elevations of 1 220 m a.s.l., 1 234 m a.s.l., 1 291 m a.s.l., 284 m a.s.l., 955 m a.s.l., 1 416 m a.s.l., 1 320 m a.s.l., 1 326 m a.s.l., 965 m a.s.l., and 805 m a.s.l. respectively (Figure 39). Please refer to Table 7 and Table 8 in APPENDIX D for logger site descriptions.

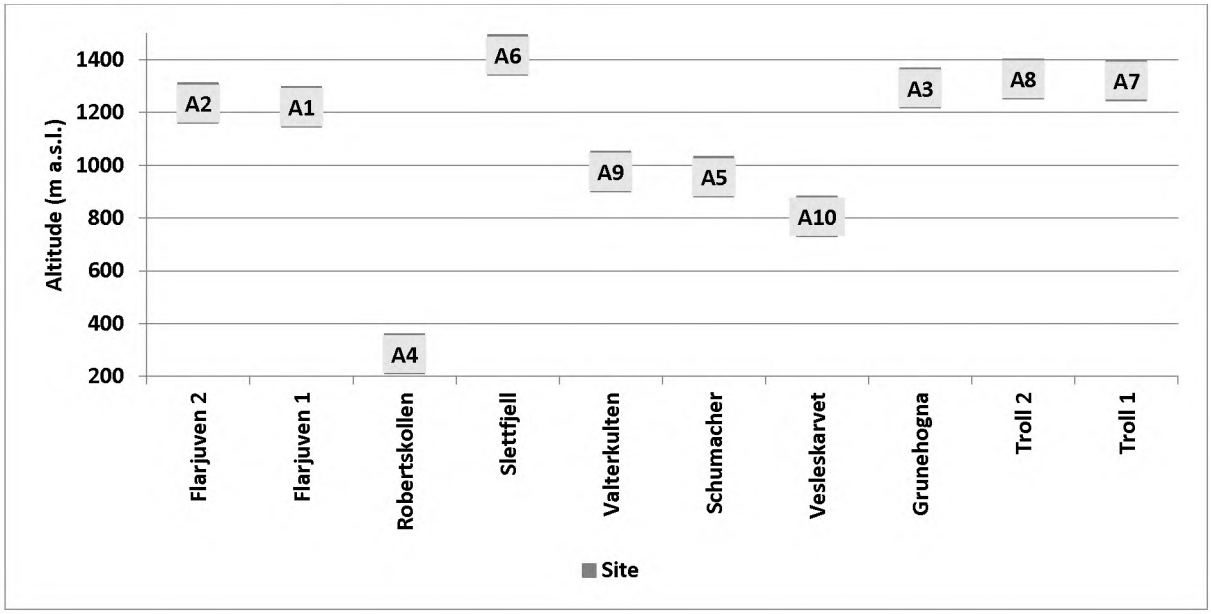


**Figure 39: Location of study sites in Dronning Maud Land, Antarctica. NOTE: the horizontal axis represents location of sites from a West to East direction and not a transect physically traversed in the field.**

### 4.3.2 Particle displacement

Frost creep is the result of one or more of the following processes: needle ice creep, diurnal frost creep and annual frost creep and, together with long-term debris production, may lead to cryoplanation/nivation (Goudie, 2004b). Diurnal, seasonal and annual frost cycles have been observed for the various sites and the assumption made that sediment movement is partly due to freeze-thaw processes. Rates (volumetric and surface) of creep is often driven by slope gradient (solifluction can occur on slopes with a gradient as low as 1°) and climate (Goudie, 2004b). Cold permafrost regions, such as Dronning Maud Land (DML), have low surface velocity rates of ± 5 $cm.a^{-1}$. In comparison, surface velocity in alpine areas may approach 100 $cm.a^{-1}$ (Goudie, 2004b), while volumetric velocity remains low. Volumetric velocity is highest in warm permafrost regions or those regions experiencing deep seasonal frost. Here 30-50 cm depth sediment masses may be moved at average surface velocity rates (Goudie, 2004b). Data on frost heave and particle movement down slope was recorded for Marion Island and the Eastern Cape. Determining movement of particles for DML was not possible due to logistical and time constraints. Several methods were employed to determine fine particle and clast heave/movement along and within a slope. These methods include the sinking of string in the ground and burying painted markers.

Soil movement is determined following the methods adapted from Pérez (1992), Holness (2004), and Ridefelt (2009). The shallow active layer and rocky substrate found in DML does not allow for the measuring of sediment movement, when using the method described by Holness (2004) and Ridefelt (2009). Subsequently, data on soil movement using lengths of string and painted markers was only collected for Marion Island and the Eastern Cape High Drakensberg. This involves measuring the vertical displacement of a length of string sunk orthogonally into the ground. A thin and hollow metal tube with string fastened inside it is placed in the ground and withdrawn, leaving the string within the ground. This string deforms as movement in the ground occurs and such movement can be measured once the string is excavated after a set amount of time. Measurable displacement of the string is used as an indicator of sediment movement and can be quantified in distance moved, as well as volume displaced. Solifluction (needle ice creep, frost creep, gelifluction, plug-like flow) occurs to various depths and at various velocities (Matsuoka, 2001). These depths and velocities reflect specific profiles. A string placed into the ground in the orthogonal will deform in shape over time as the ground undergoes solifluction, yielding profiles to those shown in Figure 40 (pg. 92). Previous research by Holness (2001b) and Boelhouwers (2003a) shows that sediment movement on Marion Island occurs in the upper portion of the ground (5-7 cm) and is likely due to diurnal frost cycles, such as needle ice events (Holness, 2004). This corresponds to profiles A and B of Figure 40 (pg. 92). At higher elevations (> 300 m a.s.l.) solifluction occurs and creep is present up to 20 cm within the ground at altitudes exceeding 1 000 m a.s.l., yielding examples of profile C of Figure 40 (pg. 92).

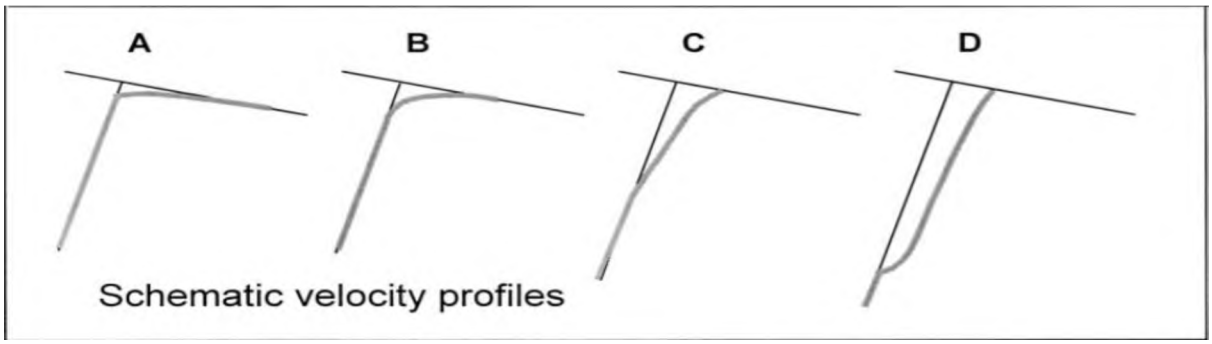


**Figure 40: Schematic velocity profiles for A) needle ice creep, B) diurnal creep, C) gelifluction, and D) plug-like flow (Matsuoka, 2001).**

Holness (2001b, 2004) examined vertical movement profiles for two sites, Junior's Kop and Katedraalkrans Nek, on Marion Island. Results agree with those by Boelhouwers (2003a), arguing for dominant sediment movement through diurnal frost cycles (Profile B of Figure 40) and needle ice, instead of solifluction. Nevertheless, the depth of displacement (12-18 cm) points to needle ice not being the only agent for particle displacement and that other forms of ice segregation must be present as well (Holness, 2004). With one of the study sites of the current study also located at Katedraalkrans the displacement of sunken string is expected to show similar profiles to those shown in Figure 41.

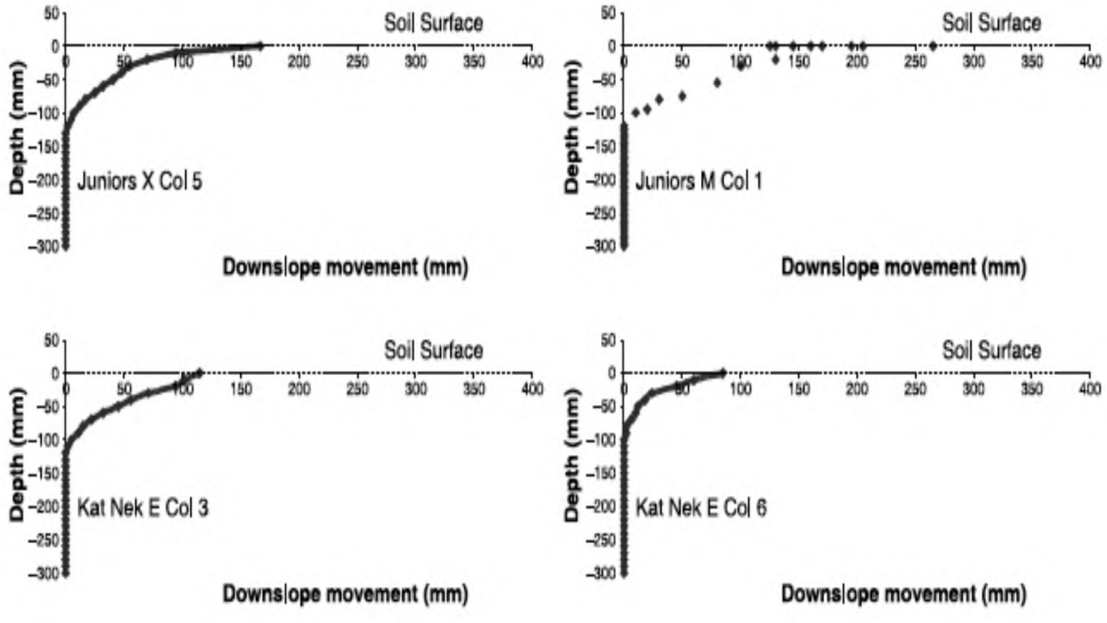


**Figure 41: Vertical movement profiles for two sites on sub-Antarctic Marion Island (Holness, 2004).**

On Marion Island a paucity of larger clasts is present down to a 20-cm depth within the soil column, although the soil surface is often characterised by a fine-gravel surface (Haussmann *et al.*, 2009b). Currently freeze-thaw cycles occur in the upper 4-7 cm of the ground (Holness and Boelhouwers, 1998), and although frost cycles at 10-cm depth have been recorded (Haussmann *et al.*, 2009a), the lack of

clasts at 20 cm depths speaks for a previously more active environment and deeper freeze-thaw cycles. Painted markers allow for an investigation into the dynamics of particle movement within the ground, as well as an indication on either frost pull or frost push mechanisms. Such markers, adapted from Pérez (1992) and Holness (2004), were buried in the ground in 25 cm x 25 cm trenches at varying depths (2 cm, 5 cm, 10 cm, 15 cm) and their displacement recorded after a period of one calendar year. Each depth had differently painted marker associated with it and each marker was of similar weight and dimension, to determine the effect diurnal frost cycles have on particle heave and displacement. The greatest care was taken to ensure the soil column was disturbed as little as possible. This was achieved by removing the soil column in layers, each layer reflecting the depth to the next marker emplacement, and carefully returning these to the excavated trench once the markers were in place. Figure 42-Figure 47 (below to pg. 93) provide an overview of the various stages of marker emplacement.

**Figure 42: Marker trench freshly dug. Scale: 50 cm.**

**Figure 43: Markers at 2 cm depth. Scale: 50 cm.**

**Figure 44: Markers at 5 cm depth. Scale: 50 cm.**

**Figure 45: Markers at 10 cm depth. Scale: 50 cm.**

**Figure 46: Markers at 15 cm depth. Scale: 50 cm.**

**Figure 47: Finalised marker trench with locational identifier. Scale: 50 cm.**

### 4.3.3 Soil characterisation

As introduced in CHAPTER 1: Introduction (pg. 1 onwards), sediment characteristics affect freeze-thaw cycles and concomitant frost heave. Pore size and grain distribution greatly influence freeze-thaw dynamics of frozen ground, while thermal conductivity and diffusivity of ground is largely controlled by grain size distribution (Goudie, 2004a). Soil structure and texture together influence nutrient, water and air supply in each volume of soil (Brady and Weil, 2016). Approximately half of the total volume of mineral soil is occupied by water and gases (Brady and Weil, 2016), and a reciprocal relationship exists between soil moisture and air temperature, as well as soil moisture and ground temperature. Mineral soil represents a porous mixture of inorganic particles, decaying organic matter, air, and water where larger particles (generally mineral fragments) are embedded in colloidal matter and other fine material (Brady and Weil, 2016). Gravelly or sandy soil occurs where larger particles dominate, whereas clayey soil occurs when mineral colloids dominate (Brady and Weil, 2016). Organic matter acts as a binding agent to form clumps and aggregates (Brady and Weil, 2016), affecting potential freeze-thaw cycles. Moisture is integral to the freeze-thaw process, and porosity and permeability of ground greatly influence moisture availability. Bulk density is a proxy for porosity, which in turn is affected by soil texture, organic content, and soil structure (Brady and Weil, 2016). To determine the control of sediment characteristics on freeze-thaw cycles sediment/soil samples were taken for each study site. A minimum of 500 g of soil was collected at each logger site, as well as at each thermo-/hygrochron set-up (10 samples for Marion Island, 8 for Ben MacDhui; 14 samples for the Elandsberg, 10 samples for Dronning Maud Land). The 500 g minimum sample weight exceeds the recommended weight of 100 g, as proposed by Briggs (1977b). To ensure maximum accuracy and precision, all samples were subjected to similar storage and transport conditions (Briggs, 1977a). Sampling of sediment/soil allows for bulk density and porosity to be determined for each site, as well as moisture and organic content, as well as soil/sediment textural fractions. These are explained in greater detail in sections 4.4.1 Bulk density and porosity (pg. 95), 4.4.2 Moisture content (pg. 95), 4.4.3 Total Organic Carbon (TOC) (pg. 97), and 4.4.4 Particle Size Analysis (PSA) (pg. 97).

## 4.4 Laboratory Analyses

Not every section detailed under 4.3 Fieldwork (pg. 79) requires a laboratory component. Soil bulk density was determined for soil characterisation, as was gravimetric water content, organic component, and particle size analyses. Furthermore, sedimentation techniques after Briggs (1977b, 1977a) were undertaken for both particle movement along slopes and soil characterisation. Particle size and fine earth fraction analyses give an indication of the depositional, erosional and weathering environment of a region (Alsharhan and El-Sammak, 2004) and effect freeze-thaw cycles. Furthermore, particle classes allow for sediment classification (Weaver and Grobler, 1981).

### 4.4.1 Bulk density and porosity

To determine bulk density and porosity, samples were removed from the field using a container of known dimensions (using Equation 2), sealed in durable plastic bags and transported to the laboratory in South Africa. Upon removal of samples from their packaging each sample was weighed and then oven-dried for 24 hours in a Labcon Forced Circulation oven (Briggs, 1977a), and the bulk density determined using Equation 3. Porosity was determined using Equation 4. Dronning Maud Land mineral soils were oven-dried at 105 °C, whereas Eastern Cape and Marion Island samples were oven-dried at 60 °C. Lower temperatures were required for the Eastern Cape and Marion Island samples, due to these soil samples having an organic component.

**Equation 2: Volume equation after Briggs (1977a).**

$$V = h\pi r^2$$

**Equation 3: Bulk density equation, where $d_b$ = bulk density, $\theta_d$ = weight of sample upon removal from the field, and V = volume of sample (Briggs, 1977a).**

$$d_b = \frac{\theta_d}{V}$$

**Equation 4: Equation to determine sediment/soil porosity, where $d_p$ = porosity, $d_b$ = bulk density, $s_d$ = soil solid density. Soil solid density is generally given as 2.65 g.cm$^{-3}$ (Manger, 1963).**

$$d_p = 1 - \frac{\theta_d}{s_d}$$

### 4.4.2 Moisture content

Moisture content, a crucial component in frost environments, may be expressed as gravimetric water content (GWC), volumetric water content (VWC), or gravimetric water content expressed as a percentage ($M_c$). Gravimetric water content (GWC) defines the mass of water per mass of dry soil, *i.e.* the soil water content; VWC is used to describe the volume of liquid water per volume of soil. The soil

water-filled pore space is expressed by dividing GWC by soil porosity and shown as a ratio or as a percentage. As such, moisture content of samples was determined where possible. This applies not only to general moisture values, but also to specific layers. For example, moisture values were determined for each layer of trenches, which had painted markers placed within them. Moisture content of each sediment/soil sample was determined by weighing each sample collected in the field ($\theta_w$) and subsequently drying samples at 60 °C or 105 °C (as applicable) in a Labcon Forced Circulation oven for 24 hours. Upon removal samples were weighed again ($\theta_d$). Gravimetric water content (GWC: $\theta_g$) is calculated using Equation 5. Volumetric water content (VWC: $\theta_v$) is calculated using Equation 6. Equation 7 shows GWC expressed as a percentage ($M_c$). Soil water-filled space ($M_p$) is calculated using Equation 8.

**Equation 5: Equation used to determine gravimetric water content (GWC) of sediment/soil samples (Black, 1965). $\theta_w$ is the weight of the sample upon removal from the field. $\theta_d$ is the weight of the sample after drying the sample at 105ºC for 24 hours (Briggs, 1977a). $\theta_g$ denotes GWC.**

$$\theta_g = \frac{(\theta_w - \theta_d)}{\theta_w}$$

**Equation 6: Equation used to determine volumetric water content (VWC) of sediment/soil samples (Black, 1965). $\theta_g$ denotes GWC, $d_b$ denotes bulk density, and $d_b$ water density. $d_b$ is generally given as 1.**

$$\theta_v = \theta_g * \frac{d_b}{d_w}$$

**Equation 7: Gravimetric water content (GWC: $\theta_g$) expressed as a percentage (Briggs, 1977a).**

$$M_c = \theta_g * 100$$

**Equation 8: Equation to determine percentage of soil water-filled space ($M_p$) per sample. $\theta_g$ denotes gravmetric water content (GWC); $d_p$ = porosity.**

$$M_p = \frac{(\theta_g)}{\theta_d}$$

### 4.4.3 Total Organic Carbon (TOC)

Organic matter of each sample was determined using loss-on-ignition (LOI). While LOI is known to contain bias *(e.g.* van Langenhoven *et al.*, 1978; Schulte *et al.*, 1991; Andersen and Krysell, 2005), the greatest care was taken to ensure minimum soil components other than organic matter were ignited during the process. Samples used for organic content determination are taken from the fine earth fraction (FEF) (coarse sand-clay), those particles smaller than 2 mm in size (Briggs, 1977a). Each sample, weighing between 5-10 g, was oven-dried in a Labcon Forced Circulation oven at 110 °C for 2 hours to remove residual moisture content (Schulte *et al.*, 1991). Once remove from the oven samples were placed in a desiccator for 30 minutes and then weighed ($W^1$) in ceramic crucibles on a Mettler AJ100 scale with precision of 0.0001g. To minimise error, crucibles were not filled more than two-thirds and samples exceeded 5 g in weight. After weighing the samples these were placed in a flash oven (muffle furnace) at 430 °C (Davies, 1974; Ben-Dor and Banin, 1989) for 6 hours, to ignite organic particles (Briggs, 1977a). A temperature of 430 °C was selected to minimise loss through the thermal breakdown of carbonates, while still ensuring effective loss of organic carbon (Schumacher, 2002). Upon removal from the oven samples were cooled in the oven to ± 150 °C and placed in a desiccator for half an hour, after which each crucible was weighed ($W^2$) (Hoskins, 2002). The difference in weight between the two samples determines the amount of organic matter in the soil/sediment (Equation 9).

**Equation 9: Organic proportion of sediment samples, expressed as a percentage (%). $W^1$ is the weight of the sample after drying at 105ºC; $W^2$ is the weight of the sample after igniting organic content at 430 °C (Davies, 1974; Briggs, 1977a; Ben-Dor and Banin, 1989).**

$$O_p = 100 - (\frac{W^2}{W^1} * 100)$$

Three LOI runs were conducted for samples from each site and the average of those three runs constitutes the organic matter component of that location. Total organic carbon (TOC) was calculated by converting the organic matter component with factors of 1.9 or 2.5 for surface and sub-surface soils respectively (Schumacher, 2002). The soil determination using the organic proportion of samples following LOI is given in Table 12 in APPENDIX E.

### 4.4.4 Particle Size Analysis (PSA)

Soil texture refers to the size of mineral particles and reflects the relative proportion of particles of different sizes (*separates*) in each volume of soil (Brady and Weil, 2016). Sieving identifies the proportion of material between 0.045-16.0 mm (4.5ø – -4ø), that is particles greater than 63 µm (Briggs, 1977a). Sieves of various sizes (8 mm; 4 mm; 2 mm; 1 mm; 0.5 mm; 0.25 mm; 0.125 mm; 0.063 mm) were arranged according to size, with the smallest sieve size located towards the base of the stack (Lubbe, 2010). Samples were dried in a Labcon Forced Circulation oven at 105 °C for 24 hours. After removal from the oven samples were disaggregated with a mortar and pestle and sieved in the sieve stack for ten minutes (Briggs, 1977a). The sediment portion in each sieve was weighed on a Mettler PC 8000 (0.0 g) scale with each sieve mesh size weighed separately to determine the dry mass proportion of sediment within each size class. The various sample fractions were subsequently separated into gravel portions (> 8000 µm), fine gravel portions (2000-8000 µm), coarse sand portions (500-2000 µm),

medium sand portions (250-500 μm) and fine sand portions (63-250 μm). The fine earth fraction (FEF: < 2 mm) was determined for all samples, as well as the proportion smaller than 63 μm (silt and clay fractions). Refer to Table 8 for sedimentation grades and sizes.

**Table 8: The three grades of the fine earth fraction (portion < 2 mm), indicated in millimetres (mm) and micrometres (μm) (Briggs, 1977a).**

| Type | Millimetre | Micrometre |
|---|---|---|
| Sand | 2-0.06 | 2000-60 |
| Silt | 0.06-0.002 | 60-2 |
| Clay | < 0.002 | < 2 |

Sediment portions smaller than 63 μm require fine particle analysis and such analyses were conducted for a subset of the sample set. These include surface sediment samples for all sites excepting those from Dronning Maud Land. This is due to these samples having little fine material (Hansen (2014); Hansen *et al.* (2014). Sediment samples obtained from trenches for painted marker movement and displacement (4.3.2 Particle displacement, pg. 91) also underwent fine particle analysis. Fine particle analyses were determined using a Malvern Mastersizer 3000 laser granulometer equipped with a Hydro LV wet dispersal unit. The Mastersizer is comparable to the SediGraph, which is a more efficient method compared to the pipette method, hydrometer and sedimentation balance method, of determining fine particle distributions (Weaver and Grobler, 1981; Lara and Matthes, 1986). Furthermore, it provides a quick, automated and reliable reproducible method for conducting fine particle analyses. Fine particle analyses are determined using laser diffraction (Mie and Frauenhofer scattering) to determine particle size distribution (Malvern Instruments Ltd., 2011). This is based on the principles of Stokes' Law (Equation 10, pg. 99) and the Beer-Lambert Law (Equation 11, pg. 99) (Weaver and Grobler, 1981; Stein, 1985; Lara and Matthes, 1986; Cramp *et al.*, 1997). The Mastersizer applies Stoke's and the Beer-Lambert laws by recording the rate of sedimentation of particles using a concentrated beam of photons. Stokes' Law determines the relationship between the rate a particle descends in a viscous medium due the force of gravity to that particle's size (Briggs, 1977a). This relationship is determined by the size of the particle (D), particle density ($\rho$), gravity ($g$), as well as the terminal velocity ($v$), density ($\rho 0$) and viscosity ($\eta$) of the liquid (Equation 10, pg. 99). Particle density is determined by the weight of a solid over the volume of the solid and not related to fineness and arrangement of solids. Mineral soils generally have particle densities within the range of 2.6-2.75 g.cm$^{-3}$ (Brady and Weil, 2016). In comparison, organic matter weighs much at 1.2-1.5 g.cm$^{-3}$ (Brady and Weil, 2016). While Stoke's Law is applied to determine the rate of movement of specific particle sizes within a viscous medium it does not truly consider absolute sizes for non-spherical particles (Lara and Matthes, 1986). Nevertheless, it explains how heavier and larger particles take shorter periods of time to settle out of liquid, with smaller and lighter particles such as clay taking up to 8 hours to settle out (Briggs, 1977a). The Beer-Lambert Law determines the relationship of how photons are attenuated when passing through a viscous medium as a function of time and height of the medium, based on the extinction coefficient, concentration and path length of the beam of photons (Equation 11, pg. 99) (Stein, 1985).

**Equation 10: Stokes' Law and how it is determined (Briggs, 1977a). The law requires the inclusion of the size of the particle (D), the terminal velocity of the particle (v); viscosity of the liquid (η), density of the particle material (ρ), density of the liquid (ρ0), and gravity (*g*).**

$$D^2 = \frac{18v\eta}{(\rho - \rho 0)\, g}$$

**Equation 11: The Beer-Lambert's Law and how it is determined (Stein, 1985). The law determines the ratio of the final beam measurements ($I_f$) to the incident beam measurements ($I_i$) based on the absorptivity of the medium (ε), the concentration of the medium (*c*), and the path length of beam (*d*).**

$$\frac{I_f}{I_i} = \exp(-\varepsilon c d)$$

Organic content of samples was removed by pre-treating 0.2 g sediment samples with a solution of 30 % hydrogen peroxide ($H_2O_2$) (Pulley *et al.*, 2015; Pulley and Rowntree, 2016). These samples were left at room temperature for 24 hours, after which they were heated to 70 °C for 4 hours (Pulley *et al.*, 2015; Pulley and Rowntree, 2016). Samples were dispersed using 5 mm of a solution of 3% sodium hexametaphosphate ($NaPO_4$) and placed into an ultrasonic bath for two minutes (Gray *et al.*, 2010). Following the ultrasonic bath, samples were added to 500 ml deionised water and placed into the Mastersizer where they were exposed to a further two minutes of ultrasonic dispersion. Analysis commenced at ± 10% obscuration (8-12%) (Blott *et al.*, 2004), determining the median (D50) particle diameter (Malvern Instruments Ltd., 2011; Pulley and Rowntree, 2016). Once the various ratios per sediment class were determined, statistical analyses were done to determine particle size distributions and similar characterisations. These are explained in greater detail in 4.5.2.2 Particle Size Analysis (PSA) statistical calculations on pg. 107.

## 4.5 Statistical Analyses

All data collected were statistically as well as geostatistically analysed and compared to evaluate trends and correlations between the sites. Geographical data vary across space and spatial relationships are generally non-stationary (Charlton *et al.*, 2006). As such, geostatistics assumes that data points are dependent on each other (Doornkamp and King, 1971; Till, 1985; Atkinson, 1999, 2001; Griffith, 2005). Autocorrelation remains a fundamental concept of geographical analyses (Atkinson, 2001), forming the basis of Tobler's First Law of Geography (Miller, 2012). However, classical statistical analyses assume data points are independent of each other. Physical geographers often investigate relationships and processes that vary from one place to another, requiring the use of non-stationary geostatistical models (Atkinson *et al.*, 2003). Combining statistics and geostatistics when analysing geographical data is a powerful analytical approach (Burrough, 2001). The nature of this study required both classical and geographical statistical analyses to be employed and statistics, as well as geostatistics were applied when performing analyses. The methods used are explained in greater detailed in 4.5.2 Statistical methods (pg. 102) and 4.6 Geographical Statistics and Modelling (pg. 107). Software used for analyses comprised the Esri suite of products, Microsoft® Excel for data preparation, as well as R Project for

Statistical Computing (R). An overview of statistical tests used to analyse which specific question is provided in Table 9. A summary of the various tests, their hypothesis and general usage is provided in Table 10 (pg. 101).

**Table 9: An overview of statistical methods employed during analyses. Please refer to the Table of Abbreviations (pg. xxxiii) and Table of Symbols (pg. xxxvi) for a list of abbreviations and symbols.**

| Investigation | Method |
|---|---|
| Comparing moisture populations | *t*-test |
| Comparing temperature populations | *t*-test |
| Determining if temperature/moisture values per sensor depth are drawn from the same population (intra-site comparison) | ANOVA |
| Determining if temperature/moisture values for all sites are drawn from the same population (inter-site comparison) | ANOVA |
| Determining if individual pairings of sample sites have similar population variances | Fisher's LSD test, Tukey HSD |
| Determining if particle size fractions for all sample sites are drawn from the same population | ANOVA |
| Determining if particle size fractions for two-sample sets are drawn from the same population | K-S |
| Determining the level of sorting (lateral and vertical) of sediment textural fractions | S |
| Determine the level of sorting per sample population | $C_u$ |
| Identify relationships amongst climate parameters and GST | Pearson's product-moment coefficient of linear correlation |
| Identifying the most important drivers of FTC | PCA |
| Determining the site's location in a CPZ, DPZ, SPZ or no permafrost zone | CPZ, DPZ, SPZ |
| Determining the number of annual days FTC occur for | Diurnal cycles below the 0 °C isotherm, coupled with moisture readings suggesting the thawing/freezing of ground moisture |
| Determining ground thermal indices | GFI, TI, FI, TSI, SO, frozen hours, number and duration of frost-thaw events, intensity of frost event, seasonal range, depth of zero amplitude, depth of base of permafrost (permafrost thickness) |

**Table 10: A summary of statistical tests, their hypothesis (if applicable) and general usage.**

| Test | Hypotheses | Usage |
|---|---|---|
| ANOVA | $H_0$: sample means are similar, *i.e.* $\mu_1 = \mu_2 = ... = \mu_i$<br>$H_a$: sample means are not similar, *i.e.* $\mu_1 \neq \mu_2 \neq ... \neq \mu_i$ | Testing equality of means of multiple populations |
| $C_u$ | $C_u < 4$: well sorted<br>$C_u > 6$: poorly sorted | Determine the level of sorting per sample population |
| *F*-test | $H_0$: sample variance is similar, $\sigma_1^2 = \sigma_2^2$<br>$H_a$: sample variance is not similar, $\sigma_1^2 \neq \sigma_2^2$ | Testing equality of variance |
| Fisher's LSD | $H_0$: the two-sample means are similar, *i.e.* $\mu_1 = \mu_2$<br>$H_a$: sample means are not similar, *i.e.* $\mu_1 \neq \mu_2$ | Testing equality of means of multiple two (pairwise) populations |
| K-S | $H_0$: The data follow a specific distribution<br>$H_a$: The data do not follow a specific distribution | Testing similarity of non-normal distributed populations |
| PCA | n/a | Identifying the principal factors in multivariate analyses |
| *r* | $r = 0$: no relationship<br>S = +1: perfect positive relationship<br>S = -1: perfect negative relationship | Calculating the strength of the relationship between two populations |
| S | S = 0: perfect sorting<br>S = 1: no lateral sorting<br>S > 1: textural fraction deficient compared to paired sample | Testing for the level of sorting between sediment textural fractions |
| S-W | $H_0$: The data are normally distributed<br>$H_a$: The data are not normally distributed | Testing normality of a distribution |
| *t*-test | $H_0$: sample means are similar, *i.e.* $\mu_1 = \mu_2$<br>$H_a$: sample means are not similar, *i.e.* $\mu_1 \neq \mu_2$ | Testing equality of means of two populations |
| Tukey HSD | $H_0$: sample means are similar, *i.e.* $\mu_1 = \mu_2 = ... = \mu_i$<br>$H_a$: sample means are not similar, *i.e.* $\mu_1 \neq \mu_2 \neq ... \neq \mu_i$ | Testing equality of means of multiple two (pairwise) populations |

### 4.5.1 Data preparation and validation

Raw data were pre-processed to enable analyses. Processing steps include removal of null values (incorrect values and no recorded value instances), applying calibration equations of sensors to data, as well as merging/splitting datasets where needed. A record of steps followed in preparing datasets for analyses is crucial to ensure and identify the suitability of each dataset to specific analyses methods and to be able to repeat the process. This metadata and all steps of the pre-processing process are available in Table 16 of APPENDIX F. All data were compiled in Microsoft® Excel and analysed in R Project for Statistical Computing (R). Furthermore, all data were normalised before analyses commenced (if

required) and probability density functions used for continuous data. Similarly, probability mass functions were used for discrete data. Normalisation of data was only required when the Shapiro-Wilk (S-W) test, or similarly the *F* test, proved a non-normal distribution. Expected values were used to determine a measure of how biased the calculated values were. Combinations of descriptive, exploratory and inferential statistical methods were used for all analyses. The power of using exploratory methods in finding connections between parameters was applicable to guide the inferential statistical methods. Predictive statistical analyses were utilised for modelling diurnal frost environments on a global scale. Methods were designed to be replicable.

### 4.5.2 Statistical methods

Descriptive statistics as well as statistical inference (hypothesis testing), using both parametric and non-parametric statistics (Till, 1985) are employed. Descriptive statistics include averages ($\mu$), medians, maximums and minimums, observed variance and standard deviations ($s$), as well as ranges. Medians were deemed a more appropriate measure of central tendency over averages, due to them being less affected by outliers and representative of central tendency when frequency distributions are narrowly spread, widely spread, clustered, or skewed (World Meteorological Organisation (WMO), 2011). The coefficient of variation (CV) of a parameter was used as a measure of that parameter's variability (Le Roux and McGeoch, 2008). Statistical inference includes the *F*-test, Shapiro-Wilk (S-W) test to determine normality and similarity of variance, Student's *t*-test for comparison testing, Kolmogorov-Smirnov (K-S) goodness-of-fit two-sample test, Fisher's least significance difference (LSD) test for multiple comparisons, Tukey Honestly Significance Difference (HSD), Analysis of Variance (ANOVA), Pearson's product-moment coefficient of linear correlation ($r$), regression analyses, as well as Principal Component Analysis (PCA). Briggs (1977b) proposes a level of significance of 0.05 ($\alpha = 0.05$), as this reflects a realistic level of certainty in physical geography, since at this level Type I and II errors are minimised (Till, 1985). As such, 0.05 reflects the lowest acceptable level for this project (Briggs, 1977b).

The *F*-test was used to determine the similarity of sample variances (Till, 1985; Williams *et al.*, 2006), before parametric tests *(e.g.* the *t*-test) were conducted (Doornkamp and King, 1971). Shapiro-Wilk tests (S-W), used to determine normality in frequentist statistics, determine normal sampling distributions for examined variables. Similarity was tested using a *t*-test for the equality of means (n is variable; mean is similar) (Doornkamp and King, 1971; Till, 1985). ANalysis Of VAriance (ANOVA) was used to compare two or more sample means of observed populations to determine whether populations were statistically similar (Doornkamp and King, 1971; Till, 1985). This statistic requires data to be tested for normal distributions (Ericson, 2004), and was used to differentiate between data sets from different study sites. In the event where ANOVA results showed that samples were indeed different, Fisher's LSD test was used to determine which population means differered (Till, 1985; Williams *et al.*, 2006). The Tukey HSD, based on the studentised range distribution ($q$), which takes the number of means compared into account, was used for multiple comparisons. Tukey HSD was employed over the *t*-test for multiple comparisons due to its greater control of committing a Type I error, decreasing family-wise error rates. For this statistical test, sample sizes also do not have to be equal.

Linear regression determines the relative influence of independent variables (Doornkamp and King, 1971; Till, 1985; Brunsdon *et al.*, 1998; Charlton *et al.*, 2006), *e.g.* ambient temperatures and soil texture, on dependent variables such as soil moisture and temperatures. Generalised linear (GLZ) models and simultaneous autoregressive models (SAR) are applied. Linear regression employs the least squares method to fit a line through a set of observations to identify relationships amongst data (Till, 1985). Predictor variables (independent variables) are modelled against response variables (dependent variables), if the calculated relationship is constant across the study area (Doornkamp and King, 1971; Till, 1985; Brunsdon *et al.*, 1998; Charlton *et al.*, 2006). This allows for determining the relative influence of independent variables, *e.g.* ambient climatic variables or soil texture, on dependent variables, *e.g.* soil temperatures. Pearson's correlation coefficient was used to determine whether two measurement variables were synchronous (Williams *et al.*, 2006), using a correlation matrix that was calculated for correlating more than two variables simultaneously (Doornkamp and King, 1971). The strength of *r* lies in the test not being reliant on variables having an equal number of observations, *i.e.* n may be variable (Till, 1985). Due to the coefficient being scaled, the final value is independent of the units of measurement for the separate populations (Williams *et al.*, 2006). The value of the coefficient indicates the strength of the relationship (Brunsdon *et al.*, 1998). A value of zero indicates no relationship or trend observed between populations (Williams *et al.*, 2006), and the $R^2$-statistic indicates how much of the total variance is explained by the linear relationship (Till, 1985). This approach is suited to determine pair-wise relationship strengths between investigated parameters. Once correlations have been identified a weighting, or interaction matrix is developed. Such weights are then used as input to geographically focused regression analyses, as well as the general frost cycle model (Equation 15 on pg. 108). Since classical linear regression applies a stationary model approach the location of geographical variables is ignored (Brunsdon *et al.*, 1998; Charlton *et al.*, 2006). As such, a non-stationary approach, such as Geographically Weighted Regression (GWR), needs to be applied. Please refer to 4.6 Geographical Statistics and Modelling (pg. 107) for an explanation of GWR.

Principal Component Analysis (PCA), an empirical orthogonal function analysis, is a statistical technique that attempts to simplify the complexity of a dataset by identifying underlying factors (or components) that explain the variance of the original dataset (World Meteorological Organisation (WMO), 2011). Through this process, the complex and multivariate dataset consisting of many correlated observations is decomposed into a new set of uncorrelated (orthogonal) functions (World Meteorological Organisation (WMO), 2011), by removing unnecessary distributions inherent to the dataset. This technique has widespread application in climatology (World Meteorological Organisation (WMO), 2011), and was used to identify the role of significant climate and other relevant parameters on freeze-thaw cycles. Furthermore, such methods are used to remove noise or redundancy in data to identify the principal causation factor(s) (Doornkamp and King, 1971). Applying PCA reduces many variables to a few, essentially summarising data (Doornkamp and King, 1971). It is often difficult, if not impossible, to isolate individual processes from, and their influence on, the landscape (Church, 2010). Any landscape is the product of synergistic (additive or amplifying) and competing processes, acting on various spatial and temporal scales (Church, 2010). Processes may interact in a non-linear way to result in chaotic (spatially diffuse) effects (Culling, 1957; Beven, 2000; Murray *et al.*, 2009), speaking to various levels of self-organisation (Phillips, 1999). Principal Component Analysis is used to identify synergistic processes and remove these from the data set. During PCA the correlation matrix is replaced by a factor-loading matrix (Doornkamp and King, 1971). The factor-loading matrix calculates which variables

load highly on specific factors. In addition, variability in the original data is explained by the importance, or loading, of each factor (eigenvalue). Only factors with an eigenvalue greater than 1 are considered in analyses and can be easily identified using a Scree plot (Doornkamp and King, 1971). Consequently, PCA was identified as the appropriate technique use in identifying significant parameters and the role each plays on soil temperature and moisture regimes in frost environments. Identifying the principal component(s) (PC) assists in determining the optimum parameters for modelling freeze-thaw cycles, their dynamics and distribution across the selected study region.

#### *4.5.2.1 Freeze-thaw cycle indices and statistical calculations*

Means and ranges provide useful indices for the evaluation of the diurnal, seasonal, and annual frost environment. These means and ranges, as discussed below, are given as equations in Table 11. Diurnal ranges are calculated by subtracting the minimum diurnal temperature from the maximum diurnal temperature. This also reflects the thermal stress index (TSI). Where less than 24 temperature (hourly) observations are recorded, the diurnal mean temperature is calculated by adding the maximum and minimum diurnal temperatures and dividing this value by two. If hourly observations are available, the average of these observations is used to determine mean diurnal temperatures. Mean monthly temperatures are calculated by dividing the sum of the mean diurnal temperatures by the number of days in the month. The seasonal range is calculated by subtracting the July mean temperature from the January mean (Boelhouwers, 2003a). The annual mean is determined by dividing the sum of the monthly mean temperatures by 12 and the surface thermal offset (SO), which is applied to any particular time frame, is calculated by subtracting mean air temperature off GST (Kotzé, 2016). Annual cumulative degree days (DD, $C.day^{-1}$) are determined by subtracting diurnal mean air temperature off mean ground surface temperature (GST) (Schoeneich, 2011). The ground freezing index (GFI), calculated on an annual basis, is an indicator of the annual frost regime and determined by summing diurnal mean GST (Schoeneich, 2011). This method approximates the Finn method, which is suitable for calculating GFI in cold regions where long seasonal freezing is common (Phukan, 1993). As such, this method of calculating the GFI is applied for this study.

**Table 11: Calculations for determining annual, seasonal and diurnal ranges and means. * using methods by the World Meteorological Organisation.**

| Symbol | Calculation | Equation |
|---|---|---|
| $T_{DR}$ / TSI | Diurnal Range / Thermal Stress Index | $T_{D:max}$-$T_{D:min}$ |
| $T_{DM}$ | Diurnal Mean | Hourly observations available *: $\Sigma T_D$ / 24<br>Hourly observations not available: ($T_{D:min}$+$T_{D:max}$)/2 |
| $T_{SR}$ | Seasonal Range | $T_{MM:Jan}$ -$T_{MM:July}$ |
| $T_{MM}$ | Monthly Mean | $\Sigma T_{DM}$ / days of the month |
| $T_{AM}$ | Annual Mean | $\Sigma T_{MM}$ / 12 |
| SO | Thermal Offset | $\Sigma$(NST / GST-$T_{AIR}$) |
| DD | Degree Days | $\Sigma$ $T_{DM: GST}$-$T_{DM: AIR}$ |

| Symbol | Calculation | Equation |
|---|---|---|
| GFI | Ground Freezing Index | $\Sigma T_{DM:\,GST}$ |
| TI | Thawing Index | $\Sigma T_{DM:>\,0\,°C\,|\,summer}$ |
| FI | Freezing Index | $\Sigma T_{DM<\,0\,°C\,|\,winter}$ |
| NST: near surface temperatures (recorded at ± 1 cm within the ground)<br>GTS: ground surface temperatures (recorded at ± 2 cm within the ground)<br>$T_{AIR}$: ambient air temperature | | |

Values used to describe the active layer include the summer thawing index (TI), the winter freezing index (FI), as well as active layer thickness through the direct measurement of ground temperature using thermistors buried at various depths within the ground (Burn, 1998). The TI reflects the accumulated DD above freezing during summer months, whereas the FI reflects the accumulated DD below freezing during winter months (Riseborough *et al.*, 2003). Although TI and FI are generally calculated only for summer and winter respectively, for this study these indices are calculated for all season (where applicable). This allows to compare locations that do not necessarily exhibit permafrost and an active layer. Active layer thickness reflects the maximum depth of thawing on an annual basis and is measured in centimetres (Christiansen, 2013). The thermal state of permafrost is given by ground temperatures measured at different depths (Christiansen, 2013). Thawing and freezing indices, derived from air temperatures, are used when ground measurements are not available. When ground measurements are present active layer and permafrost parameters are extracted directly from the recorded data. The mean temperature of permafrost provides insight into how sensitive a region is to warming global temperatures (Kawahigashi *et al.*, 2004), and these values were determined for those sites where permafrost is present. The rate of penetration of temperature change into the ground is proportional to the square root of the period of the cycle of freezing (or thawing), or the time from onset. This relationship is given in Equation 12. While this equation has inherent inaccuracies due to the complex nature of freeze events, it does serve as a guideline as to the depth of freezing cycles.

**Equation 12: The expected rate of penetration of a freezing cycle (*d*) as a function of time (Williams and Smith, 1991).**

$$d = \text{observed depth} * 1/t^{1/2}$$

The number of freeze-thaw cycles observed on a diurnal, monthly, seasonal and annual scale is determined by identifying diurnal cycles below the 0 °C isotherm and coupling these with moisture readings where either thawing or freezing of ground moisture is indicated. Moisture values were calibrated using manufacturer's instructions and thaw values extracted statistically by evaluating the variability of data recorded. Positive values with no variability were not considered for thaw events. The zero-curtain effect, when present, is investigated. The zero-curtain effect, a characteristic of wet and medium-textures soils, refers to the maintenance of temperatures at or near 0 °C in freezing or thawing ground because of the release of latent heat upon the freezing of the water (Outcalt *et al.*, 1990). Other indices calculated include (continued on next page):

1) The total number of frozen hours per sensor depth;
2) The number and duration of thaw or freeze events;
3) The intensity of the frost event determined by the absolute minimum temperature reached during the event;
4) The depth of zero amplitude or the upper limit of seasonally invariant permafrost (intersection of the minimum and maximum mean annual temperatures);
5) The annual mean permafrost surface temperature ($T_{sp}$); and
6) The calculated base of the permafrost (intersection of the mean annual temperature with the 0 °C isotherm).

Mean permafrost temperature ($T_{sp}$) is obtained by extrapolating the common linear portion of the profiles upwards. The geothermal gradient below the surface (30 °C.km$^{-1}$) was used as an indicator for determining permafrost thickness (Goudie, 2004b). Freezing depth is important to infer dynamics related to cryoturbation and the development of landforms. For example, solifluction lobes and terraces require deeper freeze-thaw cycles than those associated with needle ice (Boelhouwers *et al.*, 2003; Haussmann *et al.*, 2009b), and patterned ground is generally affected by freezing within the upper 60 cm of the ground (Campbell *et al.*, 1998). A site's location within a permafrost zone is determined using median annual near surface or ground surface temperatures (MAST or MAGT) where available, or mean annual air temperatures (MAAT) if data on ground temperatures was not available (refer to Table 12). Freeze or thaw events can also be identified visually from a temperature graph using exotherms. During the exothermic reaction, heat is released as latent heat when it freezes (Figure 48). This release of latend heat is reflects as an increase of temperature on the temperature graph (Stuart *et al.*, 2017).

**Table 12: Mean annual soil surface temperatures as an indication of permafrost zones. MAGT: mean annual near surface (± 1 cm) temperature. MAGT: mean annual ground surface (± 2 cm) temperature. MAAT: mean annual air temperature.**

| Description | MAST/MAGT | MAAT |
|---|---|---|
| Continuous Permafrost Zone (CPZ) | < -5 °C | < -8 °C |
| Discontinuous Permafrost Zone (DPZ) | -5 °C – 0 °C | -8 °C – 5 °C |
| No evidence of permafrost | > 0 °C | > 5 °C |

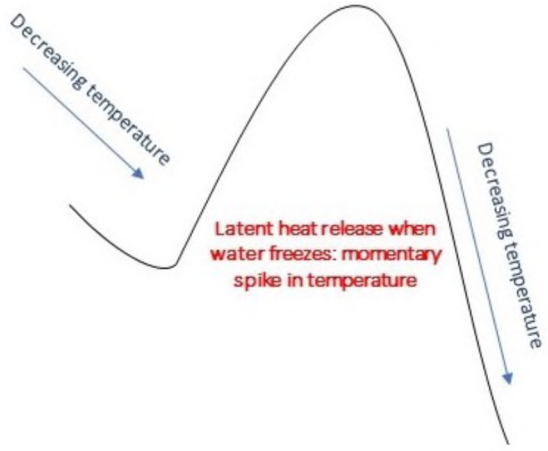


**Figure 48: Simplified diagram of an exothermic reaction.**

#### *4.5.2.2 Particle Size Analysis (PSA) statistical calculations*

Particle size analysis (PSA) includes the determination of the proportion of the fine earth fraction (FEF: particloes < 2 mm) per sample, textural classes, sorting indices, as well as lateral sorting between paired samples. The Kolmogorov-Smirnov (K-S) test was used to determine if soil samples were different. This test was used as data are already in the required format of cumulative percentages and allows for testing of population similarity of non-normal distributed populations (Till, 1985). GRADISTAT was used to perform statistical calculations (Blott and Pye, 2001). Sediment/soil ratios were plotted on ternary diagrams using Tri-plot (Graham and Midgley, 2000), to illustrate the proportions of sand, silt and clay within each sample (Briggs, 1977a). The proportion for each class per sample were calculated as a percentage of the whole and plotted on bar graphs. In addition, the cumulative percentage (coarse to fine) of each sieve class was determined and plotted. An example of a ternary diagram is given in Figure 2 in APPENDIX E. Sediment particle sizes follow lognormal distributions (Briggs, 1977b; Till, 1985). As such, these populations are transposed onto the Phi (ϕ) scale, precluding the need for normalising data (Briggs, 1977b). An overview of sediment classes and associated Phi (ϕ) scale values is provided in Table 13 of APPENDIX E. The central tendency of distributions was determined using Phi (ϕ) median (average particle size) and Phi (ϕ) mean (arithmetic average particle size) values (Briggs, 1977b). Scatter of distributions were determined with Phi (ϕ) skewness, kurtosis and sorting (Briggs, 1977b). Phi (ϕ) skewness is used to determine a coarse tail (negative skewness) or a fine tail (positive skewness) and Phi (ϕ) sorting is an indication of the dispersion of the distribution (Briggs, 1977b). Equations used to achieve each value are given in Table 13 and an overview of class descriptions are given in Table 14 (sorting indices) and Table 15 (skewness classes) of APPENDIX E.

**Table 13: Equations used during particle size analyses (Briggs, 1977a).**

| Parameter/Attribute | Equation |
|---|---|
| Phi (ϕ) mean | $\overline{\phi} = \frac{\phi 75 + \phi 50 + \phi 25}{3}$ |
| Phi (ϕ) skewness | $\frac{(\phi 84 - \phi 50)}{(\phi 84 - \phi 16)} - \frac{(\phi 50 - \phi 10)}{(\phi 90 - \phi 10)}$ |
| Phi (ϕ) sorting | $\frac{(\phi 84 - \phi 16)}{2}$ |

In addition to Phi (ϕ) sorting the uniformity coefficient ($C_u$) provides a measure of how sorted a sample is and is calculated using Equation 13 (pg. 108). Sediment where $C_u$ is less than 4 is well sorted. In comparison, a value of > 6 represents poorly sorted sediment. The coefficient gives an indication specific of geomorphic processes. For example, glacial deposits tend to have high $C_u$ values, whereas fluvial sediment will have a low $C_u$ values (Briggs, 1977b). The level of vertical sorting between pairwise textural fractions was determined using the sorting index (S) (Ballantyne and Matthews, 1983), and calculated using Equation 14 (pg. 108). This index is useful for gaining insight into the depth of freeze-thaw cycles using a proxy, such as textural fractions, for the frost cycle. An index of 0.0 reflects perfect sorting; an index of 1.0 reflects no sorting, and an index exceeding 1.0 indicates one sample deficient for that specific textural fraction compared to the comparison sample (Grab, 1997a).

**Equation 13: Uniformity coefficient ($C_u$) equation. $d_{60}$ denotes the grain size for which 60% of the sediment is finer by weight; $d_{10}$ denotes the grain size for which 10% of the sediment is finer by weight.**

$$C_u = \frac{d_{60}}{d_{10}}$$

**Equation 14: Method of calculating the sorting index (S) for pairwise textural fractions (Ballantyne and Matthews, 1983).**

$$\mathrm{S} = \frac{\%\ of\ weight\ of\ textural\ fraction\ of\ sample\ X}{\%\ of\ weight\ of\ textural\ fraction\ of\ sample\ Y}$$

#### *4.5.2.3 Modelling the diurnal frost environment*

Freeze-thaw cycles are largely influenced by air temperatures (Adlam *et al.*, 2009; Schoeneich, 2011), with reference also given to moisture availability. Wind speed (*ws*) is correlated to freeze-thaw cycles (Adlam *et al.*, 2009; Hansen, 2014), as are soil properties with loamy soils most suited to frost cycles (Osterkamp and Burn, 2003). Vegetation cover (*veg*) is also an important consideration. Frost cycles *(FTC)* are, therefore, a function of temperature (*temp*), moisture (*m*), wind speed (*ws*), soil properties (*soil*), and time (*t*). As such, a simple representation of a freeze-thaw cycle model, using available literature, can be developed. Assumptions to such a model are that landforms develop due to nonlinear and dynamic systems. Furthermore, time is the only independent factor (Phillips, 1997). However, temperature, moisture, and soil properties are not sufficient to explain all variability within the frost environment and locally important factors (*n…*) should also be considered. The state-factor model can then be written as a nonlinear dynamical system, as depicted by Equation 15. Additional locally important factors were determined during the study following statistical and geostatistical analysis.

**Equation 15: A simple freeze-thaw cycle model. FTC: frost cycles; temp: air temperatures, m: soil moisture, ws: wind speed, soil: soil properties, veg: vegetation, n…: locally important factors, and t: the independent variable of time.**

$$\frac{dFTC}{dt}, \frac{dtemp}{dt}, \frac{dm}{dt}, \frac{dws}{dt}, \frac{dsoil}{dt}, \frac{dveg}{dt}, \frac{dn\ \ldots}{dt} = f(temp, m, ws, soil, veg, n\ \ldots)$$

## 4.6 Geographical Statistics and Modelling

Geographical Information Systems (GIS) were used for spatial data modelling. Supplementary data, such as aerial imagery, cloud cover and vector data, were obtained from the South African Council of Geoscience (CGS), National Geo-Information (NGI), Moderate Resolution Imaging Spectroradiometer (MODIS), the Scientific Committee on Antarctic Research (SCAR) Antarctic Digital Database (ADD), and Quantarctica. Raw data, collected during fieldwork, were spatially interpolated using Inverse Distance Weighted (IDW) and Universal Kriging to determine the extent and distribution of frozen ground across the various study sites. Furthermore, each site surrounding each logger was investigated in terms of geomorphological landforms characteristic of diurnal frost environments. Large-scale landforms, such

as sorted circles, stone rings, ice-wedge polygons and contraction cracks were identified using GIS, if the landforms were sufficiently large enough. Digital Elevation Models (DEMs) were used to identify solifluction lobes using a topography analysis algorithm and tool in GIS. Small-scale landforms, such as needle ice, patterned ground and ice lensing were identified in the field and a record made of these. However, these data are limited in terms of when site visits were possible. Table 14 provides an overview of geostatistical methods employed and a short description thereof. The remainder of this subsection provides a detailed explanation of each method used.

**Table 14: Inferential statistical methods employed during Geographical Information Systems (GIS) analyses.**

| Investigation | Method |
|---|---|
| Identifying topographic control on observed ground temperatures | GWR, Model Builder, Identity |
| Identifying cloud cover and albedo on observed ground temperatures | Identity, Zonal Statistics |
| Interpolating elevation points across the study sites to create DEMs | IDW |
| Interpolating ground temperature values for all depths for each study site | Universal Kriging |
| Interpolating ground moisture values for all depths for each study site | Universal Kriging |
| Interpolating distribution of diurnal frost environments across the study area | Universal Kriging |

Geographical Information Systems (GIS) provide a powerful platform for creating, storing, manipulating and analysing data. They allow for the statistical exploration of spatial data and their visualisation and display (Burrough, 2001). Exploratory Spatial Data Analysis (ESDA), such as means, deviations, ranges and correlations were applied when conducting spatial data analysis. Histograms, Quantile-Quantile (QQ) plots, trend analyses, semi-variance/covariance clouds were determined using ESDA. These tools all form part of the Geostatistical Analyst toolbar in ArcMap® 10.5. In addition, Confirmatory Spatial Data Analysis (CSDA) was used for the testing of hypotheses (Burrough, 2001). GIS were utilised to spatially extrapolate the data collected to a larger area. These extrapolation values, when compared to field measurements, were used as data control points, giving a good indication of the accuracy of the analysed and calculated data points. Before data is interpolated, ESDA is calculated for the specific parameters. Histograms and QQ plots were used to determine the shape of the various distributions. This was done in addition to, and to confirm, results of classical statistical analyses, described in 4.5 Statistical Analyses (pg. 99). The histogram provides a visual representation of the shape, median, mean, skewness and kurtosis of the data. The QQ plot compares the cumulative distribution of the data to a theoretical model (normal distribution). If the data are plotted on a straight line, they follow the theoretical distribution. The semi-variogram/covariance cloud tool plots the empirical semi-variogram for paired sample locations on a graph and was used to determine the lag size to a data set. The empirical semi-variogram provides information on the spatial autocorrelation of the datasets that allows the user to subsequently fit the data to the correct empirical semi-variogram (Chang, 2012). Trend analysis was used to identify inherent trends to datasets. If no trend is apparent the projected

trend line of the graph approximates a horizontal/flat line; if a trend exists the line is drawn with a curve (Chang, 2012).

Depending on the result of ESDA, data were spatially interpolated using IDW (no trend) or Universal Kriging (inherent trend/bias). Inverse Distance Weighted (IDW) is a deterministic (exact) interpolation technique that estimates cell values in a raster from a set of sample points: the further an input point is from the cell being calculated, the less influence or weight it has on the value of that cell (Chang, 2012). Calculated values are the average of nearby points and the search radius was set to variable (n = 12), ensuring the same number of input points was used for the calculation of each raster cell. The power k was set to two, as the rate of change was set to be higher near sample points than further away (Chang, 2012). This interpolation technique was used for interpolating altitude values across study sites to create DEMs. The Solar Radiation function was used to calculate incident solar radiation for each logging site on an annual and seasonal scale. The zonal statistic function was then used to summarise freeze-thaw cycles values within slope zones, reporting the results as a table of statistics. This table was used to determine differences in freeze-thaw cycles values per slope and radiation zones; to identify possible control of these parameters (such as snow cover) to calculated freeze-thaw cycles.

Universal Kriging allows for local variation as opposed to global variation, increasing the accuracy of predicted points (Miller, 2012). Kriging is a geostatistical interpolation method, which incorporates autocorrelation in its calculations. It uses the least squares regression predictor (variance-covariance matrix) and a non-stationary mean to predict unknown values (Atkinson, 2001). Furthermore, stochastic and deterministic elements are incorporated (Chang, 2012). As such, this method was used for spatially interpolating near-surface ground temperatures. The method was employed to not only determine topographic (micro-relief) influences on recorded temperatures, but also to spatially interpolate frozen ground across the study sites. Assuming topographic control on recorded ground temperatures, positive spatial autocorrelation should occur. Points on the associated Moran scatterplot will reflect a straight line, sloping from the lower left corner to the high right-hand corner. If the scatterplot reflects a random pattern, negligible spatial autocorrelation is present (Griffith, 2005). In addition to spatially interpolating data, Kriging creates a prediction surface as well as giving an indication of the accuracy of the prediction (the error of interpolation or Kriging error) (Burrough, 2001; Chang, 2012). Furthermore, it allows for determining propagation of error, making it a powerful geostatistical interpolation technique (Burrough, 2001). Assuming these errors are normally distributed, there is a 95.5 % probability that the value predicted is the actual real-world value, plus/minus two times the square root of the value ($\pm 2\sqrt{x}$). Kriging fits a mathematical model (variography) to the number of input points specified within the search radius (Burrough, 2001), to determine the predicted raster cell value. The semi-variogram measures the spatially correlated component, with samples furthest apart having large semi-variances (Chang, 2012). To conduct Kriging, a spherical semi-variogram was used to fit a curve to the empirical semi-variogram. The spherical model is used to model a continuous decrease in spatial dependence until a threshold is reached, where autocorrelation remains level (Chang, 2012). The nugget (semi-variance at a distance of zero), range (the distance at which the semi-variance threshold is reached) and sill (threshold level) are required as inputs to Kriging (Chang, 2012), and were determined using GIS. In addition, a variable search radius

was used ensuring the same number of input points was used for the calculation of each raster cell. Finally, Universal Kriging was selected as the preferred method for interpolating near-surface temperature dynamics as it assumes an inherent overriding trend (linear with quadratic drift) within the dataset. Furthermore, it uses a non-stationary mean and a covariant structure that varies with location (Atkinson, 2001; Miller, 2012). In addition to spatially interpolating near-surface soil temperature regimes, the *'Identity'* tool was used to determine possible spatial relationships between datasets. The *'Identity'* tool overlays attributes of specified layers at a specific location. This enables the identification of similarities in attributes for sample points.

In addition to spatially interpolating near-surface soil temperature regimes, GWR was computed to determine possible spatial relationships between datasets. Geographic weighted regression (GWR) allows for the exploration of the relationships between processes and driver variables in terms of their spatial variation (Atkinson *et al.*, 2003; Charlton *et al.*, 2006), and follows a non-parametric approach (Brunsdon *et al.*, 1998). It applies weighted least squares with autocorrelation (Charlton *et al.*, 2006). This technique was employed to determine the impact of the various climate and topographical parameters on soil temperature regimes. Geographic weighted regression (GWR) uses the local window approach (Atkinson *et al.*, 2003), to determine local regression coefficients as opposed to global regression coefficients (Atkinson, 2001; Miller, 2012). Assumptions made in GWR are described by Atkinson (2001) and Charlton *et al.* (2006) and are as follows:

1) There may be some variables with a low spatial frequency that will not have been measured;
2) The dependent variable is affected by too many variables to be able to model it accurately; and
3) The nature of the relation between data points varies over space.

The result is a surface of over- or under-prediction of the spatial relationships. Geographic weighted regression (GWR) assumes that over- and under-predictions will be randomly distributed when all required parameters have been correctly identified. When over- and under-predictions cluster together on the map, not all parameters have been sufficiently identified (Propastin *et al.*, 2008). This implies that parameters incorrectly excluded or included in the analyses will be indicated by the clustered nature of the output map (Miller, 2012). The exponential weighted function, as studies have shown *(e.g.* Atkinson *et al.*, 2003), most closely approximates physical properties in geomorphology. In addition, the Gaussian error term is most commonly used in GWR (Charlton *et al.*, 2006). The exponential function with a Gaussian error term was, therefore, applied to the study. Furthermore, a univariate as opposed to multivariate model was used since the focus was not on prediction (Atkinson *et al.*, 2003). Geographic weighted regression (GWR) also requires a weighting scheme (Charlton *et al.*, 2006). To determine the relative weights of each input parameter, a correlation matrix was established using classical statistics and each parameter weighted accordingly. Soil temperature was selected as the dependent variable and climate parameters as independent variables. An adaptive kernel method was used when running the model. This is like the variable search radius of Kriging.

Finally, spatial datasets were uploaded to ArcGIS Online, providing an interactive map of frost environments for potential researchers and users. This map provides not only an overview of the entire study area, but also relevant details of each logging site. Details include geographical information (latitude, longitude m a.s.l.), state *(e.g.* relict/active), spatial characteristics *(e.g.* extent, perimeter), and other relevant information. Details on the ArcGIS Online map URLs are provided in Table 19 of APPENDIX I. Finally, the underlying data for the online map are available as a series of Excel™ spreadsheets. A summary of this spreadsheet is provided in Table 22 in APPENDIX I.

# CHAPTER 5: Results

This chapter provides an overview of results and is divided into three parts comprising the three separate study regions of the Eastern Cape of mainland South Africa, sub-Antarctic Marion Island, and Dronning Maud Land (DML) of Antarctica. Where necessary these subsections are further subdivided.

A variety of statistics and indices were calculated and these are described in detail in 4.5.2.3 Modelling the diurnal frost environment (pg. 108 onwards). Statistics and indeces calculated, their method of calculation, a short description, as well as symbols used for each idex/statistic are also provided in Table 15 below. Calculations apply to annual time scales, as well as seasonal and diurnal time scales. Seasons referred to apply to the Austral seasons, *i.e.* winter (June-August), spring (September-November), summer (December-February), and autumn (March-May).

**Table 15: Calculations for determining annual, seasonal and diurnal ranges and means. * methods of the World Meteorological Organisation.**

| Symbol | Calculation | Equation |
|---|---|---|
| DD | Degree Days | $\Sigma T_{DM:\text{ ground temperature}} - T_{DM:\text{ air temperature}}$ |
| FI | Freezing Index (calculated for winter months) | $\Sigma T_{DM< 0\,°C \mid \text{winter}}$ |
| GFI | Ground Freezing Index (calculated on an annual basis) | $\Sigma T_{DM:\text{ GST}}$ |
| $Prec_{DM}$ | Diurnal Mean Precipitation | $\Sigma Precipitation_{DM}/24$ |
| $RH_{DM}$ | Diurnal Mean Relative Humidity | $\Sigma Relative\ Humidity_{DM}/24$ |
| SO | Thermal Offset (comparing air temperatures with ground surface temperatures) | $\Sigma(NST-T_{AIR})$ |
| $T_{AM}$ | Annual Mean Temperature | $\Sigma T_{MM} / 12$ |
| $T_{D:max}$ | Maximum Diurnal Temperature | n/a |
| $T_{D:min}$ | Minimum Diurnal Temperature | n/a |
| $T_{DM}$ | Diurnal Mean Temperature | Hourly observations available *: $\Sigma T_D / 24$<br>Hourly observations not available: $(T_{D:min}+T_{D:max})/2$ |
| $T_{DR}$ / TSI | Diurnal Range / Thermal Stress Index | $T_{D:max}-T_{D:min}$ |
| TI | Thawing Index (calculated for summer months) | $\Sigma T_{DM:> 0\,°C \mid \text{summer}}$ |
| $T_{MM}$ | Monthly Mean Temperature | $\Sigma T_{DM}$ / days of the month |
| $T_{SR}$ | Seasonal Temperature Range | $T_{MM:Jan} - T_{MM:July}$ |
| $WD_{DM}$ | Mean Diurnal Wind Direction | $\Sigma Wind\ Direction_{DM}/24$ |
| $WS_{D:max}$ | Maximum Diurnal Wind Speed | n/a |
| $WS_{D:min}$ | Minimum Diurnal Wind Speed | n/a |
| $WS_{DM}$ | Mean Diurnal Wind Speed | $\Sigma Wind\ Speed_{DM}/24$ |

## 5.1 Eastern Cape

A detailed description of locations within the Eastern Cape of South Africa is given for Ben MacDhui on pg. 83 and the Elandsberg on pg. 85. Similarly, an overview of temperature and moisture sensor depths, and their respective identifiers, is given in 4.3.1 Ground temperature and moisture data (pg. 80). However, for ease of reference, site and sensor identifiers are briefly described here. Five temperature monitoring stations were erected on the slopes of Ben MacDhui and given the identifiers T1 (at highest attitude) to T5 (at lowest altitude). Seven temperature monitoring stations were erected on the Elandsberg and given the identifiers E1 (at highest attitude) to E7 (at lowest altitude). Sensors are identified using a combination of 'T' (temperature) and a subscript number, *e.g.* '5', indicating the depth of the sensor within the ground, measured in centimetres. For example, '$T_5$' represents data obtained from temperature sensors that were buried at a depth of five centimetres (5 cm) within the ground. Near surface temperatures (NST) are recorded at ± 1 cm in the ground; ground surface temperatures (GST) at ± 2 cm in the ground. A Table of Abbreviations is available on pg. xxxiii, with a Table of Symbols on pg. xxxvi.

### 5.1.1 Climate and locational parameters

Two study locations are found in the Eastern Cape of South Africa. Ben MacDhui has the highest elevation (± 3 000 m a.s.l.), and located in the High Drakensberg of the Eastern Cape (Figure 3, pg. 28). The Elandsberg is found just north of Hogsback, extending to an elevation of ± 2 000 m a.s.l. (Figure 3, pg. 28). There is no South African Weather Service (SAWS) station for Ben MacDhui, nor for the Elandsberg. However, climatic data, obtained from PACE XR5 logging stations, are available for T1 (Ben MacDhui), as well as for air temperatures at E3 (Elandsberg). Data from the nearest SAWS station at Aliwal North (for Ben MacDhui) and Fort Beaufort (for the Elandsberg) were used to determine mean annual air temperature (MAAT) for the two sites, to compare recorded air temperatures to extrapolated MAAT using the environmental lapse rate of 6.5 °C.km$^{-1}$. Furthermore, averages for 15 years of climatic data for relative humidity, air temperatures, wind speed, wind direction and precipitation were calculated for these SAWS stations. While averages do not apply specifically to Ben MacDhui nor the Elandsberg, they serve as an indication (providing the warmer temperature limit) for the expected weather for these two areas. Averages for Aliwal North are provided in Table 16. Averages for Fort Beaufort are given in Table 18 (pg. 117).

**Table 16: Climatic variables for Aliwal North from 2000-2015. All values represent diurnal averages, maximums and minimums for each parameter. Prec indicates precipitation (mm). RH reflects relative humidity (%), T indicates temperature values ( °C), WS indicates wind speed (m.s$^{-1}$), WD indicates wind direction (° off true north). DM indicates diurnal means (averages), with :min and :max indicating minimums and maximums.**

| Parameter | $Prec_{DM}$ | $RH_{DM}$ | $T_{D:min}$ | $T_{D:max}$ | $T_{DM}$ | $WS_{D:min}$ | $WS_{D:max}$ | $WS_{DM}$ | $WD_{DM}$ |
|---|---|---|---|---|---|---|---|---|---|
| Average | 1 | 56 | 6 | 24 | 15 | 1 | 5 | 3 | 175 |
| Minimum | 0 | 9 | -10 | 7 | 0 | 0 | 0 | 1 | 62 |
| Maximum | 35 | 90 | 20 | 38 | 27 | 6 | 12 | 6 | 312 |

The average diurnal mean minimum temperature of Aliwal North is 6 °C, with the average diurnal maximum temperature 24 °C. Ambient absolute minimum air temperatures reach -10 °C, while absolute maximum temperatures reach 38 °C. Mean annual air temperature (MAAT) is 15 °C, with the average wind blowing from the south (175°), with a standard deviation (*s*) of 35. While gusts of 12 $m.s^{-1}$ are recorded, the average diurnal wind speed is 3 $m.s^{-1}$ (Figure 49). Utilising the standard environmental lapse rate of 6.5 °C.$km^{-1}$ the average MAAT for Ben MacDhui ranges from 6.8 °C at T5, the site of lowest elevation, to 4.3 °C at T1, found at highest elevation (Figure 20, pg. 83). Mean annual ground surface temperature, recorded at ± 2 cm within the ground, for T1 and T4 are 6.2 °C and 7.3 °C respectively. However, extrapolated seasonal values do not always concur for seasonal MAAT recorded at T1 during the winter of 2014-2015 (Table 17).

**Table 17: Actual and extrapolated seasonal mean annual air temperatures (MAAT) for air temperatures at T1. $T_{AIR}$ reflects air temperature, measured in degree Celsius ( °C). JJA: winter. SON: spring. DJF: summer. MAM: autumn.**

| Season | Extrapolated $T_{AIR}$ | Actual $T_{AIR}$ |
|---|---|---|
| JJA | -1.7 | 0.8 |
| SON | 7.6 | 8.0 |
| DJF | 12.2 | 11.8 |
| MAM | 5.9 | 5.9 |

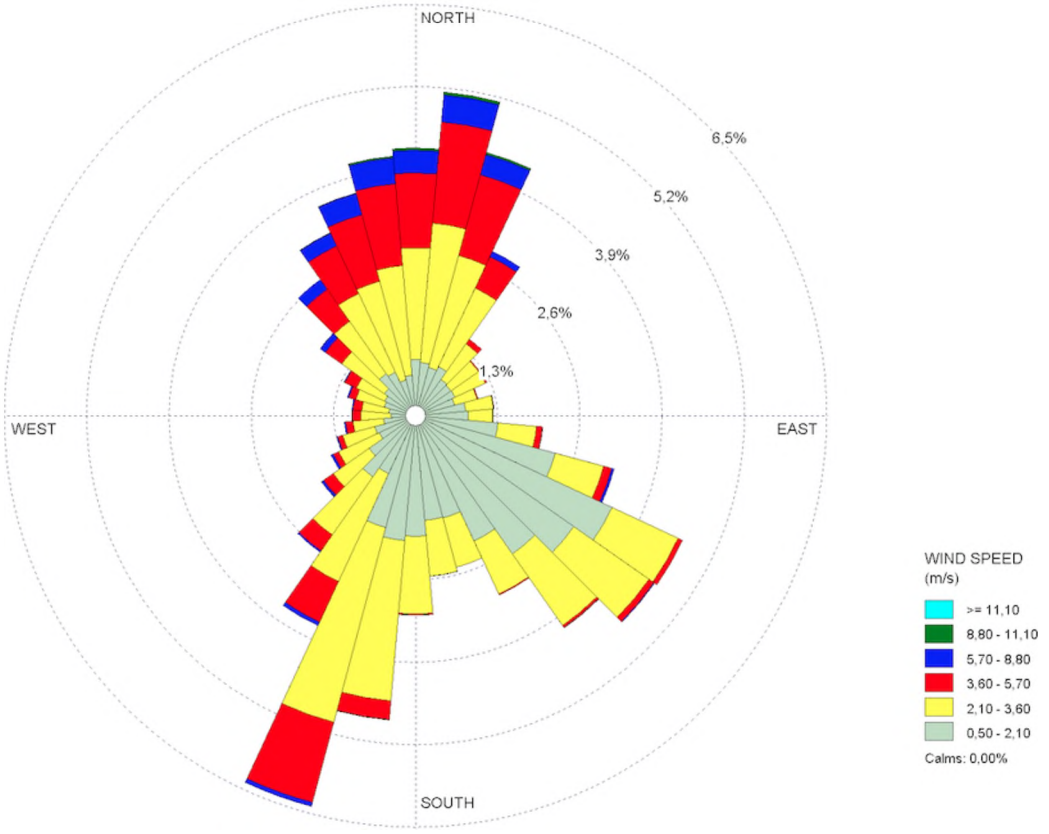


**Figure 49: Wind direction and average wind speed for Aliwal North. Interval: 1 hour; 2000-2015. Missing data: ± 1%.**

Wind measurements for T1 show a dominant southern wind (161°, *s* = 60), with average wind speeds of 3 $m.s^{-1}$. Calms are recorded ± 7% of the time (Figure 50). Wind gusts are on average twice as strong (> 6 $m.s^{-1}$) compared to the average wind speed (Figure 51, pg. 117), and stronger winds align themselves with the average wind speed direction. Peak wind gusts of 28 $m.s^{-1}$ are observed in November 2014 (Austral spring), yet more than half (± 54%) of winds exceeding 11 $m.s^{1}$ occur in winter (June-August). Gusts exceeding the required threshold for deflation to take place (wind speed > 5.4 $m.s^{-1}$) occur predominantly from June-September and November-January. Winter snowfall occurs for Ben MacDhui (*pers. obs.*) and can remain in place from a few days to a few weeks. Ambient air temperature and ground temperature at T1 show a MAAT of 6.6 °C and a MAGT of 5.4 °C. In comparison, data from Sani Pass from January 2004-2005 show MAAT of 5.8 °C and MAGT of 8.5 °C (Nel and Sumner, 2008).

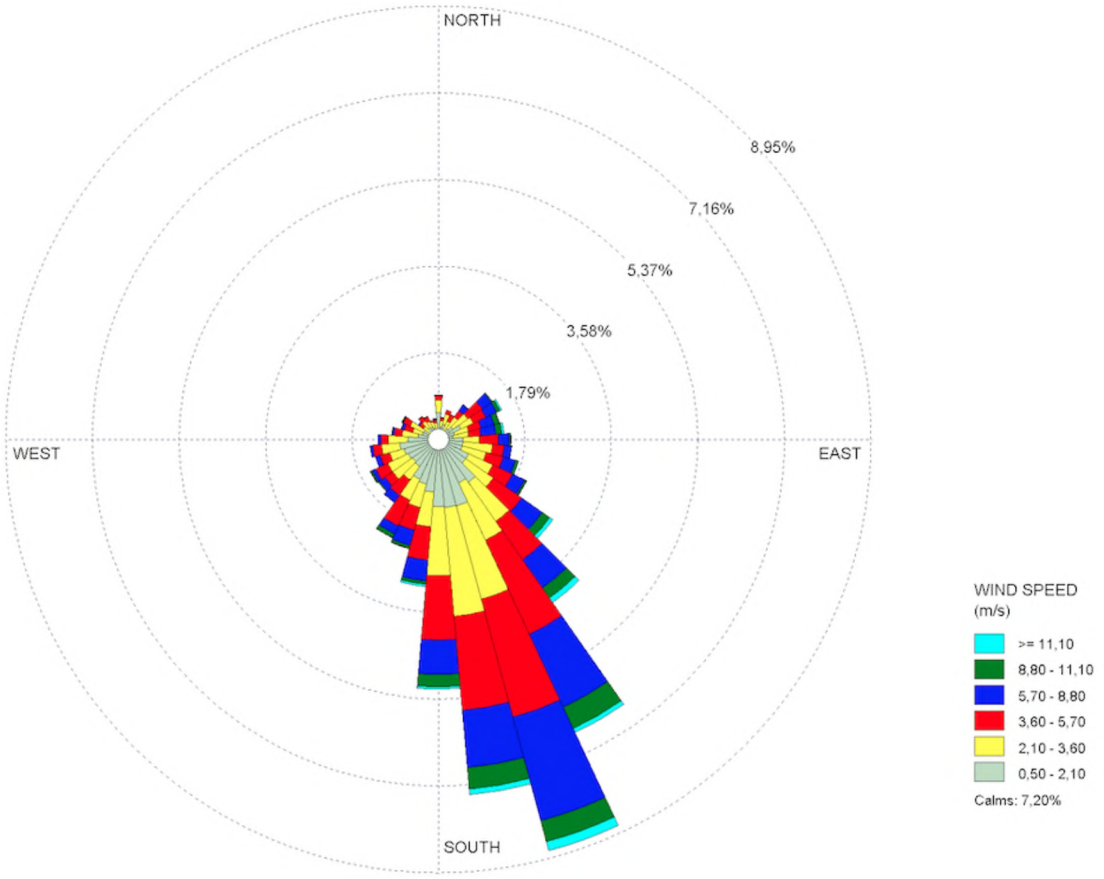


**Figure 50: Wind direction and average wind speed for T1 on Ben MacDhui. Interval: 1 hour; 2014-2015. Missing data: ± 20%.**

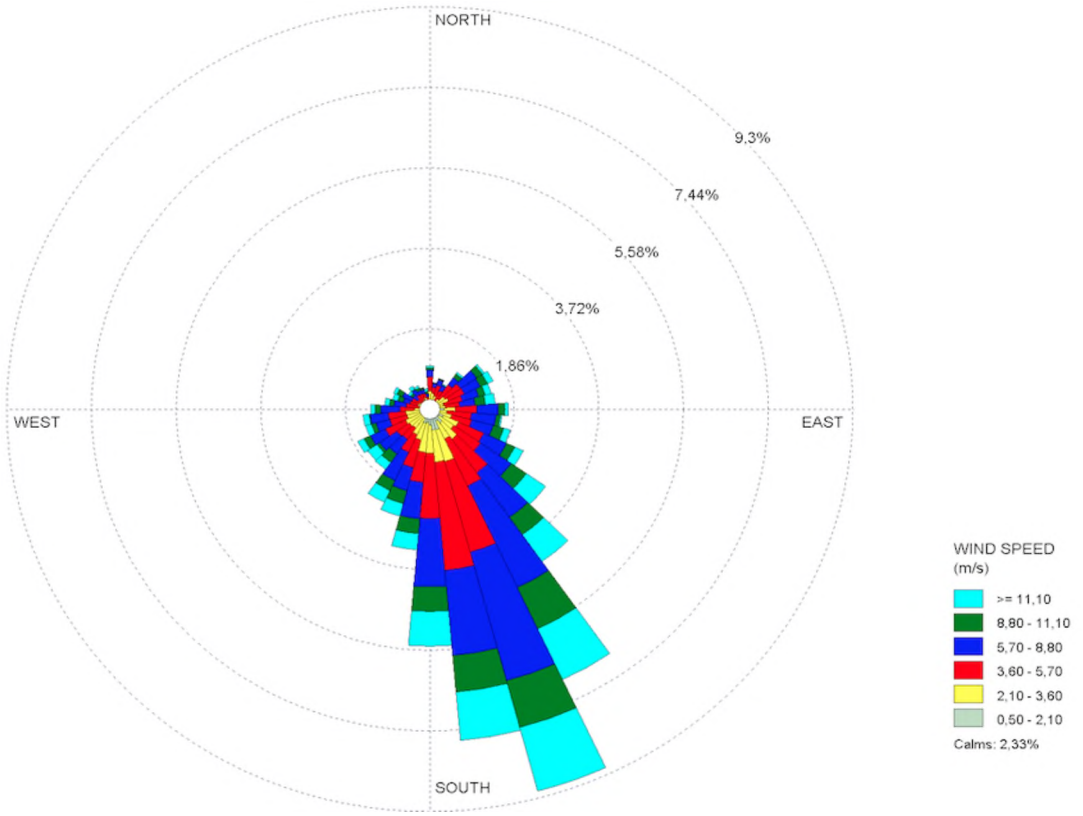


**Figure 51: Wind direction and maximum wind speed (gusts) for T1 on Ben MacDhui. Interval: 1 hour; 2014-2015. Missing data: ± 20%.**

Fort Beaufort has an average diurnal mean temperature of 12 °C and an average diurnal maximum temperature of 25 °C (Table 18). Ambient absolute air temperatures reach minimums of -2 °C, while temperatures of 45 °C are also observed. Mean annual air temperature (MAAT) is 18 °C, with an average southsouthwest wind (204°) and a standard deviation (*s*) of 35. While gusts of 17 $m.s^{-1}$ are recorded the average diurnal wind speed, like Aliwal North and T1 (refer to 5.1.2.3.1 T1, pg. 137), is 3 $m.s^{-1}$. Calms are recorded less than 1% of the time (Figure 52, pg. 118). Utilising the standard environmental lapse rate of 6.5 °C.$km^{-1}$ the average MAAT for the Elandsberg ranges from 11.4 °C at E7, the site at lowest elevation, to 7.5 °C at E1, at highest elevation. Mean annual ground surface temperature, recorded ± 2 cm within the ground, for E1-E6 range from 11.6-13.6 °C, with E7 having mean annual ground surface temperatures of 11.6 °C. Mean annual air temperature (MAAT) at E3 is 11.1 °C.

**Table 18: Climatic variables for Fort Beaufort from 2000-2015. All values represent diurnal averages, maximums and minimums for each parameter. Prec indicates precipitation (mm). RH reflects relative humidity (%), T indicates temperature values ( °C), WS indicates wind speed ($m.s^{-1}$), WD indicates wind direction (° off true north). DM indicates diurnal means (averages), with :min and :max indicating minimums and maximums.**

| Parameter | $Prec_{DM}$ | $RH_{DM}$ | $T_{D:min}$ | $T_{D:max}$ | $T_{DM}$ | $WS_{D:min}$ | $WS_{D:max}$ | $WS_{DM}$ | $WD_{DM}$ |
|---|---|---|---|---|---|---|---|---|---|
| Average | 1 | 64 | 12 | 25 | 18 | 1 | 6 | 3 | 204 |
| Minimum | 0 | 13 | -2 | 8 | 5 | 0 | 0 | 1 | 99 |
| Maximum | 47 | 93 | 24 | 45 | 31 | 6 | 17 | 10 | 354 |

Like temperature data from Ben MacDhui, extrapolated seasonal values do not concur for actual seasonal MAAT recorded at E3 from March 2015 to March 2016 (Table 19). Average temperatures are consistently higher than those determined using the environmental lapse rate of 6.5 °C.km$^{-1}$. The greatest difference between actual and calculated values is for summer (± 4 °C), with the least difference calculated for spring (±3 °C). The average difference between extrapolated and actual seasonal averages is 3 °C.

**Table 19: Actual and extrapolated seasonal mean annual air temperature (MAAT) for E3. T reflects temperature, measured in degree Celsius ( °C). JJA: winter. SON: spring. DJF: summer. MAM: autumn.**

| Season | Extrapolated T | Actual T |
|---|---|---|
| JJA | 3.8 | 7.1 |
| SON | 8.0 | 10.6 |
| DJF | 11.2 | 15.4 |
| MAM | 8.3 | 11.8 |

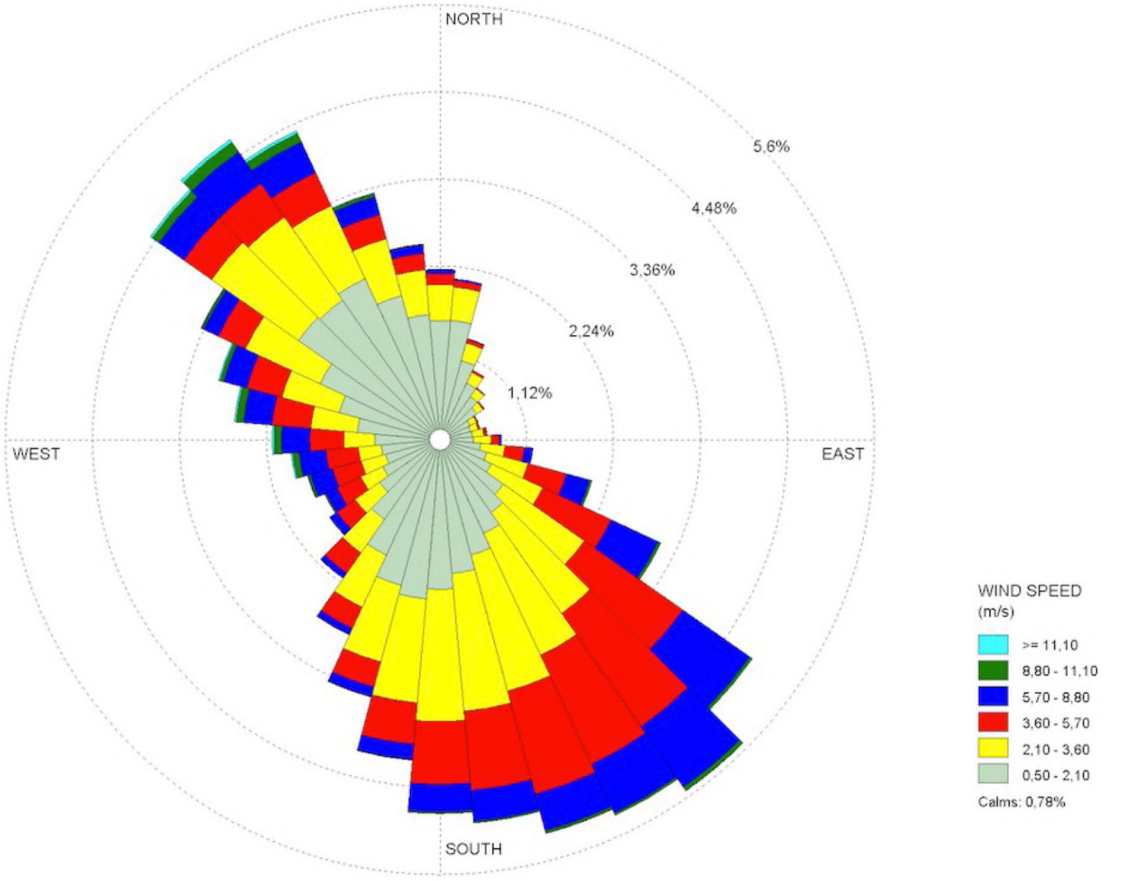


**Figure 52: Wind direction and average wind speed for Fort Beaufort. Interval: 1 hour; 2000-2015. Missing data: ± 1%.**

All locations in the Eastern Cape currently fall within the C*fb* classification of the Köppen-Geiger climate system (Kottek *et al.*, 2006). *Cfb* zones are characterised by warm, temperate, and rainy climates where the mean temperature of the coolest month is between 18 °C and -3 °C and the average temperature of the warmest month is below 22 °C. A detailed description of available climatic zonations are provided

in APPENDIX B. These systems are, furthermore, discussed in detail in CHAPTER 2: Background and Context (pg. 12 onwards). Data for the Eastern Cape show that, while all locations fall within the south temperate zone and the oceanic climate class (C) (average monthly temperatures above -3 °C and below 18 °C in the coolest month), the C*fb* class cannot be assigned to all sites. Data suggest that E3/Fort Beaufort and T1/Aliwal North are classified as *f* (precipitation occurs throughout the year) and *w* (dry winter months) respectively (Table 20). This agrees with the marginal, yet dry, periglacial environment argued to occur for the Escarpment and summits of the High Drakensberg, with MAAT of 5.8 °C at Sani Pass and annual precipitation of less than 1 000 mm (Nel and Sumner, 2008). Finally, Aliwal North and Fort Beaufort are assigned to *a* (average temperature in the warmest month above 22 °C), with E3 to *b* (average temperature in the warmest month below 22 °C). T1, with only three months showing average temperatures above 10 °C, is assigned to *c* (fewer than four months above 10 °C), placing it in the sub-tropical highland variety of C. Furthermore, T1 potentially falls within the highland periglacial zone as described by Washburn (1979), as reflected by large diurnal temperature ranges and changes over short distances in altitude and aspect. It is noted that the provided climatic conditions should be considered with caution. The temperature series recorded at T1 and E3 spans one calendar year, whereas Aliwal North and Fort Beaufort reflect 15 years of data. None of these time spans are sufficient for a climatic classification to be made. Nevertheless, the temperature averages calculated reflect expected weather conditions and can, thus, be used as a proxy for climate in this instance.

**Table 20: Average monthly air temperature, given in °C, for Aliwal North (15-year averages), Fort Beaufort (15-year averages), T1 (Ben MacDhui, 1-year averages), and E3 (Elandsberg, 1-year averages). Climatic zones are indicated in brackets.**

| Month | Aliwal North (C*wa*) | T1 (C*wc*) | Fort Beaufort (C*fa*) | E3 (C*fb*) |
|---|---|---|---|---|
| Jan | 22 | 13 | 22 | 17 |
| Feb | 21 | 12 | 22 | 16 |
| Mar | 19 | 10 | 21 | 15 |
| Apr | 14 | 6 | 18 | 10 |
| May | 11 | 5 | 16 | 11 |
| Jun | 6 | 1 | 14 | 6 |
| Jul | 7 | 0 | 13 | 6 |
| Aug | 10 | 2 | 15 | 10 |
| Sep | 14 | 8 | 16 | 10 |
| Oct | 17 | 8 | 18 | 14 |
| Nov | 19 | 8 | 19 | 11 |
| Dec | 21 | 12 | 21 | 16 |

On Ben MacDhui low tufts of grass are found near T1 and T4, with denser vegetation found near T2 and T3. Sparse grass cover and low shrub are present near T5. Evidence of frost heaving and thrusting (vertical and horizontal frost sorting), needle ice (friable surfaces) and turf banked lobes is present near T1-T4, suggesting the area to be frost active. T3 shows a sorting depth of 15 cm, with finer particles found within the first 15 cm of the ground and larger clasts found beneath this depth (*pers. obs.*). T2 and T3 are characterised by vegetation banked lobes and terracettes with sorting in evidence for the near surface. The area around T5 exhibits less frost action, with no evidence of needle ice observed and

an absence of vertical sorting. However, minimal lateral sorting is found in the area. Soil depth is variable for Ben MacDhui with depth at T1 ranging from 5-10 cm. T2 and T2 have soil depths of 30 cm and greater than 30 cm respectively, with soil at T3 moist and clayey. T4 is generally drier than T2 and T3, as observed during field visits. This is ascribed to drainage lines present in this area, as well as shallower soils of ± 20-25 cm. T5 reflects the shallowest soil depth of 2-10 cm.

Occasional snowfall occurs for the Elandsberg during winter, blanketing the ground from a few hours up to a few days (*pers. obs.*). In comparison to Ben MacDhui the Elandsberg is also more densely vegetated. E1 and E2 are characterised by low dense grass cover, with grasses increasing in height and the introduction of shrub and herbs occurring as sites decrease in elevation. Needle ice is evident for the area around E1-E3, where there is an absence of vegetation. A portion of ground near E3, which had been cleared of vegetation, showed evidence of frost heave after a cold spell. Nevertheless, no evidence of frost action is visible for E4-E7 and no frost action is evident for the entire area, wherever the ground is vegetated. Recolonisation by vegetation of cleared areas is also rapid (complete recolonisation within six months of clearance). Elandsberg soil depth and concomitant rooting depth exceeds 15 cm for all sites and field observations show high organic content of soils (humic soils).

Soil ice, in the form of needle ice, vegetation-banked lobes and terracettes, as well as patterned ground have been documented by Kück (1997) on the slopes of Ben MacDhui. These have also been noted on numerous occasions in the field. No other ground ice (segregated ice, ice veins, ice wedges) are found. Nevertheless, in addition to landforms documented by Kück (1997), several periglacial features and landforms were recorded during field visits that were not yet mentioned in literature (Table 21, pg. 121). On the slopes of Ben MacDhui, needle ice was observed down to an altitude of 2 600 m a.s.l., with frost sorting to an elevation of 2 500 m a.s.l. This is evidenced by lateral and vertical sorting of particles and the limiting of vegetation cover by frost action. The thick and frost-undisturbed vegetation downwards from 2 500 m a.s.l. suggests that frost action below this elevation is negligible, such that it is not sufficient to affect vegetation growth, agreeing with findings by Borg (2017). Turf exfoliation is noted for the High Drakensberg and such features were observed for the lower slopes of Ben MacDhui, as well as numerous terracettes (vegetation-banked lobes) at 2 940-2 960 m a.s.l. Furthermore, numerous stone lobes are located on the southward facing slope of Ben MacDhui near T3 (± 2 750 m a.s.l.). No undocumented distinct periglacial features are recorded for the Elandsberg. Evidence of needle ice was observed at E3 (end of May 2014), where vegetation had been cleared. However, thick vegetation cover precludes transient frost-related features and landforms. The bowl of the Elandsberg is characterised by block deposits. However, these are considered relict and not affected by the current climate and contemporary frost processes (Sumner and de Villiers, 2002). Periglacial features not previously indicated in the literature are provided in Table 21 (pg. 121). An overview of landforms extracted from literature and those observed in the field is given in Figure 53 (pg. 122). Images taken of landforms during field visits are provided in Table 23 (APPENDIX I).

**Table 21: Observations not reflected in the literature that were recorded during field visits to the Eastern Cape study area. Altitude is measured in meters above sea level (m a.s.l.).**

| Feature | Location | Altitude | Active/Relict |
|---|---|---|---|
| Frost sorting | Ben MacDhui | > 2 500 | Active |
| Needle ice | Elandsberg | 1 800 | Active |
| Stone lobe | Ben MacDhui | 2 750 | Relict |
| Turf exfoliation | Ben MacDhui | 2 600 | Active |
| Vegetation-banked lobes | Ben MacDhui | 2 940-2 960 | Active |

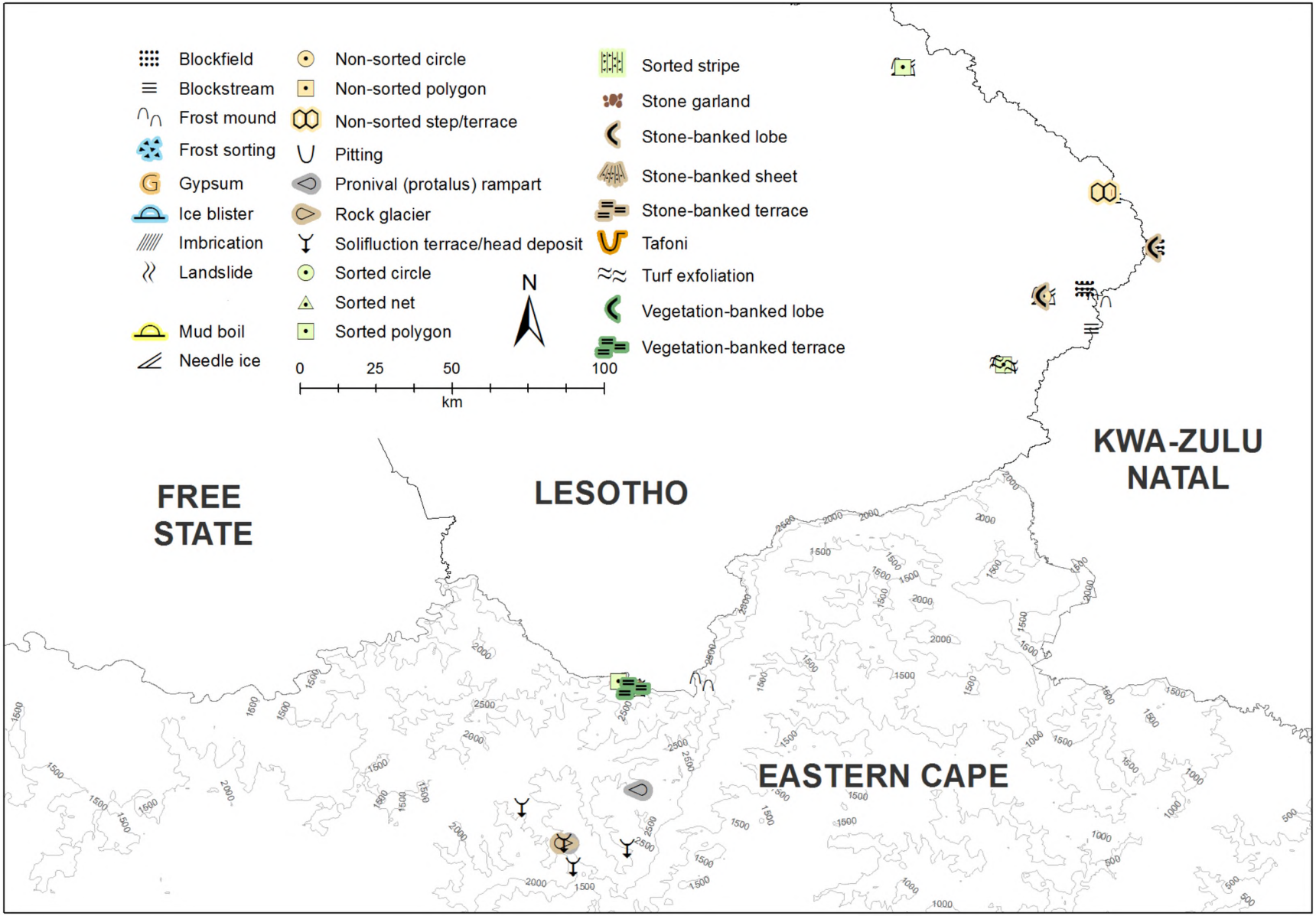


**Figure 53: Consolidated landforms observed for the Eastern Cape region.**

### 5.1.2 Ground thermal dynamics

Ground thermal dynamics are discussed with a reference to the annual, seasonal and diurnal environment. All times indicated are based on South African Standard Time (SAST; GMT+2) and represent approximations (± 1 hour). Indices, such as the freezing index (FI), thawing index (TI), ground freezing index (GFI), and thermal offset (SO) are most suited to describing an active layer and permafrost driven environment. While the Eastern Cape has neither, the use of these indices allows for a comparison to Dronning Maud Land (DML) sites. Due to sporadic data loss, not all annual calculations are possible for T2, T3 & T5. Elandsberg sites exhibit minimal data loss.

#### *5.1.2.1 Annual frost environment*

Mean annual ground surface temperatures (MAGT), reflecting mean ground temperatures recorded at ± 2 cm within the ground, show that all Eastern Cape sites, even at highest elevations, occur in a non-permafrost zone. Mean annual ground surface temperature (MAGT) is lowest for T1 (5.4 °C) and highest for E6 (13.6 °C), with Ben MacDhui sites having MAGT of ± 6 °C on average, and those for the Elandsberg ± 11 °C. Permafrost is entirely absent and the area is characterised by occasional freeze-thaw cycles during colder months. Ben MacDhui experiences short-term freezing of the ground on a scale of a few days to a couple of months; the Elandsberg shows minimal sub-zero temperatures. Mean annual ground surface temperatures (MAGT) decrease with an increase in elevation for both Ben MacDhui and the Elandsberg. Furthermore, variability of MAGT is similar for Ben MacDhui (standard deviation: *s* ± 7.5), as well as the Elandsberg (*s* ± 5.7). The exception is E7, which has a standard deviation (*s*) of ± 4.4. Mean annual ground surface temperatures (MAGT) increase from T1-T4 (5.5 °C-7.1 °C). Similarly, MAGT increase for E2-E6 (9.7 °C -13.6 °C). E1 registers higher MAGT of 11.6 °C.

At T1 on Ben MacDhui moisture levels are low, even absent, during winter although the ground is frozen down to a depth of 5-10 cm at T1 and T2 when snowfall occurs before the freeze event (*pers. obs.*). The ground at depth (10 cm) also remains frozen for the longest duration during winter and an increase in thawing events towards spring yields ground that is saturated with the lower levels still frozen. From 2 750-1 800 m a.s.l. inactive periglacial features exist (Lewis, 2008b). While potential freeze-thaw events occur at T1-T5 and E1, E2 & E5, freeze-thaw cycles are only evident for the highest elevations and none are observed for ground surface temperatures (GST) from T5-E7 (2 604-1 397 m a.s.l.). All Ben MacDhui sites exhibit ground freezing, with T1 having the greatest proportion of frozen hours of any site (Table 22, pg. 124), as well as seasonal freezing. This site also has the longest continuous frozen event at a depth of 10 cm lasting ± 2 months from June-August 2014. The number of frozen hours also increases with depth at T1, with the near surface showing the shortest duration and smallest percentage of frozen hours compared to the 10-cm depth.

**Table 22: Seasonal ranges ($T_{SR}$) and frozen period (hours, percentage and longest duration in days) for T1, T3 & T4 for 2014-2015. * insufficient data available. $T_{AIR}$ reflects air temperature; GST indicates temperature recorded at the ground surface (± 2 cm). The subscript following 'T' indicates the depth of the sensor (in centimetres) used to record ground temperature.**

| Site | $T_{SR}$ | Frozen Hours | | | | Frozen Hours % | | | | Longest Frozen Period | | | |
|---|---|---|---|---|---|---|---|---|---|---|---|---|---|
| | | $T_{AIR}$ | GST | $T_5$ | $T_{10}$ | $T_{AIR}$ | GST | $T_5$ | $T_{10}$ | $T_{AIR}$ | GST | $T_5$ | $T_{10}$ |
| T1 | 14 | 1 074 | 1 792 | 1 663 | 1 804 | 12 | 20 | 19 | 21 | 3 | 28 | 54 | 58 |
| T3 | 15 | * | 1 146 | * | * | * | 13 | * | * | * | 14 | * | * |
| T4 | 15 | * | 543 | * | * | * | 6 | * | * | * | 2 | * | * |

Interannually temperatures sstabilises with depth and greatest variability is observed for GST (Figure 54, pg. 125). Variability, expressed as standard deviation (*s*), of temperatures recorded per sensor depth shows an increase in variability from air temperature to highest variability for GST. From GST downwards, the annual mean temperature increases and levels out, with variability becoming less with increasing sensor depth. The maximum diurnal temperature is also highest for GST and least for $T_{10}$ (35 °C vs. 19 °C). Furthermore, the seasonal range in temperatures for GST, $T_5$, and $T_{10}$ at T1 is 15.7 °C, 14.8 °C and 14.3 °C respectively. Sensors closer to the surface, therefore, show they greatest variability and variability decreases as annual mean ground temperatures increases. Annual mean air temperature is greater (warmer) than those recoded within the ground. At T1 the overall absolute minimum occurs for air temperatures (-13 °C), whereas the absolute maximum is observed for GST (35 °C). While temperatures reach 44 °C for near surface temperatures (NST), those temperatures recorded at ± 1 cm within the ground, these data are not considered in evaluating the diurnal environment due to extensive data loss experienced for this sensor. Comparing GST (Figure 55, pg. 125) across sites the highest temperature is recorded at T4 (56 °C) and the lowest at T1 (-8 °C). Sites show absolute temperature ranges exceeding 40 °C for GST, with the ranges increasing with a decrease in altitude. Due to logger malfunction the seasonal temperature range is only available for T1 (12.7 °C) and T3 (12.8 °C).

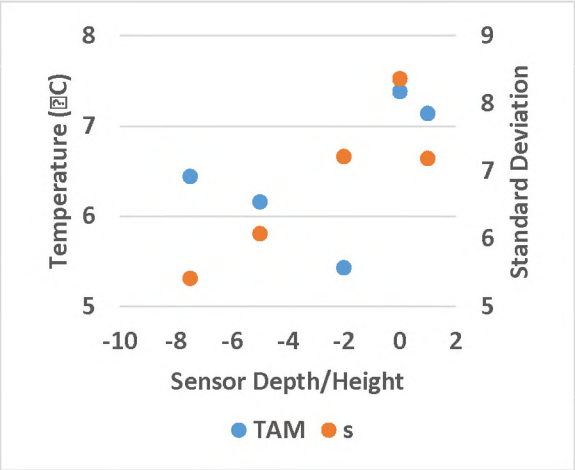


**Figure 54: Annual mean temperature ($T_{AM}$) and variability (*s*) per sensor depth for T1.**

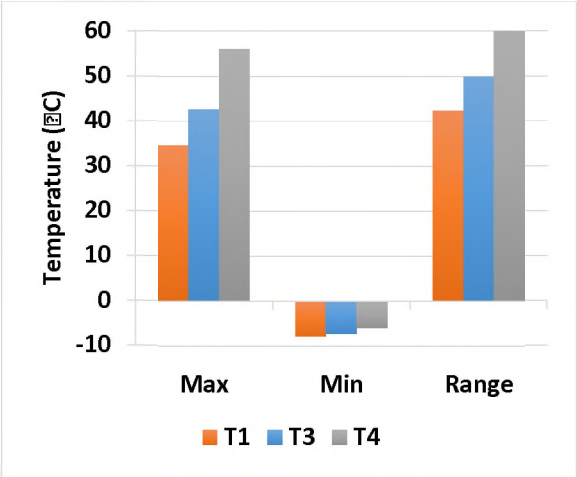


**Figure 55: Annual temperatures (maximums, minimums and ranges) for Ben MacDhui. Data gaps exist for T2 and T5. As such, T2 and T5 are not displayed here.**

At E3 in the Elandsberg ground moisture levels are elevated throughout the year. However, even during winter the ground is rarely frozen and sub-zero temperatures are only reached on isolated days, always in the early hours of the morning. For the entire observation period, spanning November 2013 to September 2015 for iButtons deployed at E1-E7, sub-zero temperatures were only reached at the depth of GST on 14 July 2015 between 05:00-08:00. Furthermore, only E1, E2 and E5 registered sub-zero temperatures. Data at E3 collected using an XR5 system show sub-zero temperatures achieved for air temperatures during winter months, as well as November, whereas all other sub-zero temperatures recorded for the other sensor depths occur exclusively during winter. Negative temperatures recorded for $T_5$ occur only on 14 July 2015 between 04:00-10:00. The longest frozen period for NST, GST, and $T_5$ are also observed on 14 July 2015 and even NST at E3, which reflect the longest continuous frozen period, shows ground frozen for less than one day (Table 23, pg. 126).

**Table 23: Seasonal ranges ($T_{SR}$) and frozen period (hours, percentage of the year, and longest duration in hours) for E1-E7 from 2013-2016. If more than one value is given within a column the first value represents 2013, the second value 2014, and the third value 2015. $T_{AIR}$ reflects air temperature; GST indicates temperature recorded at the ground surface (± 2 cm). The subscript following 'T' indicates the depth of the sensor (in centimetres) used to record ground temperature. * insufficient data available. # XR5 logging set-up, run 2015-2016.**

| Site | $T_{SR}$ | Frozen Hours | | | | | Frozen Hours % | | | | | Longest Frozen Period | | | | |
|---|---|---|---|---|---|---|---|---|---|---|---|---|---|---|---|---|
| | | $T_{AIR}$ | NST | GST | $T_5$ | $T_{10}$ | $T_{AIR}$ | NST | GST | $T_5$ | $T_{10}$ | $T_{AIR}$ | NST | GST | $T_5$ | $T_{10}$ |
| E1 | 12 | * | * | 0 \| 0 \| 4 | * | * | * | * | 0 \| 0 \| 0.05 | * | * | * | * | 0 \| 0 \| 4 | * | * |
| E2 | 13 | * | * | 0 \| 0 \| 3 | * | * | * | * | 0 \| 0 \| 0.03 | * | * | * | * | 0 \| 0 \| 3 | * | * |
| E3 | 12 | * | * | 0 \| 0 \| 0 | * | * | * | * | 0 \| 0 \| 0 | * | * | * | * | 0 \| 0 \| 0 | * | * |
| E3# | 13 | 162 | 88 | 31 | 7 | 0 | 1.85 | 1 | 0.35 | 0.08 | 0 | 20 | 17 | 15 | 7 | 0 |
| E4 | 12 | * | * | 0 \| 0 \| 0 | * | * | * | * | 0 \| 0 \| 0 | * | * | * | * | 0 \| 0 \| 0 | * | * |
| E5 | 12 | * | * | 0 \| 0 \| 2 | * | * | * | * | 0 \| 0 \| 0.02 | * | * | * | * | 0 \| 0 \| 2 | * | * |
| E6 | * | * | * | 0 \| 0 \| 0 | * | * | * | * | 0 \| 0 \| 0 | * | * | * | * | 0 \| 0 \| 0 | * | * |
| E7 | 10 | * | * | 0 \| 0 \| 0 | * | * | * | * | 0 \| 0 \| 0 | * | * | * | * | 0 \| 0 \| 0 | * | * |

Like Ben MacDhui sites, temperatures stabilise with depth at E3 and greatest variability is observed for NST, followed by GST (Figure 56). Variability, expressed as standard deviation (*s*), of temperatures recorded per sensor depth shows an increase in variability from air temperatures to highest variability observed for NST, followed by decreasing variability with increasing depth into the ground. The lowest annual mean temperature is recorded for NST (10.75 °C), followed closely by GST (10.78 °C). From GST downwards, annual mean ground temperatures increase and level out. Maximum temperatures are highest for NST and GST and least for $T_{10}$ (46 °C and 41 °C vs. 23 °C). Furthermore, seasonal ranges for NST, GST, $T_5$, and $T_{10}$ at E3 are 12.5 °C, 12.7 °C, 12.8 °C and 12.7 °C respectively. Sensors closer to the surface, like for Ben MacDhui, show they greatest variability and variability decreases as annual mean temperatures increase. Annual mean air temperatures are greater (warmer) than those recoded for sensors located within the ground. At E3 the overall absolute minimum occurs for air temperatures (-7 °C), whereas the absolute maximum is observed for NST (46 °C). Comparing GST across sites the highest temperature recorded occurs for E3 & E6 (35 °C) and the lowest at E3 (-2 °C). Sites show absolute temperature ranges (Figure 57) exceeding 30 °C for GST, with ranges variable with a change in elevation. Seasonal temperature ranges for E1-E7 average on 12 °C, while the E3 XR5 GST sensor records a seasonal temperature range of 12.7 °C.

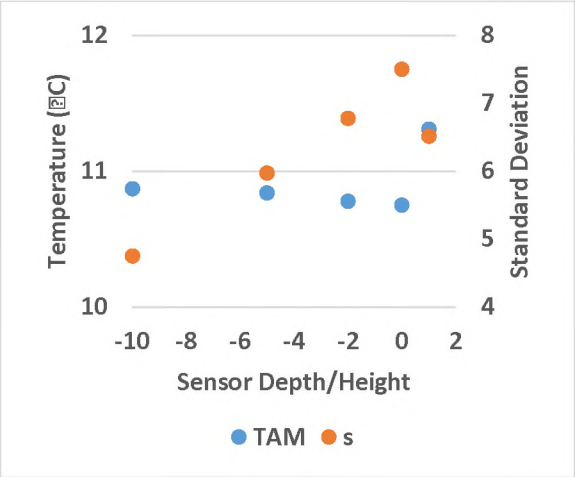


**Figure 56: Annual mean temperature ($T_{AM}$) and variability (*s*) per sensor depth for E3.**

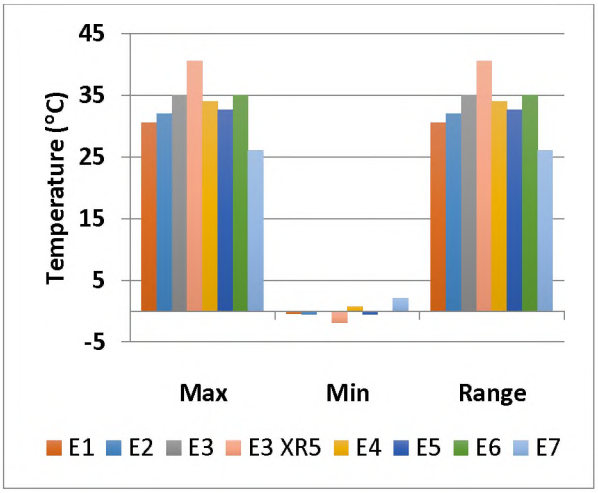


**Figure 57: Annual temperatures (maximums, minimums and ranges) for the Elandsberg. Data for E1-E7 are available for 2013-2015. Data for E3 XR5 are available 2015-2016.**

### *5.1.2.2 Seasonal frost environment*

The summer thawing index (TI) and winter freezing index (FI) are provided for ground surface temperatures (GST: ground temperatures recorded at ± 2 cm depth), for all sites, as well as air temperatures for T1 and E3. Each site is discussed in its respective subsection below.

#### 5.1.2.2.1 Ben MacDhui

Expected diurnal penetration depths (*d*) using Equation 12 (pg. 105) indicate a shallow diurnal frost environment. The deepest frost penetration on July 2014 yields an average diurnal cycle to a depth of ± 12 mm during this time and an expected average annual freezing depth of ± 0.5 cm. Seasonal freezing onset varies across sites but for ground surface temperatures (GST) (the most common freezing depth) onset is prominent for June (beginning of winter), ending in September (beginning of spring). Freezing occurring towards the end of spring is noticeable for some sites (T3 & T5), and T2 and T4 have isolated occurrences of freezing in April-May and April respectively (Table 24). Air temperatures at T1 reflect sub-zero temperatures throughout the year, except for December. Irrespective of this, most sub-zero temperatures (84%) take place during winter months of July and August. Most freeze cycles are observed for GST and the longest period of freezing is observed for $T_{10}$. Freezing is generally recorded at GST before air temperatures range below 0 °C. For diurnal cycles, as depths increase the onset of freezing occurs after the onset of freezing of the layer above. In comparison, the onset of thawing occurs before the onset of thawing of the layer above. The ground surface (0-2 cm), therefore, shows the longest potential freezing duration (first to last occurrence of freezing) for diurnal cycles with freezing duration generally becoming less with greater depth in the ground. However, annual freezing duration is greatest for $T_5$, and continuous freezing duration is greatest for $T_{10}$. As such, onset of freezing and onset of thaw are not a definitive indicator of total frozen-ground duration. Furthermore, ground freezing duration observed compares to work by Sumner (2003b) in the Lesotho Highlands at 3 220 m a.s.l., where ground at $T_5$ remained frozen for 79 days. Ground near the surface, as well as that at $T_{10}$, exhibited shorter freezing durations (56 and 52 days respectively).

**Table 24: Annual freezing period, start delay of freezing, and start delay of thaw, all given in days, for Ben MacDhui sites per sensor depth. $T_{AIR}$ reflects air temperature; GST indicates temperature recorded at the ground surface (± 2 cm). The subscript following 'T' indicates the depth of the sensor (in centimetres) used to record ground temperature.**

| Site | $T_{AIR}$ | GST | $T_5$ | $T_{10}$ |
|---|---|---|---|---|
| T1 | 45 | 75 \| **-29** \| *-1* | 75 \| **8** \| *-73* | 69 \| **5** \| *-3* |
| T2 | * | 51 \| * \| * | * | |
| T3 | * | 48 \| * \| * | * | |
| T4 | * | 23 \| * \| * | * | |
| T5 | * | | | |
| The first value in a set indicates annual freezing duration of that sensor in days. | | | | |
| **BOLD** values (second values in a set) indicate the average delay of the first sub-zero temperatures (freezing) of that layer to the one above it (the column to the left), expressed in number of days. Negative values indicate an earlier start. | | | | |

| Site | $T_{AIR}$ | GST | $T_5$ | $T_{10}$ |
|---|---|---|---|---|
| Values *italicised* (third values in a set) indicate the last sub-zero temperatures (freezing) of that layer to the one above it (the column to the left), expressed in number of days. Negative values indicate an earlier start. | | | | |
| * indicates logger failure/no data available. | | | | |
| | First occurrence of freezing in winter and last occurrence in spring. | | | |
| | First occurrence of freezing in autumn and last in spring. | | | |

The thermal offset, summer and winter mean temperatures, variability (expressed as standard deviation: *s*), as well as the summer thawing index and winter freezing index are given for T1 in Table 25. Seasonal temperatures and variability are provided for air temperatures and GST. The thermal offset for spring and summer is positive, with the greatest offset calculated for summer months. In comparison this offset is negative for autumn and winter, with the largest negative value calculated for winter. The thawing index for air temperatures and GST is highest (> 1 000) during summer. The freezing index shows lowest values during winter (-82), with zero values calculated for summer and autumn. Variability during summer is greatest for ground temperatures compared to air temperatures, although differences between GST and air temperatures are small. During winter variability is greatest for air temperatures and decreases with increasing depth into the ground. During summer GST-$T_{10}$ are warmer compared to air temperatures; for winter this relationship is reversed. Annual degree days (DD: -108) show a ground thermal regime colder than air temperatures. However, this value is small (± -0.3 per day), indicating ground temperatures and air temperatures do not differ much. Irrespective of this, a high positive ground freezing index (2 399) and a thawing index exceeding the freezing index, where even in winter months the thawing index greatly exceeds the freezing index, show an environment where ground frost is not the norm. The coldest period for T1 occurs in July, where diurnal mean maximum temperatures for GST-$T_{10}$ are 0.9 °C to -0.1 °C respectively. The deepest freeze event, to a depth of 10 cm, as well as the longest continuous frozen period for GST, spanning 28 days (Table 22, pg. 124) from 26 June (12:00) to 24 July (12:00), also occurs during this time. The longest continuous frozen event for $T_5$ lasts 54 days and occurs from 10 June (21:00) to 3 August (13:00). The longest continuous frozen event for $T_{10}$ lasts 58 days and occurs from 19 June (03:00) to 16 August (14:00).

**Table 25: Seasonal thermal indices for T1 for which data are available (2014-15). In the 'Temperature' column the first value represents the seasonal mean ($T_{SM}$); the second value the associated variability (*s*). $T_{AIR}$ reflects air temperature; GST indicates temperature recorded at the ground surface (± 2 cm); TI the thawing index; FI the freezing index; SO the thermal offset.**

| Season | $T_{AIR}$ | | | GST | | | SO |
|---|---|---|---|---|---|---|---|
| | TI | FI | Temperature | TI | FI | Temperature | |
| Winter | 701 | -89 | 0.9 / 9 | 23 | -82 | -0.5 / 0.9 | -1.3 |
| SON | 627 | -38 | 8.1 / 3.3 | 673 | -1 | 5.6 / 2.9 | 1.2 |
| DJF | 1 091 | -1 | 11.8 / 0.5 | 1 191 | 0 | 13.4 / 0.6 | 1.6 |
| MAM | 604 | -5 | 5.9 / 1.7 | 535 | 0 | 9.2 / 2.2 | -0.2 |

The ground temperature profile shows elevated average temperatures for $T_{10}$, compared to the remaining temperature sensors (Figure 58). This sensor depth exhibits the least variability of all sensors, while also having depressed diurnal maximum and diurnal minimum temperatures. Surface ground temperatures (NST and GST) show greater variability with the most extreme diurnal maximum and diurnal minimum temperatures recorded at NST, followed by GST, $T_5$ and $T_{10}$. Diurnal mean sub-zero temperatures are observed for winter months, with absolute minimum ground diurnal mean temperatures occurring on 9 July 2014 at 06:00 for GST (-7.8 °C). In comparison, work by Sumner (2003b) shows an absolute minimum temperature of -4.5 °C recorded in the Lesotho Highland at 3 200 m a.s.l. for GST during July 2000. Near surface temperature (NST) data are not available from June-October due to sensor failure and are, therefore, not included. Maximum daily mean temperatures occur during summer and spring (December-March), with absolute daily maximum ground temperatures occurring on 12 February 2015 at 15:00 for GST (44 °C). Soil moisture is variable and not available for winter. Nevertheless, soil moisture peaks during summer months (the rainfall season), reaching an average maximum during December.

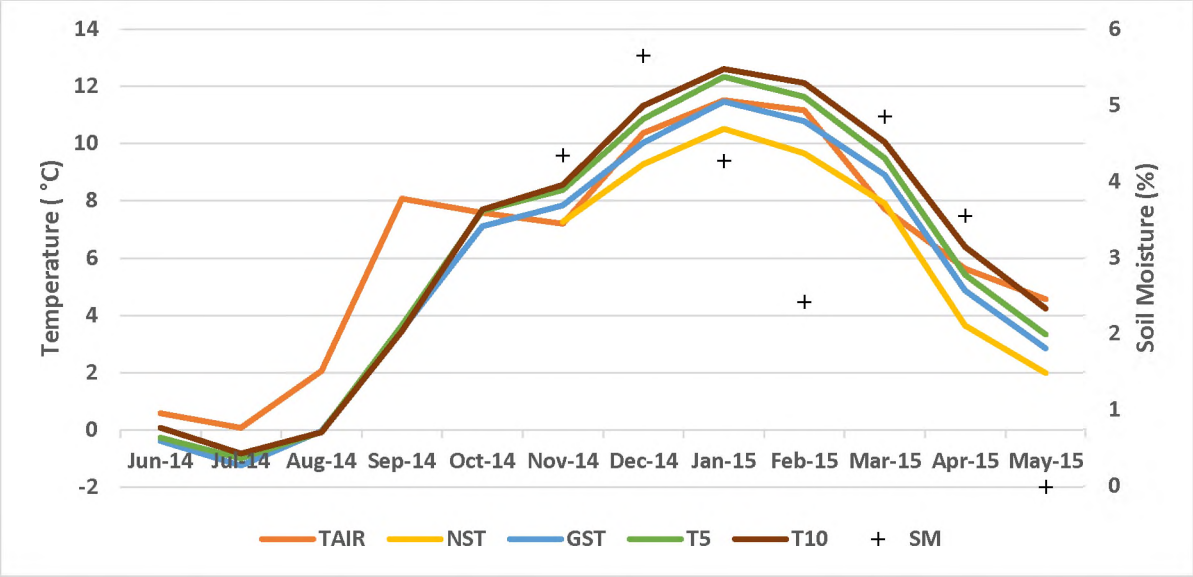


**Figure 58: Monthly means per sensor depth, as well as soil moisture (SM) for T1 (2014-15). $T_{AIR}$: air temperature. NST: ground temperature recorded at the near surface (± 1 cm). GST: temperature recorded at the ground surface (± 2 cm). The subscript following 'T' indicates the depth of the sensor (in centimetres) used to record ground temperature.**

During 2014-15 the lowest maximum air temperature at T1 is recorded during July (11.6 °C), the highest in February (26.5 °C). The lowest minimum air temperature at T1 is recorded during July and August (-13.0 °C), the highest in December (1.2 °C). This compares to maximum and minimum air temperatures of 26.2 °C and -12.8 °C presented by Kück (1997) for January and July 1996 respectively. The average duration of negative air temperatures achieved is 5 hours. However, the duration of maintaining sub-zero temperatures for air temperatures is variable (*s* ± 11). Nonetheless, the most common duration of sub-zero temperatures is one hour (21% of the time), as well as 2 and 3 hours (10% of the time for both) and 17 hours (7% of the time). Isolated instances of sub-zero temperatures maintained for more than one day occur 8% of the time, with the longest duration lasting 62 hours (± three days), starting

at 13:00 on 28 August and ending at 03:00 on 31 August. On average, temperatures dip below 0 °C at ± 14:00 and rise above 0 °C on average at ± 04:00 the following day.

For GST the lowest maximum temperature is recorded during July (11.6 °C), the highest in January (34.5 °C). The lowest minimum temperature is recorded during July (-7.8 °C), the highest in March (2.8 °C). The average duration of negative temperatures is 16 hours. However, the duration of maintaining sub-zero temperatures for GST is highly variable (*s* ± 90), due to three instances where sub-zero temperatures are maintained for longer than three days. Removing these two instances from the dataset yields *s* ± 11. The most common duration of sub-zero temperatures is 25 hours (25% of the time), as well as 14 and 16 hours (7% of the time for both) and 4 hours (7% of the time). Instances of sub-zero temperatures maintained for more than one day occur 29% of the time, with the longest duration lasting 673 hours (± 28 days), starting at 12:00 on 26 June and ending at 13:00 on 24 July. On average, temperatures dip below 0 °C at ± 16:00 and rise above 0 °C on average at ± 10:00 the following day.

At $T_5$ the lowest maximum temperature is recorded in July (0.0 °C), the highest in February (28.5 °C). The lowest minimum temperature is recorded in July (-5.7 °C), the highest in January (5.4 °C). In comparison, work by Sumner (2003b) shows an absolute minimum temperature of -2.3 °C recorded in the Lesotho Highland at 3 200 m a.s.l. during July 2000. The average duration of negative temperatures achieved is 18 hours and the duration of maintaining sub-zero temperatures is highly variable (*s* ± 254), due to two instances where sub-zero temperatures are maintained for longer than three days. Removing these two instances from the dataset yields *s* ± 10. The most common duration of sub-zero temperatures is 25 hours (16% of the time), as well as 18 hours (8% of the time). Instances of sub-zero temperatures maintained for more than one day occur 41% of the time, with the longest duration lasting 1 288 hours (± 54 days), starting at 21:00 on 10 June and ending at 13:00 on 3 August. On average, temperatures dip below 0 °C at ± 16:00 and rise above 0 °C on average at ± 11:00 the following day.

At $T_{10}$ the lowest maximum temperature is recorded during July (-0.1 °C), the highest in February (19.3 °C). The lowest minimum temperature is recorded during July (-3.3 °C), the highest in January (9.0 °C). In comparison, work by Sumner (2003b) shows an absolute minimum temperature of -0.7 °C recorded in the Lesotho Highland at 3 200 m a.s.l. during July 2000. The average duration of negative temperatures achieved is 10 hours and highly variable (*s* ± 336), due to two instances where sub-zero temperatures are maintained for longer than three days. Removing these two instances from the dataset yields *s* ± 10. The most common duration of sub-zero temperatures is 10 hours (25% of the time), as well as 1 hour (19% of the time). Instances of sub-zero temperatures maintained for more than one day occur 24% of the time, with the longest duration lasting 1 403 hours (± 58 days), starting at 03:00 on 19 June and ending at 14:00 on 16 August. On average, temperatures dip below 0 °C at ± 06:00 and rise above 0 °C on average at ± 13:00. *NOTE: percentages reflect the proportion of sub-zero temperatures only and not a proportion of all hours within one calendar year.*

#### 5.1.2.2.2 Elandsberg

Expected diurnal penetration depths (*d*) using Equation 12 (pg. 105) indicate an almost absent diurnal frost environment at a depth of ± 2 cm within the ground. The single frost penetration of July 2014 for iButtons deployed at E1, E2 and E5 yields an average diurnal cycle to a depth of ± 3 cm during this time and an expected average annual freezing depth of 13 mm. The deepest frost penetration recorded by the E3 XR5 logger during July 2015 yields a diurnal cycle to a depth of ± 3 cm during this time and an expected average annual freezing depth of 23 mm. Seasonal freezing onset occurs exclusively during July for E1, E2 and E5, whereas freezing commences during June 2015 and ends in August 2015 for E3 XR5 (Table 26). However, most freezing cycles are recorded at the near surface (NST; temperatures recorded at ± 1 cm in the ground) with ground frost largely absent for ground surface temperatures (GST: temperatures recorded at ± 2 cm in the ground). For air temperatures at E3, sub-zero temperatures are evident for June-September, as well as November with most sub-zero temperatures (92%) take place during winter months, especially the month of July (45%). At E3 the longest period of continuous freezing is recorded for NST (17 hours), followed by GST (15 hours). Freezing is observed for GST after ambient temperatures have reached sub-zero temperatures. For diurnal cycles, as depths increase the onset of freezing occurs after the onset of freezing of the layer above. In comparison, the onset of thawing occurs before the onset of thawing of the layer above. Ground surface temperatures (NST and GST), therefore, show the longest potential freezing duration (first to last occurrence of freezing) for diurnal cycles with freezing duration becoming less with greater depth in the ground.

**Table 26: Annual freezing period, start delay of freezing, and start delay of thaw, all given in days, per Elandsberg site per sensor depth. $T_{AIR}$ reflects air temperature; NST indicates temperature recorded at the near surface (± 1 cm); GST indicates temperature recorded at the ground surface (± 2 cm). The subscript following 'T' indicates the depth of the sensor (in centimetres) used to record ground temperature. # XR5 logging set-up, run 2015-2016.**

| Site | $T_{AIR}$ | NST | GST | $T_5$ | $T_{10}$ |
|---|---|---|---|---|---|
| E1 | * | * | 0.17 \| ***** \| * | * | |
| E2 | * | * | 0.13 \| ***** \| * | * | |
| E3 | * | * | 0 \| ***** \| * | * | |
| E3# | 7 | 4 \| **-21** \| *-84* | 1 \| **1** \| *-10* | 0.01 \| **18** \| *-18* | *No frost observed* |
| E4 | * | * | 0 \| ***** \| * | * | |
| E5 | * | * | 0.08 \| ***** \| * | * | |
| E6 | * | * | 0 \| ***** \| * | * | |
| E7 | * | * | 0 \| ***** \| * | * | |

The first value in a set indicates annual freezing duration of that sensor in days.

**BOLD** values (second values in a set) indicate the average delay of the first sub-zero temperatures (freezing) of that layer to the one above it (the column to the left), expressed in number of days. Negative values indicate an earlier start.

Values *italicised* (third values in a set) indicate the last sub-zero temperatures (freezing) of that layer to the one above it (the column to the left), expressed in number of days. Negative values indicate an earlier start.

* indicates logger failure/no data available.

First and last occurrence of freezing in winter.

| Site | $T_{AIR}$ | NST | GST | $T_5$ | $T_{10}$ |
|---|---|---|---|---|---|
| | First occurrence of freezing in winter and last in spring. | | | | |
| | First and last occurrence of freezing in during July. | | | | |

The ground temperature profile shows elevated average temperatures at $T_5$. At $T_{10}$, compared to the remaining temperature sensors, no sub-zero temperatures are recorded (Figure 59). Furthermore, this sensor depth exhibits the least variability of all sensors ($s \pm 2$), while also having depressed diurnal maximum and minimum temperatures. Ground surface temperatures (NST and GST) show more variability with the most extreme diurnal maximum and minimum temperatures observed for NST, followed by GST, $T_5$ and then $T_{10}$. Diurnal mean sub-zero temperatures are evident for NST and GST only in winter, with sub-zero temperatures recorded for $T_5$ on one day during July 2015. Absolute diurnal minimum ground temperature occurs on 14 July 2015 at 05:00 for NST (-4 °C). Diurnal mean temperatures exceeding 30 °C are evident from spring to summer (October-March), with absolute maximum mean ground temperatures on 28 December 2015 at 13:00 at NST (46 °C). Soil moisture is consistent throughout the year, with lower values recorded during May-June (onset of freezing), as well as before the start of the summer rains (November-December). Soil moisture peaks after the summer months, reaching an average maximum during early spring.

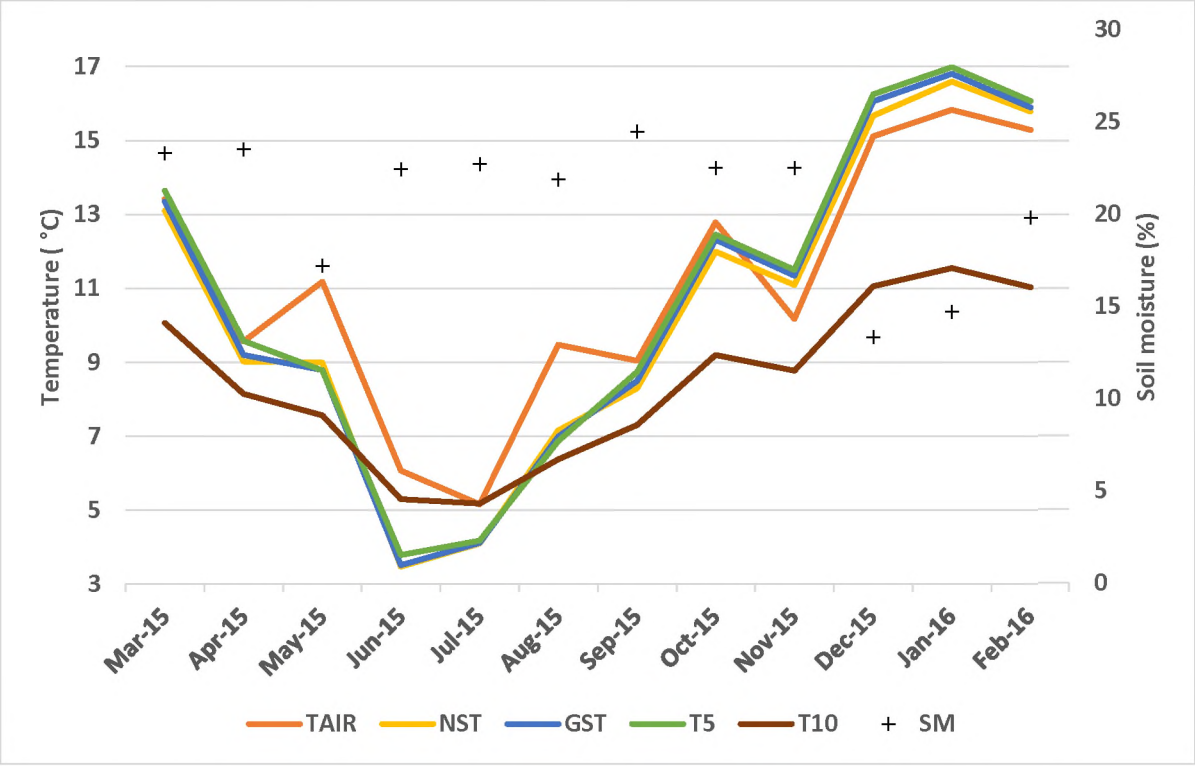


**Figure 59: Monthly means per sensor depth, as well as soil moisture (SM) for E3 (2015-16). $T_{AIR}$: air temperature. NST: ground temperature recorded at the near surface (1 cm). GST: temperature recorded at the ground surface (± 2 cm). The subscript following 'T' indicates the depth of the sensor (in centimetres) used to record ground temperature.**

The thermal offset, mean summer and winter temperatures, variability (expressed as standard deviation: *s*), as well as the summer thawing index and winter freezing index are given for E3 in **Table 27**. The thermal offset is positive for summer and autumn, with the largest positive value calculated for summer. Winter and spring register a negative offset. The thawing index for air temperatures and GST are large, with even summer months reflecting an index greater than 400 for both air and ground temperature. In comparison, the freezing index yields a value for winter but not the remaining seasons. Furthermore, the freezing index is negligible with air temperatures having a value of -8 and GST one of -1. Variability during summer is greatest for NST, next highest for GST, then $T_5$, $T_{10}$, and lowest for air temperature. This relationship is maintained in the ground during winter, although highest variability during winter is evident for air temperatures. In the ground, little differences are observed for mean temperatures in winter (s ± 1.4; seasonal mean temperature ± 4.4 °C). Annual degree days (DD: -86) show a ground thermal regime colder than air temperatures, although, like T1 on Ben MacDhui, this value is small (± -0.23 per day), indicating ground temperatures and air temperatures do not differ much. The ground freezing index is 4 131. The coldest period for E3 takes place in July 2015, where diurnal meant maximum temperatures from NST-$T_{10}$ are 13.5 °C-8.3 °C. Diurnal mean minimum temperatures for this period are -3.6 °C, -2 °C, -0.4 °C and 2 °C for NST, GST, $T_5$, and $T_{10}$ respectively. The deepest freeze event, to a depth of ± 9 cm, as well as the longest continuous frozen period for NST, spanning 17 hours (Table 23, pg. 126) takes place on 13 July from 18:00-11:00 the following day. The longest continuous frozen event for GST (15 hours) occurs the same day from 21:00-12:00 the following day. The longest continuous frozen event for $T_5$ takes place on 14 July from 04:00-11:00.

**Table 27: Seasonal thermal indices for E3 for which data are available (2015-16). In the 'Temperature' column the first value represents the seasonal mean ($T_{SM}$); the second value the associated variability (*s*). $T_{AIR}$ reflects air temperature; GST indicates temperature recorded at the ground surface (± 2 cm); TI the thawing index; FI the freezing index; SO the thermal offset.**

| Season | $T_{AIR}$ | | | GST | | | SO |
|---|---|---|---|---|---|---|---|
| | TI | FI | Temperature | TI | FI | Temperature | |
| JJA | 665 | -8 | 6.1 / 1.9 | 467 | -1 | 4.2 / 1.4 | -1.2 |
| SON | 1 042 | 0 | 10.8 / 1.7 | 1 055 | 0 | 12.1 / 1.8 | -1.9 |
| DJF | 1 478 | 0 | 15.9 / 2.2 | 1 637 | 0 | 17.0 / 2.6 | 1.3 |
| MAM | 1 077 | 0 | 11.3 / 1.8 | 1 006 | 0 | 10.1 / 2.3 | 1.2 |

#### *5.1.2.3 Diurnal frost environment*

The diurnal frost environment is presented in subdivisions of months and seasons. All temperatures are based on degree Celsius and represent approximations to the nearest degree. Thaw duration, thaw depths and proportions (percentages) are rounded to the nearest hour, centimetre and percentage respectively. Logger failure, where applicable, is indicated in the text. Each site within the Eastern Cape is discussed within its own subsection below, however a summary of calculated parameters is provided in Table 28 (pg. 136).

The lowest maximum air temperature is recorded at T1, the highest at E3. During this time, the average duration of positive air temperatures achieved at these two sites is 5 and 7 hours respectively. Sites at

greater altitude exhibit more potential freeze-thaw events, freeze-thaw cycles, as well as average freezing duration per freeze-thaw cycles than those at lower altitudes. T1 and T4, at higher altitudes compared to E1-E3 and E5, reflect occasional instances where multiple freeze-thaw cycles occur for one 24-hour period. T1, at highest elevation, also exhibits freeze-thaw cycles spanning more than one day. The lowest ground temperatures are recorded in July (mid-winter). During this time, at Ben MacDhui the ground reflects its longest frozen duration; for the Elandsberg sensors show that the ground reaches sub-zero temperatures. Freeze-thaw cycles for Ben MacDhui tend to initiate shortly after midday, with thaw observed from midnight to the early morning. Freeze-thaw cycles commence on the Elandsberg in the early morning, ending before midday. The deepest and longest freeze events occur in July for all sites except T1. At T1, which also experiences the longest duration of frozen ground and freeze-thaw cycles extending into spring, the deepest and longest freezing event occurs in August. Freezing duration is correlated to freeze-thaw cycles ($r = 0.75$, $p < 0.05$), initiation of freezing ($r = 0.84$, $p < 0.05$) but not commencement of thaw. For the Elandsberg initiation of freezing and thaw correlates strongly to freeze-thaw cycles ($r \pm 1$, $p < 0.05$; $r = 0.96$, $p < 0.05$). Average commencement of freezing for Ben MacDhui is 13:00 and thawing generally initiates by 03:00. On the Elandsberg freezing initiates by 06:00 and ends by 10:00.

**Table 28: Summary of ground thermal dynamics for those Eastern Cape sites for which freeze-thaw cycles (FTC) occur. Data are presented for 2014-2015, except for E3, which represents 2015-2016. All durations and times represent averages. If more than one value is provided per column the first value indicates frost instances at the near surface (NST: ± 1 cm depth), the second frost occurrences at the ground surface (GST: ± 2 cm depth). If only one value is provided, then GST is represented. FH: freeze hours. PFTE: potential freeze-thaw events. $T_{AIR}$: air temperature. * no data available. # XR5 set-up.**

| Site | 2014-2015 | | | | | | EVENT | | DURATION OF POSITIVE TEMPERATURES | | | |
|---|---|---|---|---|---|---|---|---|---|---|---|---|
| | $T_{AIR}$ Max | PFTE $T_{AIR}$ | PFTE | FTC | PFTE to FTC | FH to PFTE | Multiple | Over Several Days | $T_{AIR}$ | Start | End | Freezing Duration |
| T1# | 26 | 122 | 57 | 32 | 56 | 56 | Y | Y | 5 | 13:00 | 6:00 *the following day* | 18 |
| T4 | * | * | 52 | 17 | 33 | 32 | Y | N | * | 13:00 | 24:00 | 12 |
| E1 | * | * | 1 | 1 | 100 | 4 | N | N | * | 5:00 | 9:00 | 4 |
| E2 | * | * | 1 | 1 | 100 | 3 | N | N | * | 6:00 | 9:00 | 3 |
| E3# | 32 | 24 | 16 \| 6 | 4 \| 2 | 25 \| 17 | 22 \| 5 | N | N | 7 | 7:00 \| 21:00 | 14:00 \| 12:00 | 7 \| 15 |
| E5 | * | * | 1 | 1 | 100 | 2 | N | N | * | 6:00 | 8:00 | 2 |

#### 5.1.2.3.1 T1

Diurnal ranges and oscillations around 0 °C are provided in Table 29. At T1 on Ben MacDhui diurnal air temperature ranges of 10 °C are common (±71%), occurring in every month. Of the ranges, ± 27% reflect maximums above and minimums below 0 °C; *i.e.* oscillations above/below 0 °C. For GST such diurnal ranges decrease to 52% (4% >/< 0 °C), to 36% at $T_5$ (0% >/< 0 °C), and to 0.3% for $T_{10}$ (0% >/< 0 °C). Diurnal ranges exceeding 10 °C for $T_5$ and $T_{10}$ reflect positive ranges, *i.e.* daily maximum and minimum temperatures are positive. Diurnal ranges exceeding 10 °C occur predominantly during summer, with oscillations around 0 °C occurring predominantly during winter.

**Table 29: Oscillations around 0 °C (Osc), as well as diurnal ranges exceeding 10 °C ($T_{DR}$) for T1. Annual Osc (%) reflect all oscillations around 0 °C, including those where $T_{DR}$ does not exceed 10 °C. JJA: winter. SON: spring. DJF: summer. MAM: autumn.**

| Sensor | $T_{DR}$ (%) | Osc (%) | % of year | Annual Osc (%) | $T_{DR}$ (%) | | | | Osc (%) | | | |
|---|---|---|---|---|---|---|---|---|---|---|---|---|
| | | | | | JJA | SON | DJF | MAM | JJA | SON | DJF | MAM |
| $T_{AIR}$ | 71 | 27 | 19 | 28 | 16 | 30 | 33 | 22 | 62 | 21 | 3 | 14 |
| GST | 52 | 4 | 2 | 16 | 0 | 36 | 46 | 18 | 79 | 21 | 0 | 0 |
| $T_5$ | 35 | 0 | 0 | 7 | 0 | 34 | 60 | 6 | 84 | 16 | 0 | 0 |
| $T_{10}$ | ± 0 | 0 | 0 | 0 | 0 | 0 | 100 | 0 | 0 | 0 | 0 | 0 |

During 2014-15 relatively numerous sub-zero temperatures are evident for air temperatures (potential freeze-thaw events: 122). Similarly, numerous potential freeze-thaw events and freeze-thaw cycles are observed for GST and freeze events occur within the upper 10 cm of the ground. Negative air temperatures generally occur in winter (n = 77). Nevertheless, negative air temperatures are reached during spring (n = 23 occurrences), summer (n = 4 occurrences), and autumn (n = 18 occurrences). A minimum of -13 °C is reached for air temperature on 7 July 2017 at 21:00 and negative temperatures are maintained for ± 5 hours on average. Sixty-eight unique needle ice events are identified by Borg (2017), of which he uses 44 for analyses purposes. Needle ice events initiate at temperatures ranging from -0.2-2.2 °C, soil moisture values ranging from 17.4 -25.9%, and wind speeds of 0-12.9 $m.s^{-1}$ (Borg, 2017). However, of the 68 unique events identified only 57 potential freeze-thaw events are observed for GST. Of these, only 16 occur for days on which needle ice growth is determined. Thus, not every needle ice event yields a freeze-thaw cycles at GST. In addition, not every freeze-thaw cycle translates into a needle ice event. As such, the lower potential freeze-thaw events identified for GST, compared to known needle ice events, suggests that freeze events are restricted to the upper centimetre of the ground, corroborated by the expected freezing depth (*d*) of less than 1 cm for T1 (refer to 5.1.2.2.1 Ben MacDhui, pg. 128). Data are not available for NST for the whole of the period under investigation, as such, data from GST are used instead. During the observation period 32 freeze-thaw cycles for 31 separate days are recorded. More cycles are observed due to one day having two cycles taking place in a 24-hour period. Over half (56%) of potential freeze-thaw events translate into freeze-thaw cycles (Table 30, pg. 138). The amount of freeze-thaw cycles calculated is equal to the number of freeze-thaw cycles observed by Kück (1997) on Ben MacDhui during 1995 and 1996.

**Table 30: Freeze-thaw events for T1, summarised by season. * indicates underestimation of duration due to data loss. $T_{AIR}$ reflects air temperature; NST reflects ground temperature recorded at the near surface (± 1 cm); GST indicates temperature recorded at the ground surface (± 2 cm). The subscript following 'T' indicates the depth of the sensor (in centimetres) used to record ground temperature. PFTE: potential freeze-thaw events. FTC: freeze-thaw cycles. JJA: winter. SON: spring. DJF: summer. MAM: autumn.**

| Season | Potential Freezing Hours at 0 °C | | | | | PFTE | | | | | FTC |
|---|---|---|---|---|---|---|---|---|---|---|---|
| | $T_{AIR}$ | NST* | GST | $T_5$ | $T_{10}$ | $T_{AIR}$ | NST* | GST | $T_5$ | $T_{10}$ | |
| JJA | 812 | 0 | 1 680 | 1 724 | 1 644 | 77 | 0 | 45 | 20 | 15 | 25 |
| SON | 170 | 29 | 112 | 78 | 19 | 23 | 6 | 12 | 4 | 2 | 7 |
| DJF | 13 | 6 | 0 | 0 | 0 | 4 | 2 | 0 | 0 | 0 | 0 |
| MAM | 79 | 102 | 0 | 0 | 0 | 18 | 13 | 0 | 0 | 0 | 0 |
| Total | 1 074 | 137 | 1 792 | 1 802 | 1 663 | 122 | 21 | 57 | 24 | 17 | 32 |

Freeze-thaw cycles occur occasionally during spring (22%) but generally during winter months of June (25%) and August (50%), with one event during July (3%). Almost all freeze-thaw cycles represent single events, with average freezing duration of 18 hours ($s$ = 16) and freezing generally taking place from 13:00-06:00 the following day. Multiple freeze-thaw cycles are observed for 19 September 2014. The initial freeze event is shortest, lasting ± 9 hours from 00:00-09:00. The second freeze event lasts for ± 10 hours from 22:00-08:00 the following day. Deep freeze events, lasting 8 hours on average, occur for August and are associated with needle ice events (Borg, 2017). A 1-hour delay ($s$ = 6) between GST and $T_5$ is recorded and freezing is observed for ± 33 hours at $T_5$. A 15-hour delay exists between $T_5$ and $T_{10}$, with average freezing duration at $T_{10}$ ± 8 hours. The longest freeze-thaw cycle for GST initiates at 17:00 on 28 August and lasts 92 hours (± 4 days). The deepest freeze-thaw cycle takes place on 27 August, initiating at 03:00, lasting 10 hours and reaches at least 10 cm. $T_{10}$ remains frozen for most of the winter.

Twenty-one freeze-thaw cycles last longer than 10 hours (Figure 60, pg. 139). Of these 62% occur during August, with 29% during June. Isolated freezing events longer than 10 hours are observed for July and September (5% for both). For these freeze events, average freezing takes place between 16:00-04:00 two days later. When the average freezing duration is considered (18 hours, n = 13), 54% occur for August, 38% in June, with 8% in July. For these freeze events, average commencement of freezing initiates at 16:00, ending at 18:00 two days later. Variability for temperature recorded initially increases from air temperatures to GST. From GST onwards, an increase in depth into the ground yields a decrease in variability. Highest variability is evident for GST ($s$ = 7.22), lowest for $T_{10}$ ($s$ = 5.00). At GST the average diurnal temperature range approximates 5 °C, although a maximum range of 23 °C is reached. Diurnal maximum and minimum temperatures are 22 °C and -3 °C respectively. Correlations between maximum and minimum freeze duration to diurnal maximum and minimum temperatures are inconclusive, with only diurnal minimums significant ($r$ ± 0.43, $p$ < 0.05). Average diurnal maximum and minimum temperatures are 4 °C and -1 °C respectively. The average diurnal mean temperature is 1 °C.

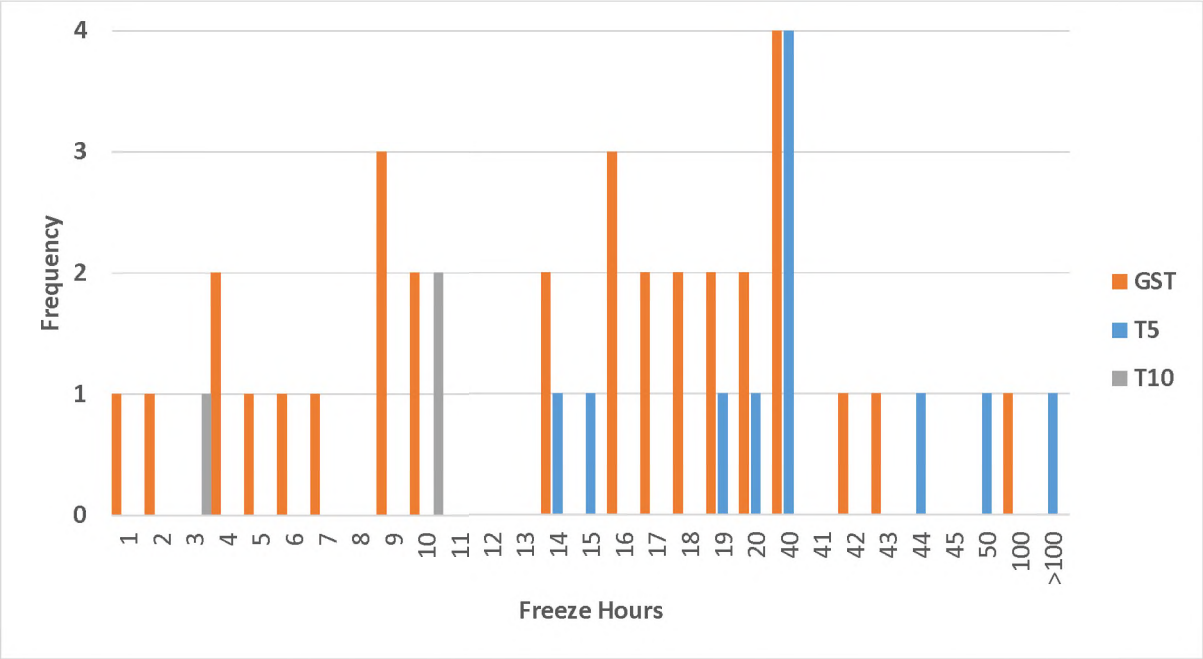


**Figure 60: Histogram of freeze duration per event per sensor depth for T1. GST: temperature recorded at the ground surface (± 2 cm). $T_5$: ground temperature recorded at 5 cm depth. $T_{10}$: ground temperature recorded at 10 cm depth.**

#### *5.1.2.3.1.1 Higher-frequency*

Higher-frequency temperature data using an XR5 system, recorded at ten-minute intervals, are available for T1 for the duration of the observation period. As such, these data are only evaluated for those seasons for which freeze-thaw cycles are evident (winter and spring).

Freeze-thaw cycles take place on eight days in June, one isolated event in July, and on 16 days in August (Figure 61, pg. 142). The remaining freeze-thaw cycles occur in spring (September: n = 3; October: n = 1; November: n = 2) (Figure 62, pg. 143). Freezing depth during this time is variable. However, freezing depth is mainly constrained to the upper centimetres of the ground, *i.e.* GST. Nevertheless, depths of 10 cm are reached on isolated days. Mid-winter reflects the lowest number of freeze-thaw cycles, due to the ground mostly frozen. The greatest intensity of any frost event during this time takes place on 24 August and reaches -2.69 °C. Diurnal temperature ranges exceeding 10 °C occur during spring. For freeze-thaw cycles taking place in winter the diurnal range is closer to 3 °C. Considering data recorded at hourly intervals, 57 potential freeze-thaw events are apparent, translating into 32 freeze-thaw cycles at GST (5.1.2.3.1 T1, pg. 137). While the number of potential freezing hours remains the same, the number of potential freeze-thaw events and freeze-thaw cycles increases when higher-frequency data are evaluated (Table 31, pg. 140). Data recorded at a shorter interval yield more potential freeze-thaw events, as well as two more freeze-thaw cycles. These cycles occur on 10 August and 19 September and have a duration of less than 1 hour. On 10 August temperatures oscillate above 0 °C and below this threshold within 30 minutes. Furthermore, the freeze-thaw cycle takes place following a period where multiple oscillations above/below 0 °C are recorded (four events within 2 hours). On 19 September one additional cycle of less than 1 hour is recorded, occurring between the two cycles already identified in

subsection 5.1.2.3.1 T1 (pg. 137). All additional cycles identified occur near or at the surface and don't reach more than 2 cm into the ground.

**Table 31: Freeze-thaw events for T1, recorded at 10-min intervals for winter (JJA) and spring (SON). Potential freeze-thaw events (PFTE) and freeze-thaw cycles (FTC) identified using hourly data are indicated in brackets. $T_{AIR}$ reflects air temperature; GST indicates temperature recorded at the ground surface (± 2 cm). The subscript following 'T' indicates the depth of the sensor (in centimetres) used to record ground temperature.**

| Season | Potential Freezing Hours at 0 °C | | | | PFTE | | | | FTC |
|---|---|---|---|---|---|---|---|---|---|
| | $T_{AIR}$ | GST | $T_5$ | $T_{10}$ | $T_{AIR}$ | GST | $T_5$ | $T_{10}$ | |
| JJA | 799 | 1 679 | 1 725 | 1 653 | 141 (77) | 65 (45) | 28 (20) | 56 (12) | 27 (25) |
| SON | 148 | 111 | 76 | 17 | 32 (23) | 13 (12) | 4 (4) | 9 (2) | 8 (7) |
| Total | 947 | 1 790 | 1 801 | 1 670 | 173 (100) | 78 (57) | 32 (24) | 65 (17) | 35 (32) |

Winter temperatures remain much lower than those evident in spring (Figure 61 on pg. 142 and Figure 62 on pg. 143 respectively). Like data recorded at hourly intervals, higher-frequency data show greatest variability of ground temperatures at GST, with the least at $T_{10}$. Soil moisture dips sharply once freezing commences, only increasing again when thawing events are recorded. Periods of sub-zero temperatures are evident at $T_5$, when GST remains above 0 °C. However, during these times $T_{10}$ is frozen. Ground snow cover is indicated on Figure 61 (pg. 142) and reflects an amelioration of variability observed. Exotherms are evident for June (5, 16-18), August (1, 5, 9, 11, 23), and September (03, 9). The zero-curtain effect is noticeable on a few isolated occasions. These all take place in August (1, 5, 9, 11), with the effect evident at a depth of approximately 2-5 cm. Thawing and freezing indices for the various sensors, given as days, are provided in Table 32. The thawing index generally decreases with increasing depth into the ground, as does the freezing index. The greatest freezing index is observed at GST, with the highest values calculated for July. In comparison, the highest thawing index is recorded for November. July reflects a thawing index approaching zero for all ground sensors. Furthermore, in July the freezing index exceeds the thawing index. In general, this relationship is reversed for other months. The balance of degree days is 135 toward the thawing index for air temperatures for winter and spring. This balance is 102, 99 and 91 for GST, $T_5$ and $T_{10}$ respectively. However, it must be noted that this balance is ± 55, 43, and 30 for GST, $T_5$ and $T_{10}$ respectively when only July is considered. Furthermore, $T_{10}$ reflects a balance skewed towards the freezing index for August. The thermal offset is skewed towards negative values from June-August, with positive values calculated for October and November.

**Table 32: The freezing index (FI) and thawing index (TI) for the various sensor depth for T1 for winter and spring 2014. $T_{AIR}$ reflects air temperature; GST indicates temperature recorded at the ground surface (± 2 cm). The subscript following 'T' indicates the depth of the sensor (in centimetres) used to record ground temperature. SO: thermal offset. DD: degree days.**

| Day | FI | | | | TI | | | | SO |
|---|---|---|---|---|---|---|---|---|---|
| | $T_{AIR}$ | GST | $T_5$ | $T_{10}$ | $T_{AIR}$ | GST | $T_5$ | $T_{10}$ | |
| June | -33 | -18 | -11 | -3 | 57 | 4 | 8 | 18 | -1.3 |
| July | -56 | -55 | -43 | -30 | 56 | 0.4 | 0 | 0 | -1.8 |
| August | -32 | -9 | -4 | -4 | 91 | 19 | 8 | 0.5 | -1.6 |
| September | -4 | -1 | -0.1 | 0 | 243 | 141 | 126 | 104 | -3.3 |

| Day | FI | | | | TI | | | | SO |
|---|---|---|---|---|---|---|---|---|---|
| | $T_{AIR}$ | GST | $T_5$ | $T_{10}$ | $T_{AIR}$ | GST | $T_5$ | $T_{10}$ | |
| October | -3 | 0 | 0 | 0 | 247 | 252 | 235 | 204 | 1.0 |
| November | -4 | -0.1 | 0 | 0 | 247 | 282 | 274 | 259 | 1.3 |
| Balance * | 135 | 102 | 99 | 91 | * Difference of DD between FI and TI | | | | |

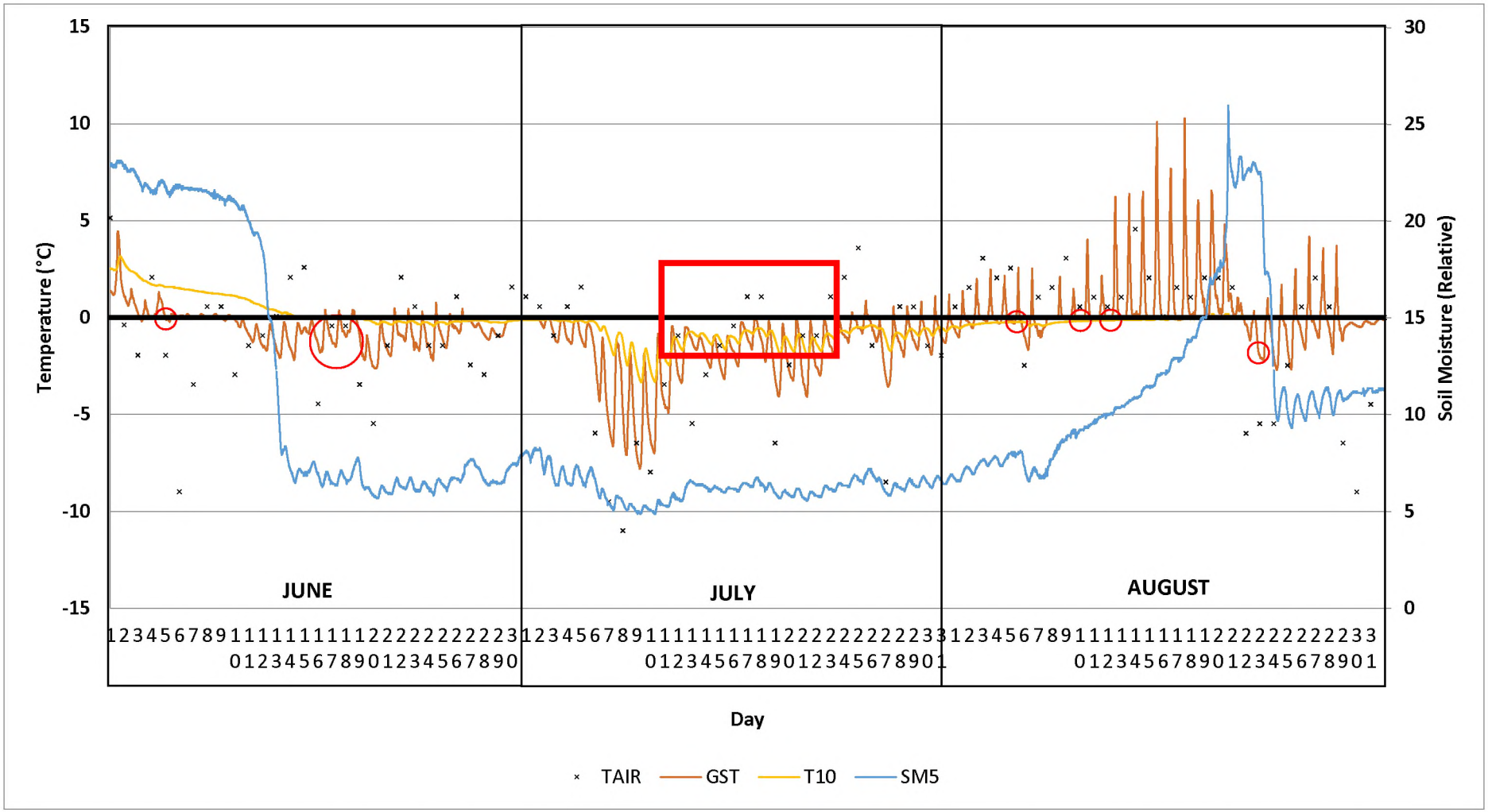


**Figure 61: Temperature and ground moisture 10-minute data at T1 for winter 2014. Black outlines delineate months; the red outline indicates a period of snow cover. Exotherms are indicated with red circles. $T_{AIR}$: air temperature. GST: recorded at ± 2 cm in the ground. The number after 'T' indicates the depth of the sensor (in centimetres) in the ground. SM: soil moisture.**

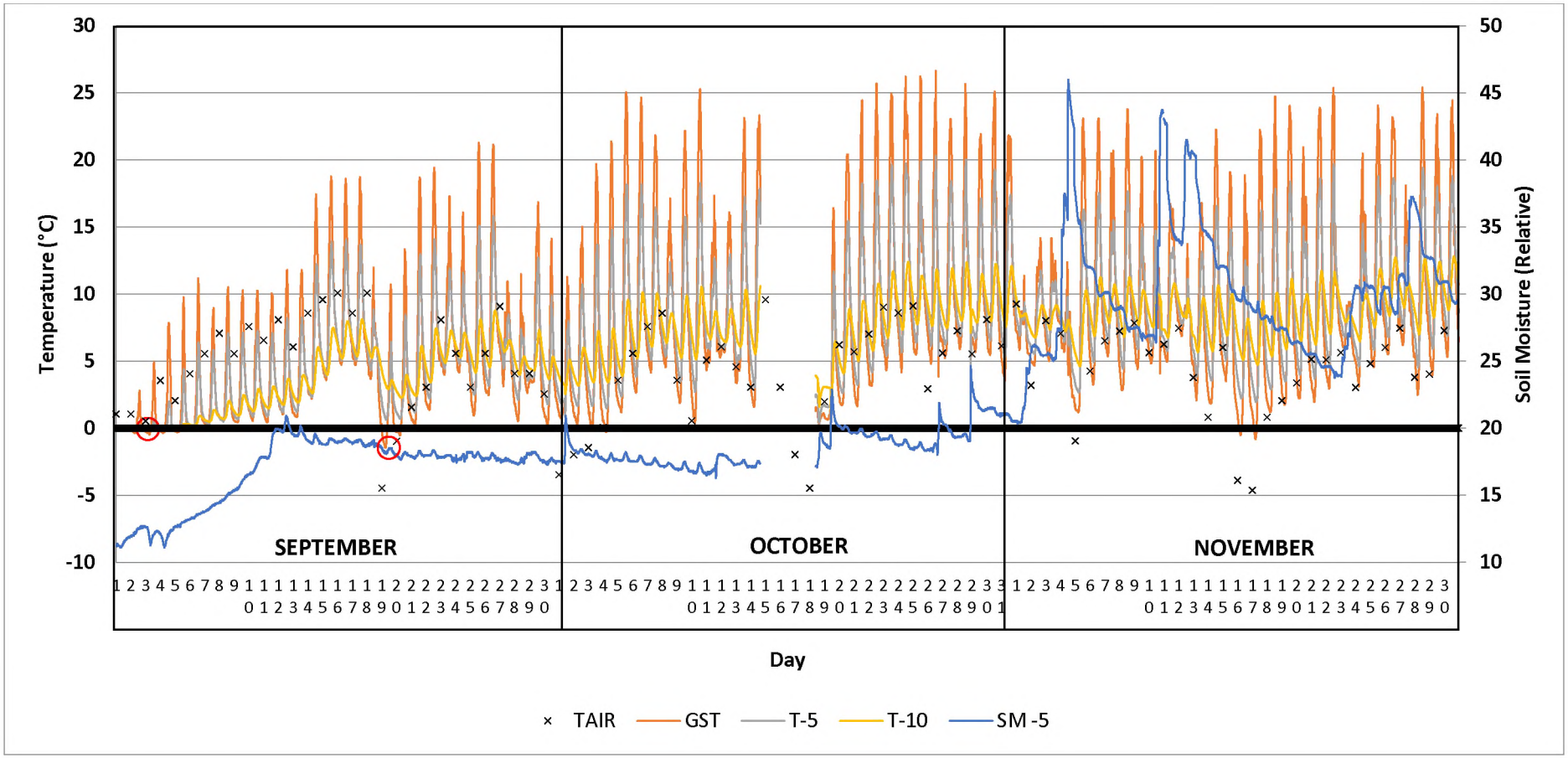


**Figure 62: Temperature and ground moisture 10-minute data at T1 for spring 2014. Black outlines delineate months. Exotherms are indicated with red circles. $T_{AIR}$: air temperature. GST: recorded at ± 2 cm in the ground. The number after 'T' indicates the depth of the sensor (in centimetres) in the ground. SM: soil moisture.**

5.1.2.3.2 T2-T5

T2, T3 and T5 experienced data loss during the observation period and the diurnal frost environment for these sites is not discussed in detail. Nevertheless, data are available for winter months, which are associated with freeze-thaw cycles (refer to 5.1.2.3.1 T1, pg. 137 onwards). T4, which has minimal data loss, is discussed in greater detail.

Diurnal ranges in the ground exceeding 10 °C are common (>= 50%), even where data loss is experienced. T4 & T5, with the most robust datasets, have diurnal ranges greater than 10 °C two-thirds of the time. Of these, T4 reflects oscillations above/below 0 °C 7% of the time and T5 19% of the time (Table 33). Diurnal temperature ranges exceeding 10 °C for all sites reflect predominantly positive ranges, *i.e.* both daily maximum and minimum temperatures are positive. For T4 and T5 the proportion of diurnal ranges that dip below 0 °C is 5% and 13% respectively. At T4, the only site where sufficient data are available for the entire calendar year, diurnal ranges exceeding 10 °C occur predominantly during spring and summer (33% & 37% respectively), with oscillations around 0 °C generally evident in winter (74%).

**Table 33: Oscillations around 0 °C (Osc), as well as diurnal ranges exceeding 10 °C ($T_{DR}$) for T2-T5 for those days where data are available. Annual Osc (%) reflect all oscillations around 0 °C, including those where $T_{DR}$ does not exceed 10 °C. * insufficient data. ± underestimation for all calculated values. JJA: winter. SON: spring. DJF: summer. MAM: autumn.**

| Site | $T_{DR}$ (%) | Osc (%) | % of year | Annual Osc (%) | $T_{DR}$ (%) | | | | Osc (%) | | | |
|---|---|---|---|---|---|---|---|---|---|---|---|---|
| | | | | | JJA | SON | DJF | MAM | JJA | SON | DJF | MAM |
| T2 | 49± | 26 | * | * | * | * | * | 99 | 70 | * | * | 30 |
| T3± | 49± | 3± | * | * | 0 | 73 | * | 27 | 93 | 7 | * | 0 |
| T4 | 64 | 7 | 5 | 15 | 2 | 33 | 37 | 28 | 74 | 24 | 0 | 2 |
| T5 | 68± | 19 | * | * | 21 | 55 | * | 24 | 76 | 24 | * | 0 |
| Months Evaluated | T2: July, October, March-May \| T3: June, July, November, December, February, March \| T4: All \| T5: July-December, April, May | | | | | | | | | | | |
| % Data Loss | T2: 51 \| T3: 40 \| T4: 0 \| T5: 26 | | | | | | | | | | | |

During the observation period, relatively numerous sub-zero temperatures are recorded at all sites. Similarly, several ground potential freeze-thaw events and freeze-thaw cycles are evident. Negative temperatures occur predominantly during winter months with the ground remaining frozen for extended periods of time. Nevertheless, negative GST are also recorded from April-October. The most common duration (> 65% of the time) of sub-zero temperatures per site is 2 hours. Maximum duration of sub-zero temperatures is maintained at T4 and T5 for 42 and 23 hours respectively (T2 & T3 cannot be evaluated). A minimum of -6.0 °C and -5.7 °C is attained for T4 and T5 respectively. June and August are the most active months for diurnal freeze-thaw cycles, with July reflecting the longest duration of when the ground is frozen. Thaw occurs on average 2 hours after positive temperatures have been reached. A decrease in freeze-thaw cycles is evident for T3 and T4 in winter, as well as T2 and T4/T5 in autumn. No freeze-thaw cycles are recorded during spring and summer (Table 34, pg. 145).

**Table 34: Freeze-thaw events for T2-T5, summarised by season. PFTE: potential freeze-thaw events. FTC: freeze-thaw cycles. * indicates period not evaluated due to data loss. JJA: winter. SON: spring. DJF: summer. MAM: autumn.**

| Season | Potential Freeze Hours at 0 °C | | | | PFTE | | | | FTC | | | |
|---|---|---|---|---|---|---|---|---|---|---|---|---|
| | T2 | T3 | T4 | T5 | T2 | T3 | T4 | T5 | T2 | T3 | T4 | T5 |
| JJA | * | 1 139 | 481 | * | * | 22 | 37 | * | * | 20 | 17 | * |
| SON | * | 7 | 59 | 112 | * | 3 | 14 | 20 | * | 0 | 0 | 0 |
| DJF | * | * | 0 | 0 | * | * | 0 | 0 | * | * | 0 | 0 |
| MAM | 160 | * | 3 | 0 | 24 | * | 1 | 0 | 8 | * | 0 | 0 |
| Total | * | * | 543 | * | * | * | 52 | * | * | * | 17 | * |

Eight freeze-thaw cycles evident in autumn at T2 yield diurnal temperature ranges exceeding 10 °C, with average maximum and minimum diurnal temperatures of 15 °C and -2 °C respectively. Variability is fairly high ($s$ ± 5.21). Freeze-thaw cycles in winter for T3 reflect diurnal ranges less than 10 °C (ranges ± 3 °C), with an average maximum and minimum diurnal temperature of 1 °C and -2 °C respectively. Variability is low at $s$ ± 0.80. No freeze-thaw cycles are recorded at T5.

Seventeen freeze-thaw cycles are recorded in winter on 16 separate days at T4. More cycles are observed due to one day having two cycles taking place in a 24-hour period and one-third (33%) of potential freeze-thaw events translate into freeze-thaw cycles. These cycles occur exclusively during winter with average freezing duration of 12 hours ($s$ = 5). Freezing generally takes place from 13:00-24:00. Multiple freeze events are observed on 28 June 2014. The initial freeze event is shortest, lasting ± 10 hours from 02:00-12:00. The second freeze event lasts ± 13 hours from 12:00-10:00 the following day. Ten freeze-thaw cycles last longer than 10 hours, as well as being longer than the average freezing duration of 12 hours (Figure 63, pg. 146). Of these 80% occur in July, with 20% in June. For these cycles, average freezing occurs from 19:00-10:00 the following day. The average diurnal temperature range approximates 5 °C, although a maximum of 9 °C is reached. Maximum and minimum diurnal temperatures are 8 °C and -6 °C respectively. Diurnal ranges don't exceed 10 °C in winter (± 5 °C), with average diurnal maximum and minimum temperatures of 4 °C and -2 °C respectively. Average diurnal mean temperatures are -1 °C, with low variability ($s$ ± 1.40). Correlations of maximum ($r$ ± 0.64) and minimum ($r$ ± 0.58) freeze duration to diurnal maximum and minimum temperatures are significance at $p < 0.01$.

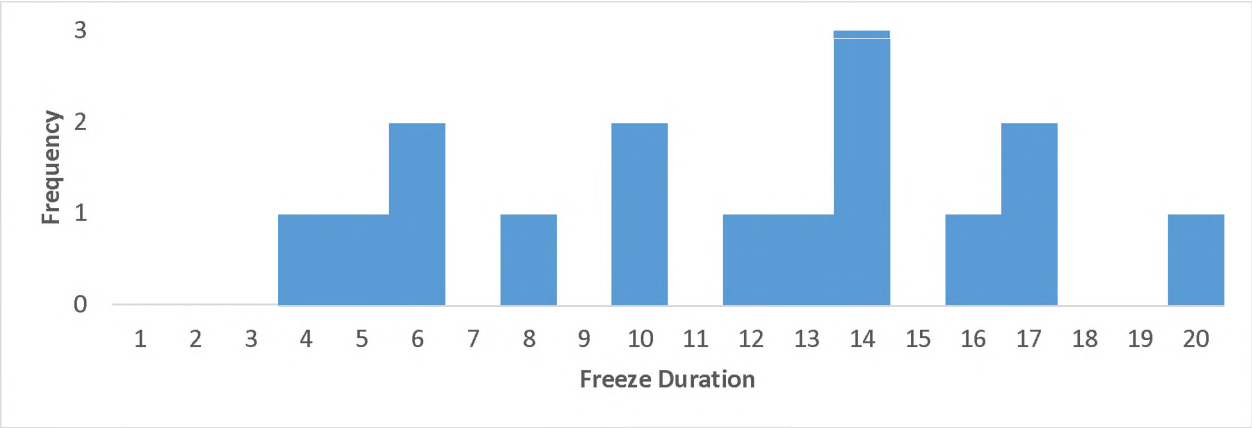


**Figure 63: Histogram of freeze duration (in hours) for ground surface temperatures (GST: ± 2 cm) at T4.**

#### 5.1.2.3.3 E1-E7

For iButtons deployed on the Elandsberg only the period of 2014-2015 is considered, since no sub-zero temperatures were recorded during 2013-2014 and 2016. Potential freeze-thaw events occur on one occasion during winter 2015 for iButtons at E1, E2 and E5. iButtons at E3-E4, and E6-E7 do not register any potential freeze-thaw events. At E1, E2 and E5 diurnal temperature ranges of 10 °C are not as common as those determined for Ben MacDhui (Table 35). However, of these ranges none reflect maximums above and minimums below 0 °C; *i.e.* oscillations above/below 0 °C. Diurnal ranges exceeding 10 °C occur predominantly during spring and summer, taking place for all months except May-July at E1, all months except May-August at E2, and for all months at E5. Oscillations around 0 °C occur only once on 14 July 2015.

**Table 35: Oscillations around 0 °C (Osc), as well as diurnal ranges exceeding 10 °C ($T_{DR}$) for E1, E2 and E5. JJA: winter. SON: spring. DJF: summer. MAM: autumn.**

| Site | DR (%) | Osc (%) | % of year | Osc (%) | $T_{DR}$ (%) | | | | Osc (%) | | | |
|---|---|---|---|---|---|---|---|---|---|---|---|---|
| | | | | | JJA | SON | DJF | MAM | JJA | SON | DJF | MAM |
| E1 | 43 | 0 | 0 | 0.3 | 1 | 39 | 41 | 19 | 100 | 0 | 0 | 0 |
| E2 | 29 | 0 | 0 | 0.3 | 0 | 41 | 51 | 8 | 100 | 0 | 0 | 0 |
| E5 | 45 | 0 | 0 | 0.3 | 11 | 40 | 7 | 42 | 100 | 0 | 0 | 0 |

Only one potential freeze-thaw event, translating into one freeze-thaw cycle for the three sites is recorded (Table 36, pg. 147). A minimum of -0.5 °C is reached at E1, E2 and E5 14 July 2017 at 05:00, 06:00 and 06:00 respectively. Negative temperatures are maintained for ± four, three, and 2 hours respectively.

**Table 36: Freeze-thaw events for E1, E2 & E5, summarised by season from spring 2014 to winter 2015. PFTE: potential freeze-thaw events. FTC: freeze-thaw cycles. JJA: winter. SON: spring. DJF: summer. MAM: autumn.**

| Season | Potential Freeze Hours at 0 °C | | | PFTE | | | FTC | | |
|---|---|---|---|---|---|---|---|---|---|
| | E1 | E2 | E5 | E1 | E2 | E5 | E1 | E2 | E5 |
| SON | 0 | 0 | 0 | 0 | 0 | 0 | 0 | 0 | 0 |
| DJF | 0 | 0 | 0 | 0 | 0 | 0 | 0 | 0 | 0 |
| MAM | 0 | 0 | 0 | 0 | 0 | 0 | 0 | 0 | 0 |
| JJA | 4 | 3 | 2 | 1 | 1 | 1 | 1 | 1 | 1 |
| Total | 4 | 3 | 2 | 1 | 1 | 1 | 1 | 1 | 1 |

At E1 the diurnal temperature range on the day of the freeze-thaw cycles is 2 °C. The maximum diurnal temperature is 2 °C, the minimum -0.5 °C. Diurnal mean temperature is 1 °C. At E2 the diurnal temperature range, maximum, minimum, and diurnal mean temperature is 3 °C, 3 °C, -0.5 °C, and 1 °C respectively. At E5 the diurnal temperature range, maximum, minimum, and diurnal mean temperature is 7 °C, 7 °C, -0.5 °C and 4 °C respectively. Correlations between maximum and minimum freeze duration to diurnal maximum and minimum cannot be calculated, since only one freeze-thaw cycle is identified.

#### 5.1.2.3.4 E3

Diurnal ranges and oscillations around 0 °C are provided in Table 37. At E3, using an XR5 logging system, diurnal ranges of 10 °C for air temperatures are common (± 63%), occurring in every month. Of the ranges, ± 4% reflect maximums above and minimums below 0 °C; *i.e.* oscillations above/below 0 °C. Near surface temperatures (NST: temperatures recorded at ± 1 cm in the ground), reflect similar values, with diurnal temperature ranges exceeding 10 °C a common occurrence (63% of the time). Of these ranges, 1% reflect oscillations above/below 0 °C. At GST such diurnal ranges decrease to 54% (0% >/< 0 °C), to 31% at $T_5$ (0% >/< 0 °C), and to 0% for $T_{10}$. All diurnal ranges exceeding 10 °C reflect positive ranges, *i.e.* both diurnal maximum and minimum temperatures are positive, except for eight instances for air temperature and two instances for NST. Diurnal ranges exceeding 10 °C occur throughout the year. However, for those sensors where ranges exceed 10 °C more than 60% (> 80% for $T_5$) occur during spring and summer. Oscillations around 0 °C occur only in winter. For air temperatures these are spread across the winter months (three each for June and July, two for August), with one occurrence each for July and August at NST.

**Table 37: Oscillations around 0 °C (Osc), as well as diurnal ranges exceeding 10 °C ($T_{DR}$) for E3. Annual Osc (%) reflect all oscillations around 0 °C, including those where $T_{DR}$ does not exceed 10 °C. $T_{AIR}$ reflects air temperature; NST reflects ground temperature recorded at the near surface (± 1 cm); GST indicates temperature recorded at the ground surface (± 2 cm). The subscript following 'T' indicates the depth of the sensor (in centimetres) used to record ground temperature. JJA: winter. SON: spring. DJF: summer. MAM: autumn.**

| Sensor | $T_{DR}$ (%) | Osc (%) | % of year | Annual Osc (%) | $T_{DR}$ (%) | | | | Osc (%) | | | |
|---|---|---|---|---|---|---|---|---|---|---|---|---|
| | | | | | JJA | SON | DJF | MAM | JJA | SON | DJF | MAM |
| $T_{AIR}$ | 63 | 4 | 2 | 7 | 15 | 29 | 32 | 24 | 100 | 0 | 0 | 0 |

| Sensor | $T_{DR}$ (%) | Osc (%) | % of year | Annual Osc (%) | $T_{DR}$ (%) | | | | Osc (%) | | | |
|---|---|---|---|---|---|---|---|---|---|---|---|---|
| | | | | | JJA | SON | DJF | MAM | JJA | SON | DJF | MAM |
| NST | 63 | 1 | ± 1 | 3 | 9 | 28 | 33 | 30 | 100 | 0 | 0 | 0 |
| GST | 54 | 0 | 0 | 1 | 4 | 31 | 38 | 27 | 0 | 0 | 0 | 0 |
| $T_5$ | 31 | 0 | 0 | ± 0 | 0 | 34 | 50 | 16 | 0 | 0 | 0 | 0 |
| $T_{10}$ | 0 | 0 | 0 | 0 | 0 | 0 | 0 | 0 | 0 | 0 | 0 | 0 |

During 2015-16 few sub-zero temperatures are evident for air temperatures (potential freeze-thaw events: 24). Similarly, a paucity of potential freeze-thaw events and freeze-thaw cycles are observed for NST and GST (potential freeze-thaw events of 16 and six respectively). Freezing occurs within the upper centimetre of the ground and at GST (± 2 cm) hardly any freezing is observed. Negative air temperatures generally occur during winter (n = 22) and negative air temperatures are reached only twice during spring (n = 2). A minimum of -7 °C is reached for air temperatures on 14 July 2015 at 03:00 and negative temperatures are maintained for ± 7 hours on average. During the observation period only four freeze-thaw cycles for three separate days are observed at NST (two on 30 June, one each for 13/14 & 31 July), with one freeze-thaw cycle at GST (13/14 July). While sub-zero temperatures are recorded at $T_5$ on 14 July no freezing occurs at this depth. Less than one third (25% & 17% respectively) of potential freeze-thaw events translate into freeze-thaw cycles at NST and GST (Table 38).

**Table 38: Freeze-thaw cycles (FTC) and potential freeze-thaw events (PFTE) for E3, summarised by season. Under 'FTC; the first value indicates FTC for NST, the second value GST. $T_{AIR}$: air temperature. NST: ground temperature recorded at the near surface (± 1 cm). GST: temperature recorded at the ground surface (± 2 cm). The subscript following 'T' indicates the depth of the sensor (in centimetres) used to record ground temperature. JJA: winter. SON: spring. DJF: summer. MAM: autumn.**

| Season | Potential Freezing Hours at 0 °C | | | | | PFTE | | | | | FTC |
|---|---|---|---|---|---|---|---|---|---|---|---|
| | $T_{AIR}$ | NST | GST | $T_5$ | $T_{10}$ | $T_{AIR}$ | NST | GST | $T_5$ | $T_{10}$ | |
| JJA | 144 | 88 | 31 | 7 | 0 | 22 | 16 | 6 | 1 | 0 | 4 \| 1 |
| SON | 18 | 0 | 0 | 0 | 0 | 2 | 0 | 0 | 0 | 0 | 0 \| 0 |
| DJF | 0 | 0 | 0 | 0 | 0 | 0 | 0 | 0 | 0 | 0 | 0 \| 0 |
| MAM | 0 | 0 | 0 | 0 | 0 | 0 | 0 | 0 | 0 | 0 | 0 \| 0 |
| Total | 162 | 88 | 31 | 7 | 0 | 24 | 16 | 6 | 1 | 0 | 4 \| 1 |

Freeze-thaw cycles occur exclusively during winter with average freezing duration of 7 hours ($s$ = 6). Freezing generally takes place from 07:00-14:00 and a 4-hour delay between NST and GST is recorded for 13/14 July with freezing observed for ± 15 hours at GST. The longest and deepest freeze-thaw cycle initiates at 17:00 on 13 July and lasts 17 hours at NST and 15 hours at GST. Multiple freeze events are observed for 30 June at NST with the initial freeze event the shortest, lasting 1 hour from 01:00-02:00. The second event is longer (6 hours) and occurs from 03:00-09:00. Only one freeze-thaw cycle lasts longer than 10 hours (Figure 64, pg. 149), registering 17 hours at NST and 15 hours at GST. This is also the only instance of a freeze-thaw cycle lasting longer than the average freezing duration of 7 hours. Variability for temperature initially increases from air temperatures to NST. From NST downwards, an increase in depth into the ground yields a decrease in variability. Highest variability is evident for NST ($s$ = 1.85), lowest for $T_{10}$ ($s$ = 0.40). At NST the average diurnal range approximates 5 °C, although a

maximum range of 9 °C is reached. At GST the average diurnal range approximates 7 °C, although a maximum of 8 °C is reached. At NST diurnal maximum is 9 °C, while diurnal minimum is -4 °C. At GST these values are 8 °C and -2 °C respectively. Correlations between maximum and minimum freeze duration to diurnal maximum and minimum temperatures are inconclusive, with only diurnal minimums having a significant correlation ($r \pm 0.96$, $p < 0.1$). For NST, average diurnal maximum, minimum and average temperatures of those days when freeze-thaw cycles occurred are 4 °C, -1 °C and 0.5 °C.

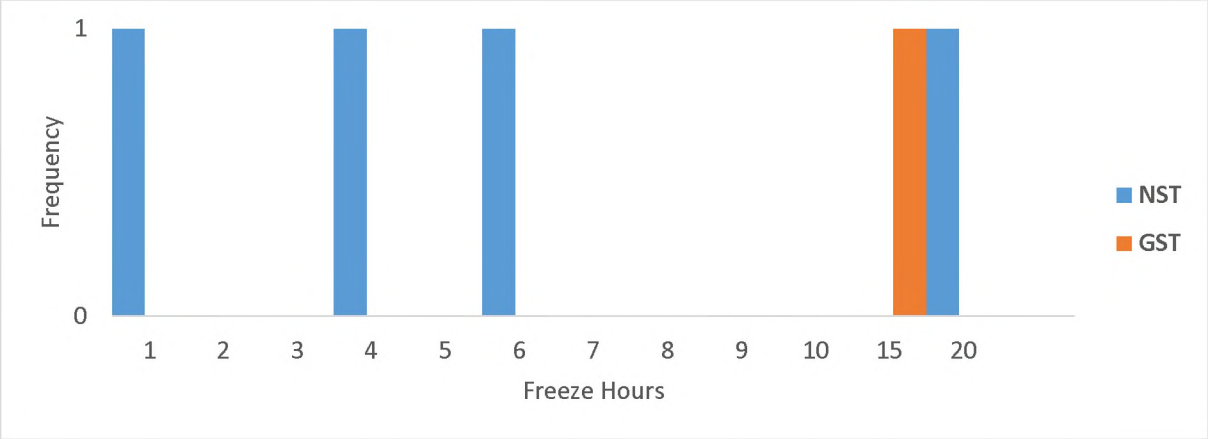


**Figure 64: Histogram of freeze duration per event per sensor depth for E3. NST: near surface (± 1 cm). GST: ground surface (± 2 cm).**

#### *5.1.2.3.4.1 Higher-frequency*

Higher-frequency temperature data using an XR5 system, recorded at ten-minute intervals, are available for E1 for the duration of the observation period and these data are evaluated only for those seasons for which freeze-thaw cycles occur at NST and GST, yielding an evaluation of the winter season.

Evaluating data recorded at an hourly interval yields six potential freeze-thaw events for NST, with four for GST. This translates into four freeze-thaw cycles at NST and one for GST (refer to 5.1.2.3.4 E3, pg. 147). At NST freeze-thaw cycles occur on three days (June: n = 2; July: n = 2). At GST only one freeze-thaw cycle is recorded (14 July) and freezing depth during this time is restricted to the upper portion of the ground. At NST two freeze-thaw cycles occur in June (30 June, 13/14 June). A further cycle takes place on 31 July. A freeze-thaw cycle at GST is evident on 13/14 July, indicating the maximum depth of freezing. The greatest intensity of any frost event during this time takes place on 14 July and reaches -3.55 °C. While diurnal ranges exceeding 10 °C occur throughout the year, the smallest proportion of these are recorded for winter months, when all freeze-thaw cycles are observed (Table 37, pg. 147). Nevertheless, diurnal ranges associated with freeze-thaw cycles approximate 10 °C. Evaluating higher-frequency data show that the number of potential freezing hours remains the same. However, the number of potential freeze-thaw events increases when higher-frequency data are evaluated (Table 39, pg. 150). Data recorded at shorter intervals yield more potential freeze-thaw events than those determined using hourly data. Although more potential freeze-thaw events are recorded with higher-frequency data, soil moisture coupled with the intensity of the potential freeze-thaw event is not

sufficient to yield more freeze-thaw cycles. Higher-frequency data confirms only one freeze-thaw cycle took take place on 14 July 2015. This is further corroborated by soil moisture dipping sharply toward the evening of 14 July, followed by a rise in soil moisture once thaw commenced in the morning of 15 July. No zero-curtain effect is observed at E3 and only one exotherm, taking place on 14 July following ground freezing, is recorded.

**Table 39: Freeze-thaw events for E3, recorded at 10-min intervals for winter 2015. Potential freeze-thaw events (PFTE) are shown, as are freeze-thaw cycles (FTC) in brackets. $T_{AIR}$: air temperature. NST: ground temperature recorded at the near surface (± 1 cm). GST: temperature recorded at the ground surface (± 2 cm). The subscript following 'T' indicates the depth of the sensor (in centimetres) used to record ground temperature. JJA: winter.**

| Season | Potential Freezing Hours at 0 °C | | | | | PFTE | | | | | FTC |
|---|---|---|---|---|---|---|---|---|---|---|---|
| | $T_{AIR}$ | NST | GST | $T_5$ | $T_{10}$ | $T_{AIR}$ | NST | GST | $T_5$ | $T_{10}$ | |
| JJA | 144 | 88 | 31 | 7 | 0 | 47 (22) | 24 (16) | 8 (6) | 1 (1) | 0 (0) | 1 (1) |

Like data recorded at hourly intervals, higher-frequency data show the greatest variability of ground temperatures at NST (*s* ± 4.13) and GST (*s* ± 3.53), with the least at $T_{10}$ (*s* ± 2.20). Soil moisture steadily decreases from June to July, with a sharp increase observed following thaw. An evaluation of these data also shows that no freeze-thaw cycles are evident for $T_5$, in agreement with the evaluation of hourly data. Thawing and freezing indices for various sensors, given as days, are provided in Table 40. The thawing index generally decrease with increasing depth into the ground, as does the freezing index for August. During June and July, the months where freeze-thaw cycles are recorded, the freezing index decreases from air temperatures to GST, where it increases again. This trend indicates the depth of freezing, as already determined using the freezing depth (discussed in 5.1.2.3.4 E3 from pg. 147 onwards). The greatest freezing index is observed at NST, followed closely by GST. Both sensors record the highest values in July (-2 and -1 respectively). In comparison, the highest thawing index is recorded in August for all sensors. Furthermore, the freezing index never exceeds the thawing index, irrespective of sensor nor month. The balance of degree days is 219 toward the thawing index for air temperatures. This balance is 162, 155, 154 and 164 for NST, GST, $T_5$ and $T_{10}$ respectively. The thawing index consistently exceeds the freezing index, indicating an environment unlikely to be affected by ground frost. The thermal offset for NST and GST is skewed towards negative values for winter months.

**Table 40: The freezing index (FI) and thawing index (TI) for the various sensor depth for E3 for winter 2015. $T_{AIR}$: air temperature. NST: ground temperature recorded at the near surface (± 1 cm). GST: temperature recorded at the ground surface (± 2 cm). The subscript following 'T' indicates the depth of the sensor (in centimetres) used to record ground temperature. SO: thermal offset. DD: degree days.**

| Day | FI | | | | | TI | | | | | SO: NST | SO: GST |
|---|---|---|---|---|---|---|---|---|---|---|---|---|
| | $T_{AIR}$ | NST | GST | $T_5$ | $T_{10}$ | $T_{AIR}$ | NST | GST | $T_5$ | $T_{10}$ | | |
| June | -1 | 0 | 0 | 0 | 0 | 184 | 118 | 116 | 121 | 144 | -2 | -2 |
| July | -6 | -2 | -1 | 0 | 0 | 178 | 135 | 131 | 132 | 146 | -1 | -1 |
| August | -1 | 0 | 0 | 0 | 0 | 303 | 235 | 219 | 210 | 203 | -2 | -3 |
| Balance * | 219 | 162 | 155 | 154 | 164 | * Difference of DD between FI and TI | | | | | | |

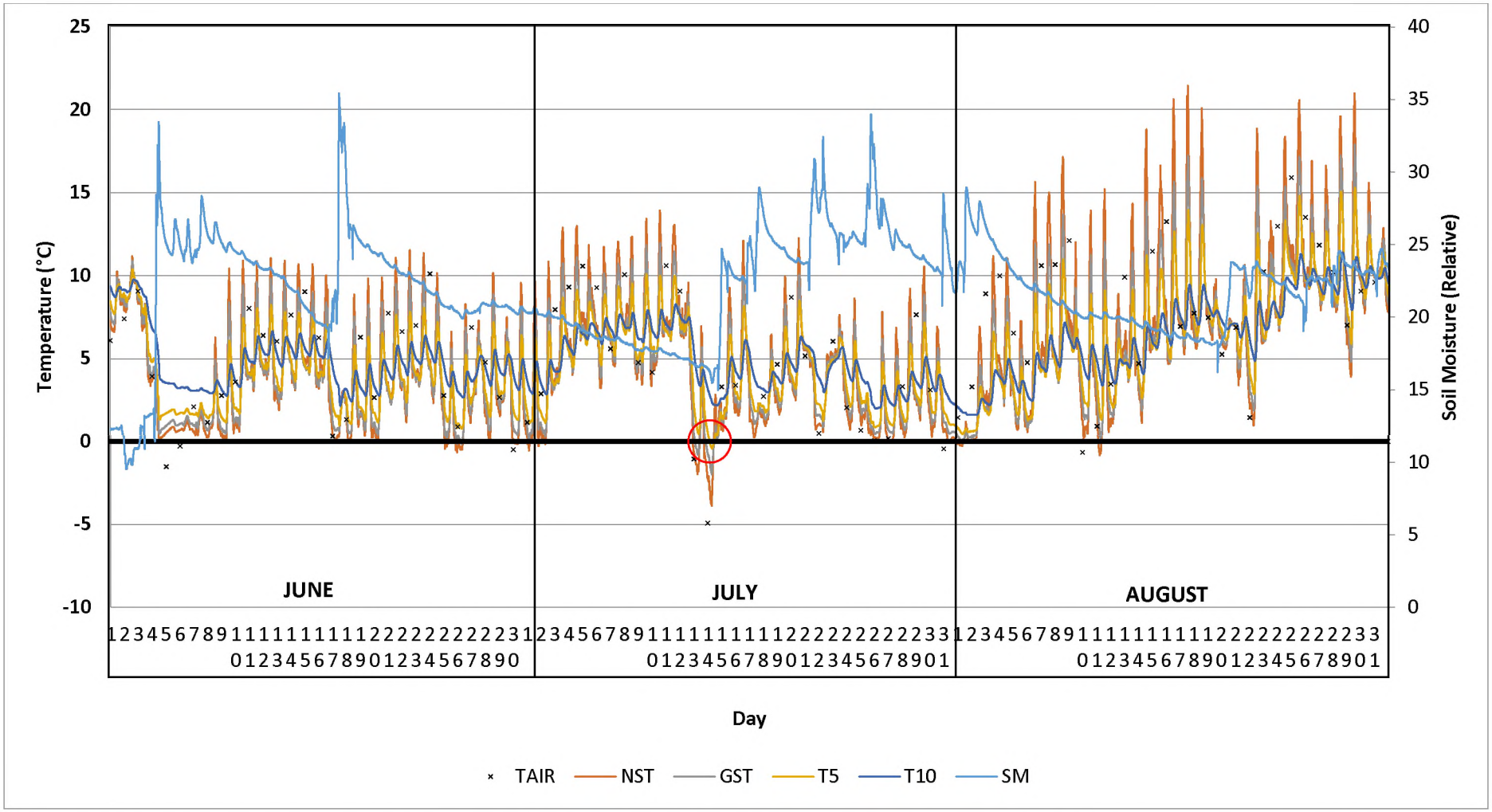


**Figure 65: Temperature and ground moisture 10-minute data at E3 for winter 2015. Black outlines delineate months. Exotherms are shown with red circles. $T_{AIR}$: air temperature. GST: recorded at ± 2 cm in the ground. The number after 'T' indicates the depth of the sensor (in centimetres) in the ground. SM: soil moisture.**

#### 5.1.2.3.5 Eastern Cape comparison

For Ben MacDhui ground surface temperatures (GST: temperatures recorded at ± 2 cm, depth), exhibit the greatest ranges, with seasonal ranges decreasing by 0.2 °C.cm$^{-1}$ increase in depth. For the Elandsberg near surface temperatures (NST: temperatures recorded at ± 1 cm, depth) and GST exhibit the greatest ranges, with seasonal ranges increasing from NST-$T_5$, after which ranges decrease (Table 41). Rate of change with depth is 0.1 °C.cm$^{-1}$ for the Elandsberg. This equates to a seasonal change in range of ± 20 °C.m$^{-1}$ for Ben MacDhui, compared to 10 °C.m$^{-1}$ for the Elandsberg.

**Table 41: Seasonal temperature averages ($T_{SM}$) and variability (*s*) for summer (DJF) and winter (JJA), as well as seasonal temperature ranges ($T_{SR}$) and the annual ground freezing index (GFI) for Eastern Cape sites. Under 'DFJ' and 'JJA' the first value reflects $T_{SM}$, the second value *s*.**

| Site | DJF | JJA | $T_{SR}$ | GFI |
|---|---|---|---|---|
| T1 | 13.4 / 0.6 | -0.5 / 0.9 | 14 | 2 399 |
| T2 | * | -0.8 / 0 .5 | * | * |
| T3 | 13.6 / 1.0 | -1.0 / 0.4 | 15 | * |
| T4 | 16.3 / 1.6 | 1.0 / 1.0 | 15 | 3 091 |
| T5 | * | 1.5 / 1.1 | * | * |
| E1 | 16.6 / 1.0 | 4.8 / 0.5 | 12 | 2 929 |
| E2 | 16.2 / 1.0 | 4.3 / 0.6 | 13 | 3 194 |
| E3 | 16.1 / 0.9 | 4.5 / 0.6 | 12 | 2 878 |
| E3# | 18.3 / 0.7 | 4.2 / 1.4 | 13 | 4 131 |
| E4 | 17.5 / 0.7 | 6.2 / 0.6 | 12 | 3 352 |
| E5 | 18.3 / 0.6 | 7.0 / 1.0 | 12 | 4 163 |
| E6 | 19.4 / 0.3 | 7.6 / 0.9 | * | 4 617 |
| E7 | 17.4 / 0.8 | 7.4 / 0.6 | 10 | 2 166 |

Seasonal ranges for all sites are not significantly different at $p \pm 0.05$. However, sites located at higher altitudes reflect longer duration of frozen ground and seasonal means increase with a decrease in elevation. Furthermore, T1 reflects freeze-thaw cycles during winter and spring with all other sites having freeze-thaw cycles only in winter. Seasonal ranges are strongly correlated to m a.s.l. ($r = 0.75$, $p < 0.05$), as are absolute minimum temperatures achieved ($r = -0.88$, $p \pm 0.00$) and freeze-thaw cycles ($r = 0.80$, $p < 0.05$). Furthermore, T1 and E3 show a high and significant correlation ($r = 0.99$, $p \pm 0.00$) when evaluated against geographical location, air and ground temperature parameters (means, maximums and minimums), potential freeze-thaw events, and freeze-thaw cycles. Higher altitudinal sites reflect seasonal ground frost; those at lower elevations do not. The thick vegetation of the Elandsberg ameliorates ambient air temperatures and freeze-thaw cycles are rare. Ben MacDhui sites are sparsely vegetated and at higher altitudes, which is reflected in more and longer freeze-thaw events. Principal Component Analysis (PCA) shows that freezing depth, freeze-thaw cycles and altitude trend together. Similarly, potential freeze-thaw events, temperature averages of GST and altitude trend together.

### 5.1.3 Sediment/soil specifics

Results from the analysis of textural and moisture properties are provided in Table 42 and Table 43 (pg. 158) respectively. Descriptive statistics are provided **Table 44** (pg. 159). Discussion of results follows each table and graphs are provided where deemed necessary.

**Table 42: Sediment physical characteristics and parameters for the Eastern Cape study sites. Total organic carbon (TOC) is expressed as a percentage; $d_b$ indicates bulk density; $d_p$ indicates porosity of samples; FEF (%) the fine earth fraction expressed as a percentage.**

| Site | Depth | TOC (%) | $d_b$ | $d_p$ | FEF (%) |
|---|---|---|---|---|---|
| ELANDSBERG | | | | | |
| E1 | Surface | 21.4 | 0.33 | 0.87 | 97.30 |
| E2 | | 12.6 | 0.46 | 0.83 | 87.47 |
| E3 | | 13.0 | 0.42 | 0.84 | 94.73 |
| E4 | | 6.5 | 0.74 | 0.72 | 87.74 |
| E5 | | 3.2 | 0.96 | 0.64 | 69.77 |
| E6 | | 2.3 | 1.16 | 0.56 | 80.23 |
| E7 | | 4.8 | 0.92 | 0.65 | 86.18 |
| BEN MACDHUI | | | | | |
| T1 | Surface | 8.3 | 0.88 | 0.67 | 59.18 |
| T2 | Surface | 7.7 | 1.01 | 0.62 | 56.15 |
| | 15 | 5.5 | 0.86 | 0.68 | 52.77 |
| T3 | Surface | 5.6 | 1.15 | 0.57 | 58.20 |
| | 15 | 4.6 | 0.92 | 0.65 | 59.19 |
| T4 | Surface | 7.8 | 0.87 | 0.67 | 73.90 |
| | 15 | 4.2 | 1.04 | 0.61 | 54.98 |
| T5 | Surface | 9.6 | 0.80 | 0.70 | 65.73 |

In the Elandsberg total organic carbon (TOC) is greatest at highest altitude and decreases with decreasing altitude to E6 where these values increase again (Figure 66, pg. 154). This is reflected in the organic soil description of Table 12 (APPENDIX E), where E1 can be considered as peat, E2 and E3 as organic soil, and E4-E7 as mineral soil with organic matter. The fine earth fraction (FEF: particle sizes < 2 mm) is high overall, decreasing as sites decrease in altitude to E5 where the fraction increases again (Figure 70, pg. 156). In general, bulk density increases with decreasing altitude (Figure 67, pg. 154). As expected, the associated porosity values decrease with decreasing altitude (Figure 67). Using bulk density as a determinant for material description, all sites, except for E6, are soils high in organic content (Table 9, APPENDIX E). E6 is classified as clay/clay loam/silt loam. Using porosity as a determinant for material description all sites have clayey-silt soils (Table 10, APPENDIX E). This reflects an average specific yield ($S_y$) between 2-18 for these sample sites (Table 11, APPENDIX E) and a specific retention of moisture of ± 7 (Robson, 1993).

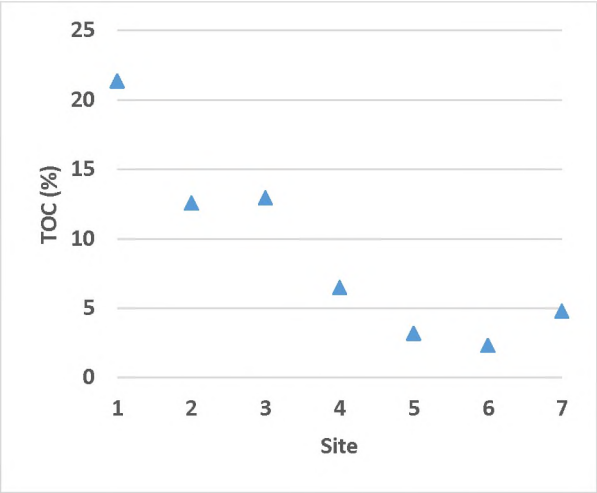


**Figure 66: Total organic carbon (TOC) expressed as a percentage for Elandsberg sites. 1-7 indicate sites E1-E7.**

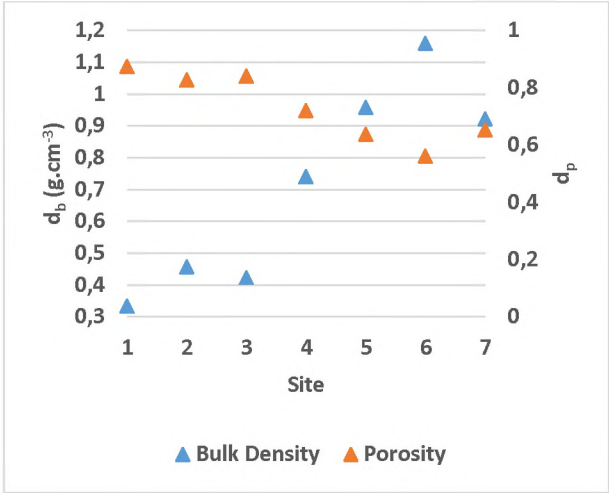


**Figure 67: Bulk density ($d_b$) and porosity ($d_p$) for Elandsberg sites. 1-7 indicate sites E1-E7.**

Total organic carbon (TOC) is comparable to organic content of ground samples taken in the Lesotho Highlands at 3 200 m a.s.l. (Sumner, 2003b). On average, Ben MacDhui samples show lower TOC (Figure 68, pg. 155) for sub-surface samples, compared to surface samples (7.79% vs. 4.77%). Similarly, the fine earth fraction is less for samples at depth (63% vs. 56% for surface and sub-surface samples respectively) (Figure 70, pg. 156). For surface samples, bulk density increases for the first 300 m of decreasing altitude, after which they decrease (Figure 69, pg. 155). The associated porosity values decrease for the first 300 m in altitudinal decrease (T1-T3), after which they increase (T4 and T5) (Figure 69, pg. 155). However, variation (expressed as standard deviation: *s*) of bulk density and porosity for surface samples is low and even less for sub-surface samples ($s$ = 0.14 and $s$ = 0.09 respectively). A comparison of surface to sub-surface samples of TOC, shows higher values for surface samples. T2 and T3 exhibit higher bulk density and associated lower porosity values for surface compared to sub-surface samples. For T4 this relationship is reversed. Like the Elandsberg, TOC decreases with deceasing altitude to T3, where it increases again. This is reflected in the organic soil description of Table 12 (APPENDIX E), where the T1 and T5 surface samples can be considered as organic soils, with all other samples as mineral soil with organic matter.

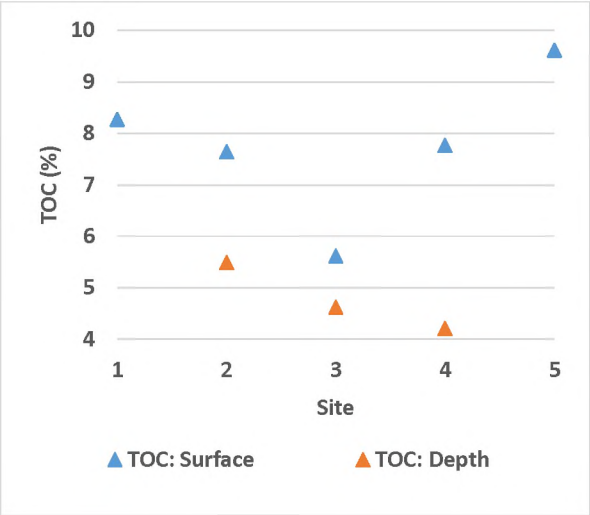


**Figure 68: Total organic carbon (TOC) expressed as a percentage for Ben MacDhui sites. 1-5 indicate sites T1-T5.**

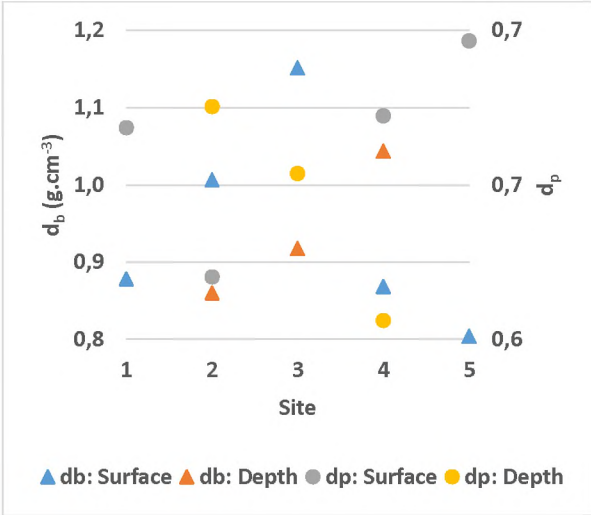


**Figure 69: Bulk density ($d_b$) and porosity ($d_p$) for Ben MacDhui sites. 1-5 indicate sites T1-T5.**

Using bulk density as a determinant for material description, surface samples for T2 and T3, as well as the sub-surface sample of T4 can be classified as clay/clay loam/silt loam, with all other sites classified as soils high in organic content (Table 9, APPENDIX E). Using porosity as a determinant for material description, all sites can be classified as clayey-silt soils (Table 10, APPENDIX E). This reflects an average specific yield ($S_y$) between 2-18 for these sample sites (Table 11, APPENDIX E) and a specific retention of moisture of ± 8-17 (Robson, 1993).

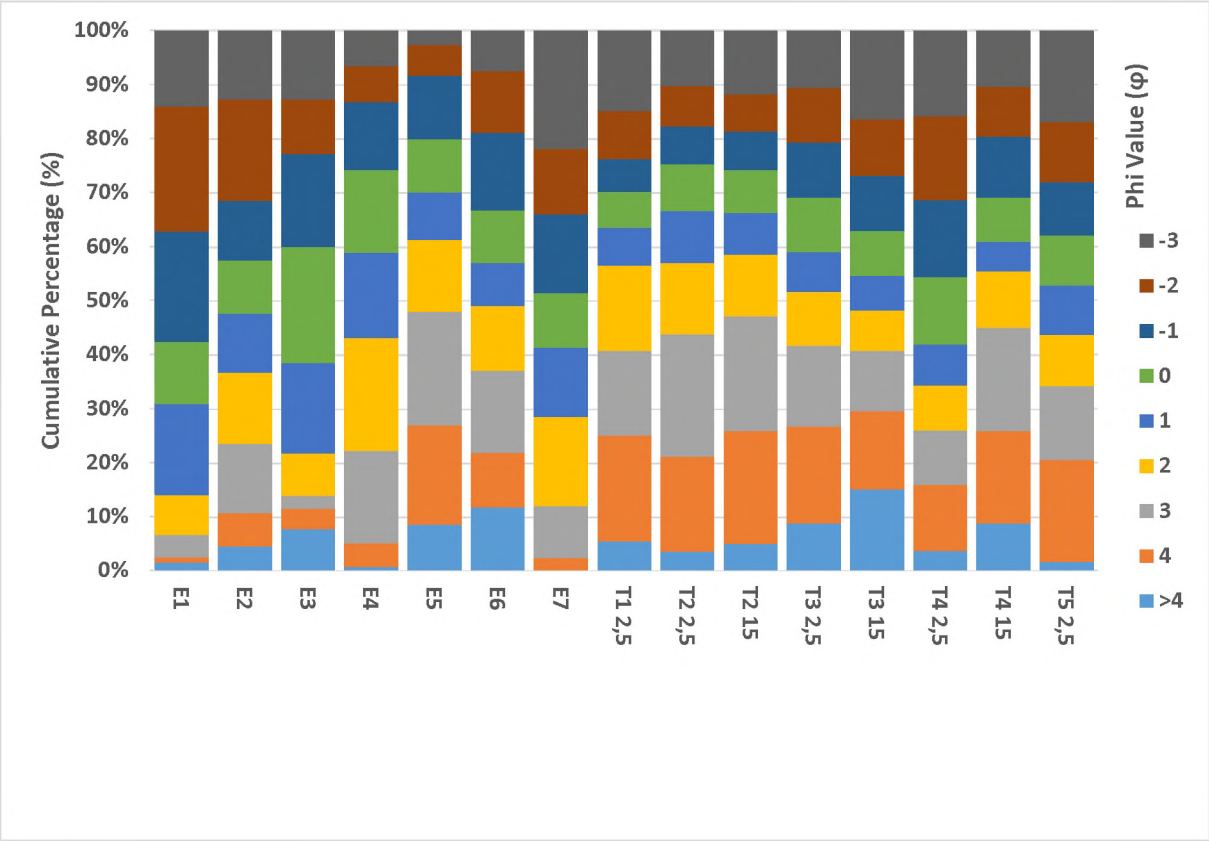


**Figure 70: Cumulative distribution of particle size distribution for Eastern Cape sampling sites, displayed using Phi (φ) values. 'E' denotes Elandsberg samples; 'T' denotes Ben MacDhui samples; 2,5 denotes surface samples; 15 denotes samples taken at 15 cm depth.**

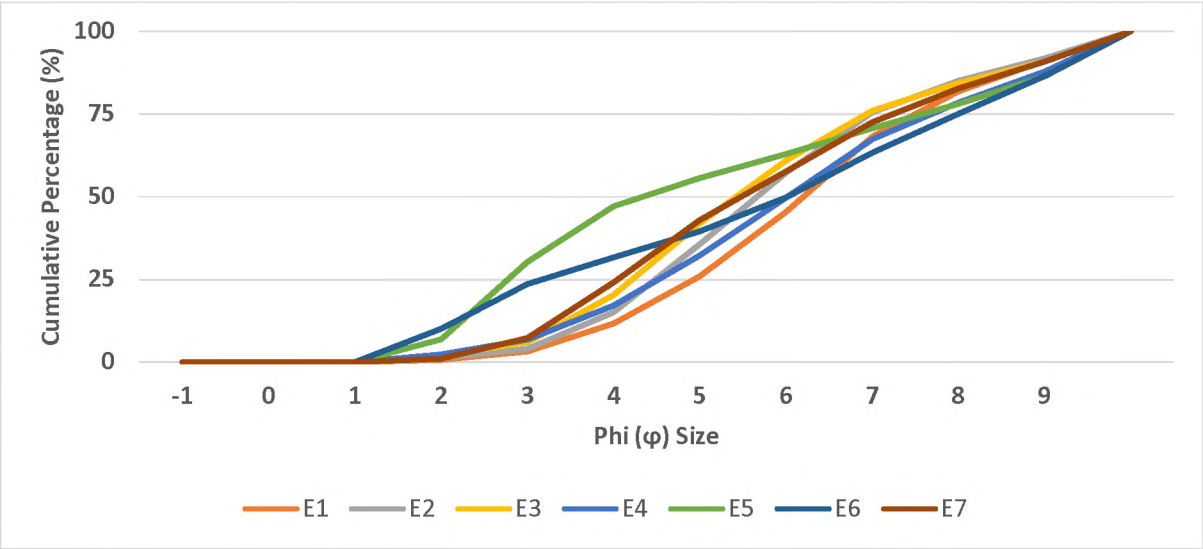


**Figure 71: Fine earth fraction analyses (φ: -1 to 9) for the Elandsberg.**

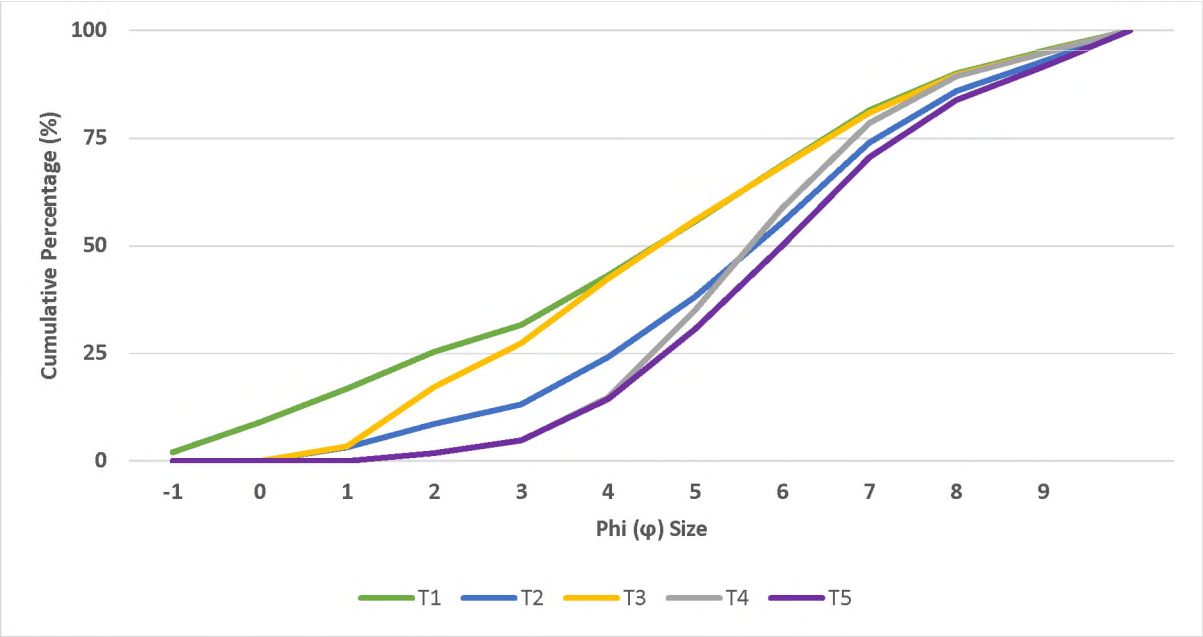


**Figure 72: Fine earth fraction analyses (φ: -1 to 9) for Ben MacDhui.**

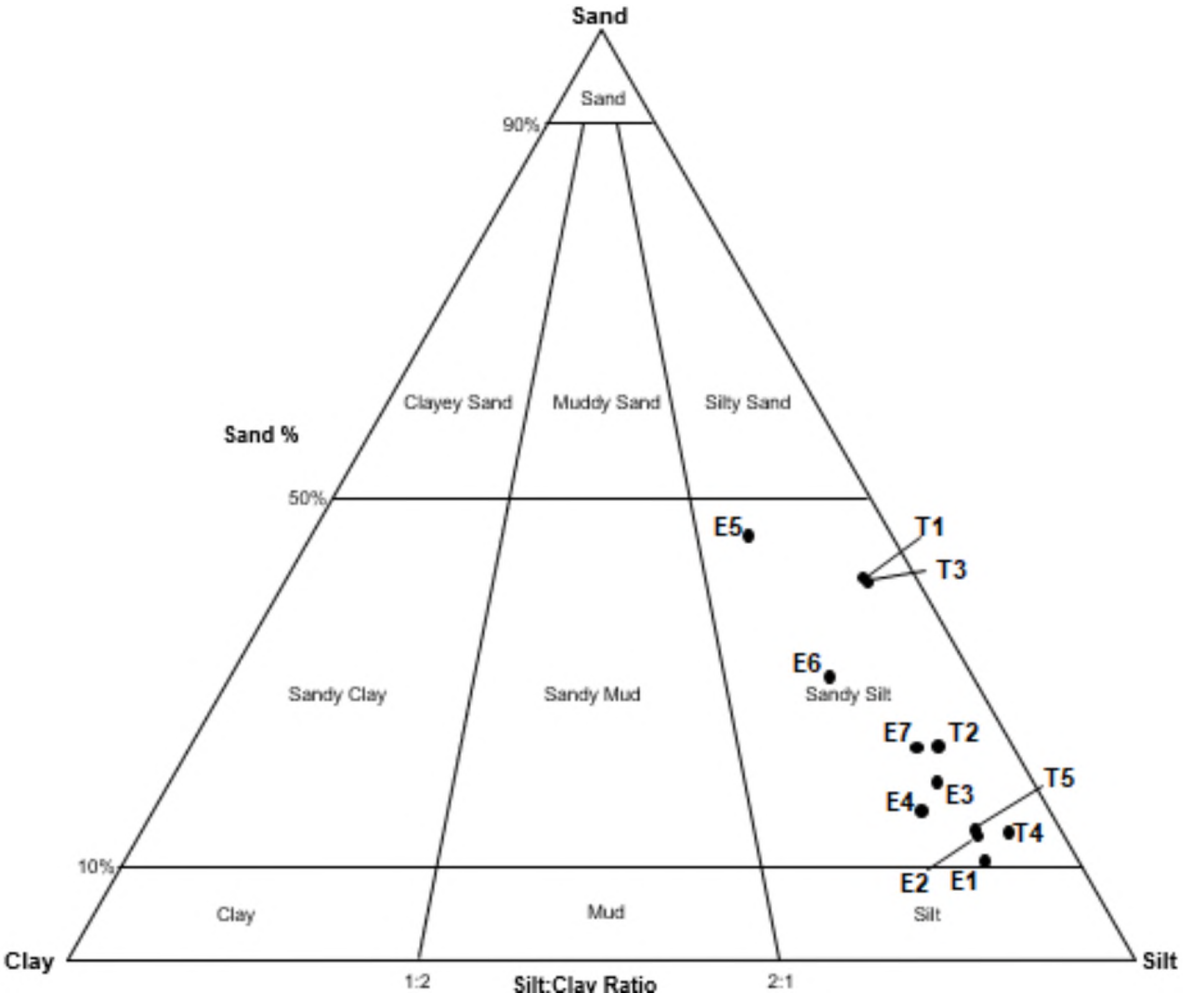


**Figure 73: Sand-silt-sand ternary diagram of Eastern Cape sediment samples. E1-E7 denotes Elandsberg samples; T1-T5 Ben MacDhui samples. The diagram reflects sediment ratios evaluated for the fine earth fraction (FEF: particles < 2mm in diameter) only.**

Proportions of the fine earth fraction are higher for the Elandsberg than for Ben MacDhui and the 50th percentile for the Elandsberg is more toward the smaller fraction than that for Ben MacDhui (Figure 70, pg. 156; Figure 71, pg. 156; Figure 72, pg. 157; Figure 73, pg, 157). All samples, irrespective of location, lack clay (Figure 73, pg, 157). Bulk density values are higher and the associated porosity values lower for the lower altitudinal Eastern Cape. Total organic carbon (TOC) is also higher for the Elandsberg than for Ben MacDhui. It is worth noting that for all samples except E1 and E3 the gravel proportion exceeds 10% and bulk density is, therefore, overestimated.

**Table 43: Sediment moisture characteristics and parameters for the Eastern Cape study sites. $\theta_v$ denotes volumetric water content; $\theta_g$ gravimetric water content; $M_c$ gravimetric water content expressed as a percentage; and $M_p$ the soil water-filled pore space.**

| Site | Depth | $\theta_v$ | $\theta_g$ | $M_c$ (%) | $M_p$ |
|---|---|---|---|---|---|
| ELANDSBERG | | | | | |
| E1 | Surface | 0.09 | 0.29 | 28.70 | 0.33 |
| E2 | | 0.13 | 0.29 | 28.84 | 0.35 |
| E3 | | 0.13 | 0.31 | 31.25 | 0.37 |
| E4 | | 0.12 | 0.17 | 16.67 | 0.23 |
| E5 | | 0.10 | 0.12 | 11.64 | 0.18 |
| E6 | | 0.13 | 0.11 | 11.27 | 0.20 |
| E7 | | 0.23 | 0.26 | 25.73 | 0.39 |
| BEN MACDHUI | | | | | |
| T1 | Surface | 0.22 | 0.25 | 25.48 | 0.00 |
| T2 | Surface | 0.25 | 0.25 | 24.51 | 0.00 |
| | 15 | 0.19 | 0.22 | 22.37 | 0.00 |
| T3 | Surface | 0.29 | 0.25 | 25.26 | 0.00 |
| | 15 | 0.28 | 0.31 | 30.70 | 0.00 |
| T4 | Surface | 0.28 | 0.32 | 31.71 | 0.00 |
| | 15 | 0.17 | 0.17 | 16.56 | 0.00 |
| T5 | Surface | 0.20 | 0.25 | 25.49 | 0.00 |

Elandsberg samples show a general increase in volumetric water content (VWC: $\theta_v$) with decreasing altitude (Figure 74, pg. 159). In comparison, gravimetric water content (GWC: $\theta_g$) shows a decreasing trend with decreasing altitude (Figure 74, pg. 159). Gravimetric water content expressed as a percentage ($M_p$) registers in the lower to medium ranges (0.39 for E7; 0.18 for E5). The highest GWC occurs for E3, which is located near a stream. The lower GWC for E4-E6 are ascribed to these sites located on steeper slopes with enhanced drainage. Averages for VWC, GWC, GWC expressed as a percentage, and soil water-filled pore space ($M_p$) are 0.14, 0.22, 22.01% and 0.29 respectively. Overall, Ben MacDhui surface samples have higher moisture values than sub-surface samples (Figure 75, pg. 159). Samples show an increase in VWC for surface samples for T1-T3, after which values decrease. Volumetric water content (VWC) for sub-surface samples increases from T2 to T3, after which it decreases. Gravimetric water content (GWC) is highly consistent for surface samples, with sub-surface samples more variable ($s$ = 0.03 and $s$ = 0.07 for surface and sub-surface samples respectively) and registering lower values on average. Averages for surface samples for VWC, GWC, GWC expressed as a

percentage, and the soil water-filled pore space ($M_p$) are 0.25, 0.26, 26.49% and 0.00 respectively. Averages for sub-surface samples for VWC, GWC, GWC expressed as a percentage, and the soil water-filled pore space ($M_p$) are 0.22, 0.23, 23.21% and 0.00 respectively.


**Figure 74: Volumetric water content (VWC) and gravimetric water content (GWC) for the Elandsberg. 1-7 denote sites E1-E7.**

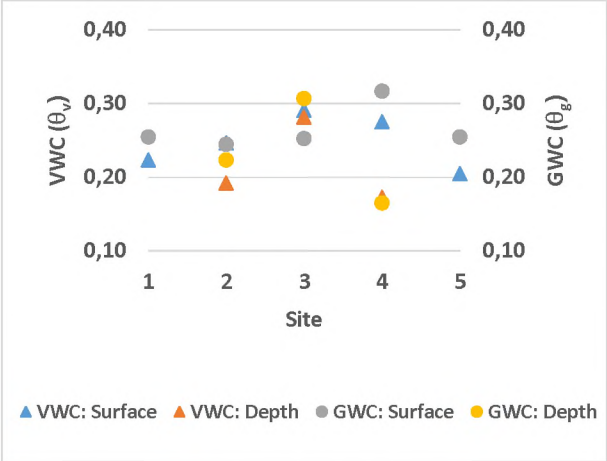


**Figure 75: Volumetric water content (VWC) and gravimetric water content (GWC) for Ben MacDhui sites. 1-5 denote sites T1-T5.**

Phi (ϕ) mean values for the Elandsberg show an increase in average particle size from the highest elevated point (E1) to E5, after which mean values decrease in size to E7. Phi (ϕ) mean values for Ben MacDhui are predominantly medium sand, except for T2 & T3 surface samples (coarse sand). The Elandsberg sites, compared to Ben MacDhui, also have greater variation in Phi (ϕ) mean values. Phi (ϕ) skewness values for Elandsberg sites are variable, with the higher altitudinal sites having a coarse tail (Figure 70, pg. 156; **Figure 71**, pg. 156). For the remaining sites this relationship is reversed. Phi (ϕ) skewness values show predominantly positively skewed populations for all Ben MacDhui samples (Figure 70, pg. 156; **Figure 72**, pg. 157). The Phi (ϕ) sorting and uniformity coefficient ($C_u$) index both indicate soil samples for the Eastern Cape to be poorly sorted. The uniformity coefficient ($C_u$) for all sites shows samples to be well graded. Applying the sorting index (S) shows no sorting and deficient samples for surface samples, compared to sub-surface samples for T2-T4. Furthermore, the sorting index indicates that surface samples at T4 are deficient for all textural sizes, when compared to sub-surface samples. No sorting is evident for coarser particles with textural fractions deficient for finer particles. The Kolmogorov-Smirnov (K-S) test shows that all samples for the Elandsberg are dissimilar at $p < 0.05$. For the Drakensberg, the T4 and T5 samples are dissimilar to all other samples at $p < 0.05$. The K-S test cannot be rejected at $p < 0.05$ for the surface samples of T1-T3 (when compared to each other). The sub-surface sample of T4 is also similar (K-S cannot be rejected at $p < 0.05$) to the surface samples of T1-T3. The paired comparisons of surface to sub-surface samples for T2 and T3 show that the K-S test cannot be rejected at $p < 0.05$. In contrast the paired comparison of T4 surface to sub-surface shows an acceptance of the null hypothesis at $p < 0.05$.

**Table 44: Phi (φ) descriptive characteristics and the uniformity coefficient ($C_u$) for Eastern Cape soil samples. 'E' denotes Elandsberg samples, 'T' Ben MacDhui samples.**

| Site | Depth | Phi (ϕ) Mean | Skewness | Sorting | $C_u$ |
|---|---|---|---|---|---|
| ELANDSBERG | | | | | |
| E1 | Surface | Fine sand | Finely negative | Very poor | Poor, uniformly graded |
| E2 | | Medium sand | | | Poor, well graded |
| E3 | | | Symmetrical | | |
| E4 | | | | | |
| E5 | | Coarse sand | Finely positive | | |
| E6 | | Medium sand | Symmetrical | | |
| E7 | | | Finely positive | | |
| BEN MACDHUI | | | | | |
| T1 | Surface | Medium sand | Positively skewed | Very poor | Poor, well graded |
| T2 | Surface | Coarse sand | | | |
| | 15 cm | Medium sand | | | |
| T3 | Surface | Coarse sand | | | |
| | 15 cm | Medium sand | Symmetrical | | |
| T4 | Surface | | | | |
| | 15 cm | | Positively skewed | | |
| T5 | Surface | | Symmetrical | | |

### 5.1.4 Sediment displacement for Ben MacDhui trenches

Moisture content for Ben MacDhui trenches shows an increase in moisture with a decrease in altitude up to T3, after which moisture values decrease (Figure 76, pg. 161). Gravimetric water content (GWC) shows an increase in moisture with depth. Total organic carbon (TOC) shows highest values occurring for the highest elevated sites and values decreasing with decreasing altitude (Figure 77, pg. 161). Higher TOC values are recorded for surface samples and TOC decreases with increasing depths into the ground. The fine earth fraction (Figure 78, pg. 161) shows an increase with depth for all sites except T2-1 and T3-2. Phi (ϕ) mean sizes are either fine gravel or coarse sand, with coarse sand generally overlying fine gravel (Table 45).

**Table 45: Phi (φ) mean textural sizes for Ben MacDhui trenches. 'C' indicates coarse sand; 'G' indicates fine gravel; 'B' indicates bedrock. 'T' denotes the sample site, whereas '1' reflects trench #1 and '2' trench #2.**

| 2,5 | G | C | C | G | G | C | C | C |
|---|---|---|---|---|---|---|---|---|
| 5 | C | G | G | | C | | | G |
| 10 | B | | | | | G | C | C |
| 15 | | B | | B | G | | | |
| Depth (cm) | T1 | | T2 | | T3 | | T4 | |
| | 1 | 2 | 1 | 2 | 1 | 2 | 1 | 2 |

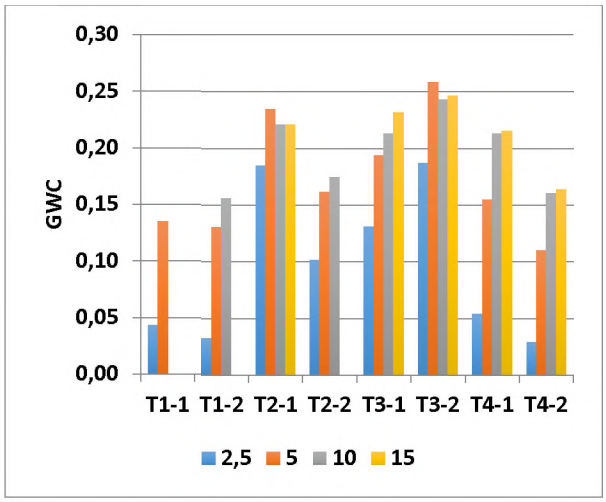


**Figure 76: Gravimetric water content (GWV) for marker trenches for Ben MacDhui. GWC is indicated for sediment depths per trench. 'T' indicates the sample site; the number following the '-' indicates the trench number.**

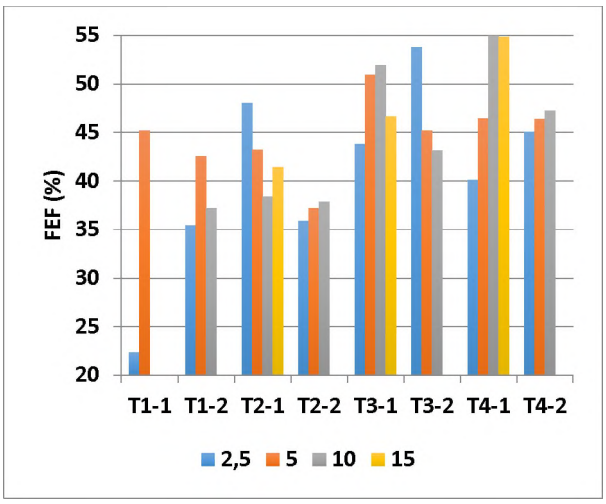


**Figure 78: The fine earth fraction (FEF) for marker trenches for Ben MacDhui. The FEF is indicated for sediment depths per trench. 'T' indicates the sample site; the number following the '-' indicates the trench number.**

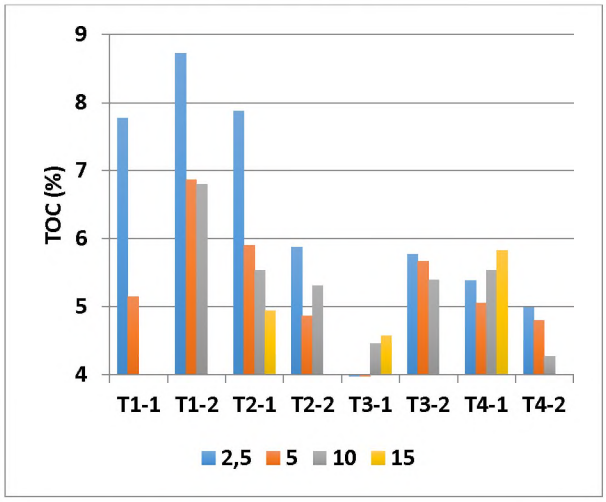


**Figure 77: Total organic carbon (TOC) for marker trenches for Ben MacDhui, shown as a percentage. TOC is indicated for sediment depths per trench. 'T' indicates the sample site; the number following the '-' indicates the trench number.**

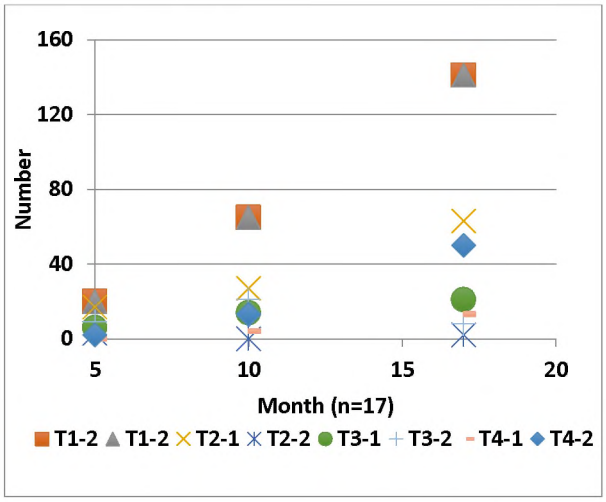


**Figure 79: Markers retrieved during site visits. The 1st visit occurred after five months; the 2nd after 10 months; the final visit at 17 months.**

Sorting is very poor for all depths for all trenches at all sites. Furthermore, Phi (ϕ) skewness indicates fine tails. As sites decrease in altitude the mean particle size also decreases, *i.e.* fine gravel dominates further upslope, whereas coarse sand dominates further downslope. No vertical sorting per trench is evident when computing the sorting index (S). Samples taken at the various depths show deficiency of textural fractions for sub-surface samples compared to surface samples, for Phi (ϕ) values of four and greater (>= 4), as well as -1 and 0. No sorting is evident in the vertical for Phi (ϕ) values of 2 and 3. All other textural fractions have variable deficient proportions and lack sorting. Analyses of particles of clay-sized fractions shows not significant disparate populations at $p < 0.05$.

Ternary diagrams are shown for trenches at T1-T4 in Figure 80-Figure 83. Sediment ratios are only evaluated for the fine earth fraction (FEF: particles < 2 mm in diameter). All trenches exhibit a paucity of clays, with the surface sample (taken at 2.5 cm) generally coarser than samples taken at the next depth (5 cm). The exception is T3 (Figure 81), where the surface sample consists of finer material than the sample taken at 5 cm depth.

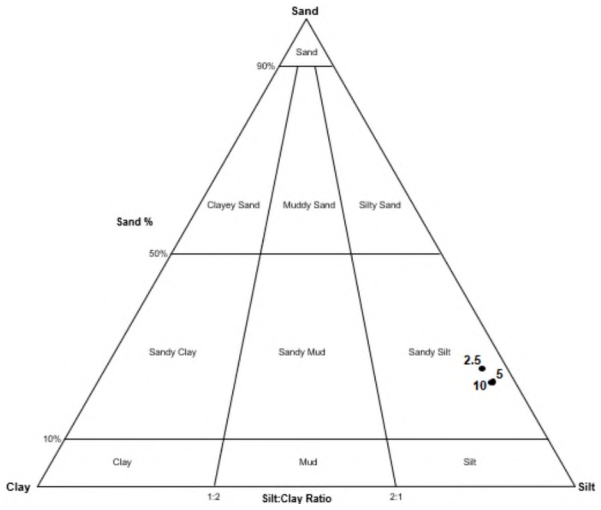


**Figure 80: Sand-silt-clay ternary diagram for trenches at T1. Numbers indicate depth of samples, in cm.**

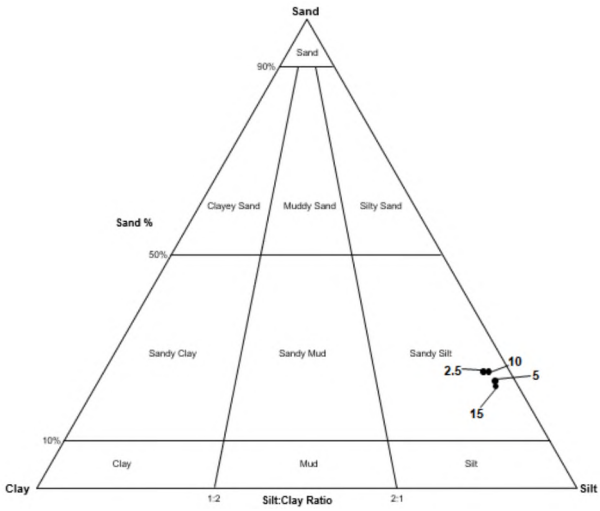


**Figure 82: Sand-silt-clay ternary diagram for trenches at T2. Numbers indicate depth of samples, in cm.**

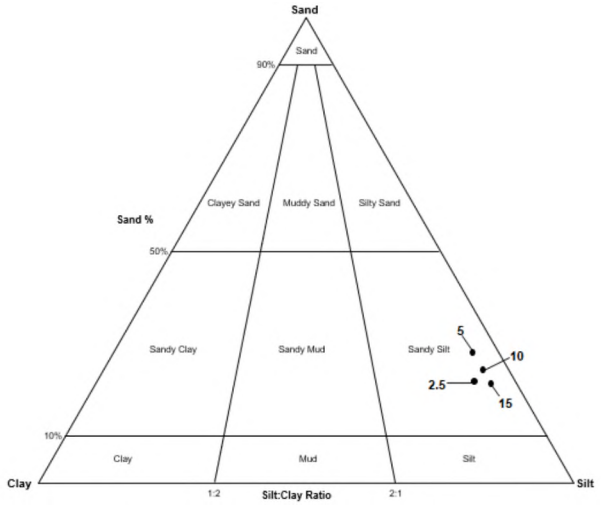


**Figure 81: Sand-silt-clay ternary diagram for trenches at T3. Numbers indicate depth of samples, in cm.**

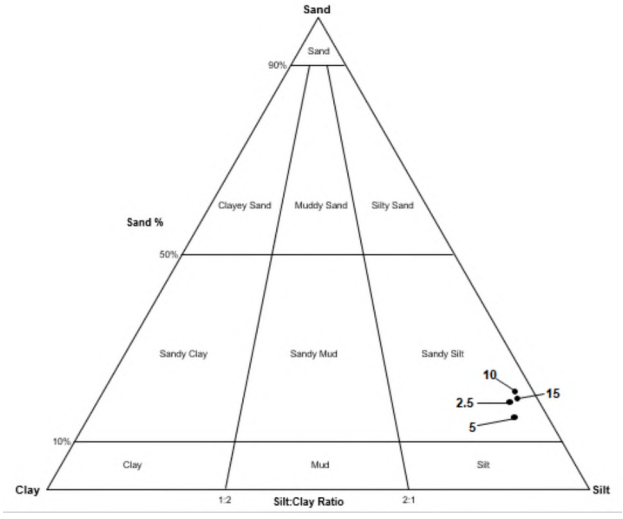


**Figure 83: Sand-silt-clay ternary diagram for trenches at T4. Numbers indicate depth of samples, in cm.**

Heave of dowels at T1 was ± 3.5 cm for the six months from April to November, with maximum heave observed over the June-August period. This heave is ± 8.5 cm for T2, ± 5 cm for T3, ± 2 cm for T4, and ± 4 cm for T5. All sites showed yellow markers heaved out (vertical displacement) during site visits and

the number of markers collected at the surface increased with time, with most markers collected after the completion of the experiment (Figure 79, pg. 161). More markers heaved for the higher elevated sites (T1 & T2) (Figure 84, pg. 163). All trenches show movement of markers deeper into the ground, *i.e.* markers placed at a certain depth moved both upward and downward into the soil column (Table 46).

**Table 46: Movement of painted markers per trench per site. Y, W, P, and B denote markers buried at 2 cm, 5 cm, 10 cm, and 15 cm depths. GS reflects the ground surface. Marker movement indicates maximum displacement of markers in the vertical.**

| Site | Trench Depth (cm) | Y | W | P | B | Marker Movement (cm) |
|---|---|---|---|---|---|---|
| T1-1 | 10 | GS-5 | 2.5-10 | | | 10 |
| T1-2 | 5 | GS-5 | 2.5-5 | | | 5 |
| T2-1 | 15 | GS-5 | 2.5-5 | 2.5-15 | 10-15 | 15 |
| T2-2 | 10 | GS-10 | 2.5-15 | 2.5-10 | | 15 |
| T3-1 | 15 | GS-10 | 5-15 | 5-15 | | 15 |
| T3-2 | 15 | GS-15 | 2.5-15 | 10-15 | | 15 |
| T4-1 | 15 | GS-10 | 2.5-5 | 10-15 | | 15 |
| T4-2 | 15 | GS-15 | 2.5-15 | 5-15 | | 15 |

Markers were also found outside the original confines of trenches (lateral displacement) (Figure 85). At T1 lateral displacement of markers is evident for 3 cm-5 cm depths. Displacement of markers outside of the confines of the trenches is greatest at T3, with ± 30% of collected markers 15 cm or more away from the central point of trenches. Almost all (± 95%) of markers heaved within the confines of trenches for T1 & T2 (minimal lateral displacement). At T4 no markers were collected greater than this threshold.

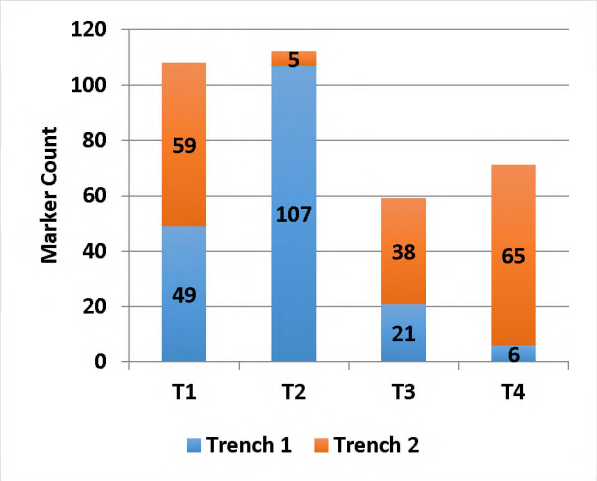


**Figure 84: Markers heaved per Ben MacDhui site, comparing marker heave amongst site trenches and total heave amongst sites.**

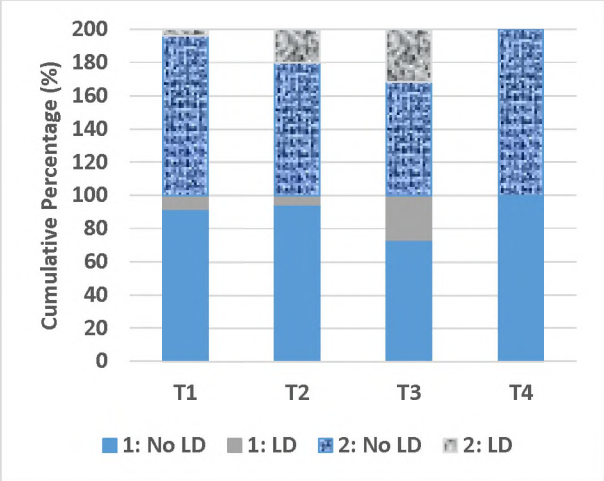


**Figure 85: Markers heaved per Ben MacDhui site, comparing percentage of markers heaved within to those heaved outside of the original confines of trenches. LD: lateral displacement. Columns to '100' reflect marker trench #1; those from '100-200' marker trench #2.**

Of 15 lengths of string sunk into the ground, 40% of sites had to be discarded due to strings pulled out, washed out or displaced through agents other than frost. Of the remaining sites ± 50 % showed no lateral movement nor deformation. Two sites registered deformation (Figure 86 and Figure 87), both located at T1. No observable deformation occurred for the first few centimetres of the ground, with maximum deformation recorded for 4-5 cm depths.

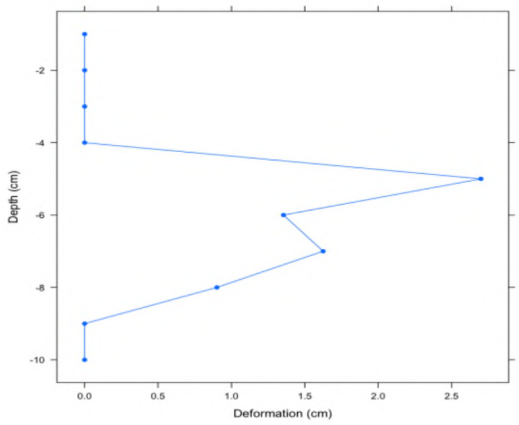


**Figure 86: String (S2) deformation for T1.**

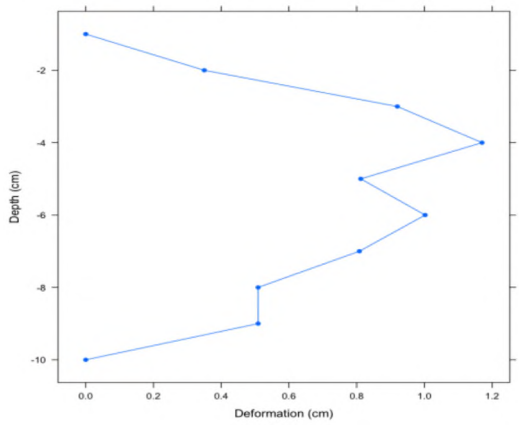


**Figure 87: String (S3) deformation for T1.**

## 5.2 Marion Island

A detailed description of locations on Marion Island is given on pg. 88. Similarly, an overview of temperature and moisture sensor depths, and their respective identifiers, is given in 4.3.1 Ground temperature and moisture data (pg. 80). However, for ease of reference site and sensor identifiers are briefly described here. Five temperature monitoring stations were erected on the Island given the identifiers M1 (at highest attitude) to M5 (at lowest altitude). Sensors are identified using a combination of 'T' (temperature) and a subscript number, *e.g.* '10', indicating the depth of the sensor within the ground, measured in centimetres. For example, '$T_{10}$' represents data obtained from temperature sensors that were buried at a depth of 10 cm. A Table of Abbreviations is available on pg. xxxiii, with a Table of Symbols on pg. xxxvi.

### 5.2.1 Climate and locational parameters

Of the five study sites on Marion Island only two record air temperatures, as well as ground temperatures. These are Katedraalkrans and Tafelberg (M1 and M2 respectively) (Figure 5, pg. 40). One additional logging station is located near M1 (Borg, 2017) and these data are used to supplement those collected at M1. The Marion Island South African Weather Service (SAWS) station is located near sea level (24 m a.s.l.), by the Marion Island research station. Data from this station were used to determine mean annual air temperature (MAAT) for those sites that do not record air temperatures. This allows for a comparison of recorded air temperatures to extrapolated MAAT using the environmental lapse rate of 6.5 °C.km$^{-1}$. Furthermore, averages for 55 years of climatic data for relative humidity, air temperatures, wind speed, wind direction and precipitation were calculated (Table 47), to identify the appropriate climatic zonation for the Island.

**Table 47: Climatic variables for Marion Island from 1960-2015. All values represent diurnal averages, maximums and minimums for each parameter. Prec indicates precipitation (mm). RH reflects relative humidity (%), T indicates temperature values ( °C), WS indicates wind speed (m.s$^{-1}$), WD indicates wind direction (° off true north). DM indicates diurnal means (averages), with :min and :max indicating minimums and maximums.**

| Parameter | $Prec_{DM}$ | $RH_{DM}$ | $T_{D:min}$ | $T_{D:max}$ | $T_{DM}$ | $WS_{D:min}$ | $WS_{D:max}$ | $WS_{DM}$ | $WD_{DM}$ |
|---|---|---|---|---|---|---|---|---|---|
| Average | 0.3 | 83 | 3 | 8 | 6 | 3 | 11 | 8 | 235-286 |
| Minimum | 0 | 28 | -12 | -1 | -3 | 0 | 0 | 0 | 0 |
| Maximum | 6 | 100 | 13 | 23 | 15 | 23 | 50 | 29 | 360 |

Average diurnal mean minimum temperature is 3 °C, with the average diurnal maximum temperature as 8 °C. Ambient air temperatures reach minimums of -12 °C, while maximums of 23 °C are also observed. Mean annual air temperature (MAAT) is 6 °C, with the average wind blowing out of the southwest to west (235-286°), with a standard deviation (*s*) of 55. While gusts of 29 m.s$^{-1}$ are recorded, the average diurnal wind speed is 8 m.s$^{-1}$ (Figure 88, pg. 166). Calms are rare (± 3% of the time) with winds exceeding 11.1 m.s$^{-1}$ a frequent occurrence (± 20% of the time). Schulze (1971) proposes a lapse rate of 4.5 °C.km$^{-1}$ for summer and a lapse rate of 4 °C.km$^{-1}$ for winter. Holness (2001a), in turn, proposes a lapse rate of 5 °C.km$^{-1}$. Using the recommended lapse rate of 5 °C.km$^{-1}$ the extrapolated

average MAAT for M1-M5 ranges from 2.1 °C at M1, the site of highest elevation, to 5.5 °C at M5, found at lowest elevation (Figure 37, pg. 88). However, extrapolated values do not concur for seasonal MAAT recorded at M1 and M2 for autumn and summer (Table 48, pg. 167). Extrapolated temperatures for M1 underestimate winter and spring and overestimate autumn temperatures by ± 1 °C. Extrapolated temperatures for summer months approximate recorded temperatures. At M2 the extrapolated summer and autumn average temperatures are respectively under- and over-estimated by ± 1 °C. Extrapolated temperatures for winter and spring approximate those recorded.

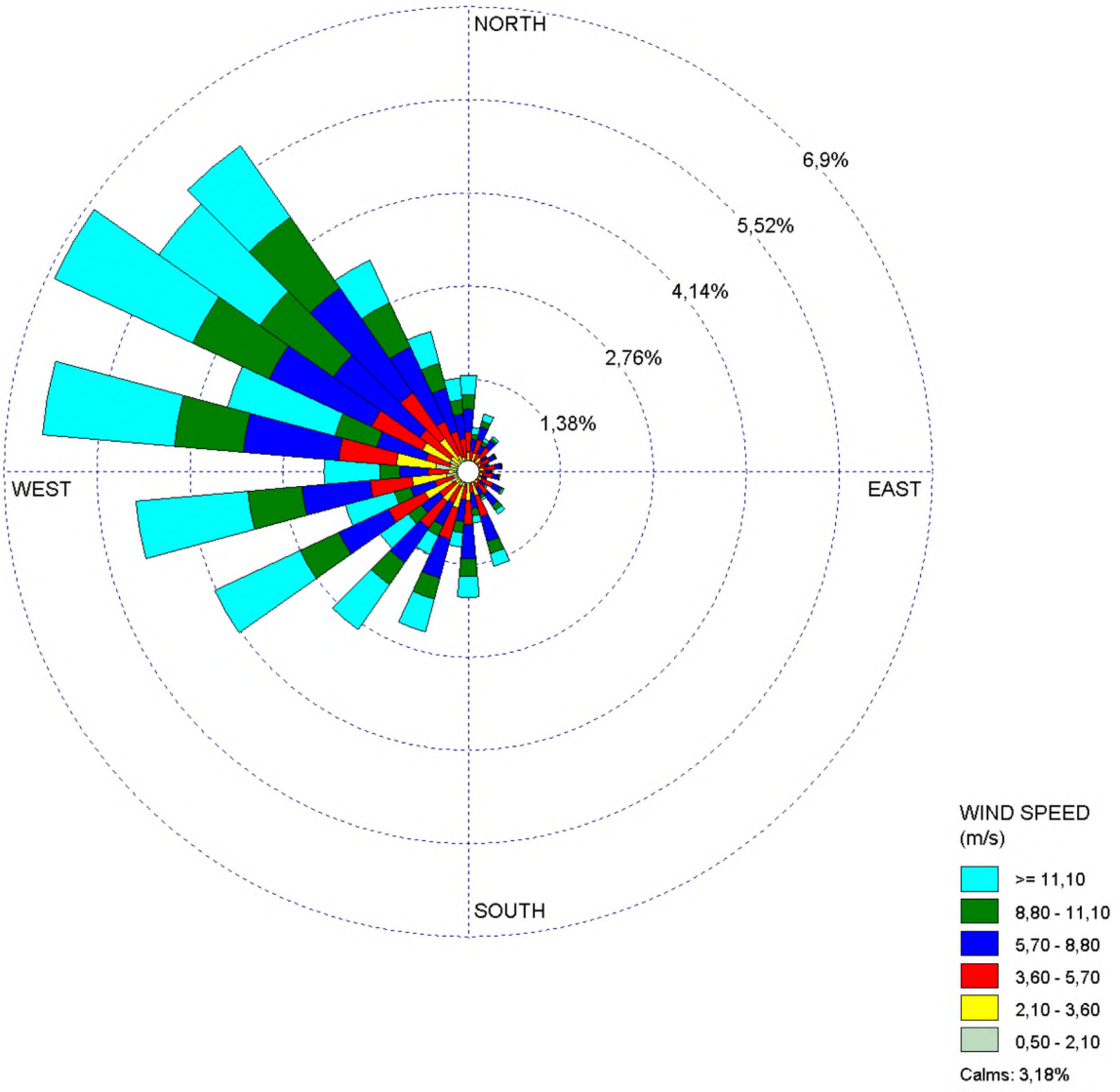


**Figure 88: Wind direction and average wind speed for Marion Island. Interval: 1 hour; 1960-2015. Missing data: ± 25%.**

**Table 48: Actual and extrapolated seasonal mean annual air temperatures (MAAT) for air temperatures at M1 and M2 (2013-2015) using a lapse rate of 5 °C.km$^{-1}$. $T_{AIR}$ reflects air temperature, measured in degree Celsius ( °C). Values in brackets indicate calculations using a 6.5 °C.km$^{-1}$ lapse rate. JJA: winter. SON: spring. DJF: summer. MAM: autumn.**

| Season | Extrapolated $T_{AIR}$ | | Actual $T_{AIR}$ | |
|---|---|---|---|---|
| | M1 | M2 | M1 | M2 |
| JJA | -0.4 | 0.8 | -1.2 | 0.7 |
| SON | 1.0 | 2.2 | -0.2 | 2.4 |
| DFJ | 3.6 (2.5) | 4.8 (5.0) | 4.1 | 5.8 |
| MAM | 2.9 | 4.1 | 1.8 | 3.2 |

Wind measurement data are available for the vicinity of M1 (Borg, 2017). Here the dominant wind direction is out of the southwest (258°) but also highly variable (*s* = 118), with an average wind speed of 1.5 m.s$^{-1}$ (Figure 89, pg. 168). However, the site experienced extensive snow cover from April-June 2014, and again from February-May 2015. This caused the anemometer to be covered by snow, affecting wind measurements (Borg, 2017). As such, the proportion of peak wind speeds, as well as calms recorded, needs to be evaluated with caution and the proportion of calms (± 60% of the time) is an overestimation of actual calm periods. Irrespective of this, where data are available gusts approximate 3 m.s$^{-1}$ on average (Figure 90, pg. 169). Average air temperature, expressed as MAAT, and ground temperature data, expressed as mean annual ground surface temperature (MAGT), for M1 show a MAAT of 0.5 °C and a MAGT of 0.6 °C. Mean annual air temperature (MAAT) at M2 is 3.1 °C and MAGT 4.6 °C.

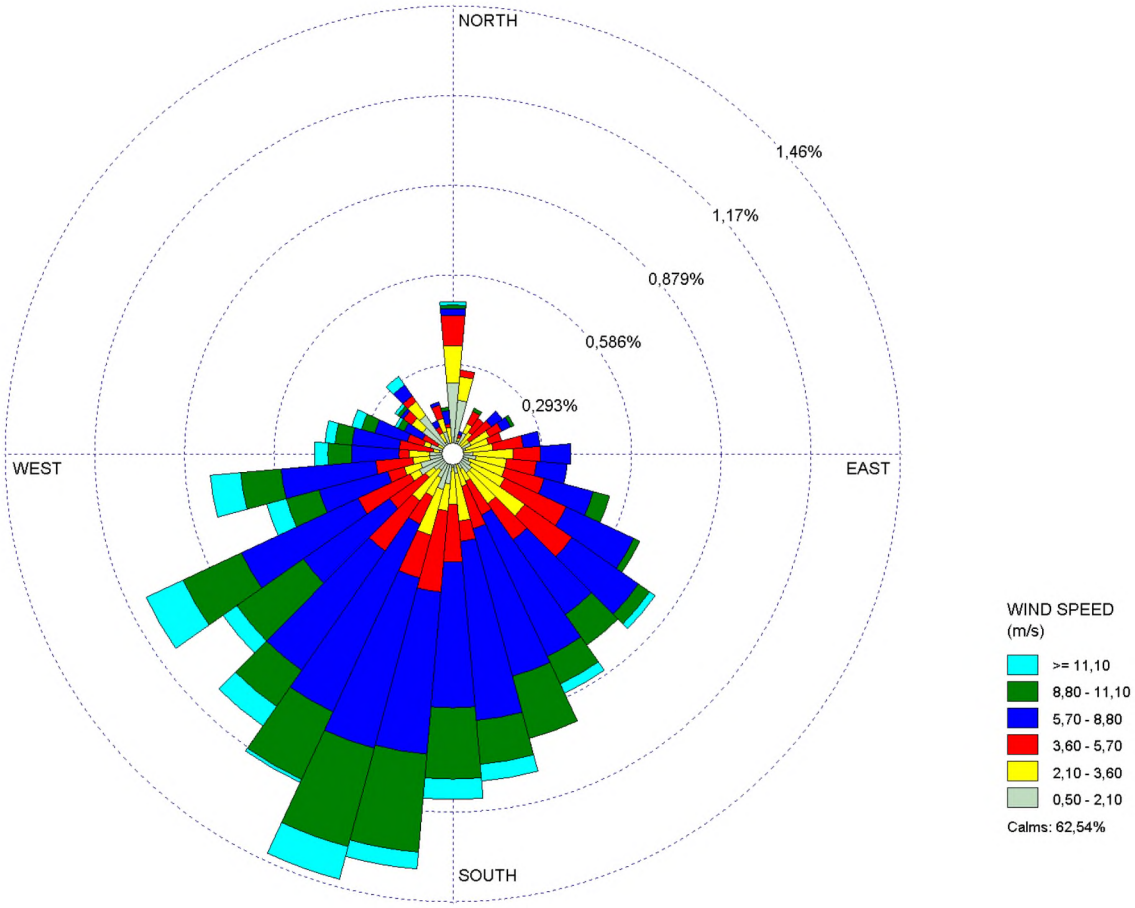


**Figure 89: Wind direction and average wind speed for the vicinity of M1. Interval: 1 hour; 2014-2015. Missing data: ± 17%.**

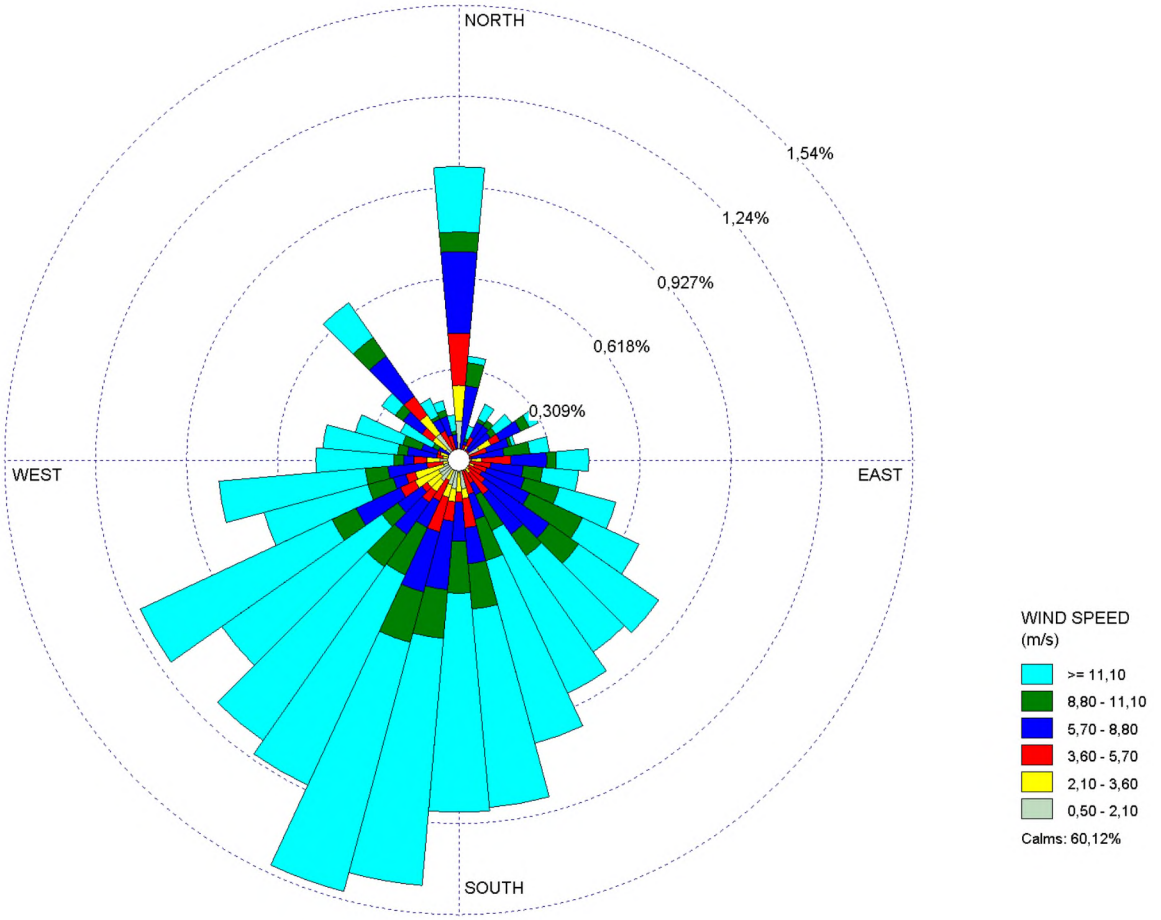


**Figure 90: Wind direction and maximum wind speed (gusts) for the vicinity of M1. Interval: 1 hour; 2014-2015. Missing data: ± 17%.**

Due to its relatively small surface area, Marion Island is generally omitted from world climatic zonation maps (Kottek *et al.*, 2006). Nevertheless, literature suggests the Island falls within the *Cfc* classification of the oceanic climate (Boelhouwers *et al.*, 2000), or within the subpolar lowlands of Washburn's (1979) periglacial zones (mean monthly temperature < -3 °C; warmest month > 10 °C). The *Cfc* classification requires no month colder than -3 °C, snowfall is common, temperatures not extreme, and winters mild. A detailed description of climatic zonation systems in use today is provided in APPENDIX B. These systems are, furthermore, discussed in detail in CHAPTER 2: Background and Context (pg. 12). Analyses show (Table 49, pg. 170) that the Island falls within the oceanic climate class (C) (average monthly temperatures above -3 °C and below 18 °C in the coolest month), with *f* (precipitation occurs throughout the year) and *c* (fewer than four months above 10 °C). This applies to the SAWS station, as well as data obtained from M1 and M2.

**Table 49: Average monthly air temperature values, given in °C, for Marion Island (55-year averages), Katedraalkrans (M1, two-year averages), and Tafelberg (M2, two-year averages). Climatic zones are shown in brackets.**

| Month | Marion Island (*Cfc*) | M1 (*Cfc*) | M2 (*Cfc*) |
|---|---|---|---|
| Jan | 8 | 4 | 5 |
| Feb | 8 | 7 | 7 |
| Mar | 8 | 3 | 5 |
| Apr | 7 | 2 | 4 |
| May | 6 | 1 | 3 |
| Jun | 5 | -1 | 1 |
| Jul | 4 | -2 | 1 |
| Aug | 4 | -1 | 1 |
| Sep | 4 | 1 | 2 |
| Oct | 5 | 1 | 3 |
| Nov | 6 | 1 | 3 |
| Dec | 7 | 2 | 5 |

Soil ice, in the form of needle ice, is common and lateral frost sorting is evident at numerous locations, as is vertical sorting (*pers. obs.*). The highest site (M1) shows a lack of vegetation cover (excepting some lichen) and no animal presence, with sediment consisting of larger clasts and gravel-sized fragments. The area in the immediate vicinity of M2 is characterised by sorted stripes orientating themselves to the wind and almost perpendicular to the slope. Lichen and bryophytes are also present, predominantly on the leeward side of clasts. M3 is characterised by vegetation-banked terraces, some grass cover and pebble and gravel sized clasts. Soil depth is 18 cm and vertical sorting is evident in the top 3-5 cm of the ground (*pers. obs.*). Below this depths sediment is gravelly and coarse. Smaller and less defined vegetation-banked terraces occur for M4, as does some grass and limited vertical sorting of the ground. The lowest altitudinal site (M5) shows greater occurrence of stone-banked lobes over vegetation-baked lobes, as well as larger boulders.

Periglacial landforms and -features are well documented (Table 3, pg. 56). However, a few processes were noted to occur at elevations not previously indicated in the literature (Table 51, pg. 171). These include needle ice, which is ubiquitous, and was observed to occur as low as 120 m a.s.l. during May 2014. Furthermore, sorted stripes occur in abundance near M2 and were also observed for Mixed Pickle. Solifluction lobes have also been recorded near Mixed Pickle. The proximity of sorted stripes near M2 required a more detailed analysis of these features. As such, these stripes are discussed in greater detail here and results presented in Table 50 (pg. 171). Stripe soil depth is ± 30 cm, with ridges approximately 2 cm wider than troughs. Troughs have a dominant orientation of 35° (northeast to southwest), with a standard deviation (*s*) of 5°. Bulk density and porosity of troughs vs. ridges are similar, although troughs exhibit slightly higher values for both. In comparison troughs have a much lower gravimetric and volumetric moisture content than ridges (moisture content: 11.6% vs. 20.6% respectively). Furthermore, the fine earth fraction (FEF: particles < 2 mm) is higher for ridges compared to troughs (16 % vs. 36% respectively). Stripes occur on level ground with a slight slope of ± 2°. The

lateral sorting index (S) is predominantly 'proportion deficient' when comparing ridge to trough samples. The larger clasts reflect poorer sorting. Phi (ϕ) values -4 and -5 for ridge to trough comparisons show no lateral sorting. In comparison, finer particle sizes reflect proportion deficiency throughout. Clasts have a mean orientation of 66°, although orientation is highly variable (standard deviation of 47°), with clasts orientated almost equally along the north-south and east-west axes. Overall clasts have an average Cailleux flatness index of 146 904, a mean diameter of 4.2 cm, and Krumbein's sphericity index on 0.5. Gypsum is in evidence on some of the larger clasts, as is moss. However, no moss or lichen are in evidence on the stripe sediment.

**Table 50: Sorted stripe characteristics, located near M2. TOC: total organic carbon, expressed as a percentage. VWC: volumetric water content. GWC: gravimetric water content. Mc: gravimetric water content expressed as a percentage. FEF: fine earth fraction (portion < 2 mm), expressed as a percentage.**

| Landform | TOC % | Bulk Density | Porosity | VWC | GWC | Mc | FEF |
|---|---|---|---|---|---|---|---|
| Trough | 4.0 | 2.4 | 0.1 | 0.3 | 0.1 | 11.6 | 16 |
| Ridge | 4.5 | 2.2 | 0.2 | 0.4 | 0.2 | 20.6 | 36 |

Landforms not previously indicated in the literature are given in Table 51. An overview of landforms extracted from literature and those observed in the field is given in Figure 91 (pg. 172). Images taken during field visits are available in Table 23. APPENDIX I. A map of points of interest on Marion Island is given in Figure 10 on pg. 52.

**Table 51: Observations not reflected in the literature that were recorded during field visits to Marion Island.**

| Feature | Location | Altitude |
|---|---|---|
| Needle ice | Katedraalkrans via First Red past Tafelberg | 120-750 |
| Solifluction terrace/head deposit | Mixed Pickle | 600 |
| Sorted stripes | Tafelberg | 370 |
| | Mixed Pickle | 275-600 |

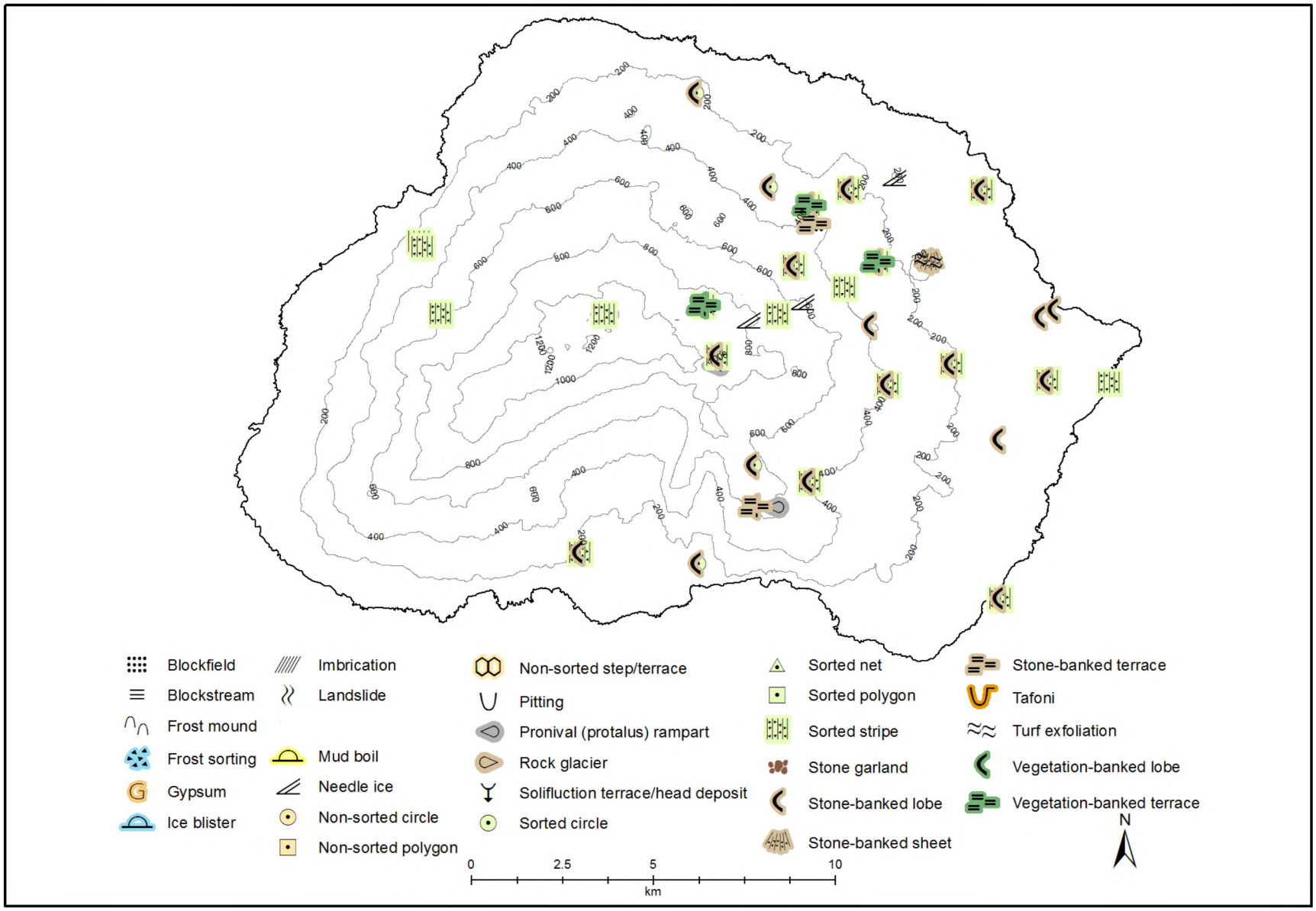


**Figure 91: Consolidated periglacial landforms observed on Marion Island.**

### 5.2.2 Ground thermal dynamics

Ground thermal dynamics are discussed with a reference to the annual, seasonal and diurnal environment. All times indicated are based on South African Standard Time (SAST; GMT+2) and represent approximations (± 1 hour). Indices, such as the freezing index (FI), thawing index (TI), ground freezing index (GFI), and thermal offset (SO) are most suited to describing an active layer and permafrost driven environment. While Marion Island has neither, the use of these indices allows for a comparison to Dronning Maud Land (DML) study sites (discussed from pg. 205 onwards). Due to sporadic data loss, not all annual calculations are possible for M1-M5.

#### *5.2.2.1 Annual frost environment*

The frost environment in Marion Island is extremely active and ground moisture ubiquitous. As such, all stations on Marion Island experienced extensive data loss and not all periods, nor sensor depths are evaluated. The most robust dataset for M1 (Katedraalkrans) is available for ambient air temperature ($T_{AIR}$) and at ± 2 cm within the ground (GST: ground surface temperature) from winter 2014 to end of spring 2015. Furthermore, data are also available for the winter months of 2014 for sensors buried at 5 cm ($T_5$), 10 cm ($T_{10}$), and 15 cm ($T_{15}$) depths. Data are available for M2 (Tafelberg) for air temperature, GST and $T_5$ from April 2014-February 2015 (except August and September 2014 for $T_5$), as well as April-September 2014 for $T_{10}$ and $T_{15}$. However, these data reflect a 3-hour frequency and, as such, mask the diurnal frost environment.

Mean annual ground frost temperatures (MAGT: recorded at ± 2 cm within the ground), show that all Marion Island sites, even at highest elevations, occur in a non-permafrost zone. Mean annual ground frost temperature is 2.9 °C at M1 and 3.2 °C at M2. Due to data loss, mean annual ground temperatures were not evaluated for iButtons deployed at M2-M5. Irrespective of this, permafrost is absent for the Island. In turn, numerous freeze-thaw cycles (FTC) are evident throughout the year. Diurnal ranges rarely exceed 10 °C, even at higher elevations. Nevertheless, M1 and M2 experience short-term freezing of the ground on a scale of a few days to a few of months. Mean annual ground temperature increases with decreasing altitude. Furthermore, ground temperature variability (expressed as standard deviation: *s*) decreases for decreasing altitude ($s$ = 4.6 at M1; $s$ = 4.0 at M2).

Ground moisture levels are high throughout the year, although these decrease in winter when the ground freezes. Seasonal frost is evident at M1 to a depth of 15 cm, with this depth frozen for almost two months (Table 52, pg. 174). No seasonal frost is evident at M2, with the longest frozen ground duration at 15-cm depth less than 11 days. However, ground freezes in July-August, like that at M1. An increase in thawing events in spring yields ground that is saturated with the lower levels still frozen. Potential freeze-thaw events (PFTE), as well as freeze-thaw cycles (FTC) are common. M2 shows such cycles throughout the year in all months. This is not the case for M2, where such cycles occur predominantly in winter and spring. Data available for iButtons from M2-M5 display no potential freeze-thaw events, nor freeze-thaw cycles.

**Table 52: Seasonal ranges ($T_{SR}$) and frozen period (hours, percentage and longest duration in days) for M1 & M2 for 2014-2015. # underestimation due to data loss. * not evaluated. $T_{AIR}$ reflects ambient air temperature; GST indicates temperature recorded at the ground surface (~ 2 cm). The subscript following 'T' indicates the depth of the sensor.**

| Site | $T_{AIR}$ | GST | $T_5$ | $T_{10}$ | $T_{15}$ |
|---|---|---|---|---|---|
| Frozen Hours | | | | | |
| M1 | 3 900 | 3 816 | 2 313# | 2 476# | 2 491# |
| M2 | 1 908 | 1 896 | * | 1 362 | 1 008 |
| Frozen Hours % | | | | | |
| Site | $T_{AIR}$ | GST | $T_5$ | $T_{10}$ | $T_{15}$ |
| M1 | 45 | 44 | 26# | 28# | 28# |
| M2 | 22 | 22 | * | 16 | 12 |
| Longest Frozen Period | | | | | |
| Site | $T_{AIR}$ | GST | $T_5$ | $T_{10}$ | $T_{15}$ |
| M1 | 213 | 240 | 330# | 646# | 1 212# |
| M2 | 5 | 9 | * | 12 | 11 |

Interannually temperatures stabilise with depth and greatest variability is observed for the ground surface (GST: recorded at ± 2 cm in the ground) (Figure 92 & Figure 94, pg. 175). At M1, temperature variability (expressed as standard deviation: *s*), shows an increase from ambient air temperature to highest values at the ground surface. From this depth (with increasing depth into the ground) mean annual ground temperature decreases, with a concomitant decrease in variability evident. The maximum diurnal temperature is greatest at the ground surface and least at 15-cm depth (29 °C vs. 10 °C). For both M1 and M2, ground temperature minimums steadily increase with greater depth in the ground (Figure 93 & Figure 95, pg. 175). At M2, temperature variability shows an increase from ambient air temperature to highest values at 5-cm depth. From this depth deeper into the mean annual ground temperature decreases, with a concomitant decrease in variability evident. The maximum diurnal temperature is greatest at the ground surface and least at 15-cm depth (23 °C vs. 10 °C). Furthermore, the seasonal temperature range decreases with increasing depth in the ground, as well as increasing at lower altitudes. The seasonal range of M1 is 3 °C; that of M2 is 5 °C. These ranges increase to 6 ° and 7 ° for M3 and M5 respectively. Temperature maximums and seasonal ranges are generally greater at M2 (at lower altitude), compared to M1 (at greater altitude). Furthermore, a decrease in altitude reflects in higher (warmer) minimum temperatures.

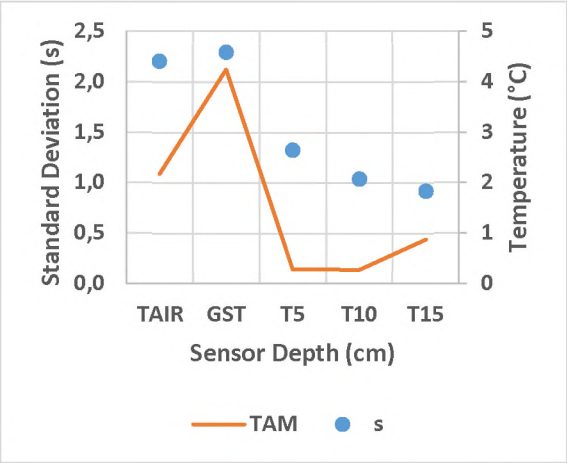


**Figure 92: Annual mean temperature ($T_{AM}$) and variability (*s*) per sensor depth for M1. $T_{AIR}$: air temperature. GST: ground surface temperature (± 2 cm in the ground). The number following 'T' indicates the depth of the sensor in centimetres.**

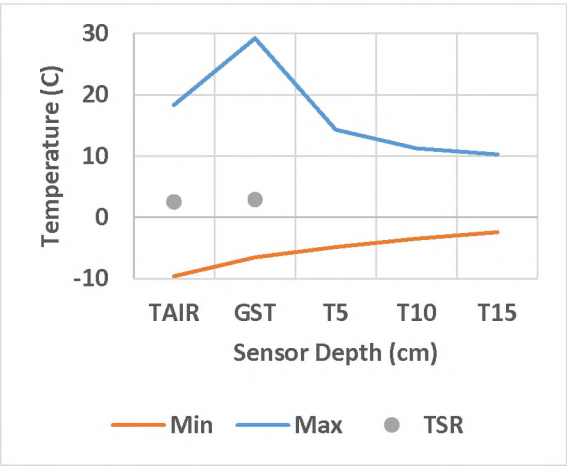


**Figure 93: Annual temperatures (maximums, minimums and ranges) for M1. $T_{SR}$: seasonal range. $T_{AIR}$: air temperature. GST: ground surface temperature (± 2 cm in the ground). The number following 'T' indicates the depth of the sensor in centimetres.**

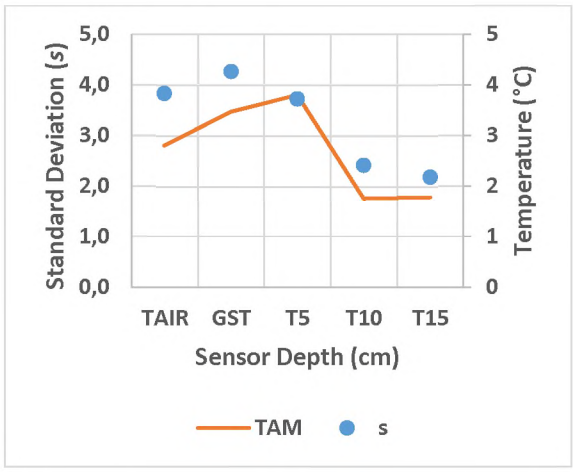


**Figure 94: Annual mean temperature ($T_{AM}$) and variability (*s*) per sensor depth for M2. $T_{AIR}$: air temperature. GST: ground surface temperature (± 2 cm in the ground). The number following 'T' indicates the depth of the sensor in centimetres.**

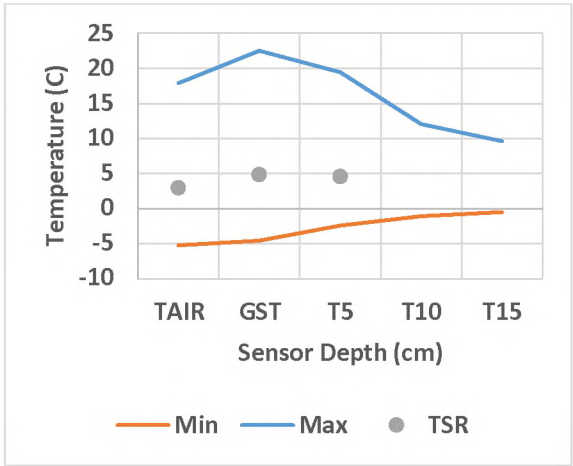


**Figure 95: Annual temperatures (maximums, minimums and ranges) for M2. $T_{SR}$: seasonal range. $T_{AIR}$: air temperature. GST: ground surface temperature (± 2 cm in the ground). The number following 'T' indicates the depth of the sensor in centimetres.**

### *5.2.2.2 Seasonal frost environment*

The summer thawing index (TI) and winter freezing index (FI) are provided for ground surface temperatures (GST), ground temperatures recorded at ± 2 cm depth, for all sites, as well as air temperatures for M1 and M2. Each site is discussed in its respective subsection below.

#### 5.2.2.2.1 M1: Katedraalkrans

Expected diurnal penetration depths (*d*) using Equation 12 (pg. 105) indicate a shallow diurnal frost environment. The deepest frost penetration at M1 in August 2014 yields an average diurnal cycle to a depth of ± 4 mm during this time and an expected average annual freezing depth of ± 0.5 cm. Ground frost is evident throughout the year, in all months and all seasons. As such, this site does not have an initiation and end period of ground frost, making such analyses not suited. Instead, Table 53 illustrates the ubiquitous nature of potential freeze-thaw events at M1. While potential freeze-thaw events occur throughout the year, at the ground surface (GST: recorded at ± 2 cm in the ground) the greatest number of cycles is evident in spring and early summer (October-December), with the least recorded for the remainder of summer (January and February). The same applies to air temperatures. At depth within the ground (15 cm) no potential freeze-thaw events are evident in August. During this time the ground at this depth is frozen.

**Table 53: Maximum potential freeze-thaw cycle (Max Cycle), as well as the percentage of these cycles of the year (Percentage of Cycles), presented in divisions of months for M1 on Marion Island. $T_{AIR}$: air temperature. GST: ground surface temperature (± 2 cm in the ground). The subscript following 'T' indicates the depth of sensors in centimetres. NOTE: percentages are calculated using available data. These percentages are overestimated for $T_5$-$T_{15}$.**

| Month | Max Cycle | | | | | Percentage of Cycles | | | | |
|---|---|---|---|---|---|---|---|---|---|---|
| | $T_{AIR}$ | GST | $T_5$ | $T_{10}$ | $T_{15}$ | $T_{AIR}$ | GST | $T_5$ | $T_{10}$ | $T_{15}$ |
| Jun-14 | 71 | 144 | 145 | 216 | 232 | 10 | 6 | 21 | 28 | 37 |
| Jul-14 | 95 | 156 | 203 | 369 | 434 | 10 | 7 | 19 | 28 | 27 |
| Aug-14 | 158 | 240 | 330 | 646 | 1178 | 10 | 9 | 15 | 22 | 0 |
| Sep-14 | 140 | 221 | * | 223 | 1212 | 5 | 6 | * | 22 | 20 |
| Oct-14 | 213 | 98 | 365 | * | * | 10 | 10 | 15 | * | * |
| Nov-14 | 72 | 42 | * | * | * | 9 | 12 | * | * | * |
| Dec-14 | 48 | 18 | * | * | * | 14 | 11 | * | * | * |
| Jan-15 | 48 | 20 | * | * | * | 5 | 7 | * | * | * |
| Feb-15 | 18 | 14 | * | * | * | 2 | 4 | * | * | * |
| Mar-15 | 44 | 19 | * | * | * | 8 | 9 | * | * | * |
| Apr-15 | 63 | 44 | * | * | * | 7 | 8 | * | * | * |
| May-15 | 45 | 64 | 104 | * | 119 | 9 | 10 | 31 | * | 17 |

The thermal offset (SO), summer (DJF), winter (JJA) temperatures and variability (expressed as standard deviation; *s*), as well as the summer thawing index (TI) and winter freezing index (FI) are given for M1 in Table 54 (pg. 177). Seasonal temperatures and variability are provided for ambient air ($T_{AIR}$) and ground temperatures (GST). The thermal offset (SO) is positive throughout, with the greatest offset calculated in summer. The ground thawing index (TI) is greatest in summer (392) and autumn (195); the freezing index (FI) shows lowest values during winter (-131) and spring (-50). Temperature variability is greatest in summer. In comparison to the Eastern Cape and Dronning Maud Land (Antarctica), thawing indices are positive for all seasons. Similarly, freezing indices are negative for all seasons. Annual degree days (DD: 344) show a ground thermal regime warmer than air temperatures. Although this value is small (± 0.9 per day), the ground freezing index is positive (722), furthermore indicating an environment where ground temperatures exceed air temperatures on average. Ground

thawing indices exceed freezing indices in all season (except winter). Air thawing indices are less than freezing indices in winter and spring, this relationship reverses in summer and autumn.

**Table 54: Seasonal thermal indices for M1 for which data are available (2014-15). In the 'Temperature' column the first value represents the seasonal mean ($T_{SM}$); the second value the associated variability (*s*). $T_{AIR}$ reflects ambient air temperature; GST indicates temperature recorded at the ground surface (± 2 cm); TI the thawing index; FI the freezing index; SO the thermal offset. JJA: winter. SON: spring. DJF: summer. MAM: autumn.**

| Season | $T_{AIR}$ | | | GST | | | SO |
|---|---|---|---|---|---|---|---|
| | TI | FI | Temperature | TI | FI | Temperature | |
| JJA | 82 | -195 | -1.3/0.09 | 51 | -131 | -0.7 / 0.26 | 0.54 |
| SON | 139 | -160 | -0.8/0.97 | 166 | -50 | 1.3 / 1.17 | 2.17 |
| DJF | 392 | -26 | 3.6/1.81 | 504 | -8 | 4.7 / 2.1 | 1.08 |
| MAM | 195 | -51 | 1.3/0.73 | 269 | -30 | 3.5 / 1.26 | 2.15 |

The coldest period for M1 is August (winter), where diurnal mean maximum temperatures for GST-$T_{15}$ range from 5.8 °C to -0.04 °C respectively. Freezing frequently occurs at 15-cm depth (and potentially beyond this depth), with the first instance of freezing at this depth recorded in early June (13 June at 19:00). The longest continuous frozen period for GST, spanning 10 days (Table 55) from 29 July (14:00) to 8 August (22:00), occurs in winter. The longest continuous frozen event for $T_5$ lasts 14 days from 26 July (05:00) to 8 August (22:00). The longest continuous frozen event at $T_{10}$ lasts 27 days from 16 July (15:00) to 12 August (12:00). The longest continuous frozen event at $T_{15}$ lasts 51 days from 13 July (20:00) to 2 August (9:00). However, it must be noted, that's the amount and percentage of frozen hours from $T_5$-$T_{15}$ are underestimated, due to logger failure for these sensors from November 2014 to May 2015. Nevertheless, frozen hours are an indication of the expected frost environment at these depths.

**Table 55: Maximum frozen hours per sensor depth for M1. GST: ground surface temperature (recorded at ±2 cm in the ground). The subscript following 'T' indicates the depth of the sensor. # underestimated.**

| Frozen Hours | $T_{AIR}$ | GST | $T_5$ | $T_{10}$ | $T_{15}$ |
|---|---|---|---|---|---|
| Max | 213 | 240 | 330# | 646# | 1212# |
| Start | 2014/10/03 16:00 | 2014/07/29 14:00 | 2014/07/26 5:00 | 2014/07/16 15:00 | 2014/07/13 20:00 |
| End | 2014/10/12 12:00 | 2014/08/08 13:00 | 2014/08/08 22:00 | 2014/08/12 12:00 | 2014/09/02 9:00 |

The ground temperature profile shows elevated average temperatures at the ground surface (GST). Sensors deeper within the ground cannot be evaluated (Figure 96, pg. 178). Temperatures at the ground surface are also consistently higher than those recorded in the air. This sensor also reflects the highest maximums (19 °C, February 2015), as well as greatest minimums (-10 °C, October 2014). Air and ground surface temperatures (GST) display greatest variability (3.7 and 3.5 respectively), with temperature variability decreasing with increasing depth in the ground. Variability is 1.8 for $T_5$, 1.1 for $T_{10}$, and 0.8 for $T_{15}$. Sub-zero temperatures are observed throughout the year, but with a prominence

in winter and spring. Maximum temperatures occur in summer and spring (February), with maximum diurnal ground means recorded on 3 February 2015 (18 °C). Soil moisture is present throughout the year and peaks during summer and spring, reaching a maximum in August (winter, attributed to snow fall) and March (attributed to rainfall).

During 2014-15 the lowest maximum air temperature at M1 is occurs in June (6.3 °C), the highest in February (18.4 °C). The lowest minimum air temperature is recorded in October (-2.2 °C), the highest in March (6.7 °C). The average duration of negative air temperatures achieved is 19 hours. However, the duration of maintaining sub-zero air temperatures is highly variable ($s$ = 28), due to four instances when air temperatures remain below 0 °C for more than 100 hours. However, removing these events from the dataset does not significantly reduce average duration (16 hours), nor variability ($s$ = 19). Nonetheless, the most common duration of sub-zero temperatures is 1 hour (17% of the time), as well as 2, 15, and 20 hours (10%, 9%, 9% respectively). Furthermore, sub-zero air temperatures less than 24 hours make up 78% of all sub-zero durations calculated.

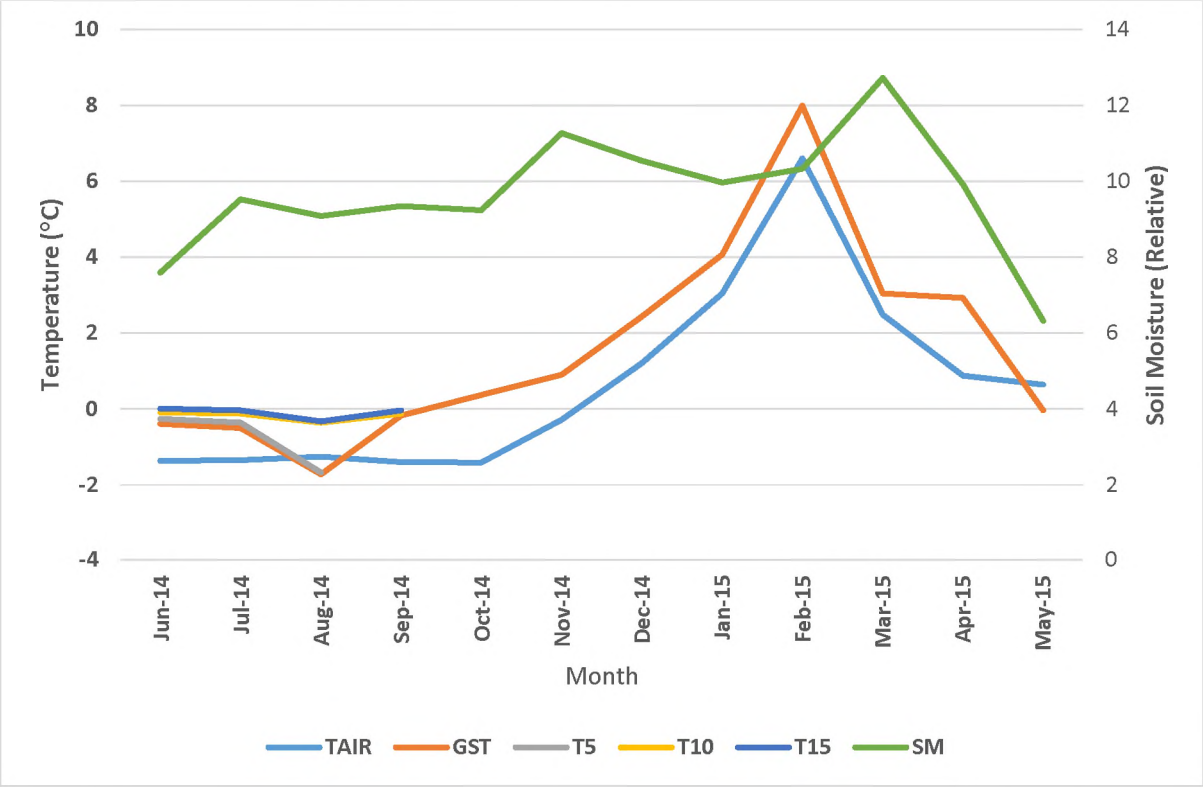


**Figure 96: Monthly means per sensor depth) for M1 (2014-15). $T_{AIR}$: ambient air temperature. GST: temperature recorded at the ground surface (± 2 cm). The number following 'T' indicates sensor depth in centimetres.**

The lowest maximum ground temperature (at GST) is recorded in August (5.8 °C), the highest in February (29.2 °C). The lowest minimum temperature is recorded in October and July (-10 °C), the highest in February (-2 °C). The average duration of negative ground temperatures achieved is 20 hours, with high variability ($s$ = 36). The most common duration of sub-zero temperature duration is 15 hours

(18% of the time), followed by 20, and 2-hour durations (14% and 8% respectively). Furthermore, sub-zero ground temperatures less than 24 hours make up 81% of all sub-zero durations calculated. Temperatures at greater depths were not evaluated.

#### 5.2.2.2.2 M2: Tafelberg

Expected diurnal penetration depths (*d*) using Equation 12 (pg. 105) indicate a shallow diurnal frost environment. The deepest and longest frost penetration at M2 in August 2014 yields an average diurnal cycle to a depth of ± 6 mm during this time and an expected average annual freezing depth of ± 0.5 cm. Like M1, ground frost is common and evident in most months seasons (Table 56). However, in comparison to M1, ground frost initiates in April and ends in December. This initiation is later with greater depth in the ground. Furthermore, ground thaw is evident earlier with greater depths in the ground. Table 56 illustrates the common nature of potential freeze-thaw events, like those at M1. While potential freeze-thaw events occur throughout most of the year, at the ground surface (GST: recorded at ± 2 cm in the ground) the greatest number of cycles occur from June-September (winter and spring), with few evident in summer and autumn. In comparison, potential freeze-thaw events for air temperatures are evident for all months, except February and March.

**Table 56: Maximum potential freeze-thaw cycle, as well as the percentage of these cycles of the year, presented in divisions of months for M2 on Marion Island. $T_{AIR}$: air temperature. GST: ground surface temperature (± 2 cm in the ground). The subscript following 'T' indicates the depth of sensors in centimetres. NOTE: percentages are calculated using available data. These percentages are overestimated for $T_5$-$T_{15}$.**

| Month | Max Cycle | | | | | Percentage of Cycles | | | | |
|---|---|---|---|---|---|---|---|---|---|---|
| | $T_{AIR}$ | GST | $T_5$ | $T_{10}$ | $T_{15}$ | $T_{AIR}$ | GST | $T_5$ | $T_{10}$ | $T_{15}$ |
| Mar-14 | 0 | 0 | 0 | 0 | 0 | 0 | 0 | 0 | 0 | 0 |
| Apr-14 | 18 | 9 | 0 | 0 | 0 | 5 | 1 | 0 | 0 | 0 |
| May-14 | 78 | 66 | 69 | 18 | 0 | 10 | 10 | 13 | 9 | 0 |
| Jun-14 | 66 | 84 | 90 | 90 | 117 | 12 | 18 | 31 | 14 | 13 |
| Jul-14 | 87 | 105 | 105 | 105 | 111 | 12 | 18 | 31 | 14 | 27 |
| Aug-14 | 114 | 204 | * | 285 | 258 | 16 | 15 | * | 23 | 33 |
| Sep-14 | 54 | 66 | * | 156 | 132 | 13 | 21 | * | 40 | 27 |
| Oct-14 | 39 | 18 | 15 | * | * | 10 | 11 | 23 | * | * |
| Nov-14 | 33 | 15 | 6 | * | * | 13 | 5 | 3 | * | * |
| Dec-14 | 12 | 3 | 0 | * | * | 5 | 1 | 0 | * | * |
| Jan-15 | 15 | 0 | 0 | * | * | 3 | 0 | 0 | * | * |
| Feb-15 | 0 | 0 | 0 | * | * | 0 | 0 | 0 | * | * |

The thermal offset (SO), summer (DJF), winter (JJA) temperatures and variability (expressed as standard deviation; *s*), as well as the summer thawing index (TI) and winter freezing index (FI) are given for M2 in Table 57 (pg. 180). Seasonal temperatures and variability are provided for ambient air ($T_{AIR}$) and ground temperatures (GST). The thermal offset (SO) is positive throughout, with the greatest offset calculated for spring and then summer. The ground thawing index (TI) is greatest in spring (311) and summer (613); the freezing index (FI) lowest during winter (-47) and spring (-25). Temperature

variability during summer is greatest for ground compared to air temperatures, and variability is greatest for air and ground temperatures in summer. In comparison to the Eastern Cape and Dronning Maud Land (Antarctica), thawing indices are positive for all seasons. Similarly, freezing indices are negative for all seasons except in summer at GST. Annual degree days (DD: 205) indicate a ground thermal regime warmer than air temperatures. Although this value is small (± 0.6 per day), the ground freezing index is positive (1 124), furthermore indicating an environment where ground temperatures exceed air temperatures. Ground thawing indices exceed freezing indices in all seasons.

**Table 57: Seasonal thermal indices for M2 for which data are available (2014-15). In the 'Temperature' column the first value represents the seasonal mean ($T_{SM}$); the second value the associated variability (*s*). $T_{AIR}$ reflects ambient air temperature; GST indicates temperature recorded at the ground surface (± 2 cm); TI the thawing index; FI the freezing index; SO the thermal offset. JJA: winter. SON: spring. DJF: summer. MAM: autumn.**

| Season | $T_{AIR}$ | | | GST | | | SO |
|---|---|---|---|---|---|---|---|
| | TI | FI | Temperature | TI | FI | Temperature | |
| JJA | 136 | -95 | 0.6/0.09 | 103 | -47 | 0.7 / 0.07 | 0.10 |
| SON | 244 | -45 | 2.2/0.86 | 311 | -25 | 3.4 / 1.14 | 1.21 |
| DJF | 499 | -1 | 5.4/1.31 | 613 | 0 | 6.3 / 1.62 | 0.88 |
| MAM | 171 | -13 | 3.3/0.32 | 169 | -5 | 3.4 / 0.46 | 0.14 |

The coldest period for M2 occurs in August (winter), where diurnal mean maximum temperatures for GST-$T_{15}$ 5.8 °C to -0.04 °C respectively. Freezing frequently occurs to 15 cm (and potentially beyond this depth), with the first instance of freezing at this depth recorded in late July (29 July at 01:00). The longest continuous frozen period for GST, spanning 9 days (Table 58) from 18-27 August (16:00-04:00), occurs in winter. The longest continuous frozen event at $T_{10}$ lasts 12 days from 27 July (13:00) to 8 August (10:00). The longest continuous frozen event at $T_{15}$ lasts 11 days from 29 July (01:00) to 8 August (19:00). However, it must be noted, that's the amount and percentage of frozen hours at $T_{10}$-$T_{15}$ are underestimated, due to logger failure for these sensors from October 2014 to February 2015. Nevertheless, frozen hours are an indication of the expected frost environment at these depths.

**Table 58: Maximum frozen hours per sensor depth for M2. GST: ground surface temperature (recorded at ±2 cm in the ground). The subscript following 'T' indicates the depth of the sensor. # underestimated.**

| Frozen Hours | $T_{AIR}$ | GST | $T_5$ | $T_{10}$ | $T_{15}$ |
|---|---|---|---|---|---|
| Max | 114 | 204 | Not evaluated. No data available in August and September | 285# | 258# |
| Start | 2014/08/18 19:00 | 2014/08/18 16:00 | | 2014/07/27 13:00 | 2014/07/29 01:00 |
| End | 2014/08/23 10:00 | 2014/08/27 04:00 | | 2014/08/08 10:00 | 2014/08/08 19:00 |

The ground temperature profile shows elevated average temperatures at the ground surface (GST). Sensors deeper within the ground cannot be evaluated (Figure 97, pg. 181). Temperatures at the ground surface are higher than those recorded in the air in spring and summer; this relationship reverses in autumn and winter. This sensor also measured the highest maximums (23 °C, February

2015). The coldest temperature, in comparison, is recorded by the air temperature sensor (-5 °C, July and October 2014). Air and ground surface temperatures (GST) display greatest variability (3.8 and 4.3 respectively), with temperature variability decreasing with increasing depth in the ground. Variability is 3.7 for $T_5$, 2.4 for $T_{10}$, and 2.2 for $T_{15}$. Sub-zero temperatures are observed for throughout the year, but with a prominence in winter and spring. Maximum temperatures occur in summer, with maximum diurnal ground means occurring on 9 February 2015 at GST (15 °C).

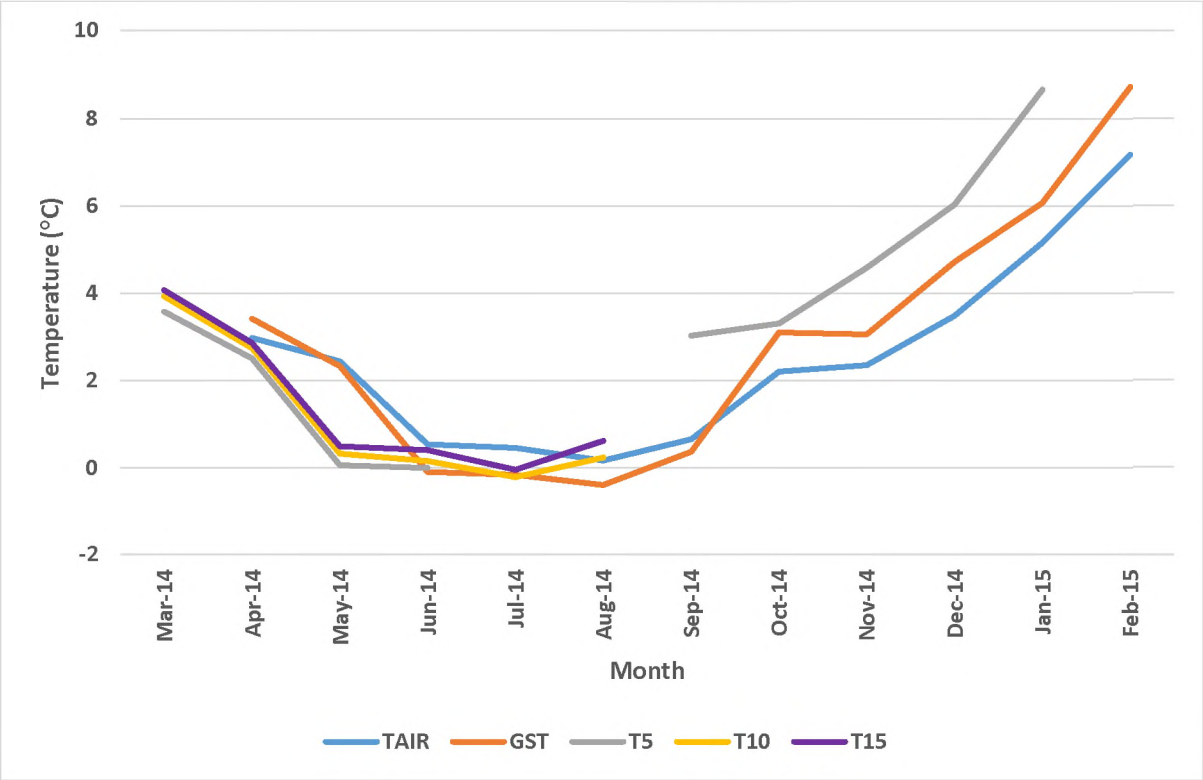


**Figure 97: Monthly means per sensor depth) for M2 (2014-15). $T_{AIR}$: ambient air temperature. GST: temperature recorded at the ground surface (± 2 cm). The number following 'T' indicates sensor depth in centimetres.**

During 2014-15 the lowest maximum air temperature at M2 is recorded in June (7.2 °C), the highest in February (17.9 °C). The lowest minimum air temperature is recorded in June and September (-5.2 °C), the highest in February (0.3 °C). The average duration of negative air temperatures achieved is 19 hours (variability: *s* = 19). However, the most common duration of sub-zero temperatures is 3 hours (18% of the time), as well as 15, 9, and 20 hours (16%, 15%, 11% respectively). Furthermore, sub-zero air temperatures less than 24 hours make up 77% of all sub-zero durations calculated. For ground temperatures (GST: ± 2 cm in the ground) the lowest maximum temperature is recorded in June (7.1 °C), the highest in February (22.5 °C). The lowest minimum temperature is recorded September (-4.6 °C), the highest in February (0.7 °C). The average duration of negative GST achieved is 3 hours (variability: *s* = 7). The most common duration of sub-zero temperature is 4 hours (20% of the time), followed by 8, 9, and 5-hour durations (14%, 13%, and 12% respectively). Furthermore, sub-zero ground temperatures less than 24 hours make up 96% of all sub-zero durations calculated. Temperatures at greater depths were not evaluated.

#### 5.2.2.2.3 iButtons: M2-M5

iButtons experienced extensive data loss throughout, ranging from 84% data loss at M2 to 34% data loss at M4. However, data are available for M2-M5 in April and May 2014, with data available for M3 from April-July 2014, as well as February and March 2015. The extent of data loss makes an evaluation of the seasonal frost environment problematic. Nevertheless, months for which data are available are evaluated and presented here.

Diurnal ranges exceeding 10 °C, as well as oscillations around 0 °C falling within this range for M2-M5 are shown in Table 59. Diurnal ranges greater than 10 °C are rare, only evident for February and March at M4 and M5. Of these ranges, no oscillations around 0 °C are apparent.

**Table 59: Oscillations around 0 °C (Osc), as well as diurnal ranges exceeding 10 °C ($T_{DR}$) for iButtons at M2-M5. Oscillations and ranges are expressed as percentages of the evaluated months.**

| Site | $T_{DR}$ (%) | | | | Osc (%) | | | |
|---|---|---|---|---|---|---|---|---|
| | Apr-14 | May-14 | Feb-15 | Mar-15 | Apr-14 | May-14 | Feb-15 | Mar-15 |
| M2 | 0 | 0 | * | * | 0 | 0 | * | * |
| M3 | 0 | 0 | 0 | 0 | 0 | 0 | 0 | 0 |
| M4 | 0 | 0 | 21 | 3 | 0 | 0 | 0 | 0 |
| M5 | 0 | 0 | 11 | 0 | 0 | 0 | 0 | 0 |

For months where data are available, no site displays frozen hours (Table 60). While negative temperatures are recorded at all sites in July, only months were 75% of data points were available were analysed with reference to frozen hours.

**Table 60: Frozen hours, where data are available, for iButton sites on Marion Island. * indicates data loss / month not evaluated.**

| Month | Frozen Hours | | | | Frozen Hours % | | | |
|---|---|---|---|---|---|---|---|---|
| | M2 | M3 | M4 | M5 | M2 | M3 | M4 | M5 |
| Apr-14 | 0 | 0 | 0 | 0 | 0 | 0 | 0 | 0 |
| May-14 | 0 | 0 | 0 | 0 | 0 | 0 | 0 | 0 |
| Jun-14 | * | 0 | * | 0 | * | 0 | * | 0 |
| Jul-14 | * | 0 | * | * | * | 0 | * | * |
| Feb-15 | * | 0 | 0 | 0 | * | 0 | 0 | 0 |
| Mar-15 | * | 0 | 0 | 0 | * | 0 | 0 | 0 |

**Table 61: Seasonal averages and variability (expressed as standard deviation: *s*) for iButton emplacement sites, where data are available, on Marion Island. The first value before '/' represents the seasonal average, the value after '/' variability. TSR represents the seasonal temperature range. * indicates data loss / season not evaluated. DJF: summer. JJA: winter.**

| Site | DJF | JJA | $T_{SR}$ |
|---|---|---|---|
| M2 | * | * | * |
| M3 | 8.9 / 1.3 | 1.6 / 0.3 | 6 |
| M4 | * | * | * |
| M5 | 11.3 / 0.9 | 3.1 / 0 | 7 |

Average seasonal temperatures and the seasonal ranges ($T_{SR}$) increase with decreasing altitude (Table 61). In comparison, variability (expressed as standard deviation: *s*) decreases with decreasing altitude. Seasonal averages are greater in summer as opposed to winter. An increase in average monthly temperatures is apparent with decreasing altitude (Table 62). During colder months (April-July), temperature variability increases with increasing altitude. In warmer months (February, March) this relationship reverses, although average monthly temperatures still increase with decreasing altitude.

**Table 62: Monthly averages and the associated variability (expressed as standard deviation: *s*) for iButton emplacement sites on Marion Island. The first value before '/' represents the seasonal average, the value after '/' variability.**

| Site | Monthly Averages | | | | | |
|---|---|---|---|---|---|---|
| | April '14 | May '14 | June '14 | July '14 | Feb '15 | March '15 |
| M2 | 4.5 / 3.0 | 3.7 / 2.9 | * | * | * | * |
| M3 | 5.2 / 2.8 | 4.1 / 2.8 | 1.6 / 1.6 | 1.7 / 1.6 | 10.2 / 3.0 | 7.0 / 2.3 |
| M4 | 5.6 / 2.8 | 4.7 / 2.6 | * | * | 10.3 / 3.5 | 8.4 / 2.8 |
| M5 | 6.2 / 2.7 | 5.1 / 2.7 | 3.1 / 1.9 | * | 12.3 / 4.0 | 7.9 / 2.2 |

### *5.2.2.3 Diurnal frost environment*

The diurnal frost environment is presented in subdivisions of months and seasons. All temperatures are based on degree Celsius and represent approximations to the nearest degree. Thaw duration, thaw depths and proportions (percentages) are rounded to the nearest hour, centimetre and percentage respectively. Logger failure, where applicable, is indicated in the text. Each site on Marion Island is discussed within its own subsection below, however a summary of calculated parameters is provided in Table 63 (pg. 184).

The lowest and highest maximum air temperatures are recorded at M1. The average duration of positive air temperatures achieved for both M1 and M2 is 19 hours, although M1 reflects a higher median diurnal cycle of 1 hour. Sites at greater altitude exhibit more potential freeze-thaw events, freeze-thaw cycles, as well as average freezing duration per freeze-thaw cycles than those at lower altitudes. At higher altitudes (M1), potential freeze-thaw events occur throughout the year; at M2 hardly any occur in summer. Both sites reflect multiple freeze-thaw cycles in one 24-hour period and both M1 and M2 exhibit freeze-thaw cycles spanning more than one day. Seasonal frost is evident at M1. The lowest ground temperatures are recorded in winter, with minimums reached in July at M1 and September at M2. During winter the ground is also often frozen, with freeze-thaw cycles only occurring

at the ground surface (GST: ± 2 cm depth). At M1, sub-zero air temperatures less than 24 hours make up 78% of all sub-zero durations calculated. At M2, sub-zero ground temperatures less than 24 hours make up 96% of all sub-zero durations calculated. For both sites, freeze-thaw cycles tend to initiate shortly after midnight or in the early morning. Freeze duration at M1 is significantly correlated to diurnal averages ($r$ ± -0.23, $p$ ± 0), diurnal ranges ($r$ ± -0.33, $p$ ± 0), and minimums ($r$ ± -0.32, $p$ ± 0). Similarly, freeze duration at M2 is significantly correlated to diurnal averages ($r$ ± -0.32, $p < 0.05$) and minimums ($r$ ± -0.30, $p < 0.05$).

**Table 63: Summary of ground thermal dynamics for M1 and M2 on Marion. Data are presented for 2014-2015. All durations and times represent averages. GST: ± 2 cm depth. FH: freeze hours. PFTE: potential freeze-thaw events. $T_{AIR}$: air temperature. * no data available.**

| Site | 2014-2015 | | | | | | EVENT | |
|---|---|---|---|---|---|---|---|---|
| | $T_{AIR}$ Max | PFTE $T_{AIR}$ | PFTE | FTC | PFTE to FTC | FH to PFTE | Multiple | Over Several Days |
| M1 | 18 | 209 | 188 | 92 | 49 | 10 | Y | Y |
| M2 | 18 | 99 | 97 | 52 | 54 | 5 | Y | Y |

5.2.2.3.1 M1: Katedraalkrans

Diurnal ranges and oscillations around 0 °C are provided in Table 64. M1 reflects few diurnal ranges ($T_{DR}$) exceeding 10 °C. This applies to all sensors. However, diurnal ranges greater than 10 °C occur throughout the year for the air sensor and spring-summer in the ground. In contrast, oscillations around 0 °C are common, occurring more than half of the year for air temperature ranges (± 54%), and at the ground surface (GST: temperature recorded at ± 2 cm in the ground; 53%). Of ranges greater than 0 °C, most occur in summer for air and ground temperature. Most oscillations around 0 °C, in turn, take place in winter for air, and spring for ground temperature.

**Table 64: Diurnal ranges exceeding 10 °C ($T_{DR}$ %), oscillations around 0 °C (Osc%) that fall into those ranges, as well all oscillations around 0 °C (Annual Osc %). $T_{AIR}$: air temperature. GST: temperature recorded at ± 2 cm in the ground. The subscript following 'T' indicates sensor depth in centimetres. * data loss/insufficient data to calculate value. JJA: winter. SON: spring. DJF: summer. MAM: autumn.**

| Sensor | $T_{DR}$ (%) | Osc (%) | Annual Osc (%) | Range >10 °C (%) | | | | Oscillations >/< 0C (%) | | | |
|---|---|---|---|---|---|---|---|---|---|---|---|
| | | | | JJA | SON | DJF | MAM | JJA | SON | DJF | MAM |
| $T_{AIR}$ | 7 | 79 | 54 | 17 | 33 | 33 | 17 | 28 | 26 | 22 | 24 |
| GST | 15 | 41 | 53 | 0 | 19 | 70 | 11 | 21 | 30 | 22 | 27 |
| $T_5$ | * | * | * | 0 | * | * | * | * | * | * | * |
| $T_{10}$ | * | * | * | 0 | * | * | * | * | * | * | * |
| $T_{15}$ | * | * | * | 0 | * | * | * | * | * | * | * |

Twenty-three unique needle ice events are identified by Borg (2017) near M1. Needle ice events initiated at temperatures ranging from -2 °C to 4.3 °C at soil moisture ranging between 0.4% and 12.5%, and wind speeds of 0 $m.s^{-1}$ to 7.5 $m.s^{-1}$ (Borg, 2017). The presence of needle ice, as observed during field visits and results presented by Borg (2017), indicate numerous freeze-thaw cycles to be present in this area. During 2014-15 relatively numerous sub-zero temperatures are evident for air

temperatures (potential freeze-thaw events: 209). Similarly, numerous potential freeze-thaw events (n = 188) and freeze-thaw cycles (n = 92) are observed for GST. Due to extensive data loss, depths from 5-15 cm cannot be evaluated. Negative air and ground temperatures reach maximum occurrence in June-August. From June-October more than 65% of all monthly air temperature hours are below 0 °C. Similarly, from June-September more than 70% of all monthly temperatures recorded at GST are below 0 °C. The fewest sub-zero temperatures are recorded in February (10% and 7% of monthly hours for air temperatures and GST). A minimum of -10 °C is reached for air temperature on 7 October at 08:00 and negative temperatures are maintained for ± 19 hours on average, although the most common cycle only spans 1 hour (discussed in 5.2.2.2.1 M1: Katedraalkrans, pg. 176). A minimum of -7 °C is reached at GST on 15 July at 03:00, with an average cycle lasting 20 hours.

During the observation period 92 freeze-thaw cycles are evident on 83 separate days. More cycles are observed due to numerous days having two cycles taking place in a 24-hour period. Almost half (49%) of potential freeze-thaw events translate into freeze-thaw cycles (Table 65). Freeze-thaw cycles occur throughout the year, with 26% in winter, 30% in spring, 20% in summer, and 24% in autumn. The greatest percentage for a single month are October and November (13%). Almost all freeze-thaw cycles represent single events, with average freezing duration of 1 hour ($s$ = 6). Freezing generally initiates between 02:00-07:00. Multiple freeze-thaw cycles in one 24-hour period are observed in June, October-December, and March. The initial freeze-event is generally shorter, with subsequent durations longer. Furthermore, multiple potential freeze-thaw events take place before a freeze-thaw cycle. And not every freeze event at GST yields a freeze event to greater depths in the ground. The ground is also frozen at depth ($T_5$-$T_{10}$) for extended periods of time. However, while the ground is frozen at depth, freeze-thaw cycles occur at the ground surface (GST).

**Table 65: Freeze-thaw events for M1, summarised by month. * indicates underestimation of duration due to data loss. $T_{AIR}$ reflects air temperature; GST indicates temperature recorded at the ground surface (± 2 cm). The subscript following 'T' indicates the depth of the sensor (in centimetres) used to record ground temperature. PFTE: potential freeze-thaw events. FTC: freeze-thaw cycles.**

| Month | PFTE | | | | | FTC |
|---|---|---|---|---|---|---|
| | $T_{AIR}$ | GST | $T_5$ | $T_{10}$ | $T_{15}$ | |
| June | 20 | 12 | 10 | 9 | 11 | 11 |
| July | 20 | 13 | 9 | 9 | 8 | 7 |
| August | 20 | 17 | 7 | 7 | 0 | 6 |
| September | 11 | 11 | * | 7 | 6 | 4 |
| October | 21 | 19 | 8 | * | * | 12 |
| November | 19 | 23 | * | * | * | 12 |
| December | 30 | 20 | * | * | * | 11 |
| January | 11 | 13 | * | * | * | 4 |
| February | 5 | 7 | * | * | * | 3 |
| March | 17 | 17 | * | * | * | 9 |
| April | 15 | 15 | * | * | * | 5 |
| May | 20 | 21 | 17 | * | 5 | 8 |
| Total | 209 | 188 | 51 | 32 | 30 | 92 |

Seventy-seven freeze-thaw cycles last longer than 10 hours (Figure 98). Of these 25% occur in September, with 10% in June and 11% in November. Of these ranges, two-thirds are evident in winter and spring. When the average freezing duration is considered (1 hours, n = 22), 14% occur in November, although two-thirds are evident from winter-spring. Temperature variability decreases with increasing depth in the ground (GST: $s$ = 3.0; $T_{15}$: $s$ = 0.9). At GST the average diurnal temperature range approximates 4 °C, although a maximum range of 24 °C is reached. Diurnal maximum and minimum temperatures are 23 °C and -4 °C respectively. Average diurnal maximum and minimum temperatures are 3 °C and -2 °C respectively. The average diurnal mean temperature is 0.3 °C. Freeze duration is significantly correlated to diurnal averages ($r$ ± -0.23, $p$ ± 0), diurnal ranges ($r$ ± -0.33, $p$ ± 0), and minimums ($r$ ± -0.32, $p$ ± 0). This only applies to freeze-thaw cycles evaluated.

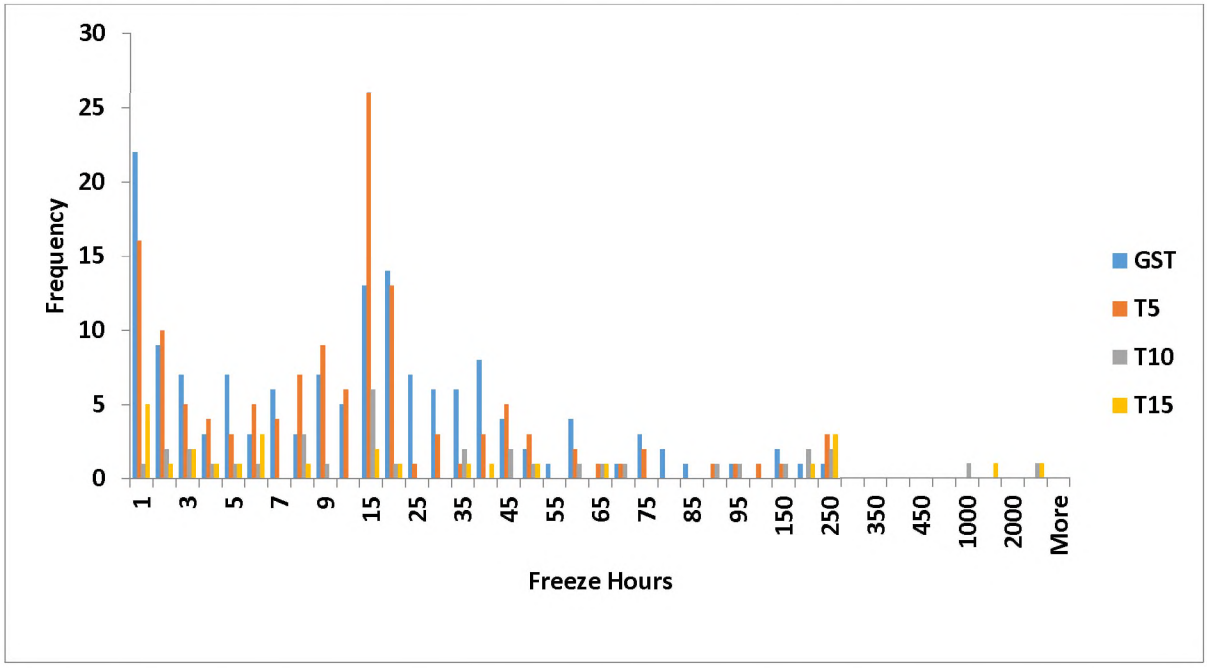


**Figure 98: Histogram of freeze duration per event per sensor depth for M1. GST: temperature recorded at the ground surface (± 2 cm). The number after 'T' indicates sensor depth in centimetres.**

#### *5.2.2.3.1.1 Higher-frequency*

High-frequency temperature data using an XR5 system, recorded at two-minute intervals, are available for M1 from 5-31 May 2015. Potential freeze-thaw events are evident for air temperature, as well as ground temperatures at 15-cm depth. As such, freeze-thaw cycles occur, although no zero-curtain effect, nor are exotherms are evident (Figure 99, pg. 189). This agrees with findings presented for M1 (5.2.2.3.1 M1: Katedraalkrans, pg. 183). Diurnal temperature ranges exceeding 10 °C are present (14 & 22 May), although the average diurnal range is less than this (7 °C, $s$ = 1.8). Furthermore, variability (expressed as standard deviation: $s$) is higher than that of lower-frequency data. Furthermore, discrepancies between potential frozen hours at 1-hour and 2-minute data are evident (Table 66, pg. 187). Lower frequency data collection masks dynamics inherent to the ground thermal regime. Potential freeze-thaw events and freeze-thaw cycles increase in number when recording temperature at higher-frequency.

**Table 66: Freeze-thaw events for M1, recorded at 2-min interval from 5-31 May 2015. Potential freeze-thaw events (PFTE) and freeze-thaw cycles (FTC) identified using 1-hourly data are indicated in brackets. $T_{AIR}$ reflects air temperature; GST indicates temperature recorded at the ground surface (± 2 cm). The subscript following 'T' indicates sensor depth in centimetres.**

| Day | Potential Freezing Hours at 0 °C | | | | PFTE | | | | FTC |
|---|---|---|---|---|---|---|---|---|---|
| | $T_{AIR}$ | GST | T5 | T15 | $T_{AIR}$ | GST | T5 | T15 | |
| 5 | 21 (21) | 22 (23) | 24 (24) | 15 (15) | 1 (1) | 7 (2) | 0 (2) | 4 (0) | 1 (1) |
| 6 | 24 (24) | 24 (24) | 24 (24) | 14 (14) | 0 (1) | 0 (0) | 0 (0) | 4 (0) | 1 (0) |
| 7 | 22 (22) | 24 (24) | 24 (24) | 24 (24) | 2 (3) | 0 (0) | 0 (0) | 0 (0) | 0 (0) |
| 8 | 9 (10) | 13 (12) | 16 (17) | 24 (24) | 1 (4) | 9 (0) | 5 (0) | 0 (0) | 0 (0) |
| 9 | 10 (9) | 17 (17) | 18 (19) | 24 (24) | 11 (0) | 10 (0) | 7 (0) | 0 (0) | 0 (0) |
| 10 | 21 (21) | 24 (24) | 24 (24) | 24 (24) | 2 (0) | 1 (0) | 0 (0) | 0 (0) | 0 (0) |
| 11 | 0 (0) | 0 (0) | 1 (1) | 8 (9) | 0 (1) | 0 (0) | 1 (0) | 13 (0) | 0 (0) |
| 12 | 0 (0) | 0 (0) | 0 (0) | 0 (0) | 0 (0) | 0 (1) | 0 (1) | 0 (0) | 0 (0) |
| 13 | 0 (0) | 0 (0) | 0 (0) | 0 (0) | 0 (0) | 0 (0) | 0 (0) | 0 (0) | 0 (0) |
| 14 | 11 (10) | 8 (7) | 5 (5) | 0 (0) | 0 (0) | 1 (0) | 5 (0) | 0 (0) | 1 (1) |
| 15 | 20 (20) | 21 (22) | 22 (22) | 0 (0) | 1 (1) | 1 (1) | 1 (1) | 0 (0) | 0 (0) |
| 16 | 8 (7) | 8 (8) | 8 (8) | 0 (0) | 2 (0) | 0 (0) | 1 (0) | 0 (0) | 1 (1) |
| 17 | 24 (24) | 24 (24) | 24 (24) | 14 (14) | 0 (0) | 0 (0) | 0 (0) | 3 (0) | 0 (0) |
| 18 | 19 (21) | 22 (22) | 24 (24) | 23 (24) | 12 (1) | 5 (1) | 1 (1) | 10 (1) | 0 (0) |
| 19 | 0 (0) | 0 (0) | 1 (1) | 0 (0) | 0 (0) | 0 (0) | 1 (0) | 1 (0) | 0 (0) |
| 20 | 0 (0) | 0 (0) | 0 (0) | 0 (0) | 0 (1) | 0 (0) | 0 (0) | 0 (2) | 0 (0) |
| 21 | 0 (0) | 0 (0) | 0 (0) | 0 (0) | 0 (0) | 0 (0) | 0 (0) | 0 (0) | 0 (0) |
| 22 | 12 (12) | 21 (22) | 18 (18) | 0 (0) | 1 (1) | 1 (2) | 3 (1) | 0 (4) | 0 (0) |
| 23 | 1 (2) | 2 (2) | 2 (2) | 0 (0) | 11 (1) | 2 (1) | 3 (0) | 0 (2) | 1 (1) |
| 24 | 13 (13) | 16 (17) | 16 (16) | 0 (0) | 5 (0) | 1 (0) | 2 (0) | 0 (0) | 1 (1) |
| 25 | 3 (1) | 10 (9) | 10 (10) | 0 (0) | 4 (0) | 4 (0) | 6 (0) | 0 (0) | 0 (0) |
| 26 | 0 (0) | 6 (6) | 6 (6) | 0 (0) | 0 (1) | 4 (1) | 3 (1) | 0 (0) | 1 (0) |
| 27 | 23 (23) | 29 (23) | 29 (23) | 0 (0) | 0 (1) | 4 (1) | 4 (1) | 0 (0) | 0 (0) |
| 28 | 9 (8) | 18 (17) | 20 (21) | 8 (8) | 12 (0) | 10 (0) | 2 (0) | 2 (0) | 0 (0) |
| 29 | 2 (3) | 6 (6) | 6 (6) | 6 (5) | 2 (1) | 3 (1) | 5 (1) | 3 (0) | 1 (1) |
| 30 | 0 (0) | 0 (0) | 0 (0) | 0 (0) | 0 (1) | 2 (0) | 2 (0) | 0 (0) | 0 (0) |
| 31 | 13 (12) | 19 (19) | 21 (20) | 0 (0) | 10 (0) | 14 (0) | 8 (0) | 0 (0) | 0 (0) |
| Total | 265 (263) | 335 (328) | 343 (339) | 184 (185) | 77 (19) | 79 (11) | 60 (9) | 40 (9) | 8 (6) |

Air and ground temperature freezing and thawing indices are variable and both indices decrease with increasing depth in the ground (Table 67, pg. 188). Like data recorded at 1-hour intervals, high-frequency data are most variable near the ground surface. The greatest freezing index is observed for air temperature on 6 May. In comparison, the highest thawing index is recorded on 11 May. The balance of degree days is ± 1 toward the thawing index, with the thermal offset ~ -0.4 and negatively skewed.

**Table 67: The freezing index (FI) and thawing index (TI) for the various sensor depths for M1 from 5-31 May. $T_{AIR}$ reflects air temperature; GST indicates temperature recorded at the ground surface (± 2 cm). The subscript following 'T' indicates the depth of the sensor (in centimetres) used to record ground temperature. SO: thermal offset. DD: degree days.**

| Day | FI | | | | TI | | | | SO |
|---|---|---|---|---|---|---|---|---|---|
| | $T_{AIR}$ | GST | $T_5$ | $T_{15}$ | $T_{AIR}$ | GST | $T_5$ | $T_{15}$ | |
| 5 | -2.1 | -1.4 | -1.2 | 0 | 0.2 | 0 | 0 | 0 | 0.6 |
| 6 | -4.3 | -2.2 | -1.6 | -0.1 | 0 | 0 | 0 | 0 | 2.0 |
| 7 | -2.5 | -1.4 | -1.2 | -0.3 | 0.1 | 0 | 0 | 0 | 1.0 |
| 8 | -1.0 | -0.7 | -0.7 | -0.2 | 1.1 | 0.3 | 0.1 | 0 | -0.6 |
| 9 | -0.5 | -0.6 | -0.4 | 0 | 1.2 | 0.4 | 0.2 | 0 | -1.0 |
| 10 | -1.4 | -1.0 | -0.8 | -0.1 | 0.2 | 0 | 0 | 0 | 0.3 |
| 11 | 0 | 0 | 0 | 0 | 7.3 | 3.2 | 1.8 | 0 | -4.1 |
| 12 | 0 | 0 | 0 | 0 | 7.1 | 5.2 | 4.1 | 1.0 | -1.9 |
| 13 | 0 | 0 | 0 | 0 | 5.0 | 4.5 | 4.3 | 3.6 | -0.5 |
| 14 | -0.8 | -0.2 | -0.1 | 0 | 2.6 | 2.7 | 2.9 | 3.8 | 0.6 |
| 15 | -1.8 | -1.4 | -1.0 | 0 | 0.2 | 0.1 | 0.1 | 0.5 | 0.3 |
| 16 | -0.6 | -0.4 | -0.2 | 0 | 1.9 | 1.8 | 1.6 | 1.5 | 0 |
| 17 | -3.0 | -2.2 | -1.7 | 0 | 0 | 0 | 0 | 0.1 | 0.8 |
| 18 | -0.9 | -0.8 | -0.7 | -0.1 | 0.1 | 0 | 0 | 0 | 0.1 |
| 19 | 0 | 0 | 0 | 0 | 4.3 | 3.9 | 3.5 | 2.1 | -0.5 |
| 20 | 0 | 0 | 0 | 0 | 4.2 | 4.0 | 3.9 | 3.7 | -0.3 |
| 21 | 0 | 0 | 0 | 0 | 6.8 | 6.7 | 6.7 | 6.4 | -0.1 |
| 22 | -1.1 | -1.4 | -0.9 | 0 | 1.9 | 0.1 | 0.1 | 1.7 | -2.1 |
| 23 | 0 | 0 | 0 | 0 | 3.3 | 2.3 | 1.8 | 0.8 | -1.0 |
| 24 | -0.7 | -0.8 | -0.6 | 0 | 1.4 | 1.2 | 1.2 | 1.9 | -0.3 |
| 25 | 0 | -0.1 | -0.1 | 0 | 1.6 | 1.4 | 1.2 | 1.2 | -0.3 |
| 26 | 0 | 0 | 0 | 0 | 2.5 | 2.0 | 2.0 | 1.7 | -0.5 |
| 27 | -2.1 | -1.8 | -1.3 | 0 | 2.6 | 2.1 | 2.1 | 2.6 | -0.1 |
| 28 | -0.4 | -0.9 | -0.9 | 0 | 2.2 | 0.5 | 0.2 | 0.1 | -2.2 |
| 29 | 0 | -0.1 | -0.1 | 0 | 3.2 | 2.7 | 2.6 | 1.5 | -0.5 |
| 30 | 0 | 0 | 0 | 0 | 2.2 | 1.9 | 1.8 | 2.3 | -0.3 |
| 31 | -0.3 | -0.6 | -0.5 | 0 | 0.2 | 0 | 0 | 0.4 | -0.4 |
| Balance * | 1.5 | 1.1 | 1.0 | 1.3 | * difference between FI and TI in DD | | | | |

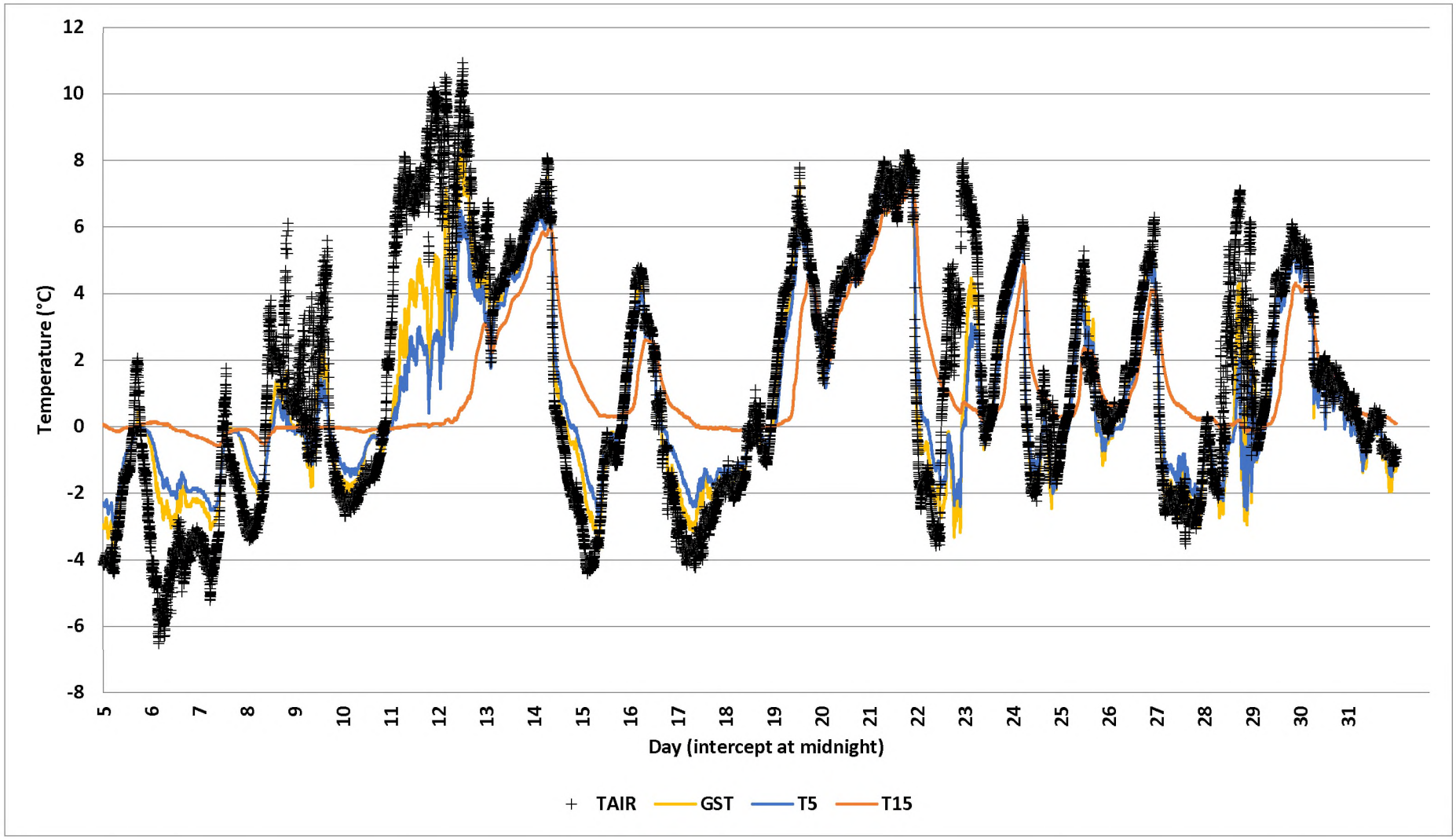


**Figure 99: Diurnal cycles for a 27-day period from 5-31 May 2015. $T_{AIR}$: air temperatures. GST: ground temperatures recorded at ± 2 cm depth. The number after T' indicates sensor depth in centimetres.**

#### 5.2.2.3.2 M2: Tafelberg

Diurnal ranges and oscillations around 0 °C are provided in Table 68. M2 reflects few diurnal ranges ($T_{DR}$) exceeding 10 °C. This applies to all sensors. No diurnal ranges greater than 10 °C occur in winter for the air sensor and in autumn in the ground. In contrast, oscillations around 0 °C are common, occurring two-thirds of the year for air temperature ranges (± 71%), and one-third of the year at the ground surface (GST: temperature recorded at ± 2 cm in the ground). Furthermore, such oscillations are evident from April-January for air temperature and from April-December for GST.

**Table 68: Diurnal ranges exceeding 10 °C ($T_{DR}$ %), oscillations around 0 °C (Osc%) that fall into those ranges, as well all oscillations around 0 °C (Annual Osc %). $T_{AIR}$: air temperature. GST: temperature recorded at ± 2 cm in the ground. The subscript following 'T' indicates sensor depth in centimetres. * data loss/insufficient data to calculate value. JJA: winter. SON: spring. DJF: summer. MAM: autumn.**

| Sensor | $T_{DR}$ (%) | Osc (%) | Annual Osc (%) | Range > 10 °C (%) | | | | Oscillations >/< 0 °C (%) | | | |
|---|---|---|---|---|---|---|---|---|---|---|---|
| | | | | JJA | SON | DJF | MAM | JJA | SON | DJF | MAM |
| $T_{AIR}$ | 2 | 71 | 36 | 0 | 57 | 29 | 14 | 41 | 37 | 8 | 14 |
| GST | 14 | 33 | 34 | 11 | 42 | 47 | 0 | 46 | 40 | 1 | 13 |
| $T_5$ | 4 | 0 | 21 | 0 | 55 | 45 | 0 | 63 | 27 | 0 | 10 |
| $T_{10}$ | 0 | 0 | 24 | 0 | * | * | * | 51 | * | * | * |
| $T_{15}$ | 0 | 0 | 13 | 0 | * | * | * | 73 | * | * | * |

During 2014-15 relatively numerous sub-zero temperatures are evident for air temperatures (potential freeze-thaw events: 98). Similarly, numerous potential freeze-thaw events (n = 97) and freeze-thaw cycles (n = 52) are observed for GST to a depth of 15 cm. Negative air and ground temperatures reach maximum occurrence in June-August. An average 45% of daily hours on these months are below 0 °C for the air temperature sensor, this proportion increases to 53% at GST. A minimum of -5 °C is reached for air temperature on 27 July at 07:00 and negative temperatures are maintained for ± 19 hours on average, although the most common cycle only spans 3 hours (discussed in 5.2.2.2.1 M2: Tafelberg, pg. 179). A minimum of -5 °C is reached at GST on 1 September at 07:00, with an average cycle lasting 3-4 hours.

During the observation period 52 freeze-thaw cycles are evident on 47 separate days. More cycles are observed due to numerous days having two cycles taking place in a 24-hour period. Over half (54%) of potential freeze-thaw events translate into freeze-thaw cycles (Table 69, pg. 191). Freeze-thaw cycles occur from May-November, with 14% in autumn, 46% in winter, and 40% in spring. None are recorded at GST in summer. While most freeze-thaw cycles take place in winter, the greatest percentage for a single month is September (21%). Almost all freeze-thaw cycles represent single events, with average freezing duration of 29 hours ($s$ = 18), whereas the median duration is 15 hours. Freezing generally taking place from 03:00-12:00 the following day. Multiple freeze-thaw cycles are observed for 21 May, 17 July, 17 and 21 September, as well as 9 October. In autumn and winter the initial freeze event is shortest, lasting ± 9 hours, occurring between 02:00-10:00. The second freeze is ± 14 hours, taking place between 16:00-15:00 the following day. In spring the initial freeze event is shortest, lasting ± 17 hours, occurring from 19:00 the previous day to 09:00 on the day. The second freeze is ± 18 hours,

taking place between 10:00-18:00 the following day. Not every freeze event at GST yields a freeze event to greater depths in the ground. Furthermore, during July-September, not every freeze-thaw cycle at GST yields thawing of the ground at greater depths. This is prominent in September, where the ground is frozen from $T_5$-$T_{15}$. Nevertheless, the ground surface experiences thaw during this time. The average delay of ground frost is ± 3 hours (*s* = 3) between GST and $T_5$. A ± 7-hour delay (*s* = 6) is noticeable from $T_5$-$T_{10}$. Furthermore, sensors at greater depth in the ground display an earlier thaw to the sensor closer to the ground surface (± 1 hour).

**Table 69: Freeze-thaw events for M2, summarised by month. * indicates underestimation of duration due to data loss. $T_{AIR}$ reflects air temperature; GST indicates temperature recorded at the ground surface (± 2 cm). The subscript following 'T' indicates the depth of the sensor (in centimetres) used to record ground temperature. PFTE: potential freeze-thaw events. FTC: freeze-thaw cycles.**

| Month | PFTE | | | | | FTC |
|---|---|---|---|---|---|---|
| | $T_{AIR}$ | GST | $T_5$ | $T_{10}$ | $T_{15}$ | |
| March | 0 | 0 | 0 | 0 | 0 | 0 |
| April | 5 | 1 | 0 | 0 | 0 | 0 |
| May | 10 | 10 | 5 | 3 | 0 | 7 |
| June | 12 | 17 | 12 | 5 | 2 | 8 |
| July | 12 | 17 | 12 | 5 | 4 | 8 |
| August | 16 | 15 | * | 13 | 5 | 8 |
| September | 13 | 20 | * | 15 | 4 | 11 |
| October | 10 | 11 | 9 | * | * | 8 |
| November | 13 | 5 | 1 | * | * | 2 |
| December | 5 | 1 | 0 | * | * | 0 |
| January | 3 | 0 | 0 | * | * | 0 |
| February | 0 | 0 | 0 | * | * | 0 |
| Total | 99 | 97 | 39 | 41 | 15 | 52 |

Forty freeze-thaw cycles last longer than 10 hours (Figure 100, pg. 192). Of these 25% occur in September, with 18% each in August and October. Cycles spanning more than 10 hours also occur on May-July (13% each), with one isolated occurrence in November. When the average freezing duration is considered (29 hours, n = 12), 67% occur in June and July. Temperature variability decreases with increasing depth in the ground (GST: *s* = 1.5; $T_{15}$: *s* = 0.9). At GST the average diurnal temperature range approximates 4 °C, although a maximum range of 19 °C is reached. Diurnal maximum and minimum temperatures are 17 °C and -4 °C respectively. Average diurnal maximum and minimum temperatures are 3 °C and -1 °C respectively. The average diurnal mean temperature is 0.5 °C. Freeze duration is significantly correlated to diurnal averages ($r$ ± -0.32, $p < 0.05$) and minimums ($r$ ± -0.30, $p < 0.05$). This only applies to freeze-thaw cycles evaluated. Average diurnal temperatures associated with freeze-thaw cycles are significantly correlated to diurnal ranges ($r$ ± 0.85, $p$ ± 0) and maximums ($r$ ± 0.72, $p$ ± 0).

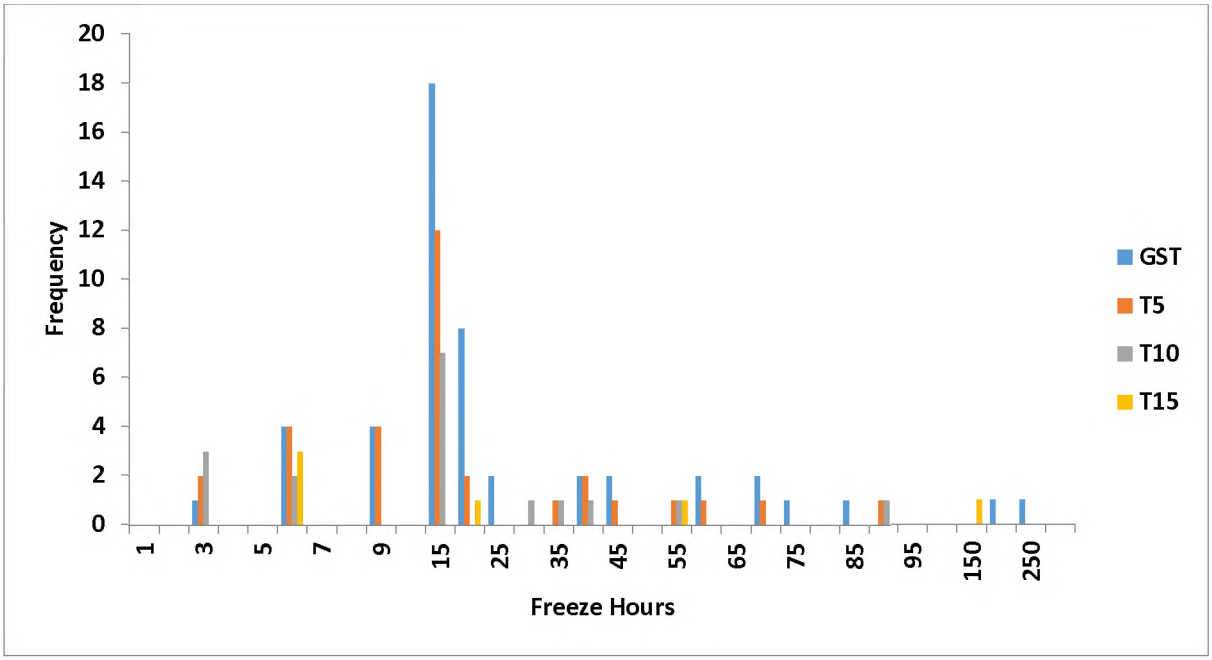


**Figure 100: Histogram of freeze duration per event per sensor depth for M2. GST: temperature recorded at the ground surface (± 2 cm). The number after 'T' indicates sensor depth in centimetres.**

#### *5.2.2.3.2.1 Higher-frequency*

Higher-frequency temperature data using an ACR system, recorded at five-minute intervals, are available for M2 from 12-24 April 2014. Potential freeze-thaw events are evident for air temperature. However, no freeze-thaw cycles are evident in the ground (Figure 101, pg. 194). Even though air temperatures reach below 0 °C, the ground remains thawed (Table 70, 192). This agrees with findings presented in For M2 (5.2.2.3.2 M2: Tafelberg, pg. 190). Diurnal temperature ranges exceeding 10 °C are not present, with the average diurnal range 1 °C ($s$ = 1.3). However, variability (expressed as standard deviation: $s$) is higher than that of lower-frequency data. Furthermore, discrepancies between potential frozen hours at 3-hour and 5-minute data are evident. Lower frequency data collection masks dynamics inherent to the ground thermal regime, like findings of M2. Potential freeze-thaw events increase in number when recording temperature at higher-frequency. While these do not translate into freeze-thaw cycles, the higher-frequency of these events is applicable to the remainder of the year. As such, the number of freeze-thaw cycles calculated at M2 (5.2.2.3.2 M2: Tafelberg, pg. 190) is an underestimation of freeze-thaw cycles.

**Table 70: Freeze-thaw events for M2, recorded at 5-min intervals from 14-24 April. Potential freeze-thaw events (PFTE) and freeze-thaw cycles (FTC) identified using 3-hourly data are indicated in brackets. $T_{AIR}$ reflects air temperature; GST indicates temperature recorded at the ground surface (± 2 cm).**

| Day | Potential Freezing Hours at 0 °C | PFTE | FTC |
|---|---|---|---|
| | $T_{AIR}$ | $T_{AIR}$ | |
| 14 | 5 (1) | 1 (1) | 0 (0) |
| 15 | 13 (15) | 1 (2) | 0 (0) |
| 21 | 1 (0) | 0 (1) | 0 (0) |

| Day | Potential Freezing Hours at 0 °C | PFTE | FTC |
|---|---|---|---|
| | $T_{AIR}$ | $T_{AIR}$ | |
| 23 | 21 (24) | 2 (9) | 0 (0) |
| Total | 40 (40) | 4 (13) | 0 (0) |

Ground temperatures register no freezing index, with marginal negative freezing indices calculated for air temperature on 14, 15, and 23 April (Table 71). In comparison, thawing indices are positive for all sensors on all days. Like data recorded at 3-hourly intervals, higher-frequency data show greatest variability of ground temperatures at GST, with the least at $T_{15}$. The thawing index generally decreases with increasing depth into the ground, as does the freezing index. The greatest freezing index is observed at for air temperature on 23 April. In comparison, the highest thawing index is recorded on 13 April. The balance of degree days is ± 4 toward the thawing index for all sensors. The thermal offset approximates 0, although skewed towards positive values.

**Table 71: The freezing index (FI) and thawing index (TI) for the various sensor depths for M2 from 12-24 April. $T_{AIR}$ reflects air temperature; GST indicates temperature recorded at the ground surface (± 2 cm). The subscript following 'T' indicates the depth of the sensor (in centimetres) used to record ground temperature. SO: thermal offset. DD: degree days.**

| Day | FI | | | | | TI | | | | | SO |
|---|---|---|---|---|---|---|---|---|---|---|---|
| | $T_{AIR}$ | GST | $T_5$ | $T_{10}$ | $T_{15}$ | $T_{AIR}$ | GST | $T_5$ | $T_{10}$ | $T_{15}$ | |
| 12 | 0 | 0 | 0 | 0 | 0 | 10.8 | 10 | 9.7 | 9.0 | 8.4 | -0.7 |
| 13 | 0 | 0 | 0 | 0 | 0 | 10.5 | 10.1 | 10 | 9.7 | 9.2 | -0.4 |
| 14 | -0.2 | 0 | 0 | 0 | 0 | 2.0 | 3.3 | 4.0 | 5.4 | 6.4 | 1.5 |
| 15 | -0.7 | 0 | 0 | 0 | 0 | 0.7 | 1.2 | 1.7 | 2.9 | 3.8 | 1.2 |
| 16 | 0 | 0 | 0 | 0 | 0 | 3.9 | 3.4 | 3.4 | 3.4 | 3.7 | -0.5 |
| 17 | 0 | 0 | 0 | 0 | 0 | 5.6 | 5.3 | 5.2 | 5.0 | 4.9 | -0.3 |
| 18 | 0 | 0 | 0 | 0 | 0 | 7.5 | 7.4 | 7.2 | 6.7 | 6.2 | -0.1 |
| 19 | 0 | 0 | 0 | 0 | 0 | 3.4 | 5.3 | 5.6 | 6.0 | 6.1 | 1.9 |
| 20 | 0 | 0 | 0 | 0 | 0 | 4.3 | 4.4 | 4.5 | 4.8 | 5.0 | 0.1 |
| 21 | 0 | 0 | 0 | 0 | 0 | 1.2 | 2.1 | 2.5 | 3.3 | 3.9 | 0.9 |
| 22 | 0 | 0 | 0 | 0 | 0 | 1.5 | 1.5 | 1.8 | 2.4 | 2.9 | 0 |
| 23 | -0.8 | 0 | 0 | 0 | 0 | 0.1 | 0.3 | 0.6 | 1.4 | 2.1 | 1.1 |
| Balance * | 3.8 | 4.1 | 4.4 | 3.9 | 0 | * difference between FI and TI in DD | | | | | |

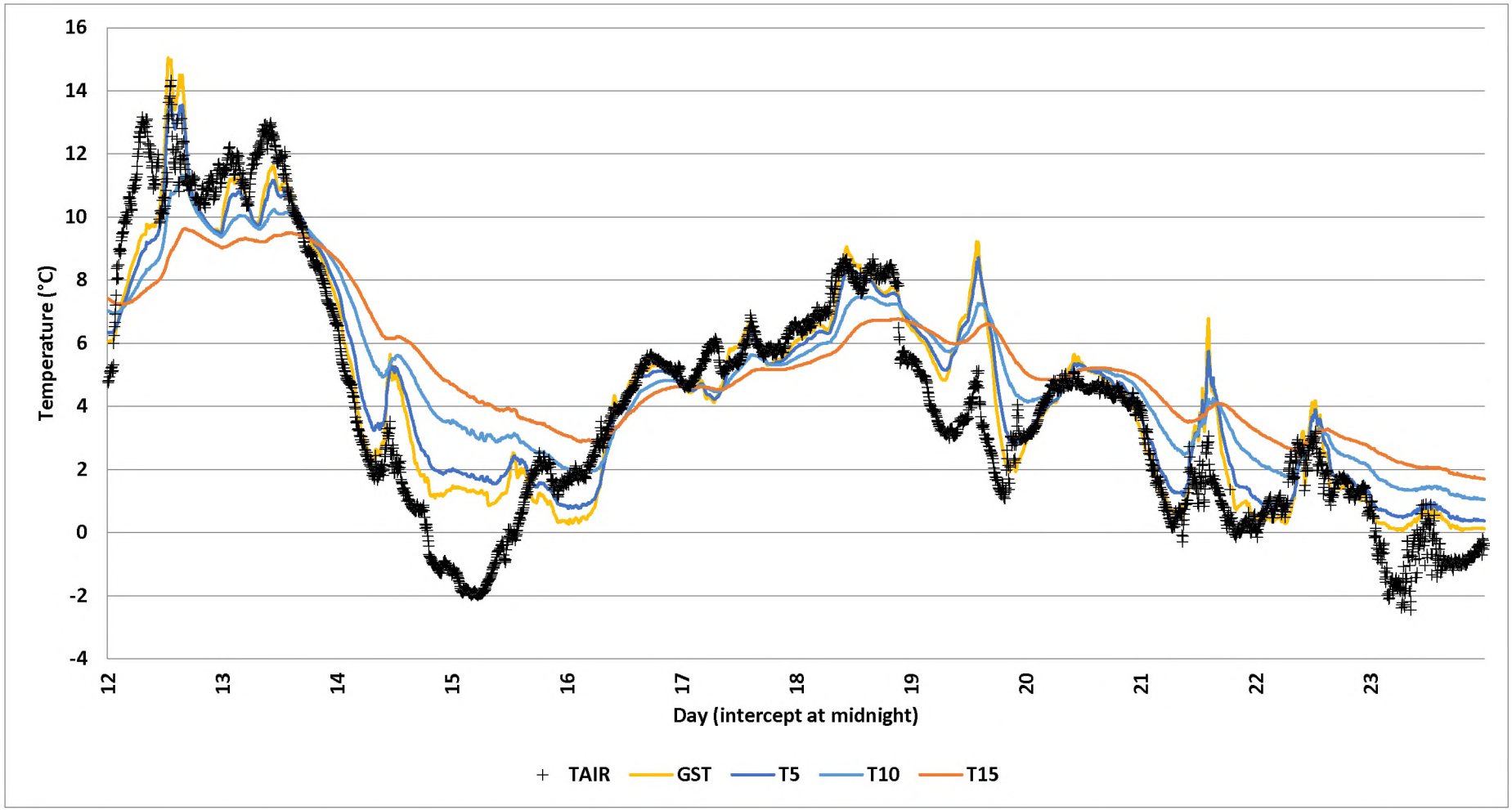


**Figure 101: Diurnal cycles for a twelve-day period from 12-24 April 2014. $T_{AIR}$: air temperatures. GST: ground temperatures recorded at ± 2 cm depth. The number after T' indicates sensor depth in centimetres.**

#### 5.2.2.3.3 iButtons: M2-M5

iButtons experienced extensive data loss throughout. However, data are available for M2-M5 in April and May 2014, with data available for M3 from April-July 2014, as well as February and March 2015. The extent of data loss, coupled with all hygrochrons yielding no usable data, makes an evaluation of the diurnal frost environment problematic. Furthermore, the lack of ground moisture data makes it impossible to infer the presence of freeze-thaw cycles. Oscillation around 0 °C are discussed in 5.2.2.2.3 iButtons: M2-M5 (pg. 182 onwards). For months and seasons where sufficient data are available to allow for analyses, no oscillations around 0 °C are evident. As such, for those times where sufficient data are available, no potential freeze-thaw events are recorded.

#### 5.2.2.3.4 Marion Island comparison

Ground surface temperatures (GST: temperatures recorded at ± 2 cm, depth), exhibit the greatest ranges, as well as temperature variability (expressed as standard deviation: *s*) (Table 72). Sites at higher altitudes reflect longer duration of frozen ground and seasonal means increase with a decrease in elevation. Furthermore, M1 reflects freeze-thaw cycles throughout the year, in comparison to M2, which reflects freeze-thaw cycles from May-November. Both sites reflect seasonal ground frost, although the duration of frozen ground is greater at M1. Moisture is also available throughout the year and not a limiting factor on freeze-thaw cycles, as argued by Holness (2001a).

**Table 72: Seasonal temperature averages ($T_{SM}$) and variability (*s*) for summer (DJF) and winter (JJA), as well as seasonal temperature ranges ($T_{SR}$) and the annual ground freezing index (GFI) for M1 and M2 on Marion Island. Under 'DFJ' and 'JJA' the first value reflects $T_{SM}$, the second value *s*.**

| Site | DJF | JJA | $T_{SR}$ | GFI |
|---|---|---|---|---|
| M1 | 4.7 / 2.1 | -0.7 / 0.26 | 3 | 722 |
| M2 | 6.3 / 1.62 | 0.7 / 0.07 | 5 | 1 124 |

### 5.2.3 Sediment/soil specifics

Results from the analyses of textural and moisture properties are provided in Table 73 (pg. 196) and Table 74 (pg. 199) respectively. Descriptive statistics are provided in **Table 75** (pg. 200). Discussion of results follows each table and graphs are provided where deemed necessary.

**Table 73: Sediment physical characteristics and parameters for Marion Island study sites. Total organic carbon (TOC) is expressed as a percentage; $d_b$ reflects bulk density; $d_p$ reflects porosity of samples; FEF (%) the fine earth fraction expressed as a percentage.**

| Site | Depth | TOC (%) | $d_b$ | $d_p$ | FEF (%) |
|---|---|---|---|---|---|
| M1 | Surface | 2.8 | 1.1 | 0.6 | 42 |
| | 15 | 2.7 | 1.0 | 0.6 | 53 |
| M2 | Surface | 4.8 | 1.4 | 0.5 | 29 |
| | 15 | 4.2 | 0.6 | 0.8 | 88 |
| M3 | Surface | 4.7 | 1.0 | 0.6 | 86 |
| M4 | Surface | 11.8 | 0.5 | 0.8 | 96 |
| | 15 | 7.4 | 0.6 | 0.8 | 95 |
| M5 | Surface | 8.2 | 0.7 | 0.8 | 68 |

On average, sub-surface samples show lower total organic carbon (TOC) compared to surface samples (4.8% vs. 5.0%). Overall TOC increases with decreasing altitude (Figure 102, pg. 197), which is reflected by the organic soil description using Table 12 (APPENDIX E), where the M1-M3 samples are mineral soils with organic matter. M4-M5 are organic soils. Bulk density for surface samples decreases from M1-M4, after which bulk density increases (Figure 103, pg. 197). The associated porosity values generally increase with a decrease in altitude (Figure 103, pg. 197). The fine earth fraction (FEF: portion < 2 mm) (Figure 104, pg. 197) is greater for samples at depth (64% vs. 79% for surface and sub-surface samples respectively). Overall variation (expressed as standard deviation: *s*) for TOC, bulk density, porosity and the FEF is higher for surface than sub-surface samples. Standard deviations (*s*) of surface samples is 3.6 for TOC, 0.4 for bulk density, 0.1 for porosity, and 28.0 for the FEF. Standard deviations (*s*) of sub-surface samples is 2.4 for TOC, 0.2 for bulk density, 0.1 for porosity, and 22.2 for the FEF. Using bulk density as a determinant for material description, the sub-surface sample of M2, as well as those of M4 and M5 are soils high in organic content, with all other sites classified as clay/clay loam/silt loam (Table 9, APPENDIX E), with M2-M4 consisting of finer proportions than M1 (Figure 106, pg. 198). Using porosity as a determinant for material description, all sites are clayey-silt soils except for the surface M2 sample, which more closely represents that of fine sand (Table 10, APPENDIX E). This reflects an average specific yield ($S_y$) between 2-21 (Table 11, APPENDIX E), and a specific retention of moisture of ± 6-8 (Robson, 1993).

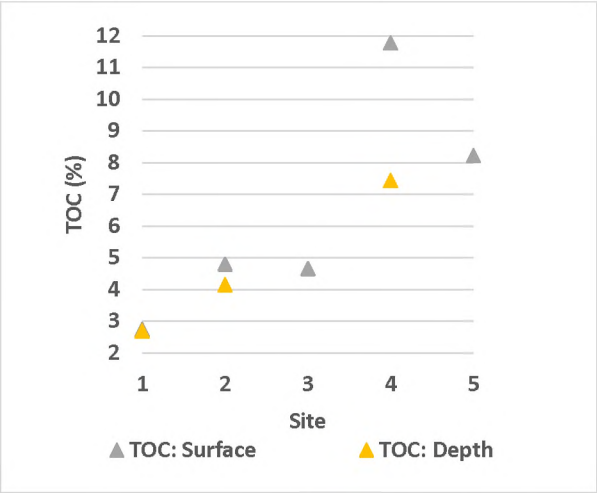


Figure 102: Total organic carbon (TOC) expressed as a percentage for Marion Island sites. 1-5 indicate sites M1-M5.

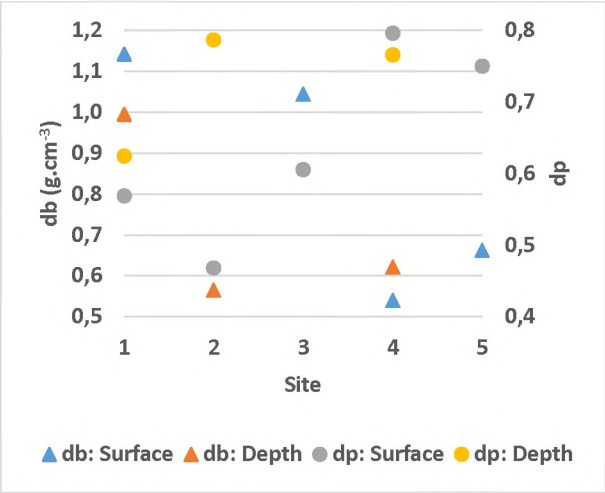


Figure 103: Bulk density ($d_b$) and porosity ($d_p$) for Marion Island sites. 1-5 indicate sites M1-M5.

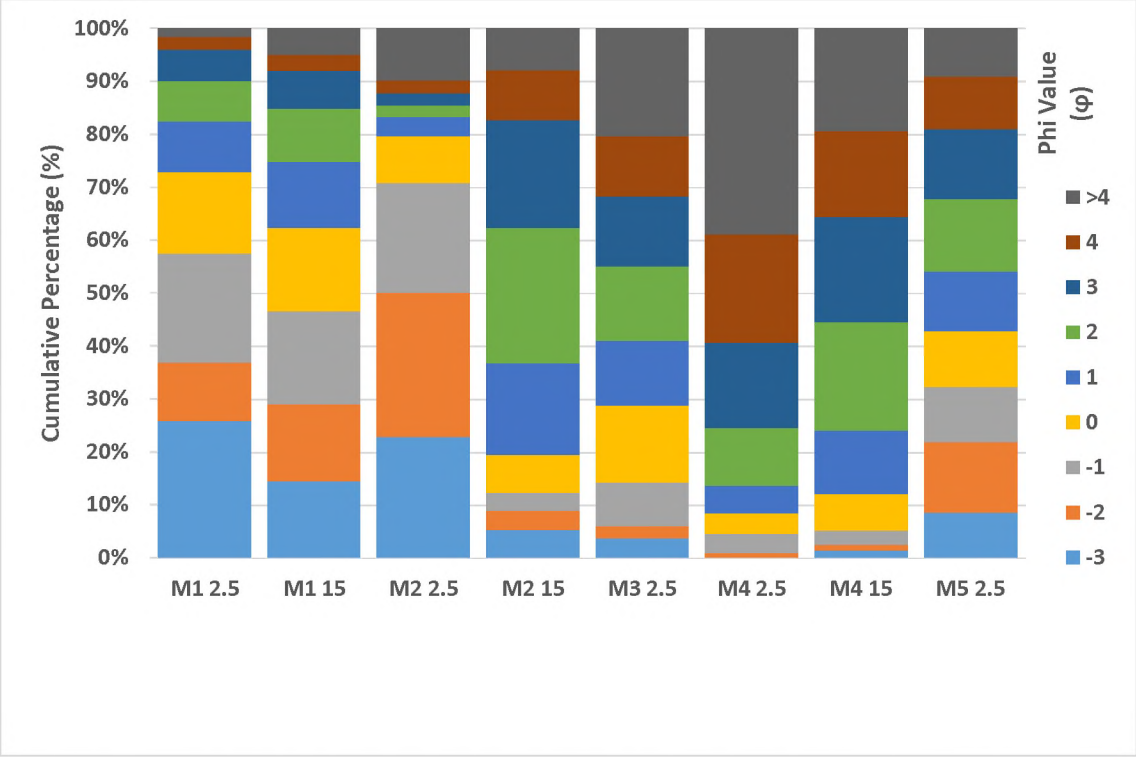


Figure 104: Cumulative distribution of particle sizes for Marion Island sampling sites, displayed using Phi (φ) values. 2.5 denotes surface samples; 15 denotes samples taken at 15-cm depth.

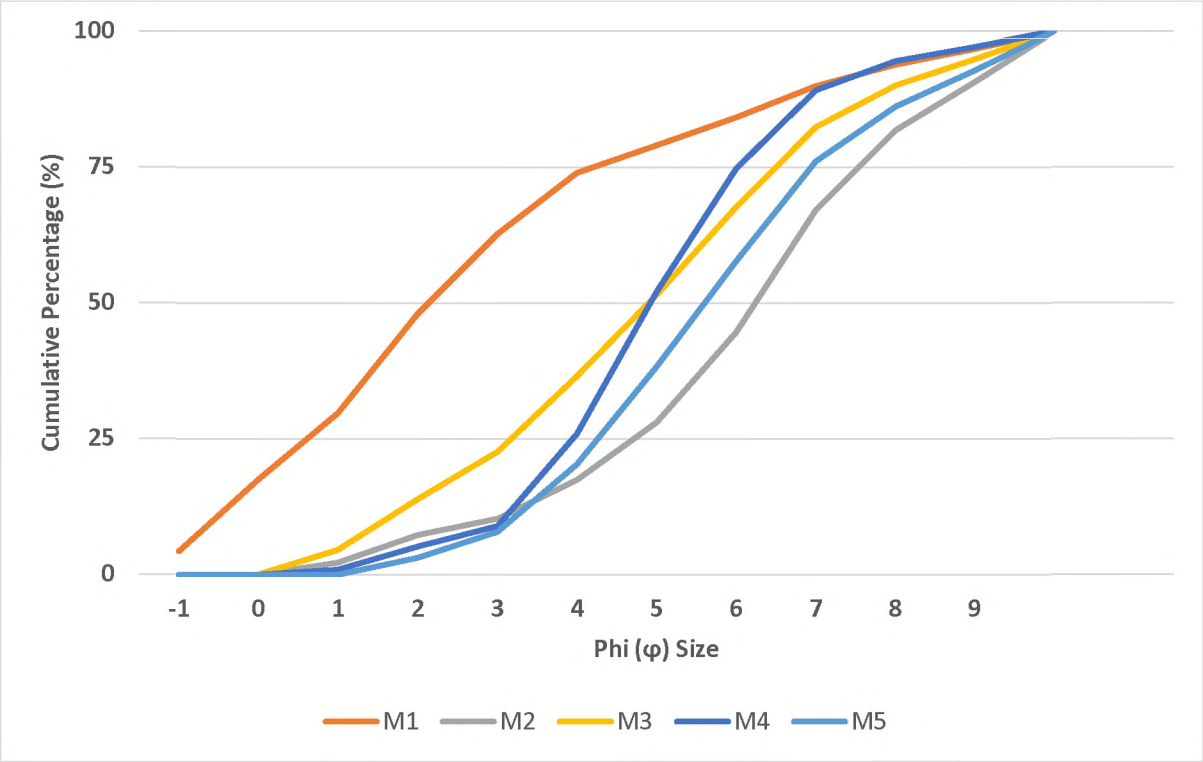


**Figure 105: Fine earth fraction analyses (φ: -1 to 9) for Marion Island sites.**

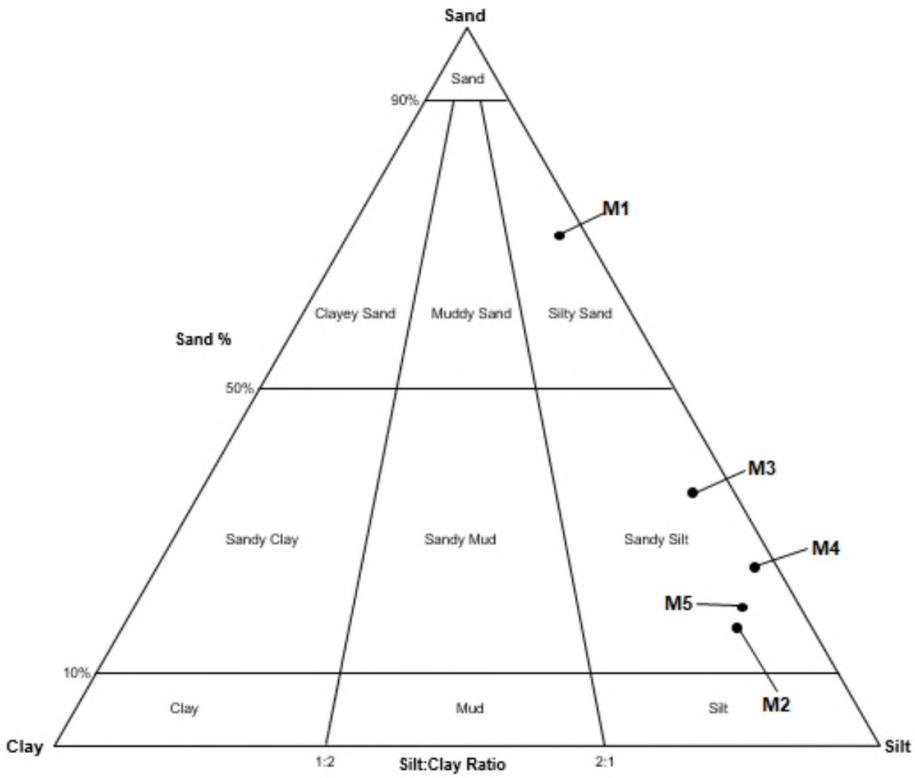


**Figure 106: Sand-silt-sand ternary diagram of Marion Island sediment samples. M1-M5 denote sample sites. The diagram reflects sediment ratios evaluated for the fine earth fraction (FEF: particles < 2mm in diameter) only.**

**Table 74: Sediment moisture characteristics and parameters for the Marion Island study sites. $\theta_v$ denotes volumetric water content; $\theta_g$ gravimetric water content; $M_c$ gravimetric water content expressed as a percentage; and $M_p$ the soil water-filled pore space.**

| Site | Depth | $\theta_v$ | $\theta_g$ | $M_c$ (%) | $M_p$ |
|---|---|---|---|---|---|
| M1 | Surface | 0.11 | 0.10 | 9.53 | 0.17 |
| | 15 | 0.14 | 0.14 | 13.82 | 0.22 |
| M2 | Surface | 0.24 | 0.17 | 16.96 | 0.36 |
| | 15 | 0.19 | 0.33 | 33.46 | 0.43 |
| M3 | Surface | 0.30 | 0.29 | 28.74 | 0.47 |
| M4 | Surface | 0.30 | 0.56 | 56.38 | 0.71 |
| | 15 | 0.33 | 0.53 | 52.53 | 0.69 |
| M5 | Surface | 0.27 | 0.40 | 40.30 | 0.54 |

Overall surface samples have higher volumetric water content (VWC: $\theta_v$) and lower gravimetric water content (GWC: $\theta_g$) than sub-surface samples (Figure 107). Samples show an increase in VWC and GWC of surface samples from M1-M4, after which ground moisture decreases. Volumetric water content (VWC) and GWC for sub-surface samples increase with decreasing altitude. Volumetric water content (VWC) and soil water-filled pore space ($M_p$) are less variable (expressed as standard deviation: *s*) for surface (VWC: $s$ = 0.08; $M_P$: $s$ = 0.20) than sub-surface samples (VWC: $s$ = 0.1; $M_P$: $s$ = 0.23). Average VWC is 0.2 for surface and sub-surface samples. Similarly, average GWC for surface and sub-surface samples is 0.3. However, when GWC is expressed as a percentage ($M_c$) this percentage rises to 30.4% and 33.3% respectively. Soil water-filled pore space ($M_p$) is 0.5 and 0.4 for surface and sub-surface samples respectively.

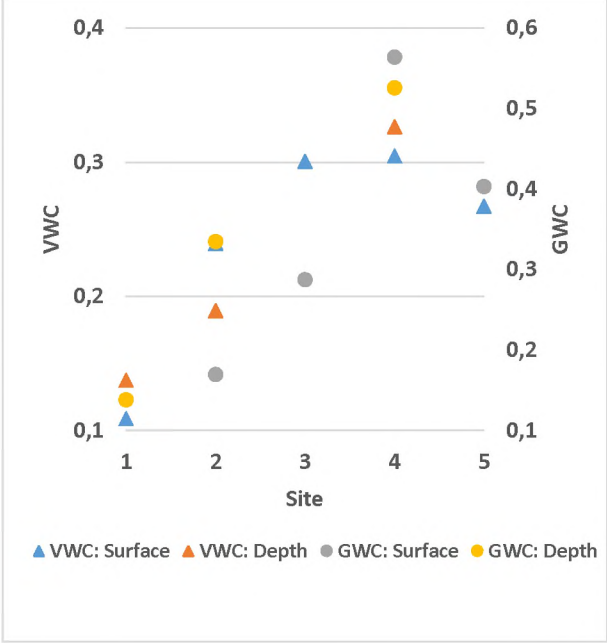


**Figure 107: Volumetric water content (VWC) and gravimetric water content (GWC) for th Marion Island sites. 1-5 denote sites M1-M5.**

Phi (ϕ) mean values for Marion Island show a decrease in average particle size from M1-M4 (higher to lower altitudes), after which mean particle size increases. Phi (ϕ) mean values for surface samples show coarser particles size for M1 and M2, when compared to sub-surface samples. Phi (ϕ) skewness values show variably skewed populations. Positive values suggest a fine tail and negative values a coarse tail (**Table 75**, pg. 200; Figure 104, pg. 197). The Phi (ϕ) sorting and uniformity coefficient ($C_u$) both indicate soil samples are poorly sorted. The uniformity coefficient ($C_u$) indicates uniformly to well graded soils. Applying the sorting index (S) shows no sorting, as well as deficient samples for M1, M2 and M4. A comparison of surface to sub-surface samples indicates no sorting for finer particle sizes, with deficient

values recorded for coarser particles (Phi (ϕ) values of -1) at the sub-surface. The only instance of vertical sorting is observed for M4 for Phi (ϕ) values of -3. At M2 sorting is evident for Phi (ϕ) values of -2, no sorting for -1, with all other textural fractions classed as deficient. Surface samples for M1 and M4 are non-sorted, when compared to sub-surface samples. At M2 surface samples are deficient when compared to sub-surface samples. The Kolmogorov-Smirnov (K-S) test shows that all samples are dissimilar at $p < 0.05$ and that the null hypothesis cannot be accepted when comparing sites to each other. This also applies to surface and sub-surface samples where the null hypothesis is rejected at $p < 0.05$ for all surface and sub-surface pairings.

**Table 75: Phi (φ) descriptive characteristics and the uniformity coefficient ($C_u$) for Marion Island soil/sediment samples.**

| Site | Depth | Phi (ϕ) Mean | Skewness | Sorting | $C_u$ |
|---|---|---|---|---|---|
| M1 | Surface | Fine gravel | Finely positive | Very poor | Extremely poor, well graded |
| | 15 cm | Coarse sand | Finely negative | | Extremely poor, uniformly graded |
| M2 | Surface | Fine gravel | Moderately positive | | |
| | 15 cm | Medium sand | Finely negative | | Poor, well graded |
| M3 | Surface | | Symmetrical | | Extremely poor, uniformly graded |
| M4 | Surface | Fine sand | Moderately negative | | Poor, uniformly graded |
| | 15 cm | | Finely negative | | Poor, well graded |
| M5 | Surface | Medium sand | Symmetrical | | Extremely poor, uniformly graded |

### 5.2.4 Sediment displacement for Marion Island trenches

Moisture content for Marion Island trenches shows a decrease in moisture with a decrease in altitude (Figure 108, pg. 201). Gravimetric water content (GWC) for M1 trenches displays an increase in moisture with depth. Trenches at M4 show a general decrease in GWC with depth. M2 and M3 show a decrease in GWC up to 10 cm depths, after which moisture increases. Total organic carbon (TOC) for trenches is lowest at highest elevations with values increasing with a decreasing altitude (Figure 109, pg. 201). Higher TOC values are recorded for surface samples and generally a decrease with increasing depths into the ground.

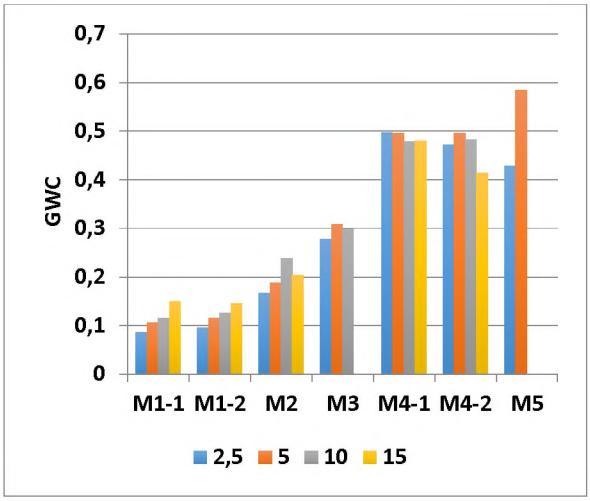


**Figure 108: Gravimetric water content (GWC) for marker trenches for Marion Island. GWC is indicated for sediment depths per trench. 'M' indicates the sample site; the number following the '-' indicates the trench number.**

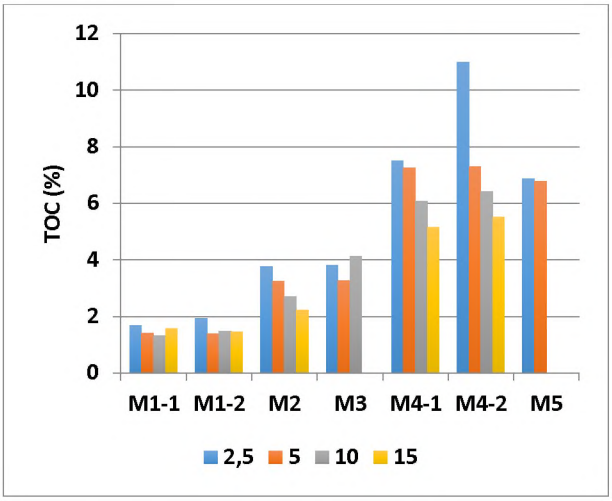


**Figure 109: Total organic carbon (TOC) for marker trenches on Marion Island, shown as a percentage. TOC is indicated for sediment depths per trench. 'M' indicates the sample site; the number following the '-' indicates the trench number.**

Variability (expressed as standard deviation: *s*) for the fine earth fraction (FEF: portion < 2 mm) (Figure 110, pg. 202), shows an increase with depth for M1 and M2. At M3 this trend is reversed, with higher proportion of fine recorded for surface samples. At M4 and M5 a general trend is less clear, with proportion of fines variable per site and depths. Phi (ϕ) mean sizes are either fine gravel or coarse to medium sand, with sand generally overlying fine gravel (Table 76, pg. 202). Sorting is very poor for all depths for all trenches at all sites. Phi (ϕ) skewness values are variable, ranging from finely negative to finely positive, suggesting no real predisposition towards fine nor coarse tails. As sites decrease in altitude mean particle size also decreases; *i.e.* fine gravel dominates further upslope, whereas sand dominates further downslope. Analyses of vertical sorting within the ground column shows that at M1 and M2 coarser particles (ϕ -4 to -1), as well as fine particles (ϕ > 3) exhibit deficiency in the upper 15 cm of the ground. For M3, particles ranging from ϕ = 0 to ϕ = -4 show deficiency in the first 15 cm of the ground. Finally, soil analyses indicate that smaller particles (ϕ > 2) and sand-sized particles (ϕ = -3) are deficient at the surface for M4, while gravel-sized particles (ϕ = -4) exhibit sorting.

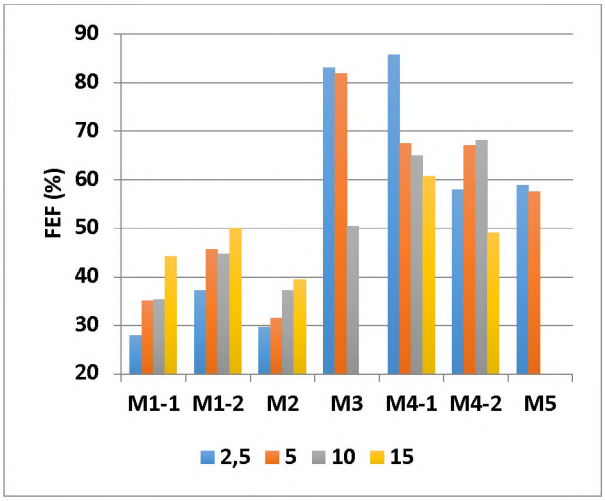


**Figure 110: Fine earth fraction (FEF) for marker trenches on Marion Island. The FEF is indicated for sediment depths per trench. 'M' indicates the sample site; the number following the '-' indicates the trench number.**

**Table 76: Phi (φ) mean textural sizes for Marion Island trenches. 'MS' indicates medium sand; 'C' indicates coarse sand; 'G' indicates fine gravel; 'B' indicates bedrock. 'M' denotes the sample site. whereas '1' reflects trench #1 and '2' trench #2.**

| | | | | | | | |
|---|---|---|---|---|---|---|---|
| 2.5 | G | G | G | MS | MS | C | C |
| 5 | | | | | | MS | |
| 10 | | | | G | C | C | B |
| 15 | | | | B | | | |
| Depth (cm) | M1 | | M2 | M3 | M4 | | M5 |
| | 1 | 2 | 1 | 1 | 1 | 2 | 1 |

Ternary diagrams are shown for trenches as Figure 111 for M1, and Figure 112-Figure 115 (pg. 203) for trenches at M2-M5. Sediment ratios are only evaluated for the fine earth fraction (FEF: particles < 2 mm in diameter). All trenches exhibit a paucity of clays. This is especially evident for M1, which has the gretest proportion of sand-sized particles compared to other sites. Surface samples (taken at 2.5 cm) are generally finer, *i.e.* have a greater proportion of silt, than samples taken at the greater depth (> 2.5 cm). Irrespective of this, samples at M2-M5 are predominantly sandy silt. The M1 samples are predominantly silty sand.

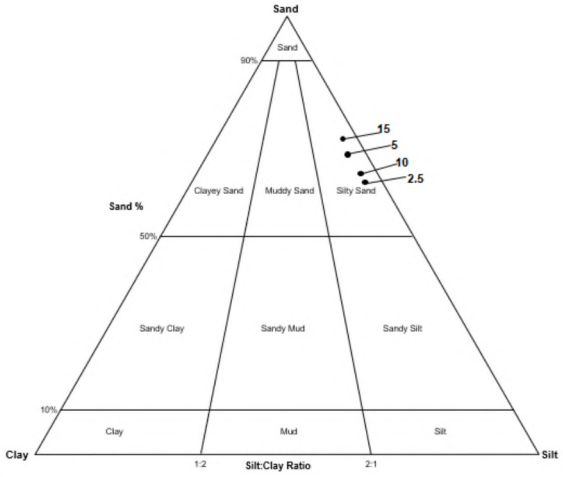


**Figure 111: Sand-silt-clay ternary diagram for trenches at M1. Numbers indicate depth of samples, in cm.**

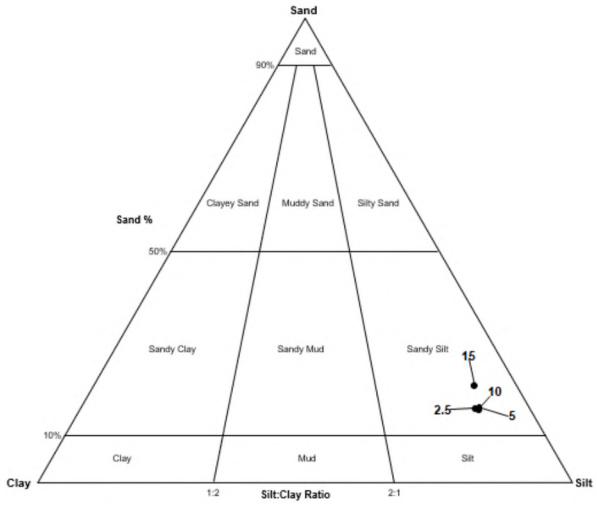


**Figure 112: Sand-silt-clay ternary diagram for trenches at M2. Numbers indicate depth of samples, in cm.**

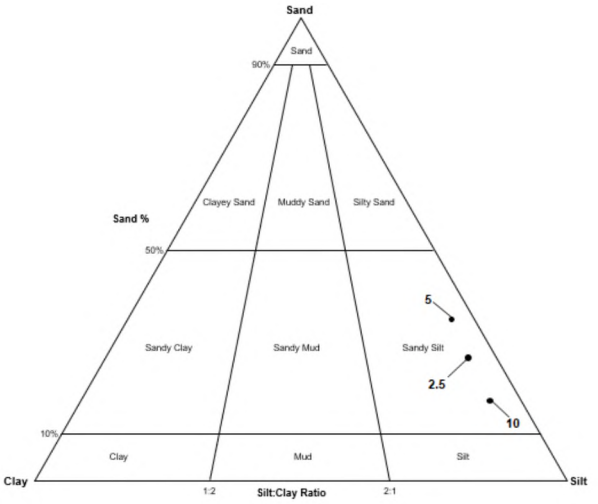


**Figure 114: Sand-silt-clay ternary diagram for trenches at M3. Numbers indicate depth of samples, in cm.**

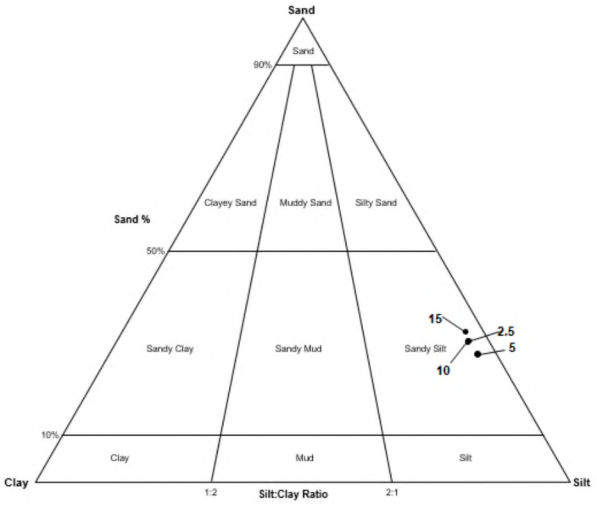


**Figure 113: Sand-silt-clay ternary diagram for trenches at M4. Numbers indicate depth of samples, in cm.**


**Figure 115: Sand-silt-clay ternary diagram for trenches at M5. Numbers indicate depth of samples, in cm.**

No vertical sorting is evident. Sub-surface samples, when compared to surface samples, suggest a deficiency of textural fractions to no sorting for all Phi (ϕ) values. The Phi (ϕ) value of 1 displays no sorting throughout. Markers were retrieved after one calendar year and numerous field visits were not possible. As such, many trenches don't have markers at the surface. This is attributed to markers being washed away following numerous rainfall events common on the Island. Instead, this analysis focuses on movement of markers within the ground column and an estimate of marker heave with time, as discussed for Ben MacDhui (5.1.4 Sediment displacement for Ben MacDhui trenches, pg. 160 and 6.1.4 Sediment displacement for Ben MacDhui trenches, pg. 287), is not possible. Heave of painted markers is evident (vertical displacement) for M1, with markers from 2-5 cm depths collected on the surface. Markers were also collected outside of the original confines of trenches (lateral displacement), with ± 45% of markers at M1 found outside the original confines of trenches. All other trenches also display

significant lateral displacement downslope (± 35 cm on average), with markers exhibiting both lateral and vertical displacement. More markers heaved at higher-elevated sites (M1 & M2). All trenches show movement of markers deeper into the ground, *i.e.* markers placed at a certain depth moved both upward and downward into the soil column (Table 77). This movement is evident for all sites, yet most noticeable at M3. Here, most markers heaved out of the ground, with less than 5% retained within the ground. Dowels for M1 displaced ± 12 cm per 12-month period. This heave is ± 12 cm for M2, ± 6 cm for M3, ± 8 cm for M4, and ± 10 cm for T5.

**Table 77: Movement of painted markers per trench per site. Y, G, T, and B denote markers buried at 2 cm, 5 cm, 10 cm, and 15 cm depths. GS reflects the ground surface. Marker movement indicates maximum displacement of markers in the vertical.**

| Site | Trench Depth (cm) | Y | G | R | B | Marker Movement (cm) |
|---|---|---|---|---|---|---|
| M1-1 | 15 | GS-15 | 5 | 5-10 | 10-15 | 15 |
| M1-2 | 15 | GS-5 | 2.5-5 | 10 | 15 | 5 |
| M2 | 15 | GS-5 | 2.5-5 | 10 | 15 | 5 |
| M3 | 10 | GS-5 | GS-5 | GS-10 | | 10 |
| M4-1 | 15 | GS-10 | 5 | 10-15 | 10-15 | 10 |
| M4-2 | 15 | GS-2.5 | 5 | 10 | 15 | 2.5 |
| M5 | 5 | GS-5 | 2.5-5 | 5 | | 5 |

Of 15 lengths of string sunk into the ground, 73% of sites had to be discarded due to strings having been heaved out. Of the remaining sites ± 20 %, all located at M1, showed no lateral movement nor deformation due to being frozen in place. One site registered deformation at M4 (Figure 116). No observable deformation occurred for the first few centimetres into the ground, with increasing deformation recorded for with increasing depth into the ground.

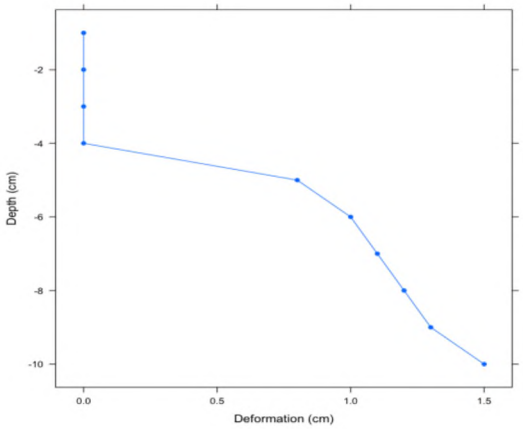


**Figure 116: String (S1) deformation for M4.**

## 5.3 Dronning Maud Land (DML), Antarctica

A detailed description of locations in Dronning Maud Land (DML) of Antarctica is given on pg. 90. Similarly, an overview of temperature and moisture sensor depths, and their respective identifiers, is given in 4.3.1 Ground temperature and moisture data (pg. 80). However, for ease of reference site and sensor identifiers are briefly described here. Ten temperature monitoring stations were used in Antarctica. Flårjuven 1, Flårjuven 2, Grunehogna Peaks, Robertskollen, Schumacherfjellet, Slettfjell, Troll Station 1, Troll Station 2, Valterkulten, and Vesleskarvet were given the identifier A1-A10 respectively. Sensors are identified using a combination of 'T' (temperature) and a subscript number, *e.g.* '15', indicating the depth of the sensor within the ground, measured in centimetres. For example, '$T_{15}$' represents data obtained from temperature sensors that were buried at a depth of 15 cm in the ground. A Table of Abbreviations is available on pg. xxxiii, with a Table of Symbols on pg. xxxvi.

### 5.3.1 Climate and locational parameters

Averages for 15 years of weather data for relative humidity, air temperature, wind speed, and wind direction for Vesleskarvet are shown in Table 78.

**Table 78: Climatic variables for Vesleskarvet from 2000-2015. All values represent diurnal averages for each parameter. RH reflects relative humidity (%), T∗ indicates temperature values ( °C), WS indicates wind speed (m.s$^{-1}$), and WD indicates wind direction (° off true north). DM indicates diurnal means (averages), with :min and :max indicating minimums and maximums.**

| Parameter | $RH_{DM}$ | $T_{D:min}$ | $T_{D:max}$ | $T_{DM}$ | $WS_{D:min}$ | $WS_{D:max}$ | $WS_{DM}$ | $WD_{DM}$ |
|---|---|---|---|---|---|---|---|---|
| Average | 65 | -19 | -14 | -17 | 5 | 16 | 11 | 104 |
| Minimum | 10 | -41 | -34 | -38 | 0 | 3 | 2 | 17 |
| Maximum | 100 | -2 | 4 | 0 | 31 | 43 | 36 | 360 |

This portion of Dronning Maud Land (DML) has an average relative humidity of 65%, although maximums of 100% are recorded occasionally, as are minimums of 10%. The average diurnal minimum is -19 °C, with the average diurnal maximum temperature -14 °C. Ambient air temperatures reach temperatures as low as -41 °C, while warm temperatures of 4 °C are also observed and the mean annual air temperature (MAAT) is -17 °C. Vesleskarvet and other locations in western Dronning Maud Land (WDML) are exposed to a predominantly easterly wind, with the average wind speed just off east (104°; occurring 80% of the time), with a variability (expressed as standard deviation: *s*) of 28 (Figure 117, pg. 206). While gusts of 43 m.s$^{-1}$ are observed, the average diurnal wind speed is 11 m.s$^{-1}$. Calms are mostly absent (< 1%), with wind speed often exceeding 11m.s$^{-1}$ (±38% of the time). Utilising the standard environmental lapse rate of 6.5 °C.km$^{-1}$ yields average air temperatures for DML sites ranging from -13 °C at A4, the site at the lowest elevation, to -21 °C for A6, located at the highest elevation. Six sites (A1-A3, A5, A7-A8) reflect MAAT of -21 °C.

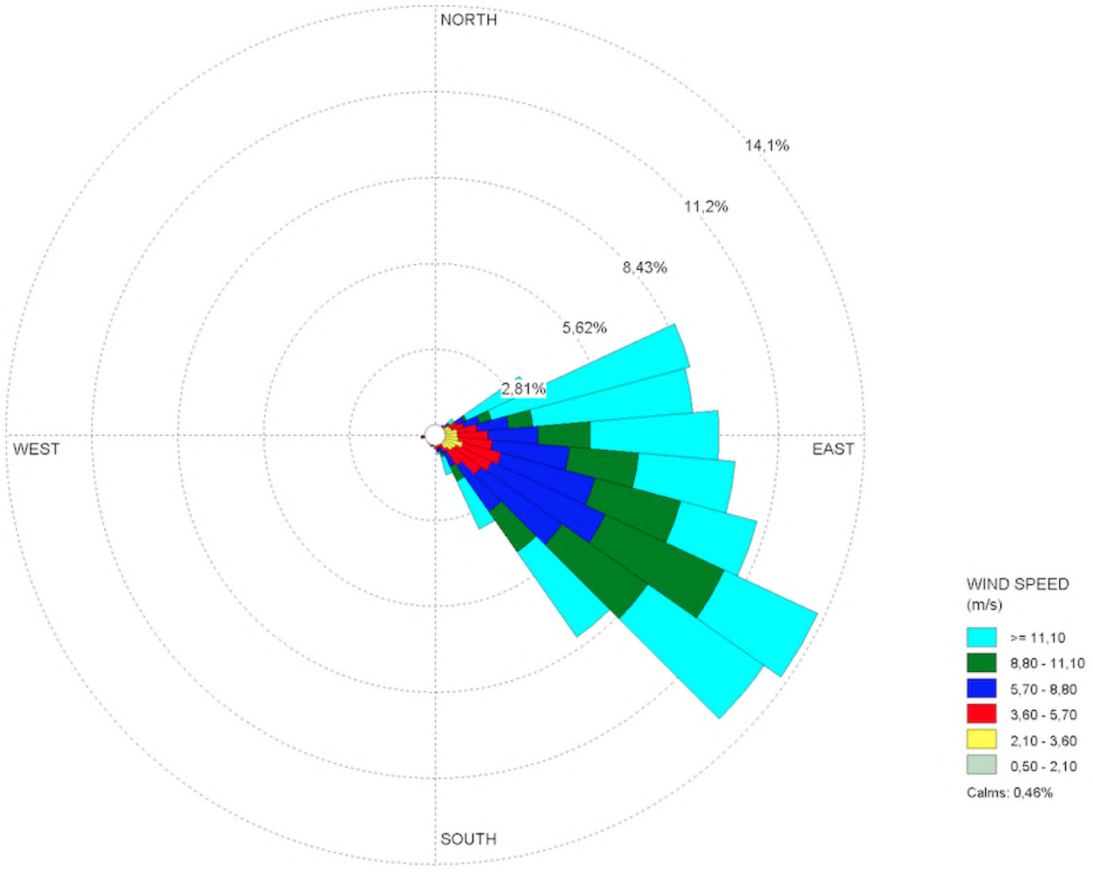


**Figure 117: Wind direction and average wind speed for Vesleskarvet. Interval: 1 hour; 2000-2015. Missing data: ±1%.**

All locations in DML currently fall within the EF classification of the Köppen-Geiger climate system (Kottek *et al.*, 2006), where temperatures of the warmest month are below 0 °C and permafrost is ubiquitous. A detailed description of various climatic zonation systems is provided in APPENDIX B. These systems are, furthermore, discussed in detail in CHAPTER 2: Background and Context (pg. 12 onwards). Data show that, while all locations fall within the polar climate zone (E) (the warmest temperatures of any month below 0 °C), sites within central Dronning Maud Land (CDML) and WDML reach temperatures exceeding 0 °C, making a classification under EF (polar ice cap climate) unsuited. While the climate is not tundra (T), temperatures exceed 0 °C for each site (Table 79, pg. 207) and, as such, cannot be placed into ET alone and must be placed within ET*f* instead. Furthermore, all sites fall most closely within the polar lowland (Washburn, 1979), and sub-polar periglacial environments (Karte, 1983). However, DML is not a periglacial zone, although it exhibits periglacial characteristics. As such, these classifications should be used with caution. It is also noted that the provided conditions only span a maximum of 15 years (Vesleskarvet). Such time spans are insufficient for a climatic classification to be made. Nevertheless, the temperature averages calculated reflect expected weather conditions and can, thus be used as a proxy for climate in this instance.

**Table 79: Average monthly temperatures for Dronning Maud Land. * data loss; underestimation of value. A1: 2008-2015; A7: 2007-2015; A10: 2009-2015; Vesleskarvet: 2000-2015; all other sites: 2013-2015.**

| Month | A1 | A2 | A3 | A4 | A5 | A6 | A7 | A8 | A9 | A10 | Vesleskarvet |
|---|---|---|---|---|---|---|---|---|---|---|---|
| Jan | -8 | -9 | -10 | -4 | -8 | -10 | -15 | -6 | -7 | -5 | -7 |
| Feb | -13 | -13 | -13 | -7 | -11 | -14 | -22 | -10 | -11 | -9 | -11 |
| Mar | -17 | -18 | -18 | -12 | -16 | -19 | -29 | -16 | -16 | -15 | -15 |
| Apr | -20 | -21 | -23 | -17 | -19 | -23 | -34 | -20 | -21 | -18 | -18 |
| May | -22 | -23 | -23 | -18 | -20 | -24 | -38 | -22 | -20 | -19 | -20 |
| Jun | -24 | -23 | -24 | -19 | -21 | -25 | -37 | -22 | -21 | -21 | -21 |
| Jul | -26 | -26 | -27 | -22 | -24 | -28 | -41 | -27 | -24 | -23 | -23 |
| Aug | -26 | -26 | -26 | -21 | -23 | -27 | -42 | -25 | -23 | -23 | -23 |
| Sep | -24 | -24 | -25 | -20 | -22 | -26 | -40 | -24 | -22 | -22 | -23 |
| Oct | -20 | -20 | -21 | -16 | -19 | -22 | -33 | -18 | -20 | -18 | -19 |
| Nov | -13 | -13 | -14 | -8 | -12 | -15 | -22 | -10 | -12 | -11 | -13 |
| Dec | -8 | -9 | -9 | -4 | -7 | -10 | -16 | -4 | -6 | -6 | -8 |
| Days > 0 °C | 97 | 0 * | 4 | 112 | 14 | 1 | 115 | 113 | 33 | 140 | 37 |

Literature covering periglacial and glacial features and landforms for CDML and WDML is not extensive and a concerted effort was made to document as many features and landforms as possible during field visits (Table 80, pg. 208). Selected images of landforms observed during field visits are available in Table 23 (APPENDIX I). Autochthonous blockfields are noted for the exposed nunataks of Flårjuven, Grunehogna, Robertskollen, Schumacherfjellet, Slettfjell, and Valterkulten. Thermal contraction polygons are found at Flårjuven, Grunehogna, Slettfjell, and sorted circles, stripes and imbrication patterns occur in the wind scoop near Grunehogna. In addition, terraces are found at Klovningen and Vassdalen in CDML, and at Flårjuven and Valterkulten in WDML. A range of sorted circles are in evidence, with those found on the Northern Buttress of the Vesleskarvet nunataks, Flårjuven, Robertskollen, Slettfjell and the brine lake on Valterkulten (all located within WDML) much smaller in diameter than those found on Klovningen in CDML. Mud boils and soil ice, in the form of needle ice, are evident wherever sufficient fines ($\phi > 4$: silt and clay) and moisture are found. Mud boils occur on Klovningen and Vassdalen in CDML, as well as in the sediment of the brine lake on Valterkulten and at Robertskollen in WDML. The permafrost at Troll (CDML) is ice-cemented, and two occurrences of vein ice occur for Grunehogna (WDML) and at Vassdalen (CDML). At Grunehogna an isolated instance of an ice wedge associated with a thermal contraction polygon is observed (Meiklejohn, 2016; *pers. comm.)*. At Vassdalen one isolated occurrence of an ice lens ± 2 cm in diameter, discovered following the excavation of a frost mound, is described (Hansen *et al.*, 2016). Frost sorting is ubiquitous, found at various levels and scales at most study sites (*pers. obs.).* In DML frost sorting is mostly mechanical, presenting as borders of coarser material around finer material. Ice blisters are observed for the water bodies near Robertskollen and Vesleskarvet in WDML, as well as near Grjotøyra in CDML. An overview of landforms extracted from the literature review and those observed in the field are given in Figure 118 (pg. 209).

**Table 80: Observations not reflected in the literature that were recorded during field visits to Dronning Maud Land.**

| Feature | Location | Altitude | Active/Relict |
|---|---|---|---|
| Blockfield | Flårjuven | 1359 | Unknown |
| | Grunehogna | 1390 | Unknown |
| | Robertskollen | 284 | Unknown |
| | Schumacherfjellet | 1230 | Unknown |
| | Slettfjell | 1435 | Unknown |
| | Valterkulten | 1100 | Unknown |
| Frost sorting | Flårjuven | 1277-1335 | Active |
| | Vassdalen | 1245 | Active |
| Ice blisters | Grjotøyra | 1310-1345 | Active |
| | Robertskollen | 440 | Active |
| | Vesleskarvet (Crystal Palace) | 750 | Active |
| Mud boil | Klovningen | 1414 | Active |
| | Robertskollen | 446 | Active |
| | Valterkulten | 1001 | Active |
| | Vassdalen | 1149 | Active |
| Non-sorted polygon | Flårjuven | 1359 | Unknown |
| | Grunehogna | 1390 | Unknown |
| | Northern Buttress, Vesleskarvet | 856 | Unknown |
| | Slettfjell | 1435 | Unknown |
| | Valterkulten | 815-1015 | Unknown |
| Non-sorted step/terrace | Flårjuven | 1280-1295 | Unknown |
| | Klovnigen | 1375-1385 | Unknown |
| | Valterkulten | 1020-1025 | Unknown |
| | Vassdalen | 1125-1140 | Unknown |
| Solifluction terrace/head deposit | Flårjuven | 1359 | Unknown |
| | Valterkulten | 1060 | Unknown |
| Sorted circle | Flårjuven | 1290 | Active |
| | Grunehogna | 10988 | Active |
| | Klovningen | 1415 | Active |
| | Robertskollen | 463 | Active |
| | Slettfjell | 1507 | Active |
| | Valterkulten | 971-1017 | Active |
| | Vesleskarvet nunataks | 856 | Active |
| Sorted stripe | Flårjuven | 1215 | Unknown |
| | Grunehogna | 1088 | Unknown |
| | Robertskollen | 445 | Unknown |

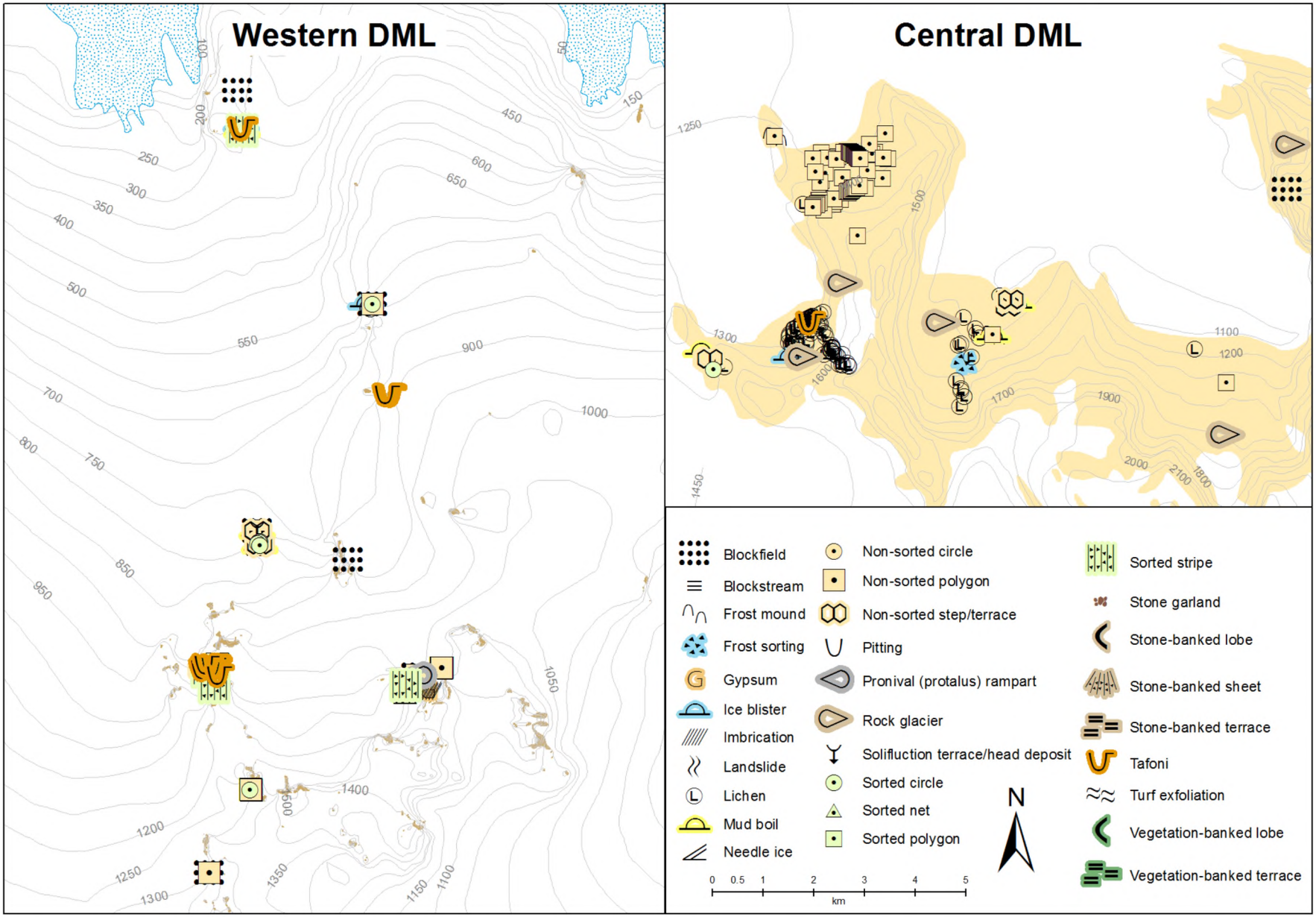


**Figure 118: Periglacial landforms, as well as lichen occurrence, observed during field visits to Dronning Maud Land.**

### 5.3.2 Ground thermal dynamics

Ground thermal dynamics are discussed with a reference to the annual, seasonal and diurnal environment. All times indicated are based on Greenwich Mean Time (GMT) and represent approximations (± one hour). Indices, such as the freezing index (FI), thawing index (TI), ground freezing index (GFI), and thermal offset (SO) are applied to allow for an intersite comparison.

#### *5.3.2.1 Annual frost environment*

Mean annual near surface temperature (MAST: ground temperature recoded at ± 1 cm depth), for all sites indicate central Dronning Maud Land (CDML) and western Dronning Maud Land (WDML) sites to fall within a continuous permafrost zone (CPZ). Mean annual near surface temperature (MAST) is lowest for A4 (Robertskollen: -14 °C), and highest for A6 (Slettfjell: -21 °C), with most sites having MAST of between -16 °C and - 19 °C. Permafrost is ubiquitous and thawing of the ground occurs in summer. Annual mean permafrost temperature for all sites ranges from -14 °C at A4 to -23 °C at A6 (Figure 119), with average permafrost temperatures -19 °C and -20 °C for WDML and CDML respectively. While temperatures fluctuate interannually, variability (expressed as standard deviation: *s*) is negligible (*s* ± 0 or *s* ± 1 for all sites). Exceptions are the sites located in the Jutulsessen of CDML, which register slightly higher variability than the WDML sites (*s* ± 2). The depth of permafrost (permafrost thickness) is less than one kilometre, ranging from 550-750 m for A10 and A6 respectively. Differences in annual meant permafrost temperatures for CDML and WDML is negligible and permafrost thickness is extrapolated to ± 650 m for the exposed and snow-free areas of these portions of Dronning Maud Land (DML).

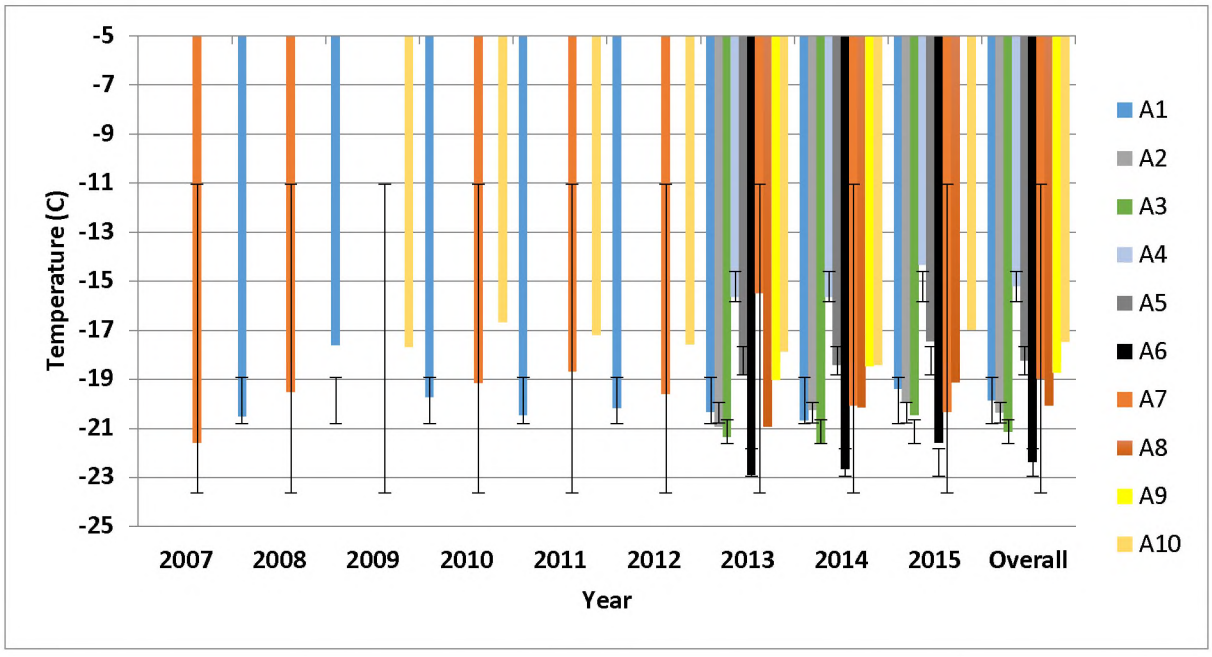


**Figure 119: Median permafrost temperature for sites located in Dronning Maud Land. Error bars (standard deviations) are indicated.**

All Dronning Maud Land (DML) sites display seasonal thaw, with A4 having the greatest proportion of thawed hours of any site (Table 81, pg. 211). A8, which had a faulty near surface sensor (at ± 1 cm in

the ground), has no data available for the first 50 cm of the ground and no estimate of frozen and thawed hours can be made at to this depth. Nevertheless, from the 50 cm-depth onwards the ground is perennially frozen, and no thaw events are observed.

**Table 81: Frozen hours per site, expressed as a percentage of hours since records began. Hours are indicated per sensor depth, with the subscript indicating the depth of the sensor. ALT: active layer thickness. $T_{AIR}$: air temperature. NST: near surface (± 1 cm depth). NOTE: western Dronning Maud Land sites (A1-A6, A9-A10) and central Dronning Maud Land sites (A7 & A8) have sensors buried at different depths.**

| Site | ALT | $T_{AIR}$ | NST | $T_{15}$ | $T_{30}$ | $T_{45}$ | $T_{60}$ |
|---|---|---|---|---|---|---|---|
| A1 | 25 | 99.0 | 96.2 | 99.4 | 100 | 100 | 100 |
| A2 | 15 | 100 | 97.8 | 100 | 100 | 100 | 100 |
| A3 | 29 | 100 | 96.4 | 99.8 | 100 | 100 | 100 |
| A4 | 58 | 98.7 | 90.9 | 93.9 | 95.4 | 97.7 | 100 |
| A5 | 29 | 99.9 | 99.0 | 99.9 | 100 | 100 | 100 |
| A6 | 12 | 100 | 99.7 | 100 | 100 | 100 | 100 |
| A9 | 29 | 99.7 | 93.6 | 97.3 | 100 | 100 | 100 |
| A10 | 16 | 99.2 | 97.1 | 99.9 | 100 | 100 | 100 |
| Site | ALT | $T_{AIR}$ | NST | $T_{50}$ | $T_{100}$ | $T_{150}$ | $T_{200}$ |
| A7 | 38 | 99.7 | 97.4 | 100 | 100 | 100 | 100 |
| A8 | < 50 | 99.0 | n/a | 100 | 100 | 100 | 100 |

Average annual temperatures stabilise with depth, with greatest variability calculated for near surface temperatures (NST: sensors buried at ± 1 cm depth) (Figure 121, pg. 212). Variability of temperatures shows a common trend for all DML sites with an increase in variability from air temperature to highest variability for NST, followed by a consistent decrease in variability to the deepest sensor (Figure 120, pg. 212). Annual mean temperatures are constant for all depths per site, *i.e.* annual means for each individual site remain within 1 °C, even at the deepest sensor. Annual maximum and minimum temperatures are shown in Figure 121 (pg. 212). Annual means are greater for air temperature, compared to ground temperature. At the depth of permafrost variability is least; depths where thawing occurs variability is greatest. Overall absolute minimums occur for air temperatures, whereas absolute maximums are observed for NST. A4 has the highest overall temperatures, with values approaching 0 °C recorded for even the deepest sensor. The highest temperature is recorded at A3 and A9 (19 °C for NST). The lowest overall temperature is recorded at A1 (-41 °C for air temperature). Central Dronning Maud Land (CDML) sites have annual air temperature ranges exceeding 50 °C, whereas none of the sites in WDML approach these range. Here ranges are in the high 30s and low 40s. In comparison, ranges observed for NST exceed 50 °C for all sites.

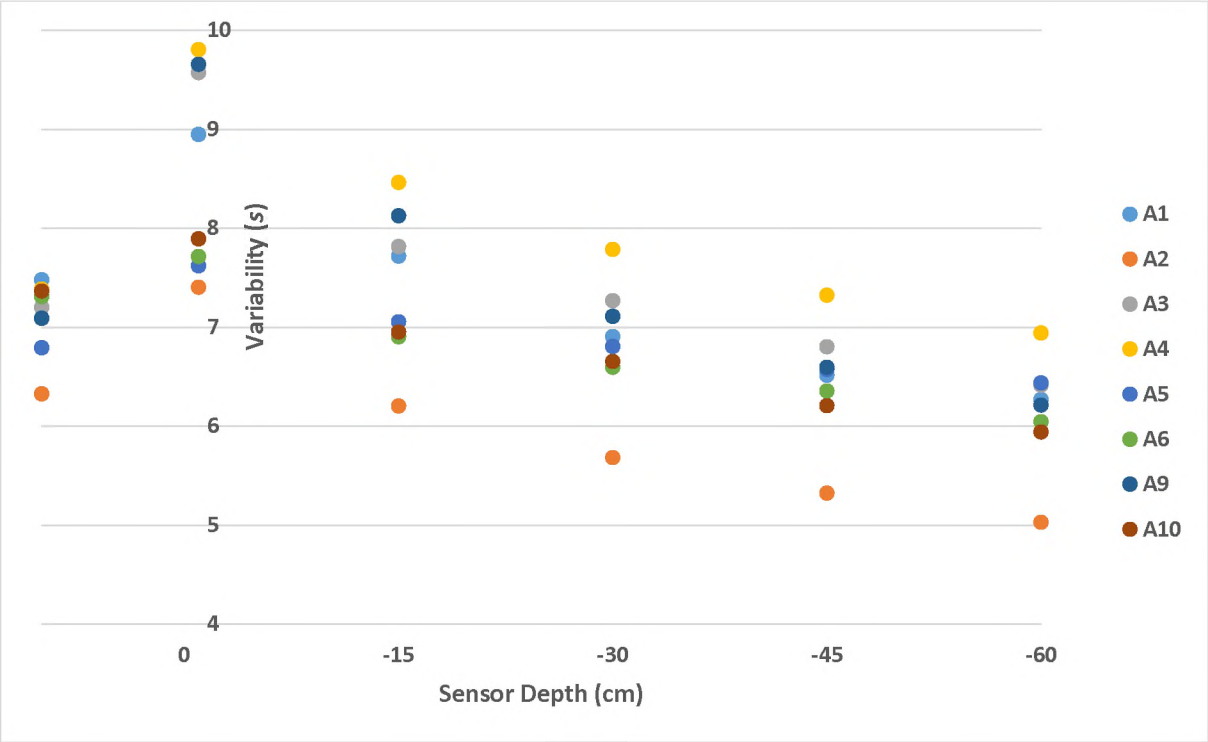


**Figure 120: Variability (shown as standard deviation: *s*) per sensor depth for western Dronning Maud Land (WDML) sites.**

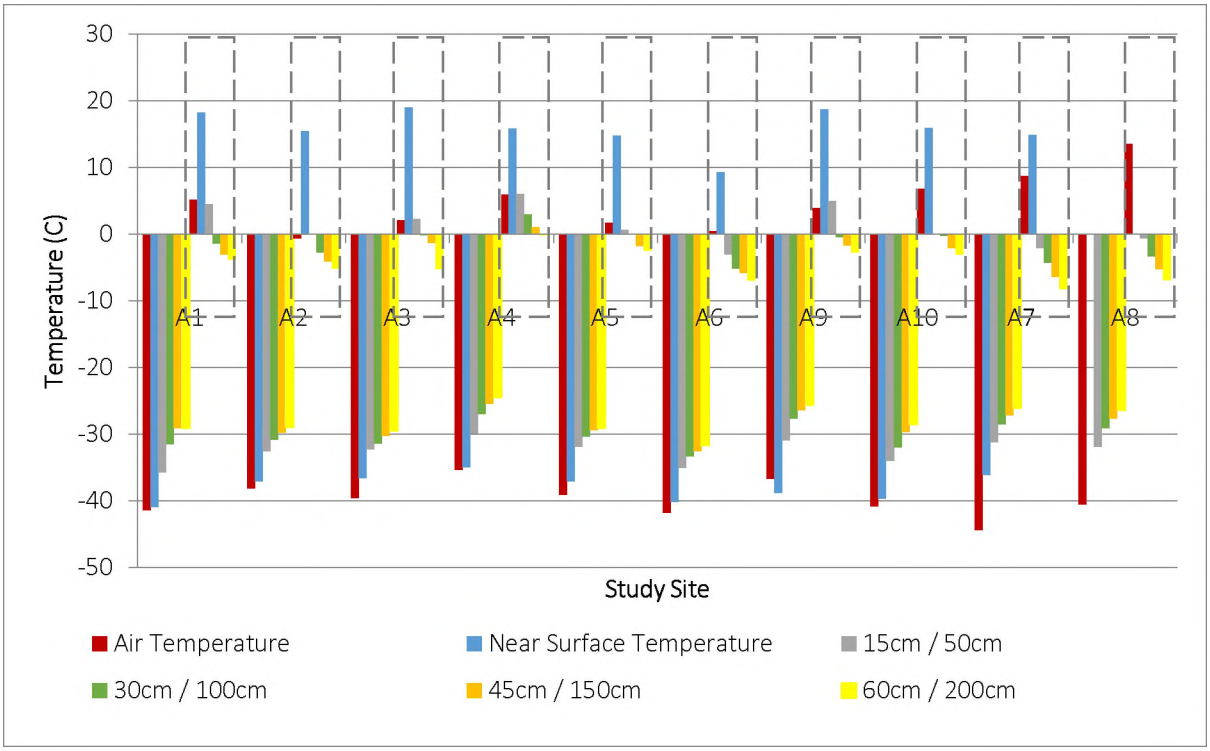


**Figure 121: Global annual minimums and maximums for Donning Maud Land (Antarctica) sites. The depth of the sensor before '/' denotes sites in western Dronning Maud Land (WDML); the depth of the sensor after '/' denotes central Dronning Maud Land (CDML) sites. A7 and A8 are in CDML, all other sites in WDML. Dashed grey rectangles indicate global maximum temperatures. All other temperatures reflect global minimums.**

Comparing temperature variability per sensor depth shows that most WDML sites (A1-6, A9-10) are comparable to each other, with CDML sites not comparable to WDML sites (Table 82). Furthermore, A4 does not correlate to A6 and A10. Nevertheless, Principal Component Analysis (PCA) calculated using all available parameters for each site (temperature minimums, maximums, averages, variability, permafrost thickness, active layer thickness, geographical location (altitude, latitude, longitude, distance to shelf/coast), potential freeze-thaw events, and freeze-thaw cycles), yields similar component loadings toward the single principal component (PC) (explained variability=0.93). Nevertheless, A4 has ± 18% less component loadings and is less correlated to other sites with an average of $r$ = 0.73 ($p$ < 0.05). This compares to average correlations of $r$ = 0.96 ($p$ < 0.05) of the remaining sites to each other. A3 and A9 have the highest overall correlation to remaining sites ($r$ = 0.98 and $r$ = 0.97 respectively, $p$ < 0.05 for both).

**Table 82: Correlation matrix and *p*-values of variability per site. Standard deviations per sensor depth are compared to each other, yielding *r*. Underlined values indicate non-significance at $p < 0.05$.**

| Site | A1 | A2 | A3 | A4 | A5 | A6 | A7 | A9 | A10 |
|---|---|---|---|---|---|---|---|---|---|
| A1 | | 0.99 | 0.97 | 0.93 | 0.98 | 0.94 | 0.87 | 0.97 | 0.95 |
| A2 | 0.99 | | 0.94 | 0.89 | 0.96 | 0.98 | 0.92 | 0.94 | 0.98 |
| A3 | 0.97 | 0.94 | | 0.99 | 1.00 | 0.86 | 0.71 | 0.99 | 0.87 |
| A4 | 0.93 | 0.89 | 0.99 | | 0.99 | 0.78 | 0.62 | 0.99 | 0.80 |
| A5 | 0.98 | 0.96 | 1.00 | 0.99 | | 0.88 | 0.75 | 1.00 | 0.89 |
| A6 | 0.94 | 0.98 | 0.86 | 0.78 | 0.88 | | 0.99 | 0.85 | 1.00 |
| A7 | 0.87 | 0.92 | 0.71 | 0.62 | 0.75 | 0.99 | | 0.72 | 0.98 |
| A9 | 0.97 | 0.94 | 0.99 | 0.99 | 1.00 | 0.85 | 0.72 | | 0.86 |
| A10 | 0.95 | 0.98 | 0.87 | 0.80 | 0.89 | 1.00 | 0.98 | 0.86 | |

#### *5.3.2.2 Seasonal frost environment*

Summer thawing (TI) and winter freezing indices (FI) are provided for air and ground temperatures recorded at the near surface (NST: ± 1 cm depth) for all sites, as well as additional sensor depths to where active layer thickness extends. Active layer thickness is variable across the region, with central Dronning Maud Land (CDML) sites (A7 & A8) and A3-A5 in western Dronning Maud Land (WDML) showing high interannual variability with variability (expressed as standard deviation: $s$) for annual active layer thickness ranging from 6-9 (Table 83, pg. 214). This compares to no significant variation for the remaining sites with $s$ ± 1-3, as argued for Vesleskarvet (A10) by Kotzé and Meiklejohn (2016). Temperature variability with increasing depth is greatest for A7 (CDML). Active layer thickness is greatest at A4; least at A6. A faulty sensor at A8 makes active layer thickness determination not possible. However, ground is permanently frozen at 50-cm depth, indicating active layer thickness less than this depth. This corroborates active layer thickness for A7, located near A8. Active layer thickness is strongly correlated to altitude ($r$ = -0.65, $p$ < 0.05), and Principal Component Analysis (PCA) shows that active layer thickness, freeze-thaw cycles and latitude trend together. Similarly, potential freeze-thaw events, near surface temperature averages, and latitude trend together. Expected diurnal frost penetration depths ($d$) (Equation 12 (pg. 105), adjusted for thawing opposed to freezing) and annual active layer thickness (Figure 122, pg. 214) show an expected shallow diurnal frost environment.

**Table 83: Variability per site (*s*) calculated for active layer thickness (ALT) and thermistors per site.**

| Variability | A1 | A2 | A3 | A4 | A5 | A6 | A7 | A8 | A9 | A10 |
|---|---|---|---|---|---|---|---|---|---|---|
| *s*: ALT | 3 | 1 | 6 | 6 | 7 | 3 | 9 | n.d. | 1 | 1 |
| *s*: T | 0.89 | 0.78 | 1.02 | 0.95 | 0.38 | 0.57 | 1.69 | 1.48 | 1.14 | 0.66 |

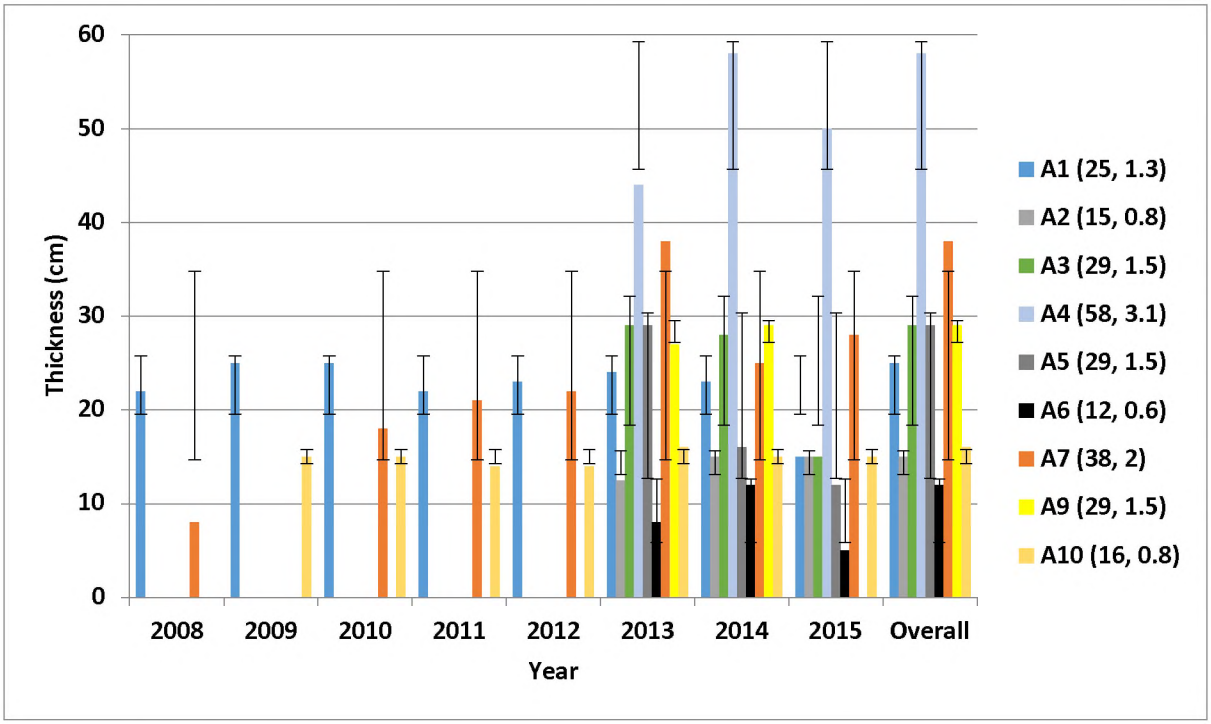


**Figure 122: Active layer thickness (ALT), measured in cm, for sites located in Dronning Maud Land (Antarctia). Error bars (standard deviations) are indicated, as is annual average ALT and the expected diurnal frost penetration (*d*) in brackets, separated by a comma. The first value indicates ALT, the second indicates *d* in centimetres.**

Onset of seasonal thaw varies for all sites but at NST (the depth of most thawing cycles), the onset is prominent for November (end of spring), ending in February (end of summer). Thaw occurring into autumn is evident at some sites (A2, A9, A10) but not common (Table 84, pg. 215). Positive air temperatures are commonly recorded in spring, with half the sites showing temperatures above 0 °C during this season. Most thaw cycles, and the longest period of thaw, are observed for near surface sensors (NST). Thawing is generally observed at NST before ambient temperatures exceed 0 °C and continues after ambient temperatures have dropped below 0 °C. As depths increase, the onset of thawing occurs after the onset of thawing of the layer (depth) above. In comparison, the onset of freezing occurs before the onset of freezing of the layer above. Near surface temperatures (NST: recorded at ± 1 cm in the ground), therefore, shows the longest thaw duration (first to last occurrence of thaw), with thaw duration becoming less with greater depth in the ground.

**Table 84: Average thaw duration, start delay of thaw, and start delay of freezing, all given in days, per Dronning Maud Land site per sensor depth. Values are indicated per sensor depth. 'T' indicates temperature data with the subscript indicating the depth of the sensor (in centimetres). Maximum extent of active layer thickness (ALT) is shown by the presence of values within that column. NOTE: western and eastern Dronning Maud Land Sites (WDML and CDML respectively) have sensors buried at different depths. $T_{AIR}$: air temperature. NST: temperature recorded at the near surface (± 1 cm depth).**

| Site | $T_{AIR}$ | NST | $T_{15}$ | $T_{30}$ | $T_{45}$ |
|---|---|---|---|---|---|
| A1 | 54 | 97 \| **-21** \| *9* | 26 \| **42** \| *-28* | | |
| A2 | * | 92 \| ***** \| * | 1 hour \| **35** \| * | | |
| A3 | 6 | 84 \| **-46** \| *38* | 1 hour \| **32** \| *-42* | | |
| A4 | 79 | 102 \| **-12** \| *6* | 65 \| **18** \| *-17* | 28 \| **17** \| *-19* | 19 \| **10** \| *-2* |
| A5 | 6 | 84 \| **-46** \| *38* | 9 \| **32** \| *-42* | | |
| A6 | 1 hour | 54 \| **-34** \| *25* | | | |
| A9 | 52 | 126 \| **-28** \| *56* | 46 \| **39** \| *-29* | | |
| A10 | 58 | 84 \| **-13** \| *17* | 1 \| **33** \| *-50* | | |
| **Site** | $T_{AIR}$ | NST | $T_{50}$ | $T_{100}$ | $T_{150}$ |
| A7 | 31 | 52 \| **-21** \| *4* | | | |
| A8 | 40 | * | | | |

| | |
|---|---|
| The first value in a set indicates annual thawed duration of that sensor in days. | |
| **BOLD** values (second values in a set) indicate the average delay of the first sub-zero temperatures (freezing) of that layer to the one above it (the column to the left), expressed in number of days. Negative values indicate an earlier start. | |
| Values *italicised* (third values in a set) indicate the last sub-zero temperatures (freezing) of that layer to the one above it (the column to the left), expressed in number of days. Negative values indicate an earlier start. | |
| * indicates logger failure/no data available. | |
| | First and last occurrence of thaw in summer. |
| | First occurrence of thaw in spring and last in summer. |
| | First and last occurrence of thaw mostly in summer. Isolated occurrence for spring and autumn. |

Consistently, the greatest seasonal range observed for any WDML site is at A4, which also has the deepest active layer (Table 85, pg. 216). Central Dronning Maud Land (CDML) sites have the greatest overall seasonal range, with active layer thickness exceeding any site except A4. However, seasonal ranges for all sites are not significantly different at $p < 0.05$. Near surface temperatures (NST) display the greatest range for all sensors. Furthermore, seasonal ranges decrease on average by 1 °C per 15 cm increase in depth for WDML sites. An average decrease of ± 3 °C is evident for each 50-cm increase in depth for CDML sites. Therefore, a seasonal change in range is ± 6.67 $°C.m^{-1}$ in WDML, compared to 6.00 $°C.m^{-1}$ in CDML.

**Table 85: Seasonal ranges ($T_{SR}$) for Dronning Maud Land (Antarctica) sites, given in °C per depth with the subscript indicating the depth of the sensor. Yellow blocks indicate depths at which seasonal thaw occurs. $T_{AIR}$: air temperatures. NST: ground temperatures recorded at ± 1 cm depth. NOTE: western Dronning Maud Land sites (A1-A6, A9-A10) and central Dronning Maud Land sites (A7 & A8) have sensors buried at different depths.**

| Site | $T_{AIR}$ | NST | $T_{15}$ | $T_{30}$ | $T_{45}$ | $T_{60}$ |
|---|---|---|---|---|---|---|
| A1 | 19 | 22 | 21 | 19 | 19 | 18 |
| A2 | 16 | 21 | 20 | 18 | 18 | 17 |
| A3 | 18 | 24 | 21 | 20 | 19 | 18 |
| A4 | 18 | 24 | 23 | 21 | 20 | 19 |
| A5 | 17 | 19 | 19 | 19 | 19 | 18 |
| A6 | 18 | 19 | 19 | 19 | 18 | 17 |
| A9 | 19 | 23 | 22 | 21 | 20 | 18 |
| A10 | 18 | 20 | 19 | 19 | 18 | 17 |
| AVERAGE: WDML | 18 | 21 | 21 | 20 | 19 | 18 |
| Site | $T_{AIR}$ | NST | $T_{50}$ | $T_{100}$ | $T_{150}$ | $T_{200}$ |
| A7 | 21 | 25 | 20 | 17 | 14 | 11 |
| A8 | 21 | n.d. | 24 | 20 | 18 | 15 |
| AVERAGE: WDML | 21 | 25 | 22 | 19 | 16 | 13 |

Seasonal frost parameters and indices are shown for A1-A10 (excepting A8) in Table 86 (pg. 220) - Table 94 (pg. 224). Frost parameters and indices include the thermal offset (SO), mean summer and winter temperatures and their associated variability (expressed as standard deviation: *s*), as well as the summer thawing index (TI) and winter freezing index (FI). Furthermore, no data values/loss of sensor data are indicated as 'n.d.'. Each site is discussed within its own subsection below.

#### 5.3.2.2.1 A1: Flårjuven 1

Seasonal frost parameters and indices for A1 are shown in Table 86 (pg. 220). The thermal offset is positive in summer and negative in winter. The exception is winter 2009, which reflects a marginally positive thermal offset. The air temperature and near surface temperature (NST) thawing index approximate zero, with freezing indices yielding large values. Variability during summer is greatest for NST, next highest for $T_{15}$ and lowest for air temperatures. This relationship is maintained for winter and little difference is observed for variability and mean temperature. Similarly, mean winter air, mean winter NST, and mean winter temperatures recorded at 15-cm depth ($T_{15}$) show little fluctuation. This contrasts to noticeably warmer summer NST. Annual degree days (> 0) reflect a ground thermal regime warmer than air temperatures. The ground freezing index lies near ± -6 000, except for 2014, when it approximates -4 000.

#### 5.3.2.2.2 Flårjuven 2

Seasonal frost parameters and indices are shown for A2 in Table 87 (pg. 220). Like A1, the summer thermal offset is positive and negative in winters. The near surface temperature (NST) thawing index

reflects a marginally positive value, with freezing indices reflecting large values for both air temperatures and NST. Variability during summer is greatest for NST and less for air temperature. This relationship is maintained in winter, although variability for air temperatures and NST is not significantly different. Few differences are evident between winter mean air and near surface temperatures. Summer NST are noticeably warmer. Annual degree days (> 0) reflect a ground thermal regime warmer than air temperatures and, like A1, the ground freezing index approximates -6 500.

#### 5.3.2.2.3 A3: Grunehogna

Seasonal frost parameters and indices are shown for A3 in Table 88 (pg. 221). Like A1 and A2, summer thermal offsets are positive and winters negative. The near surface temperature (NST) thawing index is positive, with the freezing index reflecting high negative values for both air temperature and NST. Variability during summer is greatest for NST, followed by $T_{15}$ and then air temperature. This relationship is reversed for winter with variability decreasing with increasing depth in the ground. Nevertheless, variability for air temperatures, NST, and $T_{15}$ is not significantly different. Little differences are observable in mean temperatures for winter air temperatures and NST, in comparison to summer when NST are noticeably warmer. Like A1 and A2, degree days (> 0) reflect a ground thermal regime warmer than air temperature. The ground freezing index ranges from -6 400 to -6 800.

#### 5.3.2.2.4 A4: Robertskollen

Seasonal frost parameters and indices are shown for A4 in Table 89 (pg. 221). Comparable to other Dronning Maud Land sites, summer thermal offsets are positive, in comparison to negative values for winters. The air and NST thawing indices are positive, with freezing indices reflecting high values for both air temperatures and NST. Variability in summer is greatest for NST, becoming progressively less with increasing depth into the ground. Ambient air temperatures have the second-lowest recorded variability for summer. During winter variability decreases with increasing depth into the ground. However, air temperatures display consistently high variability. Little differences are evident in mean winter temperatures for all sensors; in comparison NST is noticeably higher in summer. Like A1-A3, annual degree days (> 0) suggest a ground thermal regime warmer than air temperatures. The ground freezing index is ± 1 500 less than those calculated for A1-A3.

#### 5.3.2.2.5 A5: Schumacherfjellet

Seasonal frost parameters and indices for A5 are provided in Table 90 (pg. 222). Comparable to other western Dronning Maud Land (WDML) sites, summer thermal offsets are positive, in comparison to negative winter offsets. Near surface temperatures (NST) reflect marginally positive thawing indices, with large values calculated for freezing indices for both air temperatures and NST. Variability during summer is greatest for NST, becoming less with increasing depth into the ground. Lowest summer variability is evident for air temperatures. During winter variability decreases with increasing depth into the ground with variability for air temperature slightly lower than that of NST. Few differences are evident in mean temperatures and variability in winter. However, like other Dronning Maud Land sites, temperatures recorded at the near surface (NST) are noticeably warmer in summer. Annual degree

days reflect a variable regime with air temperatures warmer than NST during 2013 and the balance shifting to NST for the remaining two years. However, like A1-A3, the ground freezing index approximates -6 000.

#### 5.3.2.2.6 A6: Slettfjell

Seasonal frost parameters and indices for A6 are shown in Table 91 (pg. 222). Like other Dronning Maid Land sites, thermal offsets are positive in summer and negative in winter. The thawing index does not exceed zero. In comparison the freezing index is high for all years and exceeds freezing indices of all other sites. Summer air temperature variability is greater for NST than air temperatures. During winter this relationship is reversed with greater variability observed for air temperatures and less for NST. Mean winter temperature and temperature variability is similar for all sensors. In comparison, summer NST are marginally warmer. Degree days reflect an environment where air temperatures exceed ground temperatures on average. This stands in contrast to other Dronning Maud Land sites. The ground freezing index is high at more than -7 000.

#### 5.3.2.2.7 A7: Troll 1

Table 92 (pg. 223) contains seasonal frost parameters and indices for A7. None of these indices are available for A8, due to the near surface sensor failing for the duration of the study period. Comparable to western Dronning Maud Land (WDML) sites summer thermal offsets are positive, in comparison to winters, which are negative. Near surface temperature (NST) thawing indices are positive, with freezing indices yielding high negative values for both air temperatures and NST. Some thaw hours are also observed for summer 2012/13 (± 5 hours). Variability during summer is marginally greater for NST than air temperatures. During winter this relationship is reversed with greater variability evident for air temperatures, rather than NST. Few differences are present in winter air and near surface mean temperatures, as well as temperature variability. However, like all other Dronning Maud Land sites, summer NST are noticeably warmer. Like other WDML sites, annual degree (> 0) days show a ground thermal regime warmer than air temperatures with a ground freezing index near ± -6 000.

#### 5.3.2.2.8 A9: Valterkulten

Seasonal frost parameters and indices for A9 are displayed in Table 93 (pg. 223). Like other western Dronning Maud Land (WDML) sites, as well as those in central Dronning Maud Land (CDML), summer thermal offsets are positive, with winter thermal offsets negative. Near surface temperature (NST) thawing indices are positive. Like other Dronning Maud Land sites the freezing indices yield much greater values for both air temperatures and NST. Summer temperature variability is greatest for NST, becoming less with increasing depth into the ground. Air temperature variability is lowest. During winter variability also decreases with increasing depth into the ground with air temperature variability slightly lower than that of NST. Little differences are evident for winter mean temperatures, as well as temperature variability for the various sensors. In comparison, summer temperatures are noticeably warmer at the near surface (NST). Annual degree days (> 0) reflect a ground thermal regime much warmer than air temperatures with a ground freezing index near ± -5 500.

#### 5.3.2.2.9 A10: Vesleskarvet

Seasonal frost parameters and indices for A10 are shown Table 94 (pg. 224). Like previous Dronning Maud Land sites, the summer thermal offsets are positive; winter thermal offsets negative. The near surface temperature (NST) thawing index reflects positive values, with a few hours of thawing (± 7 hours) observed for air temperatures during summer 2012/13. The freezing index yields high negative values for both air temperatures and NST. Summer temperature variability is greatest for NST, then $T_{15}$ and lastly air temperatures. During winter temperature variability decreases with increasing depth into the ground, although little to no differences are observed in mean winter temperatures and variability between the various sensors. Annual degree days indicate a variable ground thermal regime where the ground temperature is cooler than air temperature from 2009-2012. In comparison, degree days suggest that ground temperatures are warmer than air temperatures from 2014-2015. The ground freezing index reflects values below -6 000.

**Table 86: Thermal indices for A1, given for summers (DJF) and winters (JJA) of the relevant years available. The first value represents average temperatures; the second value the associated variability (*s*). # underestimation: data not available for air temperatures ($T_{AIR}$) throughout. Values are indicated per sensor depth, with the subscript indicating the depth of the sensor. NST: near surface (± 1 cm). $T_{15}$: ground temperature recorded at 15 cm depth. SO: thermal offset. FI: freezing index. TI: thawing index. DD: degree days. GFI: annual ground freezing index.**

| DJF | $T_{AIR}$ | NST | $T_{15}$ | SO | TI | | JJA | $T_{AIR}$ | NST | $T_{15}$ | SO | FI | | DD | GFI |
|---|---|---|---|---|---|---|---|---|---|---|---|---|---|---|---|
| | DJF | | | | $T_{AIR}$ | NST | | JJA | | | | $T_{AIR}$ | NST | Annual | |
| 2007/08 | n.d. | n.d. | n.d. | n.d. | n.d. | 0 | 2008 | n.d. | -23.2 \| 0.7 | -24.2 \| 0.6 | n.d. | -432 | -589 | n.d. | n.d. |
| 2008/09 | n.d. | -4.4 \| 3.2 | -5.7 \| 2.7 | n.d. | 0 | 0 | 2009 | -23.3 \| 1.1 | -22.6 \| 0.9 | -23.2 \| 1.2 | 0.6 | -798 | -422 | 620 | -5 487 |
| 2009/10 | -8.6 \| 1.9 | -2.3 \| 3.3 | -3.7 \| 2.7 | 6.3 | 0 | 0 | 2010 | -25.6 \| 0.6 | -26.5 \| 0.6 | -26.1 \| 0.7 | -0.8 | -796 | -541 | 248 | -6 532 |
| 2010/11 | -8.6 \| 2.1 | -5.4 \| 3.1 | -7.1 \| 2.3 | 3.1 | 0 | 0 | 2011 | -24.9 \| 1.0 | -25.5 \| 0.8 | -25.0 \| 0.6 | -0.6 | -949 | -676 | 210 | -6 604 |
| 2011/12 | -10.1 \| 1.4 | -6.9 \| 2.5 | -8.8 \| 2.1 | 3.1 | 0 | 0 | 2012 | -25.1 \| 1.5 | -26.2 \| 1.5 | -26.1 \| 1.4 | -1.1 | -784 | -511 | 277 | -6 444 |
| 2012/13 | -6.9 \| 3.1 | -2.9 \| 4.1 | -4.6 \| 3.4 | 4.0 | n.d. | 0 | 2013 | n.d. | -25.8 \| 2.3 | -25.5 \| 2.1 | n.d. | -548 | -594 | 51 # | -6 460 |
| 2013/14 | -7.0 \| 0.5 | -5.2 \| 3.0 | -6.6 \| 2.6 | 1.9 | n.d. | 0 | 2014 | n.d. | -25.4 \| 1.0 | -25.4 \| 0.8 | n.d. | -677 | -698 | n.d. | -4 017 |
| 2014/15 | -10.7 \| 1.9 | -7.5 \| 2.4 | -8.2 \| 2.0 | 3.2 | 0 | 0 | 2015 | -26.8 \| 1.0 | -27.8 \| 1.2 | -27.3 \| 1.1 | -1.0 | -885 | -606 | 134 | -6 716 |
| 2015/16 | -9.2 \| 2.0 | -5.3 \| 3.2 | -6.5 \| 2.5 | 4.0 | n.d. | n.d. | 2016 | n.d. | n.d. | n.d. | n.d. | n.d. | n.d. | n.d. | n.d. |
| Average | -8.7 \| 1.9 | -5.9 \| 3.1 | -6.4 \| 2.5 | 3.7 | 0 | 0 | Average | -25.2 \| 1.0 | -25.4 \| 1.1 | -25.3 \| 1.1 | -0.2 | -734 | -580 | 257 | -6 037 |

**Table 87: Thermal indices for A2, given for summers (DJF) and winters (JJA) of the relevant years available. The first value represents average temperatures; the second value the associated variability (*s*). # underestimation of freezing index (FI). Values are indicated per sensor depth, with the subscript indicating the depth of the sensor. $T_{AIR}$: air temperatures. NST: near surface (± 1 cm). SO: thermal offset. TI: thawing index. DD: degree days. GFI: annual ground freezing index.**

| DJF | $T_{AIR}$ | NST | SO | TI | | JJA | $T_{AIR}$ | NST | SO | FI | | DD | GFI |
|---|---|---|---|---|---|---|---|---|---|---|---|---|---|
| | DJF | | | $T_{AIR}$ | NST | | JJA | | | $T_{AIR}$ | NST | Annual | |
| 2012/13 | n.d | n.d | n.d. | n.d. | n.d. | 2013 | -24.8 \| 2.4 | -26.0 \| 2.3 | -1.2 | -2 172 | -2 272 | 40 | -6 055 |
| 2013/14 | -7.8 \| 1.0 | -5.9 \| 3.1 | 1.9 | 0 | 6 | 2014 | n.d. | -26.2 \| 0.9 | n.d. | n.d. | -3 206 | n.d. | -6 713 |
| 2014/15 | -11.4 \| 1.2 | -7.6 \| 2.6 | 3.8 | 0 | 1 | 2015 | -26.5 \| 0.9 | -27.6 \| 1.1 | -1.1 | -2 389 | -2 475 | 119 | -6 737 |
| 2015/16 | -9.5 \| 1.8 | -5.4 \| 3.1 | 4.1 | 0 | 10 | 2016 | n.d. | n.d. | n.d. | n.d. | n.d. | n.d. | n.d. |
| Average | -9.6 \| 1.3 | -6.3 \| 3.0 | 3.3 | 0 | 6 | Average | -25.7 \| 1.6 | -26.6 \| 1.4 | -0.9 | -1 520 # | -2 651 | 80 | -6 502 |

**Table 88: Thermal indices for A3, given for summers (DJF) and winters (JJA) of the relevant years available. The first value represents average temperatures; the second value the associated variability (*s*). Values are indicated per sensor depth, with the subscript indicating the depth of the sensor. $T_{AIR}$: air temperatures. NST: near surface (± 1 cm). $T_{15}$: ground temperature recorded at 15 cm depth. SO: thermal offset. FI: freezing index. TI: thawing index. DD: degree days. GFI: annual ground freezing index.**

| DJF | $T_{AIR}$ | NST | $T_{15}$ | SO | TI | | JJA | $T_{AIR}$ | NST | $T_{15}$ | SO | FI | | DD | GFI |
|---|---|---|---|---|---|---|---|---|---|---|---|---|---|---|---|
| | DJF | | | | $T_{AIR}$ | NST | | JJA | | | | $T_{AIR}$ | NST | Annual | |
| 2012/13 | n.d | n.d | n.d | n.d. | n.d. | n.d. | 2013 | -25.3 \| 2.1 | -27.2 \| 2.0 | -26.3 \| 1.7 | -1.8 | -2 244 | -2 398 | 167 | - 6 419 |
| 2013/14 | -8.9 \| 2.3 | -3.9 \| 3.7 | -6.7 \| 2.8 | 5.1 | 0 | 57 | 2014 | -24.3 \| 1.1 | -26.0 \| 0.9 | -25.9 \| 0.6 | -1.6 | -3 060 | -3 218 | 435 | -6 692 |
| 2014/15 | -10.1 \| 1.6 | -5.2 \| 2.6 | -7.6 \| 1.7 | 4.9 | 0 | 9 | 2015 | -26.8 \| 1.1 | -28.2 \| 1.2 | -27.6 \| 1.1 | -1.4 | -2 432 | -2 544 | 305 | -6 705 |
| 2015/16 | -9.8 \| 2.0 | -4.9 \| 4.0 | -6.2 \| 2.9 | 4.9 | 0 | 17 | 2016 | n.d. | n.d. | n.d. | n.d. | n.d. | n.d. | n.d | n.d |
| Average | -9.6 \| 1.9 | -4.7 \| 3.4 | -6.8 \| 2.4 | 5.0 | 0 | 27 | Average | -25.5 \| 1.4 | -27.1 \| 1.4 | -26.6 \| 1.1 | -1.6 | -2 579 | -2 720 | 302 | -6 605 |

**Table 89: Thermal indices for A4, given for summers (DJF) and winters (JJA) of the relevant years available. The first value represents average temperatures; the second value the associated variability (*s*). Values are indicated per sensor depth, with the subscript indicating the depth of the sensor. $T_{AIR}$: air temperatures. NST: near surface (± 1 cm). The subscript following 'T' indicates the depth of the sensor (in centimetres) used to record ground temperature. SO: thermal offset. FI: freezing index. TI: thawing index. DD: degree days. GFI: annual ground freezing index.**

| DJF | $T_{AIR}$ | NST | $T_{15}$ | $T_{30}$ | $T_{45}$ | SO | TI | | Annual |
|---|---|---|---|---|---|---|---|---|---|
| | DJF | | | | | | $T_{AIR}$ | NST | GFI |
| 2012/13 | n.d | n.d | n.d | n.d | n.d | n.d. | n.d. | n.d. | -4 782 |
| 2013/14 | -3.7 \| 2.0 | 0.8 \| 3.0 | -1.3 \| 2.2 | -2.4 \| 1.7 | -2.9 \| 1.6 | 4.5 | 4 | 169 | -4 835 |
| 2014/15 | -5.4 \| 1.4 | -0.7 \| 3.0 | -1.4 \| 1.9 | -1.7 \| 1.3 | -2.9 \| 1.0 | 4.7 | 0 | 125 | -4 928 |
| 2015/16 | -4.5 \| 1.5 | 0.8 \| 3.4 | -0.2 \| 2.5 | -1.2 \| 1.9 | -2.3 \| 1.5 | 5.2 | 1 | 130 | n.d. |
| Average | -4.5 \| 1.6 | 0.3 \| 3.1 | -1.0 \| 2.2 | -1.8 \| 1.6 | -2.7 \| 1.5 | 4.8 | 2 | 141 | -4 848 |
| JJA | $T_{AIR}$ | NST | $T_{15}$ | $T_{30}$ | $T_{45}$ | SO | FI | | |
| | JJA | | | | | | $T_{AIR}$ | NST | DD |
| 2013 | -19.5 \| 1.7 | -21.6 \| 1.6 | -21.0 \| 1.4 | -20.5 \| 1.3 | -20.0 \| 1.2 | -2.1 | -1 766 | -1 940 | 61 |
| 2014 | -20.5 \| 1.1 | -21.7 \| 1.4 | -21.7 \| 1.0 | -21.5 \| 0.9 | -21.1 \| 1.0 | -1.2 | -2 522 | -2 700 | 392 |
| 2015 | -22.5 \| 1.3 | -23.7 \| 1.6 | -22.9 \| 1.5 | -22.1 \| 1.3 | -21.4 \| 1.3 | -1.2 | -1 988 | -2 108 | 244 |
| 2016 | n.d. | n.d. | n.d. | n.d. | n.d. | n.d. | n.d. | n.d. | n.d. |
| Average | -20.8 \| 1.3 | -22.3 \| 1.5 | -21.9 \| 1.3 | -21.3 \| 1.2 | -20.9 \| 1.1 | -1.5 | -2 092 | -2 249 | 232 |

**Table 90: Thermal indices for A5, given for summers (DJF) and winters (JJA) of the relevant years available. The first value represents average temperatures; the second value the associated variability (*s*). Values are indicated per sensor depth, with the subscript indicating the depth of the sensor. $T_{AIR}$: air temperatures. NST: near surface (± 1 cm). $T_{15}$: ground temperature recorded at 15 cm depth. SO: thermal offset. FI: freezing index. TI: thawing index. DD: degree days. GFI: annual ground freezing index.**

| DJF | $T_{AIR}$ | NST | $T_{15}$ | SO | TI | | JJA | $T_{AIR}$ | NST | $T_{15}$ | SO | FI | | DD | GFI |
|---|---|---|---|---|---|---|---|---|---|---|---|---|---|---|---|
| | DJF | | | | $T_{AIR}$ | NST | | JJA | | | | $T_{AIR}$ | NST | Annual | |
| 2012/13 | n.d | n.d | n.d | n.d. | n.d. | n.d. | 2013 | -22.2 \| 2.3 | -23.2 \| 2.3 | -23.0 \| 2.0 | -1.0 | -1 961 | -2 043 | -34 | -5 499 |
| 2013/14 | -7.3 \| 2.0 | -5.0 \| 2.9 | -5.3 \| 2.4 | 2.4 | 0 | 17 | 2014 | -22.5 \| 1.2 | -23.3 \| 1.1 | -23.6 \| 0.9 | -0.7 | -2 778 | -2 869 | 28 | -6 254 |
| 2014/15 | -8.7 \| 1.3 | -7.1 \| 2.1 | -6.4 \| 1.7 | 1.6 | 0 | 0 | 2015 | -24.3 \| 1.1 | -25.2 \| 1.2 | -24.8 \| 1.2 | -0.9 | -2 187 | -2 256 | 4 | -6 211 |
| 2015/16 | -8.2 \| 1.4 | -6.6 \| 2.3 | -5.6 \| 2.1 | 1.6 | 0 | 0 | 2016 | n.d. | n.d. | n.d. | n.d. | n.d. | n.d. | n.d. | n.d. |
| Average | -8.1 \| 1.6 | -6.2 \| 2.4 | -5.8 \| 2.1 | 1.9 | 0 | 6 | Average | -23.0 \| 1.5 | -23.9 \| 1.5 | -23.8 \| 1.3 | -0.9 | -2 309 | -2 389 | -1 | -5 988 |

**Table 91: Thermal indices for A6, given for summers (DJF) and winters (JJA) of the relevant years available. The first value represents average temperatures; the second value the associated variability (*s*). Values are indicated per sensor depth, with the subscript indicating the depth of the sensor. $T_{AIR}$: air temperatures. NST: near surface (± 1 cm). SO: thermal offset. FI: freezing index. TI: thawing index. DD: degree days. GFI: annual ground freezing index.**

| DJF | $T_{AIR}$ | NST | SO | TI | | JJA | $T_{AIR}$ | NST | SO | FI | | DD | GFI |
|---|---|---|---|---|---|---|---|---|---|---|---|---|---|
| | DJF | | | $T_{AIR}$ | NST | | JJA | | | $T_{AIR}$ | NST | Annual | |
| 2012/13 | n.d | n.d | n.d. | n.d. | n.d. | 2013 | -26.5 \| 2.2 | -27.2 \| 2.2 | -0.7 | -2 356 | -2 411 | -73 | -6 632 |
| 2013/14 | -9.8 \| 2.4 | -8.9 \| 2.8 | 0.9 | 0 | 0 | 2014 | -25.5 \| 1.1 | -26.6 \| 0.9 | -1.0 | -3 202 | -3 295 | 0 | -7 521 |
| 2014/15 | -11.2 \| 1.7 | -10.5 \| 2.1 | 0.7 | 0 | 0 | 2015 | -28.1 \| 1.0 | -28.9 \| 1.1 | -0.8 | -2 544 | -2 606 | -110 | -7 524 |
| 2015/16 | -10.7 \| 2.0 | -9.4 \| 2.4 | 1.3 | 0 | 0 | 2016 | n.d. | n.d. | n.d. | n.d. | n.d. | n.d. | n.d. |
| Average | -10.6 \| 2.0 | -9.6 \| 2.4 | 1.0 | 0 | 0 | Average | -26.7 \| 1.4 | -27.6 \| 1.4 | -0.9 | -2 701 | -2 771 | -61 | -7 226 |

**Table 92: Thermal indices for A7, given for summers (DJF) and winters (JJA) of the relevant years available. The first value represents average temperatures; the second value the associated variability (*s*). Values are indicated per sensor depth, with the subscript indicating the depth of the sensor. $T_{AIR}$: air temperatures. NST: near surface (± 1 cm). SO: thermal offset. FI: freezing index. TI: thawing index. DD: degree days. GFI: annual ground freezing index.**

| DFJ | $T_{AIR}$ | NST | SO | TI | | JJA | $T_{AIR}$ | NST | SO | FI | | DD | GFI |
|---|---|---|---|---|---|---|---|---|---|---|---|---|---|
| | DJF | | | $T_{AIR}$ | NST | | JJA | | | $T_{AIR}$ | NST | Annual | |
| 2006/07 | n.d. | n.d. | n.d. | n.d. | n.d. | 2007 | -25.1 \| 1.4 | -26.8 \| 1.9 | -1.7 | -2 268 | -2 419 | -115 | -6 176 |
| 2007/08 | -7.7 \| 2.0 | -4.1 \| 2.0 | 3.6 | 0 | 0 | 2008 | -25.2 \| 2.1 | -25.5 \| 2.2 | n.d. | -2 387 | -2 415 | 328 | -6 516 |
| 2008/09 | -7.1 \| 2.7 | -5.4 \| 1.9 | 1.7 | 0 | 0 | 2009 | n.d. | n.d. | n.d. | n.d. | n.d. | n.d. | n.d. |
| 2009/10 | -6.5 \| 2.1 | -3.7 \| 1.9 | 2.9 | 0 | 0 | 2010 | -26.9 \| 0.6 | -28.8 \| 0.7 | -1.8 | -2 509 | -2 638 | 196 | -6 477 |
| 2010/11 | -6.1 \| 1.7 | -4.7 \| 1.7 | 1.4 | 0 | 0 | 2011 | -23.7 \| 1.0 | -24.8 \| 0.9 | -1.0 | -2 188 | -2 297 | 229 | -6 145 |
| 2011/12 | -7.8 \| 1.1 | -5.7 \| 1.7 | 2.1 | 0 | 0 | 2012 | -24.6 \| 1.9 | -27.3 \| 1.8 | -2.6 | -2 342 | -2 397 | 257 | -6 144 |
| 2012/13 | -4.9 \| 2.6 | -1.9 \| 2.7 | 3.0 | 0.2 | 47 | 2013 | -22.8 \| 3.1 | -26.3 \| 2.0 | -3.5 | -1 216 | -2 351 | 350 | -5 712 |
| 2013/14 | -8.8 \| 2.5 | -1.2 \| 2.8 | 7.6 | 0 | 37 | 2014 | -25.12 \| 1.9 | -26.4 \| 0.7 | -1.2 | -2 391 | -2 456 | 376 | -6 434 |
| 2014/15 | -7.3 \| 1.6 | -3.3 \| 1.6 | 3.9 | 0 | 0 | 2015 | -26.6 \| 1.8 | -28.6 \| 1.8 | -2.0 | -2 356 | -2 514 | 32 | -6 482 |
| 2015/16 | -6.7 \| 1.9 | -1.9 \| 2.9 | 4.9 | 0 | 6 | 2016 | n.d. | n.d. | n.d. | n.d. | n.d. | n.d. | n.d. |
| Average | -7.0 \| 2.0 | -3.5 \| 2.1 | 3.5 | ± 0 | 11 | Average | -25.0 \| 1.7 | -26.8 \| 1.5 | -1.8 | -2 198 | -2 438 | 252 | -6 273 |

**Table 93: Thermal indices for A9, given for summers (DJF) and winters (JJA) of the relevant years available. The first value represents average temperatures; the second value the associated variability (*s*). # underestimation of the freezing index (FI). Values are indicated per sensor depth, with the subscript indicating the depth of the sensor. $T_{AIR}$: air temperatures. NST: near surface (± 1 cm). $T_{15}$: ground temperature recorded at 15 cm depth. SO: thermal offset. TI: thawing index. DD: degree days. GFI: annual ground freezing index.**

| DJF | $T_{AIR}$ | NST | $T_{15}$ | SO | TI | | JJA | $T_{AIR}$ | NST | $T_{15}$ | SO | FI | | DD | GFI |
|---|---|---|---|---|---|---|---|---|---|---|---|---|---|---|---|
| | DJF | | | | $T_{AIR}$ | NST | | JJA | | | | $T_{AIR}$ | NST | Annual | |
| 2012/13 | n.d | n.d | n.d | n.d. | n.d. | n.d. | 2013 | -22.7 \| 2.0 | -23.7 \| 2.0 | -23.3 \| 1.7 | -1.0 | -2 024 | -2 114 | 264 | -5 221 |
| 2013/14 | -5.8 \| 2.5 | -1.8 \| 3.0 | -2.7 \| 2.6 | 4.0 | 0 | 87 | 2014 | -22.7 \| 1.0 | -23.7 \| 1.1 | -23.8 \| 0.8 | -1.0 | -2 838 | -2 954 | 682 | -5 639 |
| 2014/15 | -7.6 \| 0.6 | -3.8 \| 2.3 | -3.3 \| 2.1 | 3.9 | 0 | 45 | 2015 | n.d. | -26.3 \| 1.4 | -25.2 \| 1.3 | n.d. | n.d. | -2 338 | n.d. | -5 684 |
| 2015/16 | n.d. | -2.6 \| 4.2 | -2.4 \| 3.0 | n.d. | 0 | 94 | 2016 | n.d. | n.d. | n.d. | n.d. | n.d. | n.d. | n.d. | n.d. |
| Average | -6.7 \| 1.5 | -2.7 \| 3.1 | -2.8 \| 2.6 | 4.0 | 0 | 75 | Average | -22.7 \| 1.5 | -24.6 \| 1.5 | -24.1 \| 1.3 | -1.8 | -1 621 # | -2 469 | 473 | - 5 515 |

**Table 94: Thermal indices for A10, given for summers (DJF) and winters (JJA) of the relevant years available. The first value represents average temperatures; the second value the associated variability (*s*). # underestimation of the freezing index (FI). Values are indicated per sensor depth, with the subscript indicating the depth of the sensor. $T_{AIR}$: air temperatures. NST: near surface (± 1 cm). $T_{15}$: ground temperature recoded at 15 cm depth. SO: thermal offset. TI: thawing index. DD: degree days. GFI: annual ground freezing index.**

| DJF | $T_{AIR}$ | NST | $T_{15}$ | SO | TI | | JJA | $T_{AIR}$ | NST | $T_{15}$ | SO | FI | | DD | GFI |
|---|---|---|---|---|---|---|---|---|---|---|---|---|---|---|---|
| | DJF | | | | $T_{AIR}$ | NST | | JJA | | | | $T_{AIR}$ | NST | Annual | |
| 2008/09 | n.d. | n.d. | n.d. | n.d. | n.d. | n.d. | 2009 | -20.9 \| 2.0 | -21.9 \| 1.9 | -21.5 \| 1.8 | n.d. | n.d. | n.d. | -104 | -5464 |
| 2009/10 | -6.1 \| 1.6 | -5.0 \| 1.7 | -5.4 \| 1.3 | 1.1 | 0 | 0 | 2010 | -23.6 \| 0.6 | -24.5 \| 0.6 | -24.2 \| 0.7 | -0.9 | -2 171 | -2 279 | -93 | -5 927 |
| 2010/11 | -6.2 \| 2.0 | -5.9 \| 2.3 | -6.5 \| 1.6 | 0.3 | 0 | 1 | 2011 | -21.6 \| 1.1 | -22.4 \| 0.8 | -22.0 \| 0.6 | -0.8 | -1 932 | -2 021 | -68 | -5 775 |
| 2011/12 | -8.0 \| 1.1 | -7.4 \| 1.3 | -7.3 \| 1.1 | 0.6 | 0 | 0 | 2012 | -22.0 \| 1.4 | -23.1 \| 1.4 | -23.3 \| 1.2 | -1.1 | -2 042 | -2 139 | -76 | -5 669 |
| 2012/13 | -3.8 \| 0.5 | -3.5 \| 2.2 | -4.2 \| 2.6 | 0.3 | 0.3 | 18 | 2013 | n.d. | -23.0 \| 1.5 | -22.2 \| 1.6 | n.d. | n.d. | -2 026 | n.d. | -5 600 |
| 2013/14 | -7.6 \| 2.3 | -4.6 \| 2.3 | -5.7 \| 2.0 | 3.0 | 0 | 6 | 2014 | -21.9 \| 1.2 | -23.2 \| 1.1 | -23.1 \| 0.9 | -1.3 | -2 037 | -2 152 | 72 | -5 825 |
| 2014/15 | -7.4 \| 1.3 | -5.9 \| 1.5 | -6.2 \| 1.3 | 1.5 | 0 | 11 | 2015 | -23.6 \| 1.1 | -24.8 \| 1.3 | -24.2 \| 1.2 | -1.3 | -2 090 | -2 184 | 170 | -5 642 |
| 2015/16 | -7.2 \| 1.6 | -5.7 \| 2.6 | -6.7 \| 1.9 | 1.5 | 0 | 18 | 2016 | n.d. | n.d. | n.d. | n.d. | n.d. | n.d. | n.d. | n.d. |
| Average | -6.6 \| 1.5 | -5.4 \| 2.0 | -6.0 \| 1.7 | 1.2 | 0 | 6 | Average | -22.2 \| 1.2 | -23.3 \| 1.2 | -22.9 \| 1.2 | -1.0 | -1 284 # | -1 600 | -17 | -5 700 |

#### *5.3.2.3 Diurnal thaw environment*

The discussion on the diurnal environment is separated into seasons. Most Dronning Maud Land data loggers have data from autumn 2013 – summer 2015/16, with three sites (A1, A6, A10) having longer observation periods. All temperatures are based on degree Celsius and represent approximations to the nearest degree. Thaw duration, thaw depths and proportions (percentages) are rounded to the nearest hour, centimetre and percentage respectively. Logger failure, where applicable, is indicated in the text. Furthermore, averages calculated for diurnal temperatures using the World Meteorological Organisation (WMO) (2011) method correlates (see discussion in 4.5.2.1 Freeze-thaw cycle indices and statistical calculations, pg. 104) most strongly with thaw duration (A1-5; A7-10: $r \pm 0.84$, $p \pm 0.0$; A6: 0.82, $p \pm 0.05$). As such, this method of calculating the average is preferred over standard calculations based on diurnal maximum temperature and diurnal minimum temperature. Each site within Dronning Maud Land (DML) is discussed within its own subsection below, however a summary of calculated parameters is provided in Table 95 (pg. 226).

During 2013-2016 the lowest maximum for air temperatures is recorded at A6, the highest at A4. During this time, the average duration of positive air temperatures achieved for all sites is 2 hours, the same as observed for sites with longer time series (A1, A7, A10). However, average freeze-thaw cycles calculated for A1, A7 and A10 for the period autumn 2013-2016 vs. 200*-2016 show significant decrease in numbers (103 vs. 51 respectively). This is associated with higher average diurnal maximum temperatures recorded during the longer time span (7 °C vs. 4 °C), a more than halving of potential freeze-thaw events for air temperatures and near surface temperatures (NST: temperatures recorded at ± 1 cm in the ground) (120 vs. 49 and 358 vs. 146), as well as a reduction of ± one thaw hour on average (7 vs. 6 hours). Highest diurnal maximum air temperatures are also recorded during the longer time span (9 °C for A7 and 7 °C for A10). Using data for all sites from autumn 2013-2016 show an average ground thaw duration of 8 hours, with average ground thaw duration at A4 equalling ± 18 hours. A6 exhibits the shortest average thaw duration of 5 hours. All sites, excepting A4, have a deepest thaw duration event lasting between 12-17 hours (A1-A3; A6-A9 and A5 respectively). Similarly, longest thaw duration, excepting A4, lasts between 12-18 hours (A6/A7 and A1-A9 respectively). The thaw duration of the deepest and longest thaw events for A4 is 63 and 115 hours respectively. Thaw duration is strongly correlated to freeze-thaw cycles ($r = 0.81$, $p < 0.001$), as well as to initiation of freezing following a thaw event ($r = -0.83$, $p < 0.001$). Thaw duration is strongly correlated to initiation of thaw ($r = -0.59$, $p < 0.001$). Average commencement of thaw is 10:00 and freezing generally initiates by 15:00. The notable exception is A4, where thawing commences at 08:00 and generally only ends at 02:00 the following day. Multiple thaw events within one 24-hour period are only recorded at A1, A5, and A7, with thaw events exceeding one 24-hour cycle only evident for A4. The most potential freeze-thaw events for air temperatures and NST, as well as most freeze-thaw cycles are recorded at A4. Consistently high values for these parameters are also recorded at A3 and A9.

**Table 95: Summary of ground thermal dynamics for all Dronning Maud Land sites, provided for autumn 2013-2016, as well as 200*-2016 for A1, A7, and A10. All durations and times represent averages. $T_{AIR}$: air temperatures. PFTE: potential freeze-thaw events. NST: temperature recorded at ± 1 cm depth. FTC: freeze-thaw cycles. TH: thaw hours.**

| Site | 2013-2016 | | | | | | EVENT | | DURATION OF POSITIVE TEMPERATURES | | | |
|---|---|---|---|---|---|---|---|---|---|---|---|---|
| | $T_{AIR}$ Max | PFTE $T_{AIR}$ | PFTE | FTC | PFTE to FTC (%) | TH per FTC | Multiple | Over Several Days | $T_{AIR}$ | Start: NST | End: NST | Thaw Duration |
| A1 | 5 | 95 | 138 | 84 | 61 | 5 | Y | N | 2 | 11:00 | 17:00 | 6 |
| A2 | 0 | 0 | 120 | 46 | 38 | 6 | N | N | 0 | 13:00 | 19:00 | 6 |
| A3 | 2 | 4 | 148 | 89 | 60 | 8 | N | N | 2 | 10:00 | 18:00 | 9 |
| A4 | 6 | 111 | 217 | 116 | 53 | 14 | N | Y | 5 | 8:00 | 2:00 | 18 |
| A5 | 2 | 13 | 44 | 25 | 57 | 6 | Y | N | 2 | 10:00 | 18:00 | 6 |
| A6 | 0.5 | 1 | 21 | 7 | 33 | 4 | N | N | 1 | 10:00 | 13:00 | 5 |
| A7 | 4 | 23 | 140 | 0 | 0 | 10 | N | N | 3 | n/a | n/a | n/a |
| A9 | 3 | 33 | 201 | 76 | 38 | 9 | Y | N | 4 | 11:00 | 19:00 | 8 |
| A10 | 4 | 30 | 160 | 69 | 43 | 5 | N | N | 3 | 9:00 | 16:00 | 6 |
| Site | 200* TO 2016 | | | | | | EVENT | | DURATION OF POSITIVE TEMPERATURES | | | |
| | $T_{AIR}$ Max | PFTE $T_{AIR}$ | PFTE NST | FTC | PFTE to FTC (%) | TH per FTC | Multiple | Over Several Days | $T_{AIR}$ | Start: NST | End: NST | Thaw Duration |
| A1 | 5 | 111 | 444 | 198 | 45 | 6 | Y | N | 2 | 12:00 | 17:00 | 7 |
| A7 | 9 | 109 | 314 | 18 | 6 | 8 | Y | N | 2 | 11:00 | 16:00 | 6 |
| A10 | 7 | 141 | 316 | 92 | 29 | 5 | N | N | 2 | 9:00 | 16:00 | 7 |

#### 5.3.2.3.1 A1: Flårjuven 1

Data for A1 are available from autumn 2008 to summer 2015/16 and diurnal ranges and oscillations around 0 °C are provided in Table 96. Diurnal air temperature ranges of 10 °C are rare (± 7%). Nevertheless, such ranges occur throughout the year. Of these ranges, ± 28% reflect maximums above and minimums below 0 °C, *i.e.* oscillations around 0 °C. This translates into 2% of oscillations indicative of potential freeze-thaw events that also exceed a diurnal temperature range of 10 °C, as well as 2% of oscillations when evaluating all diurnal ranges. For near surface temperatures (NST) diurnal ranges of 10 °C are more common, occurring 26% of the time since records began. Of these ranges, more than half reflect ranges where freeze-thaw events are likely (57% >/< 0 °C). This translates into 15% of oscillations indicative of potential freeze-thaw events that also exceed a diurnal temperature range of 10 °C, as well as 15% of oscillations when evaluating all diurnal ranges. At $T_{15}$ no diurnal range greater than 10 °C is recorded, although oscillations around 0 °C are (0% >/< 0 °C). Below this depth no diurnal temperature range exceeding 10 °C is observed. Diurnal ranges exceeding 10 °C occur predominantly during spring and summer. Oscillations around 0 °C are recorded predominantly during summer, with none observed in winter. Temperatures at A1 also shows days on which temperatures don't dip below 0 °C. Such ranges are observed on five days for air temperatures in summer 2014/2015.

**Table 96: Oscillations around 0 °C (Osc), as well as diurnal ranges exceeding 10 °C ($T_{DR}$) for A1. Annual Osc (%) reflect all oscillations around 0 °C, including those where $T_{DR}$ does not exceed 10 °C. $T_{AIR}$: air temperatures. NST: ground temperatures recorded at ± 1 cm depth. $T_{15}$: ground temperatures recorded at 15 cm depth. JJA: winter. SON: spring. DJF: summer. MAM: autumn.**

| Sensor | $T_{DR}$ (%) | Osc (%) | % of year | Annual Osc (%) | $T_{DR}$ (%) | | | | Osc (%) | | | |
|---|---|---|---|---|---|---|---|---|---|---|---|---|
| | | | | | JJA | SON | DJF | MAM | JJA | SON | DJF | MAM |
| $T_{AIR}$ | 7 | 28 | 2 | 2 | 15 | 34 | 35 | 17 | 0 | 5 | 85 | 10 |
| NST | 26 | 57 | 15 | 15 | 2 | 30 | 63 | 5 | 0 | 11 | 89 | 0 |
| $T_{15}$ | 0 | 0 | 0 | 2 | 0 | 0 | 0 | 0 | 0 | 0 | 100 | 0 |

During 2008-2015/16 relatively numerous positive air temperatures are recorded (potential freeze-thaw events: 111). Similarly, numerous potential freeze-thaw events and freeze-thaw cycles are observed, and thaw events occur within the upper 25 cm of the ground. Positive air temperatures generally occur during the summers of 2013/14 and 2014/15 (n = 47 and n = 31 occurrences respectively). 2014 is the only year for which positive air temperatures are attained in autumn (n = 8 occurrences) and spring (n = 7 occurrences). A maximum air temperature of 5 °C is reached on 2 December 2015 at 18:00 and positive temperatures are maintained for ± 2 hours on average. Ninety-five potential freeze-thaw events are evident from autumn 2013 to summer 2015/16. Average duration of positive temperatures achieved, as well as the diurnal maximum temperature is the same as the values recorded for the entire time span of 2008-2016.

There is no soil moisture sensor available for this site from 2008-2009 and freeze-thaw cycles are approximated for these years by comparing variability of known freeze-thaw events of 2010-2016 to the variability of potential freeze-thaw events from 2008-2009. Using this method yields 198 freeze-thaw cycles on 184 separate days from autumn 2008 to summer 2015/16. More cycles are observed

due to multiple cycles occasionally taking place in a 24-hour period. Almost half (45%) of potential freeze-thaw events translate into freeze-thaw cycles (Table 97).

**Table 97: Freeze-thaw events for A1, summarised by season. # indicates approximation of freeze-thaw cycles (FTC). PFTE: potential freeze-thaw events. $T_{AIR}$: air temperatures. NST: ground temperatures recorded at ± 1 cm depth. $T_{15}$: ground temperatures recorded at 15 cm depth.**

| Season | Potential Thaw Hours at 0 °C | | | PFTE | | | FTC |
|---|---|---|---|---|---|---|---|
| | $T_{AIR}$ | NST | $T_{15}$ | $T_{AIR}$ | NST | $T_{15}$ | |
| 2008 Autumn | 0 | 0 | 0 | 0 | 0 | 0 | 0 |
| 2008 Winter | 0 | 0 | 0 | 0 | 0 | 0 | 0 |
| 2008 Spring | 0 | 12 | 0 | 0 | 3 | 0 | 1 # |
| 2008/09 Summer | 0 | 269 | 51 | 0 | 39 | 7 | 9 # |
| 2009 Autumn | 0 | 0 | 0 | 0 | 0 | 0 | 0 # |
| 2009 Winter | 0 | 0 | 0 | 0 | 0 | 0 | 0 # |
| 2009 Spring | 0 | 20 | 0 | 0 | 4 | 0 | 2 # |
| 2009/10 Summer | 5 | 507 | 159 | 3 | 63 | 22 | 10 |
| 2010 Autumn | 0 | 0 | 0 | 0 | 0 | 0 | 0 |
| 2010 Winter | 0 | 0 | 0 | 0 | 0 | 0 | 0 |
| 2010 Spring | 0 | 32 | 0 | 0 | 14 | 0 | 12 |
| 2010/11 Summer | 12 | 349 | 11 | 9 | 55 | 2 | 18 |
| 2011 Autumn | 0 | 0 | 0 | 0 | 0 | 0 | 0 |
| 2011 Winter | 0 | 0 | 0 | 0 | 0 | 0 | 0 |
| 2011 Spring | 0 | 10 | 0 | 0 | 4 | 0 | 2 |
| 2011/12 Summer | 0 | 294 | 15 | 0 | 55 | 2 | 30 |
| 2012 Autumn | 0 | 0 | 0 | 0 | 0 | 0 | 0 |
| 2012 Winter | 0 | 0 | 0 | 0 | 0 | 0 | 0 |
| 2012 Spring | 0 | 38 | 0 | 0 | 10 | 0 | 5 |
| 2012/13 Summer | 7 | 429 | 120 | 4 | 59 | 17 | 25 |
| 2013 Autumn | 0 | 0 | 0 | 0 | 0 | 0 | 0 |
| 2013 Winter | 0 | 0 | 0 | 0 | 0 | 0 | 0 |
| 2013 Spring | 0 | 35 | 0 | 0 | 12 | 0 | 5 |
| 2013/14 Summer | 16 | 14 | 0 | 47 | 4 | 0 | 20 |
| 2014 Autumn | 9 | 0 | 0 | 8 | 0 | 0 | 0 |
| 2014 Winter | 0 | 0 | 0 | 0 | 0 | 0 | 0 |
| 2014 Spring | 7 | 14 | 0 | 7 | 4 | 0 | 4 |
| 2014/15 Summer | 64 | 202 | 0 | 31 | 47 | 0 | 20 |
| 2015 Autumn | 0 | 0 | 0 | 0 | 0 | 0 | 0 |
| 2015 Winter | 0 | 0 | 0 | 0 | 0 | 0 | 0 |
| 2015 Spring | 0 | 38 | 0 | 0 | 9 | 0 | 3 |
| 2015/16 Summer | 3 | 336 | 22 | 2 | 62 | 5 | 32 |
| Total | **123** | **2 599** | **378** | **111** | **444** | **55** | **198 #** |

Thaw events occur occasionally during spring (16%) but generally during the summer months of December (34%) and January (39%), with limited events in February (11%). Most thaw events represent single freeze-thaw cycles, with average thaw duration of 7 hours ($s$ = 4) and thaw generally occurring from 10:00-17:00. Multiple thaw events are observed on ten separate days. Of these three occur in spring and the remaining in summer. The initial thaw event is shortest, lasting ± 2 hours from 09:00-11:00. The second thaw event lasts for ± 5 hours from 12:00-17:00. Two days register three cycles. These are 29 November 2010 and 9 January 2014. For these days, the third thaw event lasts ± 3 hours from 16:00-19:00. Deep thaw events, lasting 12 hours on average, occur predominantly in December and January. A 7-hour delay ($s$ = 1) between NST and $T_{15}$ is recorded and thaw is observed for ± 7 hours at $T_{15}$. The longest thaw event of 18 hours is observed on 12 December 2012, occurring from 07:00 until 01:00 the next day. The deepest thaw event takes place on 22 December 2009, with thaw reaching 25 cm.

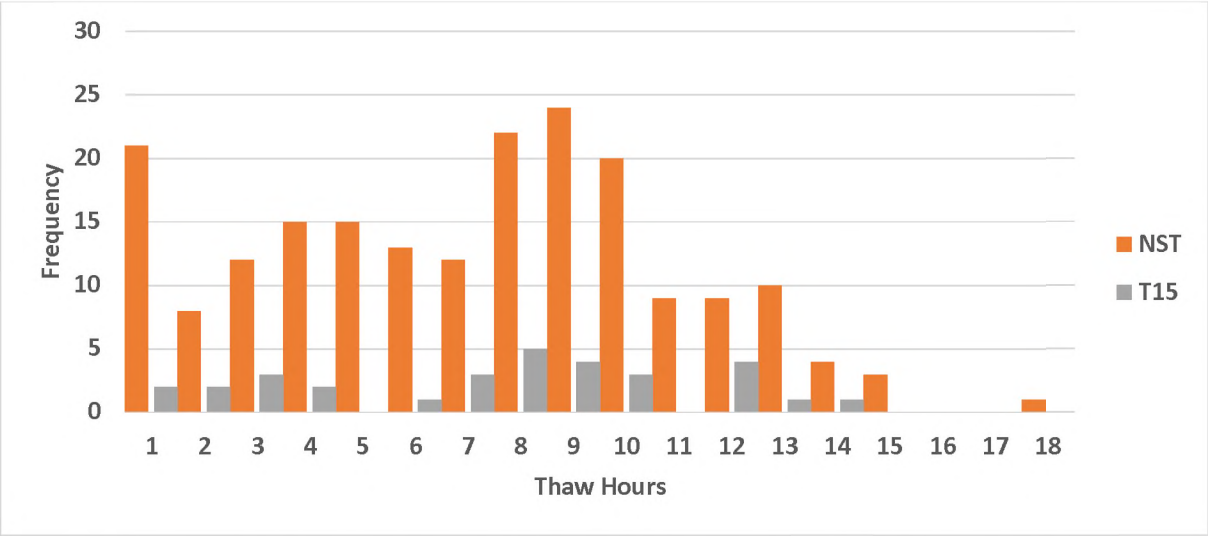


**Figure 123: Histogram of thaw duration per event per sensor depth for A1. NST: near surface (± 1 cm). $T_{15}$: temperature recorded at 15 cm depth.**

Thirty-six freeze-thaw cycles last longer than 10 hours (Figure 123). Of these 53% occur in December, with 40% during January. Isolated thaw events are evident for February (3%). For these thaw events, average thaw occurs from 07:00-11:00. When average thaw duration is considered (7 hours, n = 114), 7% occur in November, 40% in December, 48% in January, and 4% in February. For these thaw events, average commencement of thaw takes place at 10:00, ending at 17:00. Variability for temperature recorded initially increases from air temperatures to NST. From NST onwards an increase in depth into the ground yields a decrease in variability. Highest variability is observed for NST ($s$ = 8.95), lowest for $T_{60}$ ($s$ = 6.27). At NST the average diurnal temperature range is 20 °C, although a maximum diurnal range of 28 °C is reached. Maximum diurnal temperature is 18 °C, while diurnal minimum temperature is -21 °C. The greatest diurnal maximum correlates positively with maximum thaw duration ($r$ = 0.74, $p$ ± 0.0). Similarly, the coldest diurnal minimum temperature correlate positively with shortest thaw duration ($r$ = 0.75, $p$ ± 0.0). Average diurnal maximum, minimum, and mean temperatures on those days when freeze-thaw cycles are evident are 9 °C, -12 °C and -3 °C respectively.

#### 5.3.2.3.2 A2: Flårjuven 2

Data for A2 are available from autumn 2013 to summer 2015/16. Diurnal ranges and oscillations around 0 °C are provided in Table 98 (pg. 230). Diurnal air temperature ranges of 10 °C are rare (± 2%), occurring throughout the year, except for January, March, April, and December. Of these ranges, no oscillations around 0 °C are recorded. This also translates into no oscillations indicative of potential freeze-thaw events that also exceed a diurnal range of 10 °C. For near surface temperatures (NST: recorded at ± 1 cm in the ground), diurnal ranges exceeding 10 °C are more common, occurring 15% of the time since records began. Of these ranges, almost a third reflect ranges where freeze-thaw events are possible (60% >/< 0 °C). This translates into 9% of annual oscillations indicative of potential freeze-thaw events that also exceed a diurnal temperature range of 10 °C. At $T_{15}$ no diurnal temperature range greater than 10 °C is recorded, although oscillations around 0 °C are (0.2% >/< 0 °C). Below this depth no ranges exceeding 10 °C are evident. Diurnal ranges greater than 10 °C occur predominantly in summer and spring (for NST), with air temperatures registering most of these ranges in spring and winter. Oscillations around 0 °C are recorded predominantly during summer, with none observed for winter.

**Table 98: Oscillations around 0 °C (Osc), as well as diurnal ranges exceeding 10 °C ($T_{DR}$) for A2. Annual Osc (%) reflect all oscillations around 0 °C, including those where $T_{DR}$ does not exceed 10 °C. $T_{AIR}$: air temperatures. NST: ground temperatures recorded at ± 1 cm depth. $T_{15}$: ground temperatures recorded at 15 cm depth. JJA: winter. SON: spring. DJF: summer. MAM: autumn.**

| Sensor | $T_{DR}$ (%) | Osc (%) | % of year | Annual Osc (%) | $T_{DR}$ (%) | | | | Osc (%) | | | |
|---|---|---|---|---|---|---|---|---|---|---|---|---|
| | | | | | JJA | SON | DJF | MAM | JJA | SON | DJF | MAM |
| $T_{AIR}$ | 2 | 0 | 0 | 0 | 31 | 50 | 4 | 15 | 0 | 0 | 0 | 0 |
| NST | 15 | 60 | 9 | 11 | 0 | 23 | 63 | 14 | 0 | 10 | 84 | 6 |
| $T_{15}$ | 0 | 0 | 0 | ± 0 | 0 | 0 | 0 | 0 | 0 | 0 | 100 | 0 |

No potential freeze-thaw events are recorded for air temperature at A2 and thaw events occur within the upper 15 cm of the ground (active layer thickness: 15 cm). The soil moisture sensor failed for the duration of 2014 and freeze-thaw cycles are approximated for this year by comparing variability of known freeze-thaw cycles of 2013 and 2015 to potential freeze-thaw events for 2014. Using this method yields diurnal freeze-thaw cycles on 46 separate days from autumn 2013 to summer 2016. Just over a third (38%) of potential freeze-thaw events translate into freeze-thaw cycles (Table 99, pg. 231).

**Table 99: Freeze-thaw events for A2, summarised by season. # indicates approximation of freeze-thaw cycles (FTC). PFTE: potential freeze-thaw events. $T_{AIR}$: air temperatures. NST: ground temperatures recorded at ± 1 cm depth.**

| Season | Potential Thaw Hours at 0 °C | | PFTE | | FTC |
|---|---|---|---|---|---|
| | $T_{AIR}$ | NST | $T_{AIR}$ | NST | |
| 2013 Autumn | 0 | 1 | 0 | 1 | 0 |
| 2013 Winter | 0 | 0 | 0 | 0 | 0 |
| 2013 Spring | 0 | 47 | 0 | 9 | 6 |
| 2013/14 Summer | 0 | 262 | 0 | 1 | 8 # |
| 2014 Autumn | 0 | 0 | 0 | 0 | 0 # |
| 2014 Winter | 0 | 0 | 0 | 9 | 0 # |
| 2014 Spring | 0 | 10 | 0 | 1 | 3 # |
| 2014/15 Summer | 0 | 197 | 0 | 0 | 7 |
| 2015 Autumn | 0 | 0 | 0 | 0 | 0 |
| 2015 Winter | 0 | 0 | 0 | 0 | 0 |
| 2015 Spring | 0 | 1 | 0 | 1 | 1 |
| 2015/16 Summer | 0 | 250 | 0 | 37 | 21 |
| Total | **0** | **768** | **0** | **120** | **46 #** |

Thaw events occur occasionally during spring (22%) and predominantly during the summer months of December (43%) and January (30%), with limited events in February (4%). All thaw events represent single freeze-thaw cycles, with average thaw duration of 6 hours ($s$ = 3). Thaw generally occurs from 13:00-19:00. Five freeze-thaw cycles last longer than 10 hours (Figure 124, pg. 232). Of these three (60%) occur in December, with two (40%) in January. For these thaw events, average commencement of thaw occurs from 11:00-22:00. When average thaw duration is considered (6 hours, n = 30), 57% of freeze-thaw cycles take place in December, with 20% in November, 20% in January and 3% in February. For these thaw events, average commencement of thaw starts at 12:00, ending at 20:00.

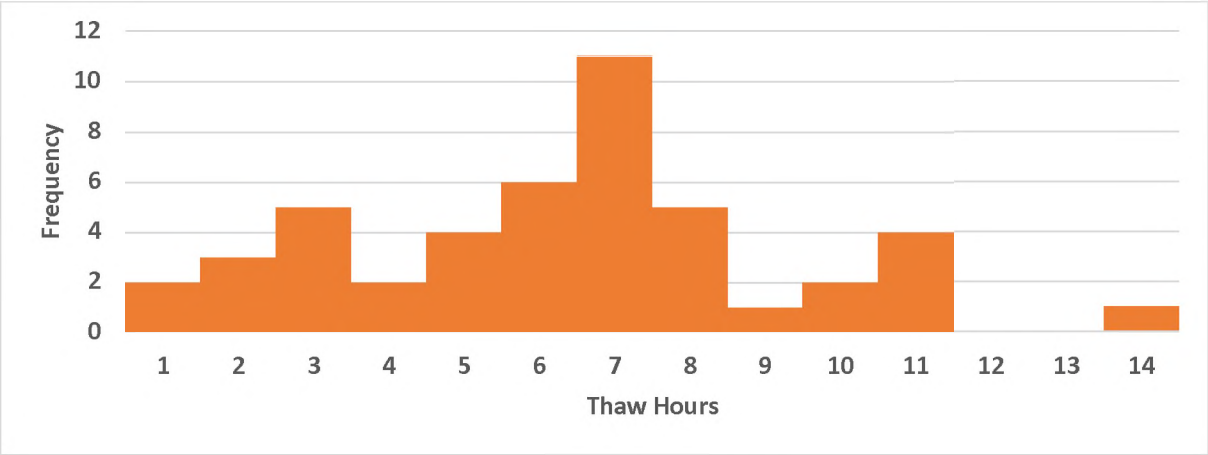


**Figure 124: Histogram of thaw duration per event per sensor at the near surface (NST) for A2.**

The deepest thaw event, lasting 10 hours, commences at 10:00 on 29 December 2015, reaching 15 cm. An 8-hour time lag between NST and $T_{15}$ is recorded. Eleven previous freeze-thaw cycles, one each day and lasting on average 7 hours are evident for the 20 days before this event. The longest thaw event of 14 hours is recorded on 3 January 2016, occurring from 10:00-24:00. Variability for temperature initially increases from air temperature to NST. From NST onwards an increase in depth into the ground yields a decrease in variability. Highest variability is evident for NST ($s$ = 7.40), lowest for $T_{60}$ ($s$ = 5.03). At NST the average diurnal temperature range approximates 20 °C, although a maximum range of 25 °C is reached. Maximum diurnal temperatures are 17 °C, while diurnal minimums reach -17 °C. The greatest diurnal maximum temperature correlates positively with maximum thaw duration ($r$ = 0.84, $p \pm 0.0$). Similarly, the coldest diurnal minimum temperature correlates positively with shortest thaw duration ($r$ = 0.55, $p \pm 0.0$). Average diurnal maximum, minimum, and mean temperatures on those days when freeze-thaw cycles take place are 6 °C, -11 °C and -4 °C respectively.

#### 5.3.2.3.3 A3: Grunehogna

Data for A3 are available from autumn 2013 to summer 2015/16 and diurnal ranges and oscillations around 0 °C are provided in Table 100 (pg. 233). Diurnal air temperature ranges of 10 °C are rare (± 4%), and only occur in January. Of these ranges, no oscillations around 0 °C are recorded. This also translates into no oscillations indicative of potential freeze-thaw events that also exceed a diurnal range of 10 °C. For near surface temperature (NST) diurnal ranges of 10 °C are more common, occurring 20% of the time since records began. Of these ranges, more than a third reflect ranges where freeze-thaw events are possible (69% >/< 0 °C). This translates into 14% of annual oscillations indicative of potential freeze-thaw events that also exceed a diurnal temperature range of 10 °C. These ranges occur predominantly during spring and summer for NST and $T_{15}$, and for spring and winter for air temperatures. At $T_{15}$ one diurnal range exceeding 10 °C is recorded (summer 2013/2014), although 10 oscillations around 0 °C are evident for the summers of 2013/2014 and 2014/2015 (1% >/< 0 °C). Below this depth no diurnal ranges greater than 10 °C are observed. Oscillations around 0 °C are evident predominantly in summer, with none observed for winter.

**Table 100: Oscillations around 0 °C (Osc), as well as diurnal ranges exceeding 10 °C ($T_{DR}$) for A3. Annual Osc (%) reflect all oscillations around 0 °C, including those where $T_{DR}$ does not exceed 10 °C. $T_{AIR}$: air temperatures. NST: ground temperatures recorded at ± 1 cm depth. $T_{15}$: ground temperatures recorded at 15 cm depth. JJA: winter. SON: spring. DJF: summer. MAM: autumn.**

| Sensor | $T_{DR}$ (%) | Osc (%) | % of year | Annual Osc (%) | $T_{DR}$ (%) | | | | Osc (%) | | | |
|---|---|---|---|---|---|---|---|---|---|---|---|---|
| | | | | | JJA | SON | DJF | MAM | JJA | SON | DJF | MAM |
| $T_{AIR}$ | 4 | 0 | 0 | 0 | 23 | 41 | 18 | 18 | 0 | 0 | 100 | 0 |
| NST | 20 | 69 | 14 | 14 | 0 | 26 | 69 | 5 | 0 | 9 | 91 | 0 |
| $T_{15}$ | ± 0 | 0 | 0 | 1 | 0 | 0 | 100 | 0 | 0 | 0 | 100 | 0 |

Almost no positive temperatures are recorded for the air sensor (potential freeze-thaw events: 4) and thaw events occur within the upper 29 cm of the ground (active layer thickness: 29 cm). Positive air temperatures, lasting on average 2 hours, are recorded on four separate days with a maximum of 2 °C reached on 10 January 2014 at 12:00. Single diurnal ground freeze-thaw cycles occur on 89 separate days between autumn 2013 and summer 2016. Almost two-thirds (60%) of potential freeze-thaw events translate into freeze-thaw cycles (Table 101).

**Table 101: Freeze-thaw events for A3, summarised by season. $T_{AIR}$: air temperatures. NST: ground temperatures recorded at ± 1 cm depth. $T_{15}$: ground temperatures recorded at 15 cm depth. PFTE: potential freeze-thaw events. FTC: freeze-thaw cycles.**

| Season | Potential Thaw Hours at 0 °C | | | PFTE | | | FTC |
|---|---|---|---|---|---|---|---|
| | $T_{AIR}$ | NST | $T_{15}$ | $T_{AIR}$ | NST | $T_{15}$ | |
| 2013 Autumn | 0 | 0 | 0 | 0 | 0 | 0 | 0 |
| 2013 Winter | 0 | 0 | 0 | 0 | 0 | 0 | 0 |
| 2013 Spring | 0 | 47 | 0 | 0 | 5 | 0 | 1 |
| 2013/14 Summer | 6 | 466 | 55 | 4 | 53 | 9 | 21 |
| 2014 Autumn | 0 | 0 | 0 | 0 | 0 | 0 | 0 |
| 2014 Winter | 0 | 0 | 0 | 0 | 0 | 0 | 0 |
| 2014 Spring | 0 | 9 | 0 | 0 | 4 | 0 | 0 |
| 2014/15 Summer | 0 | 309 | 2 | 0 | 39 | 1 | 28 |
| 2015 Autumn | 0 | 0 | 0 | 0 | 0 | 0 | 0 |
| 2015 Winter | 0 | 0 | 0 | 0 | 0 | 0 | 0 |
| 2015 Spring | 0 | 30 | 0 | 0 | 5 | 0 | 2 |
| 2015/16 Summer | 0 | 371 | 0 | 0 | 42 | 0 | 37 |
| Total | **6** | **1 232** | **57** | **4** | **148** | **10** | **89** |

Isolated thaw events occur in spring (3%) with thaw events predominantly evident in summer, particularly December (49%) and January (39%). Eight percentage of thaw events take place in February. All thaw events represent single freeze-thaw cycles, with an average thaw duration of nine

hours ($s$ = 3). Thaw generally occurs between 10:00-18:00. Deep thaw events, lasting 13 hours each, all occur in December. Two take place in 2013 (25 and 26 December), with one additional event taking place on 30 December 2014. Thaw onset is early in the morning (07:00), ending at 20:00. Time lag of thaw to the sensor at the next depth ($T_{15}$) is 6 hours. Twenty freeze-thaw cycles last longer than 10 hours (Figure 125). Of these 16 (80%) occur in December, with four in January (20%). For these thaw events, average thaw takes place between 07:00-20:00. When average thaw duration is considered (9 hours, n = 50), 70% of freeze-thaw cycles occur in December, with 30% in January. For these thaw events, average commencement of thaw occurs at 08:00, ending at 19:00.

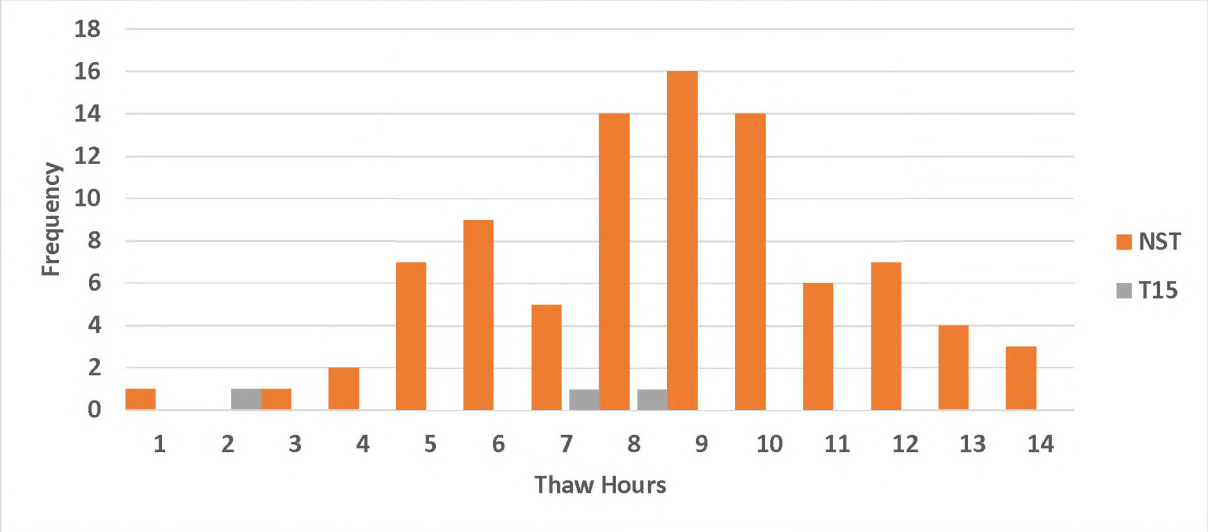


**Figure 125: Histogram of thaw duration per event per sensor depth for A3. NST: ground temperatures recorded at ± 1 cm depth. $T_{15}$: ground temperatures recorded at 15 cm depth.**

The deepest thaw event takes place on 25 December 2013, reaching 29 cm. The longest thaw duration is observed for 29 and 30 December 2015 with thaw duration of 14 hours for both days. Thaw onset is in the early morning (06:00), with freezing initiating in the evening (20:00). Temperature variability initially increases from air temperature to NST. From NST onwards an increase in depth into the ground yields a decrease in variability. Highest variability is observed for NST ($s$ = 9.58), lowest for $T_{60}$ ($s$ = 6.42). Average diurnal temperature ranges approximate 17 °C at NST, although a maximum diurnal range of 26 °C is reached. Maximum diurnal temperatures are 16 °C, while diurnal minimums reach -17 °C. The greatest diurnal maximum correlates positively with maximum thaw duration ($r$ = 0.80, $p$ ± 0.0). Similarly, the coldest diurnal minimum correlates positively with shortest thaw duration ($r$ = 0.45, $p$ ± 0.0). Average diurnal maximum, minimum, and mean temperatures on days when freeze-thaw cycles take place are 7 °C, -10 °C and -2 °C respectively.

#### 5.3.2.3.4 A4: Robertskollen

Data for A4 are available from autumn 2013 to summer 2015/16. Diurnal ranges and oscillations around 0 °C are provided in Table 102 (pg. 235). Diurnal air temperature ranges of 10 °C are rare (± 6%). Nevertheless, such ranges are recorded throughout the year. Of these ranges, oscillations around 0 °C are observed at 19%. This translates into 1% of oscillations indicative of potential freeze-thaw events

that also exceed a diurnal range of 10 °C. Annual oscillations occur less than 10% of the time. For near surface temperatures (NST) diurnal ranges of 10 °C are more common, occurring 14% of the time since records began. These ranges are observed predominantly during spring and summer. Of these ranges, three quarters reflect ranges where freeze-thaw events are possible (79% >/< 0 °C). This translates into 11% of annual oscillations indicative of potential freeze-thaw events that also exceed a diurnal range of 10 °C. Annually, oscillations indicative of potential freeze-thaw events occur 19% of the time. From $T_{15}$ deeper into the ground no ranges exceeding 10 °C are recorded. Nevertheless, some oscillations around 0 °C are evident, equating to less than 10% of the time since records began at $T_{15}$, with $T_{30}$ and $T_{45}$ reflecting 2%. Diurnal ranges exceeding 10 °C for NST occur predominantly in summer, followed by spring. For air temperatures such ranges are recorded throughout the year, with most taking place from spring to autumn. Oscillations around 0 °C are recorded only during summer from $T_{15}$ deeper into the ground. At NST such oscillations occur predominantly in summer, with a fraction also observed in spring. For air temperatures such oscillations occur predominantly during summer months, with limited oscillations observed during autumn. Ground temperatures also show days on which temperatures don't dip below 0 °C. Such ranges are observed for all sensors except air temperatures and occur exclusively during summer months.

**Table 102: Oscillations around 0 °C (Osc), as well as diurnal ranges exceeding 10 °C ($T_{DR}$) for A4. Annual Osc (%) reflect all oscillations around 0 °C, including those where $T_{DR}$ does not exceed 10 °C. $T_{AIR}$: air temperatures. NST: ground temperatures recorded at ± 1 cm depth. The subscript following 'T' indicates the depth of the sensor (in centimetres) used to record ground temperature. JJA: winter. SON: spring. DJF: summer. MAM: autumn.**

| Sensor | $T_{DR}$ (%) | Osc (%) | % of year | Annual Osc (%) | $T_{DR}$ (%) | | | | Osc (%) | | | |
|---|---|---|---|---|---|---|---|---|---|---|---|---|
| | | | | | JJA | SON | DJF | MAM | JJA | SON | DJF | MAM |
| $T_{AIR}$ | 6 | 19 | 1 | 7 | 11 | 34 | 30 | 25 | 0 | 0 | 94 | 6 |
| NST | 14 | 79 | 11 | 19 | 1 | 26 | 74 | 0 | 0 | 15 | 85 | 0 |
| $T_{15}$ | 0 | 0 | 0 | 8 | 0 | 0 | 0 | 0 | 0 | 2 | 2 | 0 |
| $T_{30}$ | 0 | 0 | 0 | 2 | 0 | 0 | 0 | 0 | 0 | 0 | 100 | 0 |
| $T_{45}$ | 0 | 0 | 0 | 2 | 0 | 0 | 0 | 0 | 0 | 0 | 100 | 0 |

Relatively numerous positive air temperatures are recorded (potential freeze-thaw events: 111). Similarly, numerous potential freeze-thaw events and freeze-thaw cycles are evident and thaw events occur within the upper 58 cm of the ground (active layer thickness: 58 cm). Positive air temperatures are registered on 81 separate days, with most of these days (n = 33) occurring during the summer of 2013/14. Positive air temperatures are reached six times for the summer of 2014/15 and 24 times for 2015/16. Isolated positive temperatures are also recorded in spring 2013 (n = 2 occurrences), and spring 2015 (n = 3 occurrences). A maximum of 6 °C is reached for air temperatures on 10 January 2014 at 12:00 and positive temperatures are maintained for ± 5 hours on average. Diurnal ground freeze-thaw cycles take place on 128 separate days between autumn 2013 and summer 2016, yielding 116 freeze-thaw cycles in total. Less freeze-thaw cycles are observed due to some cycles spanning a few days. Just over half (53%) of potential freeze-thaw events translate into freeze-thaw cycles (Table 103, pg. 236). Twenty thaw events occur during spring (18 %), with fifteen occurring toward the end of summer in February (12%). Most thaw events take place during December and January (39 events per month: 35%).

**Table 103: Freeze-thaw events for A4, summarised by season. $T_{AIR}$: air temperatures. NST: ground temperatures recorded at ± 1 cm depth. The subscript following 'T' indicates the depth of the sensor (in centimetres) used to record ground temperature. PFTE: potential freeze-thaw events. FTC: freeze-thaw cycles.**

| Season | Potential Thaw Hours at 0 °C | | | | | PFTE | | | | | FTC |
|---|---|---|---|---|---|---|---|---|---|---|---|
| | $T_{AIR}$ | NST | $T_{15}$ | $T_{30}$ | $T_{45}$ | $T_{AIR}$ | NST | $T_{15}$ | $T_{30}$ | $T_{45}$ | |
| 2013 Autumn | 0 | 0 | 0 | 0 | 0 | 0 | 0 | 0 | 0 | 0 | 0 |
| 2013 Winter | 0 | 0 | 0 | 0 | 0 | 0 | 0 | 0 | 0 | 0 | 0 |
| 2013 Spring | 7 | 108 | 6 | 0 | 0 | 3 | 15 | 2 | 0 | 0 | 5 |
| 2013/14 Summer | 226 | 1 079 | 952 | 847 | 494 | 49 | 58 | 27 | 7 | 11 | 35 |
| 2014 Autumn | 0 | 0 | 0 | 0 | 0 | 0 | 0 | 0 | 0 | 0 | 0 |
| 2014 Winter | 0 | 0 | 0 | 0 | 0 | 0 | 0 | 0 | 0 | 0 | 0 |
| 2014 Spring | 0 | 88 | 0 | 0 | 0 | 0 | 10 | 0 | 0 | 0 | 10 |
| 2014/15 Summer | 89 | 807 | 561 | 290 | 78 | 24 | 58 | 25 | 7 | 2 | 27 |
| 2015 Autumn | 0 | 0 | 0 | 0 | 0 | 0 | 0 | 0 | 0 | 0 | 0 |
| 2015 Winter | 0 | 0 | 0 | 0 | 0 | 0 | 0 | 0 | 0 | 0 | 0 |
| 2015 Spring | 4 | 93 | 0 | 0 | 0 | 3 | 11 | 0 | 0 | 0 | 5 |
| 2015/16 Summer | 110 | 907 | 749 | 353 | 56 | 32 | 65 | 33 | 8 | 3 | 34 |
| Total | **436** | **3 082** | **2 268** | **1 490** | **628** | **111** | **217** | **87** | **22** | **16** | **116** |

Average thaw duration is 18 hours ($s$ = 18) with thaw generally occurring between 08:00-02:00 the following day (Table 104). No multiple diurnal cycles are observed but numerous thaw events exceed one day, taking place during every December since observations commenced, as well as January 2014. For thaw events exceeding one day in length the longest event approaches 115 hours, spanning almost five days during December 2013. This event translates into thaw of the ground past $T_{15}$ (Table 104). Thaw onset is on 21 December 2013 at 07:00 and lasts until 02:00 on 26 December. The deepest thaw event, lasting 63 hours, commenced at 04:00 on 4 January 2014 until 19:00 on 11 January. This thaw event yields thawing of the ground past $T_{45}$ for 97 hours, reaching an approximate depth of 58 cm.

**Table 104: Thaw events exceeding one 24-hour period (one day) for A4.**

| Year | Day | Start | End | Duration (hrs) | Depth Reached (cm) |
|---|---|---|---|---|---|
| 2013 | 16 Dec | 10:00 | 22:00 + 1 Day | 35 | > 2 |
| | 21 Dec | 07:00 | 02:00 + 5 Days | 115 | > 15 |
| 2014 | 1 Jan | 03:00 | 04:00 + 1 Day | 25 | > 2 |
| | 4 Jan | 04:00 | 19:00 + 2 Days | 63 | > 45 |
| | 9 Jan | 06:00 | 21:00 + 4 Days | 111 | > 30 |
| | 16 Jan | 05:00 | 24:00 + 2 Days | 67 | > 2 |
| | 22 Dec | 06:00 | 24:00 + 3 Days | 90 | > 30 |
| | 31 Dec | 02:00 | 01:00 + 2 Days | 47 | > 2 |
| 2015 | 29 Dec | 01:00 | 22:00 +3 Days | 93 | > 2 |

The depth at which maximum duration of thaw is observed is at $T_{30}$ (±15 days), followed by $T_{45}$ (± nine days) (Table 105). The average diurnal cycle depth (*d*) for $T_{30}$ and $T_{45}$ for these times is 8 cm and 15 cm respectively. Average and maximum thaw duration increases with depth to $T_{45}$, decreasing after this depth. Similarly, variability increases with depth to $T_{45}$, after which it decreases. Time lag of thaw to the sensor at the next depth ($T_{15}$; $T_{30}$; $T_{45}$) is ± six; 17; and 37 hours respectively. Once near-thawing conditions have been reached at a specific depth subsequent delay to thaw is shortened, *i.e.* the initial delay is longer than subsequent delay to thawing events.

**Table 105: Thaw duration parameters for A4 ground sensors. $T_{AIR}$: air temperatures. NST: ground temperatures recorded at ± 1 cm depth. The subscript following 'T' indicates the depth of the sensor (in centimetres) used to record ground temperature.**

| Parameter | Thaw Duration (Hours) | | | |
|---|---|---|---|---|
| | NST | $T_{15}$ | $T_{30}$ | $T_{45}$ |
| Average | 18 | 34 | 82 | 51 |
| *s* | 18 | 51 | 88 | 57 |
| Max | 115 | 202 | 356 | 213 |
| Min | 1 | 2 | 1 | 11 |
| Delay | n/a | 6 | 17 | 37 |

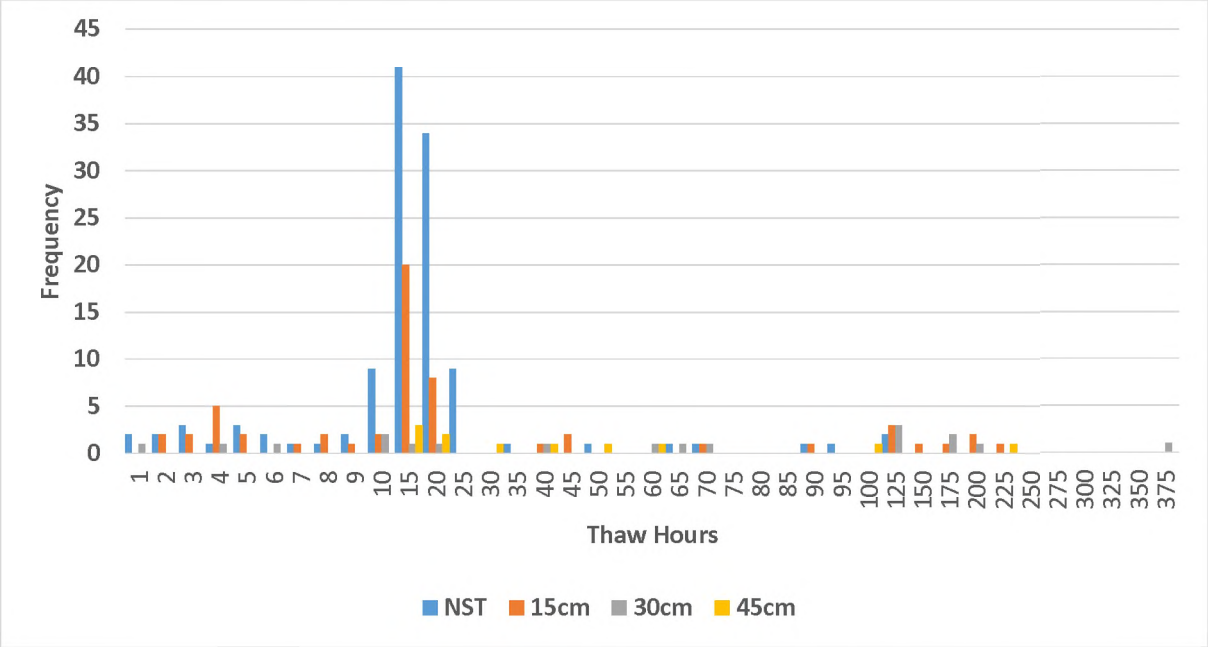


**Figure 126: Histogram of thaw duration per event per sensor depth for A4. NST: ground temperatures recorded at ± 1 cm depth. The subscript following 'T' indicates the depth of the sensor (in centimetres) used to record ground temperature.**

Of the observed freeze-thaw cycles, 92 last longer than 10 hours (Figure 126) and most freeze-thaw cycles (n = 41) last 15 hours on average. Thirty-nine (42%) freeze-thaw cycles exceeding 10 hours in duration occur in December, with 36 (39%) and six (7%) in January and February respectively. The remaining 11 freeze-thaw cycles take place during November (12%). For these thaw events, average commencement of thaw takes is 06:00, ending at 04:00 the following day. When the average thaw duration is considered (18 hours, n = 35), 66% of freeze-thaw cycles take place in December, with 34% in January. For these thaw events, average commencement of thaw is at 04:00, ending at 13:00 the following day. Variability for temperature recorded initially increases from air temperatures to NST.

From NST onwards an increase in depth into the ground yields a decrease in variability. Highest variability is evident for NST ($s$ = 9.81), lowest at $T_{60}$ ($s$ = 6.94). The average diurnal temperature range approximates 12 °C, although a maximum range of 16 °C is reached. Maximum diurnal temperature is 16 °C, while diurnal minimum is -14 °C. The greatest diurnal maximum correlates positively with maximum thaw duration ($r$ = 0.83, $p \pm 0.0$). Similarly, the coldest diurnal minimum correlates positively with shortest thaw duration ($r$ = 0.81, $p \pm 0.0$). Average diurnal maximum, minimum, and mean temperature on those days when freeze-thaw cycles occur is 8 °C, -4 °C and 2 °C respectively.

#### *5.3.2.3.4.1 Higher-frequency*

Higher-frequency temperature data using an ACR system, recorded at four-minute intervals, are available from 17-24 January 2015 (n = eight days) for air temperature, near surface temperature (NST), ground surface temperature (GST), $T_5$, $T_{10}$, $T_{15}$, and $T_{20}$. Active layer thickness for 2015 approaches 50 cm (discussed above in 5.3.2.2 Seasonal frost environment, pg. 213 onwards) and all depths record positive temperatures on 17 and 18 January. $T_5$-$T_{15}$ reflect positive temperatures on 24 January, with NST and GST for 21 January as well. During this period the highest and lowest temperatures are recorded at NST and the intensity of potential frost events (diurnal minimum temperature) ranges from -6 °C to -4 °C (17 and 19 January respectively). Four potential freeze-thaw events are recorded for NST and GST. Of these potential freeze-thaw events no freeze-thaw cycle is evident and the lack of discernible freeze-thaw cycles nor exotherms, compares with freeze-thaw cycles (or the lack thereof) during this observation period as discussed in the previous section (5.3.2.3.4 A4: Robertskollen, pg. 234). Diurnal maximums range from 17 °C to -2 °C (17 and 19 January respectively). The diurnal range is 23 °C, with minimums of -6 °C. A storm event lead to snowfall and the insulating effect of this snow is evident from 19-21 January and 22-24 January (Figure 127, pg. 239). The narrowest diurnal temperature range occurs on 19 January during the snowfall event. Diurnal mean temperature is -1 °C and sub-zero temperatures are reached every day for all sensors. Variability initially increases from air temperatures to NST and then decreases with depth into the ground. Highest variability is observed for NST ($s$ = 3.40), lowest for $T_{20}$ ($s$ = 0.60). In comparison, diurnal mean temperature decreases with depth with the highest mean temperature recorded at NST (-0.6 °C), and the lowest at $T_{20}$ (-1.2 °C). Diurnal mean air temperature is -5 °C.

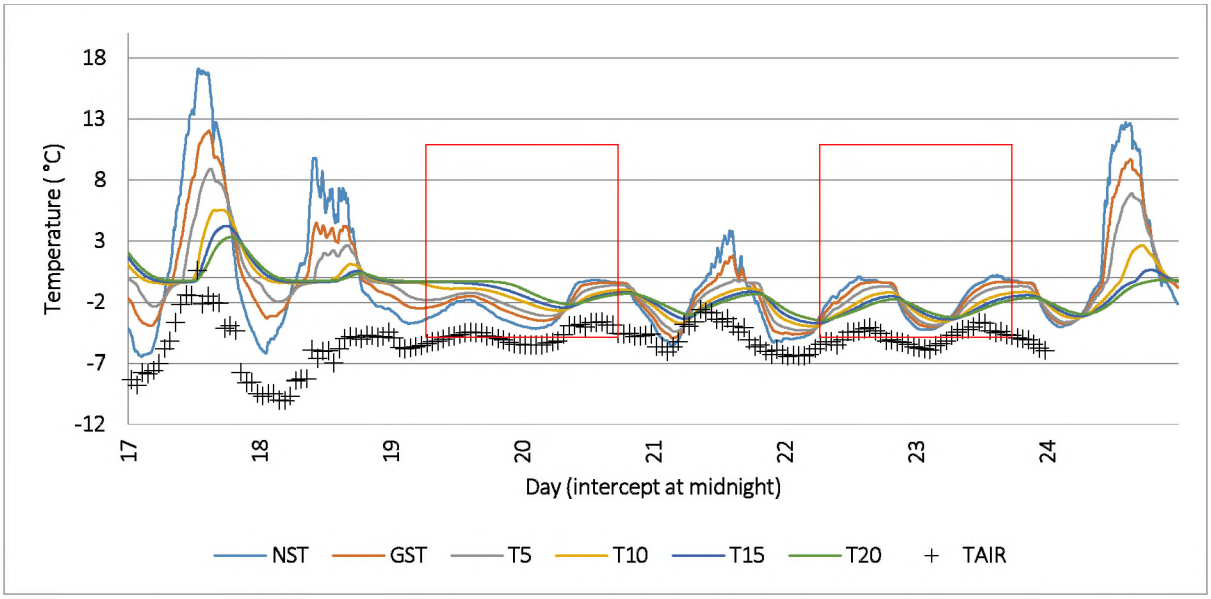


**Figure 127: Diurnal cycles for an eight-day period from 17-25 January 2015. Snowfall is indicated with red squares. NST: ground temperatures recorded at ± 1 cm depth. GST: ground temperatures recorded at ± 2 cm depth. $T_5$: ground temperatures recorded at 5 cm depth. $T_{10}$: ground temperature recorded at 10 cm depth. $T_{15}$: ground temperature recorded at 15 cm depth. $T_{20}$: ground temperature recorded at 20 cm depth. $T_{AIR}$: air temperatures.**

The thawing and freezing index for the various sensors, given as days, are listed in Table 106. Thawing indices of zero are evident during the storm event and this index decreases with increasing depth into the ground. Overall, thawing indices are marginally positive and freezing indices marginally negative with freezing indices generally exceeding thawing indices. The balance of degree days is ± 5 toward the freezing index (for air temperatures), and generally increases from NST (± 0.5) to ± 1.2 for $T_{20}$. The thermal offset is skewed towards positive values with the largest offset of 8.3 calculated for 17 January and smallest values calculated during the snowfall event.

**Table 106: The freezing index (FI) and thawing index (TI) for the various sensor depth for A4 from 17-24 January 2015. $T_{AIR}$: air temperatures. NST: ground temperatures recorded at ± 1 cm depth. GST: ground temperatures recorded at ± 2 cm depth. The subscript following 'T' indicates the depth of the sensor (in centimetres) used to record ground temperature. SO: thermal offset. DD: degree days.**

| Day | FI | | | | | | | TI | | | | | | | SO |
|---|---|---|---|---|---|---|---|---|---|---|---|---|---|---|---|
| | $T_{AIR}$ | NST | GST | $T_5$ | $T_{10}$ | $T_{15}$ | $T_{20}$ | $T_{AIR}$ | NST | GST | $T_5$ | $T_{10}$ | $T_{15}$ | $T_{20}$ | |
| 17 | -5.1 | -2.0 | -1.1 | -0.5 | -0.2 | -0.1 | -0.1 | 0.0 | 5.2 | 3.6 | 2.6 | 1.7 | 1.4 | 1.2 | 8.3 |
| 18 | -6.8 | -1.5 | -0.9 | -0.6 | -0.2 | -0.2 | -0.1 | 0.0 | 2.4 | 1.3 | 0.7 | 0.2 | 0.1 | 0.1 | 7.7 |
| 19 | -5.1 | -2.9 | -2.2 | -1.6 | -0.9 | -0.6 | -0.3 | 0.0 | 0.0 | 0.0 | 0.0 | 0.0 | 0.0 | 0.0 | 2.2 |
| 20 | -4.6 | -2.0 | -1.8 | -1.8 | -1.8 | -1.8 | -1.6 | 0.1 | 0.0 | 0.0 | 0.0 | 0.0 | 0.0 | 0.0 | 2.6 |
| 21 | -4.6 | -2.4 | -2.2 | -2.1 | -2.2 | -2.2 | -2.1 | 0.0 | 0.5 | 0.2 | 0.0 | 0.0 | 0.0 | 0.0 | 2.7 |
| 22 | -5.3 | -2.2 | -2.3 | -2.5 | -2.6 | -2.7 | -2.7 | 0.0 | 0.0 | 0.0 | 0.0 | 0.0 | 0.0 | 0.0 | 3.1 |
| 23 | -4.9 | -1.7 | -1.8 | -2.0 | -2.3 | -2.4 | -2.4 | 0.1 | 0.0 | 0.0 | 0.0 | 0.0 | 0.0 | 0.0 | 3.2 |
| 24 | -2.9 | -1.3 | -1.3 | -1.3 | -1.4 | -1.5 | -1.6 | 0.1 | 3.6 | 2.6 | 1.8 | 0.5 | 0.1 | 0.0 | 5.0 |
| Balance * | -4.9 | -0.5 | -0.7 | -0.9 | -1.1 | -1.2 | -1.2 | * Difference of DD between FI and TI | | | | | | | |

#### 5.3.2.3.5 A5: Schumacherfjellet

Data for A5 are available from autumn 2013 to summer 2015/16. Diurnal ranges and oscillations around 0 °C are provided in Table 107. Diurnal air temperature ranges of 10 °C are rare (± 6%). However, these occur throughout the year. Of these ranges, oscillations around 0 °C are recorded 4% of the time. This translates into no oscillations indicative of potential freeze-thaw events that also exceed diurnal ranges of 10 °C. For near surface temperatures (NST) diurnal ranges of 10 °C are less common, occurring 5% of the time since records began. Of these ranges, a third reflect ranges where freeze-thaw events are possible (66% >/< 0 °C). This translates into 3% of annual oscillations indicative of potential freeze-thaw events that are also greater than 10 °C. Annual oscillations indicative of potential freeze-thaw events occur 4% of the time. From $T_{15}$ deeper into the ground no diurnal ranges exceeding 10 °C are recorded. However, four oscillations around 0 °C are recorded at $T_{15}$, with one single oscillation at $T_{30}$ (0.4% >/< 0 °C and 0.1% >/< 0 °C respectively). These oscillations take place exclusively in summer. Diurnal ranges greater than 10 °C are dominant in spring and summer (at NST); such ranges for air temperatures are observed in winter and spring. Oscillations around 0 °C are recorded during summer for all sensors, although such ranges also take place during spring at NST and $T_{15}$.

**Table 107: Oscillations around 0 °C (Osc), as well as diurnal ranges exceeding 10 °C ($T_{DR}$) for A5. Annual Osc (%) reflect all oscillations around 0 °C, including those where $T_{DR}$ does not exceed 10 °C. $T_{AIR}$: air temperatures. NST: ground temperatures recorded at ± 1 cm depth. The subscript following 'T' indicates the depth of the sensor (in centimetres) used to record ground temperature. JJA: winter. SON: spring. DJF: summer. MAM: autumn.**

| Sensor | $T_{DR}$ (%) | Osc (%) | % of year | Annual Osc (%) | $T_{DR}$ (%) | | | | Osc (%) | | | |
|---|---|---|---|---|---|---|---|---|---|---|---|---|
| | | | | | JJA | SON | DJF | MAM | JJA | SON | DJF | MAM |
| $T_{AIR}$ | 6 | 4 | 0 | 1 | 29 | 44 | 18 | 9 | 0 | 0 | 100 | 0 |
| NST | 5 | 66 | 3 | 4 | 4 | 19 | 75 | 2 | 0 | 4 | 96 | 0 |
| $T_{15}$ | 0 | 0 | 0 | ± 0 | 0 | 0 | 0 | 0 | 0 | 0 | 100 | 0 |
| $T_{30}$ | 0 | 0 | 0 | ± 0 | 0 | 0 | 0 | 0 | 0 | 0 | 100 | 0 |

Few positive air temperatures are recorded (potential freeze-thaw events: 13) and thaw events occur within the upper 29 cm of the ground (active layer thickness: 29 cm). Positive air temperatures are evident on 11 separate days, with most days (n = 8) in summer 2013/14. Positive air temperatures are reached twice in summer 2014/15, once in summer 2015/16. Maximum air temperature (2 °C) is attained on 16 January 2014 at 09:00. The average duration of positive temperatures maintained is 2 hours. Twenty-five diurnal ground freeze-thaw cycles occur for 22 separate days between autumn 2013 and summer 2016. A little more than half (57%) of these translate into freeze-thaw cycles (Table 108).

**Table 108: Freeze-thaw events for A5, summarised by season. $T_{AIR}$: air temperatures. NST: ground temperatures recorded at ± 1 cm depth. $T_{15}$: ground temperatures recorded at 15 cm depth. PFTE: potential freeze-thaw events. FTC: freeze-thaw cycles.**

| Season | Potential Thaw Hours at 0 °C | | | PFTE | | | FTC |
|---|---|---|---|---|---|---|---|
| | $T_{AIR}$ | NST | $T_{15}$ | $T_{AIR}$ | NST | $T_{15}$ | |
| 2013 Autumn | 0 | 0 | 0 | 0 | 0 | 0 | 0 |
| 2013 Winter | 0 | 0 | 0 | 0 | 0 | 0 | 0 |

| Season | Potential Thaw Hours at 0 °C | | | PFTE | | | FTC |
|---|---|---|---|---|---|---|---|
| | $T_{AIR}$ | NST | $T_{15}$ | $T_{AIR}$ | NST | $T_{15}$ | |
| 2013 Spring | 0 | 1 | 0 | 0 | 1 | 0 | 0 |
| 2013/14 Summer | 14 | 201 | 30 | 10 | 30 | 4 | 8 |
| 2014 Autumn | 0 | 0 | 0 | 0 | 0 | 0 | 0 |
| 2014 Winter | 0 | 0 | 0 | 0 | 0 | 0 | 0 |
| 2014 Spring | 0 | 0 | 0 | 0 | 0 | 0 | 0 |
| 2014/15 Summer | 3 | 46 | 0 | 3 | 12 | 0 | 3 |
| 2015 Autumn | 0 | 0 | 0 | 0 | 0 | 0 | 0 |
| 2015 Winter | 0 | 0 | 0 | 0 | 0 | 0 | 0 |
| 2015 Spring | 0 | 5 | 0 | 0 | 1 | 0 | 0 |
| 2015/16 Summer | 57 | 0 | 153 | 0 | 0 | 0 | 14 |
| Total | **74** | **253** | **183** | **13** | **44** | **4** | **25** |

No thaw events occur in spring with such events predominantly taking place in December (64%), with just over a third occurring in January (36%). Average thaw duration is 6 hours ($s$ = 4) with thaw generally occurring between 10:00-18:00. Four freeze-thaw cycles last longer than 10 hours (Figure 128). Of these two (50%) take place during December, with another two in January (50%). For these thaw events, average commencement is 08:00, ending at 22:00. When the average thaw duration is considered (6 hours, n = 10), 70% of freeze-thaw cycles occur in December, with 30% in January. For these thaw events, average commencement of thaw is 09:00, ending at 19:00.

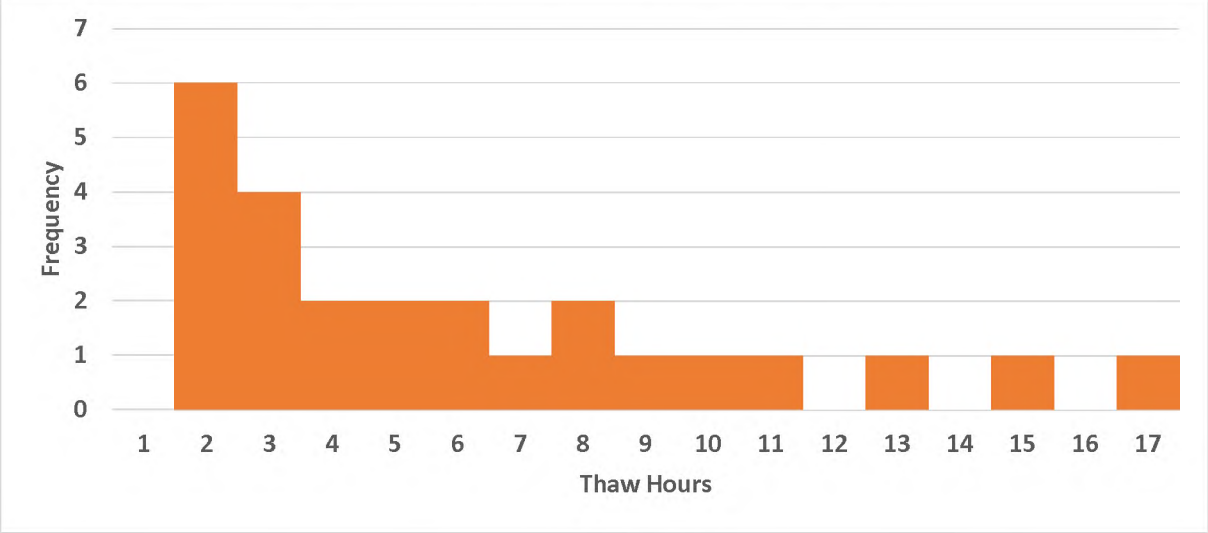


**Figure 128: Histogram of thaw duration per event per sensor at the near surface (NST) for A5.**

Multiple thaw events are evident on three days. Two freeze-thaw cycles occur on 29 and 30 December 2015, as well as two on 13 January 2016. The initial thaw event lasts ± 3 hours, commencing at 09:00. The second thaw event generally starts at 14:00 and lasts 4 hours. Deep thaw events, lasting 12 hours on average, all occur during the summer of 2013/14. Three occur between 21-23 December 2013 with

one additional event taking place on 17 January 2014. Thaw onset is in the morning, ranging from 04:00-11:00, ending at 20:00. Time lag of thaw to the sensor at the next depth ($T_{15}$) is 6 hours. The deepest thaw event occurs on 23 December 2013, reaching 29 cm. This is also the longest thaw event, lasting 17 hours. Temperature variability initially increases from air temperature to NST. From NST onwards an increase in depth into the ground yields a decrease in variability. Highest variability is calculated for NST ($s$ = 7.62), lowest for $T_{60}$ ($s$ = 6.44). The average diurnal temperature range approximates 11 °C, although a maximum range of 17 °C is reached. Maximum diurnal temperature is 9 °C, while the minimum is -11 °C. The greatest diurnal maximum temperature correlates positively with maximum thaw duration ($r$ = 0.75, $p$ ± 0.0). Similarly, the coldest diurnal minimum temperature correlates positively with shortest thaw duration ($r$ = 0.68, $p$ ± 0.0). Average diurnal maximum, minimum, and mean temperatures on those days when freeze-thaw cycles are evident are 4 °C, -7 °C and -2 °C respectively.

#### 5.3.2.3.6 A6: Slettfjell

Data for A6 are available from autumn 2008 to summer 2015/16. Diurnal ranges and oscillations around 0 °C are provided in Table 109. Diurnal air temperature ranges exceeding 10 °C are rare (± 8%). Nevertheless, such ranges occur throughout the year. Of these ranges, ± 1% reflect maximums above and minimums below 0 °C, *i.e.* oscillations around 0 °C. This translates into ± 0% of annual oscillations indicative of potential freeze-thaw events that also exceed a diurnal temperature range of 10 °C. For near surface temperatures (NST) diurnal ranges of 10 °C occur approximately the same amount of time (± 7%). Of these ranges, approximately one quarter reflect ranges where freeze-thaw events are possible (24% >/< 0 °C). This translates into 2% of annual oscillations indicative of potential freeze-thaw events whose tange is also greater than 10 °C. From $T_{15}$ deeper into the ground no diurnal ranges exceeding 10 °C are recorded, as are no oscillations around 0 °C (0% >/< 0 °C). Diurnal ranges greater than 10 °C occur throughout the year, although NST shows a higher prevalence for summer and spring. Oscillations around 0 °C are recorded predominantly during summer, with none observed for autumn and winter.

**Table 109: Oscillations around 0 °C (Osc), as well as diurnal ranges exceeding 10 °C ($T_{DR}$) for A6. Annual Osc (%) reflect all oscillations around 0 °C, including those where $T_{DR}$ does not exceed 10 °C. $T_{AIR}$: air temperatures. NST: ground temperatures recorded at ± 1 cm depth. JJA: winter. SON: spring. DJF: summer. MAM: autumn.**

| Sensor | $T_{DR}$ (%) | Osc (%) | % of year | Annual Osc (%) | $T_{DR}$ (%) | | | | Osc (%) | | | |
|---|---|---|---|---|---|---|---|---|---|---|---|---|
| | | | | | JJA | SON | DJF | MAM | JJA | SON | DJF | MAM |
| $T_{AIR}$ | 8 | 1 | 0 | 0 | 23 | 39 | 18 | 20 | 0 | 0 | 100 | 0 |
| NST | 7 | 24 | 2 | 2 | 8 | 35 | 50 | 7 | 0 | 0 | 85 | 15 |

Positive air temperatures (0.5 °C) at A6 are recorded for 1 hour on 21 December 2013 from 13:00-14:00 only. Single diurnal ground freeze-thaw cycles occur on seven separate days between autumn 2013 and summer 2016 and one third (33%) of potential freeze-thaw events translate into freeze-thaw cycles (Table 110, pg. 243).

**Table 110: Freeze-thaw events for A6, summarised by season. $T_{AIR}$: air temperatures. NST: ground temperatures recorded at ± 1 cm depth. PFTE: potential freeze-thaw events. FTC: freeze-thaw cycles.**

| Season | Potential Thaw Hours at 0 °C | | PFTE | | FTC |
|---|---|---|---|---|---|
| | $T_{AIR}$ | NST | $T_{AIR}$ | NST | |
| 2013 Autumn | 0 | 0 | 0 | 0 | 0 |
| 2013 Winter | 0 | 0 | 0 | 0 | 0 |
| 2013 Spring | 0 | 4 | 0 | 3 | 2 |
| 2013/14 Summer | 1 | 45 | 1 | 11 | 4 |
| 2014 Autumn | 0 | 0 | 0 | 0 | 0 |
| 2014 Winter | 0 | 0 | 0 | 0 | 0 |
| 2014 Spring | 0 | 0 | 0 | 0 | 0 |
| 2014/15 Summer | 0 | 32 | 0 | 7 | 1 |
| 2015 Autumn | 0 | 0 | 0 | 0 | 0 |
| 2015 Winter | 0 | 0 | 0 | 0 | 0 |
| 2015 Spring | 0 | 0 | 0 | 0 | 0 |
| 2015/16 Summer | 0 | 8 | 0 | 0 | 0 |
| Total | 1 | 89 | 1 | 21 | 7 |

Two thaw events take place during spring 2013 (November; 29%), four in January 2014 (57%), and one in December 2015 (14%). Thaw events occur within the upper 12 cm of the ground (active layer thickness: 12 cm) and average thaw duration is 5 hours ($s$ = 3) with thaw occurring between 10:00-13:00. One freeze-thaw cycle lasts longer than 10 hours (Figure 129, pg. 244), commencing at 05:00 on 10 January 2014 and ending at 17:00 the same day. When the average thaw duration is considered (5 hours, n = 3), 33% of freeze-thaw cycles take place in December, with 67% in January. For these thaw events, average commencement of thaw is 09:00, ending at 17:00. All thaw events represent single freeze-thaw cycles with deepest thaw occurring in December 2014, reaching a depth of 12 cm. This is also the longest thaw event recorded, lasting 12 hours from 05:00-17:00. Variability for temperature initially increases from air temperatures to NST. From NST onwards an increase in depth into the ground yields a decrease in variability. Highest variability is observed at NST ($s$ = 7.72), lowest at $T_{60}$ ($s$ = 6.04). The average diurnal temperature range approximates 14 °C, although maximum ranges of 19 °C are reached. Maximum diurnal temperature is 5 °C, as are minimums of -17 °C. The greatest diurnal maximum correlates positively with maximum thaw duration ($r$ = 0.86, $p < 0.05$). The coldest diurnal minimum temperatures do not correlate significantly to thaw duration. Average diurnal maximum, minimum, and mean temperature on those days when freeze-thaw cycles occur is 3 °C, -11 °C and -5 °C respectively.

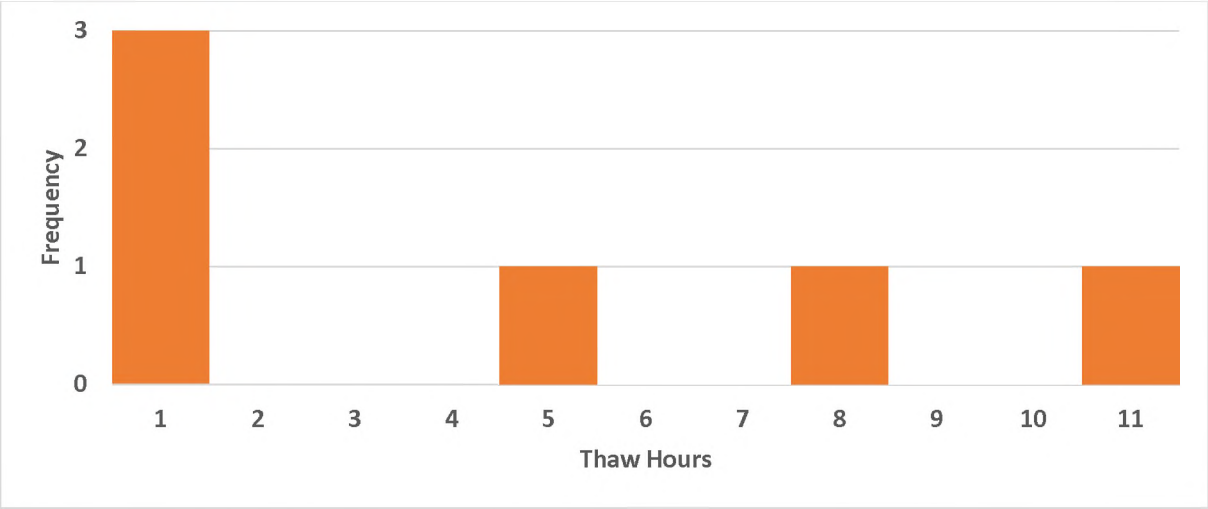


**Figure 129: Histogram of thaw duration per event per sensor at the near surface (NST) for A6.**

#### 5.3.2.3.7 A7: Troll 1

Data for A7 are available from autumn 2007 to summer 2015/16. Diurnal ranges and oscillations around 0 °C are given in Table 111. Diurnal air temperature ranges of 10 °C occur about a third of the time (± 29%). Furthermore, such ranges occur throughout the year. Nevertheless, only ± 1% of these ranges reflect maximums above and minimums below 0 °C, *i.e.* oscillations around 0 °C. This translates into approximately no annual oscillations indicative of potential freeze-thaw events whose diurnal temperature range exceeds 10 °C. However, when evaluating all diurnal ranges, the proportion of oscillations where potential freeze-thaw events may occur rises to 2%. For near surface temperature (NST) diurnal ranges of 10 °C are less common, occurring 3% of the time since records began. Furthermore, such ranges are only observed from August-February. Of these ranges, more than half reflect ranges where freeze-thaw events are possible (56% >/< 0 °C). This translates into 2% of oscillations indicative of potential freeze-thaw events that also exceed a diurnal temperature range of 10 °C. Annually, when evaluating all diurnal ranges, less than on tenth of diurnal ranges reflect those where potential freeze-thaw events may occur (9% >/< 0 °C). From $T_{50}$ deeper into the ground no diurnal ranges exceeding 10 °C are recorded, as are no oscillations around 0 °C (0% >/< 0 °C). Diurnal ranges exceeding 10 °C occur throughout the year for air temperatures, although less of such ranges are recorded for summer months. For NST most of these ranges are evident in summer, followed by approximately a third recorded in spring. Oscillations around 0 °C are recorded predominantly in summer, with none observed for autumn or winter. Such oscillations extend into autumn for air temperatures, compared to NST where these are observed only in spring and summer.

**Table 111: Oscillations around 0 °C (Osc), as well as diurnal ranges exceeding 10 °C ($T_{DR}$) for A7. Annual Osc (%) reflect all oscillations around 0 °C, including those where $T_{DR}$ does not exceed 10 °C. $T_{AIR}$: air temperatures. NST: ground temperatures recorded at ± 1 cm depth. JJA: winter. SON: spring. DJF: summer. MAM: autumn.**

| Sensor | $T_{DR}$ (%) | Osc (%) | % of year | Annual Osc (%) | $T_{DR}$ (%) | | | | Osc (%) | | | |
|---|---|---|---|---|---|---|---|---|---|---|---|---|
| | | | | | JJA | SON | DJF | MAM | JJA | SON | DJF | MAM |
| $T_{AIR}$ | 29 | 1 | ± 0 | 2 | 29 | 29 | 14 | 28 | 0 | 0 | 94 | 6 |
| NST | 3 | 56 | 2 | 9 | 2 | 30 | 63 | 5 | 0 | 7 | 93 | 0 |

Several positive air temperatures are recorded (potential freeze-thaw events: 109). While numerous potential ground freeze-thaw events are evident and thaw events occur within the upper 38 cm of the ground freeze-thaw cycles are sporadic and rare, only occurring on ten days in December 2013. Positive air temperatures is generally reached in summer (Table 112), especially those of 2009/10 and 2012/13 (n = 27 and n = 40 occurrences respectively). Positive air temperatures are reached in spring 2012 (n = 2), with a maximum air temperature of 5 °C attained at 17:00 on 13 January 2013. Positive temperatures are maintained for ± 2 hours on average. Twenty-three potential freeze-thaw events are evident in the time span of autumn 2013 to summer 2015/16. Average positive temperatures are the same as those calculated for the entire time span of 2007-2016. Average duration of positive temperatures achieved during this time is 3 hours. Maximum diurnal temperature during 2013-2016 is 4 °C (6 December 2015 at 09:00). Eighteen ground freeze-thaw cycles occur on ten separate days from autumn 2008 to summer 2015/16, all taking place in December 2013. More cycles are observed due to occasional multiple cycles taking place in a 24-hour period. Only 6% of potential freeze-thaw events translate into freeze-thaw cycles (Table 112).

**Table 112: Freeze-thaw events for A7, summarised by season. * insufficient data available. $T_{AIR}$: air temperatures. NST: ground temperatures recorded at ± 1 cm depth. PFTE: potential freeze-thaw events. FTC: freeze-thaw cycles.**

| Season | Potential Thaw Hours at 0 °C | | PFTE | | FTC |
|---|---|---|---|---|---|
| | $T_{AIR}$ | NST | $T_{AIR}$ | NST | |
| 2007/08 Summer | 2 | 25 | 2 | 8 | 0 |
| 2008 Autumn | 0 | 0 | 0 | 0 | 0 |
| 2008 Winter | 0 | 0 | 0 | 0 | 0 |
| 2008 Spring | 0 | 0 | 0 | 0 | 0 |
| 2008/09 Summer | * | * | * | * | * |
| 2009 Autumn | 0 | 0 | 0 | 0 | 0 |
| 2009 Winter | 0 | 0 | 0 | 0 | 0 |
| 2009 Spring | 0 | 0 | 0 | 0 | 0 |
| 2009/10 Summer | 62 | 149 | 27 | 28 | 0 |
| 2010 Autumn | 0 | 0 | 0 | 0 | 0 |
| 2010 Winter | 0 | 0 | 0 | 0 | 0 |
| 2010 Spring | 0 | 0 | 0 | 0 | 0 |
| 2010/11 Summer | 33 | 162 | 16 | 28 | 0 |
| 2011 Autumn | 0 | 0 | 0 | 0 | 0 |
| 2011 Winter | 0 | 0 | 0 | 0 | 0 |
| 2011 Spring | 0 | 0 | 0 | 0 | 0 |
| 2011/12 Summer | 0 | 88 | 0 | 17 | 0 |
| 2012 Autumn | 0 | 0 | 0 | 0 | 0 |
| 2012 Winter | 0 | 0 | 0 | 0 | 0 |
| 2012 Spring | 2 | 0 | 2 | 0 | 0 |
| 2012/13 Summer | 106 | 598 | 40 | 93 | 18 |
| 2013 Autumn | 0 | 0 | 0 | 0 | 0 |
| 2013 Winter | 0 | 0 | 0 | 0 | 0 |

| Season | Potential Thaw Hours at 0 °C | | PFTE | | FTC |
|---|---|---|---|---|---|
| | $T_{AIR}$ | NST | $T_{AIR}$ | NST | |
| 2013 Spring | 0 | 132 | 0 | 17 | 0 |
| 2013/14 Summer | 37 | 504 | 16 | 49 | 0 |
| 2014 Autumn | 0 | 0 | 0 | 0 | 0 |
| 2014 Winter | 0 | 0 | 0 | 0 | 0 |
| 2014 Spring | 0 | 0 | 0 | 0 | 0 |
| 2014/15 Summer | * | 246 | * | 40 | 0 |
| 2015 Autumn | 0 | 0 | 0 | 0 | 0 |
| 2015 Winter | 0 | 0 | 0 | 0 | 0 |
| 2015 Spring | 0 | 12 | 0 | 4 | 0 |
| 2015/16 Summer | 31 | 501 | 6 | 30 | 0 |
| Total | **273** | **2 417** | **109** | **314** | **18** |

Thaw events only occur in the summer of 2013 and represent a mixture of single and multiple freeze-thaw cycles, with average thaw duration of single freeze-thaw cycles 6 hours ($s$ = 5) and thaw generally occurring from 10:00-16:00. Multiple thaw events are observed on three separate days. The initial thaw event is shortest, with subsequent thaw events longer. Two thaw events occur on 25 December 2013 with the initial thaw event of 1 hour lasting from 00:00-01:00 and the subsequent event having a duration of 3 hours from 11:00-17:00. Three thaw events are observed on 27 December 2016. The initial event lasts 3 hours (00:00-03:00), the second 12 hours (10:00-22:00) and the final thaw event 1 hour (23:00-24:00). One day (28 December 2013) registers five cycles. For this day, the first-third thaw event last 1 hour from 00:00-01:00, 03:00-04:00 and 05:00-06:00 respectively. The fourth thaw event has the longest duration of 8 hours from 11:00-19:00, with the final thaw event lasting 2 hours from 20:00-22:00. The longest thaw event of 12 hours is observed over three days (20-22 December 2013). On these days thaw commences at 10:00 and ends at 22:00. Deepest thaw also takes place in this three-day period, with thaw reaching 38 cm.

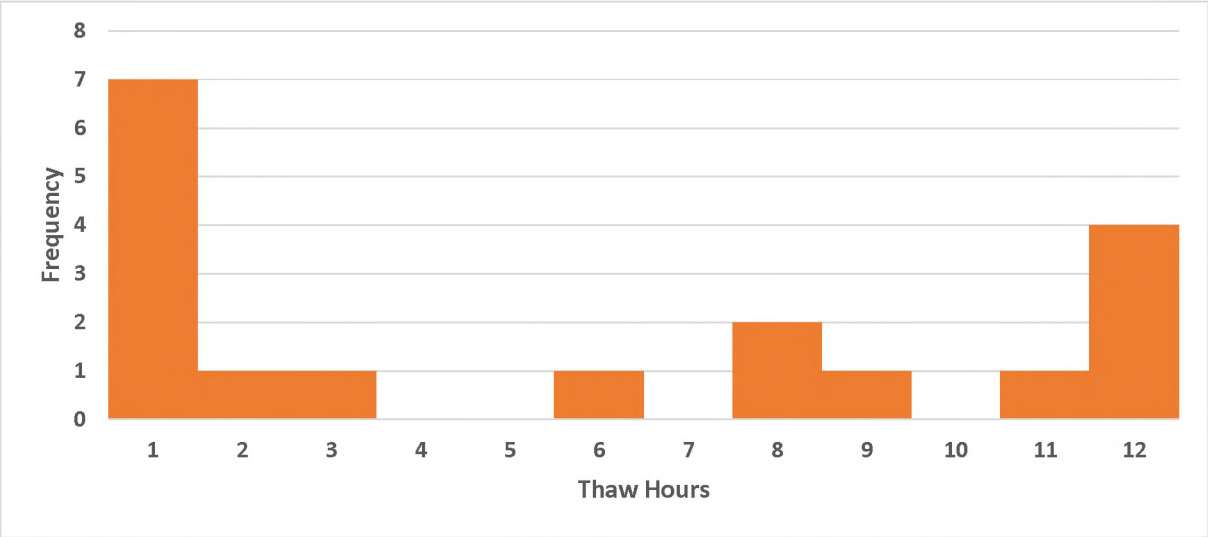


**Figure 130: Histogram of thaw duration per event per sensor at the near surface for A7.**

Five freeze-thaw cycles last longer than 10 hours (Figure 130), all occurring in December with average thaw from 10:00-22:00. When average thaw duration is considered (6 hours, n = 9), average commencement of thaw takes place at 11:00 and ends at 21:00. Temperature variability initially increases from air temperature to NST. From NST onwards an increase in depth in the ground yields a decrease in variability. Highest variability is observed for NST ($s$ = 9.49), lowest for $T_{200}$ ($s$ = 4.99). The average diurnal temperature range approximates 18 °C, although a maximum diurnal range of 23 °C is reached. Maximum diurnal temperature is 15 °C, while minimums reach -10 °C. Neither the greatest diurnal maximum temperature nor the lowest diurnal minimum temperature correlate significantly to maximum thaw duration. Average diurnal maximum, minimum, and mean temperatures on those days when freeze-thaw cycles take place are 12 °C, -6 °C and 3 °C respectively.

#### *5.3.2.3.7.1 Higher-frequency*

High-frequency temperature data using an ACR system, recorded at one-minute intervals, are available for A7 from 30 December 2013 to 7 January 2014 (n = nine days) and again for 31 December 2014 to 5 January 2015 (n = six days) for air temperatures, near surface temperatures (NST), ground surface temperatures (GST), $T_5$, $T_{10}$, $T_{15}$, and $T_{20}$. Active layer thickness for 2014 and 2015 approaches 25 and 28 cm respectively (discussed in 5.3.2.2 Seasonal frost environment, pg. 213 onwards).

##### *5.3.2.3.7.1.1 December 2013-January 2014*

During the 2014 observation period NST records positive temperatures every day, yielding nine potential freeze-thaw events (Figure 131, pg. 248). With increasing depth, not every sensor records positive temperatures. Ground surface temperatures (GST) and $T_5$ do not attain positive temperatures on 6 January; $T_{10}$ and $T_{15}$ on 6 and 7 January; $T_{20}$ from 30-31 December, as well as on 1 and 5-7 January. One freeze-thaw cycle is recorded for the late evening on 5 January, yielding an approximate 11% translation of potential freeze-thaw events to freeze-thaw cycles. This freeze-thaw cycle, identified

using an exotherm, compares with freeze-thaw cycles identified for this observation period as discussed in the previous section (5.3.2.3.7 A7: Troll 1, pg. 244). This frost event occurs near the surface and does not reach $T_5$. During the nine-day period the highest and lowest temperatures are recorded for NST. Maximum diurnal temperature is 20 °C and minimums reach -10 °C, yielding diurnal temperature ranges of 30 °C. Mean diurnal temperature is 2 °C and sub-zero temperatures are reached every day for all sensors. Furthermore, the intensity of frost events (diurnal minimum temperature) ranges from -10 °C to -7 °C (7 and 3 January respectively) at NST. In comparison, diurnal maximum temperatures attain a range of 0-20 °C (6 and 2 January respectively). The narrowest range of 9 °C is evident for 6 January, which shows the most depressed temperature values for all sensors at all depths. Variability initially increases from air temperatures to NST and then decreases with depth into the ground. Highest variability is calculated for NST ($s$ = 7.0), lowest for $T_{20}$ ($s$ = 0.53). In comparison, diurnal mean temperature decreases with depth with the highest mean temperature recorded at NST (2.2 °C). and the lowest at $T_{20}$ (-1.2 °C). Diurnal mean air temperature is -4.7 °C.

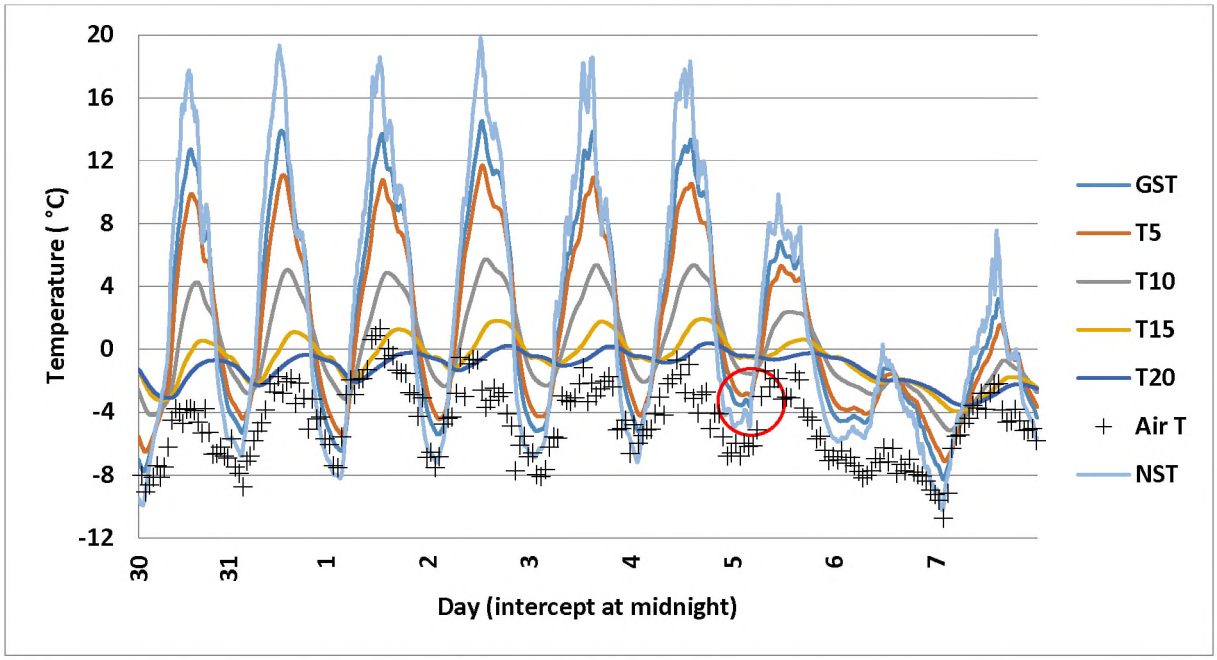


**Figure 131: Diurnal cycles for a nine-day period from 30 December 2013 to 7 January 2014. One singular freeze-thaw cycle (FTC), identified using and exotherm, is indicated by a red circle. NST: ground temperatures recorded at ± 1 cm depth. GST: ground temperatures recorded at ± 2 cm depth. The number following 'T' indicates the depth of the sensor (in centimetres) used to record ground temperature**

Thawing and freezing indices for the various sensors, given as days, are provided in Table 113 (pg. 249). The thawing index decreases with increasing depth in the ground. Thawing indices are marginally positive and freezing indices marginally negative, with freezing indices generally exceeding thawing indices. No thawing index is calculated for $T_{20}$. The balance of degree days for air temperature is ± 4 toward the freezing index. This balance generally shifts from leaning towards the thawing index at NST, GST, $T_5$ and $T_{10}$ towards the freezing index at $T_{15}$ and $T_{20}$. The freeze-thaw cycle of 5 January reflects a high positive thawing index on 4 and 5 January and concomitantly high freezing index on 3 January. The thermal offset is skewed towards positive values with the largest offset (9.0) calculated for 30 December and smallest values calculated for the depressed temperatures evident on 6 and 7 January.

**Table 113: The freezing index (FI) and thawing index (TI) for the various sensor depths for A7 from 30 December 2013 to 7 January 2014. $T_{AIR}$: air temperatures. NST: ground temperatures recorded at ± 1 cm depth. GST: ground temperatures recorded at ± 2 cm depth. The subscript following 'T' indicates the depth of the sensor (in centimetres) used to record ground temperature. SO: thermal offset. DD: degree days.**

| Day | FI | | | | | | | TI | | | | | | | SO |
|---|---|---|---|---|---|---|---|---|---|---|---|---|---|---|---|
| | $T_{AIR}$ | NST | GST | $T_5$ | $T_{10}$ | $T_{15}$ | $T_{20}$ | $T_{AIR}$ | NST | GST | $T_5$ | $T_{10}$ | $T_{15}$ | $T_{20}$ | |
| 30 | -6.8 | -2.4 | -2.0 | -1.9 | -1.5 | -1.4 | -1.8 | 0.0 | 5.5 | 4.2 | 3.2 | 1.3 | 0.1 | 0.0 | 9.0 |
| 31 | -4.7 | -1.9 | -1.4 | -1.2 | -0.8 | -0.7 | -1.1 | 0.0 | 5.8 | 4.6 | 3.6 | 1.6 | 0.3 | 0.0 | 8.4 |
| 1 | -2.7 | -2.1 | -1.6 | -1.3 | -0.8 | -0.6 | -1.0 | 0.1 | 6.4 | 5.1 | 4.1 | 1.8 | 0.4 | 0.0 | 6.9 |
| 2 | -4.0 | -2.0 | -1.4 | -1.1 | -0.6 | -0.4 | -0.6 | 0.0 | 6.8 | 5.5 | 4.6 | 2.3 | 0.6 | 0.0 | 8.8 |
| 3 | -4.3 | -1.9 | -1.4 | -1.1 | -0.6 | -0.3 | -0.5 | 0.0 | 5.9 | 4.8 | 3.9 | 1.9 | 0.5 | 0.0 | 8.3 |
| 4 | -3.9 | -1.6 | -1.1 | -0.9 | -0.5 | -0.3 | -0.4 | 0.0 | 6.2 | 5.0 | 4.2 | 2.1 | 0.7 | 0.0 | 8.5 |
| 5 | -4.3 | -1.7 | -1.2 | -1.0 | -0.5 | -0.3 | -0.4 | 0.0 | 3.0 | 2.4 | 1.9 | 0.9 | 0.2 | 0.0 | 5.7 |
| 6 | -7.5 | -4.5 | -3.8 | -3.4 | -2.5 | -1.8 | -1.7 | 0.0 | 0.0 | 0.0 | 0.0 | 0.0 | 0.0 | 0.0 | 3.1 |
| 7 | -5.0 | -2.9 | -2.7 | -2.7 | -2.8 | -2.9 | -2.9 | 0.0 | 0.8 | 0.4 | 0.1 | 0.0 | 0.0 | 0.0 | 3.0 |
| Balance * | -4.3 | 4.2 | 3.4 | 2.7 | 1.1 | -0.1 | -0.9 | * difference of DD between FI and TI | | | | | | | |

*5.3.2.3.7.1.2 December 2014-January 2015*

During the 2015 observation period NST records positive temperatures every day except on 3 January, yielding five potential freeze-thaw events (Figure 131, pg. 248). One freeze-thaw cycle is identified for the observation period on the morning of 31 December. This analysis yields one more freeze-thaw cycles than those determined using hourly data as discussed in the previous section, (5.3.2.3.7 A7: Troll 1, pg. 244). With increasing depth, not every sensor records positive diurnal temperatures. Ground surface temperatures (GST) don't reach positive temperatures on 3 and 4 January; $T_5$ and $T_{10}$ on 3-5 January; $T_{15}$ on 1-5 January; $T_{20}$ for the entire period. Highest and lowest temperatures are recorded for NST and the intensity of potential frost events (diurnal minimum temperature) ranges from -12 °C to -9 °C (2 and 5 January respectively). In comparison, diurnal maximum temperatures attain a range of 19 °C to -0.1 °C (31 December and 3 January respectively). Maximum diurnal maximum is 19 °C, minimums are -12 °C, yielding a range of 31 °C. Diurnal mean temperature is -3 °C and sub-zero temperatures are reached every day for all sensors. The narrowest diurnal temperature range of 10 °C is evident on 3 January, which shows the most depressed temperature values for all sensors at all depths. This compares to the 2014 period. Variability initially increases from air temperature to NST and then decreases with depth into the ground. Highest variability is evident for NST ($s$ = 5.2), lowest for $T_{20}$ ($s$ = 0.6). In comparison, diurnal mean temperatures decrease with depth with the highest mean temperature recorded for NST (-2.5 °C), and the lowest at $T_{20}$ (-3.6 °C). Mean diurnal air temperature is -7.4 °C. The thawing and freezing index for the various sensors, given as days, are provided in Table 114 (pg. 250). Thawing indices decrease with increasing depth in the ground. The balance of degree days for air temperature is ± 7 toward the freezing index, with the balance generally increasing with increasing depth from NST onwards. The thermal offset is skewed towards positive values with the largest thermal offset of 8.7 observed on 31 December and smallest calculated for the depressed temperatures of 3 January, like observations of the 2014 period.

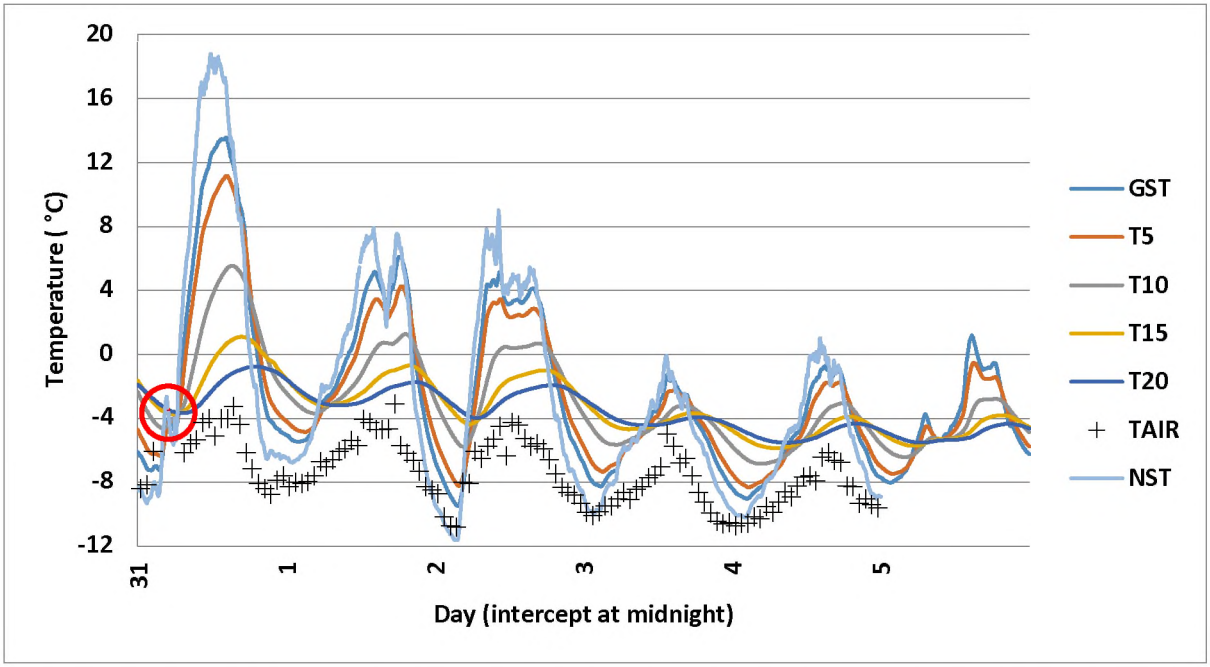


**Figure 132: Diurnal cycles for a six-day period from 31 December 2014 to 5 January 2015. The single freeze events is indicated with a red circle. NST: ground temperatures recorded at ± 1 cm depth. GST: ground temperatures recorded at ± 2 cm depth. $T_5$: ground temperatures recorded at 5 cm depth. $T_{10}$: ground temperature recorded at 10 cm depth. $T_{15}$: ground temperature recorded at 15 cm depth. $T_{20}$: ground temperature recorded at 20 cm depth. $T_{AIR}$: air temperatures.**

**Table 114: The freezing index (FI) and thawing index (TI) for the various sensors for A7 from 31 December 2014 to 5 January 2015. $T_{AIR}$: air temperatures. NST: ground temperatures recorded at ± 1 cm depth. GST: ground temperatures recorded at ± 2 cm depth. The subscript following 'T' indicates the depth of the sensor (in centimetres) used to record ground temperature. SO: thermal offset. DD: degree days.**

| Day | FI | | | | | | | TI | | | | | | | SO |
|---|---|---|---|---|---|---|---|---|---|---|---|---|---|---|---|
| | $T_{AIR}$ | NST | GST | $T_5$ | $T_{10}$ | $T_{15}$ | $T_{20}$ | $T_{AIR}$ | NST | GST | $T_5$ | $T_{10}$ | $T_{15}$ | $T_{20}$ | |
| 31 | -5.1 | -3.1 | -2.4 | -2.1 | -1.5 | -1.5 | -2.1 | 0.0 | 5.7 | 4.3 | 3.5 | 1.6 | 0.2 | 0.0 | 8.7 |
| 1 | -6.3 | -2.4 | -2.0 | -1.9 | -1.7 | -2.0 | -2.5 | 0.0 | 2.2 | 1.6 | 1.1 | 0.2 | 0.0 | 0.0 | 6.0 |
| 2 | -7.1 | -3.7 | -3.0 | -2.6 | -2.0 | -2.4 | -2.8 | 0.0 | 2.2 | 1.6 | 1.1 | 0.2 | 0.0 | 0.0 | 5.7 |
| 3 | -8.6 | -5.9 | -5.3 | -5.1 | -4.5 | -4.1 | -4.1 | 0.0 | 0.0 | 0.0 | 0.0 | 0.0 | 0.0 | 0.0 | 2.7 |
| 4 | -8.8 | -5.5 | -5.3 | -5.3 | -5.2 | -5.0 | -5.0 | 0.0 | 0.0 | 0.0 | 0.0 | 0.0 | 0.0 | 0.0 | 3.2 |
| 5 | -7.7 | -4.5 | -4.3 | -4.5 | -4.7 | -4.9 | -5.0 | 0.0 | 0.2 | 0.0 | 0.0 | 0.0 | 0.0 | 0.0 | 3.4 |
| Balance * | -7.3 | -2.5 | -2.5 | -2.6 | -2.9 | -3.3 | -3.6 | * difference in DD between FI and TI | | | | | | | |

### 5.3.2.3.8 A9: Valterkulten

Data for A9 are available from autumn 2013 to summer 2015/16. Diurnal ranges and oscillations around 0 °C are provided in Table 115 (pg. 251). Diurnal air temperature ranges of 10 °C are scarce (± 3%), although these occur throughout the year except for April and September. Of these ranges, oscillations around 0 °C are recorded 17% of the time. This translates into approximately no oscillations indicative

of potential freeze-thaw events that also exceed a diurnal temperature range of 10 °C. It must be noted that these figures are underestimated, since data for the air temperature sensor are not available for 2015. For near surface temperatures (NST) diurnal ranges of 10 °C are more common, occurring 31% of the time since records began. Of these ranges, two thirds reflect ranges where freeze-thaw events are likely (69% >/< 0 °C). This translates into 22% of annual oscillations indicative of potential freeze-thaw events that also have ranges greater than 10 °C. Annual oscillations indicative of potential freeze-thaw events occur 23% of the time. At $T_{15}$ no diurnal ranges exceeding 10 °C are recorded, although 99 oscillations around 0 °C (9% >/< 0 °C) are, occurring exclusively in summer. From $T_{30}$ deeper into the ground no ranges greater than 10 °C are recorded, as are no potential freeze-thaw events. Diurnal ranges exceeding 10 °C at NST occur predominantly in summer and spring; for air temperatures most such ranges are observed in winter and spring. Oscillations around 0 °C are recorded predominantly in summer, although such ranges also occur during spring and autumn at NST, as well as autumn for air temperatures.

**Table 115: Oscillations around 0 °C (Osc), as well as diurnal ranges exceeding 10 °C ($T_{DR}$) for A9. Annual Osc (%) reflect all oscillations around 0 °C, including those where $T_{DR}$ does not exceed 10 °C. # underestimation: data for 2015 not available. $T_{AIR}$: air temperatures. NST: ground temperatures recorded at ± 1 cm depth. $T_{15}$: ground temperature recorded at 15 cm depth. JJA: winter. SON: spring. DJF: summer. MAM: autumn.**

| Sensor | $T_{DR}$ (%) | Osc (%) | % of year | Annual Osc (%) | $T_{DR}$ (%) | | | | Osc (%) | | | |
|---|---|---|---|---|---|---|---|---|---|---|---|---|
| | | | | | JJA | SON | DJF | MAM | JJA | SON | DJF | MAM |
| $T_{AIR}$# | 3 | 17 | 0.5 | 2 | 34 | 38 | 17 | 10 | 0 | 0 | 95 | 5 |
| NST | 31 | 69 | 22 | 23 | 3 | 30 | 60 | 7 | 0 | 17 | 80 | 4 |
| $T_{15}$ | 0 | 0 | 0 | 9 | 0 | 0 | 0 | 0 | 0 | 0 | 100 | 0 |

Positive air temperatures are recorded on 33 separate days (potential freeze-thaw events: 33), with a maximum of 3 °C reached on 1 January 2014 at 14:00. These temperatures occur exclusively during summer 2013/14 and the average period of positive air temperatures is 4 hours. The soil moisture sensor failed for the duration of 2015 and ground freeze-thaw cycles are approximated for this year by comparing variability of known freeze-thaw cycles of 2013 and 2014 to potential freeze-thaw events in 2015. Using this method yields diurnal freeze-thaw cycles on 69 separate days from autumn 2013 to summer 2016. Approximately one third (38%) of potential freeze-thaw events translate into freeze-thaw cycles (Table 116).

**Table 116: Freeze-thaw events for A9, summarised by season. # indicates approximation of freeze-thaw cycles (FTC). $T_{AIR}$: air temperatures. NST: ground temperatures recorded at ± 1 cm depth. $T_{15}$: ground temperature recorded at 15 cm depth. PFTE: potential freeze-thaw events.**

| Season | Potential Thaw Hours at 0 °C | | | PFTE | | | FTC |
|---|---|---|---|---|---|---|---|
| | $T_{AIR}$ | NST | $T_{15}$ | $T_{AIR}$ | NST | $T_{15}$ | |
| 2013 Autumn | 0 | 12 | 0 | 0 | 3 | 0 | 0 |
| 2013 Winter | 0 | 0 | 0 | 0 | 0 | 0 | 0 |
| 2013 Spring | 1 | 115 | 0 | 1 | 18 | 0 | 6 |
| 2013/14 Summer | 77 | 657 | 396 | 32 | 79 | 31 | 10 |
| 2014 Autumn | 0 | 20 | 0 | 0 | 8 | 0 | 0 |
| 2014 Winter | 0 | 0 | 0 | 0 | 0 | 0 | 0 |
| 2014 Spring | 0 | 70 | 0 | 0 | 15 | 0 | 2 |
| 2014/15 Summer | 0 | 482 | 187 | 0 | 64 | 24 | 18 # |

| Season | Potential Thaw Hours at 0 °C | | | PFTE | | | FTC |
|---|---|---|---|---|---|---|---|
| | $T_{AIR}$ | NST | $T_{15}$ | $T_{AIR}$ | NST | $T_{15}$ | |
| 2015 Autumn | 0 | 2 | 0 | 0 | 2 | 0 | 0 # |
| 2015 Winter | 0 | 2 | 0 | 0 | 2 | 0 | 0 # |
| 2015 Spring | 0 | 76 | 0 | 0 | 10 | 0 | 6 # |
| 2015/16 Summer | 682 | 349 | 0 | 0 | 0 | 0 | 34 |
| Total | 760 | 1 785 | 583 | 33 | 201 | 55 | 76 # |

Most thaw events take place during summer (80%), with the remainder occurring in spring (20%). One isolated freeze-thaw cycle occurs in October 2013, representing 1% of observed freeze-thaw cycles. Cycles recorded during November amount to 19% of observed freeze-thaw cycles. Most freeze-thaw cycles occur in December (40%), with a similar amount observed for January (35%) and less in February (5%). Thaw events take place in the upper 29 cm of the ground (active layer thickness: 29 cm) and average thaw duration is 8 hours ($s$ = 6). Thaw generally occurs from 11:00-19:00. Multiple thaw events are evident on eight separate days, seven during January of 2015 and 2016, one in December 2013. The initial thaw event is shortest (2 hours), with subsequent thaw longer (6 hours). Initial thaw generally occurs from 10:00-12:00 and the subsequent one from 14:00-12:00. Twenty-seven freeze-thaw cycles last longer than 10 hours (Figure 133), commencing at 11:00 and ending at 01:00 the following day. Most of these cycles take place in December (17 freeze-thaw cycles, 63%) with ± one third (nine freeze-thaw cycles) in January and one (4%) in November. When the average thaw duration is considered (8 hours, n = 38), 53% freeze-thaw cycles take place in December, with 18% in November, and 29% in January. For these thaw events, average commencement of thaw is 11:00, ending at 24:00.

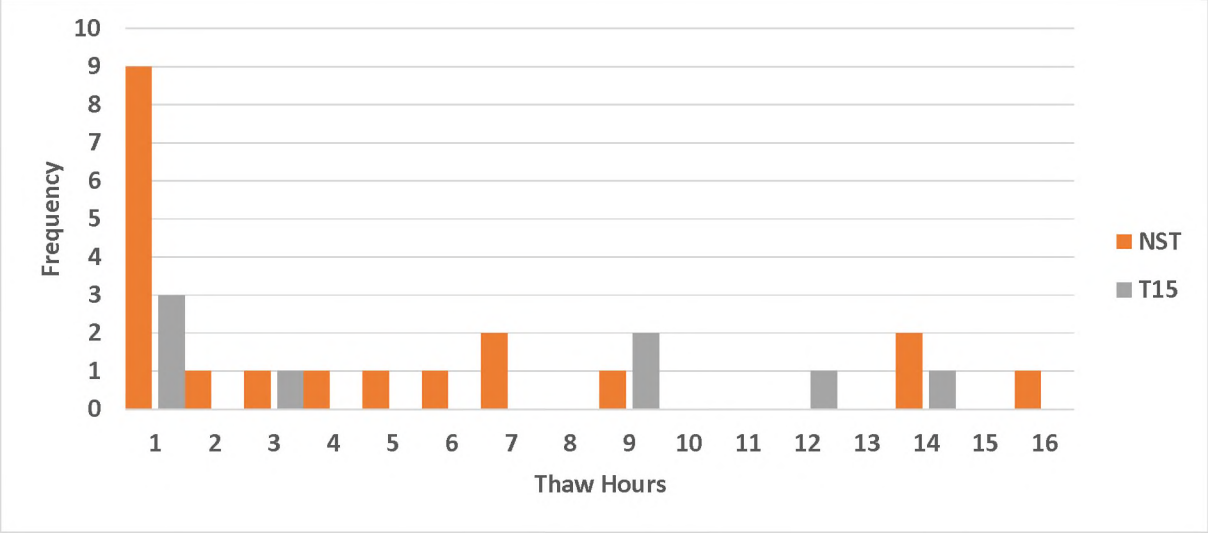


**Figure 133: Histogram of thaw duration per event per sensor depth for A9.NST: ground temperatures recorded at ± 1 cm depth. $T_{15}$: ground temperature recorded at 15 cm depth.**

Deepest thaw events occur in January 2014, reaching a depth of 29 cm. These events last 12 hours, from 08:00-19:00. The longest thaw event takes place on 29 December 2015 and lasts 18 hours from 11:00-05:00 the following day. Temperature variability initially increases from air temperatures to NST.

From NST onwards an increase in depth in the ground yields a decrease in variability. Highest variability is evident for NST ($s$ = 9.66), lowest for $T_{60}$ ($s$ = 6.21). The average diurnal temperature range approximates 16 °C, although a maximum range of 30 °C is reached. Maximum diurnal temperature is 16 °C, while minimums reach -22 °C. The greatest diurnal maximum temperatures correlate positively with maximum thaw duration ($r$ = 0.73, $p$ < 0.05). Similarly, the coldest diurnal minimum temperatures correlate significantly to thaw duration ($r$ = 0.53, $p$ < 0.05). Average diurnal maximum, minimum, and mean temperatures on those days when freeze-thaw cycles take place are 7 °C, -9 °C and -2 °C respectively.

#### 5.3.2.3.9 A10: Vesleskarvet

Data for A10 are available from autumn 2009 to summer 2015/16 and diurnal ranges and oscillations around 0 °C are provided in Table 117. Diurnal air temperature ranges of 10 °C are rare (± 7%). Nevertheless, such ranges occur throughout the year. Of these ranges, ± 19% reflect maximums above and minimums below 0 °C, *i.e.* oscillations around 0 °C. This translates into 1% of oscillations indicative of potential freeze-thaw events that also exceed a diurnal temperature range of 10 °C. When evaluating all diurnal ranges, this proportion rises to 4%. For near surface temperatures (NST) diurnal ranges of 10 °C are more common, occurring 14% of the time since records began. Furthermore, such ranges are observed for all months except April, May, July, and August. Of these ranges, almost two thirds reflect ranges where freeze-thaw events are possible (64% >/< 0 °C). This translates into 9% of oscillations indicative of potential freeze-thaw events that also exceed diurnal ranges of 10 °C. This proportion rises to 10% when all diurnal ranges are considered. At $T_{15}$ no diurnal ranges exceeding 10 °C are recorded, although oscillations around 0 °C (0% >/< 0 °C) are (on three occasions). One such oscillation is recorded on January 2010, with a further two observed for January 2013. Sensors below $T_{15}$ reflect no diurnal temperature range exceeding 10 °C, as well as not oscillations indicative of potential freeze-thaw events. Diurnal ranges greater than 10 °C are recorded throughout the year. For air temperatures such ranges occur predominantly in spring, whereas at NST these ranges are observed predominantly in summer. Oscillations around 0 °C occur predominantly in summer, although air temperatures also show a number of these in autumn. In comparison, NST exhibits such oscillations from spring through to autumn.

**Table 117: Oscillations around 0 °C (Osc), as well as diurnal ranges exceeding 10 °C ($T_{DR}$) for A10. Annual Osc (%) reflect all oscillations around 0 °C, including those where $T_{DR}$ does not exceed 10 °C. # underestimation: insufficient data available for a portion of 2013. $T_{AIR}$: air temperatures. NST: ground temperatures recorded at ± 1 cm depth. $T_{15}$: ground temperature recorded at 15 cm depth. JJA: winter. SON: spring. DJF: summer. MAM: autumn.**

| Sensor | $T_{DR}$ (%) | Osc (%) | % of year | Annual Osc (%) | $T_{DR}$ (%) | | | | Osc (%) | | | |
|---|---|---|---|---|---|---|---|---|---|---|---|---|
| | | | | | JJA | SON | DJF | MAM | JJA | SON | DJF | MAM |
| $T_{AIR}$# | 7 | 19 | 1 | 4 | 23 | 39 | 28 | 10 | 0 | 0 | 94 | 6 |
| NST | 14 | 64 | 9 | 10 | 1 | 20 | 73 | 6 | 0 | 6 | 93 | 1 |
| $T_{15}$ | 0 | 0 | 0 | ± 0 | 0 | 0 | 0 | 0 | 0 | 0 | 0 | 100 |

During the observation period relatively numerous positive air temperatures are recorded (potential freeze-thaw events: 141). Similarly, numerous potential freeze-thaw events and freeze-thaw cycles are

observed, and thaw events occur within the upper 16 cm of the ground. Positive air temperatures generally take place in summer, particularly summers of 2009/10 and 2012/13 (n = 38 and n = 37 occurrences respectively). Isolated potential freeze-thaw events occur for air temperatures during the springs of 2009, 2012 and 2015 (n = 2 for each season). A maximum air temperature of 7 °C is reached on 22 December 2010 at 13:00 and positive temperatures are maintained for ± 3 hours on average. Considering only the time span of autumn 2013 to summer 2016, potential freeze-thaw events are observed 30 times. Average duration of positive air temperatures is two and a diurnal maximum temperature is 4 °C, attained on 8 January 2013 at 11:00. There is no soil moisture sensor available for this data logger from 2008-2009 and freeze-thaw cycles are approximated for these years by comparing variability of known freeze-thaw events of 2010-2016 to variability of potential freeze-thaw events for 2008 and 2009. Using this method yields 92 single diurnal freeze-thaw cycles from autumn 2008 to summer 2016. Just under a third (29%) of potential freeze-thaw events translates into freeze-thaw cycles (Table 118).

**Table 118: Freeze-thaw events for A10, summarised by season. * insufficient data available. # approximation of freeze-thaw cycles (FTC). $T_{AIR}$: air temperatures. NST: ground temperatures recorded at ± 1 cm depth. $T_{15}$: ground temperature recorded at 15 cm depth. PFTE: potential freeze-thaw events.**

| Season | Potential Thaw Hours at 0 °C | | | PFTE | | | FTC |
|---|---|---|---|---|---|---|---|
| | $T_{AIR}$ | NST | $T_{15}$ | $T_{AIR}$ | NST | $T_{15}$ | |
| 2008/09 Summer | 0 | 0 | 0 | 0 | 0 | 0 | 0 # |
| 2009 Autumn | 0 | 0 | 0 | 0 | 0 | 0 | 0 # |
| 2009 Winter | 0 | 0 | 0 | 0 | 0 | 0 | 0 # |
| 2009 Spring | 2 | 2 | 0 | 2 | 2 | 0 | 0 # |
| 2009/10 Summer | 127 | 200 | 1 | 38 | 37 | 1 | 8 |
| 2010 Autumn | 0 | 0 | 0 | 0 | 0 | 0 | 0 |
| 2010 Winter | 0 | 0 | 0 | 0 | 0 | 0 | 0 |
| 2010 Spring | 0 | 4 | 0 | 0 | 4 | 0 | 1 |
| 2010/11 Summer | 93 | 214 | 0 | 20 | 39 | 0 | 5 |
| 2011 Autumn | 0 | 0 | 0 | 0 | 0 | 0 | 0 |
| 2011 Winter | 0 | 0 | 0 | 0 | 0 | 0 | 0 |
| 2011 Spring | 0 | 3 | 0 | 0 | 2 | 0 | 0 |
| 2011/12 Summer | 19 | 73 | 0 | 12 | 24 | 0 | 1 |
| 2012 Autumn | 0 | 0 | 0 | 0 | 0 | 0 | 0 |
| 2012 Winter | 0 | 0 | 0 | 0 | 0 | 0 | 0 |
| 2012 Spring | 8 | 16 | 0 | 2 | 2 | 0 | 0 |
| 2012/13 Summer | 142 | 342 | 10 | 37 | 46 | 2 | 8 |
| 2013 Autumn | * | 0 | 0 | * | 0 | 0 | 0 |
| 2013 Winter | * | 0 | 0 | * | 0 | 0 | 0 |
| 2013 Spring | * | 0 | 0 | * | 0 | 0 | 0 |
| 2013/14 Summer | 36 | 252 | 0 | 11 | 46 | 0 | 17 |
| 2014 Autumn | 0 | 4 | 0 | 0 | 3 | 0 | 0 |
| 2014 Winter | 0 | 0 | 0 | 0 | 0 | 0 | 0 |
| 2014 Spring | 0 | 1 | 0 | 0 | 1 | 0 | 1 |
| 2014/15 Summer | 19 | 267 | 0 | 9 | 55 | 0 | 22 |

| Season | Potential Thaw Hours at 0 °C | | | PFTE | | | FTC |
|---|---|---|---|---|---|---|---|
| | $T_{AIR}$ | NST | $T_{15}$ | $T_{AIR}$ | NST | $T_{15}$ | |
| 2015 Autumn | 0 | 0 | 0 | 0 | 0 | 0 | 0 |
| 2015 Winter | 0 | 0 | 0 | 0 | 0 | 0 | 0 |
| 2015 Spring | 2 | 37 | 0 | 2 | 10 | 0 | 6 |
| 2015/16 Summer | 13 | 259 | 0 | 8 | 45 | 0 | 23 |
| Total | **461** | **1 674** | **11** | **140** | **316** | **3** | **92 #** |

Most thaw events occur during summer (91%), with the remainder taking place during spring (November, 9%). Most freeze-thaw cycles occur in January (36%), with a less observed in December (28%) and February (27%). Thaw events occur within the upper 16 cm of the ground (active layer thickness: 16 cm) and average thaw duration is 7 hours ($s$ = 4) with thaw generally occurring between 09:00-16:00. Twenty-seven freeze-thaw cycles last longer than 10 hours (Figure 134), commencing at 07:00 and ending at 19:00. Most freeze-thaw cycles take place in December (17 freeze-thaw cycles: 63%) with ten (37%) in January. When the average thaw duration is considered (7 hours, n = 52), 52% of freeze-thaw cycles occur in January, with 35% in December, 12% in February, and 2% in November. For these thaw events, average commencement of thaw starts at 09:00, ending at 19:00.

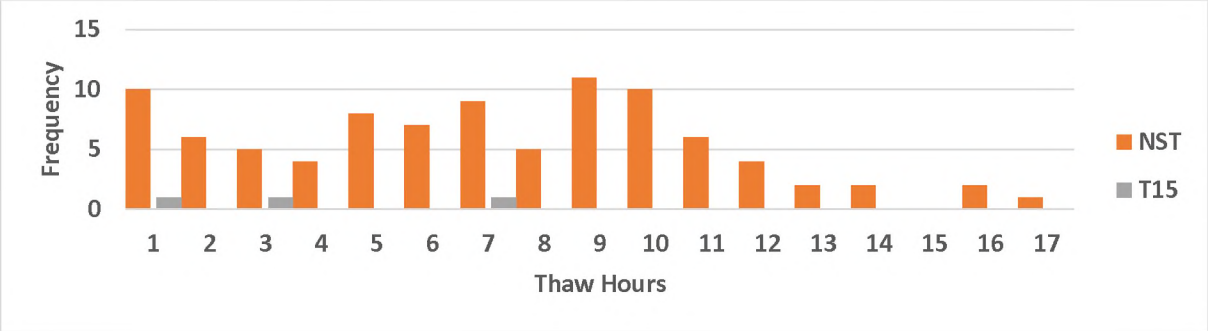


**Figure 134: Histogram of thaw duration per event per sensor depth for A10. NST: ground temperatures recorded at ± 1 cm depth. $T_{15}$: ground temperature recorded at 15 cm depth.**

The deepest thaw events (n = 3) all take place in January, once in 2010 and twice during 2013. During these events a thaw depth of 15 cm is reached, and thaw occurs for ± 13 hours at the near surface, taking place from 08:00-21:00. The longest thaw event occurs on 6 January 2013, lasting 17 hours from 06:00-23:00. This is also the deepest thaw depth reached at 16 cm and leads to a 4-hour thaw at $T_{15}$. Time lag of positive temperatures at the surface to $T_{15}$ is 7 hours. Variability for temperature recorded initially increases from air temperatures to NST. From NST onwards an increase in depth into the ground yields a decrease in variability. Highest variability is calculated for NST ($s$ = 7.89), lowest for $T_{60}$ ($s$ = 5.94). The average diurnal temperature range approximates 18 °C, although a maximum range of 33 °C is reached. Maximum diurnal temperature is 20 °C, minimums reach -20 °C. The greatest diurnal maximum temperatures correlate positively with maximum thaw duration ($r$ = 0.52, $p < 0.05$). Similarly, the coldest diurnal minimum temperatures correlate significantly to thaw duration ($r$ = 0.83, $p < 0.05$). Average diurnal maximum, minimum, and mean temperatures on those days when freeze-thaw cycles occur are 7 °C, -11 °C and -4 °C respectively.

#### *5.3.2.3.9.1 Higher-frequency*

Data, recorded at ten-minute intervals, were collected for Vesleskarvet during the 2011/12, 2013/14, and 2014/15 summer seasons using thermochron iButtons (Fairbridge technology). One-minute data are available for December 2013 and 2014, and January 2014 and 2015 using ACR systems. Similarly, one-minute data are available for XR5 systems for January 2011 and December 2015. Results from the XR5 and ACR systems are presented in their respective subsections below.

##### *5.3.2.3.9.1.1 XR5 system*

Higher-frequency temperature data, recorded at one-minute intervals with an XR5 system, are available for A10 from 19-29 January 2011 (n = ten days) for NST, and from 27-29 December 2015 for air temperatures, near surface temperatures (NST), $T_{15}$, $T_{30}$, $T_{45}$ and $T_{60}$. Active layer thickness in 2011 and 2015 approximates 15 cm.

###### *5.3.2.3.9.1.1.1 January 2011*

During the 2011 ten-day period diurnal maximum near surface temperature (NST) is 8 °C, with diurnal minimum -7 °C, yielding ranges of 15 °C (Figure 135, pg. 257). Diurnal mean temperature is -1 °C and sub-zero temperatures are reached every day, as are positive temperatures, yielding ten potential freeze-thaw events for the observation period. Of these potential freeze-thaw events one freeze-thaw cycle is recorded (10%). The freezing event is evident through an isolated exotherm on 21 January, occurring in the early morning just after midnight. This freeze-thaw cycle compares with freeze-thaw cycles identified for this observation period as discussed in the previous section (5.3.2.3.9 A10: Vesleskarvet, pg. 253). During the ten-day cycle the intensity of frost events (diurnal minimum temperature) ranges from -7 °C to -3 °C (24 and 20 January respectively). In comparison, diurnal maximum temperatures range from 1-8 °C (22 and 19 January respectively), with the warmest diurnal minimum temperature reached ± 1 day after the greatest diurnal maximum temperature recorded.

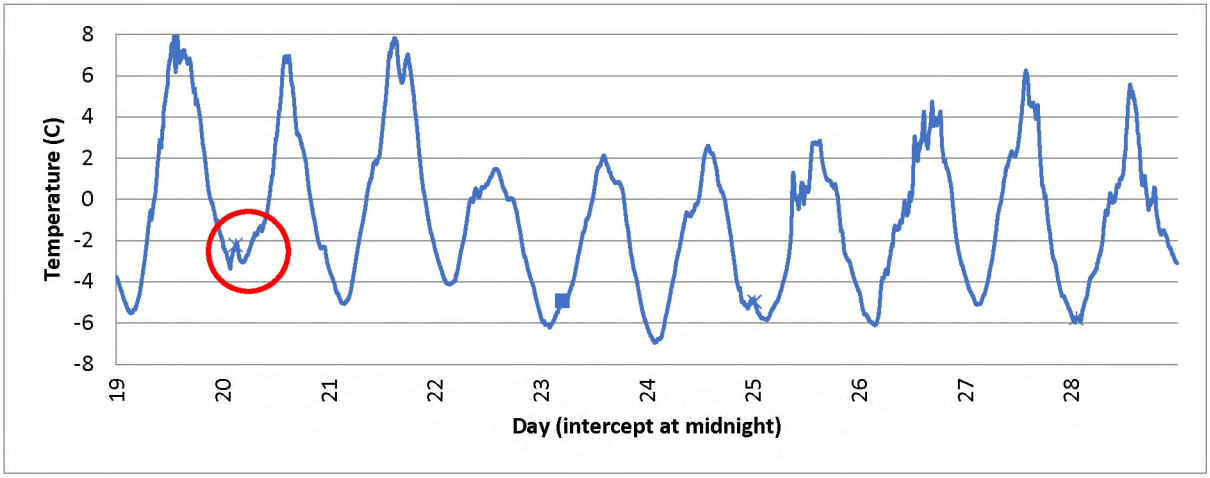


**Figure 135: Diurnal near surface temperatures (± 1 cm depth) cycles for a ten-day period from 19-29 January 2011. Exotherms are indicated with red circles.**

Temperatures are not available for air sensors and thermal offsets cannot be calculated. The thawing and freezing indices for NST, given as days, are provided in Table 119. The thawing indices are marginally positive and freezing indices marginally negative, with freezing indices generally exceeding thawing indices. The balance of degree days is ± 1 toward the freezing index. The exotherm, a proxy for freeze-thaw cycles, reflects a large thawing index and concomitantly lower freezing index. Furthermore, this exotherm is observed around midnight.

**Table 119: The freezing index (FI) and thawing index (TI) for near surface temperatures (± 1 cm depth) for the ten-day observation period in January 2011. DD: degree days. § Freeze-thaw cycles identified.**

| Day | FI | TI |
|---|---|---|
| 19 | -1.5 | 2.5 |
| 20 | -1.3 | 1.4 |
| 21 | -1.4 § | 2.3 |
| 22 | -1.8 | 0.2 |
| 23 | -2.8 | 0.3 |
| 24 | -2.8 | 0.3 |
| 25 | -2.3 | 0.5 |
| 26 | -2.0 | 1.0 |
| 27 | -2.1 | 1.2 |
| 28 | -1.8 | 0.8 |
| Balance * | -0.9 | * Difference of DD between FI and TI |

*5.3.2.3.9.1.1.2* *December 2015*

During the 2015 three-day period temperature variability initially increases from air temperature to NST (Figure 136, pg. 258). From NST onwards an increase in depth in the ground yields a decrease in variability. Highest variability is calculated for NST ($s$ = 5.96), lowest for $T_{60}$ ($s$ = 0.08). In comparison, diurnal mean temperatures decrease with depth and the highest diurnal mean temperature is recorded

at NST (-0.4 °C), the lowest at $T_{60}$ (-6 °C). Diurnal mean air temperature is -4 °C. Average diurnal temperature ranges at NST approximate 25 °C, with a maximum range of 27 °C attained. Maximum diurnal temperature is 19 °C at the near surface (NST), minimums are -9 °C. Sub-zero temperatures are reached every day for all sensors, while positive temperatures are reached for air temperatures and NST.

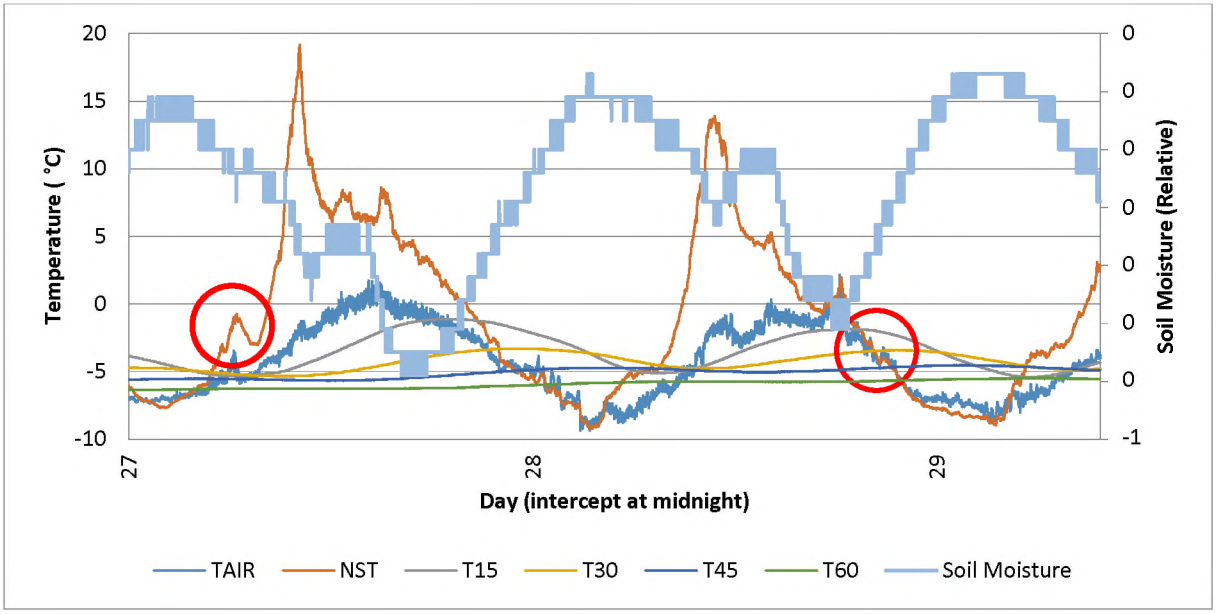


**Figure 136: Diurnal cycles for a three-day period from 27-29 December 2015. Exotherms are indicated with red circles. $T_{AIR}$: air temperatures. NST: ground temperatures recorded at ± 1 cm depth. $T_{12}$: ground temperatures recorded at 15 cm depth. $T_{30}$: ground temperature recorded at 30 cm depth. $T_{45}$: ground temperature recorded at 45 cm depth. $T_{60}$: ground temperature recorded at 60 cm depth.**

The observation period yields three potential freeze-thaw events with an average thermal offset of 3.5 for the three-day period (Table 120). One freezing event is evident (late evening on 28 December) and one thawing event (mid-morning on 27 December). These freeze-thaw cycles compare with freeze-thaw cycles identified for this observation period as discussed in the previous section (5.3.2.3.9 A10: Vesleskarvet, pg. 253). The highest thermal offset of 4.0 occurs on 27 January, which also registers the greatest diurnal maximum temperature at NST (19 °C). The thawing index for air temperatures approaches zero for all days, with greater thawing indices calculated for NST. The freezing index for NST exceeds those of air temperatures.

**Table 120: The thawing index (TI), freezing index (FI) and thermal offset (SO) for three days in 2015 at A10. # Observations only extend to noon on 29 December. DD: degree days. $T_{AIR}$: air temperatures. NST: ground temperatures recorded at ± 1 cm depth.**

| Day | TI | | FI | | SO |
|---|---|---|---|---|---|
| | $T_{AIR}$ | NST | $T_{AIR}$ | NST | |
| 27 | 0 | 177 | -3 | -138 | 4.0 |
| 28 | 0 | 107 | -4 | -198 | 2.9 |
| 29 # | 0 | 3 | -3 | -129 | 1.3 |
| Balance* | -4 | -26 | * Difference of DD between FI and TI | | |

#### *5.3.2.3.9.1.2 ACR system*

Higher-frequency temperature data, recorded at one-minute intervals with an ACR system, are available for A10 from 8-18 December 2013 (n = 10 days), 9-20 January 2014 (n = 11 days), 23-29 December 2014 (n = six days), and 12-29 January 2015 (n = 17 days) for air temperature, near surface temperature (NST), ground surface temperature (GST), $T_5$, $T_{10}$, $T_{15}$ and $T_{20}$. Active layer thickness for 2013, 2014, and 2015 is 16 cm, 15 cm, and 15 cm approximately.

##### *5.3.2.3.9.1.2.1 December 2013*

During the 2013 period diurnal maximums of 16 °C are reached at $T_5$, with minimums of -7 °C, yielding diurnal ranges of 23 °C (Figure 137, pg. 260). Diurnal mean temperature is 0 °C at NST and sub-zero temperatures are reached every day with positive temperatures attained on seven days (potential freeze-thaw events: 7). Near surface temperature (NST), ground surface temperature (GST), $T_5$, $T_{10}$ and $T_{15}$ display potential freeze-thaw events from 8-9 and 14-18 December. $T_{20}$ reaches positive temperatures on 8, 9 and 16 December. No identifiable freezing events using exotherms are evident. This lack of freeze-thaw cycles compares with freeze-thaw cycles identified for this observation period as discussed in the previous section (5.3.2.3.9 A10: Vesleskarvet, pg. 253). The deepest potential frost events (diurnal minimum temperature) are observed to $T_{10}$ during the initial potential freeze-thaw events and greatest diurnal minimum temperatures are attained by all sensors on 16 December (-5.98 °C, -6.91 °C, -6.90 °C, -7.76 °C, -7.33 °C, and -7.05 °C for air temperatures, NST, GST, $T_5$, $T_{10}$, $T_{15}$ and $T_{20}$ respectively), with $T_{10}$ registering the global diurnal minimum temperature for the observation period on this day. In comparison, the global maximum temperature for the observation period is evident for $T_5$, reaching 16 °C on 8 December. A storm event associated with drifting snow occurred between 10 and 12 December (n = 3), yielding depressed temperatures for all sensors, as well as a concomitant decrease in variability. Temperature variability initially increases from NST to $T_5$ and then decreases with depth into the ground. Highest variability is observed for $T_5$ ($s$ = 2.8), lowest for $T_{20}$ ($s$ = 1.9) and variability of air temperatures is 1.8. In comparison, diurnal mean temperature decreases with depth with the highest diurnal mean recorded for NST (-0.4 °C), and the lowest at $T_{20}$ (-2.0 °C). Diurnal mean air temperature is -3.8 °C.

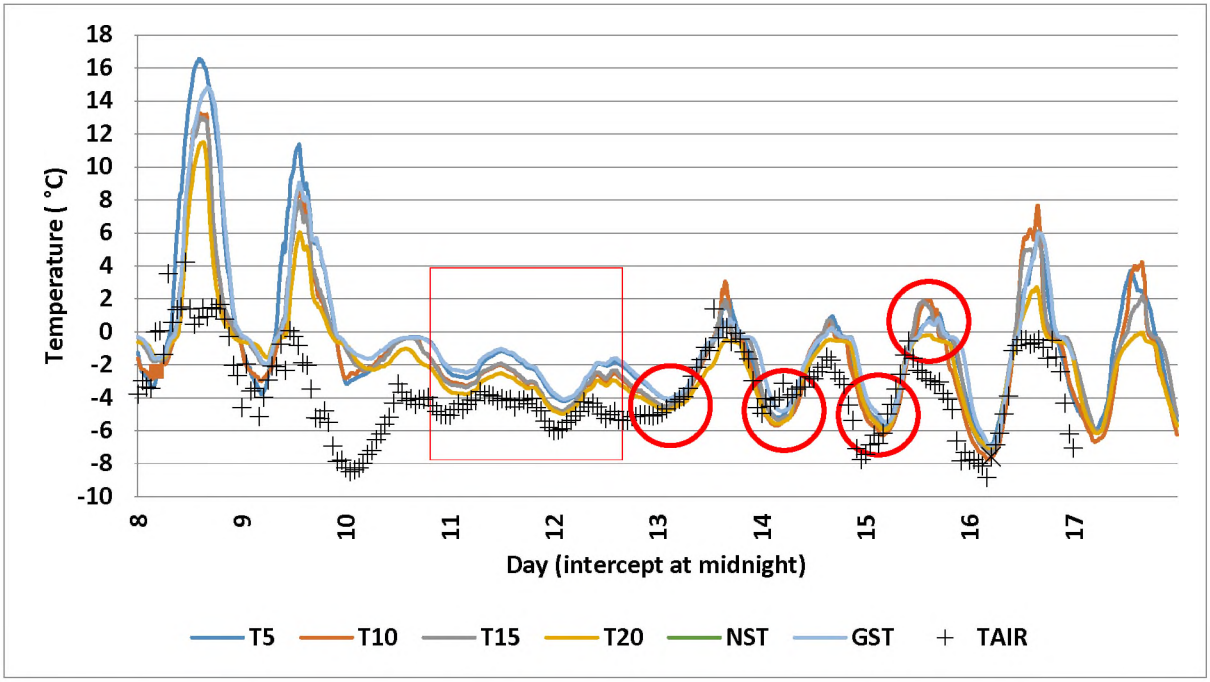


**Figure 137: Diurnal cycles for a ten-day period from 8-18 December 2013. Snowfall is indicated with a red square, freeze events with red circles. $T_{AIR}$: air temperatures. NST: ground temperatures recorded at ± 1 cm depth. GST: ground temperatures recorded at ± 2 cm depth. The numbers following 'T' indicate the depth of sensors (in centimetres) used to record ground temperature.**

The thawing and freezing indices for the various sensors, given as days, are provided in Table 121 (pg. 261). Thawing indices generally decrease with increasing depth into the ground and none are observed during the storm event. Freezing indices generally exceed thawing indices and the balance of degree days for air temperatures is ± 4 toward the freezing index. This balance increases with increasing depth into the ground. The thermal offset is skewed towards positive values with the largest thermal offset of 5.5 observed on 9 December and smallest calculated for the depressed temperatures evident during the storm event.

**Table 121: The freezing index (FI) and thawing index (TI) for the various sensor depths for A10 from 8-18 December 2013. $T_{AIR}$: air temperatures. NST: ground temperatures recorded at ± 1 cm depth. GST: ground temperatures recorded at ± 2 cm depth. The subscript following 'T' indicates the depth of the sensor (in centimetres) used to record ground temperature. SO: thermal offset. DD: degree days.**

| Day | FI | | | | | | | TI | | | | | | | SO |
|---|---|---|---|---|---|---|---|---|---|---|---|---|---|---|---|
| | $T_{AIR}$ | NST | GST | $T_5$ | $T_{10}$ | $T_{15}$ | $T_{20}$ | $T_{AIR}$ | NST | GST | $T_5$ | $T_{10}$ | $T_{15}$ | $T_{20}$ | |
| 8 | -0.8 | -0.3 | -0.4 | -0.7 | -0.8 | -0.4 | -0.4 | 0.1 | 4.9 | 5.3 | 6.3 | 3.5 | 3.7 | 2.8 | 4.6 |
| 9 | -3.5 | -0.3 | -0.4 | -1.0 | -1.0 | -0.5 | -0.4 | 0.0 | 2.2 | 2.6 | 3.4 | 1.9 | 1.9 | 1.2 | 5.5 |
| 10 | -5.6 | -0.6 | -1.0 | -1.4 | -1.6 | -1.6 | -1.9 | 0.0 | 0.0 | 0.0 | 0.0 | 0.0 | 0.0 | 0.0 | 5.0 |
| 11 | -4.4 | -1.3 | -2.0 | -2.2 | -2.9 | -2.9 | -3.4 | 0.0 | 0.0 | 0.0 | 0.0 | 0.0 | 0.0 | 0.0 | 3.1 |
| 12 | -5.1 | -2.5 | -2.8 | -2.9 | -3.6 | -3.5 | -3.9 | 0.0 | 0.0 | 0.0 | 0.0 | 0.0 | 0.0 | 0.0 | 2.6 |
| 13 | -2.3 | -1.7 | -1.7 | -2.0 | -2.3 | -2.0 | -2.8 | 0.0 | 0.1 | 0.1 | 0.2 | 0.2 | 0.2 | 0.0 | 0.6 |
| 14 | -3.7 | -1.8 | -2.1 | -2.6 | -2.8 | -2.4 | -2.8 | 0.0 | 0.0 | 0.0 | 0.1 | 0.0 | 0.1 | 0.0 | 1.9 |
| 15 | -4.3 | -1.5 | -2.1 | -2.4 | -3.0 | -2.4 | -2.7 | 0.0 | 0.1 | 0.1 | 0.1 | 0.3 | 0.3 | 0.0 | 2.9 |
| 16 | -3.9 | -2.0 | -2.3 | -2.6 | -3.0 | -2.5 | -2.6 | 0.0 | 1.0 | 1.3 | 1.1 | 1.4 | 1.2 | 0.0 | 2.9 |
| 17 | -4.8 | -1.1 | -1.6 | -2.5 | -3.1 | -2.2 | -2.9 | 0.0 | 0.7 | 0.3 | 0.8 | 0.6 | 0.3 | 0.0 | 4.4 |
| Balance * | -3.8 | -0.4 | -0.7 | -0.8 | -1.6 | -1.3 | -2.0 | * difference between FI and TI in DD | | | | | | | |

*5.3.2.3.9.1.2.2* *January 2014*

During the 2014 January period the highest and lowest temperatures are recorded for NST. Maximum diurnal temperature is 22 °C, with minimums of -8 °C, yielding diurnal temperature ranges of 30 °C (Figure 138, pg. 262). Mean diurnal temperature is 0.4 °C and positive temperatures are attained on every day except 15 January, yielding ten potential freeze-thaw events. Of these potential freeze-thaw events a few freeze-thaw cycles are recorded (40%), evidenced through isolated exotherms. Thawing is evident through on 15 January, occurring shortly after midday. Exotherms (13-15 January) occur predominantly in the late evening or approaching midnight. The deepest frost event is recorded on 13 January, reaching ± 5 cm. A freezing depth of ± 2 cm is reached on 15 January and the remaining freeze-thaw cycles occur near the surface (± 1 cm). The intensity of frost events (diurnal minimum temperatures) ranges from -8 °C to -2 °C (19 and 12 January respectively). In comparison, maximum temperature ranges from 0-22 °C (15 and 12 January respectively), with the warmest diurnal minimum reached on the day of the greatest diurnal maximum temperature. Variability initially increases from air temperature to NST and then decreases with depth into the ground. Highest variability is evident at NST ($s$ = 3.2), lowest at $T_{20}$ ($s$ = 0.4). Air temperature variability is 2.2. In comparison, diurnal mean temperatures decrease with depth with the highest diurnal mean recorded for NST (0.4 °C) and the lowest at $T_{20}$ ( -2.0 °C). Mean diurnal air temperature is -3.0 °C.

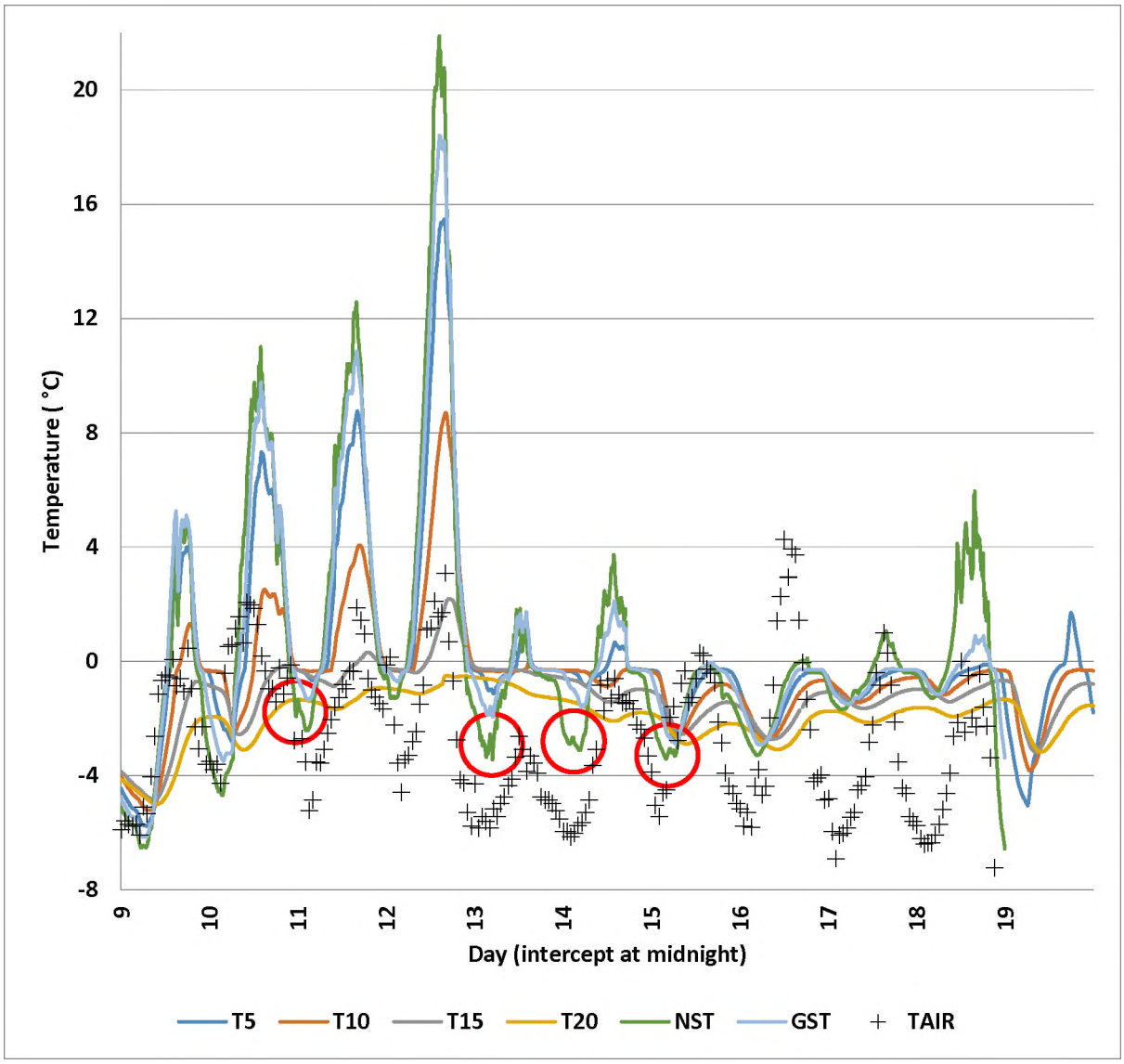


**Figure 138: Diurnal cycles for an eleven-day period from 9-20 January 2014. Exotherms are indicated with red circles. $T_{AIR}$: air temperatures. NST: ground temperatures recorded at ± 1 cm depth. GST: ground temperatures recorded at ± 2 cm depth. The subscript following 'T' indicates the depth of the sensor (in centimetres) used to record ground temperature.**

Thawing and freezing indices for the various sensors, given as days, are provided in Table 122 (pg. 263). Thawing indices decrease with increasing depth into the ground and none are observed for $T_{20}$. Freezing indices marginally exceed thawing indices ($T_{10}$-$T_{20}$), and are less than thawing indices for NST, GST and $T_5$. The balance of degree days for air temperature is ± 3 toward the freezing index. Freeze-thaw cycles are associated with high thawing indices on the day of the freeze event or on preceding days. The thermal offset is skewed towards positive values with the largest thermal offset of 7.6 observed on 12 January.

**Table 122: The freezing index (FI) and thawing index (TI) for the various sensor depth for A10 from 9-24 January 2014. $T_{AIR}$: air temperatures. NST: ground temperatures recorded at ± 1 cm depth. GST: ground temperatures recorded at ± 2 cm depth. The subscript following 'T' indicates the depth of the sensor (in centimetres) used to record ground temperature. SO: thermal offset. DD: degree days.**

| Day | FI | | | | | | | TI | | | | | | | SO |
|---|---|---|---|---|---|---|---|---|---|---|---|---|---|---|---|
| | $T_{AIR}$ | NST | GST | $T_5$ | $T_{10}$ | $T_{15}$ | $T_{20}$ | $T_{AIR}$ | NST | GST | $T_5$ | $T_{10}$ | $T_{15}$ | $T_{20}$ | |
| 9 | -2.9 | -2.8 | -2.6 | -2.5 | -2.6 | -3.1 | -3.8 | 0.0 | 0.9 | 1.1 | 0.8 | 0.2 | 0.0 | 0.0 | 0.9 |
| 10 | -0.9 | -1.2 | -0.9 | -0.7 | -0.6 | -0.9 | -1.7 | 0.4 | 1.6 | 1.3 | 0.9 | 0.3 | 0.0 | 0.0 | 2.8 |
| 11 | -1.8 | -0.5 | -0.3 | -0.2 | -0.1 | -0.4 | -1.3 | 0.2 | 4.1 | 3.7 | 3.0 | 1.3 | 0.0 | 0.0 | 5.3 |
| 12 | -2.0 | -0.3 | -0.2 | -0.1 | -0.1 | -0.1 | -0.8 | 0.5 | 6.4 | 5.8 | 4.9 | 2.7 | 0.6 | 0.0 | 7.6 |
| 13 | -4.6 | -1.1 | -0.6 | -0.4 | -0.3 | -0.4 | -0.9 | 0.0 | 0.2 | 0.2 | 0.1 | 0.0 | 0.0 | 0.0 | 3.7 |
| 14 | -3.1 | -1.0 | -0.5 | -0.3 | -0.5 | -1.0 | -1.8 | 0.0 | 0.7 | 0.4 | 0.1 | 0.0 | 0.0 | 0.0 | 2.8 |
| 15 | -2.4 | -1.6 | -1.1 | -1.0 | -1.4 | -1.8 | -2.4 | 0.0 | 0.0 | 0.0 | 0.0 | 0.0 | 0.0 | 0.0 | 0.9 |
| 16 | -2.6 | -1.4 | -1.4 | -1.4 | -1.6 | -1.9 | -2.4 | 0.8 | 0.0 | 0.0 | 0.0 | 0.0 | 0.0 | 0.0 | 0.3 |
| 17 | -3.8 | -0.7 | -0.8 | -0.8 | -1.0 | -1.3 | -1.9 | 0.1 | 0.1 | 0.0 | 0.0 | 0.0 | 0.0 | 0.0 | 3.2 |
| 18 | -4.2 | -0.9 | -0.6 | -0.5 | -0.7 | -1.0 | -1.7 | 0.0 | 1.4 | 0.1 | 0.0 | 0.0 | 0.0 | 0.0 | 4.7 |
| 19 | -6.2 | -2.9 | -2.1 | -1.8 | -1.5 | -1.7 | -2.2 | 0.0 | 1.8 | 0.2 | 0.2 | 0.0 | 0.0 | 0.0 | 5.1 |
| Balance * | -3.0 | 0.2 | 0.2 | 0.0 | -0.5 | -1.2 | -1.9 | * difference in DG between FI and TI | | | | | | | |

*5.3.2.3.9.1.2.3* *December 2014*

During the 2014 December period the most extreme temperature values are recorded for NST. Maximum diurnal temperature is 15 °C , minimums are -7 °C, yielding diurnal temperature ranges of 22 °C (Figure 139, pg. 264). Diurnal mean temperature is 1 °C and positive and sub-zero temperatures are attained daily, yielding six potential freeze-thaw events. Of these potential freeze-thaw events two freeze-thaw cycles are recorded (33%). These freeze-thaw cycles compare with freeze-thaw cycles identified for this observation period as discussed in the previous section (5.3.2.3.9 A10: Vesleskarvet, pg. 253). Freezing events are evident through isolated exotherms (26 and 27 December respectively). Exotherms occur generally in the mid to late evening. The 23 December freeze-thaw cycle reaches ± 2 cm; the 27 December freeze-thaw cycle ± 5 cm. Intensity of frost events (diurnal minimum temperature) ranges from -7 °C to -6 °C (24 and 23 December respectively). In comparison, maximum temperature ranges from 6-15 °C (28 and 27 December respectively), with freeze-thaw cycles occurring on days with high diurnal maximum temperatures. Variability initially increases from air temperatures to NST and then decreases with depth into the ground. Highest variability is calculated for NST ($s$ = 5.7), lowest for $T_{20}$ ($s$ = 0.8). Air temperature variability is 2.6. Diurnal mean temperatures decrease with depth with the highest mean recorded for NST (0.9 °C), the lowest at $T_{20}$ (-3.4 °C). Diurnal mean air temperature is -6.7 °C.

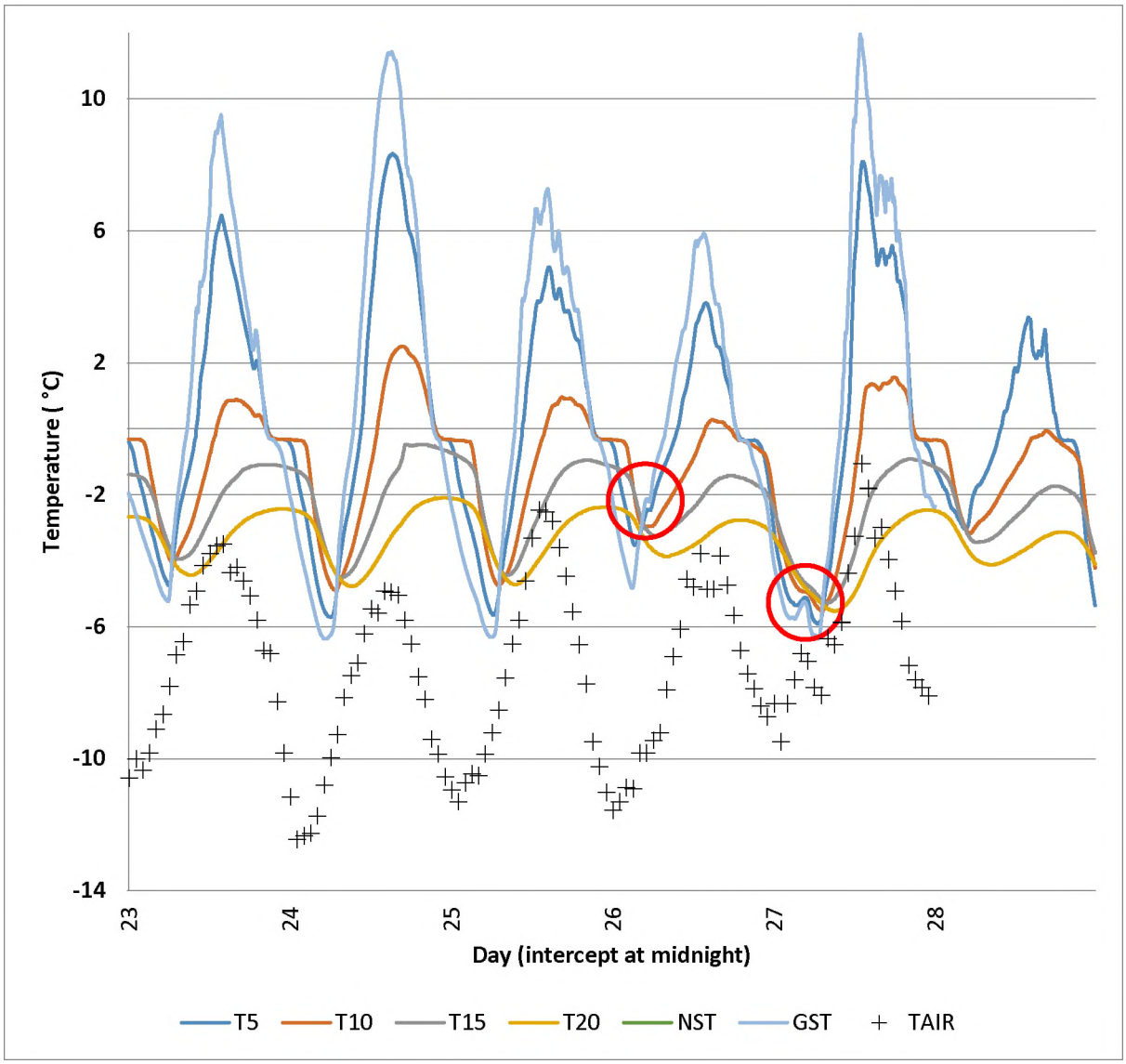


**Figure 139: Diurnal cycles for a six-day period from 23-29 December 2014. Exotherms are indicated with a red circles. $T_{AIR}$: air temperatures. NST: ground temperatures recorded at ± 1 cm depth. GST: ground temperatures recorded at ± 2 cm depth. The subscript following 'T' indicates the depth of the sensor (in centimetres) used to record ground temperature.**

Thawing and freezing indices for the various sensors, given as days, are provided in Table 123 (pg. 265). Thawing indices decrease with increasing depth into the ground and none are observed for $T_{15}$ and $T_{20}$. Freezing indices marginally exceed thawing indices for $T_{10}$-$T_{20}$ and are less than thawing indices for NST, GST and $T_5$. The balance of degree days for air temperature is ± 7 toward the freezing index and thawing indices decrease with increasing depth into the ground. Freeze-thaw cycles are associated with high thawing indices on the day of the thaw event. The thermal offset is skewed towards positive values with the largest thermal offset of 10.4 observed on 24 December.

**Table 123: The freezing index (FI) and thawing index (TI) for the various sensor depths for A10 from 23-29 December 2014. $T_{AIR}$: air temperatures. NST: ground temperatures recorded at ± 1 cm depth. GST: ground temperatures recorded at ± 2 cm depth. The subscript following 'T' indicates the depth of the sensor (in centimetres) used to record ground temperature. SO: thermal offset. DD: degree days.**

| Day | FI | | | | | | | TI | | | | | | | SO |
|---|---|---|---|---|---|---|---|---|---|---|---|---|---|---|---|
| | $T_{AIR}$ | NST | GST | $T_5$ | $T_{10}$ | $T_{15}$ | $T_{20}$ | $T_{AIR}$ | NST | GST | $T_5$ | $T_{10}$ | $T_{15}$ | $T_{20}$ | |
| 23 | -6.7 | -1.9 | -1.3 | -1.1 | -1.2 | -2.1 | -3.3 | 0.0 | 3.2 | 2.4 | 1.5 | 0.2 | 0.0 | 0.0 | 8.0 |
| 24 | -8.4 | -2.4 | -1.7 | -1.5 | -1.4 | -2.1 | -3.3 | 0.0 | 4.3 | 3.4 | 2.3 | 0.6 | 0.0 | 0.0 | 10.4 |
| 25 | -7.3 | -2.5 | -1.8 | -1.4 | -1.4 | -2.1 | -3.2 | 0.0 | 3.0 | 2.1 | 1.3 | 0.2 | 0.0 | 0.0 | 7.8 |
| 26 | -7.5 | -1.6 | -1.2 | -0.9 | -1.1 | -2.1 | -3.1 | 0.0 | 2.1 | 1.4 | 0.8 | 0.0 | 0.0 | 0.0 | 8.0 |
| 27 | -6.0 | -2.5 | -2.2 | -2.1 | -2.2 | -3.0 | -4.0 | 0.0 | 3.6 | 3.0 | 2.0 | 0.4 | 0.0 | 0.0 | 7.1 |
| 28 | -7.9 | -1.7 | -1.4 | -1.2 | -1.5 | -2.4 | -3.5 | 0.0 | 1.4 | 1.3 | 0.6 | 0.0 | 0.0 | 0.0 | 7.2 |
| Balance * | -7.3 | 0.8 | 0.7 | 0.1 | -1.2 | -2.3 | -3.4 | * difference in DG between FI and TI | | | | | | | |

*5.3.2.3.9.1.2.4* *January 2015*

During the 2015 period highest and lowest temperatures are recorded for NST. Maximum diurnal temperature is 7 °C, minimums reach -10 °C, yielding temperature ranges of 17 °C (Figure 140, pg. 266). Diurnal mean temperature at the near surface (NST) is -5 °C and sub-zero temperatures are reached daily. Positive temperatures are attained on eight days (potential freeze-thaw events: 8). Near surface temperatures (NST) and GST reflect potential freeze-thaw events on 13-17 and 26-28 January. $T_5$ reflects positive temperatures on 14-17 and 27 January, while $T_{10}$ attains positive temperatures on 16-17 January. $T_{15}$ and $T_{20}$ don't attain positive temperatures and evidence of thawing is absent. The lack of freeze-thaw cycles compares with freeze-thaw cycles identified as discussed in the previous section (5.3.2.3.9 A10: Vesleskarvet, pg. 253). A storm event associated with drifting snow occurred from 18-24 January (n = 6), yielding depressed temperatures for all sensors, as well as decrease in temperature variability. Variability initially increases from air temperatures to NST and then decreases with depth into the ground. Highest variability is observed for NST ($s$ = 2.42), lowest for $T_{20}$ ($s$ = 0.5). Air temperature variability is 2.06. Diurnal mean temperatures decrease with depth with the highest mean temperature recorded for NST (-4.6 °C), the lowest at $T_{20}$ (-6.2 °C). Diurnal mean air temperature is -6.8 °C. Thawing and freezing indices, given as days, are provided in Table 124 (pg. 267). Thawing indices decrease with increasing depth into the ground and none are observed during the storm event, $T_{15,}$ and $T_{20}$. Freezing indices generally exceed thawing indices and the balance of degree days for air temperatures is ± 6 toward the freezing index. This balance also increases with increasing depth into the ground. The thermal offset is skewed towards positive values with the largest thermal offset of 7.2 observed on 18 January and smaller values associated with depressed temperatures evident during the storm event.

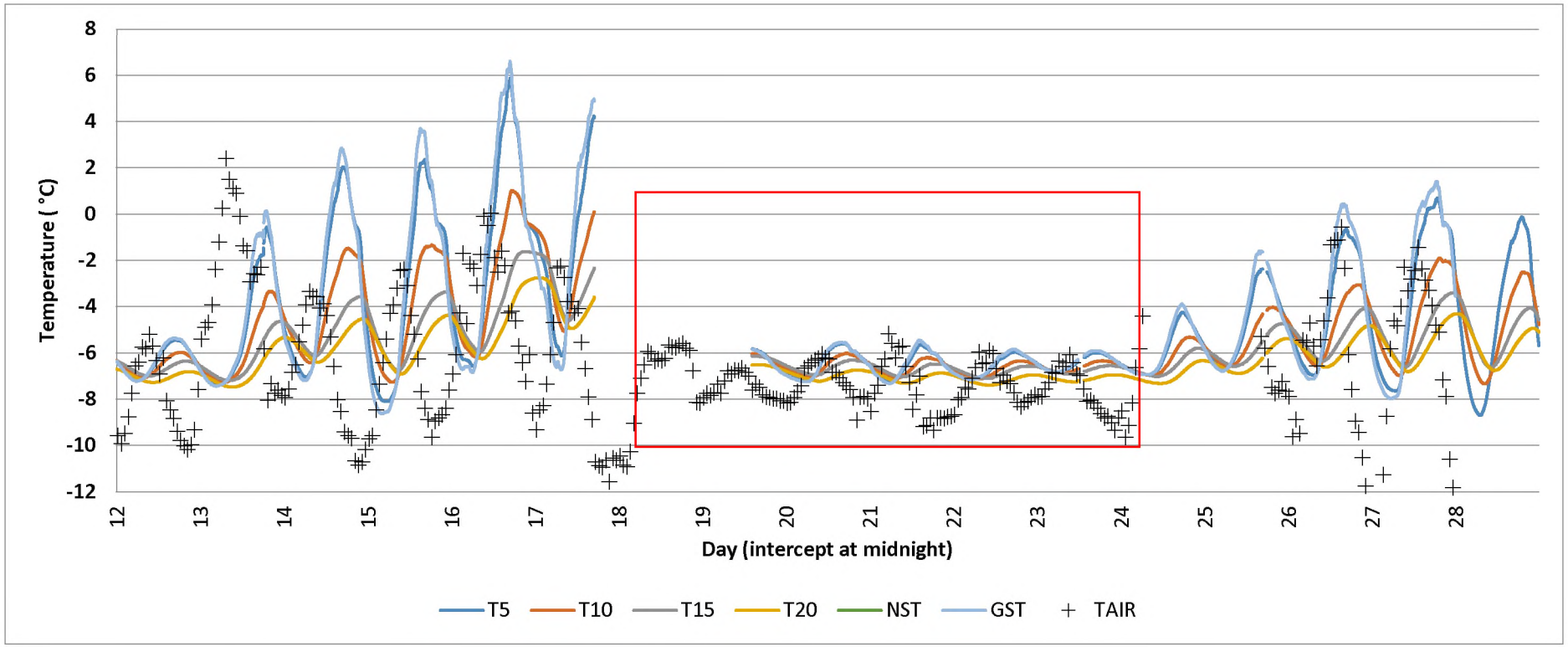


**Figure 140: Diurnal cycles for a seventeen-day period from 12-29 January 2015. No freeze-thaw cycles are recorded, and a storm event occurred 18-24 January. Snowfall is indicated with a red square. $T_{AIR}$: air temperatures. NST: ground temperatures recorded at ± 1 cm depth. GST: ground temperatures recorded at ± 2 cm depth. The subscript following 'T' indicates the depth of the sensor (in centimetres) used to record ground temperature.**

**Table 124: The freezing index (FI) and thawing index (TI) for the various sensor depths for A10 from 12-29 January 2015. $T_{AIR}$: air temperatures. NST: ground temperatures recorded at ± 1 cm depth. GST: ground temperatures recorded at ± 2 cm depth. The subscript following 'T' indicates the depth of the sensor (in centimetres) used to record ground temperature. SO: thermal offset. DD: degree days.**

| Day | FI | | | | | | | TI | | | | | | | SO |
|---|---|---|---|---|---|---|---|---|---|---|---|---|---|---|---|
| | $T_{AIR}$ | NST | GST | $T_5$ | $T_{10}$ | $T_{15}$ | $T_{20}$ | $T_{AIR}$ | NST | GST | $T_5$ | $T_{10}$ | $T_{15}$ | $T_{20}$ | |
| 12 | -8.0 | -6.4 | -6.3 | -6.3 | -6.5 | -6.7 | -7.0 | 0.0 | 0.0 | 0.0 | 0.0 | 0.0 | 0.0 | 0.0 | 1.6 |
| 13 | -3.3 | -4.5 | -4.6 | -4.9 | -5.7 | -6.3 | -6.8 | 0.3 | 0.0 | 0.0 | 0.0 | 0.0 | 0.0 | 0.0 | -1.4 |
| 14 | -6.9 | -3.6 | -3.4 | -3.3 | -4.0 | -4.9 | -5.6 | 0.0 | 0.5 | 0.4 | 0.3 | 0.0 | 0.0 | 0.0 | 3.8 |
| 15 | -6.6 | -4.0 | -3.8 | -3.6 | -4.2 | -5.0 | -5.7 | 0.0 | 0.8 | 0.6 | 0.4 | 0.0 | 0.0 | 0.0 | 3.3 |
| 16 | -3.7 | -2.7 | -2.6 | -2.5 | -2.8 | -3.9 | -4.8 | 0.0 | 1.9 | 1.6 | 1.2 | 0.1 | 0.0 | 0.0 | 2.8 |
| 17 | -7.2 | -2.2 | -2.0 | -1.7 | -1.8 | -2.3 | -2.8 | 0.0 | 1.2 | 0.7 | 0.4 | 0.0 | 0.0 | 0.0 | 5.7 |
| 18 | -7.2 | 0.0 | 0.0 | 0.0 | 0.0 | 0.0 | 0.0 | 0.0 | 0.0 | 0.0 | 0.0 | 0.0 | 0.0 | 0.0 | 7.2 |
| 19 | -7.5 | -2.6 | -2.6 | -2.6 | -2.6 | -2.6 | -2.7 | 0.0 | 0.0 | 0.0 | 0.0 | 0.0 | 0.0 | 0.0 | 1.0 |
| 20 | -7.2 | -6.5 | -6.4 | -6.4 | -6.5 | -6.6 | -7.0 | 0.0 | 0.0 | 0.0 | 0.0 | 0.0 | 0.0 | 0.0 | 0.8 |
| 21 | -7.6 | -6.5 | -6.5 | -6.5 | -6.6 | -6.7 | -7.1 | 0.0 | 0.0 | 0.0 | 0.0 | 0.0 | 0.0 | 0.0 | 1.1 |
| 22 | -7.3 | -6.5 | -6.5 | -6.6 | -6.7 | -6.8 | -7.2 | 0.0 | 0.0 | 0.0 | 0.0 | 0.0 | 0.0 | 0.0 | 0.8 |
| 23 | -7.68 | -5.89 | -5.91 | -5.93 | -6.09 | -6.20 | -6.54 | 0.00 | 0.00 | 0.00 | 0.00 | 0.00 | 0.00 | 0.00 | 1.3 |
| 24 | -1.83 | -5.71 | -5.80 | -5.88 | -6.27 | -6.54 | -6.97 | 0.00 | 0.00 | 0.00 | 0.00 | 0.00 | 0.00 | 0.00 | 1.6 |
| 25 | -2.64 | -4.33 | -4.47 | -4.60 | -5.16 | -5.53 | -6.00 | 0.00 | 0.00 | 0.00 | 0.00 | 0.00 | 0.00 | 0.00 | 2.4 |
| 26 | -7.02 | -4.20 | -4.19 | -4.36 | -5.03 | -5.47 | -6.02 | 0.00 | 0.19 | 0.03 | 0.00 | 0.00 | 0.00 | 0.00 | 3.1 |
| 27 | -6.22 | -3.56 | -3.36 | -3.39 | -4.36 | -5.03 | -5.63 | 0.00 | 0.30 | 0.21 | 0.06 | 0.00 | 0.00 | 0.00 | 2.9 |
| 28 | -8.93 | -4.35 | -4.14 | -4.12 | -4.52 | -4.81 | -5.25 | 0.00 | 0.03 | 0.03 | 0.00 | 0.00 | 0.00 | 0.00 | 4.0 |
| Balance * | -6.3 | -4.0 | -4.1 | -4.1 | -4.6 | -5.0 | -5.5 | * difference in DG between FI and TI | | | | | | | |

### 5.3.3 Sediment/soil specifics

Sediment textural properties are provided in Table 125 and discussed in the text following the table. Sediment moisture characteristics are given in **Table 126** (pg. 270) and discussed thereafter. Descriptive statistics are provided in **Table 127** (pg. 271) and discussed in the text following the table. Graphs are provided where deemed necessary.

**Table 125: Sediment physical characteristics and parameters for Dronning Maud Land study sites. Total organic carbon (TOC) is expressed as a percentage, $d_b$ reflects bulk density, $d_p$ indicates porosity of samples, and FEF (%) the fine earth fraction expressed as a percentage.**

| Site | Depth | TOC (%) | $d_b$ | $d_p$ | FEF (%) |
|---|---|---|---|---|---|
| A1 | Surface | 0.3 | n.d. | n.d. | 36.12 |
| A2 | | 0.5 | 1.69 | 0.36 | 57.89 |
| A3 | | 0.3 | 1.75 | 0.34 | 49.77 |
| A4 | | 0.3 | 1.83 | 0.31 | 46.86 |
| A5 | | 0.2 | 1.76 | 0.34 | 43.44 |
| A6 | | 0.8 | 1.86 | 0.30 | 42.69 |
| A7 | | 0.1 | 1.92 | 0.28 | 67.44 |
| A8 | | 0.1 | 1.89 | 0.29 | 68.84 |
| A9 | | 0.3 | 1.49 | 0.44 | 35.55 |
| A10 | | 0.6 | 1.97 | 0.26 | 43.35 |

Fine earth fraction (FEF: particles < 2 mm) proportions and total organic carbon (TOC) are low for Dronning Maud Land (DML) samples (Table 125; Figure 142, pg. 269). In comparison, bulk density values are high and porosity low (Figure 142, pg. 269). Fine earth fraction (FEF) proportions are well below 90% (Figure 143, pg. 269), suggesting that bulk density values are overestimated for these samples. Furthermore, FEF analyses for A10 (Vesleskarvet) samples show a lack of clay and silt-sized particles (Figure 144, pg. 270). Using organic matter content ($O_p$) as the classifier (Table 12, APPENDIX E), samples are classed as mineral soils. Using bulk density and porosity as classifiers (Table 9 and Table 10, APPENDIX E), samples are classed as sand or fine sand-fine gravel respectively. This reflects average specific yield ($S_y$) between 21-27 (Table 11, APPENDIX E) and a specific retention of moisture at ± 6 (Robson, 1993).

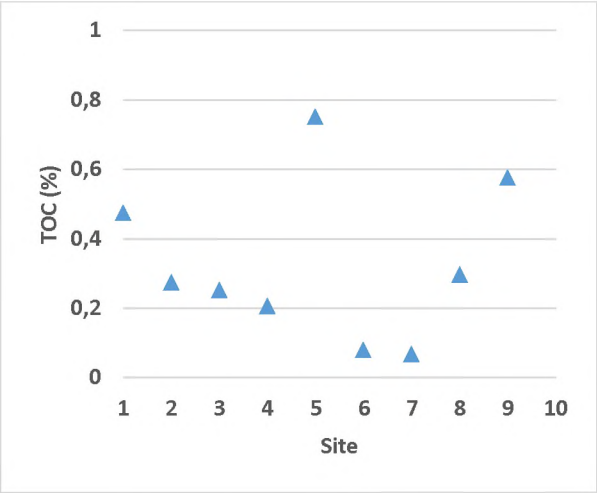


Figure 141: Total organic carbon (TOC) expressed as a percentage for Dronning Maud Land sites. 1-10 indicate sites A1-A10.

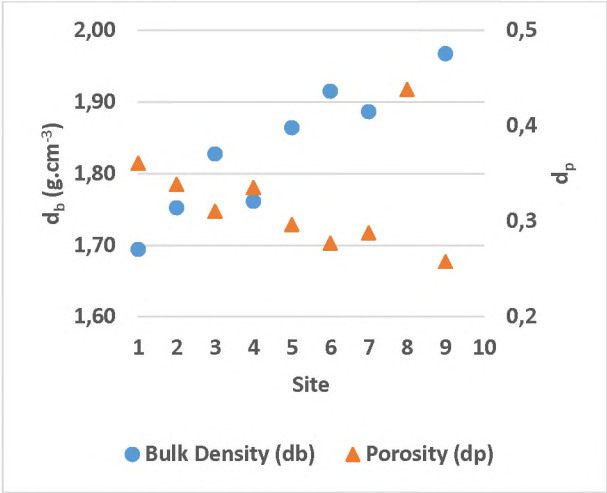


Figure 142: Bulk density ($d_b$) and porosity ($d_p$) for Dronning Maud Land sites. 1-10 indicate sites A1-A10.

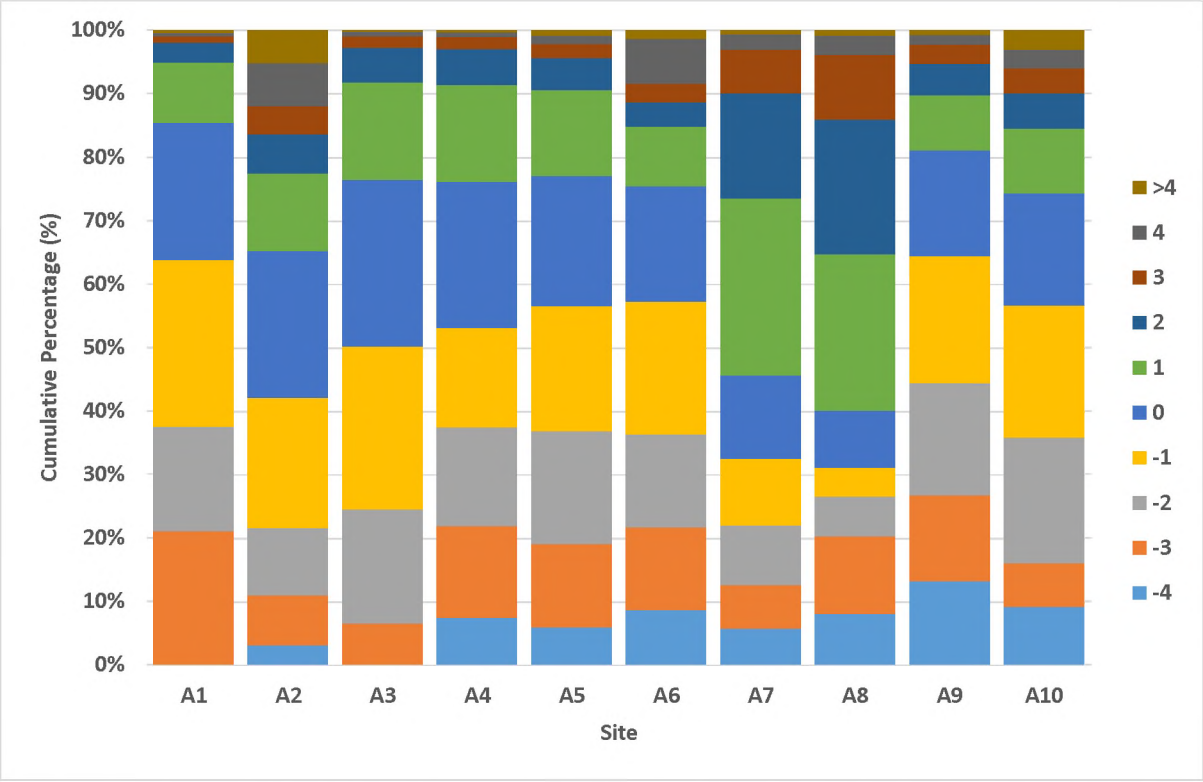


Figure 143: Cumulative particle size distribution of Dronning Maud Land sampling sites, displayed using Phi (φ) values.


**Figure 144: Sand-silt-sand ternary diagram of A10 (Vesleskarvet) sediment samples. The diagram reflects sediment ratios evaluated for the fine earth fraction (FEF: particles < 2mm in diameter) only.**

**Table 126: Sediment moisture characteristics and parameters for Dronning Maud Land study sites. $\theta_v$ denotes volumetric water content; $\theta_g$ gravimetric water content; $M_c$ gravimetric water content expressed as a percentage; $M_p$ the soil water-filled pore space.**

| Site | Depth | $\theta_v$ | $\theta_g$ | $M_c$ (%) | $M_p$ |
|---|---|---|---|---|---|
| A1 | Surface | n.d. | n.d. | n.d. | n.d. |
| A2 | Surface | 0.15 | 0.09 | 8.64 | 0.24 |
| A3 | Surface | 0.03 | 0.02 | 1.85 | 0.05 |
| A4 | Surface | 0.05 | 0.03 | 2.83 | 0.09 |
| A5 | Surface | 0.11 | 0.06 | 6.42 | 0.19 |
| A6 | Surface | 0.04 | 0.02 | 2.02 | 0.07 |
| A7 | Surface | 0.00 | 0.00 | 0.19 | 0.01 |
| A8 | Surface | 0.06 | 0.03 | 3.09 | 0.11 |
| A9 | Surface | 0.06 | 0.04 | 4.31 | 0.10 |
| A10 | Surface | 0.20 | 0.10 | 10.25 | 0.40 |

Moisture samples were obtained during summers and as such, give an indication of expected summer ground moisture content. Dronning Maud Land samples exhibit low moisture contents (**Table 126**, pg. 270; Figure 145). Volumetric water content (VWC: $\theta_v$) registers consistently below ± 0.2, with gravimetric water content (GWC: $\theta_g$) consistently below 0.1 ($M_c$ < ± 10%). Averages for VWC, GWC, GWC expressed as a percentage ($M_c$), and the soil water-filled pore space ($M_p$) are 0.08, 0.04, 4.40% and 0.14 respectively. A10 exhibits the highest VWC at 0.2, followed by A2. Higher VWC values for these sites are reflected in higher soil water-filled pore spaces. Nevertheless, moisture values are low for DML sites and freeze-thaw processes are hampered due to the paucity of moisture.


**Figure 145: Volumetric water content (VWC) and gravimetric water content (GWC) for Dronning Maud Land sites. 1-10 denote sites A1-A10.**

**Table 127: Phi (φ) descriptive characteristics and the uniformity coefficient ($C_u$) for Dronning Maud Land sediment samples.**

| Site | Depth | Phi (ϕ) Mean | Skewness | Sorting | $C_u$ |
|---|---|---|---|---|---|
| A1 | Surface | Fine gravel | Finely negative | Very poor | Very poor, well graded |
| A2 | | Coarse sand | Finely positive | | Extremely poor, well graded |
| A3 | | | | | Very poor, well graded |
| A4 | | Fine gravel | Symmetrical | | Extremely poor, uniformly graded |
| A5 | | | | | |
| A6 | | | Finely positive | | Extremely poor, well graded |
| A7 | | Coarse sand | Negative | | |
| A8 | | Fine gravel | | | |
| A9 | | | Symmetrical | | |
| A10 | | | Finely positive | | |

Phi (ϕ) mean values for central and western Dronning Maud Land (CDML and WDML) show predominantly coarse sediment, with fine gravel dominating (A1, A4-A6, A8-A10). Phi (ϕ) skewness values show variably skewed populations, with negative values suggesting predominantly coarse fragments and *vice versa* (Table 127). Samples are poorly sorted. The Phi (ϕ) sorting and uniformity coefficient ($C_u$) both indicate sediment samples to be extremely to very poorly sorted and well graded. The Kolmogorov-Smirnov (K-S) test shows that most samples for Dronning Maud Land are dissimilar at $p < 0.05$. The null hypothesis for the K-S tests cannot be rejected at $p < 0.05$ for A4-A5 (Robertskollen and Schumacherfjellet) and A6-A10 (Slettfjell-Vesleskarvet).

## 5.4 Modelling the Diurnal Frost Environment

The control on freeze-thaw cycles and potential freeze-thaw events observed can be determined by evaluating specific parameters against each other. These were identified in Table 5 (pg. 75) and quantified where possible using data collected during the study. The various subsections below address each of these parameters. Each parameter, its relevance to freeze-thaw cycles, and implications is discussed below.

### 5.4.1 Air temperatures, ground temperatures, soil moisture, wind speed and direction

When evaluating ground temperatures, A1 reflects oscillations around 0 °C 15 % on an annual basis at the near surface (NST: recorded at ± 1 cm in the ground), reducing to 2% to the depth of the active layer. At NST of A2, 9% of diurnal cycles reflect oscillations around 0 °C, reducing to almost none to the depth of the active layer. For NST at A3, 14% of diurnal cycles reflect oscillations around 0 °C, reducing to 1% to the depth of the active layer. The percentage of diurnal cycles at A4-A10 (excluding A7) at NST are 19%, 4%, 2%, 7%, 23%, and 10% respectively. At the depth of the active layer such diurnal ranges reduce to ± 0%, ± 0%, 2%, ± 0%, 9%, and ± 0% for A5-A10 (excluding A8) respectively. Ambient air temperatures are highly correlated with NST and ground surface temperatures (GST: ± 2 cm in the ground), although greater variability is explained by principal component (PC) when using GST over NST. For those data in Dronning Maud Land (DML) where NST and GST observation points are available (ACR systems: NST-$T_{20}$), the variability associated with GST for the principal component equals 0.8 versus that of NST of 0.7. And while air temperature is correlated most strongly with NST ($r$ = 0.9, $p$ < 0.05); GST at $r$ = 0.6 ($p$ < 0.05) is correlated most strongly to sensor depths within the ground when compared to NST. Conducting Principal Component Analysis (PCA) for air temperatures, GST, $T_5$, $T_{10}$, $T_{15}$ and $T_{20}$ for western Dronning Maud Land (WDML) sites shows principal components of 0.8 and 0.2 in terms of the proportion of variance on average for PC1 and PC2. For PC1 these various parameters (sensor depths) share ± equal component loadings, although small differences are apparent. Ambient air temperature scores consistently lower compared to other parameters (± 50% compared to the average component loading), as does $T_{20}$ on occasion (25% compared to average component loading). In comparison, $T_5$ and $T_{10}$ frequently score higher component loadings (on par with average component loading). A6 in central Dronniing Maud Land (CDML) behaves differently to WDML sites in that component loadings for all parameters, excepting $T_{20}$, equate to each other. $T_{20}$ contributes 25% less of the component loadings toward the principal component. An evaluation of PC2 (where applicable) shows that loadings reverse (a positive relationship reverts to a negative relationship) from $T_5$/$T_{10}$ onwards. This is mirrored by the correlation coefficient, which shows that GST is most strongly correlated to $T_5$ and $T_{10}$, less for $T_{15}$ and even less to $T_{20}$ (all at $p$ < 0.05). A7 in CDML again behaves differently where higher values for the correlation coefficient are alculated for $T_{15}$ and only a significant drop in correlation occurs for $T_{20}$.

Volumetric water content (VWC) exhibits the strongest and most significant correlation to gravimetric water content (GWV), GWC expressed as a percentage($M_c$), and soil water-filled pore space ($M_p$) ($r$ ± 0.99, $p$ ± 0.00). Evaluating temperature populations for DML study sites together with soil moisture shows all sites having only one principal component. A10 is the exception with two principal

components (Table 128). Component loadings for all sites fall into a narrow range and it is difficult to remove variables based on their loadings. The exception is soil moisture, which consistently scores lower across the sites. Average active layer thickness also yields into higher component loadings. $T_{15}$ and $T_{30}$ show high component loadings for all WDML sites. For CDML $T_{50}$ and $T_{100}$ exhibit high component loadings.

**Table 128: Component loadings for principal components (PC) for Dronning Maud Land sites for the various temperature and moisture parameters. Sensors depths are indicated with a subscript. WDML: western Dronning Maud Land. CDML: central Dronning Maud Land. $T_{AIR}$: air temperatures. NST: ground temperatures recorded at ± 1 cm depth. The subscript following 'T' indicates the depth of the sensor (in centimetres) used to record ground temperature. SM: soil moisture. Var: proportion of variance per PC. Values in bold represent variables contributing the greatest variance towards the PC. Yellow blocks indicate to the depth the average active layer thickness (ALT) is recorded. * Active layer thickness unknown.**

| WDML | $T_{AIR}$ | NST | $T_{15}$ | $T_{30}$ | $T_{45}$ | $T_{60}$ | SM | Var |
|---|---|---|---|---|---|---|---|---|
| A1 | 0.38 | 0.39 | **0.40** | **0.40** | **0.40** | 0.39 | 0.27 | 0.86 |
| A2 | 0.38 | 0.39 | **0.40** | **0.40** | **0.40** | 0.39 | 0.25 | 0.86 |
| A3 | 0.38 | 0.40 | **0.41** | **0.41** | **0.41** | 0.40 | 0.17 | 0.83 |
| A4 | 0.39 | 0.40 | **0.41** | **0.41** | **0.41** | **0.41** | 0.09 | 0.82 |
| A5 | 0.39 | 0.40 | **0.41** | **0.41** | **0.41** | 0.40 | 0.16 | 0.83 |
| A6 | 0.38 | 0.39 | **0.41** | **0.41** | 0.40 | 0.40 | 0.22 | 0.85 |
| A9 | 0.38 | 0.37 | **0.40** | **0.40** | **0.40** | **0.40** | 0.27 | 0.85 |
| A10: PC1 | 0.38 | 0.40 | **0.42** | **0.42** | **0.42** | 0.41 | 0.05 | 0.79 |
| A10: PC2 | -0.04 | -0.05 | 0.02 | 0.04 | **0.06** | **0.08** | -0.99 | 0.14 |
| CDML | $T_{AIR}$ | NST | $T_{50}$ | $T_{100}$ | $T_{150}$ | $T_{200}$ | ctiv | Var |
| A7 | 0.35 | 0.41 | **0.42** | **0.42** | 0.41 | 0.39 | 0.17 | 0.78 |
| A8 * | 0.40 | n/a | **0.46** | **0.46** | **0.46** | 0.44 | -0.13 | 0.77 |

Evaluating temperature populations for DML study sites together with soil moisture shows soil moisture component loadings are lowest overall, except for PC2 of A10 where soil moisture contributes the highest loading toward the PC (Table 128). Calcualtion the correlation coefficient for sensor depths and soil moisture for DML sites shows that air temperatures is most strongly correlated to NST $r = 0.96$ for WDML and $r = 0.87$ for CDML; $rp < 0.0001$). However, $T_{15}$ and $T_{30}$ score consistently highest coefficients to all other sensor depths for all sites in WDML except A4, for which $T_{15}$-$T_{45}$ consistently score the highest coefficients. For CDML this relationship is apparent for $T_{50}$ (Table 129, pg. 274). Consistently highest coefficients for soil moisture occur for sensor depths to which active layer thickness occurs. These values are shown in the fifth column of Table 129 (pg. 274). Values in bold represent composite coefficients exceeding the average coefficient for soil moisture to all other sensors for that site; values italicised represent composite coefficients 0.01 less than averagecoefficient for soil moisture compared to all other sensors for that site; values neither bolded nor italicised represent composite coefficients equal to the average coefficient for soil moisture to all other sensors for that site.

**Table 129: Average correlations ($p < 0.0001$) for specific sensor depths ($T_{15}$, $T_{30}$, $T_{45/50}$) to all other sensors for Dronning Maud Land sites. Active layer thickness (ALT) is shown, as is the average correlation of sensors at which ALT occurs with respect to soil moisture (SM-ALT).**

| Site | $T_{15}$ | $T_{30}$ | $T_{45}$ / $T_{50}$ | SM-ALT | ALT |
|---|---|---|---|---|---|
| A1 | 0.96 | 0.96 | 0.94 | **0.59** | 25 |
| A2 | 0.97 | 0.97 | 0.96 | **0.56** | 15 |
| A3 | 0.97 | 0.96 | 0.96 | **0.35** | 29 |
| A4 | 0.97 | 0.97 | 0.96 | *0.16* | 58 |
| A5 | 0.97 | 0.97 | 0.96 | 0.32 | 29 |
| A6 | 0.97 | 0.96 | 0.95 | *0.44* | 12 |
| A7 | n/a | | 0.81 | **0.34** | 38 |
| A8 | | | 0.94 | *0.20* | n/a |
| A9 | 0.96 | 0.95 | 0.94 | **0.58** | 29 |
| A10 | 0.94 | 0.94 | 0.94 | **0.11** | 16 |

Evaluating diurnal mean, maximum temperature, minimum temperature, and thaw duration for WDML sites shows that one principal component is identified for each site with each variable contributing in a similar manner in terms of loadings (Table 130). For years where deeper active layer thickness is observed component loadings of sensors deeper within the ground (using higher-frequency ACR systems) contribute similarly to the principal compoennt as those sensors at shallower depths. This suggests that as active layer thickness increases the observations recorded at increasing depths within the ground increase in significance. A7 in CDML is the only site in DML where two principal compponents are evident. Diurnal temperature range, variability (expressed as standard deviation: *s*), and diurnal temperature range computed using diurnal maximum temperature and diurnal minimum temperature do not contribute significantly to component loadings.

**Table 130: Component loadings for diurnal mean temperatures ($T_{DM}$), diurnal maximum temperatures ($T_{D:max}$), diurnal minimum temperatures ($T_{D:min}$), and thaw duration for Dronning Maud Land study sites. Var: variance. Values separated by ';' represent *r* for the variable and thaw duration. Values separated by '/' indicate loadings for principal components (PC 1 and PC 2 respectively). § indicates *r* not significant at $p < 0.05$.**

| Site | $T_{DM}$ | $T_{D:max}$ | $T_{D:min}$ | Thaw Duration | PC 1 Var | PC 2 Var |
|---|---|---|---|---|---|---|
| A1 | 0.5; 0.8 | 0.5; 0.7 | 0.5; 0.8 | 0.5 | 0.9 | n/a |
| A2 | 0.6; 0.8 | 0.5; 0.8 | 0.4; 0.4 | 0.5 | 0.7 | n/a |
| A3 | 0.6; 0.9 | 0.5; 0.8 | 0.4; 0.5 | 0.5 | 0.8 | n/a |
| A4 | 0.5; 0.5 | 0.5; 0.5 | 0.5; 0.5 | 0.4 | 0.8 | n/a |
| A5 | 0.5; 0.8 | 0.5; 0.8 | 0.5; 0.7 | 0.5 | 0.8 | n/a |
| A6 | 0.5; 0.8 | 0.5; 0.9 | 0.5; 0.6 § | 0.5 | 0.8 | n/a |
| A7 | 0.7; 0.1 § \| -0.3 | 0.6; -0.2 § \| 0.4 | 0.5; 0.2 § \| 0.8 | 0.0 | 0.6 § | 0.3 |
| A8 | n/a | | | | | |
| A9 | 0.6; 0.7 | 0.5; 0.7 | 0.5; 0.5 | 0.5 | 0.8 | n/a |
| A10 | 0.6; 0.9 | 0.4; 0.5 | 0.5; 0.8 | 0.5 | 0.8 | n/a |

Diurnal ranges exceeding 10 °C, compared to oscillations indicative of potential freeze-thaw events for Dronning AMud Land (DML) sites show a significant relationship for these parameters when evaluating ground temperatures ($r \pm 0.81$, $p \pm 0.01$). An evaluation of air temperatures shows no such relationship ($r \pm 0.07$, $p \pm 0.86$). Comparing air temperature oscillations indicative of potential freeze-thaw events to active layer thickness and diurnal freezing depth ($d$) shows a significant relationship ($r \pm 0.70$, $p < 0.05$), as well as mean annual air temperature (MAAT: $r \pm 0.91$, $p \pm 0$). The same comparison using ground temperatures shows a lack of a significant relationship for these parameters. Nevertheless, comparing these oscillatrions to freeze-thaw cycles indicates a significant relationship ($r \pm 0.69$, $p < 0.05$). Correlating air temperure diurnal ranges exceeding 10 °C, evaluated against oscillations indicative of potential freeze-thaw events, for all sites suggests a strong and significant relationship ($r \pm 0.79$, $p < 0.01$). Furthermore, such ranges are strongly correlated to MAAT ($r \pm 0.94$, $p \pm 0$), as well as mean annual ground temperature (MAGT: $r \pm 0.89$, $p \pm 0$). The same comparison using ground temperatures shows a lack of a significant relationship for these parameters.

Freeze-thaw cycles evaluated together with wind speed and direction for data sets from Vesleskarvet (Antarctica) and Ben MacDhui (Eastern Cape of mainland South Africa) indicate that wind direction is not significant on the ground thermal regime, whereas wind speed is a significant parameter at $p < 0.05$.

### 5.4.2 Soil properties

Principal Component Analysis (PCA) shows that bulk density explains the variability of both porosity and permeability and a high and significant correlation is calculated for bulk density and porosity ($r \pm$-0.99, $p \pm 0.00$). Phi ($\phi$) mean and the fine earth fraction (FEF: particles < 2 mm in diameter) exhibit a strong correlation ($r = 0.88$, $p \pm 0.02$), as do organic content ($O_p$) and total organic carbon (TOC) ($r \pm 0.99$, $p \pm 0.00$). Principal Component Analysis (PCA) for bulk density, Phi ($\phi$) mean, organic content, and soil moisture shows that sediment properties trend together, with moisture properties trending together on a separate principal components.

### 5.4.3 Vegetation, snow and cloud cover

Sites on mainland South Africa are variably vegetated. Vegetation has a significant and negative control on freeze-thaw cycles at $p < 0.05$. The effect of snow cover on potential freeze-thaw events and freeze-thaw cycles in the Elandberg and High Drakensberg of South Africa is presented in 5.1.2.3 Diurnal frost environment (pg. 134 onwards). Dronning Maud Land snow cover is discussed for A4 (5.3.2.3.4 A4: Robertskollen, pg. 234) and A10 (5.3.2.3.9 A10: Vesleskarvet, pg. 253). Here the presence of snow provides an insulating effect, maintaining and ameliorating ground temperatures. In DML snow cover reduces variability (expressed as standard deviation: $s$) of all ground temperature sensors, particularly near and ground surface temperatures (NST: recorded at ± 2 cm in the ground; GST: recorded at ±2 cm in the ground). No freeze-thaw cycle nor potential freeze-thaw events are recorded for periods when snowfall is verifiably present. Similarly, on Marion Island snow cover reduces snow temperature variability, although the depth of frost cycles increases during times of snow cover. The same applies

to freeze-thaw cycles evident on Ben MacDhui in the Eastern Cape when ground snow cover is present. Cloud cover was evaluated for all sites. Although cloud cover has a negative effect on freeze-thaw cycles., *i.e.* less freeze-thaw cycles are recorded when cloud cover is present, these results must be considered with caution. Cloud cover is not available at hourly frequency. As such, results reflect daily cover, whereas freeze-thaw cycles may occur at much higher-frequency.

### 5.4.4 Altitude

An altitudinal gradient is also present in the Eastern Cape and on Marion Island. On Ben MacDhui (Eastern Cape) absolute maximum annual ground temperatures increase at ± 5.9 °C per 100 m increase in altitude. Seasonal ranges, in contrast, decrease at ± 5.5 °C per 100 m increase in altitude. Absolute minimum ground temperatures only decrease with ± 0.4 °C per 100 m increase in altitude, similar to average ground temperatures decreasing with ± 0.6 °C per 100 m increase in altitude. In the Elandsberg average ground temperatures decrease by ± 1.0 °C per 100 m increase in altitude. Annual absolute maximum ground temperatures, as well as seasonal ranges decrease by ± 0.8 °C for every 100 m increase in altitude. Like Ben MacDhui, changer per altitude is less for absolute minimum ground temperatures. These temperature decrease by ± 0.1 °C for every increase in altitude. The smaller temperature changes calculated for minimum temperatures are attributed to the insolating effect of vegetation.

Work by Hedding (2006) at Ned's North and Ned's South (± 800 m a.s.l.), showed that the greatest maximum and minimum ground temperatures occur at the near surface. At Ned's South, no seasonal freeze was recorded at the near surface, with 225 potential freeze-thaw events (potential freeze-thaw events: oscillations around 0 °C) observed. Similarly, at Ned's North no seasonal freezing occurred, with 192 potential freeze-thaw events recorded. The longest seasonal freeze at Ned's South occurred at 75 cm within the ground (71 days), decreasing to 26 and 12 days at 50 cm and 25 cm respectively. Similarly, the longest seasonal freeze at Ned's North occurred at 75 cm within the ground (81 days), decreasing to 45 and 30 days at 50 cm and 25 cm respectively. The average diurnal range at Ned's North was 4.6 °C, compared to the average diurnal range at Ned's South of 6 °C. At 25 cm in the ground this range is 1.4 °C and 0.8 °C respectively. A similar trend is evident with maximum diurnal ranges observed. At Ned's North, a range of 21.1 °C is observed for the near surface, compared to a maximum diurnal range of 9.3 °C at 25 cm. At Ned's South, a maximum diurnal range of 24.3 °C is recorded, compared to a maximum diurnal range of 3.9 °C at 25 cm. Both sites showed a decrease of potential freeze-thaw events from the near surface to a depth of 75 cm within the ground. Similarly, median ground temperatures at Ned's North and Ned's South for the near surface and 25 cm depths were 1.9 °C and 1.3 °C, and 1.8 °C and 1.2 °C respectively. Bierman (2014), at Katedraalkrans (± 750 m a.s.l.), determined absolute maximum, absolute minimum, and mean near surface soil temperatures to be 25.6 °C, -10.7 °C, and 2.3 °C respectively. Mean air temperatures were calculated to be 0.2 °C, with 118 frost days recorded during the observation period (April 1999-April 2000). Furthermore, near surface soil temperatures at Katedraalkrans are not as strongly correlated to air temperatures ($r$ ± 0.74, $p < 0.01$), when compared to sites closer to the coast, or the Central Highland. Nevertheless, similar to Hedding (2006), an increase in potential freeze-thaw events is evident when moving from the coastal areas further inland toward the Central Highland. These trends are confirmed by data from M1 and M2.

Seasonal ranges increase with increasing altitude and distance from the coast. Furthermore, colder temperatures are recorded at higher elevations, as is longer seasonal frost.

In Dronning Maud Land, an increase in altitude is associated with a decrease in mean annual air temperature (MAAT) and an increase in freeze-thaw cycles: an increase in altitude reflects a strong negative relationship to freeze-thaw cycles at $r = -0.7$ ($p < 0.01$). In comparison, an increase in altitude reflects a strong positive relationship to potential freeze-thaw events observed for air temperatures and near surface temperatures ($r = 0.7$ for both, $p < 0.05$). (Near surface temperatures are measured at ± 1 cm within the ground.) Furthermore, potential freeze-thaw events for $T_{30}$ and $T_{45}$ for Dronning Maud Land sites correlate to altitude ($r = -0.85$, $p \pm 0.02$ and $r = -0.85$, $p \pm 0.01$ respectively). Altitude is strongly correlated to averages calculated per sensor depth and to maximum temperatures recorded at $T_{60}$ for these sites ($r > -0.76$, $p < 0.05$ and $r = -0.79$, $p \pm 0.02$ respectively). Similarly, altitude is strongly correlated to minimum temperatures observed for air temperatures for all sensors ($r = -0.80$, $p \pm 0.02$ and $r > -0.75$, $p \pm 0.02$ respectively). The deepest sensors also exhibit the strongest and most significant correlations to minimum temperatures observed ($r = -0.91$, $p \pm 0.00$). Principal Component Analysis (PCA) shows that altitude is inversely related to active layer thickness and freeze-thaw cycles with high component loadings calculated (loadings > 0.40).

### 5.4.5 Latitude and distance from the ice shelf/ocean

In the Eastern Cape, latitude and longitiude are strongly correlated to means calculated for ground surface temperature (GST: $r > 0.86$. $p < 0.01$), as well as minimums recorded $r > 0.93$. $p \pm 0.00$). In comparison, distance to the coast correlates more strongly than latitude/longiture to means and minmums recorded at GST ($r > -0.87$. $p < 0.01$ and $r > -0.93$. $p < 0.001$ respectively). Nevertheless, like Dronning Maud Land (DML) sites (discussed below), latitude, longitude ($r > 0.46$. $p \pm 0.3$), and distance to the coast ($r > 0.64$. $p \pm 0.1$) are not as strongly correlated to maximum temperatures recorded at GST. For Eastern Cape locations distance to the coast correlates more strongly to potential freeze-thaw events and freeze-thaw cycles at GST, as well as temperatures variables calculated (means, maximums, minimums). Correlations of latitude, longitude, and distance to the coast to potential freeze-thaw events and freeze-thaw cycles at GST are similar at $r = 0.99$ ($p \pm 0.00$) and $r = 0.94$ ($p \pm 0.01$) respectively.

In Dronning Maud Land (DML), an increase in latitude is associated with a reduction in mean annual air temperature (MAAT), affecting freeze-thaw cycles. Latitude is strongly correlated to temperature averages calculated per sensor depth ($r > 0.89$, $p < 0.02$ for all), with air temperatures, ground temperatures (NST: recorded at ± 1 cm in the ground; GST: recorded at ± 2 cm in the ground) and the deepest sensor most strongly correlated ($r = 0.91$, $p < 0.002$; $r = 0.92$, $p < 0.002$ and $r = 0.93$, $p < 0.001$ respectively). Similarly, latitude is strongly correlated to minimum air temperature. Furthermore, air temperatures correlate most strongly with $T_{15}$ and $T_{30}$ ($r = 0.93$, $p < 0.001$; $r = 0.94$, $p < 0.001$ and $r = 0.93$, $p < 0.001$ respectively). In comparison, latitude is not correlated to maximum temperatures except for $T_{60}$ ($r = 0.83$, $p \pm 0.01$).

Principal Component Analysis (PCA) shows that distance to the shelf for each DML site is inversely related to freeze-thaw cycles. While component loadings towards the Principal component are high, the loadings are consistently lower than those shown by altitude at an average of ± 10%. Potential freeze-thaw events for $T_{30}$ and $T_{45}$ correlate to distance of the site to the ice shelf ($r$ = -0.66, $p < 0.05$ for both). Similarly, distance to shelf is strongly correlated to minimum air and ground temperature ($r$ = -0.83, $p \pm 0.01$ and $r > -0.78$, $p \pm 0.02$ respectively), with the deepest sensor exhibiting the strongest and most significant correlation to minimum temperatures observed ($r$ = -0.82, $p \pm 0.01$). While distance to shelf correlates strongly at $r \pm -0.67$ to temperature averages calculated per sensor depth, the required confidence interval is not achieved ($p < 0.1$). Similarly, maximums observed per sensor depth are not significant for a site's distance to the shelf.

### 5.4.6 Microtopography and locational specifics

Aspect-related control on freezing observed in thúfur in the High Drakensberg has been noted by Grab (2005). Here southern and south-western aspects receive less sunlight and freeze before the northern/north-eastern aspects. Borg (2012) noted differences in needle ice growth on northern (52%) and southern (64%) aspects at two locations (Abisko, northern Sweden and Sani Pass, southern Africa). He argued for positive feedback loops between animal-induced trampling reducing vegetation cover and needle ice restricting re-vegetation of surfaces. As such, aspect control on frost cycles in the three chosen study regions was investigated.

Higher-frequency temperature data are available for A10 in Dronning Maud Land (DML) for 19-29 January 2011 (n = ten days). Sensors were placed in the ground for the four main cardinal directions (north, east, south west) and recorded temperature at one-minute intervals. Data show that the north-facing aspect has the greatest diurnal maximum temperature and diurnal temperature range, followed by the next-highest diurnal maximum temperature for the west-facing aspect (Figure 146, pg. 279). In comparison, the west-facing aspect registers warmer diurnal minimum temperature, followed by the northern aspect. The southern aspect consistently registers the lowest diurnal maximum, minimum, range, and mean temperature and has the lowest variability (expressed as standard deviation: $s$) observed over the ten-day period ($s$ = 2.67). In comparison, the northern aspect exhibits the greatest variability ($s$ = 4.82). The diurnal cycle displays the greatest diurnal temperature range for the northern aspect and a delay in diurnal maximum temperature between northern and western aspects is observed.

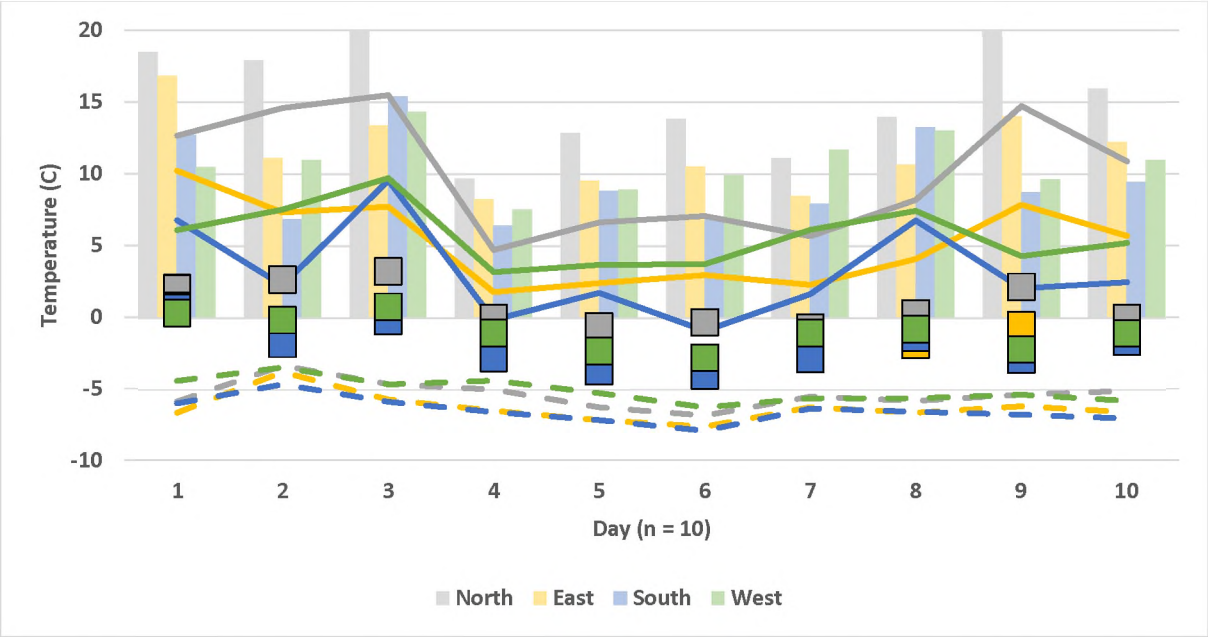


**Figure 146: Diurnal maximums ($T_{D:max}$), minimums ($T_{D:min}$), ranges ($T_{DR}$), and means ($T_{DM}$) observed at A10, presented per aspect, over a ten-day period. $T_{D:max}$ is indicated by a solid line., $T_{D:min}$ is indicated by a dashed line. $T_{DR}$ is shown by columns. $T_{DM}$ is shown as squares.**

Analysis Of Variance (ANOVA) for the four aspects shows that the various aspects are significantly difference at $p < 0.01$. Pairwise comparisons of the various aspects shows that the northern aspect is consistently and significantly different to other aspects for diurnal maximum, minimum, range, mean temperature, as well as variability (Table 131). One exception is diurnal minimum temperature in relation to the western aspect, where no significance is found at $p < 0.05$. Eastern and southern aspects exhibit similarity of evaluated parameters. The thawing index for the north, east, south, and west aspects is 2.6, 0.9, 0.5 and 1.0 respectively. The freezing index for the north, east, south, and west aspects is -1.7, -2.3, -2.6 and -2.1 respectively. The longest warm period on average for the ten-day period is evident the northern aspect, with the shortest period recorded for the southern aspect (**Table 132**, pg. 280). Temperatures above 0 °C are reached first for the northern aspect, followed by the eastern aspect with the southern and western aspect registering similar initial warming times. In comparison, the northern and western aspects register similar times for when temperatures reach sub-zero levels. Sub-zero temperatures are reached first for the eastern aspect, followed by the southern-facing side and only then for the northern and western aspects.

**Table 131: Student's t-test at $p < 0.05$ for diurnal maximum ($T_{D:max}$), minimum ($T_{D:min}$), ranges ($T_{DR}$), means ($T_{DM}$), and variability (expressed as standard deviation: $s$) per aspect-pairing over a ten-day period in January 2011.**

| Parameter | Significance |
|---|---|
| $T_{D:max}$ | Not for E-S and E-W |
| $T_{D:min}$ | Not for E-S and N-W |
| $T_{DR}$ | Not for E-S, E-W and S-W |
| $T_{DM}$ | Not for E-S, E-W and S-W |
| $s$ | Not for E-W and S-W |

**Table 132: Temperatures registering above 0 °C for four aspects at A10 (Vesleskarvet, Antarctica) over the ten-day period in January 2011.**

| Aspect | Start | End | Duration |
|---|---|---|---|
| North | 7:45 | 19:51 | 12:06 |
| East | 9:15 | 17:29 | 8:13 |
| South | 11:38 | 18:59 | 6:37 |
| West | 11:56 | 19:53 | 7:57 |

A series of iButtons were set up across the Northern Buttress of Vesleskarvet (Antarctica), simultaneously recording ground surface temperatures (GST: recorded at ± 2 cm in the ground), and air temperature. Gradient and aspect differed for each site and geographic weighted regression (GWR) was run to determine control on these aspect and gradient changes on GST. While variations occur, these are not significant at $p < 0.05$. Research by Hall (1998b), showed that rock temperatures on northern aspects in a location in Antarctica (Rothera Island) were not warmer than their southern counterparts. In contrast, aspect is argued to exert a control on the weathering of surfaces for a blockfield in DML (Hansen *et al.*, 2013). While the authors contradict each other, Hall (1998b) evaluates temperature data collected at high-frequency (1-minute data), Hansen *et al.* (2013) focus on hardness of rock surfaces determined using a Schmidt Hammer. As such, due to differences in methods and topics, based on these studies, a definitive conclusion on aspect control cannot be made.

To evaluate aspect on a macroscale environmental forcings, a case study of ground temperature and moisture (relative humidity measured in percentage) was done at Sani Pass (Lesotho), with respect to north and south facing slopes. South facing slopes exhibit significantly colder ($p < 0.05$) median temperatures compared to north facing slopes (Table 133). In comparison, south facing slopes exhibit significantly higher ($p < 0.05$) median soil moisture content compared to north facing slopes (Table 133).

**Table 133: Comparison of ground temperature and moisture with relation to aspect.**

| Parameter | North Facing Slope | South Facing Slope | *p* Value |
|---|---|---|---|
| Median Temperature ( °C) | 16 | 11 | 0.001 |
| Median Moisture (relative humidity; %) | 30 | 40 | 0.01 |

# CHAPTER 6: Discussion of Findings

This chapter presents a discussion of results, subdivided into the three study locations. Results, presented in CHAPTER 5: Results (pg. 113 onwards), are discussed for the Eastern Cape (below – pg. 293), Marion Island (from pg. 288-293), and Dronning Maud Land (DML), Antarctica (pg. 293-300). Each section is subdivided into various subsections, like subdivisions of CHAPTER 5: Results. Finally, the chapter concludes with a discussion on modelling the frost environment (6.4 Modelling the Diurnal Frost Environment, pg. 300).

## 6.1 Eastern Cape

Results, presented in CHAPTER 5: Results (pg. 114-165), are discussed for the Eastern Cape and evaluated for climate and site-specific characteristics (6.1.1 Climate and locational parameters, below), ground thermal properties (6.1.2 Ground thermal dynamics, pg. 282), soil characteristics (6.1.3 Sediment/soil specifics, pg. 285), and particle displacement within the ground (6.1.4 Sediment displacement: Ben MacDhui, pg. 287).

### 6.1.1 Climate and locational parameters

South African Weather Service (SAWS) data, as well as limited weather data recorded using XR5 logging set-ups for Ben MacDhui and the Elandsberg, conclusively show both sites to fall outside of any permafrost-affected area. This applies to utilising measurements for both mean annual air temperature (MAAT) and mean annual ground surface temperature (MAGT). Even at highest elevation (T1), ground and air temperatures exceed the required threshold for permafrost to occur. This agrees with global climatic zone delineation, as well as the argument of multiple authors *(e.g.* Boelhouwers, 1994; Grab, 1997c, 1998; Boelhouwers and Meiklejohn, 2002; Lewis, 2008a). Deep seasonal freezing is also not in evidence, excluding this area from periglacial zones as defined by Goudie (2004b). Furthermore, MAAT recorded at T1 on Ben MacDhui is 6.6 °C, with MAAT for E3 on the Elandsberg 11.1 °C. This excludes these locations from Karte's (1983) definition of sub-tropical periglacial environments, where MAAT needs to be from < 3-6 °C. However, MAAT at T1 almost falls within these thresholds. As such, the high altitudes of Ben MacDhui can be classed as sub-periglacial, as already argued for in CHAPTER 3: Study Area and Site Description (3.1 Eastern Cape, pg. 27 onwards).

Irrespective of this, both sites exhibit air temperatures and GST below 0 °C throughout the year and diurnal frost cycles occur here. This is indicated by turf exfoliation, frost sorting, observations on needle ice during field visits, and ubiquitous terracettes on the slopes of Ben MacDhui. Minimal evidence is also available for the Elandsberg, where evidence of frost sorting and friable surfaces occur on isolated instances for the higher-elevated sites. The Elandsberg is the most densely vegetated site of all the study areas (Eastern Cape, Marion Island, Dronning Maud Land), followed by Ben MacDhui. For Ben MacDhui a vegetation gradient is apparent, with vegetation becoming less and concentrated more on grass with increasing elevation. The Elandsberg is densely vegetated throughout and the soil

characterised by deep rooting depths and high organic content. The higher MAGT for E1 is attributed to this denser vegetation cover and humic soils. This continuous vegetation cover for the Elandsberg, thus, becomes a limiting factor on freeze-thaw cycles. For Ben MacDhui a more complex relationship between vegetation and freeze-thaw cycles exist. Diurnal frost can locally affect vegetation growth when freeze-thaw cycles are active, and their intensity exceeds the threshold required for hampering vegetation growth. Where this threshold is not met, *i.e.* insufficient cycles of in sufficient intensity, vegetation growth is not affected.

Average air temperatures show Aliwal North, Fort Beaufort, and T1 to fall outside of C*fb*, as delineated by Kottek *et al.* (2006). Weather observed at E3 show it to remain within the C*fb* classification. The shift of climatic classification illustrates the importance of delineating zones at the appropriate scale to each specific study. While the C*fb* classification is not wrong when applied at certain scales, local specifics are ignored. This is particularly important when considering freeze-thaw cycles, due to their short-term and often low frequency nature. Furthermore, the C*wc* class assigned to T1 exemplifies the importance of assigning sites to the appropriate climatic zones. Freeze-thaw cycles are much more likely to occur in a C*wc* setting, than a C*fb* setting. This is illustrated for T1, where much more freeze-thaw cycles occur compared to E3. A MAAT between ± 4.8 °C and ± 6.1 °C near Ben MacDhui at an altitude of 2 750 m a.s.l. (Lewis, 2008b), is like MAAT calculated from data for Aliwal North. However, actual MAAT do not agree with those extrapolated, with calculated values lower than those recorded *in situ*. This agrees with previous findings by Nel and Sumner (2008) for Sani Pass, where MAAT were higher than those extrapolated by Grab (1994, 1997c). Extrapolated MAAT for summer agrees with recorded temperatures. Similarly, extrapolated MAAT for spring and autumn fall within 1 °C of actual temperatures recorded. However, recorded winter temperatures are much higher than extrapolated ones, suggesting that the environmental lapse rate of 6.5 °C.km$^{-1}$ exaggerates the actual lapse rate. The same applies to extrapolated temperatures from Fort Beaufort, as applied to the Elandsberg. The region is known to experience highly seasonal precipitation, with ± 80% of precipitation falling in the summer months between October and March (Tyson *et al.*, 1976; Hanvey and Marker, 1992) and, for the escarpment and High Drakensberg, only 10% of precipitation falls during winter months (Nel and Sumner, 2008). This yields dry winters and suggests that the dry lapse rate of 5 °C.km$^{-1}$ should be applied to dry seasons, *i.e.* winter. For the Elandsberg the dry lapse rate, applied to extrapolated temperatures for the whole calendar year, yields calculated averages within 1 °C of recorded temperatures. This also has implications on calculating MAAT for paleoclimatic conditions, providing more evidence that the Eastern Cape region was more likely to have exhibited periglacial conditions, rather than glaciation. While average wind speed is not sufficient for deflation to occur (Brady and Weil, 2016), wind gusts exceed the required wind speed threshold and with most of these occurring during winter, when most freeze-thaw cycles also occur, deflation is expected during these months.

### 6.1.2 Ground thermal dynamics

Previous work by Kück (1997) shows Ben MacDhui air temperatures to oscillate above/below zero 40% of time, with oscillations for ground surface temperatures (GST: temperatures recorded at ± 2 cm in the ground) 20% of the time. This suggests the presence of freeze-thaw cycles and the suitability of the area to diurnal freezing and thawing. At T1 diurnal ranges exceeding 10 °C occur throughout the year.

In comparison, such ranges recorded in the ground reflect ranges exceeding 10 °C take place in summer. The deeper within the ground, the greater the likelihood that such ranges take place during summer. Oscillations indicative of potential freeze-thaw events show a dominance in winter, with none recorded for summer nor autumn for any sensors within the ground. Furthermore, while almost one third of air temperature oscillations indicative of potential freeze-thaw events make up diurnal ranges exceeding 10 °C, this proportion reduces to 4% at GST. At E3, diurnal air temperature ranges exceeding 10 °C also occur throughout the year. Within the ground a prevalence for spring to autumn is observed, with an increasing dominance for summer at greater deepths the ground. In comparison, oscillations indicative of potential freeze-thaw events occur only in winter. Furthermore, few diurnal ranges translate into potential freeze-thaw events. Comparing such figures to those of DML of Antarctica (6.3.2 Ground thermal dynamics, pg. 294 onwards) for both general locations, diurnal air temperature ranges exceeding 10 °C are not necessarily an indicator of potential freeze-thaw events. For both locations, potential freeze-thaw events make up a greater proportion of all diurnal ranges than only those reflecting a 10 °C difference. Furthermore, in the Eastern Cape oscillations indicative of potential freeze-thaw events occur in winter, with those in DML summer. This is indicative of the general climate found at each study location and further underlines the importance of above and below 0 °C oscillations, over a simple analysis of diurnal ranges. Furthermore, rate of change of temperature with depth is greater for higher altitudes in the Eastern Cape, than sites located at lower altitudes. This reflects the ameliorating effect of vegetation cover on ground temperatures, which is further shown in temperatures recorded. This applies even when the altitudinal gradient is considered.

The highest sites (T1-T4) are the only sites exhibiting longer-duration (> few days) freezing of the ground, while also having numerous freeze-thaw cycles. On Ben MacDhui ground freezes on a seasonal basis. The upper 2-3 cm are the most active potion of the ground, as exhibited by lowest annual mean temperatures and highest variability (expressed as standard deviation: *s*), and freeze-thaw cycles predominantly occur within this band of the ground. However, needle ice events identified by Borg (2017), do not necessarily translate into freeze-thaw cycles to a depth of 2 cm. Therefore, while needle ice is an important component of the frost environment, its presence near the surface limits its role in deeper cryoturbation. Nevertheless, this process does make the surface more friable and prone to deflation and other erosional processes. Furthermore, Borg (2017), argues for needle ice leading to heave and toppling regarding sediment displacement following each event. Duration of seasonal freezing and highest freeze-thaw cycles activity observed compares to work by Sumner (2003b), who shows seasonal freezing in the Lesotho Highland at 3 200 m a.s.l., with highest frost activity occurring in the upper 5 cm of the ground. At T1 air temperatures show 77 potential freeze-thaw events for the winter months during the year of observation, with 45 potential freeze-thaw events observed for GST. This translates into 25 freeze-thaw cycles at GST for the observation period. This compares well to results from Sani Pass where ± 71 potential freeze-thaw events and ± 44 potential freeze-thaw events were observed during the winters of 2003 and 2004 (Nel and Sumner, 2008). Furthermore, most freeze-thaw cycles occur during winter, as shown by Nel and Sumner (2008) at Sani Pass. Furthermore, average freeze duration at T1 is 18 hours near the ground surface (GST); at T4 average freeze duration is 12 hours. As such, frost cycles in the Drakensberg tend to occur on a diurnal basis and although seasonal ground frost is present, diurnal frost cycles dominate.

An increase in thaw events in spring yields a thawed and saturated near surface layer, underlain by a frozen layer. With the ground frozen for extended periods at 10-cm depth, the freezing front can extend from the surface downwards, as well as from the sub-surface upwards. This agrees with findings by Kück (1997), and while solifluction was not specifically investigated, these conditions are, nevertheless, suitable for solifluction. Furthermore, saturated ground over a frozen sub-layer and ambient temperatures that show oscillations above/below 0 °C in the presence of sufficient ground moisture, yields an environment suited for freeze-thaw cycles. Finally, the high proportion of diurnal ranges (> 10 °C), agreeing with findings by Kück (1997), makes the site suitable to such cycles. Diurnal freezing has been observed to 2 550 m a.s.l. on Ben MacDhui (Lewis *et al.*, 1994), and field data shows potential freeze-thaw events to just below 2 600 m a.s.l. However, while potential freeze-thaw events are recorded for the Elandsberg down to 1 400 m a.s.l., no freeze-thaw cycles are observed for GST at this altitude. While potential freeze-thaw events are observed for air temperatures for the Elandsberg, these do not generally translate into freeze-thaw cycles observed within the ground. The single freeze-thaw cycles recorded in the observation period can easily be described as an outlier. Nevertheless, the presence of this cycle shows that the Elandsberg has the potential for freeze-thaw cycles to take place. Field visits show that limited heave is present when vegetation cover is removed, suggesting that frost cycles occur only at the near surface (< 1 cm depth), with the dense vegetation cover of the Elandsberg limiting ground frost penetration. In comparison, the Eastern Cape Drakensberg is characterised by a sparser vegetation cover and freeze-thaw cycles occur here.

Thermal offsets for summer are consistently positive for T1 and E3, reflecting warmer GST than air temperatures. In comparison, thermal offsets for winter are negative, reflecting colder GST compared to air temperatures. However, degree days are negative, suggesting GST to be colder, compared to air temperatures, on an annual basis. This contradicts previous finding by Nel (2008), who shows that in the High Drakensberg ground temperatures are generally warmer than air temperatures. Irrespective of this, a negative thermal offset in winter speaks for a lack of snow cover and sparse vegetation, which would otherwise have provided an insulating effect on the ground temperature regime. Furthermore, the geographic area investigated by Nel (2008) is not the same investigated here. Finally, degree days are calculated using average air and ground temperatures. The thermal offset is calculated using raw data points and when such calculations are done the result is a positive value, contradicting the negative value determined for degree days. As such, degree days are not as suited in determining the dominant environment (air versus ground), if data points exceeding single daily averages are available. This agrees with the recommendation of the World Meteorological Association (WMO), which suggests daily averages based on 24 hourly temperature points, instead of calculating daily average temperatures using diurnal minimum and maximum temperatures (World Meteorological Association (WMO), 2011). As such, degree days potentially mask the fine-scale variability of temperatures, which the thermal offset does not.

The freezing index is low for T1 and absent for E3. Instead, the thawing index dominates, as is expected for areas where no permafrost is present. Nevertheless, the freezing index calculated for T1 suggests an environment where sub-zero temperatures are possible (as is the case) and where freeze-thaw cycles can be expected. When the freezing index is zero no freeze-thaw cycles are expected (E3-E7).

Furthermore, the thawing index at T1 shows that ground temperatures steadily decrease with depth. In comparison, at E3 the thawing index decreases up to GST, where it increases again. This suggests that the thawing may be used as a proxy for the lower limit of the freezing depth. This is corroborated by the depth of the single freeze-thaw cycle at E3. At T1 sensors only extended to 10 cm in the ground. However, with the ground at this depth frozen for extended periods of time in winter, and freeze-thaw cycles determined to this depth, it is possible that freeze-thaw cycles extend beyond this depth. The high balance of degree days toward the thawing index at E3 indicates an environment where ground frost is exceedingly rare. While this balance is also toward the thawing index at T1, values are less than those calculated for E3, suggesting ground frost is more likely to occur here. This is corroborated by freeze-thaw cycles at GST determined for T1 (32) and E3 (1). Nevertheless, the consistently greater thawing index compared to the freezing index highlights the paucity of freeze-thaw cycles present at either site.

### 6.1.3 Sediment/soil specifics

The higher-elevated Elandsberg sites are situated in the bowl of the doleritic mountain that comprises the Elandsberg. A wetland is found in the depression of this bowl, as well as a small stream. As such, E1-E3 are found in a different environment to E4-E7, which are located on a slope. E1-E3 are characterised by higher organic content, as well as higher fine earth fraction proportions when compared to E4-E7. As expected, high values for total organic carbon (TOC) also translate into lower bulk density and higher porosity values. This suggests that, apart from being located at higher altitudes on the Elandsberg, these sites also have greater freeze-thaw potential when considering only soil characteristics. Meentemeyer and Zippin (1981) argue that percentage of fines ($\phi > 4$: silt and clay) in the soil column increases, reaching a threshold at 16%, the amount of moisture required for frost processes to occur decreases. Boelhouwers and Meiklejohn (2002), argue frost cycles are common in frost-susceptible loam-rich soils with a fine fraction between 7-57%. Silty-loamy soils have high freezing potential. The Elandsberg, in comparison to the other two study regions (Marion Island and Dronning Maud Land [DML]), has the highest TOC and fine earth fraction, increasing the suitability of the soil for freezing taking place. The lower TOC recorded for Ben MacDhui makes these sites potentially less suitable for freezing to occur. However, fine earth fraction proportions on the Elandsberg greatly exceed thresholds proposed by Meentemeyer and Zippin (1981), and Boelhouwers and Meiklejohn (2002), with fine earth fraction proportions for Ben MacDhui closer to these thresholds. Furthermore, a suitability of ground frost occurrence needs to be considered together with external parameters such as altitude and mean annual air temperature (MAAT). As such, the Elandsberg has few potential freeze-thaw events and virtually no freeze-thaw cycles (see 5.1.2 Ground thermal dynamics, pg. 123). The dense vegetation cover and lower altitude limit freeze-thaw cycles. Limited freeze-thaw cycles, high TOC, low bulk density and high porosity make this site the most suited for agricultural practises.

On the Elandsberg porosity values are similar regarding intersite comparisons and the ground column is expected to retain similar amounts of moisture from E1-E7. At Ben MacDhui bulk density values are unexpected, being lower at the surface compared to the sub-surface. This implies a loosening of the surface layer through, *e.g.* freeze-thaw cycles and the concomitant removal of coarser particles through frost heave. Such cycles change bulk density and porosity. Cryoturbation leads to a mixing of soil, with

particles moved up and down within the soil column. That portion of the ground where freeze-thaw cycles occur, exhibits a paucity of certain textural fractions, as illustrated by sediment samples collected on Ben MacDhui. The deficiency of Phi (ϕ) sizes -1 and zero near the surface suggests the removal of these particles through freeze-thaw cycles. The deficiency of particles of Phi (ϕ) sizes >= 4 can be attributed to the aggradation properties of clays, which can subsequently be removed following freeze-thaw cycles. Furthermore, the contention that contemporary periglacial landforms near Ben MacDhui are largely driven by needle ice (Boelhouwers and Meiklejohn, 2002), is corroborated by fieldwork observations, data recorded, and recent work by Borg (2017).

On the slopes of Ben MacDhui all sites show higher TOC for surface samples compared to sub-surface samples. This is expected, as vegetation and roots grow near the surface. Organic content affects bulk density: the greater this proportion, the lower the ground's porosity. Furthermore, the higher proportion of organic particles makes the surface area of the ground more susceptible to freeze-thaw cycles. T2 and T4 have higher fine earth fraction proportions at the sub-surface, indicating the removal of fines (ϕ > 4: silt and clay) from the surface layer. Ice segregation and frost heave generally occur in fine-grained soils and the variable distribution of fines has implications on freeze-thaw cycles and frost heave. Uniformity coefficients ($C_u$) consistently show poor sorting and well graded samples. While $C_u$ values are more sorted than those determined for Dronning Maud Land sites (5.3.3 Sediment/soil specifics, pg. 268), the ground remains unsorted. Since samples reflect ground weathering *in situ* this is to be expected. Moisture values are also higher for the Eastern Cape compared to Marion Island and DML. At Ben MacDhui Volumetric Water Content (VWC) is greater at the surface. This shows the higher moisture-holding capacity, and concomitant freeze-thaw cycles potential for surface layers compared to sub-surface layers. And while VWC expressed as a percentage ($M_c$) suggests that the Elandsberg is more suited to freeze-thaw cycles compared to Ben MacDhui (where $M_c$ equates to ± 0), almost no potential freeze-thaw events and no freeze-thaw cycles are observed near the ground surface on the Elandsberg (refer to 5.1.2 Ground thermal dynamics, pg. 123). This indicates the importance of locational parameters such as textural properties and fractions, vegetation cover, as well as altitude on the presence and distribution of freeze-thaw cycles. More so for the Elandsberg, but also for Ben MacDhui, high porosity and moisture retention values, as well as low specific yield ($S_Y$) values, indicate that the sediment column can retain ground moisture. Moisture is a crucial component to freeze-thaw cycles, albeit not potential freeze-thaw events, and frost heave cannot occur without the presence of ground moisture. However, the presence of moisture does not necessarily translate into freeze-thaw cycles, as exemplified by a lack of landforms associated with diurnal freeze-thaw cycles for *e.g.* the Elandsberg.

Kolmogorov-Smirnov (K-S) tests for the Elandsberg show that sediment samples at different altitudes are statistically different, attributed to the well-developed soil and thick vegetation cover found in the region. Deep weathering with sufficient moisture and biotic activity leads to different soil populations, as exhibited in the Elandsberg. In contrast, the lack of outright rejection of the null hypothesis of the K-S test for Ben MacDhui suggests the shallower and younger soils found at this site translate into similar populations. Exceptions are the lowest-altitudinal sites, which are statistically different. This suggests the importance external topographical factors, such as gradient, which lends itself to different erosional

regimes and environments. Furthermore, the downslope movement of material yields a deeper colluvium further downslope, as argued by Kück (1997).

### 6.1.4 Sediment displacement: Ben MacDhui

Moisture is a limiting factor to freeze-thaw cycles and the increase in gravimetric water content (GWC) with depth per trench suggests loss of moisture to environmental parameters, such as deflation, with greater depths insulated from moisture loss. Winter months in the Drakensberg are also drier and windier, potentially increasing deflation and encouraging needle ice growth. The surface is the dominant zone of root growth, which is reflected in surface samples having higher total organic carbon (TOC) values. Freeze-thaw cycles are more frequent in material consisting of a greater proportion of fines and organic matter. The smaller proportion of fines ($\phi > 4$) near the surface has two implications: 1) fines have been removed through deflation following freeze-thaw cycles, when the ground surface becomes more friable; or 2) fines slowly settle deeper within the ground column through the forces of gravity and water. Furthermore, the layers nearer the surface show a deficiency of particles within the coarse sand and fine gravel classes ($\phi < 0$). Coarser particles within the ground migrate upwards in the direction of the freezing front when soil is frozen at the surface (Hallet, 1990), yielding patterned ground with coarser particles on the surface, and a relatively coarse-particle-poor sediment column (sorting). Although sediment samples on Ben MacDhui are not sorted, the sorting index (S) does show deficiency of particles between the various depths. Deficiency of particles at Ben MacDhui, therefore, are likely of all three sorting mechanisms: 1) uplift of particles when freezing occurs from the top, 2) sorting as particles migrate away from the freezing plane approaching from the top or sides, and 3) mechanical sorting (Corte, 1966). The coarser textural fraction recorded further upslope is also less suitable for the occurrence of freeze-thaw cycles, while the finer textural fraction further downslope is more suited to these cycles occurring. And while no sorting is in evidence within trenches, the deficiency of Phi ($\phi$) values four and greater (silt and clay), suggests the removal of these sized particles from the portion of the ground where frost cycles are shown to occur. Compared to coarser particles, finer particles can be sorted under a wider range of freezing conditions (Easterbrook, 1999).

Frost heave is shown through heave of dowels and painted markers. Heave of dowels increases from T1 to T3, after which it decreases. All trenches exhibit vertical movement of markers within the top 2 cm of the ground with most sites showing movement down to 15cm. This is slightly deeper than the proposed depth of 10 cm for freeze-thaw cycles as argued by Boelhouwers and Meiklejohn (2002). Markers originally buried at greater depths (± 10-15 cm) do not heave all the way to the surface. However, marker buried at shallowest depths are found at 15 cm depths. Higher elevated sites exhibit more heave of painted markers, which is attributed to a higher proportion of TOC, a greater proportion of fines and shallow soil, as well as lower temperatures. Lateral displacement of markers is greatest for T3, which shows the highest proportion of ground moisture. High moisture readings at this site are attributed to high fine earth fraction proportions, since a greater proportion of fines enhances the ground's water holding capacity. For the higher-elevated sites (T1 & T2) vertical movement exceeds lateral displacement. It must be noted that the soil depth at higher elevations is shallower and that suitable locations for trenches were rare. At T3 soil is much deeper and occurs for a larger area making lateral displacement more likely. When freezing takes place the larger-sized markers migrate upwards

in the direction of heat flow and the movement of markers indicate the presence of freeze-thaw cycles. As markers migrate upward during freezing events the number of markers near the surface/heaved out increases within time, explaining the increase of number of markers retrieved with time. The soil column at the various site shows a greater proportion of fines ($\phi > 4$: silt and clay) at greater depths within the ground. Simultaneously the layers near the surface (± 2-5 cm) shows a lack of coarse sand and fine gravel sized particles ($\phi < 0$). This illustrates that the near surface loses fine particles through deflation, potentially at increased rates following freeze-thaw cycles, as well as larger-sized particles through these freeze events.

Analyses into deformation of the ground using sunken strings shows that little lateral displacement is evident across the study sites. T3, which shows high lateral movement through painted markers yields no usable string data. Nevertheless, limited lateral displacement is evident for T1 when using painted markers and this site shows deformation of two strings. Here strings show the greatest deformation at ± 4-5 cm and no displacement is evident below 10 cm. This shows similar results as those recorded for painted markers, which show greatest lateral displacement at ± 5 cm. In comparison, T4 shows no lateral displacement of painted markers and strings retrieved here yield the same data. At T4 bulk density and porosity values act as one would expect (bulk density increases with depth). Furthermore, sub-surface and surface samples are statistically different when using the Kolmogorov-Smirnov (K-S) test. Seventeen freeze-thaw cycles occur at this site, with an average freeze duration of 12 hours. As such, freeze-thaw cycles lead to the migration of particles toward the freezing front (as discussed above), leading to a decrease in bulk density closer to the surface. The paucity of slope deformation highlights the dominance of diurnal freeze-thaw cycles over long-term and deeper freezing fronts leading to solifluction. The abundance of frost sorting at the surface and a visible lack of coarser particles near the surface further supports this.

## 6.2 Marion Island

Similar to discussion of Eastern Cape results, this section is further subdivided into subsections on local parameters and climate (6.2.1 Climate and locational parameters, pg. 288), thermal dynamics of the ground (6.2.2 Ground thermal dynamics, pg. 289), soil characteristics (6.2.3 Sediment/soil specifics, pg. 289), and displacement of particles within the ground (6.2.4 Sediment displacement, pg. 291). Results presented in CHAPTER 5: Results (pg. 165-205), are discussed in detail. Please refer to the various subsections listed above.

### 6.2.1 Climate and locational parameters

South African Weather Service (SAWS), as well as the limited weather data recorded using XR5 logging set-ups for M1 (Katedraalkrans) and M2 (Tafelberg) on Marion Island show both sites to fall outside of any permafrost affected area. This applies to utilising measurements for both mean annual air temperatures (MAAT), as well as mean annual ground surface temperatures (MAGT: temperatures recorded at ± 2 cm within the ground). As such, there is no evidence of permafrost nor an active layer on the Island. M1, at highest elevation, shows that ground and air temperatures exceed the required

threshold for permafrost to occur. With decreasing altitude, from M1-M5, ground temperatures increase, reflecting an absence of permafrost on the Island. This agrees with, *e.g.* Hedding (2008), who argues for an absence of permafrost. Irrespective of this, Marion Island has an active frost environment that lacks seasonal patterns. Frost cycles occur throughout the year for all calendar months, as argued by *e.g.* Boelhouwers *et al.* (2003) and Nel (2009). M1 reflects the most active frost environment, with air and ground temperatures below 0 °C throughout the year. However, freeze-thaw cycles are shallow, suggesting dominant frost processes by needle ice. Further indications of frost action are turf exfoliation, frost sorting, and vegetation and stone banked lobes and terraces. High ground moisture values, a lack of vegetation cover, frost-susceptible soils and a temperature regime suited for numerous fluctuations around 0 °C make Marion Island an idea environment for diurnal frost cycles.

Average air temperatures for the SAWS station, as well as at M1 and M2, show the Island to fall within the *Cfc* classification. This climatic zone requires average air temperatures where no month is colder than -3 °C or warmer than 18 °C, where snowfall is common, and precipitation occurs throughout the year, temperatures are not extreme, and winters mild (refer to APPENDIX B for an overview of this zone). The thermal offset, as well as positive ground freezing indices, indicate an environment where ground temperatures are warmer than air temperatures. Extrapolated air temperatures show that the higher-elevated site (M1) is colder by ± 1 °C than extrapolated temperatures, for all seasons excepting summer. Extrapolated temperatures for summer approximate recorded temperatures. At M2 the extrapolated summer and autumn average temperatures are respectively under- and over-estimated by ± 1 °C. Extrapolated temperatures for winter and spring approximate those recorded. This suggests that the proposed lapse rate by Holness (2001a) is not entirely suited for autumn, as well as winter. Irrespective of this, the *Cfc* climatic classification is highly suited to ground frost occurrence, specifically diurnal frost cycles. This is reflected in the high number of potential freeze-thaw events and freeze-thaw cycles observed for the Island, as well as already published and argued for in the literature (*e.g.* Holness, 2003a; Boelhouwer *et al.*, 2003, 2008; Nel *et al.*, 2009). This high ratio of potential freeze-thaw events to freeze-thaw cycles is further aided by high ground moisture levels. In areas of large and constant amounts of precipitation water percolating into the ground yields mass heat transfer, while simultaneously increasing heat conductivity of the soil column, diminishing the zero-curtain effect (Boelhouwers, 2003a). Marion Island received almost continuous precipitation and the isothermal regimes are achieved within the ground reflect the largely isothermal ambient temperature regime of the Island.

### 6.2.2 Ground thermal dynamics

Seasonal frost is evident for M1 but not M2. This agrees with Boelhouwers *et al.* (2003), who argue for no seasonal frost below the altitude of Katedraalkrans. The calculated average freeze-thaw cycle of 20 hours at M1 and 19 at M2, as well as ground frozen in August, agrees with Hausmann et al. (2009a), who argue that at an altitude like M2, mean freeze-thaw cycle duration is 20 hours and longest frost duration in August. However, while average frozen duration is 20 hours at M1, the most common cycle spans one hour. As such, short and more frequent frost cycles are evident at higher altitudes.

Diurnal ground oscillations around 0 °C at M1 occur throughout the year, with 30% in spring, yielding more than 190 days on which potential freeze-thaw events take place. Most freeze-thaw cycles occur from October-December, as well as June. This is attributed to colder conditions in winter, which lead to the ground is frozen for extended periods of time from 5-15 cm depths. These conditions limit potential freeze-thaw events and freeze-thaw cycles, with not every potential frost event reflecting a freeze-thaw cycle. Nevertheless, more than half of potential events yield freeze-thaw cycles. This is attributed to frequent oscillations around 0 °C, narrow diurnal ranges (4 ° C), and high ground moisture levels.

At M2 most freeze-thaw cycles occur from June-September, with ground frost not extending beyond a few days. At his lower altitude, no ground frost is evident from December-March. Diurnal ground oscillations around 0°C are common, evident on more than 124 days of the year. Like M2, the greatest number of such oscillations occurs in spring (40%). In contrast to M1, most freeze-thaw cycles at M2 occur in winter. Irrespective of this, for both sites, temperatures stabilize with increasing depth in the ground, with the least variability (expressed as standard deviation: *s*) recorded at greatest depth. When multiple cycles are evident within one 24-hour period, the initial event is shorter, followed by a longer cycle. Furthermore, freezing generally initiates in the early morning, when the lowest air and ground temperatures are reached. Finally, like results from the Eastern Cape and Dronning Maud Land, the frequency of data collection impacts the amount of frost cycles calculated. Data recoded at higher-frequency, such as 2 or 5-minute intervals, yields more potential freeze-thaw events, as well as freeze-thaw cycles.

### 6.2.3 Sediment/soil specifics

All sites on Marion Island are characterised by fairly low organic content, with the total organic carbon (TOC) increasing with decreasing altitude. Furthermore, sub-surface samples show slightly higher TOC compared to surface samples (6.44% vs. 4.76), as well as a fine earth fraction (FEF: particles < 2 mm in diameter) proportion greater at 15 cm depth within the ground compared to the surface. This suggests a removal of fines from surface samples or the enrichment of this layer by clasts being cycles up through the ground column. Furthermore, the absence of vegetation cover at most sites removes the input of organic matter through roots and leaves. That organic proportion present in the soil may, thus, settle further into the ground column. This may occur due to cycling of the ground through frost cycles, leading to changes in bulk density and porosity. Coupled with frequent snow and rain fall, finer particles settle deeper into the ground, yielding lower TOC and fines at the surface. Furthermore, lower TOC and fine proportions make surface samples less suited for freeze-thaw cycles to occur. Organic content affects bulk density: the greater this proportion, the lower the ground's porosity. Irrespective of this, bulk density and soil porosity, clayey-silt rich soils and high moisture content make the soil on Marion Island highly frost-susceptible. The higher variation recorded for soil parameters for surface samples also shows a more dynamic environment at the ground surface, when compared to sub-surface samples. As such, it is suggested that frost cycles are most active in the upper portion of the ground (0-2 cm) and the greater variation observed in this layer is attributed to dynamic aspects introduced by frequent and shallow freeze-thaw cycles. These lead to the removal of fines, as well as sorting, as is evident for M4. Ice segregation and frost heave generally occur in fine-grained soils and the variable

distribution of fines has implications for freeze-thaw cycles and frost heave. Uniformity coefficients ($C_u$) consistently show poor sorting and well graded samples. While these coefficients are more sorted than those determined for Dronning Maud Land (DML) (5.3.3 Sediment/soil specifics, pg. 268), the ground column remains unsorted. However, that portion of the ground column where freeze-thaw cycles occur, exhibits a paucity of certain textural fractions. As such, while surface soil samples are on average not sorted, with more sorting evident for sub-surface samples (± 15 cm depth), data for M4 suggests sorting in various particle sizes, indicating this site to be especially frost active. Bulk density, soil porosity and a relatively high organic proportion, furthermore, make this site most suited to ground frost occurrence.

Differences in soil organic matter, bulk density, porosity, and proportions of fines are not significant between surface and sub-surface samples. As such, freeze-thaw cycles extend beyond 2.5 cm (the depth at which surface samples were sampled), deeper into the ground to where subsurface samples were collected (app 15 cm). However, the small differences calculated for TOC, bulk density, porosity, and proportion of fines for surface samples indicate that the upper portion of the ground is exposed to more freeze-thaw cycles and greater frost heave. This is further corroborated by the Kolmogorov-Smirnov (K-S) test, which clearly shows that surface and sub-surface samples do not represent similar populations. As such, soil properties indicate an environment where freeze-thaw cycles occur predominantly in the upper few centimetres of the ground, as well as also suggesting that freeze-thaw cycles can also extend deeper into the ground.

Like soil samples evaluated for the Elandsberg, high porosity and moisture retention values, as well as low specific yield ($S_y$), indicate that the sediment column for Marion Island sites can retain ground moisture. This stands in contrast to DML sites, such as A7 in central Dronning Maud Land (CDML). Moisture is a crucial component to freeze-thaw cycles and frost heave cannot occur without the presence of ground moisture. The K-S tests for Marion Island show that sediment samples at different altitudes are statistically different. This is evident by soil textural sizes becoming increasingly coarse with increasing elevation. Lower sites with higher organic content, thus, promote a disparate frost environment compared to higher-elevated sites that are associated with coarse soils and lower organic proportions.

### 6.2.4 Sediment displacement: Marion Island

Similar to Ben MacDhui sites (6.1.4 Sediment displacement: Ben MacDhui, pg. 287), the increase in gravimetric water content (GWC) with depth per trench suggests loss of moisture to environmental parameters, such as deflation, with depths deeper within the ground insulated from moisture loss. Freeze-thaw cycles are more frequent in material consisting of a greater proportion of fines and organic matter. M2 has a higher proportion of fines in the fine earth fraction (particles < 2 mm in diameter), when compared to the other sites. The area has numerous and visible landforms and -features associated with diurnal freezing and thawing, such as sorted stripes, frost sorting and evidence of needle ice. A higher proportion of fine increases the potential of freeze-thaw cycles occurring, as displayed by the larger area of M2, as well as analyses of the ground thermal regime at this site.

Furthermore, the smaller proportion of fines at M1 and M2 near the surface has many implications, as discussed previously (refer to 5.2.3 Sediment/soil specifics, pg. 195 onwards). First, fines have been removed through deflation following freeze-thaw cycles, when the ground surface becomes more friable; or second, fines slowly settle deeper into the ground column through the forces of gravity and water. Furthermore, surface layer particles are on average finer than those of sub-surface samples. This suggests removal of certain particle sizes through numerous freeze-thaw cycles. Finally, while most samples exhibit no sorting, sub-surface compared to surface samples show deficiency in various textural fractions. Coarser particles migrate upwards in the direction of the freezing front when soil is frozen at the surface (Hallet, 1990), yielding coarser particles on the surface, and a relatively coarse-particle-poor sediment column at the depth of maximum freezing. Sorting, or the deficiency of certain particle sizes for soil on Marion Island is, therefore, likely due to all three sorting mechanisms: 1) uplift of particles when freezing occurs from the top, 2) sorting as particles migrate away from the freezing plane approaching from the top or sides, and 3) mechanical sorting (Corte, 1966). This applies most to M2, which shows the greatest level of textural size deficiency when comparing sub-surface to surface samples. The coarser textural fraction recorded further upslope at M1 is also less suited for the occurrence of freeze-thaw cycles, while the finer textural fraction further downslope more suited to these cycles occurring. And while limited to no sorting is in evidence within trenches, the deficiency of Phi ($\phi$) values > 4 (silt and clay), suggests the removal of these particles from the portion of the ground when freeze-thaw cycles take place. Compared to coarser particles, finer particles can be sorted under a wider range of freezing conditions (Easterbrook, 1999).

The heave of painted markers indicates the presence of freeze-thaw cycles, as does the displacement of dowels. The displacement of markers in the vertical, as well as laterally, suggest Marion Island to have an active frost environment. Furthermore, markers suggest cycling within the ground, with markers migrating to lower depths, as well as to the surface. The lack of significant lateral displacement at M1 is attributed to the level surface of this site. In contrast, the slight gradient of other sites reflects greater lateral displacement of markers at these locations. Furthermore, analyses into deformation of the ground using sunken strings reflects lack of lateral deformation at M1, with limited lateral movement evident for M4. The deficiency of fine particles, as well as coarse sand / fine gravel particles for all trenches for all sites, furthermore, shows that the near surface loses fine particles through deflation, potentially at increased rates following freeze-thaw cycles, as well as larger-sized particles through these freeze-thaw cycles. While string displacement is not sufficient to infer creep, lateral displacement of markers downslope is indicative of soil creep. Since most strings were no longer in place upon return to study sites, an inference (based on the data) of which creep is active in the area cannot be made. However, literature (*e.g.* Holness, 2001a; Boelhouwers, 2003b) indicates solifluction (gelifluction and plug-like flow) to be absent at the altitudes of M1-M5. As such, lateral displacement of markers downslope, as well as the maximum depth of these trenches, suggest creep to be due to needle ice creep and/or diurnal creep. Furthermore, the absence of permafrost at the study sites excludes plug-like flow as a mechanism of soil deformation.

Haussmann *et al.* (2010a) obtained 10Be concentrations at 0–1, 1–2, 7–8, 8–9, 11–12, 12–13 and 17–18 cm. These equate to the near surface, 10 cm and 20 cm for the current project. Haussmann *et al.'s*

study shows that general 10Be concentrations decrease with depth within the soil. One of the reasons for this trend is given as physical (particle related) transport of 10Be from the lower horizons within the profile. This mixing of soil is evident on the Island, as evidenced by marker movement within the examined soil profiles and heave of dowels with both marker movement and heave of dowels greatest for M1-M3. Heave of ± 10 cm was observed at M1 and M2, confirming research by Haussmann *et al.* (2009a) who record complete heave (on an annual basis) of 10 cm dowels placed in sediment of Tafelberg. Holness (2004) reports heave of 15 cm dowels for Katedraalkrans Nek (750 m a.s.l.) and First Red Hill (550 m a.s.l.), suggesting that ice lensing must also be considered as a geomorphic process on the Island. This is due to needle ice being effective up to ± 10 cm into the ground and any displacement exceeding this depth attributed to ice lensing. However, the current study did not record heave exceeding 10 cm at Katedraalkrans (M1), and greater significance is given to diurnal frost processes, such as needle ice, as a mechanism of sediment displacement. This is, furthermore, corroborated by Borg (2017).

## 6.3 Dronning Maud Land (DML), Antarctica

Results from Dronning Maud Land of Antarctica are presented in CHAPTER 5: Results (pg. 205-272). This section serves for the discussion of these results. Please refer to the various subsections (6.3.1 Climate and locational parameters, pg. 293; 6.3.2 Ground thermal dynamics, pg. 294; 6.3.3 Sediment/soil specifics, pg. 299) for a detailed discussion of each.

### 6.3.1 Climate and locational parameters

Annual average temperatures calculated for Dronning Maud Land (DML) are low and the coldest calculated for the three study areas. Humidity values area low overall and little precipitation is recorded in the area (Reijmer and Broeke, 2001), as supported by field observations. Most precipitation is received during storm events that are driven by the dominant easterly winds, as argued by Hansen (2014). During these events drifting snow accumulates, generally on the windward side, becoming a potential moisture bank during periods of warmer temperatures. Nevertheless, surface moisture is almost absent for all sites and while diurnal maximum temperature can reach 4 °C the entire area is characterised by a dry and cold climate with high winds. Landforms recorded speak to both glacial and periglacial origins. Ubiquitous thermal contraction polygons reflect a permafrost-dominated environment. Nevertheless, sorted circles, needle ice evidence and frost sorting, while not as common, are all in evidence for numerous sites, reflecting a diurnal environment with low intensity freeze-thaw cycles. DML is, thus, an area where annual and seasonal frost interplays with seasonal and diurnal thaw and concomitant freeze-thaw cycles. Average air temperatures show all sites to fall within ET*f*, and not ET as delineated by Kottek *et al.* (2006). This illustrates the importance of delineating zones at the appropriate scale to your specific study. ET, which requires temperatures to never to reach above 0 °C, prevent freeze-thaw cycles from occurring. In comparison, the ET*f* classification allows freeze-thaw cycles to take place.

### 6.3.2 Ground thermal dynamics

The Antarctic region is characterised by annual frost with seasonal thaw and freeze-thaw cycles of low frequency and generally low intensity. While the area experiences no darkness in summer, diurnal cycles are, nevertheless, present. In Dronning Maud Land (DML) thaw cycles average on 12-18 hours for A6/A7 and A1-9 respectively, although longer cycles are evident for A4 (maximum thaw duration: 115 hours), with multiple cycles within one 24-hour period recorded at A1, A5, and A7. As such, the thaw environment in DML tends to occur on a diurnal scale during warmer months (predominantly summer months). Furthermore, thaw cycles reach a maximum of 58 cm (at A4), with deepest thaw of 12 cm recorded at A6. This yields an average thaw depth (or active layer thickness) of 28 cm for the region. Active layer thickness for central Dronning Maud Land (CDML) is 38 cm, for western Dronning Maud Land (WDML) it is 27 cm. As such, the area is characterised by an overriding deep and annual frost environment, indicative of permafrost environments. Nevertheless, evidenceof diurnal thaw cycles reflects the presence of a diurnal frost environment and, with a projected global increase in ambient air temperatures, this environment is expected to become more active and significant. All DML sites are in a continuous permafrost zone (CPZ) and the expected shallow active layer thickness and freezing depth (*d*) recorded for all sites reflects the dominance of annual frost. Thawing occurs predominantly during summer months, although isolated thaw takes place during spring and autumn. High values calculated for the freezing index further indicate an environment in which annual freezing dominates, interspersed by sporadic seasonal and diurnal thawing. Sites at lowest elevation experience consistently longer thaw hours, yet thaw hours expressed as an annual percentage are low overall and the DML study region is characterised by permafrost and annual frozen conditions with limited seasonal (summer) thaw. This is shown by variability (expressed as standard deviation: *s*) at permafrost depths registering lowest values and variability within the active layer highest per site. Seasonal ranges reflect a positive relation to active layer thickness with sites of large seasonal ranges showing deepest active layers *(e.g.* A4 and A7). Higher-altitudinal sites have lower annual mean temperatures than those at lower elevations. Permafrost thickness is consistent at ± 650m and active layer thickness ranges from 12 cm at A6 to 58 cm at A4. Considering only sites in WDML located at high altitudes (m a.s.l. > 1 000 m) active layer thickness ranges from 12 cm at A6 to 29 for A3 and A5. This is close to the active layer thickness proposed by Vieira *et al.* (2010) and comparable to those of the McMurdo Sound-Dry Valleys for mountainous and dry areas (Campbell *et al.*, 1998). In comparison, active layer thickness reaches its greatest extent for DML sites in December and January and not during February, as proposed by Turner *et al.* (2009). Longest ground thaw duration (45% and 34% for December and January respectively) and most freeze-thaw cycles (58% and 39% for December and January respectively) also occur during these months, as opposed for February.

Active layer thickness is significantly correlated to altitude and Principal Component Analysis (PCA) suggests that active layer thickness, freeze-thaw cycles and latitude trend together. This suggests that an increase in elevation translates into a decrease in active layer thickness, a relationship apparent for DML sites. Furthermore, an increase in latitude reflects a decrease in active layer thickness and freeze-thaw cycles observed, *i.e.* as sites move closer located to the South Pole the active layer becomes thinner and concomitant freeze-thaw cycles decrease in number. However, altitude overrides the effect of latitude when sites are in proximity to each other. Maximum diurnal air temperature, potential freeze-thaw events, freeze-thaw cycles, thaw duration, initiation of thaw and subsequent

commencement of freezing, as well as average diurnal minimum, maximum, and mean temperature suggest an altitudinal gradient with sites located at lowest elevation (A4) exhibiting higher values and those at higher elevation (A6 or A7) lower values. Variability and temperature means are highest for near surface temperatures (NST: recorded at ± 1 cm in the ground), compared to sensors located at greater depths, as well as air temperatures. This is reflected in less potential freeze-thaw events recorded for air temperatures compared to NST. Nevertheless, air temperature impact and forces NST and ground surface temperatures (GST: recorded at ± 2 cm in the ground), and warmer air temperatures translates into higher ground temperatures and associated variability. Most WDML sites show no significant change in interannual active layer thickness. Notable exceptions are A3 and A4. A3 has signs to be an indicator site for the remaining WDML sites and A4 has the deepest active layer thickness, as well as most variable ground temperature regime. Furthermore, high variability calculated for ground temperature at A3 is reflected in high variability of active layer thickness. Furthermore, this site exhibits the second-highest average ground thaw duration (9 hours). A4 has the highest average ground thaw duration (18 hours).

Diurnal ranges exceeding 10 °C are rare for air temperatures in WDML, with A6 reflecting the highest proportion at 8% (average ± 5% for all WDML sites). Sites located in CDML show a much greater proportion at 29%. The proportion of such ranges also increases with a decrease in average air temperatures, *i.e.* A4, located at lowest altitude has a much smaller proportion of these ranges compared to A6, located at highest elevation. Furthermore, most of these ranges reflect daily minimums and maximums below 0 °C, *i.e.* not oscillations around 0 °C. In comparison, NST reflects higher proportions of such ranges when compared to air temperatures. In WDML the highest proportion of these ranges is recorded at A9 (31%), with the lowest at A5 (5%). In CDML relatively low number of such ranges are recorded at NST (±3%). All sites show that a diurnal range of 10 °C for air temperatures is not always sufficient for inferring potential freeze-thaw events within the ground, with sites generally reflecting more oscillations indicative of potential freeze-thaw events outside of this range, than potential freeze-thaw events within the 10 °C diurnal range. This implies that in DML large diurnal air temperature ranges indicate cold ranges, *i.e.* where both minimums and maximums fall below 0 °C (as mentioned above). This is reflected in the greatest proportion of such ranges occurring during winter and autumn months. Nevertheless, when evaluating ground temperatures, it is apparent that such large ranges are in fact indicative of potential freeze-thaw events, with the majority of these ranges taking place during summer, with approximately a third during spring. While diurnal ranges exceeding 10 °C occur throughout the year at all sites, certain sites show a dominance for spring, followed by summer months (A2/A3/A5/A6/A7/A9), with the remainder reflecting a greater proportion for spring months followed by winter months (A1/A4/A10). In comparison, an evaluation of ground temperature ranges reflects a dominance during summer months, with approximately a third occurring in spring. This holds true for all sites, irrespective of locating. Finally, oscillations around 0 °C at NST occur predominantly during summer months, with such oscillations reflecting earlier thawing within the ground (spring and summer), than the air (summer and autumn).

Highest temperatures are consistently recorded for the near surface (NST) and freeze-thaw cycles occur within this band of the ground. Freeze-thaw cycles identified using exotherms generally occur in the

late evening and in the region of -2 °C, suggesting freezing occurs in this area below 0 °C. Irrespective of this, thawing of the ground generally commences during the mid-morning (09:00), close to the time of maximum solar radiation received (midday) and extends into the evening (19:00). Freeze-thaw cycles are evident where variability is greatest, and temperatures reach higher maximums, such as those observed for NST. Temperatures and variability are invariable are highest for NST and GST, d decreasing with increasing depth into the ground. Snow cover not only has a dampening effect on ground temperatures in terms of maximums and minimums recorded, but also on a narrowing of diurnal temperature range and a lowering of variability. Higher freezing indices and lower thermal offsets are also observed during storm and snowfall events and no freeze-thaw cycles are observed when snow covers the ground. Longest thaw duration for most sites occurs at NST and the thermal properties of the ground must be considered for sensors located at this depth, with sensors registering positive temperatures before such are recorded for air temperatures. The exception is A4, which registers longest thaw duration at $T_{30}$ and $T_{45}$ and not NST, indicative of the greater active layer thickness (58 cm) at this site. Time lag observed in thaw duration as depth within the ground increases shows that temperatures dissipate with increasing depth and thaw, if present, at deeper sensors is consistently of shorter duration with a later initiation to sensors closer to the surface. Ambient air temperatures can, therefore, be used as an indicator for ground thaw when this delay is considered. Using this method shows that on average NST shows signs of thawing ± one calendar month before positive temperatures are recorded for air temperatures. Similarly, NST shows signs of freezing ± one calendar month after sub-zero temperatures are recorded for air temperatures. Where the active layer extends beyond NST, an average delay in thawing at $T_{15}$ of 33 days, associated with an earlier onset of freezing of 26 days is observed. Thawing delay appears to be on the scale of months, rather than days, further speaking for an environment driven by long-term cold temperature regimes and not diurnal cycles.

Thermal offsets for summer are consistently positive for all sites, reflecting warmer NST and GST than air temperatures. In comparison, thermal offsets in winter are consistently negative for all sites, reflecting colder NST and GST compared to air temperatures. Overall annual thermal offsets are positive, indicating warmer ground temperatures than air temperatures. This reflects the insulating effect of snow on ground temperature regimes. This supports findings for A1, A4, A6 and A10 as argued by Kotzé (2016). Thawing indices for all sites are low with freezing indices dominating. Thawing indices for air temperatures and NST at A1 and A6 (at greatest altitude) are zero. Thawing indices for NST are positive for A2-A5, A9 (n = three years), A6 (n = ten years), as well as A10 (n = eight years). Here thawing index values are 17, 83, 424, 17, 226, 90, and 54 days respectively. Thawing indices for air temperatures are five days at A4 (n = three years), 5 hours for A7 (n = ten years), and 7 hours at A10 (n = eight years). Thawing indices for both air temperatures and NST, as well as high thawing indices compared to other sites, indicate the greater thawing potential at A4, which is reflected in this site having the greatest active layer thickness for all sites. The longest ground thaw is observed here between $T_{30}$ and $T_{45}$, suggesting that active layer thickness normally extends to these depths. As such, duration of ground thaw, as well as thawing indices may be used to infer active layer thickness.

High freezing indices are observed for all sensors for all years for all sites with a variably greater index calculated for air temperatures compared to NST. A greater freezing index for air temperatures is

evident for A1. In comparison, greater freezing indices at NST are evident at A3, A4, A5, A6, A7, reflecting shallower and less variable active layers. A2, A9 and A10 cannot be definitively calculated due to sporadic sensor failure for air temperatures. Nevertheless, freezing indices differences between air temperatures and NST for all sites are negligible and greater thawing indices associated with lower freezing indices reflect a deeper active layer. Similarly, smaller positive differences between thermal offsets for summer and winter reflect a shallower active layer. This is exemplified for A6 where thermal offset differences between summer and winter are 0.1. In comparison, greater positive values (thermal offset > 3.00) between summer and winter reflect a deeper active layer (> 25 cm). This is evident for A1, A3, A4, and A9. Lower freezing indices, as well as greater thawing indices and thermal offsets are associated with freeze-thaw cycles yet even when freeze-thaw cycles occur the balance of the freezing index to the thawing index is skewed toward the freezing index. This indicates the dominant quality of the environment, which is characterised by annual frost.

Annual degree days vary across sites, with degree days generally positive, reflecting a warmer ground regime. Notable exceptions are A5, A6, and A10. A5 shows negative degree days for 2013, A6 for 2013 and 2015 and A10 for 2009-2012. However, overall degree days and thermal offsets show that NST is warmer than air temperatures and that snow cover is present throughout, insulating the ground, yielding warmer ground temperatures compared to air temperatures. Ground freezing indices indicate a frost-driven regime. However, A4, which registers most freeze-thaw cycles and the lowest altitude has noticeable lower ground freezing indices compared to the remaining DML sites. In comparison, A6, located at highest altitude and with the lowest number of freeze-thaw cycles, has noticeably higher ground freezing indices. A6 also shows negative thermal offsets, indicating colder air temperatures than GST and a concomitant lack of snow cover during the year. All sites, without exception, register higher thermal offsets during 2014. This year was warmer than averages and thermal offset suggest that A6 had greater snow coverage in this year.

Positive temperatures maintained for air temperatures range from lasting 0 hours at A2 and 1 hour at A6 to 5 hours at A4. Between 6-45% of potential freeze-thaw events translate into freeze-thaw cycles for DML sites, with an average of ± 6% for CDML and 44% for WDML. While certain freeze-thaw cycles span more than one day, as observed for A4, and other sites exhibit multiple freeze-thaw events within a day, such as for A1, A5 and A9, most freeze-thaw cycles fall within the diurnal cycle. Freeze-thaw cycles are restricted to each site's active layer, specifically the upper portion of this layer, *i.e.* most freeze-thaw cycles only penetrate the upper few centimetres of the ground, as shown by the calculated expected diurnal freezing depth ($d$). This holds true for all sites except A4, where more frequent and deeper diurnal cycles are observed. This higher-frequency of potential freeze-thaw events and calculated freeze-thaw cycles is reflected in active sorted circles found here. Furthermore, Kotzé (2016) shows that these landforms are more active when compared to similar landforms found for A1 and A6. This is reflected in A4 having the highest number of freeze-thaw cycles of any DML site, the only site where cycles span several days and the longest thaw duration on average (18 hours). Furthermore, this site experiences the earliest average thaw initiation time (08:00), as well as the latest freeze initiation time (02:00 the following day). A1 has a high potential freeze-thaw events to freeze-thaw cycles conversion rate (45% for autumn 2008-2016; 61% for autumn 2013-2016), which is reflected in active

sorted circles found here (Kotzé, 2016). A9 shows thawing in spring and autumn, as well as the third-highest average thaw duration at NST recorded for any site (8 hours). It is also the only site where positive NST are recorded during October. High values for potential freeze-thaw events and freeze-thaw cycles for A9 suggest external locational parameter forcings on ground thermal dynamics. Here logger and sensors are in a depression/bowl near a brine lake and the emittance of longwave radiation (emissivity) from the surrounding rust-coloured doleritic rocks potentially increases the duration of positive temperatures recorded here for NST, as well as more freeze-thaw cycles having been calculated. The pond is also generally warmer and remains unfrozen for longer than similar water bodies found in the area (Marshall *et al.*, 1995), further having a potential warming effect on NST and associated ground thaw hours. The lower ground freezing index calculated for A9 gives further credence to the notion that the depression causes longwave radiation to be reflected inwards, increasing NST and GST and yielding high degree day values with concomitant lower-than-expected ground freezing indices. A3 consistently shows long ground thaw duration, a high number of potential freeze-thaw events and freeze-thaw cycles, as well as a high conversion of potential freeze-thaw events to freeze-thaw cycles (60%). This may be ascribed to the logger and sensor located on a scree slope (Krynauw, 1986). Logger and sensors do not exhibit significantly warmer air temperatures nor longer positive temperatures maintained for air temperatures when compared to sites at similar elevation (A5 & A7) and sediment textural descriptions (A1 & A2). Therefore, the gradient and composition of the scree slope potentially affect temperature and moisture dynamics of the ground, yielding higher freeze-thaw cycles and longer thaw durations.

The lack of change of positive air temperatures from 2013-2016 compared to longer time spans suggests little change in ambient temperatures in the last ten years for the region. In comparison, the halving of freeze-thaw cycles, potential freeze-thaw events and reduction in thaw hours since records began suggests a cooling trend for the area. However, summer of 2012/13 was unseasonably warm with highest temperatures, a thawing index exceeding zero (where a zero index is normally apparent: refer to 5.3.2.2.7 A7: Troll 1 (pg. 218) and 5.3.2.2.9 A10: Vesleskarvet (pg. 219) respectively), and an increase in freeze-thaw cycles recorded. A7 specifically only registers freeze-thaw cycles during this period. Furthermore, the warm summer of 2012/13 is associated with high temperature variability and mean temperatures for all sensors for A1, A6 and A10 (observations are not available for the remaining sites for those months). Removing this season from the dataset shows no significant warming nor cooling trend for the area. Multiple thaw events occur almost exclusively during summer, specifically January, with initial thaw generally commencing in the mid-morning (09:00-10:00) and last 2 hours. The main thaw event generally lasts 6 hours from 12:00-18:00 and is followed by subsequent events of shorter duration (± 1-2 hours). Several shorter thaw events followed by a longer event highlight how longer thaw duration is related to a lowering of threshold temperatures. Shorter periods of warming elevate ground temperatures compared to average conditions. Subsequent warming periods, thus, more readily yield extended thawing of the ground. This is also evident at A2, where the deepest and longest thaw event is preceded by eleven freeze-thaw cycles of an average of 7 hours each in the preceding twenty days. However, multiple thaw events do not translate into more freeze-thaw cycles. Instead, correlations between thaw duration and freeze-thaw cycles calculated indicate that higher numbers of freeze-thaw cycles yield longer thaw hours observed in the ground. This is exemplified by A4, the site with the highest number of freeze-thaw cycles and the only site where thaw events exceed one 24-hour period. Similarly, correlations between thaw duration and commencement of freezing

following a thaw event suggest that later commencement of freezing indicates longer duration of thaw. Finally, the strong positive and significant correlation between diurnal maximum temperature with maximum thaw duration shows that maximum temperatures translate into longer thaw observed in the ground. While initiation time of ground thaw is significantly correlated to thaw hours, as is diurnal minimum temperature with minimum thaw duration, these relationships are not as strong as those of freezing initiation, freeze-thaw cycles, and diurnal maximum temperatures.

Central Dronning Maud Land (CDML) is geologically distinct to WDML sites, which is reflected in lower moisture values and freeze-thaw cycles. Limited freeze-thaw cycles are observed for A7 in CDML and only during the 2012/13 summer, which, as already discussed, was warmer than average. The active layer here can be most closely described as the layer overlying permafrost that exhibits warmer temperatures without the frequent thawing and freezing of moisture. However, occasional freezing and thawing of the ground does take place. While CDML does exhibit above 0 °C ground temperatures, the ground cannot be called active in the truest sense and the lack of freeze-thaw cycles explains the lack of features such as sorted circles and evidence of needle ice. High temperatures variability with increasing sensor depth at A7 in CDML may be ascribed to the coarse-grained and sandy material and concomitant lack of moisture, since such material is associated with deeper freezing fronts and enhanced air movement. This translates into higher variability, as well as a variable interannual active layer thickness. Both are observed at this site. Furthermore, high air temperature variability also indicates the continental location of the site, since temperature extremes increase with increasing distance from the coast, as argued by Kotzé (2016) for A1 and A7. Nevertheless, although variability is slightly higher for CDML than WDML, an evaluation of the thermal state of the permafrost,, seasonal ranges and seasonal change shows little variation with no significance in terms of the annual frost environment. Similarly, small differences in annual temperature ranges between CDML and WDML exist, yet these do not translate into noticeable greater annual ranges for NST and GST. As such, it can be argued that the permafrost environment remains similar for all sites, with variations only present in the seasonal and diurnal thaw environment. Furthermore, PCA shows that DML sites relate to each other with no site significantly more important than another and the small differences observed, such as for variability, between CDML and WDML sites are found to be statistically insignificant. Nevertheless, A4 exhibits consistently less component loadings and is less correlated to the other sites, suggesting a different environment to the remaining sites. The high correlations exhibited by A3 and A9 to other sites suggest that these sites may be used as indicator sites for the locations within WDML and warrant further investigation.

### 6.3.3 Sediment/soil specifics

Ryan *et al.* (1989) and Ravindra and Chaturvedi (2011) argue for a deglaciation of Dronning Maud Land (DML) at 10 000 BP and the poorly developed soils with low bulk density, poor sorting, well graded samples, a paucity of organic content and moisture all reflect an environment recently deglaciated. Furthermore, the region is dominated by ice and cold temperatures, such as found in a continuous permafrost zone (CPZ). While fine earth fraction (FEF) proportions are low and bulk density values thus overestimated, all Dronning Maud Land (DML) samples exhibit a lack of fines ($\phi > 4$: silt and clay) with coarse material (coarse sand/fine gravel) dominating in the area. Ice segregation and frost heave

generally occur in fine-grained soils and the lack of fines, therefore, has implications for freeze-thaw cycles and frost heave. Uniformity coefficients ($C_u$) consistently show very poor sorting and well graded samples, furthermore indicating glaciated material with a lack of fines. Uniformity coefficients ($C_u$) can be attributed to an environment in which weathering occurs at lower rates, limiting the production of fines. The cold climate of the Antarctic does limit chemical weathering rates, although both mechanical and chemical weathering are present (Hall, 2002). Nevertheless, the Maud Belt has experienced little surface weathering since exposure (McGibbon, 2014).

Low porosity and moisture retention values, as well as high specific yields ($S_y$), indicate that the sediment column is limited in terms of retaining ground moisture. Moisture is a crucial component to freeze-thaw cycles, albeit not potential freeze-thaw events, and frost heave cannot occur without the presence of ground moisture. This lack of moisture partially explains the lack of landforms such as sorted circles and evidence of frost sorting, when compared to permafrost associated landforms such as thermal contraction polygons. Low total organic carbon (TOC) values agree with to those calculated by Steele *et al.* (1994) for Vesleskarvet and Shrivastava *et al.* (Shrivastava *et al.*, 2014) for the Jutulsessen. Organic content affects bulk density: the greater this proportion, the lower the ground's porosity. This has implications for freeze-thaw cycles, since a paucity of organic content generally translates into a lower freeze-thaw cycle potential. A10 reflects the highest moisture values yet even these are low. Low moisture contents (± 3% on average for all sites except A10), are comparable to those of the shallow active layer observed for continental Antarctica (Bockheim and Hall, 2002). However, the ice-cemented permafrost suggests a gravimetric moisture content of at least 5% (Campbell *et al.*, 1998), which is calculated for A2, A5, and A10. While other sites score below this threshold, it is noted that moisture values represent point samples and do not reflect annual moisture values. Nevertheless, the lack of surface water translates into the absence of discernible ice content of the permafrost and active layer thickness tends to 25 cm, like observations for McMurdo Sound (Campbell *et al.*, 1998). Furthermore, it is argued that soil moisture is a limiting factor for freeze-thaw cycles in DML.

Finally, A7 in CDML of Antarctica exhibits an atypical frost environment with a paucity of freeze-thaw cycles, when compared to the WDML sites. The paucity of freeze-thaw cycles for this area is explained by high porosity values and a coarse-grained sediment, which generally has low permeability. Furthermore, water-holding capacity of sandy material is low due to large pore spaces present in the column of ground and drainage enhanced in sandy soils (Brady and Weil, 2016). Finally, when unfrozen water content is low frost heave becomes limited (Osterkamp and Burn, 2003). The lack of needle ice evidence, frost heave and sorted circles for the Jutulsessen compared to WDML can, thus, be attributed to these factors.

## 6.4 Modelling the Diurnal Frost Environment

The subsections below provide a discussion on the various parameters analysed and how these affect the annual seasonal, and diurnal frost environment.

### 6.4.1 Air temperatures, ground temperatures, soil moisture, wind speed and direction

Highest mean annual average temperatures (MAAT) for all study areas (Eastern Cape, Marion Island, Dronning Maud Land (DML) of Antarctica) are recorded at the ground surface (1-2 cm depth). Furthermore, temperatures stabilise with depth. In areas of permafrost and snowfall, such as those of DML, positive thermal offsets indicate the insolating effect snow has on ground temperatures. In permafrost areas, greatest temperature variability occurs for depths that thaw during summer and to which active layer thickness is present. In non-permafrost areas, highest variability of temperature regimes occurs where seasonal freezing of the ground occurs. As such, highest variability occurs to the depth of freeze-thaw cycles. Seasonal ranges are high for all sites with Eastern Cape, Marion Island and DML all exhibiting seasonal range exceeding 30 °C. Seasonal ranges are, therefore, not significant ($p < 0.05$). However, diurnal temperature ranges, maximums, and minimums reflect significance ($p < 0.05$). Furthermore, freezing depth is shallow for Eastern Cape sites, as well as Marion Island, with depths recorded in the centimetre range. In DML, sites exhibit shallow thawing depths, with thaw for all investigated sites not extending beyond 60 cm. Shallow freezing depths observed for the Eastern Cape and Marion Island is reflective of diurnal and limited seasonal freezing, whereas the shallow thawing depths of DML reflect diurnal and limited seasonal (summer) thaw.

The effect of climate change on the frost regime must also be considered. An estimated 25% decrease in potential freeze-thaw events is expected to occur with a 1 °C increase in temperature (Boelhouwers, 2003a). This will be associated with the halving of the freezing depth from 20 cm to 10 cm at 1 000 m a.s.l. on Marion Island. Furthermore, a potential reduction of 25% of sediment movement rates is expected. Hedding (2006) provides, for two sites on Marion Island, further estimations of the reduction in potential freeze-thaw events under a warming climate. Considering a change of + 1 °C, potential freeze-thaw events at Ned's North will decrease from 233 to 89 at the near surface. When an increase of 2 °C is considered, potential freeze-thaw events at the near surface will decrease to 50. For both scenarios, no potential freeze-thaw events will occur at 50 cm or deeper within the ground. Similarly, a one degree increase in climate will decrease potential freeze-thaw events at Ned's South from 276 to 181 at the near surface. When an increase of 2 °C is considered, potential freeze-thaw events will decrease to 115. In both scenarios, no potential freeze-thaw events will reach 25 cm within the ground.

Evaluating near surface and ground surface temperature (NST and GST, respectively) against each other using Principal Component Analysis (PCA), shows that GST explains greater variability of the dataset compared to NST. It can, therefore, be concluded that GST is the preferred depth (or parameter) for recording ground temperature when evaluating ground freeze-thaw cycles. Dronning Maud Land (DML), with simpler systems, allows for an evaluation of freeze-thaw cycles using temperature variability (expressed as standard deviation: s) extracted from verified freeze-thaw cycles. However, this does not apply to the more complex environment of Marion Island, nor the Drakensberg. Furthermore, central Dronning Maud Land (CDML) sites exhibit differences in behaviour, when compared to western Dronning Maud Land (WDML) sites. The active layer thickness of 38 cm reflects depths shallower than this depth behaving as one unit, which correlates with air temperatures and is shown by PCA analyses and correlation calculations for sensors ranging from NST to $T_{20}$. The warmer year of 2013 reflects slightly adjusted component loadings for those sites where data are available. For

A10, which registers active layer thickness of 16 cm for 2013, component loadings, as they apply to $T_{20}$, are no longer different to those of sensor at shallower depths.

The evenly distributed component loadings per principal component (PC) suggest that all temperature populations are of significance at each site. Two PCs calculated for A10, using all available temperature and moisture populations, suggests that this site behaves differently to the remaining DML sites. PC2 of A10 displays high component loading for soil moisture, trending together with air temperatures, NST and $T_{15}$. This relationship is reversed for $T_{30}$-$T_{60}$ and suggests soil moisture affects thermistors down to $T_{15}$. Simultaneously it can be argued that air temperatures affect soil moisture. Active layer thickness is associated with higher component loadings per PC for all sites. This suggests that component loadings could be potentially used, in the absence of other data, as a proxy for determining active layer thickness. Similarly, correlation coefficients ($r$) corroborate component loading values, where the highest correlations (across sensors) are calculated for sensor depths for the average calculated active layer thickness per site, *i.e.* correlations are highest at depths to which the active layer occurs. Furthermore, soil moisture values generally register higher than average correlations with depths that are within the active layer. This suggests that the correlation coefficient ($r$) could potentially be used as a proxy for determining active layer thickness for these sites, or sites like those of the study area. It can also be inferred that the highest correlation exhibited by $T_{50}$ to all other layers of A8 suggests that active layer thickness is closer to this depth than NST or $T_{100}$. This corresponds to the actual measured active layer thickness of 38 cm for A7. Principal Component Analysis (PCA), furthermore, shows that computed diurnal temperature ranges using the World Meteorological Organisation (WMO) method (World Meteorological Organisation (WMO), 2011), as well as diurnal maximum temperature and diurnal minimum temperature, explain sufficient of the variance when evaluated against thaw duration of freeze-thaw cycles. Diurnal maximum temperature is also more appropriate for inferring thaw duration when using a combined score of component loading and the correlation coefficient. As such, it can be concluded that the variable of diurnal mean and maximum temperature, suffices to infer characteristics of freeze-thaw cycles, such as duration of thaw.

A7, located in central Dronning Maud Land (CDML), behaves differently to sites located in western Dronning Maud Land (WDML). Here thaw duration is neither correlated strongly, or significantly, to any of diurnal mean, maximum, minimum, range, and temperature variability (expressed as standard deviation: $s$). An evaluation of freeze-thaw cycles shows that a minimum of these, when compared to other study sites, are observed for A7. This explains the lack of correlation and component loadings for thaw duration against calculated diurnal parameters. Similarly, the low proportion of identified freeze-thaw cycles at A6 reflects the lack of significant correlation of thaw duration to diurnal minimum temperature for this site. Diurnal ranges exceeding 10 °C, compared to oscillations around 0 °C show that over a large area (DML, Marion Island, Eastern Cape), air temperature reflects a strong relationship ($r \pm 0.79$, $p < 0.01$) with ground temperatures. As expected, such ranges are also strongly correlated to mean annual air temperatures ($r \pm 0.94$, $p \pm 0$). However, diurnal ranges exceeding 10 °C, which were used as an indicator of freeze-thaw cycles by Kück (1997) in the Eastern Cape, are not applicable for inferring freeze-thaw cycles on Marion Island, or in DML. On Marion Island, due to the mild oceanic climate, diurnal ranges rarely exceed this threshold. In DML, such ranges occur but tend to not breach

0 °C. As such, each site must be evaluated separately, when inferring diurnal ranges with reference to freeze-thaw cycles and potential freeze-thaw events. Furthermore, local climatic drivers and thresholds are need to be considered. For DML, the threshold for freeze-thaw cycles focuses on positive temperatures reached at the ground surface; in the Eastern Cape the threshold focuses on sub-zero temperatures reached at the ground surface. As such, freeze-thaw cycles take place predominantly during summer and winter respectively. Nevertheless, the underlying requirements remain the same across the sites.

Soil moisture is a crucial component of freeze-thaw cycles occurring, and volumetric water content (VWC) can be used as an indicator for gravimetric water content (GWC), as well as GWV is expressed as a percentage ($M_c$), and the soil water-filled pore space ($M_p$). This is inferred from the strong and significant correlations of these parameters. The lack of soil moisture at A7 and A8 also translates into a paucity of freeze-thaw cycles at these sites. Soil moisture exhibits consistently less loadings on PCs in the DML dataset and could potentially be removed from each individual dataset. A possible explanation is the paucity of freeze-thaw cycles determined for DML. While numerous potential freeze-thaw events are observed, freeze-thaw cycles are few. Since soil moisture is a requirement for freeze-thaw cycles but not potential freeze-thaw events, PCA suggests that in an environment where freeze-thaw cycles are rare soil moisture recordings are less significant. While snow cover ameliorates ground temperatures, it does not significantly improve the availability of soil moisture to freezing events. Macroclimatic forcings, such as air temperatures, exert a significantly greater control on freeze-thaw cycles observed ($p < 0.05$) than the availability of snow and ice as a source of meltwater.

### 6.4.2 Soil properties

Due to encouraged granulation and aeration freeze-thaw cycles and associated heave yield lower bulk densities and higher porosities. This is due to material losing bulk density and cohesion following such cycles (Williams and Smith, 1991). Bulk density, porosity, as well as permeability were thus investigated regarding freeze-thaw cycles.

Bulk density is an indicator of soil compaction and represents the dry weight of sediment compared to a known volume (McKenzie *et al.*, 2002). Higher densities indicate low sediment porosity and sediment compaction, affecting and restricting the movement of water through sediment (McKenzie *et al.*, 2002), which in turn affects freeze-thaw cycles. High bulk densities, thus indicate low porosities and *vice versa*. Furthermore, porosities affect permeability. As such, literature suggests that bulk density, porosity, and permeability are complementary indicators. This is confirmed through statistical analyses, based on correlation coefficients (r) and Principal Component Analysis (PCA). While porosity affects the amount of water the ground can hold, which is crucial to freeze-thaw cycles, and permeability determines the ability of water to move within the ground, another important factor in the evaluation of freeze-thaw cycles identified by PCA, is bulk density, which explains the variability of both porosity and permeability. The expected high and significant correlation of bulk density with porosity, furthermore, supports this analysis. Phi ($\phi$) mean and the fine earth fraction (particle sizes < 2 mm in diameter) in turn are complementary indicators, as shown by their strong correlation. Similarly, organic content ($O_p$) and

total organic carbon (TOC) are paired as shown by their high and significant correlation. Principal Component Analysis (PCA) suggests that the soil property parameter is ideally composed of bulk density, Phi ($\phi$) mean, and organic content ($O_p$) when evaluating freeze-thaw cycles. Other parameters may be excluded.

### 6.4.3 Vegetation, snow and cloud cover

Cloud cover data are available from the Moderate Resolution Imaging Spectroradiometer (MODIS) on the NASA Terra and Aqua satellites. Images are taken at 10:30 a.m. descending node (Terra), or 1:30 p.m. ascending node (Aqua). However, even at such a resolution, inferences regarding the diurnal frost environment are difficult to make. Instead, ambient air temperatures and ground moisture (refer to 5.4.1 Air temperatures, ground temperatures, soil moisture, pg. 272), provide a greater indication of ameliorating/enhancing effects on freeze-thaw cycles. While cloud cover is not excluded as a parameter, problems of scale exist. Freeze-thaw cycles range from a few seconds to 24 hours (diurnal), while cloud cover images are recorded at scales of hours to days. As such, evaluating cloud cover impacts on freeze-thaw cycles is problematic. Nevertheless, cloud cover decreases the presence of freeze-thaw cycles, as presented by Campbell *et al.* (1998), and attributed to slower rates of heating and cooling.

Ambient air temperature greatly affects ground temperatures (refer to 5.4.1 Air temperatures, ground temperatures, soil moisture, pg. 272). However, not every potential freeze-thaw event yields a freeze-thaw cycle. This is ascribed to, amongst others, soil textural properties, soil moisture content, as well as snow and vegetation cover. Freeze-thaw cycles may limit vegetation cover due to frost processes damaging root, stem and leaf structures. Concomitantly, a lack of vegetation cover increases the potential for frost processes to occur. Feedback loops and thresholds between ground frost penetration and sparse vegetation cover must, therefore, be considered. A relationship is apparent between vegetation cover and ground freeze-thaw cycles. Data from the Eastern Cape show that dense vegetation cover limits ground frost penetration. Furthermore, removal of this vegetation cover enhances ground frost penetration. Therefore, vegetation cover and ground frost are correlated, and specific thresholds must be met for ground frost to occur in an area that is vegetated. Vegetation cover decreases the likelihood of ground frost occurring, providing an insulating effect, maintaining and ameliorating ground temperatures. In Dronning Maud Land, the Eastern Cape, and on Marion Island, snow cover reduces variability (expressed as standard deviation: *s*) of ground temperatures at all depths, particularly at the near surface sensor (NST: recorded at ± 1 cm) and the ground surface sensor (GST: recorded at ±2 cm depth), preventing freeze-thaw cycles from occurring. Instead, snow cover leads to longer freeze durations.

### 6.4.4 Altitude

An increase in altitude reflects an increase in potential freeze-thaw events for all Dronning Maud Land (DML) sites and a decrease in freeze-thaw cycles and active layer thickness, as exhibited by strong correlations of altitude to frost cycles and temperatures recorded per sensor depth. This suggests that

soil moisture is a limiting factor in frost environments. In DML, while more potential freeze-thaw events are observed with increasing altitude, these do not translate into more freeze-thaw cycles, but rather the increasing elevation translates into a decrease in freeze-thaw cycles. Principal Component Analysis (PCA) suggests that the contribution of altitude to active layer thickness and freeze-thaw cycles is greater than that of distance to the shelf/ocean of each site. As such, altitude is evaluated as the more significant contributor compared to distance from the ice shelf/ocean to the frost environment. While correlations to near surface temperatures (NST: recorded at ± 1 cm in the ground) are not as apparent, strong and significant correlations exist to temperature variables for deeper depths. This suggests that altitude influences temperature observed and that higher elevations reflect in colder temperatures deeper within the ground, *i.e.* not affected by short-term fluctuations of incoming solar radiation as experienced by the near surface. A similar relationship is observed in the Eastern Cape Drakensberg and on Marion Island. Elevation is strongly correlated to recorded temperature, as well as potential freeze-thaw events and freeze-thaw cycles. Nevertheless, in the Eastern Cape, significant relationships exist between altitude and ground minimums and means. In Dronning Maud Land strong relationships exist between altitude and ground mean, maximum, and minimum temperatures. This suggests that altitude affects minimum temperatures to a greater extent in the marginal environment of the Eastern Cape, than in the other two locations. Furthermore, in Dronning Maud Land an increase in elevation yields less freeze-thaw cycles recorded. In the Eastern Cape an increase in altitude yields more freeze-thaw cycles. The same applies to Marion Island, with an altitudinal gradient apparent. This is due to DML being characterised by annual frost, Marion Island by seasonal frost, and the Eastern Cape by sporadic seasonal frost (if at all).

### 6.4.5 Latitude and distance from the ice shelf/ocean

Ground temperature averages, calculated for the various temperature depths, correlates with increasing latitude. Furthermore, the greater the increase in latitude, the greater this correlation. The fact that the temperature at the deepest sensor at each Dronning Maud Land (DML) site occurs within permafrost, is most strongly correlated with latitude, suggests that at this depth less variability is observed, and that the more dynamic environment of the surface is indicative of the active layer thickness. Similarly, variability is greatest at the depth to which freeze-thaw cycles penetrate on Marion Island and in the Eastern Cape.

In DML, temperature minimums calculated at various depths in the ground are strongly correlated to latitude and distance from the ice shelf, suggesting that colder conditions are impacted by these parameters, in comparison to warmer conditions which do not correlate at a significant level. Increasing distance to the shelf shows a strong negative relationship to freeze-thaw cycles calculated, suggesting that the shelf has a potential ameliorating effect on ambient temperatures, with sites further inland potentially more dynamic and variable. Another factor of importance is that freeze-thaw cycles require a suitable medium, such as soil or sediment. Such mediums are not present at the ice shelf and the relationship exhibited between distance to the shelf and freeze-thaw cycles can be attributed to this fact. Nevertheless, of the eight nunataks evaluated for DML the sites furthest from the ice shelf reflect less freeze-thaw cycles, indicating that distance from the ice shelf does have a forcing on ground dynamics regarding the frost environment. This is, furthermore, shown by the correlation of potential

freeze-thaw events to $T_{30}$ and $T_{45}$ in that only A4 exhibits potential freeze-thaw events at these depths. This site is also closest from the ice shelf. Nevertheless, of the parameter of latitude and distance to the shelf, latitude is determined as the more significant contributor when evaluating the frost environment. In the Eastern Cape distance from the coast has a greater forcing on potential freeze-thaw events and freeze-thaw cycles recorded at the ground surface (GST). However, this inference is not conclusive since the topography of the Eastern Cape is such that an increase in elevation is observed as distance to the coast increases. The same applies to Marion Island, where distance from the coast translates into an increase in altitude. As such, altitude exerts greater forcing on freeze-thaw cycles, as opposed to distance from the coast.

### 6.4.6 Microtopography and locational specifics

Macrotopographial factors significantly affect ground temperature and moisture dynamic. In comparison, microtopographical factors are not significant.

Aspect-related control on freezing observed in thúfur in the High Drakensberg has been noted by Grab (2005). Here southern and south-western aspects receive less sunlight and freeze before the northern/north-eastern aspects. Differences in needle-ice growth on northern and southern aspects at locations in Abisko (Sweden) and Sani Pass (South Africa) were noted by Borg (2012). He argued for positive feedback loops between animal-induced trampling reducing vegetation cover and needle ice restricting re-vegetation of surfaces. Furthermore, Hansen *et al.,* (2013) argue for aspect-controlled weathering on a blockfield in western Dronning Maud Land of Antarctica. Higher-frequency ground temperature data, collected A10 in Dronning Maud Land (DML) from 19-29 January 2011 (n = ten days), show that aspects are significantly different. The north-facing aspect, followed by the west-facing aspect, has the greatest diurnal maximum and temperature ranges. The southern aspect consistently registers the lowest diurnal maximum, minimum, range, and mean temperature and has the lowest variability (expressed as standard deviation: *s*). Furthermore, the diurnal cycle displays the greatest diurnal temperature range for the northern aspect. As such, the northern aspect, which greater solar radiation, is consistently warmer and significantly different to other aspects. Furthermore, analyses from Sani Pass indicate the effect of aspect on ground temperature and moisture dynamics, with south-facing slopes significantly ($p < 0.05$) colder and with higher soil moisture compared to north facing slopes. In contrast, geographic weighted regression (GWR) of ground temperature recorded across a selected area (Northern Buttress of Vesleskarvet, Antarctica), indicates that slight locational differences in aspect and gradient are not significant at $p < 0.05$. As such, microtopographic control is not significant on observed temperature and moisture regimes, although macrotopography on a regional scale affects freeze-thaw cycles. Due to the lack of a significant impact of microtopography on freeze-thaw cycles, it is concluded that such locational characteristics don't skew or affect data observed per area, *i.e.* the control of slight differences in slope and aspect on each separate area of interest (Ben MacDhui, Elandsberg, Marion Island, central Dronning Maud Land (CDML), western Dronning Maud Land (WDML) is not sufficient to significantly affect observed freeze-thaw cycles. In contrast, macroscale parameters must be considered.

## 6.5 Sediment Movement and Feature Comparison

Dronning Maud Land of Antarctica is dominated by annual frost and seasonal thaw events; Marion Island by seasonal frost events and a lack of permafrost; mainland South Africa only registers short-duration frost of a few weeks at a time. Each investigated area features landforms, such as polygons, solifluction lobes, and sorted circles. Landforms, thus, exhibit azonality. Furthermore, a cohort of processes yield these forms, suggesting a measure of equifinality to be present. Analyses suggest that the three geographical areas represent a similar morphogenetic region with respect to the diurnal environment. Self-organisation in landforms suggests that the processes, at various spatial and temporal scales, act synergistically. Such organisation may be divided into landforms of two-dimensional periodicity (sand dunes, dust ripples, beach cusps *etc.*), three-dimensional patterns (thermal contraction polygons, patterned ground), large-scale periodic patterns (volcanoes, rifts), and scale-invariant structures (drainage patterns) (Hallet, 1990). Furthermore, climatic zones might delineate specific geomorphic systems, yet not all relevant sub-systems. Each sub-system, dependent on the applied scale, may have further sub-systems inherent to it. Open systems dictate that multiple processes, inputs and outputs may be present, suggesting self-organisation and equifinality. Landforms resulting from annual and deep seasonal frost cycles dominate the Antarctic landscape with thermal contraction polygons ubiquitous for the snow and ice-free portions of Dronning Maud Land (DML). Other common landforms include rock glaciers, openwork block deposits and solifluction terraces. The long polar night experienced at this latitude is reflected in deep permafrost and landforms found here are largely attributed to permafrost dynamics and not as much fluctuations on a diurnal basis. Therefore, such landforms correctly indicate the presence of long-term (seasonal and annual) frost cycles. Landforms found for DML also exist for the highest elevations on Marion Island. However, these do not reflect the contemporary frost environment. Instead, contemporary landforms indicate an environment where medium- to short-term (seasonal and diurnal) frost processes are active. In the High Drakensberg of the Eastern Cape on mainland South Africa, such landforms, as are common in Antarctica, including Dronning Maud Land (DML), are considered relict and indications of a colder paleoclimate and environment. Such landforms, therefore, fit within current climatic zonations and cannot be considered azonal in the truest sense. The proper evaluation of frost cycles in terms of their duration (long-, medium-, short-term), is reflected in landforms of the appropriate scale. Nevertheless, landforms caused by shallow and high-frequency frost cycles (those associated with diurnal cycles) are also present in DML, with frost sorting, mud boils and sorted circles notable examples. Marion Island exhibits a plethora of such landforms at a great altitudinal range. Furthermore, frost sorting is common for the slopes of Ben MacDhui. It can, therefore, be argued that landforms associated with shallow and high-frequency frost cycles, *i.e.* diurnal frost cycles, exhibit azonality and occur across zones.

Painted marker trenches also indicate cycling of material within the ground. These cycles cause particles to move towards the freezing front, yielding deficiency of specific textural fraction to the depth of freeze-thaw cycles. While the dominant direction of movement is towards the ground surface, the cyclical nature of these processes is evident in particles moving deeper into the ground. Furthermore, lateral movement of particles is also in evidence. As such, freeze-thaw processes yield lateral and vertical movement of particles deficiency of certain textural fractions likely due to all three sorting mechanisms: 1) uplift of particles when freezing occurs from the top, 2) sorting as particles migrate

away from the freezing plane approaching from the top or sides, and 3) mechanical sorting (refer to Corte, 1966).

## 6.6 Modelling the Frost Environment

An evaluation of all parameters allows for an estimation of the freeze-thaw cycle model. Frost cycles *(FTC)* are predominantly a function of temperature (*temp*), with the greatest weighting given to this parameter. This is followed by soil moisture (*m*), which is given the next-highest weighting. Soil properties (*soil*) for inclusion in the model are the proportion of fines (particles < 2 mm in diameter), gravimetric water content (GWC), and organic proportion ($O_p$). The overriding factor of latitude and latitude is also included. Here an increase in latitude from increases the occurrence of freeze-thaw cycles, with a maximum reached in the mid-latitudes. When moving from mid-latitudes toward the polar regions, fewer freeze-thaw cycles occur. An increase in altitude also yields more freeze-thaw cycles, but must be considered with the relative location of an area. The high altitudes of the high latitudes produce fewer freeze-thaw cycles; in the mid-latitudes this relationship is reversed. Vegetation and snow cover exert some control on ground frost, but not as much as other parameters discussed here. Nevertheless, these parameters should also be included in the freeze-thaw cycle state factor model. Finally, time (*t*) needs to be evaluated in terms of diurnal, monthly, seasonal, or annual scales. The state-factor model can then be written as depicted by Equation 16. Factors decrease with weighting towards the left, *i.e.* temperature has the greatest weighting and, as such, has the first place in the equation.

**Equation 16: The adjusted freeze-thaw cycle model. FTC: frost cycles; temp: air temperatures, m: soil moisture, soil: soil properties [FEF: fine earth fraction, VWC: volumetric water content, $O_p$: organic component), veg: vegetation, snow: snow cover, and t: the independent variable of time (evaluated on diurnal, monthly, seasonal, and annual scales). 1; 2: consideration given to the geographical location of the site.**

$$\frac{dF}{dt}, \frac{dtemp}{dt}, \frac{dm}{dt}, \frac{dlat}{dt}, \frac{dalt}{dt}, \frac{dsoil}{dt}, \frac{dveg}{dt}, = f(temp, m, lat[1;2], alt\,[1;2], soil[FEF, VWC, Op], veg/snow[1;2])$$

## 6.7 Zonality vs. Azonality

Arguments can be made for and against azonality of landforms and processes. Polygons are found at each site, although those in Dronning Maud Land (DML) ascribed to thermal contraction, and those on the slopes of Ben MacDhui in the Eastern Cape of mainland South Africa to desiccation, as well as thermal contraction. Furthermore, polygons differ in size, with those in DML largest, and those on Ben MacDhui smallest. Additionally, the Eastern Cape polygons are sorted, as well as non- sorted. Those in DML are generally non-sorted.

While Dronning Maud Land (DML) soils lack clays and silt, freezing of the substrate still occurs in the polar environment where low sub-zero temperatures are common. Moisture is required and in continental Antarctica the ground, which often lacks moisture, does not necessarily experience freeze-thaw cycles. Holness (2001a) argues that moisture is not a limiting factor on freeze-thaw cycles on

Marion Island and the ubiquitous freeze-thaw cycles on the Island affirm this assertion. Irrespective if this, soils of the Eastern Cape have much higher proportion of clay and silt particles, suggesting suitability for freeze-thaw cycles. However, thick vegetation cover, especially on the Elandsberg, negates the impact of sub-zero air temperatures, thereby minimising ground freeze-thaw activity. The same applies to Marion Island, where Haussmann *et al.* (2009a, 2009b) showed an insulating effect of *Azorella selago* on ground temperatures. However, it must be noted, that this study shows that frost processes at Ben MacDhui and the Elandsberg don't have a significant impact on vegetation growth and cover, as argued by Borg (2017) and Kück (1997) for Ben MacDhui.

On Marion Island, soil contains both clay and silt, receives a high degree of precipitation throughout the year (required for ground moisture), and lacks thick vegetation cover. As such, freeze-thaw cycles are common and this location the most active in terms of diurnal freeze-thaw cycles and potential freeze-thaw events. Animal impacts are negligible to non-existent for Ben MacDhui and the Elandsberg. Ben MacDhui is not intensely grazed when freeze-thaw cycles are common (winter and spring). The Elandsberg is not utilised for animal husbandry where the study was conducted. As such, no inference can be made in terms of animal presence on freeze-thaw cycles at these locations. The same applies to DML of Antarctica and Marion Island, where no animal presence is noticeable near logger locations. Instead, vegetation cover exerts a greater influence, as discussed above, especially for the Eastern Cape.

While the highest number of freeze-thaw cycles occur in regions with low annual temperature ranges, the fewest cycles are observed in high latitudes and in continental climates (Goudie, 2004a). Where permafrost occurs, freeze-thaw cycles occur only within the active layer. Furthermore, the depth of the active layer determines the depth of freeze-thaw cycles. In non-permafrost environments, the depth of such cycles increases with latitude (Goudie, 2004a). Zonality does not specifically apply to the periglacial environment, but rather to the investigated climatic zones, which do not all account for the periglacial environment. However, results show that Ben MacDhui is classed as sub-periglacial and here azonality of form is apparent. The DML sites, while exhibiting limited periglacial characteristics, are appropriately located in the Polar climatic zone. Yet landforms such as sorted circles, non-sorted polygons, and terraces occur at all sites. Marion Island, which is distinctly periglacial, as already argued by Boelhouwers *et al.* (2003), features a whole range of periglacial landforms. As such, an argument is made for both azonality of processes (specifically diurnal and short-term frost processes), as well as landforms. Equifinality is thus achieved by more than one process yielding similar landforms. Finally, as argued by *e.g.* Beven (1996; 2000), and Phillips (2007), global parameters are not sufficient to model local parameters, masking local characteristics. As such, climatic geomorphology, when taken in the context of geomorphological investigations, should include local parameters in climate zone delineation, instead of global parameters. This allows for more appropriately delineated zones, applicable to specific scientific investigations. Current climatic zones should be used as a starting point, but not the defining parameter when evaluating climatic regions. Specifically, climatic zones should not be used to infer specific processes nor landforms, but should, rather, be used as a tool to predict processes and landforms. Each geographical location should be evaluated individually, and processes and landforms described and inferred following site-specific investigations.

Definitions of the periglacial environment allow climatic zonation to be made across zones. As such, the periglacial environment is azonal and processes within it, therefore, azonal as well. Each site investigated in this research have periglacial characteristics. While permafrost is not present on Marion Island, nor the Drakensberg, seasonal frost is, allowing for a periglacial classification to be applied. Irrespective of the above arguments, current climatic zonation systems do not truly consider the periglacial environment and, as such, do not allow for azonality of processes, nor their resultant landforms. Freeze-thaw cycles occur predominantly within a periglacial, or cold-climate setting. However, the lack of a definitive definition for these environments makes their inclusion within climatic classifications problematic. Furthermore, climatic classification systems are largely based on annual temperatures, with the occasional inclusion of moisture values. Using temperature as a proxy for the soil-moisture balance is critiqued. Analyses show that moisture values, within the periglacial environment, should be given greater consideration, as already argued by Thorn and Hall (2002). Even though a clear relationship between temperature and moisture is apparent, this relationship is not always linear and varies depending on parameters such as organic matter, vegetation cover, snow or cloud cover, and even human surface modifications. Annual averages mask seasonal and diurnal characteristics, introducing additional complexity by not considering appropriate levels of scale. Broad zone delineation is appropriate for determining long-term processes, such as annual freeze cycles, and current climatic systems, specifically those where permafrost occurs. However, high-frequency and short-duration processes acting on diurnal scales are not adequately provided for under current climatic classifications, and it is these processes that exhibit azonality. Furthermore, contemporary landforms formed through such high-frequency processes occur across zones. While current climatic delineations do not specifically exclude the presence of diurnal frost cycles, the overall zonal descriptions do not sufficiently address their presence nor absence. As such, current climatic zonations should include aspects of diurnal frost cycles in their delineations. However, such cycles are impacted by several factors and zonation is complex. Phillips (1999) proposes that increased complexity generally yields divergence of form and spatial patterns. This is due to conditionality within geomorphic systems, where landscapes and landforms may develop differently due to thresholds either exceeded or not. The comparatively more complex systems of the Drakensberg and on Marion Island yield a greater variety of landforms than those of DML. The Drakensberg and Marion Island also feature paleolandforms, which can be evaluated as examples of equifinality and azonality of landforms. However, the project takes this into account, and paleolandforms are not considered in the evaluation of azonality of landforms. Rather, contemporary and temporal landforms are the focus. This study also uses the definition of the periglacial environment as one where freeze-thaw processes are present and not only permafrost. This increases the global geographic range of periglacial environments to 35% of the Earth's land surface (Washburn, 1979; Goudie, 2004b).

Morphogenetic regions are useful for identifying common landforms. However, not all landforms and processes are addressed, yielding the exclusion of such landforms and processes from these regions. This yields an azonality of landforms and processes – not that these processes or landforms are absent from specific regions but rather that classification systems simply make no allowance for their presence. The inclusion of more delineating parameters does increase the complexity of any climatic classification system and this complexity eventually yields equifinality, as argued by Beven (2000). Convergence of form is transitory, perceived as a local (temporary) equilibrium state. Although contemporary processes yield the same landforms and override historical features (equilibrium view: Phillip, 2007), natural

systems are open-state systems and yield a non-equilibrium state, a state that is most common in such systems (non-equilibrium view: Phillips, 2007). Azonality, as shown in this project, shows that global factors, such as temperature and precipitation values used for climatic zonal delineation, force landscape evolution. However, local contingent factors, such as geology, vegetation and aspect, are crucial in determining landscape evolution, and concomitant landform morphology, as well. Although arguments have been made against equifinality as a concept within geomorphology by *e.g.* Haines-Young and Petch (1983), simplexity requires that a measure of equifinality is present. Applying these at specific scales, as proposed by Phillips (1997), such as those applicable to periglacial environments and diurnal frost processes, allows for an argument to be made for convergence of form and equifinality. Each zone features landforms, such as polygons, solifluction lobes, and sorted circles. Landforms, thus, exhibit azonality. Patterned ground occurs in all investigated climatic zones, or specifically, study locations and frost processes are integral to the formation of all these landforms. Patterned ground, as an example of self-organisation (Phillips, 1999), is not unique to the periglacial environment and does not occur only due to cold-climate processes (Goudie, 2004b). For example, patterned ground found in the tropics is the result of the swelling of clay particles; desiccation polygons occurs due to contraction of the ground following desiccation events; and, in dry regions patterns, such as the Namibian faery circles (Tschinkel, 2015), may result from vegetation banding of faunal influences (Goudie, 2004b). Characteristic features found in cold environments, such as angular clasts, are also found in hot environments, suggesting azonality of landforms and/or processes. Such features, therefore, don't necessarily indicate frost weathering and may instead be attributed to salt weathering, thermal stress, hydration, dilatation and fire-induced spalling (Boelhouwers *et al.*, 2002). Furthermore, mechanical weathering due to wetting and drying is active in cold regions (Hall, 2002) and frost-weathered debris does not necessarily have to have one specific form (Hall and Thorn, 2011). However, cold environments with sensitive threshold levels – required to effect change within the present geomorphic system – as those found in DML and sub-Antarctic, are more sensitive to small changes than those where threshold levels are higher (Barsch, 1993; Boelhouwers, 2003a; Boelhouwers *et al.*, 2003; Nel, 2012). Azonality of landforms is also implied by Bourke *at al.* (2007), who discuss tafoni and their occurrence across a range of climatic zones. For the current study, it is apparent that convergence of form, or equifinality, exits, with landform and -features common to all three. However, frost cycles, common in cold environments, are also known to occur in hot-desert environments (Sumner *et al.*, 2004b) and their presence for all three sites, as mentioned above, suggests an azonality of processes. As such, it is paramount that the azonal nature of processes acting over a long period of time (Meiklejohn and Hall, 1997; André, 2003; Boelhouwers, 2004), and non-linear weathering rates (Sumner *et al.*, 2009), are parameters considered when investigating frost cycles across the various study sites.

# CHAPTER 7: Conclusion and Recommendations for Future Studies

This chapter addresses limitations to the study, as well as recommendations and avenues of further research. Findings are summarised as well. A comprehensive list of references (pg. 317) concludes this document.

## 7.1 Limitations

Limitations are discussed in two separate subsections. Logging equipment failure commences below; limitations pertaining to the theoretical framework and application to this project are discussed in the next subsection (7.1.2 Theoretical application from pg. 312 onwards).

### 7.1.1 Logging equipment failure

iButton hygrochrons were the most unreliable logger used during the study with a high failure rate recorded (± 60% for hygochorns, ± 20% for thermochrons). While previous studies by *e.g.* Johnson *et al.* (2005) have shown these loggers to be watertight and durable, the high failure rate of this study confirms work by Wolaver and Sharp (2007), who reported an approximate 40% failure rate of iButtons. However, the study by Wolaver and Sharp (2007) was limited to eight thermochrons of which three failed after being submerged in water for seven weeks. The small sample size and the fact that loggers were submerged in water and not soil, a requirement for this study, led to iButtons being selected as a preferred logger. Nevertheless, high rainfall on Marion Island and the Elandsberg translated into a high failure rate for specifically hygrochrons, making these loggers ultimately unsuited to high-rainfall areas. Thermochrons fared better, although a high failure rate was also recorded evident. A period of use of 1-2 months is ideal to minimise iButton failure rates. Leaving these loggers in the field for longer periods inevitably leads to some of the deployed loggers failing.

XR5 loggers were the most reliable in terms of hardware and software specifics. However, due to the high visibility of these logging stations, issues around theft and animal interference were apparent. An XR5 on the Elandsberg was damaged by animals, with porcupines chewing through its protective Pelican casing, as well as cabling and thermistors. Furthermore, fallow deer used the pole that secured the radiation shield above the ground as a scratching pole, damaging the radiation shield and air temperature thermistor in the process. Finally, the National Aeronautics and Space Agency's (NASA) Soil Moisture Active Passive (SMAP) moisture product was not suitable for inclusion in the study due to the sensor failing in the latter part of 2015. Furthermore, the product is collected at large scales and, as such, not suited for inclusion in analyses. Nevertheless, ground moisture values determined in the study contribute to current knowledge on ground moisture in the three selected study areas.

### 7.1.2 Theoretical application

Geomorphological research may be applied through holistic approaches and open-system analyses require the acknowledgement of multiple processes and agents contributing towards landforms and -features. However, it is never truly possible to isolate and identify each contributing factor or agent. While this research has contributed to a greater understanding of frost environments in three disparate study regions, the outcomes of the research reflect an approximation of reality and not utmost reality. Furthermore, climatic geomorphology is applied as a framework. Limitations to this framework apply and are acknowledged. Furthermore, the application of climatic geomorphology has been critiqued and discussed. Furthermore, calculations of freeze-thaw cycles are estimated based on available data. Numbers should not be seen as exact, nor definitive, but rather as a guideline and indication of the frost environment. In other words, freeze-thaw cycle estimations indicate the presence or absence of such cycles within a region, allowing for inferences on landforms associated with such processes.

## 7.2 Considerations and Recommendations

While the purpose of the study was not to investigate agricultural production in cold or cold-marginal zones, results of the study may contribute toward agricultural management and practises in these areas. Investigtions in the High Drakensberg and Elandsberg of mainland South Africa showed that a better understanding of ground thermal regimes may assist farmers in better management of cropland and pastures.

Agricultural production is particularly sensitive to climate variability and climate change can potentially alter the current geographical lines of where freeze-thaw cycles occur. This can effectively open currently colder regions to agricultural production in the future, whereas currently productive areas could become less suitable in the future (Holz and Cooperative Research Centre for Antarctic Climate and Ecosystems (Australia), 2010; Hardcastle and Renwick, 2013). The current project has improved our understanding of freeze-thaw environments at the investigated locations and it is hoped that the results will be useful for predicting the shift of viable agricultural zones due to a changing climate. Furthermore, while vegetation cover should be considered when evaluating the presence of freeze-thaw cycles, as discussed in Chapter 1: Introduction (pg. 1 onwards), the dampening effect of plant cover on soil temperatures is also of interest to land management and farming activities (Hutchinson *et al.*, 2000; Smith, 2012). In colder climate zones, temperatures and accumulated heat values, which are externally driven and cannot be controlled, are crucial limiting factors on pasture growth rates characteristics (Hutchinson *et al.*, 2000). Plant and pasture growth is not only determined by air temperatures, but also by rainfall seasonality, solar radiation received, soil nutrients and fertiliser used, as well as plant ecotype and pests (Hutchinson *et al.*, 2000; Roche *et al.*, 2009; Li *et al.*, 2011; Smith, 2012). Hutchinson *et al.* (2000) note that growing degree days (GDD), which are linked to air temperature and expressed as accumulated heat, account for 75% of the variability of total pasture growth. However, annual variation of pasture growth rates cannot be explained by the parameters mentioned above alone (Smith, 2012). Soil temperatures should also be considered. Improved farming management practises require the use of data on climatic variables, as well as soil characteristics (Hutchinson *et al.*, 2000). This project has contributed towards understanding the soil temperature

regime for the High Drakensberg, as well as that of the Elandsberg and it is hoped that these results will allow farmers within these areas to improve their management practises. It is also suggested that a more detailed study, focusing on soil temperature regimes in the higher-intensity areas of the Elandsberg region, is initiated.

In addition to the above, it is suggested that a more robust approach for equifinality modelling is explored. Equifinality is a feature of natural and open models. This study has collected a wealth of data and determined significant parameters to the frost environment across various geographical settings. To fully acknowledge the non-linearity of processes and the non-stationarity of parameters across geographical space (Beven and Freer, 2001; Beven, 2006), it is suggested that data from this study are used within a Generalised Likelihood Uncertainty Estimation (GLUE) model using a uniform Monte Carlo simulation approach, as described by Beven and Binley (1992). This will allow for the expansion of the stochastic identification model to an equifinality one, while still considering hypothesis testing or Bayesian updating when mapping (Beven, 2006). These have been applied to a certain degree here, through objectives (4.1.1 Objective 1-4.1.5 Objective 5, pg. 72-77) largely achieved using statistical and geostatistical methods, as described in 4.5.2 Statistical Methods (pg. 99) and 4.5.3 Geographical Statistics and Modelling (pg. 108).

Finally, while the online resources for making this study's data available to a greater audience works well it is, nevertheless, recommended that the data are stored by the South African Environmental Observation Network (SAEON) and managed by their data custodians. This ensures reliable and accurate metadata capturing and storage of spatial data in an integrated, easily accessible and central database. It is also suggested that these data are made available as a standalone plug-in to the Quantarctica project, currently managed by the Norwegian Polar Institute, as well as being made available through the Global Terrestrial Network for Permafrost (GTN-P).

## 7.3 Conclusions and Final Remarks

This study has attempted to provide a new insight into frost-environment-derived landforms in three very different settings. It has furthered our understanding of frost environments in the Eastern Cape Drakensberg, an area requiring further study as argued by Boelhouwers and Meiklejohn (2002). Investigations have contributed to several national and international projects already active within the region and the research has improved our knowledge of and application of climatic zones in geomorphology. Furthermore, the investigation of frost environments, and how these relate to the regional landscape, has provided data for the interpretation of associated landforms, as well as improving our understanding of Southern Hemisphere frost cycles, active layer dynamics, and permafrost. Finally, the study has contributed to our understanding of how climate and local parameters impact landscape dynamics in these settings.

This study has shown that the greatest forcing on freeze-thaw cycles is air temperatures, yet other parameters of textural size and moisture availability have an ameliorating effect on these cycles. Snow cover decreases such cycles in the polar environment, while increasing the depth of these cycles in a mid-latitudinal setting. Sufficient organic content can make a material more susceptible to freeze-thaw cycles, whereas thick vegetation cover will lessen their impact. Nevertheless, external factors, such as the textural properties, organic content, vegetation cover, expected moisture (derived from annual precipitation), mean seasonal air temperatures, and mean annual air temperatures should be aggregated when delineating climatic zones. Because textural properties and organic content require *in situ* sampling such an approach could become cumbersome and increase the complexity of such delineation. Nevertheless, this will greatly improve climatic zonation with respect to the frost environment.

Climatic classification systems by, *e.g.* Köppen (1936) and Walter (1985), provide an elegant way to delineate zones and dominant processes. However, climatic zones are defined using annual temperature and moisture averages, and to a limited extent seasonal and monthly averages. Thonthwaite (1948), stressed the importance of multi-decision criteria analysis, as well as using natural break points within climatic data. Such an approach approximates the multiple controls evident in geomorphic systems, as argued by Phillips (2007). However, annual averages mask seasonal and diurnal dynamics, leading to the exclusion of processes acting at a shorter time scale from these broad climatic zones. Furthermore, most climatic classification systems are based on only a few parameters. While this is largely limited due to the lack of data, soil moisture, which is crucial in determining a frost-driven environment, is largely ignored. As such, while climatic classifications provide a useful framework for working at regional and global scale, such classifications are not suited to working at smaller geographic areas, nor when considering processes that are ephemeral or are only active for a short time span. While current climatic classifications do not exclude diurnal frost processes from their delineations, such processes are not addressed in detail. Since the global temperature is increasing and diurnal processes are generally sensitive to small fluctuations in temperature (*e.g.* Boelhouwesr, 2003a; Hedding, 2006), climatic systems are not suited to determine diurnal frost processes and their geographic distribution.

Climatic geomorphology makes use of a reductionist approach, applying the equilibrium worldview. However, the perfect landscape approach (Phillips, 2007) lends itself to this study in numerous ways. While global laws are applied, such as the thermodynamics of freezing and volumetric expansion of water, local (boundary) conditions exert a significant control on resultant landforms and processes. An example is the effect of vegetation. Thick vegetation cover depresses the effect of cyclical freezing and thawing, supressing evidence of these cycles. In contrast, temperatures of a few degrees colder can override the ameliorating effect of vegetation of freeze-thaw cycles. Equifinality is evaluated and shown to exist to a certain extent, *i.e.* in the ergodic and topological sense and a divergence of form applies. This is shown by the azonal nature of landforms. Landforms due to the frost environment are evaluated and the evidence shows that such landforms do occur across the investigated climatic zones. However, these are only present when the process can override local restrictive parameters, such as vegetation cover and unsuited textural sizes. In that sense, equifinality is present for different initiating conditions

and various scales, yet the process of freeze-thaw cycles remains the one attributed to the investigated landforms. Freeze-thaw cycles are azonal when placed within broadly delineated climatic zones. However, these processes become zonal when appropriate restrictive parameters (forcings) are considered in their mapping. Convergence of form exists in the sense that patterned ground is evident across Dronning Maud Land (DML) sites, irrespective of local conditions and assumed initial conditions. However, for example in the Elandsberg, evidence of freeze-thaw cycles is only present when vegetation cover is removed. It can, therefore, be argued that periglacial landforms only present when the thresholds of bounding conditions of site-specific characteristics are exceeded. Nevertheless, within the frost environments specific landforms are found, irrespective of the chaotic elements of each different setting. Self-organisation is present through evidence of patterned ground, suggesting equifinality at this level. The azonality of the freeze-thaw process and azonality of landforms speaks to the divergence of landforms argued by Phillips (1999, 2005). As such, climatic zonation and equifinality must be applied at appropriate scale levels to be relevant.

Azonality of processes is apparent. While the intensity, frequency and duration of frost processes are variable across climatic zones, their presence is ubiquitous. These diurnal controls are dominant in the warmer seasons of the permafrost environment; apparent throughout the year in the maritime climate of Marion Island; evident in the cold season of the temperate Drakensberg. Diurnal and seasonal frost processes are, therefore, azonal. Furthermore, landforms derived from such processes occur across climatic zones. As such, azonality with respect to the frost environment, measured at seasonal and diurnal scales, exists with reference to processes and landforms. It is suggested that delineating climatic zones is based on average minimum air temperatures, seasonal air temperatures, ground average temperatures and moisture values, as well as soil/sediment properties, and vegetation cover. This allows for a finetuning of zone delineation. Moisture is an integral component of the frost environment, with phase changes potentially yielding soil heave, as well ground subsidence. It is the phase change of ground moisture, driven by temperature dynamics, that yield periglacial features and excluding ground moisture from climatic zonations leads to the exclusion, or incorrect delineation, of this environment within current climatic classification systems. The project has shown that local characteristics and dynamics are ignored when zones are defined using macro-scale processes, as argued Graham and Midgley (2000). Furthermore, the project results agree with Mensching (1984), who argues that over-simplification of zones and processes leads to the exclusion of significant processes.

# References


Adlam, L.S., Balks, M.R., Seybold, C.A., Campbell, D.I., 2009. *Temporal and spatial variation in active layer depth in the McMurdo Sound Region,* Antarctica. Antarctic Science 22, 45–52.

Alsharhan, A.S., El-Sammak, A.A., 2004. Grain-size analysis and characterization of sedimentary environments of the United Arab Emirates coastal area. *Journal of Coastal Research* 202, 464–477.

Andersen, K.J., Krysell, M., 2005. *Dry matter (DM), loss on ignition (LOI) and total organic carbon (TOC).* ECN (Energy Research Centre of the Netherlands), Petten, Netherlands.

André, M.-F., 2003. Do periglacial landscapes evolve under periglacial conditions? *Geomorphology* 52, 149–164.

André, M-F., Hall, K., Bertran, P., Arocena, J. 2008. Stone runs in the Falklands: Periglacial or tropical? *Geomorphology,* 95, 524-543.

Ashcroft, M.B., Gollan, J.R., 2012. Fine-resolution (25 m) topoclimatic grids of near-surface (5 cm) extreme temperatures and humidities across various habitats in a large (200 × 300 km) and diverse region. *International Journal of Climatology* 32, 2134 – 2148.

Atkinson, P.M., 1999. Geographical information science: geostatistics and uncertainty. *Progress in Physical Geography* 23, 134–142.

Atkinson, P.M., 2001. Geographical information science: GeoComputation and nonstationarity. *Progress in Physical Geography* 25, 111–122.

Atkinson, P.M., German, S.E., Sear, D.A., Clark, M.J., 2003. Exploring the relations between riverbank erosion and geomorphological controls using geographically weighted logistic regression. *Geographical Analysis* 35, 58–82.

Australian Antarctic Data Centre, 2016. *SCAR Composite Gazetteer* [WWW Document]. URL https://data.aad.gov.au/aadc/gaz/scar/ (accessed 9.7.16).

Ballantyne, C.K., Harris, C., 1994. *The Periglatiation of Great Britain*. Cambridge University Press, Cambridge.

Ballantyne, C.K., Matthews, J.A., 1982. The development of sorted circles on recently deglaciated terrain, Jotunheimen, Norway. *Arctic and Alpine Research* 14, 341–354.

Ballantyne, C.K., Matthews, J.A., 1983. Desiccation cracking and sorted polygon development, Jotunheimen, Norway. *Arctic and Alpine Research* 15, 339–349.

Bargagli, R., 2005. *Antarctic Ecosystems: Environmental Contamination, Climate Change, And Human Impact*. Springer.

Barsch, D., 1993. Periglacial geomorphology in the 21st century. *Geomorphology* 7, 141–163.

Barton, J.M., Klemd, R., Allsopp, H.L., Auret, S.H., Copperthwaite, Y.E., 1987. The geology and geochronology of the Annandagstoppane granite, Western Dronning Maud Land, Antarctica. *Contributions to Mineralogy and Petrology* 97, 488–496.

Bate, G.C., Smith, V.R., 1983. Photosynthesis and respiration in the sub-Antarctic tussock gras *Poa cookii*. *New Phytologist* 95, 533–543.

Bauer, W., 2009. Permian sedimentary cover, Heimefrontfjella, western Dronning Maud Land (East Antarctica). *Polarforschung* 79, 39–42.

Ben-Dor, E., Banin, A., 1989. Determination of organic matter content in arid zone soils using a simple "loss-on-ignition" method. *Communiucations in Soil Science and Plant Analysis* 20, 1675–1695.

Beven, K., 1996. Equifinality and uncertainty in geomorphological modelling, *in*: Rhoads, B.L., Thorn, C.E. (Eds.), *The Scientific Nature of Geomorphology*: *Proceedings of the 27th Binghamton Symposium in Geomorphology, 27-29 September, 199*6. Wiley, Chichester; New York, p. 289.

Beven, K., 2000. Uniqueness of place and the representation of hydrological processes. *Hydrology and Earth System Sciences* 4, 203–213.

Beven, K., 2006. A manifesto for the equifinality thesis. *Journal of Hydrology* 320, 18–36.

Beven, K., Binley, A., 1992. The future of distributed models: Model calibration and uncertainty prediction. *Hydrological Processes* 6, 279–298.

Beven, K., Freer, J., 2001. Equifinality, data assimilation, and uncertainty estimation in mechanistic modelling of complex environmental systems using the GLUE methodology. *Journal of Hydrology* 249, 11–29.

Bierman, S., 2014. *Synoptic circulation patterns and its relationship with ground thermal characteristics along an altitudinal transect on sub-Antarctic Marion Island* (MSc). Fort Hare, East London, South Africa.

Birnie, R.V., Thom, G., 1982. Preliminary observations on two rock glaciers in South Georgia, Falkland Islands Dependencies. *Journal of Glaciology* 28, 377–386.

Black, C.A., 1965. *Methods of Soil Analysis: Part I Physical and Mineralogical Properties*. American Society of Agronomy, Madison, Wisconsin, USA.

Blake, B.J., 1996. *Microclimate and prediction of photosynthesis at Marion Island* (MSc). University of the Free State, Bloemfontein, South Africa.

Bliss, A., Hock, R., Cogley, J.G., 2013. A new inventory of mountain glaciers and ice caps for the Antarctic periphery. *Annals of Glaciology* 54, 191–199.

Blott, S.J., Croft, D.J., Pye, K., Saye, S.E., Wilson, H.E., 2004. Particle size analysis by laser diffraction. *Geological Society, London, Special Publications* 232, 63–73.

Blott, S.J., Pye, K., 2001. GRADISTAT: a grain size distribution and statistics package for the analysis of unconsolidated sediments. *Earth Surface Processes and Landforms* 26, 1237–1248.

Bockheim, J.G., 1995. Permafrost distribution in the southern circumpolar region and its relation to the environment: A review and recommendations for further research. *Permafrost and Periglacial Processes* 6, 27–45.

Bockheim, J.G., Hall, K.J., 2002. Permafrost, active-layer dynamics and periglacial environments of continental Antarctica: Periglacial and permafrost research in the Southern Hemisphere. *South African Journal of Science* 98, 82–90.

Boelhouwers, J.C., 1991a. Periglacial evidence from the western Cape Mountains, South Africa: A progress report. *Permafrost and Periglacial Processes* 2, 13–20.

Boelhouwers, J.C., 1991b. Present-day periglacial activity in the Natal Drakensberg, Southern Africa: A short review. *Permafrost and Periglacial Processes* 2, 5–12.

Boelhouwers, J.C., 1994. Periglacial landforms at Giant's Castle, Natal Drakensberg, South Africa. *Permafrost and Periglacial Processes* 5, 129–136.

Boelhouwers, J.C., 1995. Present day soil frost activity at the Hex River Mountains, Western Cape, South Africa. *Zeitschrift für Geomorphologie* 39, 237–248.

Boelhouwers, J.C., 2003a. Sensitivity and responses to climate change in the Subantarctic periglacial environment, in*:* Phillips, M., Springman, S.M., Arenson, L.U. (Eds.), *Permafrost: Proceedings of the 8th International Conference on Permafrost, Zurich, Switzerland, 21-25 July 2003*. A.A. Balkema Publishers, Lisse [Netherlands]; Exton, PA.

Boelhouwers, J.C., 2003b. Quaternary slope development in the Lesotho highlands: review and alternative model: research in action. *South African Journal of Science* 99, 44–46.

Boelhouwers, J.C., 2004. New perspectives on autochthonous blockfield development. *Polar Geography* 28, 133–146.

Boelhouwers, J.C., 2007. *Plot- and slope-scale topographic and vegetation control on ground temperature spatial variability: synoptic-scale observations from Marion Island*. Presented at the South African National Antarctic Programme, P.I., Post-doc and Student Symposium, October 2007, Centre for Invasion Biology, Stellenbosch.

Boelhouwers, J.C., Holness, S.D., Meiklejohn, K.I., Sumner, P.D., 2002. Observations on a blockstream in the vicinity of Sani Pass, Lesotho highlands, Southern Africa. *Permafrost and Periglacial Processes* 13, 251–257.

Boelhouwers, J.C., Holness, S.D., Sumner, P.D., 2000. Geomorphological characteristics of small debris flows on Junior's Kop, Marion Island, maritime sub - Antarctic. *Earth Surface Processes and Landforms* 25, 341–352.

Boelhouwers, J.C., Holness, S.D., Sumner, P.D., 2003. The maritime Subantarctic: a distinct periglacial environment. *Geomorphology* 52, 39–55.

Boelhouwers, J.C., Holness, S.D., Sumner, P.D., Nel, W., 2001. *Cryogenic Landforms and Processes on Marion Island* (Final Report submitted to the South African Committee for Antarctic Research (SACAR), April 1996 – March 2001). South African Committee for Antarctic Research (SACAR), Pretoria, South Africa.

Boelhouwers, J.C., Meiklejohn, K.I., 2002. Quaternary periglacial and glacial geomorphology of southern Africa: review and synthesis. *South African Journal of Science* 98, 47–54.

Boelhouwers, J.C., Meiklejohn, K.I., Holness, S.D., Hedding, D.W., 2008. Geology, geomorphology and climate change, *in*: Chown, S.L., Froneman, P.W. (Eds.), *The Prince Edward Islands: Land-Sea Interactions in a Changing Ecosystem*. SUN MeDIA, Stellenbosch, pp. 65–96.

Borg, C.-J., 2012. *Mechanisms controlling valley assymmetry development at Abisko, northern Sweden and Sani Pass, southern Africa* (MSc). Uppsala Universitet, Uppsala, Sweden.

Borg, C.-J., 2017. *Identifying growth criteria and sediment movement mechanisms of needle ice using high-frequency environmental and visual monitoring* (PhD). Rhodes University, Grahamstown, South Africa.

Bourke, M.C., Brearley, J.A., Haas, R., Viles, H.A., 2007. *A Photographic Atlas of Rock Breakdown Features in Geomorphic Environments*. Planetary Science Institute, Tucson, Arizona.

Brady, N.C., Weil, R.R., 2016. The Nature and Properties of Soils, 15th ed. Pearson, Columbus.

Bremer, H., 2004. Morphogenetic region, *in*: Goudie, A.S. (Ed.), *Encyclopedia of Geomorphology*. Routledge, London; Madison Avenue, N.Y., pp. 694–696.

Briggs, D.J., 1977a. *Soils, Sources and Methods in Geography*. Butterworths, London ; Boston.

Briggs, D.J., 1977b. *Sediments, Sources and Methods in Geography*. Butterworths, London; Boston.

British Antarctic Survey, 2016. *SCAR Antarctic Digital Database* [WWW Document]. URL http://www.add.scar.org/home/add7 (accessed 4.20.16).

Brunsdon, C., Fotheringham, S., Charlton, M., 1998. Geographically weighted regression-modelling spatial non-stationarity. *Journal of the Royal Statistical Society, Series D (The Statistician)* 47, 431–443.

Büdel, J., 1951. Die Klimazonen des Eiszeitalters. *Eiszeitalter und Gegenwart* 1, 16–26.

Büdel, J., 1953. Die "periglazial"-morphologischen Wirkungen des Eiszeitklimas auf der ganzen Erde: (Beiträge zur Geomorphologie der Klimazonen und Vorzeitklimate IX.) (The Morphological Effects of Climates outside the Glaciated Areas during the Ice Age). *Erdkunde* 7, 249–266.

Burn, C.R., 1998. The active layer: two contrasting definitions. *Permafrost and Periglacial Processes* 9, 411–416.

Burrough, P.A., 2001. GIS and geostatistics: Essential partners for spatial analysis. *Environmental and Ecological Statistics* 8, 361–377.

Campbell, I.B., Claridge, G.G.C., Campbell, D.I., Balks, M.R., 1998. Permafrost properties of the McMurdo Sound-Dry Valley Region of Antarctica, *in*: Lewkowicz, A.G., Allard, M. (Eds.), *Permafrost: Proceedings of the 7th International Conference on Permafrost, Yellowknife, Canada, 23 - 27 June 1998.* Collection Nordicana, Centre d'études nordiques, Université Laval, Québec, Yellowknife, Canada, pp. 121–126.

Carbutt, C., Edwards, T.J., 2003. The flora of the Drakensberg alpine centre. *Edinburgh Journal of Botany* 60, 581–607.

Chamberlin, T.C., 1987. The method of multiple working hypotheses. *The Journal of Geology* 5, 837–848.

Chang, K.-T., 2012. *Introduction to Geographic Information Systems*, 6th ed. McGraw-Hill, New York.

Charlton, M., Fotheringham, S., Brunsdon, C., 2006. NCRM Methods Review Papers, NCRM/006. *Geographically Weighted Regression (Review Paper*). ESRC (Economic and Social Research Council), Ireland.

Chorley, R.J., Kennedy, B.A., 1971. *Physical Geography: A Systems Approach*. Prentice-Hall International, London.

Chown, S.L., Froneman, P.W., 2008. *The Prince Edward Islands: Land-Sea Interactions in a Changing Ecosystem.* SUN MeDIA.

Chown, S.L., Lee, J.E., Shaw, J.D., 2008. Conservation of Southern Ocean islands: Invertebrates as exemplars. *Journal of Insect Conservation* 12, 277–291.

Chown, S.L., le Roux, P.C., Ramaswiela, T., Kalwij, J.M., Shaw, J.D., McGeoch, M.A., 2012. Climate change and elevational diversity capacity: do weedy species take up the slack? *Biology Letters* 9, 20120806–20120806.

Chown, S.L., Smith, V.R., 1993. Climate change and the short-term impact of feral house mice at the sub-Antarctic Prince Edward Islands. *Oecologia* 96, 508–516.

Christiansen, H.H., 2013. *Global Terrestrial Network on Permafrost (GTN-P): Strategy and Implementation Plans 2012-2016*, *in*: Session 15. Presented at the GCOS/WCRP Terrestrial Observation Panel for Climate, Geneva, Switzerland.

Church, M., 2010. The trajectory of geomorphology. *Progress in Physical Geography* 34, 265–286.

Clark, G.M., Hedges, J., 1992. *Origin of certain high-elevation local broad uplands in the Central Appalachians south of the glacial border, U.S.A. - a paleoperiglacial hypothesis*, *in*: Dixon, J.C., Abrahams, A.D. (Eds.), *Periglacial Geomorphology: Proceedings of the 22nd Binghamton Symposium in Geomorphology*. Wiley, Chichester; New York, pp. 31–61.

Cohen, J., Stewart, I., 1994. *The Collapse of Chaos: Discovering Simplicity in a Complex World*. Viking, New York.

Condy, P.R., Van Aarde, R.J., Bester, M.N., 1978. The seasonal occurrence and behaviour of killer whales Orcinus orca, at Marion Island. *Journal of Zoology* 184, 449–464.

Conradie, E.C., Smith, V.R., 2012. Spatial variation in soil chemistry on a sub-Antarctic island. *Open Journal of Soil Science* 02, 111–115.

Cooke, R.U., Reeves, R.W., 1976. Arroyos and environmental change in the American South-West, *Oxford Research Studies in Geography*. Clarendon Press, Oxford.

Corte, A.E., 1966. Particle sorting by repeated freezing and thawing. *Biutetyn Peryglacjany* 51, 175–240.

Cramp, A., Lee, S.V., Herniman, J., Hiscott, R.N., Manley, P.L., Piper, D.J.W., Deptuck, M., Johnston, S.K., Black, K.S., 1997. Interlaboratory comparison of sediment grain-sizing techniques: data from Amazon fan upper levee complex sediment, *in*: Flood, R.D., Piper, D.J.W., Klaus, A., Peterson, L.C. (Eds.), *Proceedings of the Ocean Drilling Program, 155 Scientific Results*. Ocean Drilling Program, pp. 217–228.

Crawford, R.J.M., Cooper, J., Dyer, B.M., Greyling, M.D., Klages, N.T.W., Ryan, P.G., Petersen, S.L., Underhill, L.G., Upfold, L., Wilkinson, W., de Villiers, M.S., du Plessis, S., du Toit, M., Leshoro, T.M., Makhado, A.B., Mason, M.S., Merkle, D., Tshingana, D., Ward, V.L., Whittington, P.A., 2003. Populations of surface-nesting seabirds at Marion Island, 1994/95–2002/03. *African Journal of Marine Science* 25, 427–440.

Crawford, R.J.M., Dyer, B.M., Cooper, J., Underhill, L.G., Unit, A.D., 2006. Breeding numbers and success of Eudyptes penguins at Marion Island, and the influence of mass and time of arrival of adults. *CCAMLR Science* 13, 175–190.

Crawford, R., Makhado, A., Upfold, L., Dyer, B., 2008. Mass on arrival of rockhopper penguins at Marion Island correlated with breeding success. *African Journal of Marine Science* 30, 185–188.

Culling, W.E.H., 1987. Equifinality: Modern approaches to dynamical systems and their potential for geographical thought. *Transactions of the Institute of British Geographers* 12, 57–72.

Culling, W.E.H., 1957. Multicyle streams and the equilibrium theory of grade. *Journal of Geology* 65, 259–274.

Dallmann, W.K., Norwegian Polar Institute, Norwegian Antarctic Research Expedition, 1990. *Geology Around the Norwegian Antarctic Station "Troll", Jutulsessen, Dronning Maud Land*. Norsk Polarinstitutt, Oslo.

Dartnall, H.J.G., Smith, V.R., 2012. Freshwater Invertebrates of Sub-Antarctic Marion Island. *African Zoology* 47, 203–215.

Davies, B.E., 1974. Loss-on-ignition as an estimate of soil organic matter. *Soil Science Society of America, Proceedings* 38, 150–151.

de Villiers, A.F., 1976. Littoral ecology of Marion and Prince Edward Islands (Southern Ocean). *South African Journal of Antarctic Research Supplement 1*, 1–40.

de Villiers, S., 2000. *The development of a spatial database for research into cryogenic processes and landforms in southern Africa* (MA). University of Pretoria, Pretoria, South Africa.

Diop, S., Stapelberg, F., Tegegn, K., Ngubelanga, S., Heath, L., 2011. *A review on problems soils in South Africa* (No. 2011-0062). Council for Geoscience, Western Cape, South Africa.

Doornkamp, J.C., King, C.A.M., 1971. *Numerical Analysis in Geomorphology: An Introduction*. Hodder & Stoughton Education, London.

Easterbrook, D.J., 1999. *Surface Processes and Landforms*, 2nd ed. Prentice-Hall International, New Jersey.

Elvevold, S., Ohta, Y. (Eds.), 2010. *Nature Environment Map H.U. Sverdrupfjella: Dronning Maud Land, East Antarctica 1:150 000, Temakart*. Norwegian Polar Institute, Tromsø.

Ericson, K., 2004. Geomorphological surfaces of different age and origin in granite landscapes: an evaluation of the Schmidt hammer test. *Earth Surface Processes and Landforms* 29, 495–509.

Essenwanger, O.M., 2001. *General climatology 1C: Classification of Climates*. Elsevier, Amsterdam.

Fahey, B.D., 1973. An analysis of diurnal freeze-thaw and frost heave cycles in the Indian Peake Region of the Colorado Front Range. *Arctic and Alpine Research* 269–281.

Fey, M.V., 2010. Soils of South Africa. Cambridge University Press, Cambridge ; New York.

Field, C.V., Schmidt, G.A., Koch, D., Salyk, C., 2006. Modeling production and climate-related impacts on 10Be concentration in ice cores. *Journal of Geophysical Research* 111.

Fitchett, J.M., Grab, S.W., Bamford, M.K., Mackay, A.W., 2016. A multi-disciplinary review of late Quaternary palaeoclimates and environments for Lesotho. *South African Journal of Science* 112, 1–9.

French, H.M., 2000. Does Lozinski's periglacial realm exist today? A discussion relevant to modern usage of the term "periglacial." *Permafrost and Periglacial Processes* 11, 35–42.

French, H.M., 1996. *The Periglacial Environment*, 2nd ed. Addison Wesley Longman Ltd., Harlow.

French, H.M., Demitroff, M., 2001. Cold-climate origin of the enclosed depressions and wetlands ("spungs") of the Pine Barrens, southern New Jersey, USA. *Permafrost and Periglacial Processes* 12, 337–350.

Gabriel, A.G.A., Chown, S.L., Barendse, J., Marshall, D.J., Mercer, R.D., Pugh, P.J.A., Smith, V.R., 2001. Biological invasions of Southern Ocean islands: the Collembola of Marion Island as a test of generalities. *Ecography* 24, 421–430.

Galvin, J.F.P., 2008. The weather and climate of the tropics: Part 6 – Monsoons. *Weather* 63, 129–137.

Gerrard, A.J., 1984. Multiple working hypotheses and equifinality in geomorphology: Comments on the recent article by Haines-Young and Petch. *Transactions of the Institute of British Geographers* 9, 364–366.

Golynsky, A.V., Grikurov, G.E., Kamene, E.N., 1997. Geological significance of regional magnetic anomalies in Coats Land and Western Dronning Maud Land. *Polarforschung* 67, 91–99.

Goudie, A.S. (Ed.), 2004a. *Encyclopedia of Geomorphology: Volume 1*. Routledge : International Association of Geomorphologists, London ; New York.

Goudie, A.S. (Ed.), 2004b. *Encyclopedia of Geomorphology: Volume 2*. Routledge : International Association of Geomorphologists, London ; New York.

Goudie, A.S., 2004c. Climatic geomorphology, *in*: Goudie, A.S. (Ed.), *Encyclopedia of Geomorphology*. Routledge, London; Madison Avenue, N.Y., pp. 162–164.

Grab, S.W., 1994. Thúfur in the Mohlesi Valley, Lesotho, Southern Africa. *Permafrost and Periglacial Processes* 5, 111–118.
Grab, S.W., 1997a. Annually re-forming miniature sorted patterned ground in the High Drakensberg, Southern Africa. *Earth Surface Processes and Landforms* 22, 733–745.
Grab, S.W., 1997b. *An evaluation of the periglacial geomorphology in the High Drakensberg and associated environmental implications*. University of Natal, Pietermaritzburg, South Africa.
Grab, S.W., 1997c. Thermal regime for a thufa apex and its adjoining depression, Mashai Valley, Lesotho. *Permafrost and Periglacial Processes* 8, 437–445.
Grab, S.W., 1998. Non-sorted patterned ground in the High Drakensberg, Southern Africa: Some New Data. *The Geographical Journal* 164, 19–31.
Grab, S.W., 1999. Block and debris deposits in the High Drakensberg, Lesotho, Southern Africa: Implications for high altitude slope processes. *Geografiska Annaler: Series A, Physical Geography* 81, 1–16.
Grab, S.W., 2000. Stone-banked lobes and environmental implications, High Drakensberg, Southern Africa. *Permafrost and Periglacial Processes* 11, 177–187.
Grab, S.W., 2001. Needle ice observations from the High Drakensberg, Lesotho. *Permafrost and Periglacial Processes* 12, 227–231.
Grab, S.W., 2002a. Turf exfoliation in the High Drakensberg, Southern Africa. *Geografiska Annaler: Series A, Physical Geography* 84, 39–50.
Grab, S.W., 2002b. Characteristics and palaeoenvironmental significance of relict sorted patterned ground, Drakensberg plateau, southern Africa. *Quaternary Science Reviews* 21, 1729–1744.
Grab, S.W., 2005. Earth hummocks (thúfur): new insights to their thermal characteristics and development in eastern Lesotho, southern Africa. *Earth Surface Processes and Landforms* 30, 541–555.
Grab, S.W., Mills, S.C., Carr, S.J., 2012. Periglacial and glacial geomorphology, *in*: Holmes, P., Meadows, M. (Eds.), *Southern African Geomorphology: Recent Trends and New Directions.* SUN MeDIA, Bloemfontein, pp. 233–267.
Graham, D.J., Midgley, N.G., 2000. Graphical representation of particle shape using triangular diagrams: an Excel spreadsheet method. *Earth Surface Processes and Landforms* 25, 1473–1477.
Grantham, G.H., Jackson, C., Moyes, A.B., Groenewald, P.B., Harris, P.D., Ferrar, G., Krynauw, J.R., 1995. The tectonothermal evolution of the Kirwanveggen-H.U. Sverdrupfjella areas, Dronning Maud Land, Antarctica. *Precambrian Research* 75, 209–229.
Gray, A.B., Pasternack, G.B., Watson, E.B., 2010. Hydrogen peroxide treatment effects on the particle size distribution of alluvial and marsh sediments. *The Holocene* 20, 293–301.
Gremmen, N.J.M. (Ed.), 1981. *The Vegetation of the Subantarctic Islands Marion and Prince Edward*. Springer.
Gremmen, N.J.M., Chown, S.L., Marshall, D.J., 1998. Impact of the introduced grass Agrostis stolonifera on vegetation and soil fauna communities at Marion Island, sub-Antarctic. *Biological Conservation* 85, 223–231.
Gremmen, N.J.M., Smith, V.R., 1999. New records of alien vascular plants from Marion and Prince Edward Islands, sub-Antarctic. *Polar Biology* 21, 401–409.
Gremmen, N.J.M., Smith, V.R., van Tongeren, O.F.R., 2003. Impact of trampling on the vegetation of subantarctic Marion Island. Arctic, *Antarctic, and Alpine Research* 35, 442–446.
Griffith, D.A., 2005. Spatial Autocorrelation, *in*: Kempf-Leonard, K. (Ed.*), Encyclopedia of Social Measurement*. Elsevier/Academic Press, San Diego, California, pp. 581–590.
Grobler, D.C., Toerien, D.F., Smith, V.R., 1987. Bacterial activity in soils of a sub-Antarctic island. *Soil Biology and Biochemistry 19*, 485–490.
Groenewald, P.B., Moyes, A.B., Grantham, G.H., Krynauw, J.R., 1995. East Antarctic crustal evolution: geological constraints and modelling in western Dronning Maud Land. *Precambrian Research* 75, 231–250.

Grosch, E.G., Bisnath, A., Frimmel, H.E., Board, W.S., 2007. Geochemistry and tectonic setting of mafic rocks in western Dronning Maud Land, East Antarctica: implications for the geodynamic evolution of the Proterozoic Maud Belt. *Journal of the Geological Society* 164, 465–475.

Guetter, P.J., Kutzbach, J.E., 1990. A modified Köppen classification applied to model simulations of glacial and interglacial climates. *Climatic Change* 16, 193–215.

Guglielmin, M., 2012. Advances in permafrost and periglacial research in Antarctica: A review. *Geomorphology* 155-156, 1–6.

Gyamfi, C., Ndambuki, J.M., Salim, R.W., 2016. Spatial variability modeling of soil erodibility index in relation to some soil properties at field scale. *Environment and Natural Resources Research* 6, 16.

Hagen, J.O., 1997. Blue ice field studies in the Jutulsessen and Troll areas, *in*: Orheim, O. (Ed.), *Report of the Norwegian Antarctic Research Expedition 1992/93*, Meddelelser / Norsk Polarinstitutt. Norsk Polarinstitutt, Oslo, pp. 82–84.

Haines-Young, R.H., Petch, J.R., 1983. Multiple working hypotheses: Equifinality and the study of landforms. *Transactions of the Institute of British Geographers* 8, 458–466.

Hall, B.L., 2009. Holocene glacial history of Antarctica and the sub-Antarctic islands. *Quaternary Science Reviews* 28, 2213–2230.

Hall, K.J., 1977. Some observations on the former sea levels of Marion Island. *South African Journal of Antarctic Research* 7, 19–22.

Hall, K.J., 1979. Sorted stripes orientated by wind action: Some observations from sub-Antarctic Marion Island. *Earth Surface Processes and Landforms* 4, 281–289.

Hall, K.J., 1981. Observations on stone-banked lobes of Marion Island. *South African Journal of Science* 77, 129–131.

Hall, K.J., 1982. Rapid deglaciation as an initiator of volcanic activity: An hypothesis. *Earth Surface Processes and Landforms* 7, 45–51.

Hall, K.J., 1990. Quaternary glaciations in the Southern Ocean: Sector 0° Long to 180° Long, *in:* Clapperton (Ed.), *Quaternary Science Review,* 9, 217-228.

Hall, K.J., 1997. Zoological erosion in permafrost environments: A possible origin of dells? *Polar Geography* 21, 1–9.

Hall, K., 1998a. Nivation or cryoplanation: Different terms, same features? *Polar Geography* 22, 1–16.

Hall, K.J., 1998b. Rock temperatures and implications for cold region weathering: II. New data Rothera, Adelaide Island (Antarctica). *Permafrost and Periglacial Processes,* 9, 47-55.

Hall K.J., 2013. Mechanical Weathering in Cold Regions. *in:* Shrader, J.F. (Ed.) *Treatise on Geomorphology*. Elsevier, San Diego: Academic Press. pp. 258-276.

Hall, K., 2010. The shape of glacial valleys and implications for southern African glaciation. *South African Geographical Journal* 92, 35–44.

Hall, K.J., 2002. Review of Present and Quaternary periglacial processes and landforms of the maritime and sub-Antarctic region. *South African Journal of Science* 98, 71–81.

Hall, K., Boelhouwers, J., Driscoll, K., 1999. Animals as erosion agents in the alpine zone: Some data and observations from Canada, Lesotho, and Tibet. *Arctic, Antarctic, and Alpine Research* 31, 436.

Hall, K.J., Arocena, J.M., Boelhouwers, J.C., Liping, Z., 2005. The influence of aspect on the biological weathering of granites: observations from the Kunlun Mountains, China. *Geomorphology* 67, 171–188.

Hall, K.J., Meiklejohn, K.I., 2011. Glaciation in southern Africa and in the sub-Antarctic, *in*: Horne, D.J., Holmes, J.A., Rodrigues-Lazaro, J. (Eds.), *Developments in Quaternary Sciences*. Elsevier, pp. 1081–1085.

Hall, K.J., Meiklejohn, K.I., Bumby, A., 2011. Marion Island volcanism and glaciation. *Antarctic Science* 23, 155–163.

Hall, K.J., Thorn, C.E., Matsuoka, N., Prick, A., 2002. Weathering in cold regions: some thoughts and perspectives. *Progress in Physical Geography* 26, 577–603.

Hall, K., Thorn, C., 2011. The historical legacy of spatial scales in freeze-thaw weathering: Misrepresentation and resulting misdirection. *Geomorphology* 130, 83–90.

Hall, K. and Walton, D.W.H. 1992. Rock weathering, soil development and colonisation under a changing climate. *Philosophical Transactions of the Royal Society,* B, 338, 269-277.

Hallet, B., 1990. Spatial self-organization in geomorphology: from periodic bedforms and patterned ground to scale-invariant topography. *Earth-Science Reviews* 29, 57–75.

Hansen, C.D., 2014. *The characterisation of an openwork block deposit, Northern Buttress, Vesleskarvet, Dronning Maud Land, Antarctica* (MSc). Rhodes University, Grahamstown, South Africa.

Hansen, C.D., Meiklejohn, K.I., Dwight, R.A., Scott, D.A., Rudolph, E.M., 2014. An investigation into morphology and dynamics of thermal contraction crack polygons found at Mimelia in the Jutulsessen, Antarctica, *in*: An*tarctic Permafrost, Periglacial, Snow, Firn and Ice-Free Environment*. Presented at the XXXIII Scientific Committee on Antarctic Research Open Science Conference (SCAR OSC).

Hansen, C.D., Loubser, M.J., Rudolph, E.M., 2016a. Observations on frost mounds in the Jutulsessen, Antarctica, *in: Antarctic Permafrost, Periglacial Processes and Soil Development*. Presented at the XXXIV Scientific Committee on Antarctic Research Open Science Conference (SCAR OSC), Kuala Lumpur, Malaysia.

Hansen, C.D., Meiklejohn, K.I., Nel, W., 2016b. The ground thermal regime of Troll, in the Jutulsessen of Antarctica: 2007-2016, *in*: *Antarctic Permafrost, Soils and Periglacial Environments* (co-Organized by SCAR). Presented at the 11th International Conference on Permafrost (ICOP), Potsdam, Germany.

Hansen, C.D., Meiklejohn, K.I., Nel, W., Loubser, M.J., Van Der Merwe, B.J., 2013. Aspect-controlled weathering observed on a blockfield in Dronning Maud Land, Antarctica. *Geografiska Annaler: Series A, Physical Geography* 95, 305–313.

Hansen, G., Aspmo, K., Berg, T., Edvardsen, Kã¥., Fiebig, M., Kallenborn, R., Krognes, T., Lunder, C., Stebel, K., Schmidbauer, N., Solberg, S., Yttri, K.E., 2009. Atmospheric monitoring at the Norwegian Antarctic station Troll: measurement programme and first results*. Polar Research* 28, 353–363.

Hanvey, P.M., Marker, M.E., 1992. Present-day periglacial microforms in the Lesotho Highlands: Implications for present and past climatic conditions. *Permafrost and Periglacial Processes* 3, 353–361.

Hardcastle, L., Renwick, J., 2013. *Impacts of climate change on key primary industries on the Kāpiti Coast*. Kāpiti Coast District Council, Paraparaumu, New Zealand.

Harris, S.A., 1981. Climatic relationships of permafrost zones in areas of low winter snow-cover. *Arctic* 34, 64–70.

Haussmann, N.S., Aldahan, A., Boelhouwers, J.C., Possnert, G., 2010a. 10Be application to soil development on Marion Island, southern Indian Ocean. *Nuclear Instruments and Methods in Physics Research Section B: Beam Interactions with Materials and Atoms* 268, 1058–1061.

Haussmann, N.S., Boelhouwers, J.C., McGeoch, M.A., 2009a. Fine scale variability in soil frost dynamics surrounding cushions of the dominant vascular plant species (Azorella selago) on sub-Antarctic Marion Island. G*eografiska Annaler: Series A, Physical Geography* 91, 257–268.

Haussmann, N.S., McGeoch, M.A., Boelhouwers, J.C., 2009b. Interactions between a cushion plant (Azorella selago) and surface sediment transport on sub-Antarctic Marion Island. *Geomorphology* 107, 139–148.

Haussmann, N.S., McGeoch, M.A., Boelhouwers, J.C., 2010b. Contrasting nurse plants and nurse rocks: The spatial distribution of seedlings of two sub-Antarctic species. *Acta Oecologica* 36, 299–305.

Hedding, D.W., 2006. *Geomorphology and geomorphological responses to climate change in the interior of sub-Antarctic Marion Island* (MSc). University of Pretoria, Pretoria, South Africa.

Hedding, D.W., 2008. Spatial inventory of landforms in the recently exposed central highland of sub-Antarctic Marion Island. *South African Geographical Journal* 90, 11–21.

Hedding, D.W., 2014. *On the identification, genesis and paleoenvironmental significance of pronival ramparts* (PhD). University of Pretoria, Pretoria, South Africa.

Hedding, D.W., Meiklejohn, K.I., Le Roux, J.J., Loubser, M.J., Davis, J.K., 2010. Some observations on the formation of an active pronival rampart at Grunehogna Peaks, Western Dronning Maud Land, Antarctica. *Permafrost and Periglacial Processes* 21, 355–361.

Hedding, D.W., Sumner, P.D., Holness, S.D., Meiklejohn, K.I., 2007. Formation of a pronival rampart on sub-Antarctic Marion Island. *Antarctic Science* 19.

Hefferan, K., O'Brien, J., 2010. *Earth Materials*. Wiley-Blackwell, Chichester, West Sussex, UK; Hoboken, NJ.

Hjort, J., Luoto, M., 2009. Interaction of geomorphic and ecologic features across altitudinal zones in a subarctic landscape. *Geomorphology* 112, 324–333.

Hodgson, D.A., Graham, A.G.C., Roberts, S.J., Bentley, M.J., Cofaigh, C. 6.,Verleyen, E., Jomelli, V., Favier, V.M., Brunstein, D., Calhoun, E.A., Saunders, K., Macintosh, A., Hall, K.J., McGlone, M., Van der Putten, N. 2014. ACE Community Antarctic Ice Sheet reconstruction - sub-Antarctic Islands. *Quaternary Science Reviews,* 100, 1-9.

Hoffman, T., Todd, S., Ntshona, Z., Turner, S., 1999. Land *Degradation in South Africa*. Department of Environmental Affairs and Tourism, Pretoria, South Africa.

Holden, J., 2007. A plea for more careful presentation of near-surface air temperature data in geomorphology. *Earth Surface Processes and Landforms* 32, 1433–1436.

Holness, S.D., 2001a. *Periglacial slope processes, landforms and environment at Marion island, Maritime Subantarctic* (PhD). University of the Western Cape, Cape Town, South Africa.

Holness, S.D., 2001b. The orientation of sorted stripes in the maritime subantarctic, Marion Island. *Earth Surface Processes and Landforms* 26, 77–89.

Holness, S.D., 2003a. The periglacial record of Holocene environmental change, subantarctic Marion Island. *Permafrost and Periglacial Processes* 14, 69–74.

Holness, S.D., 2003b. Sorted circles in the maritime Subantarctic, Marion Island. *Earth Surface Processes and Landforms* 28, 337–347.

Holness, S.D., 2004. Sediment movement rates and processes on cinder cones in the maritime Subantarctic (Marion Island). *Earth Surface Processes and Landforms* 29, 91–103.

Holness, S.D., Boelhouwers, J.C. 1998. Some observations on Holocene changes in periglacial activity at Long Ridge, Marion Island. *South African Journal of Science* 94, 399–403.

Holz, G.K., Cooperative Research Centre for Antarctic Climate and Ecosystems (Australia), 2010. *Climate futures for Tasmania: impacts on agriculture technical report*. Antarctic Climate and Ecosystems Cooperative Research Centre, Hobart, Tasmania.

Hornberger, G.M., Spear, R.C., 1981. Approach to the preliminary analysis of environmental systems. *Journal of Environmental Research* 12, 7–18.

Hoskins, B., 2002. *Organic Matter by Loss on Ignition*. University of Maine.

Hubbart, J., Link, T., Campbell, C., Cobos, D., 2005. Evaluation of a low-cost temperature measurement system for environmental applications. *Hydrological Processes* 19, 1517–1523.

Huggett, R.J., 2007. Fundamentals of Geomorphology. Routledge, London; Madison Avenue, N.Y.

Humlum, O., Christiansen, H.H., 1998. Mountain climate and periglacial phenomena in the Faeroe Islands. *Permafrost and Periglacial Processes* 9, 189–211.

Hunter, D.R., Krynauw, J.R., Le Roex, A.P., Groenewald, P.B., Harris, C., Corner, B., Grantham, G.H., Bergh, H.W., Moyes, A.B., 2013. A recent history of South African earth science research in Antarctica and adjacent regions. *Journal of Antarctic Research* 21, 173–173.

Hutchinson, G.K., Richards, K., Risk, W.H., 2000. *Aspects of accumulated heat patterns (growing degree-days) and pasture growth in Southland*. Presented at the Proceedings of the New Zealand Grassland Association, New Zealand Grassland Association, pp. 81–85.

Huyser, O., Ryan, P.G., Cooper, J., 2000. Changes in population size, habitat use and breedingbiology of lesser sheathbills (Chionis minor) at Marion Island: impacts of cats, mice and climate change? *Biological Conservation* 92, 299–310.

ICSU, 2010. *Advisory Note "Science communication."* Presented at the Science Communication: Responsibilities of the Scientific Community and the Media, ICSU, Bogotá, Columbia, p. 2.

Inkpen, R., Hall, K. J. 2016. Using morphospaces to understand tafoni development. *Geomorphology,* 261, 193-199.

Isaksson, E., Karlén, W., 1994. High resolution climatic information from short firn cores, western Dronning Maud Land, Antarctica. *Climatic Change* 26, 421–434.

Ishikawa, M., 2003. Thermal regimes at the snow–ground interface and their implications for permafrost investigation. *Geomorphology* 52, 105–120.

IUSS Working Group WRB, 2015. *World Reference Base for Soil Resources 2014*, update 2015 International soil classification system for naming soils and creating legends for soil maps (World Soil Resources Report No. 106). Food and Agricultural Organisation of the United Nations, Rome.

Jevon, W.S., 1918. *Elementary Lessons in Logic: Deductive and Inductive: With Copious Questions and Examples, and a Vocabulary of Logical Terms*. Macmillan, London.

Johnson, A.N., Boer, B.R., Woessner, W.W., Stanford, J.A., Poole, G.C., Thomas, S.A., O'Daniel, S.J., 2005. Evaluation of an inexpensive small-diameter temperature logger for documenting ground water–river interactions. *Ground Water Monitoring & Remediation* 25, 68–74.

Johnson, M.R., Anhaeusser, C.R., Thomas, R.J., Geological Society of South Africa (Eds.), 2006. *The Geology of South Africa.* Geological Society of South Africa, Johannesburg.

Jones, A., Chown, S., Ryan, P., Gremmen, N.J., Gaston, K., 2003. A review of conservation threats on Gough Island: a case study for terrestrial conservation in the Southern Oceans. *Biological Conservation* 113, 75–87.

Jones, B.M., Grosse, G., Arp, C.D., Miller, E., Liu, L., Hayes, D.J., Larsen, C.F., 2015. Recent Arctic tundra fire initiates widespread thermokarst development. *Scientific Reports* 5, 15865.

Kalvová, J., Halenka, T., Bezpalcová, K., Neme\vsová, I., 2003. Köppen climate types in observed and simulated climates. *Studia Geophysica et Geodaetica* 47, 185–202.

Karte, J., 1983. Periglacial Phenomena and their Significance as climatic and edaphic indicators. *GeoJournal* 7, 329–340.

Kawahigashi, M., Kaiser, K., Kalbitz, K., Rodionov, A., Guggenberger, G., 2004. Dissolved organic matter in small streams along a gradient from discontinuous to continuous permafrost. *Global Change Biology* 10, 1576–1586.

Kennicutt, M.C., Chown, S.L., Cassano, J.J., Liggett, D., Massom, R., Peck, L.S., Rintoul, S.R., Storey, J.W.V., Vaughan, D.G., Wilson, T.J., Sutherland, W.J., 2014. Polar research: Six priorities for Antarctic science. *Nature* 512, 23–25.

Kennicutt, M.C., Chown, S.L., Cassano, J.J., Liggett, D., Peck, L.S., Massom, R., Rintoul, S.R., Storey, J., Vaughan, D.G., Wilson, T.J., Allison, I., Ayton, J., Badhe, R., Baeseman, J., Barrett, P.J., Bell, R.E., Bertler, N., Bo, S., Brandt, A., Bromwich, D., Cary, S.C., Clark, M.S., Convey, P., Costa, E.S., Cowan, D., Deconto, R., Dunbar, R., Elfring, C., Escutia, C., Francis, J., Fricker, H.A., Fukuchi, M., Gilbert, N., Gutt, J., Havermans, C., Hik, D., Hosie, G., Jones, C., Kim, Y.D., Le Maho, Y., Lee, S.H., Leppe, M., Leitchenkov, G., Li, X., Lipenkov, V., Lochte, K., López-Martínez, J., Lüdecke, C., Lyons, W., Marenssi, S., Miller, H., Morozova, P., Naish, T., Nayak, S., Ravindra, R., Retamales, J., Ricci, C.A., Rogan-Finnemore, M., Ropert-Coudert, Y., Samah, A.A., Sanson, L., Scambos, T., Schloss, I.R., Shiraishi, K., Siegert, M.J., Simões, J.C., Storey, B., Sparrow, M.D., Wall, D.H., Walsh, J.C., Wilson, G., Winther, J.G., Xavier, J.C., Yang, H., Sutherland, W.J., 2015. A roadmap for Antarctic and Southern Ocean science for the next two decades and beyond. *Antarctic Science* 27, 3–18.

Keskitalo, J., Leppäranta, M., Arvola, L., 2013. First records of primary producers of epiglacial and supraglacial lakes in western Dronning Maud Land, Antarctica. *Polar Biology* 36, 1441–1450.

Kiernan, K., McConnell, A., 1999. Geomorphology of the sub-Antarctic Australian territory of Heard Island-McDonald Island. *Australian Geographer* 30, 159–195.

King, C.A.M., 1966. *Techniques in Geomorphology*. Edward Arnold, Great Britain.

Kleinhans, I., 2006. A *critical appraisal of regional geotechnical mapping in South Africa*(MSc). University of Pretoria, Pretoria, South Africa.

Kleman, J., Glasser, N.F., 2007. The subglacial thermal organization (STO) of ice sheets. *Quaternary Science Reviews* 25, 585–587.

Knight, J., 2012. The shape of glacial valleys: comment on Hall (2010). *South African Geographical Journal* 94, 1–3.

Koaze, T., Nogami, M., Iwata, S., 1974. Paleoclimatic significance of fossil periglacial phenomena in Hokkaidô, Northern Japan. *The Quaternary Research (Daiyonki-Kenkyu)* 12, 177–191.

Köppen, W., 1936. Das Geographische System der Klimate, *in*: Köppen, W., Geiger, R. (Eds.), *Handbuch der Klimatologie*, 3. Gebrüder Borntraeger, Berlin, pp. 1–44.

Kottek, M., Grieser, J., Beck, C., Rudolf, B., Rubel, F., 2006. World Map of the Köppen-Geiger climate classification updated. *Meteorologische Zeitschrift* 15, 259–263.

Kotzé, C., 2016. *Active layer dynamics at four borehole sites in Western Dronning Maud Land, Antarctica* (MSc). Rhodes University, Grahamstown, South Africa.

Kotzé, C., Meiklejohn, K.I., 2016. Temporal variability of ground thermal regimes on the northern buttress of the Vesleskarvet nunatak, western Dronning Maud Land, Antarctica. *Antarctic Science* 1–9.

Krynauw, J.R., 1986. *The petrology and geochemistry of intrusions at selected nunataks of the Ahlmannryggen and Giaeverryggen, Western Dronning Maud Land, Antarctica* (PhD). University of Natal, Durban, South Africa.

Kück, K.M., 1997. *Periglacial features in the vicinity of Tiffindell Ski Resort, North East Cape Drakensberg, South Africa, and their implications for the development of the resort* (MSc). Rhodes University, Grahamstown, South Africa.

Kück, K.M., Lewis, C.A., 2002. Terracettes and active gelifluction terraces in the Drakensberg of the province of the Eastern Cape, South Africa: A process study. *South African Geographical Journal* 84, 214–225.

Kumar, P.P., 2011a. Cryogenesis, *in*: Singh, V.P., Singh, P., Haritashya, U.K. (Eds.), *Encyclopedia of Snow, Ice and Glaciers*. Springer, Dortrecht, p. 171.

Kumar, P.P., 2011b. Cryoturbation, *in*: Singh, V.P., Singh, P., Haritashya, U.K. (Eds.), *Encyclopedia of Snow, Ice and Glaciers*. Springer, Dortrecht, p. 173.

La Grange, J.J., 1954. The South African station on Marion Island, 1948–53. *Polar Record* 7, 155–158.

Lara, O.G., Matthes, W.J., 1986. *The SediGraph as an alternative to the pipet*. Presented at the 4th Federal Interagency Sedimentation Conference. Subcommittee on Sedimentation of the Interagency Advisory Committee on Water Data, Las Vegas, Nevada, pp. 1.1–1.12.

Lee, J.E., Le Roux, P.C., Meiklejohn, K.I., Chown, S.L., 2013. Species distribution modelling in low-interaction environments: Insights from a terrestrial Antarctic system. *Austral Ecology* 38, 279–288.

le Roex, A.P., Chevallier, L., Verwoerd, W.J., Barends, R., 2012. Petrology and geochemistry of Marion and Prince Edward Islands, Southern Ocean: Magma chamber processes and source region characteristics. *Journal of Volcanology and Geothermal Research* 223-224, 11–28.

Le Roux, P.C., 2008. Climate and climate change, *in*: Chown, S.L., Froneman, P.W. (Eds.), *The Prince Edward Islands: Land-Sea Interactions in a Changing Ecosystem*. SUN MeDIA, Stellenbosch, pp. 39–64.

le Roux, P.C., McGeoch, M.A., 2008. Changes in climate extremes, variability and signature on sub-Antarctic Marion Island. *Climatic Change* 86, 309–329.

Lewis, C.A., 1988. Periglacial features in southern Africa: an assessment. *Palaeoecology of Africa* 19, 357–370.

Lewis, C.A., 1994. Protalus ramparts and the altitude of the Local Equilibrium Line during the last glacial stage in Bokspruit, East Cape Drakensberg, South Africa. *Geografiska Annaler. Series A, Physical Geography* 76, 37–48.

Lewis, C.A., 2005. Late Glacial and Holocene palaeoclimatology of the Drakensberg of the Eastern Cape, South Africa. *Quaternary International, Highlights of Quaternary Research in Southern Africa* 129, 33–48.

Lewis, C.A., 2008a. Glaciations and glacial features, *in*: Lewis, C.A. (Ed.), *Geomorphology of the Eastern Cape, South Africa*. NISC, Grahamstown, pp. 127–148.

Lewis, C.A., 2008b. Periglacial features, *in*: Lewis, C.A. (Ed.), *Geomorphology of the Eastern Cape, South Africa*. NISC, Grahamstown, pp. 149–185.

Lewis, C.A., 2008c. Late Quaternary climatic changes, and associated human responses, during the last ± 45 000 yr in the Eastern and adjoining Western Cape, South Africa. *Earth-Science Reviews* 88, 167–187.

Lewis, C.A., 2008d. Late Pleistocene and early Holocene foragers in southern Africa, *in*: Pearsall, D.M. (Ed.), *Encyclopedia of Archaeology*. Elsevier/Academic Press, San Diego, California, pp. 86–93.

Lewis, C.A., Hanvey, P.M., 1988. Sedimentology of debris slope accumualtions at Rhodes, eastern Cape Drakensberg, South Africa, *in*: Dardis, G.F., Moon, B.P. (Eds.), *Geomorphological Studies in Southern Africa*. Balmena, Rotterdam, pp. 365–381.

Lewis, C.A., Hanvey, P.M., 1993. The remains of rock glaciers in Bottelnek, East Cape Drakensberg, South Africa. *Transactions of the Royal Society of South Africa* 48, 265–289.

Lewis, C.A., Hydrological Research Unit (Rhodes University), Southern African Society for Quaternary Research, 1994. *Field Guide to the Quaternary Glacial, Periglacial and Colluvial Features of the East Cape Drakensberg*. Published on behalf of the Southern African Society for Quaternary Research by the Department of Geography, Rhodes University, Grahamstown.

Li, F., Snow, V., Holzworth, D., 2011. Modelling the seasonal and geographical pattern of pasture production in New Zealand. New *Zealand Journal of Agricultural Research* 54, 331–352.

Liljedahl, A., Hinzman, L., Busey, R., Yoshikawa, K., 2007. Physical short-term changes after a tussock tundra fire, Seward Peninsula, Alaska. *Journal of Geophysical Research* 112, F02S07.

Lozinski, W., 1909. Über die mechanische Verwitterung der Sandsteine im Gemässigten Klima. *Bulletin International de l'Académie des Sciences de Cravocie class des Sciences Mathématiques et Naturelles* 1.

Lubbe, N.R., 2010. *Soil characteristics and pedogenesis on Sub-Antarctic Marion Island* (MSc). University of Pretoria, Pretoria, South Africa.

Mackay, J.R., 1981. Active layer slope movement in a continuous permafrost environment, Garry Island, Northwest Territories, Canada. *Canadian Journal of Earth Sciences* 18, 1666–1680.

Malvern Instruments Ltd., 2011. *Mastersizer 3000 User Manual*. Malvern Instruments Ltd.

Manger, G.E., 1963. *Porosity and bulk density of sedimentary rocks* (USGS Numbered Series No. 1144-E), Bulletin. U.S. G.P.O.

Marschall, H.R., Hawkesworth, C.J., Leat, P.T., 2013. Mesoproterozoic subduction under the eastern edge of the Kalahari-Grunehogna Craton preceding Rodinia assembly: The Ritscherflya detrital zircon record, Ahlmannryggen (Dronning Maud Land, Antarctica). *Precambrian Research* 236, 31–45.

Marshall, D.J., Crafford, J.E., Krynauw, J.R., Drummond, A.E., Newton, I.P., 1995. The biology, physico-chemistry and geology of a nunatak pond at Valterkulten, western Dronning Maud Land, Antarctica. South African *Journal of Antarctic Research* 25, 9–16.

Matsuoka, N., 2001. Solifluction rates, processes and landforms: a global review. *Earth-Science Reviews* 55, 107–134.

McDougall, I. a. N., Verwoerd, W., Chevallier, L., 2001. K–Ar geochronology of Marion Island, Southern Ocean. *Geological Magazine* 138, 1–17.

McGibbon, D., 2014. *Shear Zones of the Maud Belt, Antarctica: Kinematics and eeformation mechanisms* (MSc). University of Cape Town, Cape Town.

McKenzie, N., Coughlan, K., Cresswell, H., Australian Collaborative Land Evaluation Program, Natural Heritage Trust (Australia), 2002. *Soil physical measurement and interpretation for land evaluation*. CSIRO Pub., Collingwood, Vic.; [Great Britain].

Meentemeyer, V., Zippin, J., 1981. Soil moisture and texture controls of selected parameters of needle ice growth. *Earth Surface Processes and Landforms* 6, 113–125.
Meiklejohn, K.I., 2011. Marion's disappearing ice cap, *in*: Zietsman, L., South African Environmental Observation Network, Department of Science and Technology (Eds.), *Observations on Environmental Change in South Africa*. SUN MeDIA, Stellenbosch, pp. 57–62.
Meiklejohn, K.I., Hall, K.J., 1997. Aqueous geochemistry as an indicator of chemical weathering on southeastern Alexander Island, Antarctica. *Polar Geography* 21, 101–112.
Mensching, H.G., 1984. Julius Büdel und sein Konzept der Klima-Geomorphologie - Rückschau und Würdigung. *Erdkunde* 38, 157–167.
Miller, J.A., 2012. Species distribution models: Spatial autocorrelation and non-stationarity. *Progress in Physical Geography* 36, 681–692.
Mills, S.C., Grab, S.W., Carr, S.J., 2009. Recognition and palaeoclimatic implications of late Quaternary niche glaciation in eastern Lesotho. *Journal of Quaternary Science* 24, 647–663.
Mndawe, M.B., Ndambuki, J., Kupolati, W.K., 2013. *Revision of the Macro Climatic Regions of Southern Africa* (SSRN Scholarly Paper No. ID 2343006). Social Science Research Network, Rochester, NY.
Mortimer, E., Van Vuuren, B.J., Meiklejohn, K.I., Chown, S.L., 2012. Phylogeography of a mite, Halozetes fulvus, reflects the landscape history of a young volcanic island in the sub-Antarctic. *Biological Journal of the Linnean Society* 105, 131–145.
Moyes, A.B., 1993. The age and origin of the Jutulsessen granitic gneiss, Gjelsvikfjella, Dronning Maud Land. *South African Journal of Antarctic Research* 23, 25–32.
Moyes, A.B., Krynauw, J.R., Barton, J.M., 1995. The age of the Ritscherflya Supergroup and Borgmassivet Intrusions, Dronning Maud Land, Antarctica. Antarctic Science 7, 87–97.
Mucina, L., Rutherford, M.C. (Eds.), 2006. *The Vegetation of South Africa, Lesotho and Swaziland*. Strelitzia; South African National Biodiversity Institute, Pretoria.
Murray, A.B., Lazarus, E., Ashton, A., Baas, A., Coco, G., Coulthard, T., Fonstad, M., Haff, P., McNamara, D., Paola, C., Pelletier, J., Reinhardt, L., 2009. Geomorphology, complexity, and the emerging science of the Earth's surface. *Geomorphology* 103, 496–505.
Myers-Smith, I.H., Harden, J.W., Wilmking, M., Fuller, C.C., McGuire, A.D., Chapin, F.S., 2008. Wetland succession in a permafrost collapse: interactions between fire and thermokarst. *Biogeosciences* 5, 1273–1286.
National Aeronautics Space Agency (Nasa), 2014. *SMAP: Handbook - Soil Moisture Active Passive*. National Aeronautics Space Agency (Nasa).
National Aeronautics Space Agency (Nasa), 2015. *Soil Moisture Active Passive (SMAP)*. National Aeronautics Space Agency (Nasa).
National Aeronautics Space Agency (Nasa), 2016a. *MODIS Moderate Resolution Imaging Spectroradiometer [*WWW Document]. URL http://modis.gsfc.nasa.gov/data/
National Aeronautics Space Agency (Nasa), 2016b. *LAADS Web Level 1 and Atmosphere Archive and Distribution System* [WWW Document]. URL https://ladsweb.nascom.nasa.gov/data/search.html
Natural Heritage Trust (Australia), 2001. *Australian Agriculture Assessment 2001*. National Land and Water Resources Audit, Turner, A.C.T.
Nel, W., 2001. A *spatial inventory of glacial, periglacial and rapid mass movement forms on part of Marion Island: implications for Quaternary environmental change* (MSc). University of Pretoria, Pretoria, South Africa.
Nel, W., 2008. *On the climate of the Drakensberg: rainfall and surface-temperature attributes, and associated geomorphic effects* (PhD). University of Pretoria, Pretoria, South Africa.
Nel, W., 2012. A preliminary synoptic assessment of soil frost on Marion Island and the possible consequences of climate change in a maritime sub-Antarctic environment. *Polar Research* 31.
Nel, W., Boelhouwers, J.C., 2014a. Synoptic classification and decadal change in air circulation patterns at Marion Island, 1960-2009, *in*: *Antarctica and the Southern Ocean in the 21st Century*.

Presented at the Scientific Committee on Antarctic Research Open Science Conference, SCAR, Auckland, New Zealand, p. 1003.
Nel, W., Boelhouwers, J.C., 2014b. First observations on needle ice formation in the sub-Antarctic. *Antarctic Science* 26, 327–328.
Nel, W., Boelhouwers, J.C., Zilindile, M.B., 2009. The effect of synoptic scale weather systems on sub-surface soil temperatures in a diurnal frost environment: Preliminary observations from sub-Antarctic Marion Island. *Geografiska Annaler: Series A, Physical Geography* 91, 313–319.
Nel, W., Sumner, P.D., 2008. Rainfall and temperature attributes on the Lesotho-Drakensberg Escarpment Edge,Southern Africa. *Geografiska Annaler: Series A, Physical Geography* 90, 97–108.
Newton, I.P., 1994. Climatic data from Robertskollen, Dronning Maud Land, Antarctica, January 1993 to January 1995. *South African Journal of Antarctic Research* 24, 103–110.
Noone, D., Turner, J., Mulvaney, R., 1999. Atmospheric signals and characteristics of accumulation in Dronning Maud Land, Antarctica. *Journal of Geophysical Research* 104, 19191–19211.
Norwegian Polar Institute, 2016. *Quantarctica* [WWW Document]. URL http://www.quantarctica.org/ (accessed 4.20.16).
Nossov, D.R., Jorgenson, M.T., Kielland, K., Kanevskiy, M.Z., 2013. Edaphic and microclimatic controls over permafrost response to fire in interior Alaska. *Environmental Research Letters* 8, 035013.
Odoni, N.A., 2007. *Exploring equifinality in a landscape evolution model* (PhD). University of Southampton, Southampton, UK.
Ohta, Y., Tørudbakken, B.O., Shiraishi, K., 1990. Geology of Gjelsvikfjella and western Mühlig-Hofmannfjella, Dronning Maud Land, east Antarctica. *Polar Research* 8, 99–126.
Orheim, O. (Ed.), 1997. *Report of the Norwegian Antarctic Research Expedition 1992/93*, Meddelelser / Norsk Polarinstitutt. Norsk Polarinstitutt, Oslo.
Orheim, O., Lucchitta, B., 1990. Investigating cliamte change by digital analysis of blue ice, *in*: *Proceedings of the Symposium on Ice and Climate, Seattle, Washington, USA, 21-25 August 1989*. International Glaciological Society, p. 211.
Osmaston, H.A., Harrison, S.P., 2005. The Late Quaternary glaciation of Africa: A regional synthesis. *Quaternary International* 138-139, 32–54.
Osterkamp, T.E., Burn, C.R., 2003. *Permafrost*, in: Curry, J.A., Pyle, J.A. (Eds.), *Encyclopedia of Atmospheric Sciences*. Elsevier, pp. 1717–1729.
Outcalt, S.I., 1971. An algorithm for needle Ice growth. *Water Resources Research* 7, 394–400.
Outcalt, S.I., 1972. The simulation of subsurface sffects on the diurnal surface thermal regime in cold regions. *Arctic* 25, 305–307.
Outcalt, S.I., Nelson, F.E., Hinkel, K.M., 1990. The zero-curtain effect: Heat and mass transfer across an isothermal region in freezing soil. *Water Resources Research* 26, 1509–1516.
Peel, M.C., Finlayson, B.L., McMahon, T.A., 2007. Updated world map of the Köppen-Geiger climate classification. *Hydrology and Earth System Sciences* 11, 1633–1644.
Pérez, F.L., 1992. Miniature sorted striped in the Páramo de Piedras Blancas (Venezuela Andes), *in*: Dixon, J.C., Abrahams, A.D. (Eds.), *Periglacial Geomorphology: Proceedings of the 22nd Binghamton Symposium in Geomorphology*. Wiley, Chichester; New York, pp. 125–157.
Perritt, S., 2001. The *Ahlmannryggen Group, Western Dronning Maud Land, Antarctica* (BScHons). University of Natal, Durban, South Africa.
Phillips, J.D., 1997. Simplexity and the reinvention of equifinality. *Geographical Analysis* 29, 1–15.
Phillips, J.D., 1999. Divergence, convergence, and self-organization in landscapes. *Annals of the Association of American Geographers* 89, 466–488.
Phillips, J.D., 2005. Weathering instability and landscape evolution. *Geomorphology* 67, 255–272.
Phillips, J.D., 2007. The perfect landscape. *Geomorphology* 84, 159–169.
Phukan, A. (Ed.), 1993. *Frost in Geotechnical Engineering: Proceedings of the 2nd International Symposium on Frost in Geotechnical Engineering, Anchorage, USA, 28 June - 1 July 1993*. Balkema, Rotterdam.

Priesnitz, K., 1988. Cryoplanation, *in*: Clark, M.J. (Ed.), *Advances in Periglacial Geomorphology*. Wiley, Chichester; New York, pp. 49–69.

Prince Edward Islands Management Plan Working Group (Ed.), 1996. *Prince Edward Islands Management Plan (EMP)*. Deptartment of Environmental Affairs & Tourism (DEAT) Directorate Antarctica and Islands, Pretoria, South Africa.

Propastin, P., Kappas, M., Erasmi, S., 2008. Application of geographically weighted regression to investigate the impact of scale on prediction uncertainty by modelling relationship between vegetation and climate. *International Journal of Spatial Data Infrastructures Research* 3, 73–94.

Pulley, S., Foster, I., Antunes, P., 2015. The uncertainties associated with sediment fingerprinting suspended and recently deposited fluvial sediment in the Nene river basin. *Geomorphology* 228, 303–319.

Pulley, S., Rowntree, K., 2016. Stages in the life of a magnetic grain: Sediment source discrimination, particle size effects and spatial variability in the South African Karoo. *Geoderma* 271, 134–143.

Ravindra, R., Chaturvedi, A., 2011. Antarctica, *in*: Singh, P., Haritashya, U.K. (Eds.), *Encyclopedia of Snow, Ice and Glaciers*. Springer, Dortrecht, pp. 45–54.

Rea, B., Whalley, W.B., Rainey, M.M., Gordon, J.E., 1996. Blockfields, old or new? Evidence and implications from some plateaus in northern Norway. *Geomorphol*ogy 15, 109–121.

Reijmer, C.H., Broeke, M.R.V.D., 2001. Moisture source of precipitation in Western Dronning Maud Land, Antarctica. *Antarctic Science* 13.

Rempel, A.W., 2011. Frost, *in*: Singh, V.P., Singh, P., Haritashya, U.K. (Eds.), *Encyclopedia of Snow, Ice and Glacier*s. Springer, Dortrecht, pp. 303–306.

Republic of South Africa, 2007. Id*entification of Problematic Soils in Southern Africa: Technical Notes for Civil and Structural Engineers (No. PW2006/1)*. Department of Public Works, Pretoria, South Africa.

Republic of South Africa, 1981. *Reconnaissance Geological Map of the Ahlmannryggen Area, Western Dronning Maud Land, Antarctica*. SR29-30/15 (part) and SR29-30/16 Sheet 1.

Rhoads, B.L., Thorn, C.E., 1996. Toward a Philosophy of Geomorphology, *in*: Rhoads, B.L., Thorn, C.E. (Eds.), *The Scientific Nature of Geomorphology*: *Proceedings of the 27th Binghamton Symposium in Geomorphology, 27-29 September, 199*6. Wiley, Chichester; New York, pp. 115–143.

Ridefelt, H., 2009. *Spatial and temporal variations of solifluction and related environmental parameters in the Abisko Mountains, Northern Sweden* (PhD). Uppsala Universitet, Uppsala, Sweden.

Riseborough, D.W., Springman, S.M., Arenson, L.U., 2003. Thawing and freezing indices in the active layer, *in*: Phillips, M., Springman, S.M., Arenson, L.U. (Eds.), *Permafrost: Proceedings of the 8th International Conference on Permafrost, Zurich, Switzerland, 21-25 July 2003*. A.A. Balkema Publishers, Lisse [Netherlands] ; Exton, PA, pp. 953–958.

Robson, S.G., 1993. *Techniques from estimating specific yield retention from grain-sized data and geophysical logs from clastic bedrock aquifers (Open File Report No. 93-4198*), Water-Resources Investigations Report. United States Department of the Interior, U.S. Geological Survey, Denver, Colorado.

Rocha, A.V., Loranty, M.M., Higuera, P.E., Mack, M.C., Hu, F.S., Jones, B.M., Breen, A.L., Rastetter, E.B., Goetz, S.J., Shaver, G.R., 2012. The footprint of Alaskan tundra fires during the past half-century: implications for surface properties and radiative forcing. *Environmental Research Letters* 7, 044039.

Roche, J.R., Turner, L.R., Lee, J.M., Edmeades, D.C., Donaghy, D.J., Macdonald, K.A., Penno, J.W., Berry, D.P., 2009. Weather, herbage quality and milk production in pastoral systems. 3 inter-relationships and associations between weather variables and herbage growth rate, quality and mineral concentration. *Animal Production Science* 49, 211–221.

Rotschky, G., Holmlund, P., Isaksson, E., Mulvaney, R., Oerter, H., Van Den Broeke, M.R., Winther, J.-G., 2007. A new surface accumulation map for western Dronning Maud Land, Antarctica, from interpolation of point measurements. *Journal of Glaciology* 53, 385–398.

Rouault, M., Mélice, J.-L., Reason, C.J.C., Lutjeharms, J.R.E., 2005. Climate variability at Marion Island, Southern Ocean, since 1960. *Journal of Geophysical Research* 110, C05007.

Rubel, F., Kottek, M., 2010. Observed and projected climate shifts 1901-2100 depicted by world maps of the Köppen-Geiger climate classification. *Meteorologische Zeitschrift* 19, 135–141.

Rudolph, E.M., 2015. *Surface characteristics of rock glaciers in the Jutulsessen, Dronning Maud Land, Antarctica* (MSc). Rhodes University, Grahamstown, South Africa.

Ryan, P.G., Watkins, B.P., 1989. The influence of physical factors and ornithogenic products on plant and arthropod abundance at an Inland Nunatak group in Antarctica. P*olar Biology* 10, 151–160.

Ryan, P.G., Watkins, B.P., Lewis Smith, R.I., Dastyeh, H., Eicker, A., Foissner, W., Heatwole, H., Miller, W.R., Thompson, G., 1989. Biological survey of Robertskollen, western Dronning Maud Land: area description and preliminary species list. *South African Journal of Antarctic Research* 19, 10–20.

Sack, D., Orme, A.R., 2013. 1.1 Introduction to the Foundations of Geomorphology, *in*: Shrader, J.F. (Ed.) *Treatise on Geomorphology*. Elsevier, San Diego: Academic Press. pp. 1–10.

Schoeneich, P., 2011. *Guide lines for monitoring GST - Ground Surface Temperatures (No. 3 – 2.2.2011*). Permanet Alpine Space.

Schulte, E.E., Kaufmann, C., Peters, J.B., 1991. The influence of sample size and heating time on soil weight loss-on-ignition. *Communications in Soil Science and Plant Analysis* 22, 159–168.

Schulze, B.R., 1971. *The Climate of Marion Island, in: Marion and Prince Edward Islands: Report on the South African Biological and Geological Expeditions 1965–1966*. A.A. Balkema Publishers, Cape Town, pp. 16–31.

Schumacher, B.A., 2002. *Methods for the determination of total organic carbon (TOC) in soils and sediments*. National ESD (Ed.). EPA.

Schuur, E.A.G., Bockheim, J., Canadell, J.G., Euskirchen, E., Field, C.B., Goryachkin, S.V., Hagemann, S., Kuhry, P., Lafleur, P.M., Lee, H., Mazhitova, G., Nelson, F.E., Rinke, A., Romanovsky, V.E., Shiklomanov, N., Tarnocai, C., Venevsky, S., Vogel, J.G., Zimov, S.A., 2008. Vulnerability of permafrost carbon to climate change: Implications for the global carbon cycle. *BioScience* 58, 701.

SciDev.Net, 2010. *Communication: a responsibility of all scientists* [WWW Document]. SciDev.Net. URL http://www.scidev.net/index.cfm?originalUrl=global/communication/editorials/communication-a-responsibility-of-all-scientists.html (accessed 5.16.16).

Scientific Committee on Antarctic Research, 2017. *Strategic Plan 2017-2022: Connecting and Building Antarctic Research*.

Seppälä, M. 2004. *Wind as a Geomorphic Agent in Cold Climates*. Studies in Polar Research, Cambridge University Press, UK.

Shrivastava, P.K., Dharwadkar, A., Asthana, R., Roy, S.K., Swain, A.K., Beg, M.J., 2014. The sediment properties of glacial diamicts from the Jutulsessen area of Gjelsvikfjella, East Antarctica: A reflection of source materials and regional climate. *Polar Science* 8, 264–282.

Skinner, B.J., 2004. *Dynamic Earth: An Introduction to Physical Geology*, 5th ed. J. Wiley & Sons, Hoboken, NJ.

Smith, L.C., 2012. Long term pasture growth patterns for Southland New Zealand: 1978 to 2012, *in*: *Proceedings New Zealand Grasslands Association. New Zealand Grassland Association, Gore, New Zealand*, pp. 147–152.

Smith, V.R., 2002. Climate change in the Sub-Antarctic: an illustration from Marion Island. C*limatic Change* 52, 345–357.

Smith, V.R., French, D.D., 1988. Patterns of variation in the climates, soils and vegetation of some Subantarctic and Antarctic islands. *South African Journal of Botany* 54, 35–46.

Smith, V.R., Steenkamp, M., 2001. Classification of the terrestrial habitats on Marion Island based on vegetation and soil chemistry. *Journal of Vegetation Science* 12, 181–198.

Soil Survey Staff, 1999. *Soil Taxonomy: A Basic System of Soil Classification for Making and Interpreting Soil Surveys*, 2nd ed. Natural Resources Conservation Service. U.S. Department of Agriculture Handbook.

Steele, W.K., Balfour, D.A., Harris, J.M., Dastych, H., Heyns, J., Eicker, A., 1994. Preliminary biological survey of Vesleskarvet, northern Ahlmannryggen, western Queen Maud Land: site of South Africa's new Antarctic base. *South African Journal of Antarctic Research* 24, 57–65.

Stein, R., 1985. Rapid grain-size analyses of clay and silt fraction by SediGraph 5000D: Comparison with Coulter Counter and Atterberg methods. *Journal of Sedimentary Petrology* 55, 590–593.

Stewart, J., 2011. *Antarctica: An Encyclopedia*. McFarland, Jefferson, N.C.

Strahler, A.N., 1974. *Physical Geography*, 4th ed. Wiley, New York.

Strahler, A.N., 1989. *Elements of Physical Geography*, 4th ed. Wiley, New York.

Stuart, A., Bruchkov, A., Guodong, C., 2017. *Geocryology: Characteristics and Use of Frozen Ground and Permafrost Landforms*. CRC Press.

Summerfield, M.A., 1999. *Global Geomorphology: An Introduction to the Study of Landforms*, 8th ed. Addison Wesley Longman, Harlow.

Sumner, P.D., 2003a. *On the geomorphic evidence for a Late Quaternary periglaciation of the Main Escarpment Region of Eastern Southern Africa* (PhD). University of Pretoria, Pretoria, South Africa.

Sumner, P.D., 2003b. A contemporary winter ground thermal profile in the Lesotho highlands and implications for active and relict soil frost phenomena. *Earth Surface Processes and Landforms* 28, 1451–1458.

Sumner, P.D., 2004a. Geomorphic and Climatic Implications of Relict Openwork Block Accumulations Near Thabana-Ntlenyana, Lesotho. *Geografiska Annaler: Series A, Physical Geography* 86, 289–302.

Sumner, P.D., 2004b. Relict sorted patterned ground in Lesotho. *Permafrost and Periglacial Processes* 15, 89–93.

Sumner, P.D., 2004c. Comment on: 'Characteristics and palaeoenvironmental significance of relict sorted patterned ground, Drakensberg plateau, southern Africa.' *Quaternary Science Reviews* 23, 1201–1204.

Sumner, P.D., 2004d. Rock weathering rates on Subantarctic Marion Island. *Arctic, Antarctic, and Alpine Research* 36, 123–127.

Sumner, P.D., de Villiers, S., 2002. On the Pleistocene palaeoenvironmental evidence from the Amatola screes. *South African Journal of Science* 98, 598–601.

Sumner, P.D., Hall, K.J., Van Rooy, L., Meiklejohn, K.I., 2009. Rock weathering on the eastern mountains of southern Africa: Review and insights from case studies. *Journal of African Earth Sciences* 55, 236–244.

Sumner, P.D., Meiklejohn, K.I., 2004. On the development of autochthonous blockfields in the grey basalts of sub-Antarctic Marion Island. *Polar Geography* 28, 120–132.

Sumner, P.D., Meiklejohn, K.I., Boelhouwers, J.C., Hedding, D.W., 2004a. Climate change melts Marion Island's snow and ice. *South African Journal of Science* 100, 395–398.

Sumner, P.D., Nel, W., Hedding, D.W., 2004b. Thermal attributes of rock weathering: Zonal or azonal? A Comparison of Rock Temperatures in Different Environments. *Polar Geography* 28, 79–92.

Sumner, P.D., Nel, W., Holness, S.D., Boelhouwers, J.C., 2002. Rock weathering characteristics as relative-age indicators for glacial and post-glacial landforms on Marion Island. *South African Geographical Journal* 84, 153–157.

Thamban, M., Laluraj, C.M., Naik, S.S., Chaturvedi, A., 2011. Reconstruction of Antarctic climate change using ice core proxy records from the coastal Dronning Maud Land, East Antarctica. *Journal of the Geological Society of India* 78, 19–29.

Thorn, C.E., 1992. Periglacial geomorphology: What, where, when?, *in*: Dixon, J.C., Abrahams, A.D. (Eds.), *Periglacial Geomorphology*. Wiley, Chichester, West Sussex, UK; Hoboken, NJ, pp. 1–31.

Thorn, C.E., Hall, K.J., 2002. Nivation and cryoplanation: the case for scrutiny and integration. *Progress in Physical Geography* 26, 533–550.
Thornthwaite, C.W., 1948. An approach toward a rational classification of climate. *Geographical Review* 38, 55–94.
Till, R., 1985. *Statistical Methods for the Earth Scientist: An Introduction*. Macmillan, London.
Tosh, C.A., de Bruyn, P.J.N., Bester, M.N., 2008. Preliminary analysis of the social structure of killer whales, Orcinus orca, at subantarctic Marion Island. *Marine Mammal Science* 24, 929–940.
Troll, C., 1948. Der subnivale oder periglaziale Zyklus der Denudation. *Erdkunde* 2, 1–21.
Tschinkel, W.R., 2015. Experiments testing the causes of Namibian fairy circles. *PLOS ONE* 10, e0140099.
Turner, J., Bindschadler, R.A., Convey, P., di Prisco, G., Fahrbach, E., Gutt, J., Hodgson, D.A., Mayewski, P.A., Summerhayes, C.P., 2009. *Antarctic Climate Change and the Environment*. SCAR (Scientific Committee on Antarctic Research), Cambridge.
Twidale, C.R., Lageat, Y., 1994. Climatic geomorphology: a critique. *Progress in Physical Geography* 18, 319–334.
Tyson, P.D., Preston-Whyte, R.A., Schulze, R.E., 1976. *The Climate of the Drakensberg*. Natal Town and Regional Planning Commission, Pietermaritzburg.
van Everdingen, R.O., 1985. *Unfrozen Permafrost and Other Taliks (US Army CRREL Special Report No. 85-5101-105)*, Proceedings on the Workshop on Permafrost Geophysics. Golden, Colorado.
van Everdingen, R.O. 1998. *Multi-Language Glossary of Permafrost and Related Ground-Ice Terms. International Permafrost Association*. University of Calgary Press.
van Langenhoven, A.D., van der Gaast, S.J., Eisma, D., 1978. A comparison of the effectiveness of eight methods for removal of organic matter from clay. *Clays and Clay Minerals* 26, 361–364.
Verma, K., Bhattacharya, S., Ansari, A.M.A., Srivastava, P.K., Dharwadkar, A., 2014. Geomorphic control on the formation of mixed layer clays by progressive degradation of biotite: A case study from Jutulsessen Gjelsvikfjella, East Antarctica. *Journal of the Geological Society of india* 83, 532–534.
Verwoerd, W.J., 1971. Geology, *in*: van Zinderen Bakker, J.M., Winterbottom, R.A., Dyer, R.A. (Eds.), *Marion and Prince Edward Islands: Report on the South African Biological and Geological Expeditions 1965–1966*. A.A. Balkema Publishers, Cape Town, pp. 40–62.
Vieira, G.T., Bockheim, J., Guglielmin, M., Balks, M., Abramov, A.A., Boelhouwers, J.C., Cannone, N., Ganzert, L., Gilichinsky, D.A., Goryachkin, S., López-Martínez, J., Meiklejohn, K.I., Raffi, R., Ramos, M., Schaefer, C., Serrano, E., Simas, F., Sletten, R., Wagner, D., 2010. Thermal state of permafrost and active-layer monitoring in the Antarctic: Advances during the international polar year 2007-2009. *Permafrost and Periglacial Processes* 21, 182–197.
Viles, H.A., 2005. Can stone decay be chaotic? *in:* AV, Turkington (Ed.), *Stone Decay in the Architectural Environment*. Geological Society of America Special Papers, 390, 11–16.
von Bertalanffy, L., 1968. *General System Theory: Foundations, Development, Applications*, 1st ed. Braziller, New York.
von Elverfeldt, K., 2012. *System Theory in Geomorphology*, Springer Theses. Springer, Dordrecht.
Walter, H., 1985. *Vegetation of the Earth and Ecological Systems of the Geo-biosphere*. Springer Berlin Heidelberg, Berlin, Heidelberg.
Wang, M., Overland, J.E., 2004. Detecting Arctic climate change using Köppen climate classification. *Climatic Change* 67, 43–62.
Warburton, J., 2013. 8.19 Patterned Ground and Polygons, *in*: Shrader, J.F. (Ed.) *Treatise on Geomorphology*. Elsevier, San Diego: Academic Press. pp. 298–312.
Washburn, A.L., 1979. *Geocryology: A Survey of Periglacial Processes and Environments*. Edward Arnold, London.
Weaver, A. van B., Grobler, D.C., 1981. An evaluation of the sedigraph as a standard method of sediment particle size analysis. *Water SA* 7, 79–87.
Weinert, H.H., 1980. *The Natural Road Construction Materials of Southern Africa*. Academica.

Weinert, H.H., 1984. Climate and the durability of South African road aggregates. *Bulletin of the International Association of Engineering Geology* 29, 463–466.

Whalley, W.B., Rea, B., Rainey, M.M., 2004. Weathering, blockfields, and fracture systems and the implications for long-term landscape formation: some evidence from Lyngen and Øksfordjøkelen areas in north Norway. *Polar Geography* 28, 93–119.

Williams, P.J., Smith, M.W., 1991. *The Frozen Earth: Fundamentals of Geocryology*. Cambridge University Press, Cambridge.

Williams, T.A., Sweeney, D.J., Anderson, D.R. (Eds.), 2006. *Contemporary Business Statistics with Microsoft Excel*. South-Western College Pub, Cincinnati, Ohio.

Wolaver, B.D., Sharp, J.M., 2007. Thermochron iButton: limitation of this inexpensive and small-diameter temperature logger. *Ground Water Monitoring and Remediation* 27, 127–128.

World Meteorological Organisation (WMO), 2011. *Guide to Climatological Practices*, 3rd ed. WMO, Geneva.

Yeloff, D., Mauquoy, D., Barber, K., Way, S., van Geel, B., Turney, C.S.M., 2007. Volcanic ash deposition and long-term vegetation change on subantarctic Marion Island. *Arctic, Antarctic, and Alpine Research* 39, 500–511.

Zhou, H., Dick, H.J.B., 2013. Thin crust as evidence for depleted mantle supporting the Marion Rise. *Nature* 494, 195–200.

# On High-Altitude and High-Latitude Frost Environments: Supplementary Material

A thesis submitted in fulfilment of the requirements for the degree of

DOCTOR OF PHILOSOPHY (PhD)

OF

RHODES UNIVERSITY

BY

CHRISTEL DOROTHEE HANSEN

8 MARCH 18

SUPERVISOR

PROFESSOR K.I. MEIKLEJOHN (GEOGRAPHY DEPARTMENT, RHODES UNIVERSITY)

CO-SUPERVISOR

ASSOCIATE PROFESSOR W. NEL (DEPARTMENT OF GEOGRAPHY AND ENVIRONMENTAL SCIENCE, UNIVERSITY OF FORT HARE)

*The assistance of the National Research Foundation (NRF) and the German Academic Exchange Service (DAAD) is hereby acknowledged. Opinions expressed, and conclusions arrived at are that of the author and are not necessarily to be attributed to the NRF or DAAD or any affiliated entities.*

## Plagiarism Declaration

I, CHRISTEL DOROTHEE HANSEN, hereby declare that this thesis is my own original work, that all assistance and sources of information have been properly acknowledged, and that this work has not been presented to any other University for a higher degree.

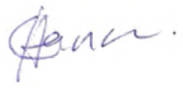

Christel D Hansen

# Summary

This document contains supplementary information to the thesis *'On High-Altitude and High-Latitude Frost Environments'* and is also available a digitally on a CD.

# Table of Figures

# Table of Tables

# Appendix A: Conceptual Model of Climatic Zone Delineation

The graphic contained in this appendix provides an overview of how current climatic zones are delineated under the current classification systems.

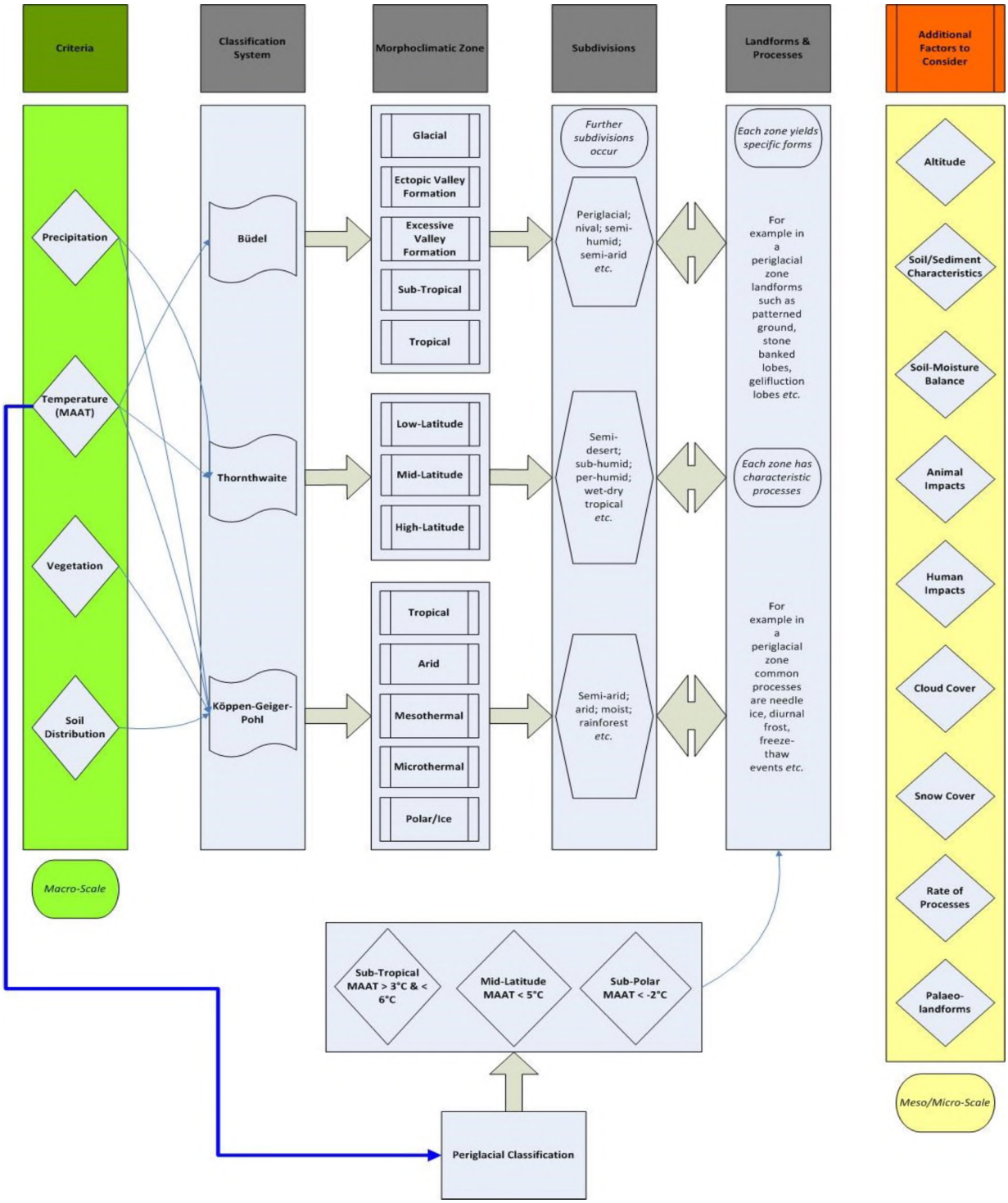


Figure 1: Conceptual model of climatic zone determination using current classification systems.

# Appendix B: Climate Classification Systems

This appendix contains information to a selection of climate classification systems. These include the Köppen classification (Table 1), Köppen-Geiger (Table 2), Walter (Table 3), subdivision of periglacial climates (Table 4), and other general models (Table 5).

Table 1: Köppen climatic zone classification system. Adapted from Köppen (1936) and Guetter and Kutzbach (1990).

| Climate Group | Description | Climate Type |
|---|---|---|
| A | Tropical rainy climates (equatorial zone): temperature of the coolest month exceeds 18 °C. | *Af; Aw* |
| | Rainfall in the driest month exceeds 60 mm. This zone is characterised by evergreen tropical rainforest. | *Af* |
| | Rainfall in the driest month is less than 60 mm. This zone is characterised by tropical deciduous forests and savannas. | *Aw* |
| B | Dry climates (arid zone): annual rainfall is less than the amounts given by the following formulae (MAR for mean annual rainfall; T for temperature in degrees Celsius):<br>1. MAR = 2T: winter rainfall area;<br>2. MAR = 2T + 7: all-year-round precipitation; and<br>3. MAR = 2T + 14: summer rainfall area. | *BS; BW* |
| | Semi-arid climates: rainfall exceeds one-half the amount given by the formulae for the boundary between dry and humid climates. This zone is characterised by grasslands, dry tropical savannas, and low shrubs.<br>1. T + 14 ≤ R < 2T + 28 for summer rain areas;<br>2. T + 7 ≤ R < 2T + 14 no marked dry season; and<br>3. T ≤ R < 2T for winter rain areas. | *BS* |
| | Arid climates: rainfall is less than one half the amount given by the formulae for the boundary between dry and humid climates. Vegetation is sparse or lacking.<br>1. R < T + 14 for summer rain areas;<br>2. R < T + 7 no marked dry season; and<br>3. R < T for winter rain areas. | *BW* |
| C | Warm temperate and rainy climates (temperate zone): temperature of the coolest month is between 18 °C and -3 °C. | *Cs; Cw; Cf* |
| | Summer drought area: rainfall of the wettest winter month exceeds that of the driest summer month at least three times. This zone is characterised by trees adapted to summer dryness, such as some oaks, eucalyptus or olives. | *Cs* |
| | Winter drought area: rainfall of the wettest summer month exceeds that of the driest winter months by at least ten times. This zone is characterised by deciduous forests, subtropical evergreen forests. | *Cw* |
| | No drought. This zone is characterised by deciduous forests, subtropical evergreen forests. | *Cf* |
| D | Boreal climates (snow zone): temperature of the coolest month is less than - | *Dw; Df* |

| Climate Group | Description | Climate Type |
|---|---|---|
| | 3 °C and the temperature of the warmest month exceeds 10 °C. This zone is characterised by evergreen coniferous forest. Mixed deciduous and evergreen forests occur near the southern boundary. | |
| | Winter drought regions: rainfall of the wettest summer month is at least ten times that of the driest winter month. | *Dw* |
| | No drought period. | *Df* |
| E | Snow and ice climates (polar zone): temperature of the warmest month is below 10°C. | *ET; EF* |
| | Tundra climate: temperature of the warmest month exceeds 0 °C. This zone is characterised by tundra vegetation, *i.e.* no trees. | *ET* |
| | Perpetual frost area (permafrost): temperature of the warmest month is below 0 °C. | *EF* |

Table 2: Köppen-Geiger climatic zone classification system (Köppen-Geiger-Pohl). Adapted from Köppen (1936) and Kottek et al. (2006).

| Climate Group | Description | Climate Type |
|---|---|---|
| A | Tropical rainy climates (equatorial): mean temperature of the coolest month exceeds 18 °C. | *Af; Am; As; Aw* |
| | Rainfall in the driest month exceeds 60 mm. This zone is characterised by evergreen tropical rainforest. | *Af* |
| | Rainfall in the driest month is less than 60 mm. Equatorial monsoon area. This zone is characterised by evergreen tropical rainforest. | *Am* |
| | Rainfall in the driest month is less than 60 mm with dry summers. This zone is characterised by tropical deciduous forests and savannas. | *As* |
| | Rainfall in the driest month is less than 60 mm with dry winters. This zone is characterised by tropical deciduous forests and savannas. | *Aw* |
| B | Dry climates (arid): annual rainfall is less than the amounts given by the following formulae (MAR for mean annual rainfall; T for temperature in degrees Celsius):<br>1. MAR = 2T: winter rainfall area;<br>2. MAR = 2T + 7: all-year-round precipitation; and<br>3. MAR = 2T + 14: summer rainfall area. | *BS (k&h); BW (k&h)* |
| | Semi-arid climates: rainfall exceeds one-half the amount given by the formulae for the boundary between dry and humid climates. These are arid but cold steppes. | *BSk* |
| | Semi-arid climates: rainfall exceeds one-half the amount given by the formulae for the boundary between dry and humid climates. These are arid and hot steppes. | *BSh* |
| | Arid climates: rainfall is less than one half the amount given by the formulae for the boundary between dry and humid climates. These are arid but cold deserts. | *BWk* |
| | Arid climates: rainfall is less than one half the amount given by the formulae for the boundary between dry and humid climates. These are arid but hot deserts. | *BWh* |
| C | Warm temperate rainy climates: mean temperature of the coolest month | *Cs (a-c);* |

| Climate Group | Description | Climate Type |
|---|---|---|
| | is between 18 °C and -3 °C. | *Cw (a-c); Cf (a-c)* |
| | Summer drought area: rainfall of the wettest winter month exceeds that of the driest summer month at least three times. Summers are classified as hot. This zone is characterised by trees adapted to summer dryness, such as some oaks, eucalyptus or olives. | *Csa* |
| | Summer drought area: rainfall of the wettest winter month exceeds that of the driest summer month at least three times. Summers are classified as warm. This zone is characterised by trees adapted to summer dryness, such as some oaks, eucalyptus or olives. | *Csb* |
| | Summer drought area: rainfall of the wettest winter month exceeds that of the driest summer month at least three times. Summers are classified as cool. This zone is characterised by trees adapted to summer dryness, such as some oaks, eucalyptus or olives. | *Csc* |
| | Winter drought area: rainfall of the wettest summer month exceeds that of the driest winter months by at least ten times. Summers are classified as hot. This zone is characterised by deciduous forests, subtropical evergreen forests. | *Cwa* |
| | Winter drought area: rainfall of the wettest summer month exceeds that of the driest winter months by at least ten times. Summers are classified as warm. This zone is characterised by deciduous forests, subtropical evergreen forests. | *Cwb* |
| | Winter drought area: rainfall of the wettest summer month exceeds that of the driest winter months by at least ten times. Summers are classified as cool. This zone is characterised by deciduous forests, subtropical evergreen forests. | *Cwc* |
| | No drought. Summers are classified as hot. This zone is characterised by deciduous forests, subtropical evergreen forests. | *Cfa* |
| | No drought. Summers are classified as warm. This zone is characterised by deciduous forests, subtropical evergreen forests. | *Cfb* |
| | No drought. Summers are classified as cool. This zone is characterised by deciduous forests, subtropical evergreen forests. | *Cf* |
| D | Boreal climates (snow): mean temperature of the coolest month is less than -3°C and the temperature of the warmest month exceeds 10 °C. This zone is characterised by evergreen coniferous forest. Mixed deciduous and evergreen forests occur near the southern boundary. | *Dw (a-d); Df (a-d); Ds (a-d)* |
| | Winter drought regions: rainfall of the wettest summer month is at least ten times that of the driest winter month. Summers are classified as hot. | *Dwa* |
| | Winter drought regions: rainfall of the wettest summer month is at least ten times that of the driest winter month. Summers are classified as warm. | *Dwb* |
| | Winter drought regions: rainfall of the wettest summer month is at least ten times that of the driest winter month. Summers are classified as cool. | *Dwc* |
| | Winter drought regions: rainfall of the wettest summer month is at least ten times that of the driest winter month. Extremely continental. | *Dwd* |
| | No drought period (fully humid). Summers are classified as hot. | *Dfa* |
| | No drought period (fully humid). Summers are classified as warm. | *Dfb* |
| | No drought period (fully humid). Summers are classified as cool. | *Dfc* |
| | No drought period (fully humid), extremely continental. | *Dfd* |
| | Summer drought regions: rainfall of the wettest summer month is at least | *Dsa* |

| Climate Group | Description | Climate Type |
|---|---|---|
| | ten times that of the driest winter month. Summers are classified as hot. | |
| | Summer drought regions: rainfall of the wettest summer month is at least ten times that of the driest winter month. Summers are classified as warm. | *Dsb* |
| | Summer drought regions: rainfall of the wettest summer month is at least ten times that of the driest winter month. Summers are classified as cool. | *Dsc* |
| | Summer drought regions: rainfall of the wettest summer month is at least ten times that of the driest winter month. Extremely continental. | *Dsd* |
| E | Ice climates (polar): mean temperature of the warmest month is below 10 °C. | *ET; EF* |
| | Tundra climate: temperature of the warmest month exceeds 0 °C. This zone is characterised by tundra vegetation, *i.e.* no trees. | *ET* |
| | Perpetual frost area (permafrost): temperature of the warmest month is below 0 °C. | *EF* |

Table 3: Climate classification predominantly based on precipitation values (Walter, 1985).

| Climate Group | Climate Types | Zonal Vegetation |
|---|---|---|
| I | Equatorial (humid) with diurnal climate. | Evergreen tropical rain forest. |
| II | Tropical (humido-arid) with summer rains. | Tropical deciduous forests or savannas. |
| III | Subtropical-arid (arid desert climate). | Subtropical desert vegetation. |
| IV | Winter rain and summer drought (arido-humid). | *Sclerophyllous* woody plants. |
| V | Warm (humid) temperate (maritime). | Temperate evergreen forests. |
| VI | Typical temperate with a short period of frost (nemoral). | Nemoral broadleaf-deciduous forests (bare in winter). |
| VII | Arid temperate with a cold winter (continental). | Steppe to desert with cold winters. |
| VIII | Cold-temperate (boreal). | Boreal coniferous forests (taiga). |
| IX | Arctic and Antarctic (polar). | Tundra vegetation (treeless). |

Table 4: Climate classification of periglacial climates (Washburn, 1979).

| Location | Temperature Classes | Description |
|---|---|---|
| Polar lowlands | Mean temperature of coldest month < -3 °C. | Ice caps, bare rock and tundra vegetation, climate influenced by latitude. |
| Subpolar lowlands | Mean temperature of coldest month < -3 °C and of warmest month > 10 °C. | Taiga type of vegetation, climate influenced by latitude. |
| Mid-latitude lowlands | Mean temperature of coldest month < -3 °C and of four warmest months > 10 °C. | Climate influenced by latitude. |
| Highlands | Climate influenced by altitude and latitude, aspect exerts an influence, diurnal ranges tend to be high. | |

Table 5: Climate classification based on predominantly temperature and precipitation values (Strahler, 1989).

| Climate Group | Climate Types | Climate Type Divisions |
|---|---|---|
| I: Low-latitude | 1: West equatorial<br>2: Monsoon and trade-littoral<br>3: Wet-dry tropical<br>4: Dry tropical | *s* – semi-arid (steppe): sufficient precipitation to support steep grassland.<br>*sd* – semi-desert: transition between desert and semi-desert.<br>*d* – desert: evapotranspiration exceeds precipitation; scarce to no vegetation.<br>*sh* – sub-humid: evapotranspiration approximates precipitation.<br>*h* – humid: precipitation exceeds evapotranspiration.<br>*p* – per humid: precipitation greatly exceeds evapotranspiration. |
| II: Mid-latitude | 5: Dry subtropical<br>6: Moist subtropical<br>7: Mediterranean<br>8: Marine west-coast<br>9: Dry mid-latitude<br>10: Moist continental | |
| III: High-latitude | 11: Boreal forest<br>12: Tundra<br>13: Ice sheet | |

# Appendix C: SCAR Horizon Scan Questions

This section provides an overview of the SCAR Horizon Scan questions that have relevance to the periglacial environment regarding permafrost and active layer dynamics. Questions with relevance to the current project are indicated in grey. The list of clusters and questions are sourced from Kennicutt et al. (2014, 2015), unless otherwise indicated.

Table 6: An overview of the SCAR Horizon Scan questions applicable to the periglacial environment with a specific focus made on those relevant to the current study.

| Question Number | Cluster | Question Description | Relevance to Research Project |
|---|---|---|---|
| 10 | Antarctic atmosphere and global connections | Will there be release of greenhouse gases stored in Antarctic and Southern Ocean clathrates, sediments, soils, and permafrost as climate changes? | N/A |
| 20 | Southern Ocean and sea ice in a warming world | How do extreme events affect the Antarctic cryosphere and Southern Ocean? | N/A |
| 22 | | How will climate change affect the physical and biological uptake of $CO_2$ by the Southern Ocean? | N/A |
| 23 | | How will changes in freshwater inputs affect ocean circulation and ecosystem processes? | N/A |
| 39 | Dynamic earth – probing beneath Antarctic ice | What are and have been the rates of geomorphic change in different Antarctic regions, and what are the ages of preserved landscapes? | Yes |
| 42 | | How will permafrost, the active layer and water availability in Antarctic soils and marine sediments change in a warming climate, and what are the effects on ecosystems and biogeochemical cycles? | Yes |
| 48 | Antarctic life on the precipice | Which ecosystems and food webs are most vulnerable in the Antarctic and Southern Ocean, and which organisms are most likely to go extinct? | N/A |
| 49 | | How will threshold transitions vary over different spatial and temporal scales, and how will they impact ecosystem functioning under future environmental conditions? | N/A |
| 50 | | What are the synergistic effects of multiple stressors and environmental change drivers on Antarctic and Southern Ocean biota? | N/A |
| 53 | | What is the exposure and response of Antarctic organisms and ecosystems to atmospheric contaminants (*e.g.* black carbon, mercury, sulphur, etc.), and are the sources and distributions of these contaminants changing? | N/A |
| 59 | | How will linkages between marine and terrestrial systems change in the future? | N/A |
| 60 | | What are the impacts on changing seasonality and transitional events on Antarctic and Southern Ocean marine ecology, biogeochemistry, and energy flow? | N/A |

# Appendix D: Study Site Parameter and Data Logging Overview

The table below provides an overview of the various site parameters, as well as data logging set-ups per site. Not all approaches were used for the various sites. Similarly, different loggers and sensors, as well as field experiments were used across the sites.

Table 7: Study site locations and their descriptive parameters. These include, geographical location information, as well as vegetation and geology specifics. DD: decimal degrees. m.a.s.l.: meters above sea level. CDML: central Dronning Maud Land. WDML: western Dronning Maud Land.

| Area | Site | Identifier | Latitude (DD) | Longitude (DD) | Elevation (m.a.s.l.) | Vegetation | Biome | Geology | Climate (Köppen-Geiger) |
|---|---|---|---|---|---|---|---|---|---|
| Eastern Cape | Ben MacDhui | T1 | 30.65° S | 27.94° E | 2993 | Lesotho Highland basalt grassland | Drakensberg grassland | Basaltic lava, with minor sandstone, tuff and agglomerate in the lower part of the succession in places | *Cfb* |
| | | T2 | 30.65° S | 27.94° E | 2909 | | | | |
| | | T3 | 30.65° S | 27.94° E | 2802 | | | | |
| | | T4 | 30.65° S | 27.94° E | 2711 | | | | |
| | | T5 | 30.66° S | 27.94° E | 2604 | | | | |
| | Elandsberg | E1 | 32.49° S | 26.88° E | 1997 | Amatole mistbelt grassland | Drakensberg grassland | A network of dolerite sills, sheets and dykes, mainly intrusive into the Karoo Supergroup | |
| | | E2 | 32.50° S | 26.89° E | 1902 | | | | |
| | | E3 | 32.51° S | 26.91° E | 1803 | | | | |
| | | E4 | 32.50° S | 26.91° E | 1702 | | | | |
| | | E5 | 32.50° S | 26.92° E | 1611 | | | | |
| | | E6 | 32.50° S | 26.92° E | 1504 | | | | |
| | | E7 | 32.51° S | 26.93° E | 1397 | | | | |
| Marion Island | Katedraalkrans | M1 | 46.90° S | 37.77° E | 765 | Sub-Antarctic polar desert | Polar desert | Grey lava | Not included |
| | Tafelberg | M2 | 46.89° S | 37.79° E | 450 | Sub-Antarctic fellfield | Sub- Antarctic tundra biome | | |

| Area | Site | Identifier | Latitude (DD) | Longitude (DD) | Elevation (m.a.s.l.) | Vegetation | Biome | Geology | Climate (Köppen-Geiger) |
|---|---|---|---|---|---|---|---|---|---|
| | | M3 | 46.89° S | 37.80° E | 363 | Sub-Antarctic fellfield | | | |
| | | M4 | 46.88° S | 37.82° E | 228 | Sub-Antarctic fellfield | | | |
| | | M5 | 46.88° S | 37.84° E | 87 | Sub-Antarctic fellfield | | | |
| Antarctica (WDML) | Flårjuven 1 | A1 | 72.01° S | 3.39° W | 1220 | None | Polar desert | Mafic sills | EF |
| | Flårjuven 2 | A2 | 72.02° S | 3.39° W | 1234 | | | | |
| | Grunehogna Peaks | A3 | 72.05° S | 2.79° W | 1291 | | | Dioritic and quartz-diorite pegmatitic sills | |
| | Robertskollen | A4 | 71.48° S | 3.33° W | 284 | | | Gabbronorite and doleritic dykes | |
| | Schumacherfjellet | A5 | 71.91° S | 2.97° W | 1230 | | | Mafic sills | |
| | Slettfjell | A6 | 72.13° S | 3.27° W | 1435 | | | | |
| | Valterkulten | A9 | 71.90° S | 3.23° W | 975 | | | | |
| | Vesleskarvet | A10 | 71.69° S | 2.84° W | 805 | | | | |
| Antarctica (CDML) | Troll 1 | A7 | 72.01° S | 2.53° E | 1320 | | Polar desert | Granitic gneisses (orthogneisses) | |
| | Troll 2 | A8 | 72.01° S | 2.53° E | 1326 | | | | |

Table 8: Research activities for each study site including logger sensors and type, experiment set-up and additional information. An 'X' indicates the instrument or sensor is present for that specific study site. DD: decimal degrees. m.a.s.l.: meters above sea level. CDML: central Dronning Maud Land. WDML: western Dronning Maud Land.

| Area | Site | Identifier | Latitude (DD) | Longitude (DD) | Elevation (m.a.s.l.) | XR5 | ACR | Decagon EC5 | Thermochron | Hygrochron | String Emplacement | Painted Marker |
|---|---|---|---|---|---|---|---|---|---|---|---|---|
| Eastern Cape | Ben MacDhui | T1 | 30.65° S | 27.94° E | 2993 | X | X | X | X | X | X | X |
| | | T2 | 30.65° S | 27.94° E | 2909 | | | | X | X | X | X |
| | | T3 | 30.65° S | 27.94° E | 2802 | | | | X | X | X | X |
| | | T4 | 30.65° S | 27.94° E | 2711 | | | | X | X | X | X |
| | | T5 | 30.66° S | 27.94° E | 2604 | | | | X | X | X | X |
| | Elandsberg | E1 | 32.49° S | 26.88° E | 1997 | | | | X | X | | |
| | | E2 | 32.50° S | 26.89° E | 1902 | | | | X | X | | |
| | | E3 | 32.51° S | 26.91° E | 1803 | X | | X | X | X | | |
| | | E4 | 32.50° S | 26.91° E | 1702 | | | | X | X | | |
| | | E5 | 32.50° S | 26.92° E | 1611 | | | | X | X | | |
| | | E6 | 32.50° S | 26.92° E | 1504 | | | | X | X | | |
| | | E7 | 32.51° S | 26.93° E | 1397 | | | | X | X | | |
| Marion Island | Katedraalkrans | M1 | 46.90° S | 37.77° E | 765 | X | X | X | | | X | X |
| | Tafelberg | M2 | 46.89° S | 37.79° E | 450 | X | X | X | X | X | X | X |
| | | M3 | 46.89° S | 37.80° E | 363 | | | | X | X | X | X |
| | | M4 | 46.88° S | 37.82° E | 228 | | | | X | X | X | X |
| | | M5 | 46.88° S | 37.84° E | 87 | | | | X | X | X | X |
| Antarctica (WDML) | Flårjuven 1 | A1 | 72.01° S | 3.39° W | 1220 | X | X | X | | | | |
| | Flårjuven 2 | A2 | 72.02° S | 3.39° W | 1234 | X | X | X | | | | |
| | Grunehogna Peaks | A3 | 72.05° S | 2.79° W | 1291 | X | X | X | | | | |
| | Robertskollen | A4 | 71.48° S | 3.33° W | 284 | X | X | X | | | | |
| | Schumacherfjellet | A5 | 71.91° S | 2.97° W | 1230 | X | X | X | | | | |
| | Slettfjell | A6 | 72.13° S | 3.27° W | 1435 | X | X | X | | | | |
| | Valterkulten | A9 | 71.90° S | 3.23° W | 975 | X | X | X | | | | |

| Area | Site | Identifier | Latitude (DD) | Longitude (DD) | Elevation (m.a.s.l.) | XR5 | ACR | Decagon EC5 | Thermochron | Hygrochron | String Emplacement | Painted Marker |
|---|---|---|---|---|---|---|---|---|---|---|---|---|
| | Vesleskarvet | A10 | 71.69° S | 2.84° W | 805 | X | X | X | | | | |
| Antarctica (CDML) | Troll 1 | A7 | 72.01° S | 2.53° E | 1320 | X | X | X | | | | |
| | Troll 2 | A8 | 72.01° S | 2.53° E | 1326 | X | X | X | | | | |

# Appendix E: Statistical Descriptions, Ranges and Classes

Terms used throughout statistical and laboratory analyses often need to be defined and assigned to classes, to standardise all terms used. Tables below show terms, such as levels of skewness and kurtosis, and their specific range of values. Furthermore, porosity, specific yield values, and particle size classes are indicated as well as an example of a soil texture diagram.

Table 9: Bulk density values for selected particle sizes (Brady and Weil, 2016).

| Material | Dry Density (g/cm$^3$) |
|---|---|
| Sand | 1.52 (1.20-1.80 g.cm-$^3$) |
| Sandy loam | 1.44 (1.20-1.80 g.cm-$^3$) |
| Loam | 1.36 |
| Silt loam | 1.28 (1.0-1.6 g.cm-$^3$) |
| Clay loam | 1.28 (1.0-1.6 g.cm-$^3$) |
| Clay | 1.2 (1.0-1.6 g.cm-$^3$) |
| Soil high in organics | 0.5 |

Table 10: Porosity values for selected particle sizes adapted from Brady and Weil (2016).

| Material | Porosity | Porosity (%) | Average (%) |
|---|---|---|---|
| Coarse gravel | 0.24-0.26 | 24-36 | 30 |
| Fine gravel | 0.25-0.38 | 25-38 | 31.5 |
| Coarse sand | 0.31-0.46 | 31-46 | 38.5 |
| Fine sand | 0.26-0.53 | 26-53 | 39.5 |
| Silt | 0.34-0.61 | 34-61 | 47.5 |
| Clay | 0.34-0.60 | 34-60 | 47 |

Table 11: Specific yield ($S_y$) values assigned to particle size distribution classes adapted from Brady and Weil (2016).

| Material | Maximum | Minimum | Average |
|---|---|---|---|
| Coarse gravel | 26 | 12 | 22 |
| Medium gravel | 26 | 13 | 23 |
| Fine gravel | 35 | 21 | 25 |
| Gravelly sand | 35 | 20 | 25 |
| Coarse sand | 35 | 20 | 27 |
| Medium sand | 32 | 15 | 26 |
| Fine sand | 28 | 10 | 21 |
| Silt | 19 | 3 | 18 |
| Sandy clay | 12 | 3 | 7 |
| Clay | 5 | 0 | 2 |

Table 12: Soil determination with reference to organic matter following loss on ignition (LOI) (Huang et al., 2009).

| Soil Organic Description | Proportion (%) |
|---|---|
| Peat | > 30 |
| Organic Soil | < 30 & > 15 |
| Mineral soil with organic matter | < 15 & > 3 |
| Mineral soil | < 3 |

Table 13: Size grades of sedimentary particles after Briggs (1977a) and Strahler (1989).

| Phi Size (ø) | Millimetres (mm) | Micrometres (µm) | Wentworth Grade |
|---|---|---|---|
| -5.0 | 32 | 32 000 | Coarse gravel<br>------- 20.0 mm ------- |
| -4.0 | 16 | 16 000 | Medium gravel<br>------- 6.0 mm ------- |
| -3.0 | 8 | 8 000 | |
| -2.0 | 4 | 4 000 | Fine gravel<br>------- 2.0 mm ------- |
| -1.0 | 2 | 2 000 | |
| 0.0 | 1 | 1 000 | Coarse sand<br>------- 0.6 mm ------- |
| 1.0 | 0.5 | 500 | Medium sand<br>------- 0.2 mm ------- |
| 2.0 | 0.25 | 250 | |
| 3.0 | 0.125 | 125 | Fine sand<br>------- 0.06 mm ------- |
| 4.0 | 0.063 | 63 | |
| 5.0 | 0.032 | 32 | Coarse silt<br>------- 0.02 mm ------- |
| 6.0 | 0.016 | 16 | Medium silt<br>------- 0.006 mm ------- |
| 7.0 | 0.008 | 8.0 | |
| 8.0 | 0.004 | 4.0 | Fine silt<br>------- 0.002 mm ------- |
| 9.0 | 0.002 | 2.0 | Clay |

Table 14: Descriptive terms and ranges used for sediment sorting classes (Briggs, 1977a).

| Description | Range |
|---|---|
| Very well sorted | < 0.35 |
| Well sorted | 0.35 – 0.50 |
| Moderately well sorted | 0.50 – 0.70 |
| Moderately sorted | 0.70 – 1.00 |
| Poorly sorted | 1.00 – 2.00 |
| Very poorly sorted | 2.00 – 4.00 |
| Extremely poorly sorted | > 4.00 |

Table 15: Descriptive terms and ranges used for skewness classes (adapted from Briggs (1977a) and Williams *et al.* (2006).

| Description | Range |
|---|---|
| Highly negatively skewed | < -1.62 |
| Negatively skewed | -1.0 – -1.62 |
| Moderately negatively skewed | -0.3 – -1.0 |
| Finely negatively skewed | -0.3 – -0.1 |
| Symmetrical | -0.1 – 0.1 |
| Finely positively skewed | 0.1 – 0.3 |
| Positively skewed | 0.3 –1.0 |
| Very positively skewed | 1.0 – 1.62 |
| Highly positively skewed | > 1.62 |

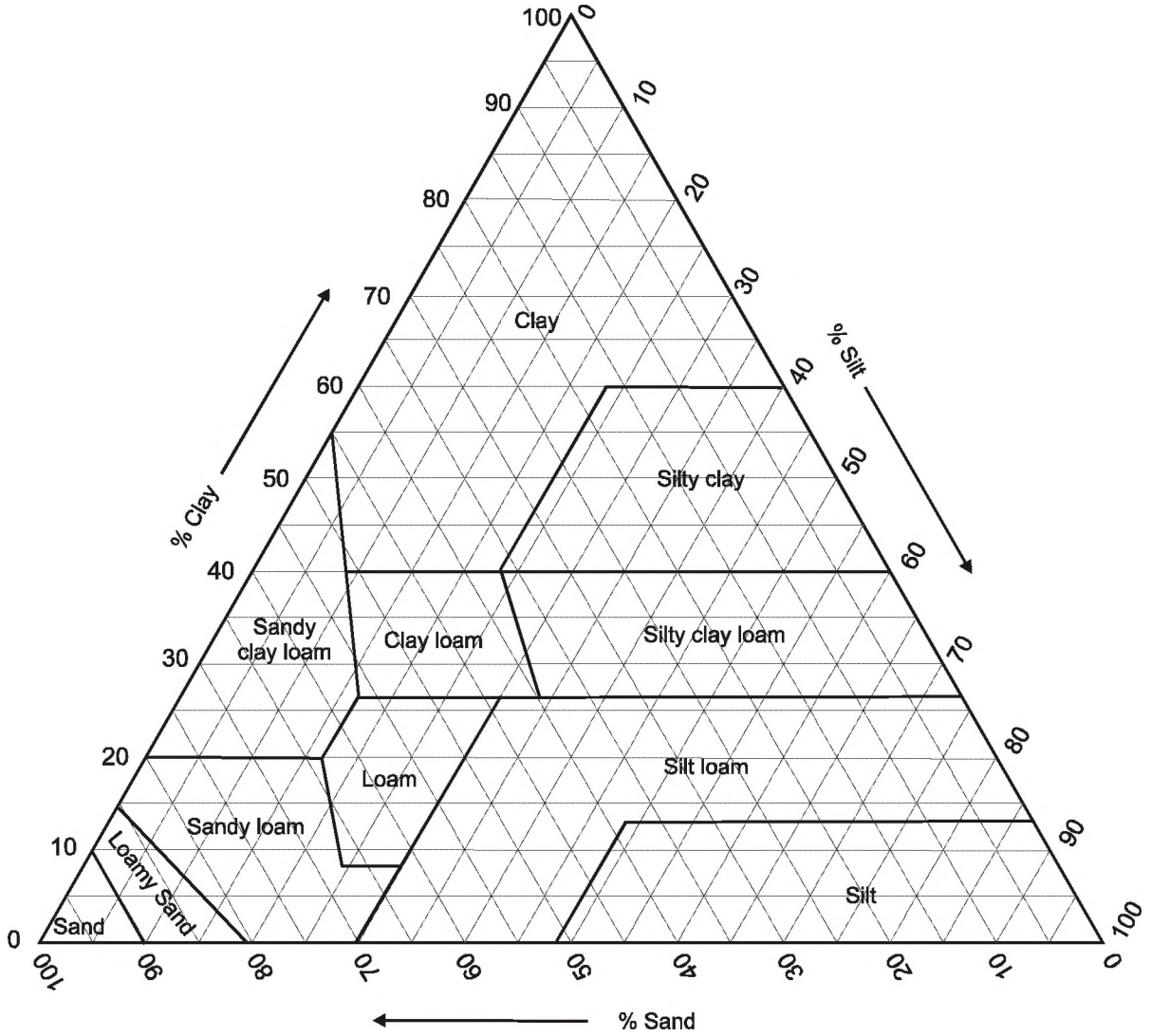


Figure 2: Soil texture diagram, based on sand, silt and clay content (Briggs, 1977b).

# Appendix F: Pre-Processing Steps

Recording steps conducted during pre-processing are crucial to ensure the integrity and suitability of datasets to analyses processes. The table below lists the various steps in pre-processing all separate datasets. All steps were recorded in separate files with each file listing the method of pre-processing steps, as well as data cleaning methods employed.

Table 16: A summary of pre-processing and data cleaning steps as they apply to the various datasets.

| Description | Instrument |
|---|---|
| Sensors were calibrated per manufacturer instructions. In addition, iButtons were calibrated in a controlled temperature bath. | All |
| All data series were aligned i.t.o. date of recording. | ACR, Decagon EC5, iButtons, XR5 |
| Null values (21.9) were removed, as were values when sensors malfunctioned (as applicable). | Decagon EC5 |
| Calibration (polynomial) equation applied to series (Kotzé, 2016), as well as the manufacturer's calibration equation of $U(\%Vol) = 0.119\ mV - 40.1$. | Decagon EC5 |
| Null values (86.639/-41.365) were removed, as were values when sensors malfunctioned (as applicable). | iButtons (hygrochrons, thermochrons) |
| One calendar month given for stabilisation of ground temperatures. This was done for all sites (Antarctica, Marion Island, South Africa) to ensure standardisation of methodology. If logging commenced halfway through a month the remainder of that month, as well as the next month of sampled data were excluded from analyses. | XR5 |
| Null values (-49.99) were removed, as were values when sensors malfunctioned (as applicable). | XR5 |

# Appendix G: Data Specifics

Below follows a list of all data used and their description. The nature of data (discrete or continuous), time series of collection and availability of data are provided. GWC: gravimetric water content. VWC: volumetric water content. TOC: total organic carbon.

Table 17: Summary of data used for the project, their nature, geographical area of collection, as well as data gaps (if applicable). $ supplemented by ACR data.

| Data Set | Set-Up | Type | Time Frame | Area | Subset | Data Gap(s) |
|---|---|---|---|---|---|---|
| Bulk Density | n/a | Discrete | 2015 | Antarctica | Flårjuven (2) (A2) | |
| | | | | | Grunehogna (A3) | |
| | | | | | Robertskollen (A4) | |
| | | | | | Schumacherfjellet (A5) | |
| | | | | | Slettfjell (A6) | |
| | | | | | Troll (1) (A7) | |
| | | | | | Troll (2) (A8) | |
| | | | | | Valterkulten (A9) | |
| | | | | | Vesleskarvet (A10) | |
| | | | | Eastern Cape | Elandsberg (E1) | |
| | | | | | Elandsberg (E2) | |
| | | | | | Elandsberg (E3) | |
| | | | | | Elandsberg (E4) | |
| | | | | | Elandsberg (E5) | |
| | | | | | Elandsberg (E6) | |
| | | | | | Elandsberg (E7) | |
| | | | | | Ben MacDhui (T1) | |
| | | | | | Ben MacDhui (T2) | |
| | | | | | Ben MacDhui (T3) | |
| | | | | | Ben MacDhui (T4) | |
| | | | | | Ben MacDhui (T5) | |
| | | | 2014 | Marion Island | Katedraal (M1) | |
| | | | | | Tafelberg (M2) | |
| | | | | | 350 (M3) | |

| Data Set | Set-Up | Type | Time Frame | Area | Subset | Data Gap(s) |
|---|---|---|---|---|---|---|
| | | | | | 250 (M4) | |
| | | | | | 100 (M5) | |
| GWC/VWC/Porosity/Soil Particle Distribution/TOC | | Ratio | 2015 | Antarctica | Flårjuven (2) (A2) | |
| | | | | | Grunehogna (A3) | |
| | | | | | Robertskollen (A4) | |
| | | | | | Schumacherfjellet (A5) | |
| | | | | | Slettfjell (A6) | |
| | | | | | Troll (1) (A7) | |
| | | | | | Troll (2) (A8) | |
| | | | | | Valterkulten (A9) | |
| | | | | | Vesleskarvet (A10) | |
| | | | | Eastern Cape | Elandsberg (E1) | |
| | | | | | Elandsberg (E2) | |
| | | | | | Elandsberg (E3) | |
| | | | | | Elandsberg (E4) | |
| | | | | | Elandsberg (E5) | |
| | | | | | Elandsberg (E6) | |
| | | | | | Elandsberg (E7) | |
| | | | | | Ben MacDhui (T1) | |
| | | | | | Ben MacDhui (T2) | |
| | | | | | Ben MacDhui (T3) | |
| | | | | | Ben MacDhui (T4) | |
| | | | | | Ben MacDhui (T5) | |
| | | | 2014 | Marion Island | Katedraal (M1) | |
| | | | | | Tafelberg (M2) | |
| | | | | | 350 (M3) | |
| | | | | | 250 (M4) | |
| | | | | | 100 (M5) | |
| Soil Moisture | XR5 (Decagon EC-5) | Continuous | 2008-2016 | Antarctica | Flårjuven (1) (A1) | |
| | | | 2013-2016 | | Flårjuven (2) (A2) | |
| | | | | | Grunehogna (A3) | |
| | | | | | Robertskollen (A4) | |
| | | | | | Schumacherfjellet (A5) | |

| Data Set | Set-Up | Type | Time Frame | Area | Subset | Data Gap(s) |
|---|---|---|---|---|---|---|
| | | | | | Slettfjell (A6) | |
| | | | 2007-2016 | | Troll (1) (A7) | |
| | | | 2013-2016 | | Troll (2) (A8) | 2013 |
| | | | | | Valterkulten (A9) | |
| | | | 2009-2015 | | Vesleskarvet (A10) | |
| | | | 2015-2016 | Eastern Cape | Elandsberg (E3) | |
| | | | | | Ben MacDhui (T1) | |
| | | | 2014-2016 | Marion Island | Katedraal (M1) | |
| | | | 2015-2016 | | Tafelberg (M2) | |
| | iButton (hygrochron DS1922S/ DS1921Z) | | 2013-2016 | Eastern Cape | Elandsberg (E1) | |
| | | | | | Elandsberg (E2) | |
| | | | | | Elandsberg (E3) | |
| | | | | | Elandsberg (E4) | |
| | | | | | Elandsberg (E5) | |
| | | | | | Elandsberg (E6) | |
| | | | | | Elandsberg (E7) | |
| | | | 2014-2015 | | Ben MacDhui (T1) | |
| | | | | | Ben MacDhui (T2) | Aug-Sep, Nov-Dec 2014, Jan-Feb 2015 |
| | | | | | Ben MacDhui (T3) | Jun 2014-15 |
| | | | | | Ben MacDhui (T4) | Sep-Dec 2014 |
| | | | | | Ben MacDhui (T5) | Jan-Jun 2015 |
| | | | | Marion Island | Tafelberg (M1) | No data available |
| | | | | | 350 (M2) | |
| | | | | | 250 (M3) | |
| | | | | | 100 (M4) | |
| Temperature | XR5 (PT900 series) | | 2008-2016 | Antarctica | Flårjuven (1) (A1) | 2013/14 (air |

| Data Set | Set-Up | Type | Time Frame | Area | Subset | Data Gap(s) |
|---|---|---|---|---|---|---|
| | | | | | | temp), 2015 (45cm) |
| | | | 2013-2016 | | Flårjuven (2) (A2) | 2014[$] |
| | | | | | Grunehogna (A3) | |
| | | | | | Robertskollen (A4) | |
| | | | | | Schumacherfjellet (A5) | |
| | | | | | Slettfjell (A6) | |
| | | | 2007-2016 | | Troll (1) (A7) | May-Dec 2009, Jul-Dec 2014[$] |
| | | | 2013-2016 | | Troll (2) (A8) | |
| | | | | | Valterkulten (A9) | 2013 (air temp), 2015[$] |
| | | | 2009-2016 | | Vesleskarvet (A10) | 2013 (air temp, near surface[$]) |
| | | | 2015-2016 | Eastern Cape | Elandsberg (E3) | |
| | | | 2015 | | Ben MacDhui (T1) | |

| Data Set | Set-Up | Type | Time Frame | Area | Subset | Data Gap(s) |
|---|---|---|---|---|---|---|
| | | | 2014-2015 | Marion Island | Katedraal (M1) | Nov 2014-April 2015 ($T_5$-$T_{15}$); Se 2014 ($T_5$); Oct 2014 ($T_{10}$ & $T_{15}$); May 2015 ($T_{10}$) |
| | ACR (low temperature probe (ET-004-GP) | | 2013-2016 | Antarctica | Flårjuven (2) (A2) | |
| | | | | | Grunehogna (A3) | |
| | | | | | Robertskollen (A4) | |
| | | | | | Schumacherfjellet (A5) | |
| | | | | | Slettfjell (A6) | |
| | | | | | Troll Centre | |
| | | | | | Troll Crack | |
| | | | | | Valterkulten (A9) | |
| | | | | | Vesleskarvet (A10) | |
| | | | 2014-2015 | Marion Island | Tafelberg (M2) | Aug & Sep 2015 ($T_5$); Oct 2014-Feb 2015 ($T_{10}$ & $T_{15}$) |
| | iButton (thermochron DS1923) | | 2013-2015 | Eastern Cape | Elandsberg (E1) | |
| | | | | | Elandsberg (E2) | |
| | | | | | Elandsberg (E3) | |
| | | | | | Elandsberg (E4) | |
| | | | | | Elandsberg (E5) | |
| | | | | | Elandsberg (E6) | |

| Data Set | Set-Up | Type | Time Frame | Area | Subset | Data Gap(s) |
|---|---|---|---|---|---|---|
| | | | | | Elandsberg (E7) | |
| | | | 2014-2015 | | Ben MacDhui (T1) | |
| | | | | | Ben MacDhui (T2) | Aug-Sep, Nov-Dec 2014, Jan-Feb 2015 |
| | | | | | Ben MacDhui (T3) | Aug-Oct 2014, Jan, Apr-May 2015 |
| | | | | | Ben MacDhui (T4) | |
| | | | | | Ben MacDhui (T5) | Jan-Mar 2015 |
| | | | 2014-2015 | Marion Island | Tafelberg (M1) | June 2014-Mar 2015 |
| | | | | | 350 (M3) | Sep-Nov 2014; Jan 2015 |
| | | | | | 250 (M4) | June 2014; Aug 2014-Jan 2015 |
| | | | | | 100 (M5) | Jul-Aug 2014; Nov-Dec 2014 |

# Appendix H: Logger Specifications

The table below provides a description of logger and sensors specifications.

Table 18: Summary of loggers and sensors used, as well as their relevant specifications.

| Type | Logging System | Range | Resolution | Accuracy |
|---|---|---|---|---|
| Decagon EC-5 | XR5-SE | Calibration dependent; up to 0-100% VWC with polynomial equation | 0.1% VWC (mineral soil) | ±3% VWC, most mineral soils, up to 8 dS/m<br>±1-2% VWC with soil specific calibration |
| Hygrochron DS1923 | n/a | Temp: -20°C to +85°C, Humidity: 0%RH to 100%RH | 0.0625 / 0.5°C (temp), 0.06% / 0.4% (hum) | ±0.5°C (temp), ± 5% (hum) |
| Low temperature probe (ET-004-GP) | ACR SmartReader Plus 8 (SRP-008) | -60°C to 55°C (-75°F to 130°F) | 0.03°C (0.05°F) @ 25°C; better than 0.07°C (0.12°F) between -25°C and 70°C (-13°F and 158°F); better than 0.13°C (0.23°F) between -40°C and -25°C (-40°F and -13°F) | ±0.2°C over the range of 0°C to 70°C (± 0.3°F over the range of 32°F to 158°F) |
| PT900 Series Temperature Probe | XR5-SE | | 0.02°C at 25°C | 0.1°C |
| Thermochron DS1921Z | n/a | -5°C to +26°C | 0.125°C | ± 1°C |
| Thermochron DS1922S | n/a | -40°C to +85°C | 0.0625°C | ± 0.5°C |

# Appendix I: Science Communication and Outreach

This section provides an overview of the dissemination of scientific data as an ArcGIS Online Map Resource (pg. 22), engagement with the public through the digital Project Website and Facebook Page (pg. 24), and a database of landforms found across the study region in the Landform Database (pg. 26).

The compilation of a landform database forms the basis of OBJECTIVE 3. Features have been obtained from literature, as well as during field visits to the various sites. Information is provided in tabular format in the table below and includes data on geographic location, data source, landform characteristics (where available), as well as the nature of the landform. Locations are extracted from the literature and when not provided, were obtained using Google Maps™. Caution should be used when viewing locations of landforms extracted from literature. Exact locations are provided in those instances when the landform was recorded during field visits. The absence of specific landforms from an area is indicated with '*None observed*' in the table. However, this does not indicate that such features are truly absent from an area, but rather that no evidence of such landforms is present in the literature and none have been observed in the field. This table serves as an accompaniment to the online map resource. Details on engagement with the public and dissemination of scientific outcomes through digital and popular media are an integral component of OBJECTIVE 5.

## ArcGIS Online Map Resource

The online map, powered by ArcGIS Online, provides an interactive method for viewers to view periglacial landforms found for the three study sites. The online map integrates into the project's website (Project Website and Facebook Page, pg. 24) and a document is provided on the database sources, accuracy, timeframe of observations, and relevant metadata. Additional information on copyright, data usage and ownership, as well as a general disclaimer are also provided in this document, which is available through the project's website. The various links to the map and the supporting documentation are given in Table 19 (pg. 23).

The ArcGIS Online map is best navigated with the use of bookmarks. Bookmarks have been created for:

- Home (full view extent);
- Eastern Cape (full view extent of all Eastern Cape recorded landforms and features);
- Elandsberg, Eastern Cape, South Africa;
- Tiffindell Ski Resort, Ben MacDhui, Eastern Cape, South Africa;
- Marion Island, Southern Ocean, South Africa;
- Western Dronning Maud Land, Antarctica; and
- Jutulsessen (central Dronning Maud Land), Antarctica.

Table 19: The various URLs for viewing the ArcGIS Online Resource map of periglacial and other relevant landforms.

| Description | URL |
|---|---|
| Direct Link | http://www.arcgis.com/home/webmap/viewer.html?webmap=67d7776e7d1f49e7bf385dc68f75ab04 |
| Alternative Link 1 | http://arcg.is/2fHStCJ |
| Alternative Link 2 | https://www.arcgis.com/apps/Embed/index.html?webmap=67d7776e7d1f49e7bf385dc68f75ab04&extent=-48.0811,-72.7532,118.5596,-1.545&home=true&zoom=true&scale=true&search=true&searchextent=true&legend=true&basemap_gallery=true&disable_scroll=true&theme=light |
| Website Link | https://geomorphologyantarctica.wordpress.com/data/landform-database/ |
| Supporting Documentation | https://geomorphologyantarctica.files.wordpress.com/2017/06/landform_database_online_map_literary_references_supporting_documentation3.pdf |

## Project Website and Facebook Page

The project website, Facebook page and Twitter account allow for the dissemination of scientific output and interaction with individuals outside of the scientific community. Digital media reach many people and allow for an interactive environment and engagement with the public and are an integral component of OBJECTIVE 5. Project website and Facebook page links are provided in Table 20. For ease of navigating the website shortcuts and links are provided in the Table 21.

Table 20: URLs to the project website and Facebook page are provided here.

| Details | Information | URL |
|---|---|---|
| Facebook page | The project's Facebook page, which is updated on a weekly basis and targets the public and their engagement with polar science. | https://www.facebook.com/RhodesAntarctica/ |
| Project website | The project's website is updated on a weekly basis and focuses more on engagement with the scientific community. Nevertheless, a focus is also on engagement with the public. | https://geomorphologyantarctica.wordpress.com/ |
| Twitter account | The Twitter account is linked to the project's website and updated when new posts appears on the website. | https://twitter.com/RhodesAntarctic/<br><br>Handle: @RhodesAntarctic |

Table 21: Details and URLs for the various site, data and logger parameters as they are available through the project's ('Landscape Processes in Antarctic Ecosystems') website.

| Details | Information | URL |
|---|---|---|
| Academic output | References to conference presentations, posters and articles published in academic journals published by participants to the project. | https://geomorphologyantarctica.wordpress.com/publications-and-awards/publications-and-presentations/ |
| Study site information | Study site information on the Antarctic study sites only. | https://geomorphologyantarctica.wordpress.com/data/site-information/ |
| Logger information | Temperature and moisture logger set-ups and sensors for the Antarctic sites only. However, the same set-up and specifications are used for Marion Island and Eastern Cape (South Africa) sites. | https://geomorphologyantarctica.wordpress.com/data/temperature-logging/ |
| Landform database | The database, also provided in Table 22 (pg. 26), provides a list of landforms and notable features observed in the field, as well as listed in the relevant literature. | https://geomorphologyantarctica.wordpress.com/data/landform-database/ |

## Landform Database

Table 22: Landform database for the three study sites. Active or relict landforms ares indicated when known. *Includes pingo, palsa, thúfur. § Disputed. DD: decimal degrees. m.a.s.l.: meters above sea level. EC: Eastern Cape, MI: Marion Island, DML: Dronning Maud Land, Antarctica. *pers. obs.*: personal observation. Note: lichen are not periglacial features but are included here due to their presence at all study areas and sites.

| Feature | Site | Location | Active/Relict | Source | Latitude (DD) | Longitude (DD) | Altitude (m.a.s.l.) |
|---|---|---|---|---|---|---|---|
| Blockfield | EC | Giant's Castle | Relict | (Boelhouwers, 1991, 1994) | -29.345075 | 29.48149167 | 3 140-3 300 |
| | | Thabana-Ntlenyana, Lesotho | Relict | (Sumner, 2004) | -29.46795833 | 29.27311389 | 3 482 |
| | MI | Above 450 m.a.s.l. and below 750 m.a.s.l. | Relict | (Boelhouwers, 2003; Sumner and Meiklejohn, 2004) | -46.8947 | 37.7492 | > 450 and < 750 |
| | | Long Ridge | Relict | (Sumner and Meiklejohn, 2004) | -46.8742 | 37.7886 | 400 |
| | | Tafelberg | Relict | (Sumner and Meiklejohn, 2004) | -46.8836 | 37.8117 | 200 |
| | | Tate's Hill | Relict | (Sumner and Meiklejohn, 2004) | -46.9139 | 37.8161 | 400 |
| | DML | Basen | Active | (Boelhouwers, 2004) | -73.0433 | -13.4083 | 443 |
| | | Flårjuven | Unknown | *pers. obs.* | -72.026 | -3.409 | 1 359 |
| | | Grunehogna | Unknown | *pers. obs.* | -72.046 | -2.769 | 1 390 |
| | | Jutulsessen (flat-topped ridges) | Unknown | (Dallmann et al., 1990) | -72.0167 | 2.75 | 1 800-2 000 |
| | | Northern Buttress, Vesleskarvet | Active | (Hansen et al., 2013; Hansen, 2014) | -71.667 | -2.855 | 856 |
| | | Robertskollen | Unknown | *pers. obs.* | -71.477 | -3.333 | 284 |
| | | Schumacherfjellet | Unknown | *pers. obs.* | -71.912 | -2.971 | 1 230 |

| Feature | Site | Location | Active/Relict | Source | Latitude (DD) | Longitude (DD) | Altitude (m.a.s.l.) |
|---|---|---|---|---|---|---|---|
| | | Slettfjell | Unknown | *pers. obs.* | -72.128 | -3.293 | 1 435 |
| | | Valterkulten | Unknown | *pers. obs.* | -71.887 | -3.227 | 1 100 |
| Blockstream / Stone lobe | EC | Ben MacDhui | Relict | *pers. obs.* | -30.652025 | 27.93181944 | 2 750 |
| | | Bottlenek Valley, Barkly East § | Relict | (Lewis and Hanvey, 1993) | -31.10808889 | 27.731075 | ~ 1 840 |
| | | Elandsberg | Relict | (Sumner and de Villiers, 2002) | -32.51219167 | 26.89050278 | 1 740 |
| | | Giant's Castle | Relict | (Boelhouwers, 1994) | -29.345075 | 29.48149167 | 3 140-3 300 |
| | | Njesuthi-Mafadi Summit, Lesotho Drakensberg | Relict | (Grab, 1999) | -29.20237222 | 29.35706111 | 3 400 |
| | | Sani Pass, Lesotho Drakensberg | Relict | (Boelhouwers et al., 2002) | -29.58797778 | 29.29219722 | 3 000-3 200 |
| | | Thabana-Ntlenyana, Lesotho | Relict | (Sumner, 2004) | -29.46795833 | 29.27311389 | 3 482 |
| | MI | Feldmark Plateau (Beret Hill) | Relict | (Holness, 2001a) | -46.9444 | 37.7686 | 750 |
| | | Long Ridge South | Relict | (Holness and Boelhouwers, 1998) | -46.8847 | 37.7817 | 500 |
| Frost mound * | EC | Bell River Valley & Tina Head | Active | (Lewis, 2008a) | -30.63141111 | 28.13961944 | > 2 550 |
| | | Ben MacDhui | Active | (Kück, 1997) | -30.64829167 | 27.93525556 | 2 650; 2 780; > 2 900 |
| | | KwaZulu Natal Drakensberg | Active | (Boelhouwers, 1991) | -29.49013333 | 29.14902222 | ~ 3 000 |
| | | Mafadi Valley, Lesotho Drakensberg | Active | (Grab, 1998) | -29.69157778 | 29.03261944 | up to 3 482 |

| Feature | Site | Location | Active/Relict | Source | Latitude (DD) | Longitude (DD) | Altitude (m.a.s.l.) |
|---|---|---|---|---|---|---|---|
| | | Mashai Valley, Lesotho Drakensberg | Active | (Grab, 1997a, 2005) | -29.69157778 | 29.03261944 | ~ 2 950 |
| | | Mashai Valley, Lesotho Drakensberg | Active | (Grab, 1998) | -29.69157778 | 29.03261944 | up to 3 482 |
| | | Mohlesi Valley, Lesotho Drakensberg | Active | (Grab, 1994) | -29.49508333 | 29.31548611 | 2 750-3 360 |
| | | Tlaeeng Pass, Lesotho Highlands | Active | (Hanvey and Marker, 1992) | -28.81184167 | 28.73378056 | 3 275 |
| | DML | Nonshøgda | No longer in evidence | (Dallmann et al., 1990) | -72 | 2.516666667 | 1 331 |
| | | Vassdalen | Unknown | (Hansen et al., 2016) | -72.03333333 | 2.6465 | 1 184 |
| Frost sorting | DML | Flårjuven | Active | *pers. obs.* | -72.01766535 | -3.419327326 | 1 295 |
| | | Flårjuven | Active | *pers. obs.* | -72.02089171 | -3.421707284 | 1 295 |
| | | Flårjuven | Active | *pers. obs.* | -72.01574028 | -3.398245247 | 1 335 |
| | | Flårjuven | Active | *pers. obs.* | -72.01518204 | -3.423365979 | 1 289 |
| | | Flårjuven | Active | *pers. obs.* | -72.01712798 | -3.430784969 | 1 292 |
| | | Flårjuven | Active | *pers. obs.* | -72.01577799 | -3.425698997 | 1 283 |
| | | Flårjuven | Active | *pers. obs.* | -72.016929 | -3.429287039 | 1 291 |
| | | Flårjuven | Active | *pers. obs.* | -72.01632902 | -3.426523022 | 1 277 |
| | | Flårjuven | Active | *pers. obs.* | -72.01618896 | -3.397618029 | 1 318 |
| | | Flårjuven | Active | *pers. obs.* | -72.01628099 | -3.397088042 | 1 319 |
| | | Flårjuven | Active | *pers. obs.* | -72.01639599 | -3.395255003 | 1 317 |
| | | Flårjuven | Active | *pers. obs.* | -72.01217604 | -3.38543904 | 1 246 |
| | | Vassdalen | Active | *pers. obs.* | -72.03854199 | 2.631073035 | 1 244 |
| Gypsum | DML | Flårjuven | Active | *pers. obs.* | -72.02128071 | -3.4222076 | 1 297 |

| Feature | Site | Location | Active/Relict | Source | Latitude (DD) | Longitude (DD) | Altitude (m.a.s.l.) |
|---|---|---|---|---|---|---|---|
| | | Flårjuven | Active | *pers. obs.* | -72.01848191 | -3.42206276 | 1 293 |
| | | Flårjuven | Active | *pers. obs.* | -72.01624998 | -3.427093998 | 1 270 |
| | | Flårjuven | Active | *pers. obs.* | -72.01502102 | -3.423078982 | 1 294 |
| | | Flårjuven | Active | *pers. obs.* | -72.01552402 | -3.42442302 | 1 291 |
| | | Flårjuven | Active | *pers. obs.* | -72.015607 | -3.424500972 | 1 290 |
| | | Flårjuven | Active | *pers. obs.* | -72.01641401 | -3.42668999 | 1 279 |
| | | Flårjuven | Active | *pers. obs.* | -72.01565696 | -3.423309987 | 1 288 |
| | | Flårjuven | Active | *pers. obs.* | -72.01645098 | -3.390821982 | 1 317 |
| | | Flårjuven | Active | *pers. obs.* | -72.011953 | -3.384720962 | 1 248 |
| | | Flårjuven | Active | *pers. obs.* | -72.01538304 | -3.392268028 | 1 309 |
| | | Flårjuven | Active | *pers. obs.* | -72.01374002 | -3.416129965 | 1 280 |
| | | Flårjuven | Active | *pers. obs.* | -72.01542302 | -3.412760021 | 1 287 |
| | | Flårjuven | Active | *pers. obs.* | -72.01508699 | -3.413117006 | 1 292 |
| | | Flårjuven | Active | *pers. obs.* | -72.01389701 | -3.415993005 | 1 276 |
| | | Flårjuven | Active | *pers. obs.* | -72.01344699 | -3.417342994 | 1 284 |
| | | Flårjuven | Active | *pers. obs.* | -72.01341597 | -3.417426981 | 1 285 |
| | | Grunehogna | Active | *pers. obs.* | -72.04863333 | -2.716933333 | 1 067 |
| | | Slettfjell | Active | *pers. obs.* | -72.13653197 | -3.304775041 | 1 516 |
| | | Valterkulten | Active | *pers. obs.* | -71.8972096 | -3.2280502 | 1 068 |
| | | Valterkulten | Active | *pers. obs.* | -71.89664416 | -3.227113271 | 1 026 |
| | | Valterkulten | Active | *pers. obs.* | -71.89658649 | -3.226747066 | 1 030 |
| | | Valterkulten | Active | *pers. obs.* | -71.89705797 | -3.227709979 | 1 026 |
| | | Valterkulten | Active | *pers. obs.* | -71.89732603 | -3.227346037 | 1 020 |
| | | Valterkulten | Active | *pers. obs.* | -71.89705102 | -3.227223996 | 1 022 |
| Ice blister | DML | Grjotøyra | Active | *pers. obs.* | -72.03866667 | 2.530594444 | 1 310-1 345 |
| | | Robertskollen | Active | *pers. obs.* | -71.480 | -3.220 | 440 |

| Feature | Site | Location | Active/Relict | Source | Latitude (DD) | Longitude (DD) | Altitude (m.a.s.l.) |
|---|---|---|---|---|---|---|---|
| | | Vesleskarvet (Crystal Palace) | Active | *pers. obs.* | -71.66343611 | -2.852772222 | 750 |
| Imbrication | MI | Long Ridge South | Relict | (Holness and Boelhouwers, 1998) | -46.8847 | 37.7817 | 500 |
| | | Tafelberg area | Relict | (Haussmann et al., 2009b) | -46.8836 | 37.8117 | 300 |
| | DML | Flårjuven | Unknown | *pers. obs.* | -72.01496596 | -3.396352865 | 1 341 |
| | | Flårjuven | Unknown | *pers. obs.* | -72.01746527 | -3.419025075 | 1 294 |
| | | Flårjuven | Unknown | *pers. obs.* | -72.01420899 | -3.395381989 | 1 317 |
| | | Flårjuven | Unknown | *pers. obs.* | -72.01386399 | -3.395367991 | 1 316 |
| | | Flårjuven | Unknown | *pers. obs.* | -72.01616599 | -3.398415986 | 1 317 |
| | | Flårjuven | Unknown | *pers. obs.* | -72.01727098 | -3.43161704 | 1 295 |
| | | Flårjuven | Unknown | *pers. obs.* | -72.01736301 | -3.431195011 | 1 293 |
| | | Grunehogna | Active | *pers. obs.* | -72.04978333 | -2.716066667 | 1 071 |
| | | Grunehogna | Active | *pers. obs.* | -72.04875 | -2.71665 | 1 061 |
| Landslide | EC | Howison's Poort § | Relict | (Lewis, 2008b) | -31.10808889 | 27.731075 | ~ 485 |
| Lichen | DML | Flårjuven | Active | *pers. obs.* | -72.01646514 | -3.418279504 | 1 287 |
| | | Flårjuven | Active | *pers. obs.* | -72.01587179 | -3.417753372 | 1 289 |
| | | Flårjuven | Active | *pers. obs.* | -72.01561497 | -3.424506001 | 1 290 |
| | | Flårjuven | Active | *pers. obs.* | -72.01644402 | -3.427637983 | 1 278 |
| | | Flårjuven | Active | *pers. obs.* | -72.01568797 | -3.425185019 | 1 287 |
| | | Flårjuven | Active | *pers. obs.* | -72.01582904 | -3.417522032 | 1 285 |
| | | Flårjuven | Active | *pers. obs.* | -72.016411 | -3.391890004 | 1 316 |
| | | Flårjuven | Active | *pers. obs.* | -72.01648534 | -3.418430798 | 1 298 |
| | | Grjotøyra | Active | *pers. obs.* | -72.03428306 | 2.762943842 | 1 099 |
| | | Grjotøyra | Active | *pers. obs.* | -72.03823345 | 2.550284145 | 1 375 |

| Feature | Site | Location | Active/Relict | Source | Latitude (DD) | Longitude (DD) | Altitude (m.a.s.l.) |
|---|---|---|---|---|---|---|---|
| | | Grjotøyra | Active | *pers. obs.* | -72.03281782 | 2.542052027 | 1 271 |
| | | Grjotøyra | Active | *pers. obs.* | -72.03078202 | 2.549145967 | 1 271 |
| | | Grjotøyra | Active | *pers. obs.* | -72.03195901 | 2.540937904 | 1 291 |
| | | Grjotøyra | Active | *pers. obs.* | -72.03402087 | 2.532217791 | 1 284 |
| | | Grjotøyra | Active | *pers. obs.* | -72.03487633 | 2.530145282 | 1 285 |
| | | Grjotøyra | Active | *pers. obs.* | -72.03528713 | 2.529898351 | 1 288 |
| | | Grjotøyra | Active | *pers. obs.* | -72.03544504 | 2.529887203 | 1 289 |
| | | Grjotøyra | Active | *pers. obs.* | -72.03637359 | 2.529783016 | 1 287 |
| | | Grjotøyra | Active | *pers. obs.* | -72.03672295 | 2.531289412 | 1 288 |
| | | Grjotøyra | Active | *pers. obs.* | -72.03673963 | 2.531640194 | 1 290 |
| | | Grjotøyra | Active | *pers. obs.* | -72.03656025 | 2.533256812 | 1 287 |
| | | Grjotøyra | Active | *pers. obs.* | -72.03661867 | 2.533485554 | 1 290 |
| | | Grjotøyra | Active | *pers. obs.* | -72.03664105 | 2.53449834 | 1 288 |
| | | Grjotøyra | Active | *pers. obs.* | -72.03196219 | 2.540333066 | 1 288 |
| | | Grjotøyra | Active | *pers. obs.* | -72.03674901 | 2.534669666 | 1 289 |
| | | Grjotøyra | Active | *pers. obs.* | -72.03768033 | 2.535168473 | 1 293 |
| | | Grjotøyra | Active | *pers. obs.* | -72.03801359 | 2.536009513 | 1 300 |
| | | Grjotøyra | Active | *pers. obs.* | -72.03662756 | 2.54005068 | 1 297 |
| | | Grjotøyra | Active | *pers. obs.* | -72.03632036 | 2.539856974 | 1 293 |
| | | Grjotøyra | Active | *pers. obs.* | -72.03609807 | 2.53983493 | 1 292 |
| | | Grjotøyra | Active | *pers. obs.* | -72.03308897 | 2.541762181 | 1 288 |
| | | Grjotøyra | Active | *pers. obs.* | -72.0325843 | 2.541604936 | 1 288 |
| | | Grjotøyra | Active | *pers. obs.* | -72.03260416 | 2.541495217 | 1 287 |
| | | Grjotøyra | Active | *pers. obs.* | -72.03254649 | 2.542442204 | 1 285 |
| | | Grjotøyra | Active | *pers. obs.* | -72.03285788 | 2.536616027 | 1 286 |
| | | Grjotøyra | Active | *pers. obs.* | -72.03289342 | 2.546582865 | 1 289 |

| Feature | Site | Location | Active/Relict | Source | Latitude (DD) | Longitude (DD) | Altitude (m.a.s.l.) |
|---|---|---|---|---|---|---|---|
| | | Grjotøyra | Active | *pers. obs.* | -72.03288948 | 2.547364309 | 1 285 |
| | | Grjotøyra | Active | *pers. obs.* | -72.03299048 | 2.547607217 | 1 285 |
| | | Grjotøyra | Active | *pers. obs.* | -72.03715746 | 2.553614359 | 1 361 |
| | | Grjotøyra | Active | *pers. obs.* | -72.03752962 | 2.553954665 | 1 378 |
| | | Grjotøyra | Active | *pers. obs.* | -72.03498672 | 2.535792924 | 1 279 |
| | | Grjotøyra | Active | *pers. obs.* | -72.03289912 | 2.536520222 | 1 285 |
| | | Grjotøyra | Active | *pers. obs.* | -72.03350195 | 2.534676539 | 1 285 |
| | | Grjotøyra | Active | *pers. obs.* | -72.03363505 | 2.534353333 | 1 286 |
| | | Grjotøyra | Active | *pers. obs.* | -72.03390109 | 2.532883398 | 1 286 |
| | | Grjotøyra | Active | *pers. obs.* | -72.03396865 | 2.53266396 | 1 284 |
| | | Grjotøyra | Active | *pers. obs.* | -72.03397024 | 2.532425076 | 1 285 |
| | | Grjotøyra | Active | *pers. obs.* | -72.03379925 | 2.542185299 | 1 289 |
| | | Grjotøyra | Active | *pers. obs.* | -72.03171099 | 2.541986983 | 1 280 |
| | | Grjotøyra | Active | *pers. obs.* | -72.03421097 | 2.549029039 | 1 294 |
| | | Grjotøyra | Active | *pers. obs.* | -72.03449797 | 2.550139977 | 1 292 |
| | | Grjotøyra | Active | *pers. obs.* | -72.03517598 | 2.550956961 | 1 297 |
| | | Grjotøyra | Active | *pers. obs.* | -72.03659998 | 2.554364037 | 1 352 |
| | | Grjotøyra | Active | *pers. obs.* | -72.03693601 | 2.555031991 | 1 369 |
| | | Grjotøyra | Active | *pers. obs.* | -72.03704104 | 2.55488296 | 1 370 |
| | | Grjotøyra | Active | *pers. obs.* | -72.037048 | 2.55506401 | 1 372 |
| | | Grjotøyra | Active | *pers. obs.* | -72.03714103 | 2.554998966 | 1 374 |
| | | Grjotøyra | Active | *pers. obs.* | -72.03750397 | 2.554005962 | 1 382 |
| | | Grjotøyra | Active | *pers. obs.* | -72.03761302 | 2.55443302 | 1 387 |
| | | Grjotøyra | Active | *pers. obs.* | -72.03180503 | 2.542376993 | 1 282 |
| | | Grjotøyra | Active | *pers. obs.* | -72.03774604 | 2.554926965 | 1 396 |
| | | Grjotøyra | Active | *pers. obs.* | -72.037984 | 2.555973027 | 1 410 |

| Feature | Site | Location | Active/Relict | Source | Latitude (DD) | Longitude (DD) | Altitude (m.a.s.l.) |
|---|---|---|---|---|---|---|---|
| | | Grjotøyra | Active | *pers. obs.* | -72.03801099 | 2.556214007 | 1 412 |
| | | Grjotøyra | Active | *pers. obs.* | -72.038185 | 2.557052029 | 1 423 |
| | | Grjotøyra | Active | *pers. obs.* | -72.03842103 | 2.558268998 | 1 439 |
| | | Grjotøyra | Active | *pers. obs.* | -72.03842598 | 2.558426997 | 1 441 |
| | | Grjotøyra | Active | *pers. obs.* | -72.03813496 | 2.561146002 | 1 452 |
| | | Grjotøyra | Active | *pers. obs.* | -72.03961504 | 2.56393902 | 1 507 |
| | | Grjotøyra | Active | *pers. obs.* | -72.04009901 | 2.565233018 | 1 529 |
| | | Grjotøyra | Active | *pers. obs.* | -72.031799 | 2.542503979 | 1 283 |
| | | Grjotøyra | Active | *pers. obs.* | -72.03193403 | 2.542749988 | 1 285 |
| | | Grjotøyra | Active | *pers. obs.* | -72.03205498 | 2.54300396 | 1 285 |
| | | Grjotøyra | Active | *pers. obs.* | -72.03210804 | 2.543207975 | 1 286 |
| | | Grjotøyra | Active | *pers. obs.* | -72.032216 | 2.543555992 | 1 285 |
| | | Grjotøyra | Active | *pers. obs.* | -72.04001804 | 2.564729014 | 1 563 |
| | | Grjotøyra | Active | *pers. obs.* | -72.03294396 | 2.545673009 | 1 287 |
| | | Grjotøyra | Active | *pers. obs.* | -72.03311697 | 2.546014991 | 1 289 |
| | | Grjotøyra | Active | *pers. obs.* | -72.03228531 | 2.542038197 | 1 291 |
| | | Grjotøyra | Active | *pers. obs.* | -72.0329303 | 2.542001233 | 1 289 |
| | | Grjotøyra | Active | *pers. obs.* | -72.03305771 | 2.541765701 | 1 289 |
| | | Grjotøyra | Active | *pers. obs.* | -72.03455807 | 2.542429799 | 1 294 |
| | | Grjotøyra | Active | *pers. obs.* | -72.03982953 | 2.559216656 | 1 477 |
| | | Grjotøyra | Active | *pers. obs.* | -72.03997755 | 2.560836207 | 1 491 |
| | | Grjotøyra | Active | *pers. obs.* | -72.03998116 | 2.561583035 | 1 498 |
| | | Grjotøyra | Active | *pers. obs.* | -72.03116038 | 2.547177728 | 1 287 |
| | | Grjotøyra | Active | *pers. obs.* | -72.03154142 | 2.542534405 | 1 287 |
| | | Grjotøyra | Active | *pers. obs.* | -72.03156129 | 2.542520408 | 1 287 |
| | | Grjotøyra | Active | *pers. obs.* | -72.03179564 | 2.541974075 | 1 289 |

| Feature | Site | Location | Active/Relict | Source | Latitude (DD) | Longitude (DD) | Altitude (m.a.s.l.) |
|---|---|---|---|---|---|---|---|
| | | Grjotøyra | Active | *pers. obs.* | -72.03188424 | 2.541414583 | 1 289 |
| | | Grjotøyra | Active | *pers. obs.* | -72.03247843 | 2.541042427 | 1 286 |
| | | Grjotøyra | Active | *pers. obs.* | -72.0324206 | 2.541391198 | 1 284 |
| | | Grjotøyra | Active | *pers. obs.* | -72.01184663 | 2.534599928 | 1 291 |
| | | Robertskollen | Active | *pers. obs.* | -71.48806209 | -3.209913606 | 468 |
| | | Slettfjell | Active | *pers. obs.* | -72.1387546 | -3.299086997 | 1 497 |
| | | Slettfjell | Active | *pers. obs.* | -72.138523 | -3.293272639 | 1 481 |
| | | Troll | Active | *pers. obs.* | -72.04125596 | 2.493847031 | 1 506 |
| | | Valterkulten | Active | *pers. obs.* | -71.89727297 | -3.227585005 | 1 014 |
| | | Valterkulten | Active | *pers. obs.* | -71.89711397 | -3.226685962 | 1 029 |
| | | Valterkulten | Active | *pers. obs.* | -71.89655699 | -3.229341013 | 1 036 |
| | | Valterkulten | Active | *pers. obs.* | -71.89543901 | -3.224589983 | 1 082 |
| | | Vassdalen | Active | *pers. obs.* | -72.03750506 | 2.634931225 | 1 235 |
| | | Vassdalen | Active | *pers. obs.* | -72.04637211 | 2.629632354 | 1 342 |
| | | Vassdalen | Active | *pers. obs.* | -72.03548963 | 2.62724678 | 1 259 |
| | | Vassdalen | Active | *pers. obs.* | -72.04452901 | 2.631808966 | 1 322 |
| | | Vassdalen | Active | *pers. obs.* | -72.0445265 | 2.631827993 | 1 323 |
| | | Vassdalen | Active | *pers. obs.* | -72.04358948 | 2.630005013 | 1 314 |
| | | Vassdalen | Active | *pers. obs.* | -72.04321959 | 2.63000099 | 1 306 |
| | | Vassdalen | Active | *pers. obs.* | -72.03057884 | 2.629485084 | 1 223 |
| | | Vassdalen | Active | *pers. obs.* | -72.04181604 | 2.627044022 | 1 299 |
| | | Vassdalen | Active | *pers. obs.* | -72.03521797 | 2.628727024 | 1 250 |
| | | Vassdalen | Active | *pers. obs.* | -72.03323876 | 2.637356361 | 1 211 |
| | | Vassdalen | Active | *pers. obs.* | -72.03243988 | 2.636496127 | 1 215 |
| | | Vassdalen | Active | *pers. obs.* | -72.03412598 | 2.638974991 | 1 198 |
| | | Vassdalen | Active | *pers. obs.* | -72.02643885 | 2.649691924 | 1 150 |

| Feature | Site | Location | Active/Relict | Source | Latitude (DD) | Longitude (DD) | Altitude (m.a.s.l.) |
|---|---|---|---|---|---|---|---|
| | | Vassdalen | Active | *pers. obs.* | -72.02643885 | 2.649691924 | 1 150 |
| | | Vesleskarvet | Active | *pers. obs.* | -71.66980891 | -2.847480364 | 850 |
| | | Vesleskarvet | Active | *pers. obs.* | -71.66979139 | -2.84687737 | 846 |
| | | Vesleskarvet | Active | *pers. obs.* | -71.67076251 | -2.840341497 | 838 |
| | | Vesleskarvet | Active | *pers. obs.* | -71.67073972 | -2.839090163 | 837 |
| Mud boil | DML | Klovningen | Active | *pers. obs.* | -72.03829598 | 2.479630988 | 1 415 |
| | | Klovningen | Active | *pers. obs.* | -72.03829598 | 2.479630988 | 1 415 |
| | | Robertskollen | Active | *pers. obs.* | -71.48806821 | -3.210036149 | 446 |
| | | Valterkulten | Active | *pers. obs.* | -71.89727599 | -3.227351988 | 1 039 |
| | | Valterkulten | Active | *pers. obs.* | -71.89732402 | -3.22748702 | 1 029 |
| | | Valterkulten | Active | *pers. obs.* | -71.89730398 | -3.227559021 | 1 028 |
| | | Valterkulten | Active | *pers. obs.* | -71.89733097 | -3.227592967 | 1 027 |
| | | Valterkulten | Active | *pers. obs.* | -71.89728999 | -3.227609983 | 1 027 |
| | | Valterkulten | Active | *pers. obs.* | -71.89724497 | -3.227696987 | 1 027 |
| | | Valterkulten | Active | *pers. obs.* | -71.897235 | -3.227652982 | 1 027 |
| | | Valterkulten | Active | *pers. obs.* | -71.89721002 | -3.227691036 | 1 027 |
| | | Valterkulten | Active | *pers. obs.* | -71.89723198 | -3.22746397 | 1 025 |
| | | Valterkulten | Active | *pers. obs.* | -71.89725998 | -3.227378977 | 1 025 |
| | | Valterkulten | Active | *pers. obs.* | -71.89728797 | -3.227256015 | 1 038 |
| | | Valterkulten | Active | *pers. obs.* | -71.89728504 | -3.227229025 | 1 037 |
| | | Valterkulten | Active | *pers. obs.* | -71.89728697 | -3.227263978 | 1 035 |
| | | Valterkulten | Active | *pers. obs.* | -71.89731999 | -3.227316029 | 1 033 |
| | | Valterkulten | Active | *pers. obs.* | -71.89729803 | -3.227331033 | 1 031 |
| | | Valterkulten | Active | *pers. obs.* | -71.89732896 | -3.227379983 | 1 032 |
| | | Valterkulten | Active | *pers. obs.* | -71.89732804 | -3.227446033 | 1 029 |
| | | Valterkulten | Active | *pers. obs.* | -71.89733298 | -3.227443015 | 1 029 |

| Feature | Site | Location | Active/Relict | Source | Latitude (DD) | Longitude (DD) | Altitude (m.a.s.l.) |
|---|---|---|---|---|---|---|---|
| | | Valterkulten | Active | *pers. obs.* | -71.8833 | -3.2333 | 1 001 |
| | | Vassdalen | Active | *pers. obs.* | -72.02760494 | 2.659724308 | 1 128 |
| | | Vassdalen | Active | *pers. obs.* | -72.03333333 | 2.6465 | 1 149 |
| Needle Ice | EC | Ben MacDhui | Active | (Kück, 1997) | -30.64829167 | 27.93525556 | > 1 800 |
| | | High Lesotho Drakensberg | Active | (Grab, 2001) | -29.49013333 | 29.14902222 | > 2 750 |
| | | KwaZulu Natal Drakensberg | Active | (Boelhouwers, 1991) | -29.49013333 | 29.14902222 | up to 3 842 |
| | | Tlaeeng Pass, Lesotho Highlands | Active | (Hanvey and Marker, 1992) | -28.81184167 | 28.73378056 | 3 275 |
| | MI | First Red Hill (Cinder cone) | Active | (Holness, 2004) | -46.8936 | 37.785 | 550 |
| | | Junior's Kop | Active | (Boelhouwers et al., 2000) | -46.8833 | 37.8303 | 306 |
| | | Junior's Kop (Cinder cone) | Active | (Holness, 2004) | -46.8833 | 37.8303 | 200 |
| | | Katedraalkrans | Active | (Borg, 2017) | -46.8967 | 37.7761 | ~ 750 |
| | | Katedraalkrans Nek (Cinder cone) | Active | (Holness, 2004) | -46.8967 | 37.7761 | 750 |
| | | Katedraalkrans via First Red past Tafelberg | Active | *pers. obs.* | -46.8947 | 37.7492 | 120-750 |
| | | Ned's Kop | Active | (Hedding, 2006) | -46.8983 | 37.7656 | ~ 800 |
| | | Ned's Hill (Cinder cone) | Active | (Holness, 2004) | -46.8983 | 37.7656 | 750 |
| | | Tafelberg | Active | (Haussmann et al., 2009a) | -46.8836 | 37.8117 | 300 |
| | | Twisted Sister (Cinder cone) | Active | (Holness, 2004) | -46.86276944 | 37.81764167 | 150 |
| | DML | Vesleskarvet nunataks | Active | (Hedding et al., 2010) | -71.674 | -2.85 | 856 |

| Feature | Site | Location | Active/Relict | Source | Latitude (DD) | Longitude (DD) | Altitude (m.a.s.l.) |
|---|---|---|---|---|---|---|---|
| Non-sorted circle | EC | KwaZulu Natal Drakensberg | Active | (Boelhouwers, 1991, 1994) | -29.49013333 | 29.14902222 | up to 3 842 |
| | | Tlaeeng Pass, Lesotho Highlands | Active | (Hanvey and Marker, 1992) | -28.81184167 | 28.73378056 | 3 275 |
| Non-sorted polygon | EC | Ben MacDhui | Active | (Kück, 1997) | -30.64829167 | 27.93525556 | > 2 755 |
| | | Mafadi Summit | Active | (Grab, 1997b) | -29.18191667 | 29.32774167 | 3 410 |
| | | Tlaeeng Pass, Lesotho Highlands | Active | (Hanvey and Marker, 1992; Grab, 1997b, 2005) | -28.81184167 | 28.73378056 | 3 275 |
| | MI | Central Highland | Relict | (Hedding, 2008) | -46.8972 | 37.7136 | 950 |
| | | Central Highland | Active | (Sumner and Meiklejohn, 2004) | -46.8972 | 37.7136 | 750 |
| | DML | Brugdedalen | Unknown | (Rudolph, 2015) | -72.03992 | 2.7820833 | 1 325 |
| | | Flårjuven | Unknown | *pers. obs.* | -72.01191667 | -3.384555556 | 1 247 |
| | | Flårjuven | Unknown | *pers. obs.* | -72.01177778 | -3.384388889 | 1 242 |
| | | Flårjuven | Unknown | *pers. obs.* | -72.01172222 | -3.383861111 | 1 242 |
| | | Flårjuven | Unknown | *pers. obs.* | -72.01158333 | -3.384111111 | 1 242 |
| | | Flårjuven | Unknown | *pers. obs.* | -72.01155556 | -3.384416667 | 1 242 |
| | | Flårjuven | Unknown | *pers. obs.* | -72.01220202 | -3.382687513 | 1 256 |
| | | Flårjuven | Unknown | *pers. obs.* | -72.01209054 | -3.382800417 | 1 253 |
| | | Flårjuven | Unknown | *pers. obs.* | -72.01190606 | -3.382811313 | 1 253 |
| | | Flårjuven | Unknown | *pers. obs.* | -72.0118592 | -3.382949531 | 1 255 |
| | | Flårjuven | Unknown | *pers. obs.* | -72.01203086 | -3.383820998 | 1 250 |
| | | Flårjuven | Unknown | *pers. obs.* | -72.01196305 | -3.383780764 | 1 250 |
| | | Flårjuven | Unknown | *pers. obs.* | -72.01194176 | -3.384207655 | 1 250 |
| | | Flårjuven | Unknown | *pers. obs.* | -72.0119758 | -3.384434301 | 1 249 |
| | | Flårjuven | Unknown | *pers. obs.* | -72.01190153 | -3.384138085 | 1 252 |

| Feature | Site | Location | Active/Relict | Source | Latitude (DD) | Longitude (DD) | Altitude (m.a.s.l.) |
|---|---|---|---|---|---|---|---|
| | | Flårjuven | Unknown | *pers. obs.* | -72.01183749 | -3.383892663 | 1 252 |
| | | Flårjuven | Unknown | *pers. obs.* | -72.011939 | -3.384777959 | 1 248 |
| | | Flårjuven | Unknown | *pers. obs.* | -72.01196297 | -3.384874016 | 1 247 |
| | | Flårjuven | Unknown | *pers. obs.* | -72.01190304 | -3.384623984 | 1 248 |
| | | Flårjuven | Unknown | *pers. obs.* | -72.01188896 | -3.38491098 | 1 249 |
| | | Flårjuven | Unknown | *pers. obs.* | -72.01182299 | -3.385139974 | 1 247 |
| | | Flårjuven | Unknown | *pers. obs.* | -72.01177203 | -3.385170987 | 1 247 |
| | | Flårjuven | Unknown | *pers. obs.* | -72.01186398 | -3.384705959 | 1 250 |
| | | Flårjuven | Unknown | *pers. obs.* | -72.01180204 | -3.384447042 | 1 249 |
| | | Flårjuven | Unknown | *pers. obs.* | -72.01175904 | -3.384437989 | 1 249 |
| | | Flårjuven | Unknown | *pers. obs.* | -72.01176197 | -3.384331036 | 1 248 |
| | | Flårjuven | Unknown | *pers. obs.* | -72.01175996 | -3.384307986 | 1 248 |
| | | Flårjuven | Unknown | *pers. obs.* | -72.01164496 | -3.38421897 | 1 247 |
| | | Flårjuven | Unknown | *pers. obs.* | -72.011694 | -3.384081004 | 1 247 |
| | | Flårjuven | Unknown | *pers. obs.* | -72.01163096 | -3.384311004 | 1 248 |
| | | Flårjuven | Unknown | *pers. obs.* | -72.01156701 | -3.384250989 | 1 247 |
| | | Flårjuven | Unknown | *pers. obs.* | -72.01157598 | -3.384159962 | 1 247 |
| | | Flårjuven | Unknown | *pers. obs.* | -72.01156198 | -3.383810017 | 1 247 |
| | | Flårjuven | Unknown | *pers. obs.* | -72.01164496 | -3.383996012 | 1 246 |
| | | Flårjuven | Unknown | *pers. obs.* | -72.01164597 | -3.383809011 | 1 247 |
| | | Flårjuven | Unknown | *pers. obs.* | -72.01170397 | -3.383685965 | 1 247 |
| | | Flårjuven | Unknown | *pers. obs.* | -72.01170196 | -3.38376903 | 1 242 |
| | | Flårjuven | Unknown | *pers. obs.* | -72.01176298 | -3.383980002 | 1 247 |
| | | Grjotlia | Unknown | (Rudolph, 2015) | -72.017 | 2.5666666 | 1 602 |
| | | Grjotøyra | Unknown | *pers. obs.* | -72.02721 | 2.66775 | 1 132 |
| | | Grjotøyra | Unknown | *pers. obs.* | -72.02726 | 2.66794 | 1 133 |

| Feature | Site | Location | Active/Relict | Source | Latitude (DD) | Longitude (DD) | Altitude (m.a.s.l.) |
|---|---|---|---|---|---|---|---|
| | | Grjotøyra | Unknown | *pers. obs.* | -72.02731 | 2.66828 | 1 135 |
| | | Grjotøyra | Unknown | *pers. obs.* | -72.02739 | 2.66844 | 1 137 |
| | | Grjotøyra | Unknown | *pers. obs.* | -72.02746 | 2.66872 | 1 140 |
| | | Grjotøyra | Unknown | *pers. obs.* | -72.02744 | 2.66913 | 1 142 |
| | | Grjotøyra | Unknown | *pers. obs.* | -72.02771 | 2.67012 | 1 153 |
| | | Grjotøyra | Unknown | *pers. obs.* | -72.02777 | 2.67055 | 1 157 |
| | | Grjotøyra | Unknown | *pers. obs.* | -72.02777 | 2.67094 | 1 157 |
| | | Grjotøyra | Unknown | *pers. obs.* | -72.02783 | 2.67106 | 1 160 |
| | | Grjotøyra | Unknown | *pers. obs.* | -72.02757 | 2.67178 | 1 157 |
| | | Grjotøyra | Unknown | *pers. obs.* | -72.02749 | 2.67170 | 1 156 |
| | | Grjotøyra | Unknown | *pers. obs.* | -72.02741 | 2.67161 | 1 154 |
| | | Grjotøyra | Unknown | *pers. obs.* | -72.02735 | 2.67145 | 1 150 |
| | | Grjotøyra | Unknown | *pers. obs.* | -72.02729 | 2.67121 | 1 148 |
| | | Grjotøyra | Unknown | *pers. obs.* | -72.02726 | 2.67104 | 1 147 |
| | | Grjotøyra | Unknown | *pers. obs.* | -72.02725 | 2.67085 | 1 142 |
| | | Grjotøyra | Unknown | *pers. obs.* | -72.02725 | 2.67052 | 1 144 |
| | | Grjotøyra | Unknown | *pers. obs.* | -72.02720 | 2.67027 | 1 141 |
| | | Grjotøyra | Unknown | *pers. obs.* | -72.02719 | 2.66988 | 1 137 |
| | | Grunehogna | Unknown | *pers. obs.* | -72.049 | -2.793 | 1 390 |
| | | Grunehogna | Unknown | *pers. obs.* | -72.04936111 | -2.791055556 | 1 546 |
| | | Grunehogna | Unknown | *pers. obs.* | -72.04925 | -2.7905 | 1 534 |
| | | Grunehogna | Unknown | *pers. obs.* | -72.04969444 | -2.790722222 | 1 521 |
| | | Grunehogna | Unknown | *pers. obs.* | -72.04994444 | -2.791 | 1 515 |
| | | Grunehogna | Unknown | *pers. obs.* | -72.05016667 | -2.790583333 | 1 509 |
| | | Grunehogna | Unknown | *pers. obs.* | -72.05047222 | -2.789388889 | 1 499 |
| | | Grunehogna | Unknown | *pers. obs.* | -72.05047222 | -2.788638889 | 1 493 |

| Feature | Site | Location | Active/Relict | Source | Latitude (DD) | Longitude (DD) | Altitude (m.a.s.l.) |
|---|---|---|---|---|---|---|---|
| | | Grunehogna | Unknown | *pers. obs.* | -72.04944444 | -2.788583333 | 1 479 |
| | | Grunehogna | Unknown | *pers. obs.* | -72.04933333 | -2.788583333 | 1 479 |
| | | Grunehogna | Unknown | *pers. obs.* | -72.04927778 | -2.78825 | 1 476 |
| | | Mimelia | Active | (Dallmann et al., 1990; Lee et al., 2013; Hansen et al., 2014) | -72.00661111 | 2.579444444 | 1 130-1 350 |
| | | Mimelia | Active | *pers. obs.* | -72.00230 | 2.57181 | 1 175 |
| | | Mimelia | Active | *pers. obs.* | -72.01160 | 2.55204 | 1 500 |
| | | Mimelia | Active | *pers. obs.* | -72.00540 | 2.57058 | 1 256 |
| | | Mimelia | Active | *pers. obs.* | -72.01070 | 2.55609 | 1 482 |
| | | Mimelia | Active | *pers. obs.* | -72.00260 | 2.54384 | 2 060 |
| | | Mimelia | Active | *pers. obs.* | -72.00200 | 2.57427 | 2 020 |
| | | Mimelia | Active | *pers. obs.* | -72.00680 | 2.55649 | 1 353 |
| | | Mimelia | Active | *pers. obs.* | -72.00320 | 2.55321 | 2 040 |
| | | Mimelia | Active | *pers. obs.* | -72.01160 | 2.55134 | 1 504 |
| | | Mimelia | Active | *pers. obs.* | -72.01090 | 2.54870 | 1 329 |
| | | Mimelia | Active | *pers. obs.* | -72.00310 | 2.58218 | 2 030 |
| | | Mimelia | Active | *pers. obs.* | -72.00344 | 2.54722 | 2 050 |
| | | Mimelia | Active | *pers. obs.* | -72.00240 | 2.57283 | 2 030 |
| | | Mimelia | Active | *pers. obs.* | -72.00750 | 2.54462 | 1 318 |
| | | Mimelia | Active | *pers. obs.* | -71.99875 | 2.57969 | 2 030 |
| | | Mimelia | Active | *pers. obs.* | -72.00620 | 2.54653 | 1 303 |
| | | Mimelia | Active | *pers. obs.* | -72.00072 | 2.57100 | 2 100 |
| | | Mimelia | Active | *pers. obs.* | -72.01110 | 2.55255 | 1 495 |
| | | Mimelia | Active | *pers. obs.* | -72.00950 | 2.56036 | 1 457 |
| | | Mimelia | Active | *pers. obs.* | -72.00781 | 2.54369 | 1 322 |

| Feature | Site | Location | Active/Relict | Source | Latitude (DD) | Longitude (DD) | Altitude (m.a.s.l.) |
|---|---|---|---|---|---|---|---|
| | | Mimelia | Active | *pers. obs.* | -72.00850 | 2.56247 | 1 430 |
| | | Mimelia | Active | *pers. obs.* | -72.00210 | 2.55843 | 2 100 |
| | | Mimelia | Active | *pers. obs.* | -72.00367 | 2.53889 | 2 030 |
| | | Mimelia | Active | *pers. obs.* | -72.01270 | 2.54667 | 1 469 |
| | | Mimelia | Active | *pers. obs.* | -72.00230 | 2.55668 | 2 100 |
| | | Mimelia | Active | *pers. obs.* | -72.00600 | 2.54094 | 2 020 |
| | | Mimelia | Active | *pers. obs.* | -72.00300 | 2.57940 | 2 040 |
| | | Mimelia | Active | *pers. obs.* | -72.01070 | 2.55223 | 1 477 |
| | | Mimelia | Active | *pers. obs.* | -72.00850 | 2.56985 | 1 356 |
| | | Mimelia | Active | *pers. obs.* | -72.00360 | 2.55253 | 2 020 |
| | | Mimelia | Unknown | *pers. obs.* | -72.00215 | 2.55972 | 1 136 |
| | | Mimelia | Unknown | *pers. obs.* | -72.00229 | 2.55993 | 1 132 |
| | | Mimelia | Unknown | *pers. obs.* | -72.00229 | 2.56032 | 1 134 |
| | | Mimelia | Unknown | *pers. obs.* | -72.00233 | 2.56081 | 1 135 |
| | | Mimelia | Unknown | *pers. obs.* | -72.00246 | 2.56149 | 1 139 |
| | | Mimelia | Unknown | *pers. obs.* | -72.00245 | 2.56149 | 1 139 |
| | | Mimelia | Unknown | *pers. obs.* | -72.00254 | 2.56214 | 1 141 |
| | | Mimelia | Unknown | *pers. obs.* | -72.00252 | 2.56216 | 1 142 |
| | | Mimelia | Unknown | *pers. obs.* | -72.00253 | 2.56244 | 1 144 |
| | | Mimelia | Unknown | *pers. obs.* | -72.00258 | 2.56252 | 1 147 |
| | | Mimelia | Unknown | *pers. obs.* | -72.00260 | 2.56270 | 1 147 |
| | | Mimelia | Unknown | *pers. obs.* | -72.00265 | 2.56296 | 1 148 |
| | | Mimelia | Unknown | *pers. obs.* | -72.00277 | 2.56319 | 1 152 |
| | | Mimelia | Unknown | *pers. obs.* | -72.00277 | 2.56347 | 1 154 |
| | | Mimelia | Unknown | *pers. obs.* | -72.00279 | 2.56366 | 1 156 |
| | | Mimelia | Unknown | *pers. obs.* | -72.00281 | 2.56390 | 1 157 |

| Feature | Site | Location | Active/Relict | Source | Latitude (DD) | Longitude (DD) | Altitude (m.a.s.l.) |
|---|---|---|---|---|---|---|---|
| | | Mimelia | Unknown | *pers. obs.* | -72.00294 | 2.56409 | 1 159 |
| | | Mimelia | Unknown | *pers. obs.* | -72.00298 | 2.56433 | 1 161 |
| | | Mimelia | Unknown | *pers. obs.* | -72.00308 | 2.56456 | 1 165 |
| | | Mimelia | Unknown | *pers. obs.* | -72.00311 | 2.56487 | 1 168 |
| | | Mimelia | Unknown | *pers. obs.* | -72.00321 | 2.56508 | 1 170 |
| | | Mimelia | Unknown | *pers. obs.* | -72.00329 | 2.56535 | 1 173 |
| | | Mimelia | Unknown | *pers. obs.* | -72.00332 | 2.56573 | 1 177 |
| | | Mimelia | Unknown | *pers. obs.* | -72.00335 | 2.56593 | 1 179 |
| | | Mimelia | Unknown | *pers. obs.* | -72.00337 | 2.56635 | 1 181 |
| | | Mimelia | Unknown | *pers. obs.* | -72.00926 | 2.55930 | 1 337 |
| | | Mimelia | Unknown | *pers. obs.* | -72.00912 | 2.56025 | 1 326 |
| | | Mimelia | Unknown | *pers. obs.* | -72.00923 | 2.56082 | 1 337 |
| | | Mimelia | Unknown | *pers. obs.* | -72.00906 | 2.56171 | 1 339 |
| | | Mimelia | Unknown | *pers. obs.* | -72.00896 | 2.56223 | 1 339 |
| | | Mimelia | Unknown | *pers. obs.* | -72.00873 | 2.56289 | 1 331 |
| | | Mimelia | Unknown | *pers. obs.* | -72.00859 | 2.56368 | 1 332 |
| | | Mimelia | Unknown | *pers. obs.* | -72.00851 | 2.56439 | 1 326 |
| | | Mimelia | Unknown | *pers. obs.* | -72.00851 | 2.56509 | 1 327 |
| | | Mimelia | Unknown | *pers. obs.* | -72.00814 | 2.56637 | 1 325 |
| | | Nonshøgda | Unknown | (Dallmann et al., 1990) | -72 | 2.516666667 | 1 331 |
| | | Northern Buttress, Vesleskarvet | Unknown | *pers. obs.* | -71.668 | -2.852 | 856 |
| | | Slettfjell | Unknown | *pers. obs.* | -72.155 | -3.238 | 1 435 |
| | | Slettfjell | Unknown | *pers. obs.* | -72.13806401 | -3.299597958 | 1 511 |
| | | Slettfjell | Unknown | *pers. obs.* | -72.13806996 | -3.299469966 | 1 509 |
| | | Slettfjell | Unknown | *pers. obs.* | -72.13802897 | -3.299737014 | 1 508 |

| Feature | Site | Location | Active/Relict | Source | Latitude (DD) | Longitude (DD) | Altitude (m.a.s.l.) |
|---|---|---|---|---|---|---|---|
| | | Slettfjell | Unknown | *pers. obs.* | -72.13804004 | -3.299930971 | 1 509 |
| | | Slettfjell | Unknown | *pers. obs.* | -72.13776402 | -3.299685968 | 1 506 |
| | | Slettfjell | Unknown | *pers. obs.* | -72.13783803 | -3.299176013 | 1 506 |
| | | Slettfjell | Unknown | *pers. obs.* | -72.137875 | -3.299194034 | 1 506 |
| | | Slettfjell | Unknown | *pers. obs.* | -72.13786603 | -3.298436981 | 1 504 |
| | | Slettfjell | Unknown | *pers. obs.* | -72.13773997 | -3.298198013 | 1 503 |
| | | Slettfjell | Unknown | *pers. obs.* | -72.13811296 | -3.299121028 | 1 504 |
| | | Slettfjell | Unknown | *pers. obs.* | -72.13663599 | -3.301685974 | 1 505 |
| | | Slettfjell | Unknown | *pers. obs.* | -72.136754 | -3.300806042 | 1 502 |
| | | Slettfjell | Unknown | *pers. obs.* | -72.13671796 | -3.300788021 | 1 501 |
| | | Slettfjell | Unknown | *pers. obs.* | -72.13667303 | -3.300705962 | 1 501 |
| | | Slettfjell | Unknown | *pers. obs.* | -72.13671503 | -3.300520973 | 1 501 |
| | | Slettfjell | Unknown | *pers. obs.* | -72.13674797 | -3.300557015 | 1 501 |
| | | Slettfjell | Unknown | *pers. obs.* | -72.13678401 | -3.300622981 | 1 502 |
| | | Slettfjell | Unknown | *pers. obs.* | -72.136797 | -3.300679978 | 1 501 |
| | | Slettfjell | Unknown | *pers. obs.* | -72.13682198 | -3.301085997 | 1 502 |
| | | Slettfjell | Unknown | *pers. obs.* | -72.13678401 | -3.301132014 | 1 502 |
| | | Slettfjell | Unknown | *pers. obs.* | -72.13741601 | -3.300171029 | 1 497 |
| | | Slettfjell | Unknown | *pers. obs.* | -72.13741198 | -3.300316036 | 1 497 |
| | | Slettfjell | Unknown | *pers. obs.* | -72.13739798 | -3.300437992 | 1 497 |
| | | Slettfjell | Unknown | *pers. obs.* | -72.13746403 | -3.300416032 | 1 497 |
| | | Slettfjell | Unknown | *pers. obs.* | -72.13746697 | -3.300130041 | 1 497 |
| | | Troll | Unknown | *pers. obs.* | -72.04018601 | 2.489146963 | 1 499 |
| | | Troll | Unknown | *pers. obs.* | -72.01094147 | 2.54359086 | 1 414 |
| | | Troll | Unknown | *pers. obs.* | -72.01103660 | 2.54401683 | 1 418 |
| | | Troll | Unknown | *pers. obs.* | -72.01145461 | 2.54387274 | 1 427 |

| Feature | Site | Location | Active/Relict | Source | Latitude (DD) | Longitude (DD) | Altitude (m.a.s.l.) |
|---|---|---|---|---|---|---|---|
| | | Troll | Unknown | *pers. obs.* | -72.01159400 | 2.54271948 | 1 422 |
| | | Troll | Unknown | *pers. obs.* | -72.01183422 | 2.54234145 | 1 423 |
| | | Troll | Unknown | *pers. obs.* | -72.01185912 | 2.54117696 | 1 298 |
| | | Troll | Unknown | *pers. obs.* | -72.01213296 | 2.54073758 | 1 416 |
| | | Troll | Unknown | *pers. obs.* | -72.01230705 | 2.54024480 | 1 414 |
| | | Valterkulten | Unknown | (Marshall et al., 1995) | -71.894 | -3.235 | 1 006 |
| | | Valterkulten | Unknown | *pers. obs.* | -71.89418483 | -3.22928544 | 1 014 |
| | | Valterkulten | Unknown | *pers. obs.* | -71.89417653 | -3.22976120 | 1 015 |
| | | Valterkulten | Unknown | *pers. obs.* | -71.89424224 | -3.22970764 | 1 015 |
| | | Valterkulten | Unknown | *pers. obs.* | -71.89469797 | -3.23113088 | 1 019 |
| | | Valterkulten | Unknown | *pers. obs.* | -71.89565174 | -3.23216463 | 1 004 |
| | | Valterkulten | Unknown | *pers. obs.* | -71.89533097 | -3.23402692 | 815 |
| | | Valterkulten | Unknown | *pers. obs.* | -71.89537078 | -3.23380019 | 846 |
| | | Valterkulten | Unknown | *pers. obs.* | -71.89544094 | -3.23401124 | 1 004 |
| | | Valterkulten | Unknown | *pers. obs.* | -71.89577320 | -3.23434426 | 817 |
| | | Valterkulten | Unknown | *pers. obs.* | -71.89608484 | -3.23386892 | 995 |
| | | Valterkulten | Unknown | *pers. obs.* | -71.89668431 | -3.23379289 | 987 |
| | | Valterkulten | Unknown | *pers. obs.* | -71.89661415 | -3.23380999 | 988 |
| | | Vassdalen | Unknown | (Rudolph, 2015) | -72.03333333 | 2.6465 | 1 163 |
| Non-sorted step/terrace | EC | Mafadi Valley, Lesotho Drakensberg | Active | (Grab, 1997b, 2005) | -29.18191667 | 29.32774167 | 3 400 |
| | DML | Flårjuven | Unknown | *pers. obs.* | -72.01694434 | -3.418594832 | 1 295 |
| | | Flårjuven | Unknown | *pers. obs.* | -72.01676697 | -3.428975986 | 1 287 |
| | | Flårjuven | Unknown | *pers. obs.* | -72.01666002 | -3.428755039 | 1 286 |
| | | Flårjuven | Unknown | *pers. obs.* | -72.01657402 | -3.428701982 | 1 282 |

| Feature | Site | Location | Active/Relict | Source | Latitude (DD) | Longitude (DD) | Altitude (m.a.s.l.) |
|---|---|---|---|---|---|---|---|
| | | Flårjuven | Unknown | *pers. obs.* | -72.01652097 | -3.428382967 | 1 281 |
| | | Flårjuven | Unknown | *pers. obs.* | -72.01650102 | -3.42827199 | 1 279 |
| | | Flårjuven | Unknown | *pers. obs.* | -72.01648702 | -3.428040985 | 1 277 |
| | | Flårjuven | Unknown | *pers. obs.* | -72.01647696 | -3.427888015 | 1 274 |
| | | Flårjuven | Unknown | *pers. obs.* | -72.01690796 | -3.429261977 | 1 291 |
| | | Klovningen | Unknown | *pers. obs.* | -72.03989298 | 2.484128969 | 1 385 |
| | | Klovningen | Unknown | *pers. obs.* | -72.03993296 | 2.484281017 | 1 384 |
| | | Klovningen | Unknown | *pers. obs.* | -72.03997303 | 2.484445972 | 1 383 |
| | | Klovningen | Unknown | *pers. obs.* | -72.03994998 | 2.484782003 | 1 382 |
| | | Klovningen | Unknown | *pers. obs.* | -72.03995802 | 2.484850986 | 1 381 |
| | | Klovningen | Unknown | *pers. obs.* | -72.03997001 | 2.484947965 | 1 380 |
| | | Klovningen | Unknown | *pers. obs.* | -72.03996498 | 2.485344009 | 1 377 |
| | | Valterkulten | Unknown | *pers. obs.* | -71.89657627 | -3.226853432 | 1 030 |
| | | Valterkulten | Unknown | *pers. obs.* | -71.89665983 | -3.226911686 | 1 028 |
| | | Valterkulten | Unknown | *pers. obs.* | -71.89675187 | -3.226978406 | 1 024 |
| | | Valterkulten | Unknown | *pers. obs.* | -71.89682093 | -3.227072284 | 1 022 |
| | | Valterkulten | Unknown | *pers. obs.* | -71.89689294 | -3.22712115 | 1 020 |
| | | Valterkulten | Unknown | *pers. obs.* | -71.893 | -3.229 | 1 006 |
| | | Vassdalen | Unknown | *pers. obs.* | -72.02834398 | 2.654929021 | 1 139 |
| | | Vassdalen | Unknown | *pers. obs.* | -72.02709398 | 2.656257972 | 1 124 |
| Pitting | DML | Flårjuven | Unknown | *pers. obs.* | -72.01520752 | -3.396777743 | 1 337 |
| Pronival (protalus) rampart | EC | Mount Enterprise farm (between Ugie & Barkly East) § | Relict | (Lewis, 2008a) | -31.10808889 | 27.731075 | ~ 2 160 |
| | | Kilmore § | Relict | (Lewis, 1994; Lewis et al., 1994) | -30.95 | 27.95 | ~ 2 000 |

| Feature | Site | Location | Active/Relict | Source | Latitude (DD) | Longitude (DD) | Altitude (m.a.s.l.) |
|---|---|---|---|---|---|---|---|
| | MI | Black Haglet Valley | Active | (Hedding et al., 2007) | -46.90958333 | 37.75388889 | 900 |
| | | Central Highland (Delta Kop) | Active | (Hedding, 2008) | -46.8972 | 37.7136 | ~ 1 000 |
| | | Snok cirque backwall | Relict | (Boelhouwers et al., 2008) | -46.9444 | 37.7756 | 550-600 |
| | DML | Grunehogna | Active | (Hedding et al., 2010) | -72.041 | -2.763 | 1 390 |
| Rock glacier | EC | Bottlenek Valley, Barkly East § | Relict | (Lewis and Hanvey, 1993; Lewis et al., 1994; Lewis, 2005) | -31.10808889 | 27.731075 | ~ 1 840 |
| | DML | Brugdedalen | Relict | (Rudolph, 2015) | -72.04913056 | 2.783266667 | 1 500 |
| | | Grjotlia | Relict | (Rudolph, 2015) | -72.02551389 | 2.559438889 | 1 530 |
| | | Grjotøyra | Relict | (Dallmann et al., 1990; Rudolph, 2015) | -72.03884722 | 2.538944444 | 1 475 |
| | | Jutuldalen | Active | (Rudolph, 2015) | -71.99726389 | 2.812338889 | 1 340 |
| | | Vassdalen | Relict | (Rudolph, 2015) | -72.03175833 | 2.616916667 | 1 260 |
| Solifluction terrace/head deposit/frost creep | EC | Ben MacDhui | Active | (Kück, 1997) | -30.64829167 | 27.93525556 | 2 755-2 765 |
| | | Bottlenek Valley, Barkly East § | Relict | (Lewis, 2008a) | -31.10808889 | 27.731075 | ~ 1 840 |
| | | Buttermead farm § | Relict | (Lewis, 2008a) | -31.002175 | 27.60756944 | ~ 1 800 |
| | | Dynevor Park § | Relict | (Lewis, 2008a) | -31.17788889 | 27.75901389 | ~ 1 980 |
| | | Giant's Castle | Active | (Boelhouwers, 1991, 1994) | -29.345075 | 29.48149167 | 3 140-3 300 |
| | | Kilchurn § | Active | (Lewis et al., 1994) | -31.12474167 | 27.91842222 | 1 920 |
| | MI | Bill Briggs (Long Ridge) | Relict | (Holness and Boelhouwers, 1998) | -46.8658 | 37.8011 | 350 |

| Feature | Site | Location | Active/Relict | Source | Latitude (DD) | Longitude (DD) | Altitude (m.a.s.l.) |
|---|---|---|---|---|---|---|---|
| | | Central Highland; No Name Peak | Relict | (Hedding, 2006, 2008) | -46.8972 | 37.7136 | > 750; ~ 950 |
| | | Long Ridge South | Relict | (Holness and Boelhouwers, 1998) | -46.8847 | 37.7817 | 500 |
| | | Mixed Pickle High | Unknown | *pers. obs.* | -46.89738889 | 37.65461111 | 600 |
| | | Tafelberg | Relict | (Holness and Boelhouwers, 1998; Boelhouwers et al., 2008) | -46.8836 | 37.8117 | 300 |
| | DML | Flårjuven | Unknown | *pers. obs.* | -72.006 | -3.393 | 1 359 |
| | | Valterkulten | Unknown | *pers. obs.* | -71.852 | -3.305 | 1 060 |
| Sorted circle | EC | KwaZulu Natal Drakensberg | Active | (Boelhouwers, 1991, 1994) | -29.345075 | 29.48149167 | 3 140-3 300 |
| | | Mashai Valley, Lesotho Drakensberg § | Relict | (Grab, 1997b) | -29.69157778 | 29.03261944 | 2 950 |
| | | Tlaeeng Pass, Lesotho Highlands | Active | (Hanvey and Marker, 1992) | -28.81184167 | 28.73378056 | 3 275 |
| | MI | At all altitudes, excluding the coastal area | Active | (Boelhouwers et al., 2003) | -46.8947 | 37.7492 | All altitudes |
| | | Beret Hill | Active | (Holness, 2003a) | -46.9342 | 37.7681 | 750 |
| | | Delta Extension | Active | (Boelhouwers et al., 2003) | -46.9072 | 37.7544 | 1 000 |
| | | Eduard | Active | (Holness, 2003a) | -46.8653 | 37.7728 | 350 |
| | | Fred's Hill | Active | (Boelhouwers et al., 2003) | -46.9086 | 37.8389 | 290 |

| Feature | Site | Location | Active/Relict | Source | Latitude (DD) | Longitude (DD) | Altitude (m.a.s.l.) |
|---|---|---|---|---|---|---|---|
| | | Greyheaded-Albatross Ridge | Active | (Boelhouwers et al., 2003; Holness, 2003a) | -46.9561 | 37.7056 | 100 |
| | | Hansen Point | Active | (Boelhouwers et al., 2003) | -46.9128 | 37.8958 | 10 |
| | | Kildalkey Bay | Active | (Boelhouwers et al., 2003; Holness, 2003a) | -46.9664 | 37.8575 | 70 |
| | | Long Ridge North | Active | (Boelhouwers et al., 2003; Holness, 2003a) | -46.8697 | 37.7869 | 200 |
| | | Long Ridge South | Active | (Boelhouwers et al., 2003; Holness, 2003a) | -46.8847 | 37.7817 | 500 |
| | | Repettos Hill | Active | (Holness, 2003a) | -46.8422 | 37.7458 | 300 |
| | | Skua Ridge | Active | (Boelhouwers et al., 2003; Holness, 2003a) | -46.8656 | 37.8492 | 90 |
| | | Stoney Ridge | Active | (Boelhouwers et al., 2003; Holness, 2003a) | -46.9125 | 37.8736 | 150 |
| | | Tafelberg | Active | (Boelhouwers et al., 2003; Holness, 2003a) | -46.8836 | 37.8117 | 450 |
| | | Tate's Hill | Active | (Boelhouwers et al., 2003; Holness, 2003a) | -46.9139 | 37.8161 | 460 |
| | | Upper Haglet Valley | Active | (Boelhouwers et al., 2003) | -46.9381 | 37.7883 | 850 |
| | | Watertunnel | Active | (Holness, 2003a) | -46.9586 | 37.7483 | 100 |
| | DML | Flårjuven | Active | *pers. obs.* | -72.01498398 | -3.423040006 | 1 291 |
| | | Flårjuven | Active | *pers. obs.* | -72.01507299 | -3.423113013 | 1 293 |

| Feature | Site | Location | Active/Relict | Source | Latitude (DD) | Longitude (DD) | Altitude (m.a.s.l.) |
|---|---|---|---|---|---|---|---|
| | | Flårjuven | Active | *pers. obs.* | -72.01539603 | -3.423818015 | 1 290 |
| | | Flårjuven | Active | *pers. obs.* | -72.01551296 | -3.424428971 | 1 291 |
| | | Flårjuven | Active | *pers. obs.* | -72.01639398 | -3.393985983 | 1 320 |
| | | Flårjuven | Active | *pers. obs.* | -72.01 | -3.393 | 1 359 |
| | | Grunehogna | Active | *pers. obs.* | -72.04215 | -2.787916667 | 1 088 |
| | | Klovningen | Active | *pers. obs.* | -72.05 | 2.486666667 | 1 415 |
| | | Robertskollen | Active | *pers. obs.* | -71.49089249 | -3.234328916 | 500 |
| | | Robertskollen | Active | *pers. obs.* | -71.49125073 | -3.234643573 | 463 |
| | | Robertskollen | Active | *pers. obs.* | -71.49127864 | -3.234656984 | 463 |
| | | Robertskollen | Active | *pers. obs.* | -71.49127102 | -3.234575763 | 462 |
| | | Slettfjell | Active | *pers. obs.* | -72.13747703 | -3.302728012 | 1 507 |
| | | Valterkulten | Active | *pers. obs.* | -71.89399305 | -3.22715216 | 1 002 |
| | | Valterkulten | Active | *pers. obs.* | -71.89403378 | -3.22738895 | 1 004 |
| | | Valterkulten | Active | *pers. obs.* | -71.89400654 | -3.22744050 | 1 004 |
| | | Valterkulten | Active | *pers. obs.* | -71.89401140 | -3.22711277 | 1 002 |
| | | Valterkulten | Active | *pers. obs.* | -71.89435833 | -3.22928033 | 1 016 |
| | | Valterkulten | Active | *pers. obs.* | -71.89430268 | -3.22944243 | 1 016 |
| | | Valterkulten | Active | *pers. obs.* | -71.89431827 | -3.22980436 | 1 017 |
| | | Valterkulten | Active | *pers. obs.* | -71.89420662 | -3.22989170 | 1 015 |
| | | Valterkulten | Active | *pers. obs.* | -71.89409304 | -3.22921051 | 1 012 |
| | | Valterkulten | Active | *pers. obs.* | -71.89546097 | -3.23410101 | 1 004 |
| | | Valterkulten | Active | *pers. obs.* | -71.89733240 | -3.22750806 | 971 |
| | | Valterkulten | Active | *pers. obs.* | -71.89732301 | -3.22758785 | 971 |
| | | Valterkulten | Active | *pers. obs.* | -71.89734204 | -3.22719734 | 969 |
| | | Vesleskarvet nunataks | Active | *pers. obs.* | -71.667 | -2.851 | 856 |

| Feature | Site | Location | Active/Relict | Source | Latitude (DD) | Longitude (DD) | Altitude (m.a.s.l.) |
|---|---|---|---|---|---|---|---|
| Sorted net | MI | Bill Briggs (Long Ridge) | Relict | (Holness and Boelhouwers, 1998) | -46.8658 | 37.8011 | 350 |
| Sorted polygon | EC | Ben MacDhui | Active | (Kück, 1997) | -30.64829167 | 27.93525556 | > 2 900 |
| | | Eastern Cape Drakensberg | Active | (Lewis, 1988) | -30.62815833 | 27.89296667 | 2 550 |
| | | Mashai Valley, Lesotho Drakensberg | Active | (Grab, 1997b) | -29.69157778 | 29.03261944 | 2 420; 2 950 |
| | | Tlaeeng Pass, Lesotho Highlands | Active | (Hanvey and Marker, 1992) | -28.81184167 | 28.73378056 | 3 275 |
| | MI | Central Highland | Active | (Hedding, 2008) | -46.8972 | 37.7136 | > 750 |
| Sorted stripe | EC | KwaZulu Natal Drakensberg | Active | (Boelhouwers, 1991, 1994; Grab, 1997b) | -29.345075 | 29.48149167 | up to 3 842 |
| | MI | At all altitudes, excluding the coastal area | Active | (Boelhouwers et al., 2003) | -46.8947 | 37.7492 | All altitudes |
| | | Bill Briggs (Long Ridge) | Active (4-7 cm depth) | (Holness and Boelhouwers, 1998) | -46.8658 | 37.8011 | 350 |
| | | Central Highland (Delta Kop) | Active | (Hedding, 2006, 2008) | -46.8972 | 37.7136 | ~ 1 000 |
| | | Delta Extension | Active | (Boelhouwers et al., 2003) | -46.9072 | 37.7544 | 1 000 |
| | | Fred's Hill | Active | (Holness, 2001b; Boelhouwers et al., 2003) | -46.9086 | 37.8389 | 290 |
| | | Greyheaded-Albatross Ridge | Active | (Holness, 2001b; Boelhouwers et al., 2003) | -46.9561 | 37.7056 | 100 |

| Feature | Site | Location | Active/Relict | Source | Latitude (DD) | Longitude (DD) | Altitude (m.a.s.l.) |
|---|---|---|---|---|---|---|---|
| | | Hansen Point | Active | (Boelhouwers et al., 2003) | -46.9128 | 37.8958 | 10 |
| | | Katedraalkrans | Active | (Boelhouwers et al., 2003) | -46.8967 | 37.7761 | 750 |
| | | Kildalkey Bay | Active | (Holness, 2001b; Boelhouwers et al., 2003) | -46.9664 | 37.8575 | 70 |
| | | Long Ridge North | Active | (Holness, 2001b; Boelhouwers et al., 2003) | -46.8697 | 37.7869 | 200 |
| | | Long Ridge South | Active (10-15 cm depth) | (Holness, 2001b; Boelhouwers et al., 2003) | -46.8847 | 37.7817 | 500 |
| | | Mixed Pickle | Active | *pers. obs.* | -46.87958333 | 37.6465 | 275 |
| | | Mixed Pickle | Active | *pers. obs.* | -46.88077778 | 37.64772222 | 300 |
| | | Mixed Pickle High | Active | *pers. obs.* | -46.89738889 | 37.65461111 | 600 |
| | | Skua Ridge | Active | (Holness, 2001b; Boelhouwers et al., 2003) | -46.8656 | 37.8492 | 100 |
| | | Stoney Ridge | Active | (Holness, 2001b; Boelhouwers et al., 2003) | -46.9125 | 37.8736 | 150 |
| | | Tafelberg | Active | (Holness, 2001b; Boelhouwers et al., 2003) | -46.89 | 37.8 | 368 |
| | | Tafelberg | Active (5-10 cm depth) | (Holness, 2001b) | -46.8836 | 37.8117 | 300 |
| | | Tafelberg Extension | Active | (Holness, 2001b; Boelhouwers et al., 2003) | -46.8836 | 37.8117 | 400 |

| Feature | Site | Location | Active/Relict | Source | Latitude (DD) | Longitude (DD) | Altitude (m.a.s.l.) |
|---|---|---|---|---|---|---|---|
| | | Tate's Hill | Active | (Holness, 2001b; Boelhouwers et al., 2003) | -46.9139 | 37.8161 | 460 |
| | | Upper Haglet Valley | Active | (Holness, 2001b; Boelhouwers et al., 2003) | -46.9381 | 37.7883 | 850 |
| | DML | Flårjuven | Unknown | *pers. obs.* | -72.01794748 | -3.420232153 | 1 295 |
| | | Flårjuven | Unknown | *pers. obs.* | -72.01 | -3.395 | 1 215 |
| | | Grunehogna | Active | *pers. obs.* | -72.04215 | -2.787916667 | 1 088 |
| | | Robertskollen | Unknown | *pers. obs.* | -71.48808681 | -3.210103791 | 444 |
| Stone garland | EC | Ben MacDhui | Relict | (Kück, 1997) | -30.64829167 | 27.93525556 | 2 730-2 895 |
| Stone-banked lobe | EC | Giant's Castle | Active | (Boelhouwers, 1991, 1994) | -29.345075 | 29.48149167 | 3 140-3 300 |
| | | High KwaZulu-Natal/Lesotho Drakensberg | Active | (Grab, 2000) | -29.49013333 | 29.14902222 | > 3 300 |
| | MI | Albatross Lakes | Relict | (Holness, 2003b) | -46.8967 | 37.8714 | 50 |
| | | Beret Hill | Relict | (Holness, 2003b) | -46.9342 | 37.7681 | 750 |
| | | Bill Briggs (Long Ridge) | Relict for risers exceeding app. One meter; active for those below | (Holness and Boelhouwers, 1998) | -46.8658 | 37.8011 | 350 |
| | | Black Haglet Valley | Relict | (Holness, 2003b) | -46.9381 | 37.7883 | 700 |
| | | Delta Extension | Relict | (Holness, 2003b) | -46.9072 | 37.7544 | 1 000 |
| | | Eduard | Relict | (Holness, 2003b) | -46.8653 | 37.7728 | 600 |
| | | Feldmark Plateau | Relict (risers of 3 m) | (Holness, 2001a) | -46.9444 | 37.7686 | 600-750 |
| | | Fred's Hill | Relict | (Holness, 2003b) | -46.9086 | 37.8389 | 290 |
| | | Greyheaded-Albatross Ridge | Relict | (Holness, 2003b) | -46.9561 | 37.7056 | 100 |

| Feature | Site | Location | Active/Relict | Source | Latitude (DD) | Longitude (DD) | Altitude (m.a.s.l.) |
|---|---|---|---|---|---|---|---|
| | | Junior's Kop | Relict | (Hall, 1981) | -46.8833 | 37.8303 | 150 |
| | | Kerguelen Rise | Relict | (Holness, 2003b) | -46.9272 | 37.8567 | 250 |
| | | Kildalkey Bay | Relict | (Hall, 1981; Holness, 2003b) | -46.9664 | 37.8575 | 70 |
| | | Long Ridge North | Relict | (Hall, 1981; Holness, 2003b) | -46.8697 | 37.7869 | 200 |
| | | Long Ridge South | Relict for risers exceeding app. One meter; active for those below | (Holness and Boelhouwers, 1998) | -46.8847 | 37.7817 | 500 |
| | | Macaroni Bay | Relict | (Sumner et al., 2002) | -46.89491944 | 37.87620556 | 40 |
| | | Piew Crags | Relict | (Sumner et al., 2002) | -46.8992 | 37.81 | 400 |
| | | Repettos Hill | Relict | (Holness, 2003b) | -46.8422 | 37.7458 | 75 |
| | | Skua Ridge | Relict | (Holness, 2003b) | -46.8656 | 37.8492 | 90 |
| | | Stoney Ridge | Relict | (Hall, 1981; Holness, 2003b) | -46.9125 | 37.8736 | 100 |
| | | Tafelberg | Relict | (Hall, 1981; Holness, 2003b) | -46.8836 | 37.8117 | 450 |
| | | Tate's Hill | Relict | (Holness, 2003b) | -46.9139 | 37.8161 | 450 |
| | | Watertunnel | Relict | (Holness, 2003b) | -46.9586 | 37.7483 | 150 |
| Stone-banked sheet | MI | Junior's Kop | Active | (Boelhouwers et al., 2003) | -46.8833 | 37.8303 | 150 |
| Stone-banked terrace | MI | Feldmark Plateau | Relict (risers of 4 m) | (Holness, 2001a) | -46.9444 | 37.7686 | 600-750 |
| | | Feldmark Plateau | Relict (risers of 6 m) | (Nel, 2001) | -46.9444 | 37.7686 | 600-750 |
| | | Long Ridge | Relict (larger landforms)/Active | (Holness and Boelhouwers, 1998) | -46.8742 | 37.7886 | 200-550 |

| Feature | Site | Location | Active/Relict | Source | Latitude (DD) | Longitude (DD) | Altitude (m.a.s.l.) |
|---|---|---|---|---|---|---|---|
| | | | (smallest landforms) | | | | |
| Tafoni | DML | Flårjuven | Unknown | *pers. obs.* | -72.01439699 | -3.395819021 | 1 312 |
| | | Flårjuven | Unknown | *pers. obs.* | -72.01602601 | -3.417906007 | 1 383 |
| | | Flårjuven | Unknown | *pers. obs.* | -72.01601403 | -3.417884968 | 1 290 |
| | | Flårjuven | Unknown | *pers. obs.* | -72.01351899 | -3.418615032 | 1 281 |
| | | Flårjuven | Unknown | *pers. obs.* | -72.01377103 | -3.418895993 | 1 281 |
| | | Flårjuven | Unknown | *pers. obs.* | -72.01443697 | -3.421190036 | 1 286 |
| | | Flårjuven | Unknown | *pers. obs.* | -72.01447603 | -3.42151098 | 1 292 |
| | | Flårjuven | Unknown | *pers. obs.* | -72.01459698 | -3.421995034 | 1 292 |
| | | Flårjuven | Unknown | *pers. obs.* | -72.01480703 | -3.422891982 | 1 292 |
| | | Flårjuven | Unknown | *pers. obs.* | -72.01609399 | -3.385830978 | 1 308 |
| | | Flårjuven | Unknown | *pers. obs.* | -72.01440596 | -3.388753999 | 1 299 |
| | | Flårjuven | Unknown | *pers. obs.* | -72.01398603 | -3.395596985 | 1 311 |
| | | Flårjuven | Unknown | *pers. obs.* | -72.015261 | -3.421988999 | 1 280 |
| | | Flårjuven | Unknown | *pers. obs.* | -72.016599 | -3.428267967 | 1 280 |
| | | Flårjuven | Unknown | *pers. obs.* | -72.01760801 | -3.429774027 | 1 291 |
| | | Flårjuven | Unknown | *pers. obs.* | -72.01549804 | -3.397897985 | 1 310 |
| | | Flårjuven | Unknown | *pers. obs.* | -72.01519503 | -3.413088005 | 1 292 |
| | | Flårjuven | Unknown | *pers. obs.* | -72.01343802 | -3.416732037 | 1 282 |
| | | Flårjuven | Unknown | *pers. obs.* | -72.01341497 | -3.417417007 | 1 284 |
| | | Flårjuven | Unknown | *pers. obs.* | -72.01337004 | -3.417698974 | 1 283 |
| | | Grjotøyra | Unknown | *pers. obs.* | -72.03302074 | 2.541742232 | 1 275 |
| | | Lorentzenpiggen | Unknown | *pers. obs.* | -71.75780447 | -2.78778831 | 955 |
| | | Lorentzenpiggen | Unknown | *pers. obs.* | -71.75751429 | -2.79200415 | 932 |
| | | Lorentzenpiggen | Unknown | *pers. obs.* | -71.75748479 | -2.79208328 | 932 |

| Feature | Site | Location | Active/Relict | Source | Latitude (DD) | Longitude (DD) | Altitude (m.a.s.l.) |
|---|---|---|---|---|---|---|---|
| | | Lorentzenpiggen | Unknown | *pers. obs.* | -71.75744363 | -2.79224387 | 932 |
| | | Lorentzenpiggen | Unknown | *pers. obs.* | -71.75751513 | -2.79263967 | 932 |
| | | Lorentzenpiggen | Unknown | *pers. obs.* | -71.75725940 | -2.79622125 | 915 |
| | | Lorentzenpiggen | Unknown | *pers. obs.* | -71.75732779 | -2.79723991 | 915 |
| | | Lorentzenpiggen | Unknown | *pers. obs.* | -71.75733659 | -2.79790409 | 915 |
| | | Lorentzenpiggen | Unknown | *pers. obs.* | -71.75755042 | -2.80051958 | 904 |
| | | Lorentzenpiggen | Unknown | *pers. obs.* | -71.75746383 | -2.80146128 | 904 |
| | | Robertskollen | Unknown | *pers. obs.* | -72.02398002 | -3.37987002 | 534 |
| | | Robertskollen | Unknown | *pers. obs.* | -71.48878603 | -3.208416011 | 514 |
| | | Robertskollen | Unknown | *pers. obs.* | -71.48886801 | -3.208312998 | 512 |
| | | Robertskollen | Unknown | *pers. obs.* | -71.48854497 | -3.208469991 | 507 |
| | | Robertskollen | Unknown | *pers. obs.* | -71.48846702 | -3.208877016 | 505 |
| | | Robertskollen | Unknown | *pers. obs.* | -71.48845503 | -3.208996961 | 502 |
| | | Robertskollen | Unknown | *pers. obs.* | -71.48839602 | -3.208727986 | 498 |
| | | Robertskollen | Unknown | *pers. obs.* | -71.48831799 | -3.208810966 | 495 |
| Turf exfoliation | EC | Ben MacDhui | Active | *pers. obs.* | -30.64829167 | 27.93525556 | 2 600 |
| | | Mashai Valley, Lesotho Drakensberg | Active | (Grab, 2002) | -29.69157778 | 29.03261944 | 2 900-3 100 |
| | MI | At all altitudes where vegetation is present, excluding the coastal area | Active | (Boelhouwers et al., 2003) | -46.8947 | 37.7492 | All altitudes |
| | | Junior's Kop | Active | (Boelhouwers et al., 2003) | -46.8833 | 37.8303 | 150 |
| Vegetation-banked lobe | MI | At all altitudes, excluding the highest areas | Active | (Boelhouwers et al., 2003) | -46.8947 | 37.7492 | All altitudes |

| Feature | Site | Location | Active/Relict | Source | Latitude (DD) | Longitude (DD) | Altitude (m.a.s.l.) |
|---|---|---|---|---|---|---|---|
| Vegetation-banked terrace | EC | Ben MacDhui | Active | *pers. obs.* | -30.64971004 | 27.93585498 | 2 957 |
| | | Ben MacDhui | Active | *pers. obs.* | -30.64970199 | 27.93583201 | 2 954 |
| | | Ben MacDhui | Active | *pers. obs.* | -30.64970098 | 27.93581801 | 2 955 |
| | | Ben MacDhui | Active | *pers. obs.* | -30.64972001 | 27.93582397 | 2 954 |
| | | Ben MacDhui | Active | *pers. obs.* | -30.64973401 | 27.93581801 | 2 953 |
| | | Ben MacDhui | Active | *pers. obs.* | -30.64972403 | 27.93591499 | 2 949 |
| | | Ben MacDhui | Active | *pers. obs.* | -30.64973099 | 27.93592203 | 2 949 |
| | | Ben MacDhui | Active | *pers. obs.* | -30.64968699 | 27.935901 | 2 949 |
| | | Ben MacDhui | Active | *pers. obs.* | -30.64971599 | 27.93590401 | 2 949 |
| | | Ben MacDhui | Active | *pers. obs.* | -30.64971599 | 27.93591298 | 2 949 |
| | | Ben MacDhui | Active | *pers. obs.* | -30.64975899 | 27.93594902 | 2 948 |
| | | Ben MacDhui | Active | *pers. obs.* | -30.64977399 | 27.93593997 | 2 948 |
| | | Ben MacDhui | Active | *pers. obs.* | -30.64978296 | 27.93593402 | 2 947 |
| | | Ben MacDhui | Active | *pers. obs.* | -30.64978598 | 27.93593603 | 2 946 |
| | | Ben MacDhui | Active | *pers. obs.* | -30.64978497 | 27.93594198 | 2 947 |
| | | Ben MacDhui | Active | *pers. obs.* | -30.64981196 | 27.93599001 | 2 944 |
| | | Ben MacDhui | Active | *pers. obs.* | -30.64978899 | 27.93600501 | 2 944 |
| | | Ben MacDhui | Active | *pers. obs.* | -30.64977298 | 27.93604198 | 2 944 |
| | | Ben MacDhui | Active | *pers. obs.* | -30.64981196 | 27.93602404 | 2 944 |
| | | Ben MacDhui | Active | *pers. obs.* | -30.64982898 | 27.93601298 | 2 943 |
| | | Ben MacDhui | Active | *pers. obs.* | -30.64984004 | 27.93596101 | 2 940 |
| | | Ben MacDhui | Active | *pers. obs.* | -30.64986602 | 27.93597501 | 2 942 |
| | | Ben MacDhui | Active | *pers. obs.* | -30.64990902 | 27.93592002 | 2 941 |
| | | Ben MacDhui | Active | *pers. obs.* | -30.64992998 | 27.93586101 | 2 942 |
| | | Ben MacDhui | Active | *pers. obs.* | -30.64993903 | 27.935902 | 2 939 |
| | | Ben MacDhui | Active | (Kück, 1997) | -30.64829167 | 27.93525556 | 2 755-2 765 |

| Feature | Site | Location | Active/Relict | Source | Latitude (DD) | Longitude (DD) | Altitude (m.a.s.l.) |
|---|---|---|---|---|---|---|---|
| | MI | At all altitudes, excluding the highest areas | Active | (Boelhouwers et al., 2003) | -46.8947 | 37.7492 | All altitudes |
| | | Long Ridge (Long Ridge South; Bill Briggs; Long Ridge North) | Relict (larger landforms)/Active (smallest landforms) | (Holness and Boelhouwers, 1998) | -46.8697 | 37.7869 | 200-550 (500; 350; 200) |
| | | Tafelberg (but common throughout fellfield) | Active/Relict (state may be identified by surface sediment mobility) | (Haussmann et al., 2009a, 2009b) | -46.8836 | 37.8117 | 300 |

## Landform Images

This section provides a selection of images taken of andforms during field visits to the various sites. The table below is not a summative assessment of landforms found at each site, but rather provides examples of landforms obersved in the field. Furthermore, no description and characterisation of landforms is provided. Instead, the images serve as examples of landforms specific to each site. An exhaustive list and associated database of images is available from Landscape Processes in Antarctic Ecosystems upon request.

Table 23: Images taken of landforms and specific features during field visits.

| | | |
|---|---|---|
| 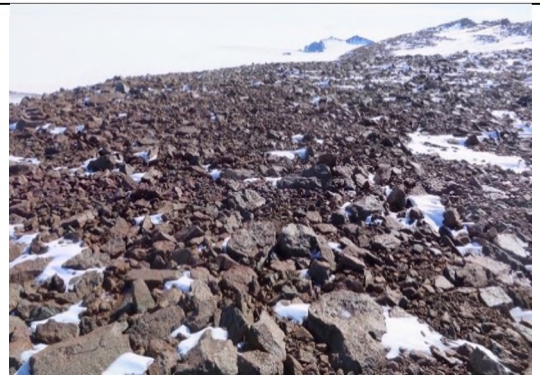 Figure 3: Blockfield (Flårjuven, Antarctica). | 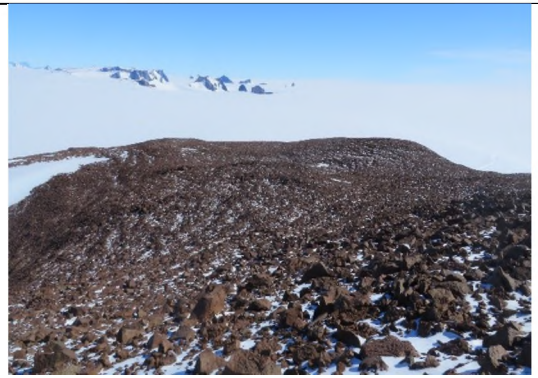 Figure 4: Blockfield (Valterkulten, Antarctica). |  Figure 5: Blockfield (Vesleskarvet, Antarctica). |

Figure 6: Blockstream (Ben MacDhui, South Africa).

Figure 7: Blockstream (Gaika's Kop, South Africa) (Meiklejohn, 2016).

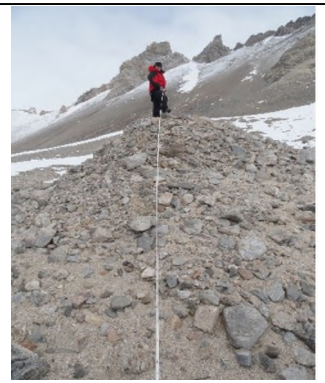

Figure 8: Frost mound (Vassdalen, Antarctica) (Loubser, 2016).

Figure 9: Frost sorting (Grjotøyra, Antarctica).

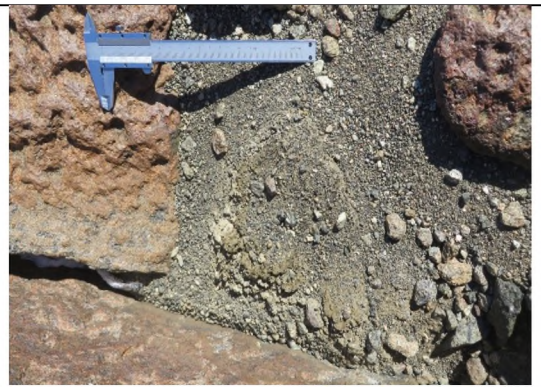

Figure 10: Frost sorting (Lorentzenpiggen, Antarctica).

Figure 11: Frost sorting (Trollkammen/Trollveikja, Antarctica).

Figure 12: Frost sorting (Ben MacDhui, South Africa).

Figure 13: Frost sorting (Elandsberg, South Africa).

Figure 14: Frost sorting (Grjotfjellet, Antarctica).

Figure 15: Frost sorting (Vassdalen, Antarctica).

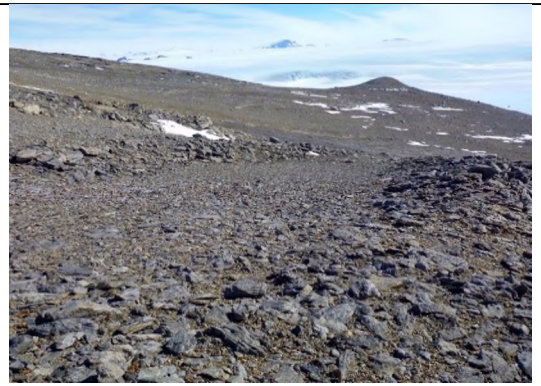

Figure 16: Gelifluction lobes (Trollkammen/Trollveikja, Antarctica).

Figure 17: Ice blister (Grjotøyra, Antarctica).

Figure 18: Ice blister (Crystal Palace, Antarctica) (Van Aswegen, 2011).

Figure 19: Ice lensing (Vassdalen, Antarctica) (Loubser, 2016).

Figure 20: Ice wedging (polygons) (Grunehogna, Antarctica) (Meiklejohn, 2017).

Figure 21: Mud boils (Trollkammen/Trollveikja, Antarctica).

Figure 22: Mud boils (Valterkulten, Antarctica).

Figure 23: Mud boils (Vassdalen, Antarctica).

Figure 24: Pitting (Lorentzenpiggen, Antarctica).

Figure 25: Pitting (Vesleskarvet, Antarctica).

Figure 26: Rock glacier (Grjotøyra, Antarctica).

Figure 27: Rock glacier (Sessegen, Antarctica).

Figure 28: Rock glacier (Tommelen, Antarctica).

Figure 29: Rock glacier (Vassdalen, Antarctica).

Figure 30: Sorted circle (Flårjuven, Antarctica).

Figure 31: Sorted circle (Klovningen, Antarctica).

Figure 32: Sorted circles (Lorentzenpiggen, Antarctica).

Figure 33: Sorted (rock) circle (Robertskollen, Antarctica.

Figure 34: Stripe formation (Flårjuven, Antarctica).

Figure 35: Stripe formation (Flårjuven, Antarctica).

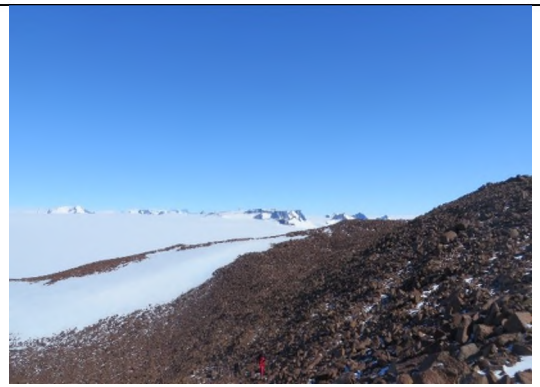

Figure 36: Stripe formation (Valterkulten, Antarctica).

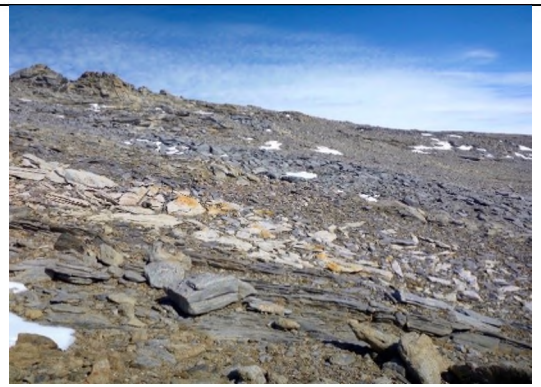

Figure 37: Stripe formation (Trollkammen/Trollveikja, Antarctica).

Figure 38: Sorted stripes (Tafelberg, Marion Island).

Figure 39: Tafoni (Flårjuven, Antarctica).

Figure 40: Tafoni and lichen (Grjotfjellet, Antarctica).

Figure 41: Tafoni (Grjotøyra, Antarctica).

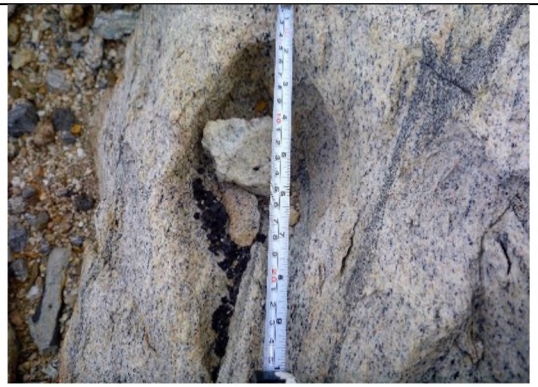

Figure 42: Tafoni (Klovningen, Antarctica).

Figure 43: Tafoni (Lorentzenpiggen, Antarctica).

Figure 44: Tafoni (Robertskollen, Antarctica).

Figure 45: Tafoni (Schumacherfjellet, Antarctica).

Figure 46: Tafoni (Trollkammen/Trollveikja, Antarctica).

Figure 47: Tafoni (Vassdalen, Antarctica).

Figure 48: Steps/terraces (Valterkulten, Antarctica).

Figure 49: Tafoni (Vesleskarvet, Antarctica).

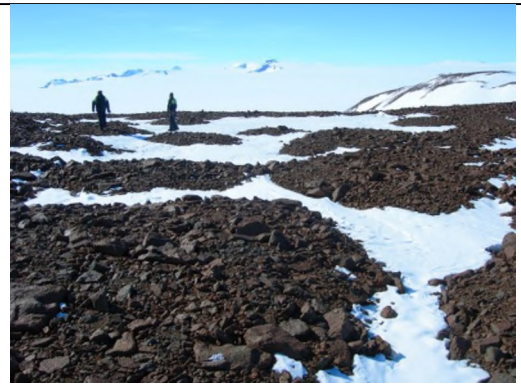

Figure 50: Thermal contraction polygons (Flårjuven, Antarctica).

Figure 51: Thermal contraction cracks (Delta Extension, Marion Island) (Meiklejohn, 2017).

Figure 52: Thermal contraction cracks (Grjotøyra, Antarctica).

Figure 53: Desiccation cracks (Grjotøyra, Antarctica).

Figure 54: Thermal contraction polygons with seepage line (Mimelia, Jutulsessen, Antarctica) (Loubser, 2011).

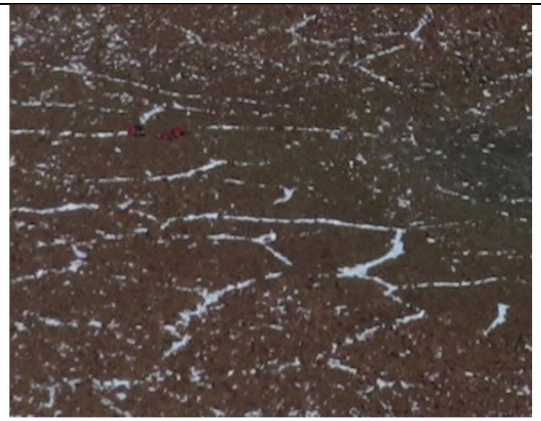

Figure 55: Thermal contraction polygons and brine pond (Valterkulten, Antarctica).

Figure 56: Thermal contraction polygons (Vassdalen, Antarctica).

Figure 57: Thermal contraction cracks (Vassdalen, Antarctica).

Figure 58: Thermal contraction cracks (Vassdalen, Antarctica).

Figure 59: Thermal contraction polygon (Vassdalen, Antarctica).

Figure 60: Needle-ice (Ben MacDhui, South Africa).

Figure 61: Needle-ice, friable surface (Ben MacDhui, South Africa).

Figure 62: Needle-ice (Ben MacDhui, South Africa).

Figure 63: Needle-ice (friable surface) (Elandsberg, South Africa).

Figure 64: Needle-ice (Gaika's Kop, South Africa) (Meiklejohn, 2016).

# References


Boelhouwers, J.C., 1991. Present-day periglacial activity in the Natal Drakensberg, Southern Africa: A Short Review. *Permafrost and Periglacial Processes*. 2, 5–12. doi:10.1002/ppp.3430020104

Boelhouwers, J.C., 1994. Periglacial landforms at Giant's Castle, Natal Drakensberg, South Africa. *Permafrost and Periglacial Processes*. 5, 129–136. doi:10.1002/ppp.3430050302

Boelhouwers, J.C., 2003. Sensitivity and responses to climate change in the Subantarctic periglacial environment, *in:* Phillips, M., Springman, S.M., Arenson, L.U. (Eds.), *Permafrost: Proceedings of the 8th International Conference on Permafrost*, Zurich, Switzerland, 21-25 July 2003. A.A. Balkema Publishers, Lisse [Netherlands]; Exton, PA.

Boelhouwers, J.C., 2004. New perspectives on autochthonous blockfield development. *Polar Geography*. 28, 133–146.

Boelhouwers, J.C., Holness, S.D., Meiklejohn, K.I., Sumner, P.D., 2002. Observations on a blockstream in the vicinity of Sani Pass, Lesotho highlands, Southern Africa. *Permafrost and Periglacial Processes.* 13, 251–257. doi:10.1002/ppp.428

Boelhouwers, J.C., Holness, S.D., Sumner, P.D., 2000. Geomorphological characteristics of small debris flows on Junior's Kop, Marion Island, maritime sub - Antarctic. *Earth Surface Processes and Landforms.* 25, 341–352. doi:10.1002/(SICI)1096-9837(200004)25:4<341::AID-ESP58>3.0.CO;2-D

Boelhouwers, J.C., Holness, S.D., Sumner, P.D., 2003. The maritime Subantarctic: a distinct periglacial environment. *Geomorphology*. 52, 39–55. doi:10.1016/S0169-555X(02)00247-7

Boelhouwers, J.C., Meiklejohn, K.I., Holness, S.D., Hedding, D.W., 2008. Geology, geomorphology and climate change, *in: The Prince Edward Islands: Land-Sea Interactions in a Changing Ecosystem*. SUN MeDIA, Stellenbosch, pp. 65–96.

Borg, C.-J., 2017. *Identifying growth criteria and sediment movement mechanisms of needle ice using high-frequency environmental and visual monitoring* (PhD). Rhodes University, Grahamstown, South Africa.

Brady, N.C., Weil, R.R., 2016. *The nature and properties of soils*, Fifteenth edition. ed. Pearson, Columbus.

Briggs, D.J., 1977a. *Soils, Sources and methods in geography*. Butterworths, London ; Boston.

Briggs, D.J., 1977b. *Sediments, Sources and methods in geography*. Butterworths, London; Boston.

Dallmann, W.K., Norsk polarinstitutt, Norwegian Antarctic Research Expedition, 1990. *Geology around the Norwegian Antarctic station "Troll", Jutulsessen, Dronning Maud Land*. Norsk Polarinstitutt, Oslo.

Grab, S.W., 1994. Thúfur in the Mohlesi Valley, Lesotho, Southern Africa. *Permafrost and Periglacial Processes.* 5, 111–118. doi:10.1002/ppp.3430050205

Grab, S.W., 1997a. Thermal regime for a thufa apex and its adjoining depression, Mashai Valley, Lesotho. *Permafrost and Periglacial Processes.* 8, 437–445. doi:10.1002/(SICI)1099-1530(199710/12)8:4<437::AID-PPP264>3.0.CO;2-O

Grab, S.W., 1997b. Annually re-forming miniature sorted patterned ground in the High Drakensberg, Southern Africa. *Permafrost and Periglacial Processes.* 22, 733–745. doi:10.1002/(SICI)1096-9837(199708)22:8<733::AID-ESP764>3.0.CO;2-L

Grab, S.W., 1998. Non-sorted patterned ground in the High Drakensberg, Southern Africa: Some New Data. *The Geographical Journal.* 164, 19–31. doi:10.2307/3060542

Grab, S.W., 1999. Block and debris deposits in the High Drakensberg, Lesotho, Southern Africa: Implications for high altitude slope processes. *Geografiska Annaler: Series A, Physical Geography.* 81, 1–16. doi:10.1111/j.0435-3676.1999.00045.x

Grab, S.W., 2000. Stone-banked lobes and environmental implications, High Drakensberg, Southern Africa. *Permafrost and Periglacial Processes.* 11, 177–187. doi:10.1002/1099-1530(200007/09)11:3<177::AID-PPP349>3.0.CO;2-R

Grab, S.W., 2001. Needle ice observations from the High Drakensberg, Lesotho. *Permafrost and Periglacial Processes.* 12, 227–231. doi:10.1002/ppp.371

Grab, S.W., 2002. Turf exfoliation in the High Drakensberg, Southern Africa. *Geografiska Annaler: Series A, Physical Geography.* 84, 39–50. doi:10.1111/j.0435-3676.2002.00160.x

Grab, S.W., 2005. Earth hummocks (thúfur): new insights to their thermal characteristics and development in eastern Lesotho, southern Africa. *Earth Surface Processes and Landforms*. 30, 541–555. doi:10.1002/esp.1150

Guetter, P.J., Kutzbach, J.E., 1990. A modified Köppen classification applied to model simulations of glacial and interglacial climates. *Climatic Change.* 16, 193–215.

Hall, K.J., 1981. Observations on stone-banked lobes of Marion Island. *South African Journal of Science.* 77, 129–131.

Hansen, C.D., 2014. *The characterisation of an openwork block deposit, Northern Buttress, Vesleskarvet, Dronning Maud Land, Antarctica* (MSc). Rhodes University, Grahamstown, South Africa.

Hansen, C.D., Loubser, M.J., Rudolph, E.M., 2016. Observations on frost mounds in the Jutulsessen, Antarctica, *in: Antarctic Permafrost, Periglacial Processes and Soil Development*. Presented at the XXXIV Scientific Committee on Antarctic Research Open Science Conference (SCAR OSC), Kuala Lumpur, Malaysia.

Hansen, C.D., Meiklejohn, K.I., Dwight, R.A., Scott, D.A., Rudolph, E.M., 2014. An investigation into morphology and dynamics of thermal contraction crack polygons found at Mimelia in the Jutulsessen, Antarctica, *in: Antarctic Permafrost, Periglacial, Snow, Firn and Ice-Free Environment*. Presented at the XXXIII Scientific Committee on Antarctic Research Open Science Conference (SCAR OSC).

Hansen, C.D., Meiklejohn, K.I., Nel, W., Loubser, M.J., Van Der Merwe, B.J., 2013. Aspect-controlled Weathering Observed on a Blockfield in Dronning Maud Land, Antarctica. *Geografiska Annaler: Series A, Physical Geography.* 95, 305–313.

Hanvey, P.M., Marker, M.E., 1992. Present-day periglacial microforms in the Lesotho Highlands: Implications for present and past climatic conditions. *Permafrost and Periglacial Processes.* 3, 353–361. doi:10.1002/ppp.3430030409

Haussmann, N.S., Boelhouwers, J.C., McGeoch, M.A., 2009a. Fine scale variability in soil frost dynamics surrounding cushions of the dominant vascular plant species (Azorella selago) on sub-Antarctic Marion Island. *Geografiska Annaler: Series A, Physical Geography.* 91, 257–268. doi:10.1111/j.1468-0459.2009.00368.x

Haussmann, N.S., McGeoch, M.A., Boelhouwers, J.C., 2009b. Interactions between a cushion plant (Azorella selago) and surface sediment transport on sub-Antarctic Marion Island. *Geomorphology*. 107, 139–148. doi:10.1016/j.geomorph.2008.12.002

Hedding, D.W., 2008. Spatial inventory of landforms in the recently exposed central highland of sub-Antarctic Marion Island. *South African Geographical Journal.* 90, 11–21. doi:10.1080/03736245.2008.9725307

Hedding, D.W., 2006. *Geomorphology and geomorphological responses to climate change in the interior of sub-Antarctic Marion Island* (MSc). University of Pretoria, Pretoria, South Africa.

Hedding, D.W., Meiklejohn, K.I., Le Roux, J.J., Loubser, M.J., Davis, J.K., 2010. Some observations on the formation of an active pronival rampart at Grunehogna Peaks, Western Dronning Maud Land, Antarctica. *Permafrost and Periglacial Processes.* 21, 355–361. doi:10.1002/ppp.698

Hedding, D.W., Sumner, P.D., Holness, S.D., Meiklejohn, K.I., 2007. Formation of a pronival rampart on sub-Antarctic Marion Island. *Antarctic Science.* 19. doi:10.1017/S0954102007000582

Holness, S.D., 2001a. *Periglacial slope processes, landforms and environment at Marion island, Maritime Subantarctic* (PhD). University of the Western Cape, Cape Town, South Africa.

Holness, S.D., 2001b. The orientation of sorted stripes in the maritime subantarctic, Marion Island. *Earth Surface Processes and Landforms.* 26, 77–89. doi:10.1002/1096-9837(200101)26:1<77::AID-ESP161>3.0.CO;2-N

Holness, S.D., 2003a. Sorted circles in the maritime Subantarctic, Marion Island. *Earth Surface Processes and Landforms.* 28, 337–347. doi:10.1002/esp.430

Holness, S.D., 2003b. The periglacial record of Holocene environmental change, subantarctic Marion Island. *Permafrost and Periglacial Processes.* 14, 69–74. doi:10.1002/ppp.439

Holness, S.D., 2004. Sediment movement rates and processes on cinder cones in the maritime Subantarctic (Marion Island). *Earth Surface Processes and Landforms.* 29, 91–103. doi:10.1002/esp.1015

Holness, S.D., Boelhouwers, J.C., 1998. Some observations on Holocene changes in periglacial activity at Long Ridge, Marion Island. *South African Journal of Science.* 94, 399–403.

Huang, P.-T., Patel, M., Santagata, M.C., Bobet, A., 2009. *Classification of organic soils* (Open File Report No. FHWA/IN/JTRP-2008/2). Purdue University, USA.

Kennicutt, M.C., Chown, S.L., Cassano, J.J., Liggett, D., Massom, R., Peck, L.S., Rintoul, S.R., Storey, J.W.V., Vaughan, D.G., Wilson, T.J., Sutherland, W.J., 2014. Polar research: Six priorities for Antarctic science. *Nature.* 512, 23–25. doi:10.1038/512023a

Kennicutt, M.C., Chown, S.L., Cassano, J.J., Liggett, D., Peck, L.S., Massom, R., Rintoul, S.R., Storey, J., Vaughan, D.G., Wilson, T.J., Allison, I., Ayton, J., Badhe, R., Baeseman, J., Barrett, P.J., Bell, R.E., Bertler, N., Bo, S., Brandt, A., Bromwich, D., Cary, S.C., Clark, M.S., Convey, P., Costa, E.S., Cowan, D., Deconto, R., Dunbar, R., Elfring, C., Escutia, C., Francis, J., Fricker, H.A., Fukuchi, M., Gilbert, N., Gutt, J., Havermans, C., Hik, D., Hosie, G., Jones, C., Kim, Y.D., Le Maho, Y., Lee, S.H., Leppe, M., Leitchenkov, G., Li, X., Lipenkov, V., Lochte, K., López-Martínez, J., Lüdecke, C., Lyons, W., Marenssi, S., Miller, H., Morozova, P., Naish, T., Nayak, S., Ravindra, R., Retamales, J., Ricci, C.A., Rogan-Finnemore, M., Ropert-Coudert, Y., Samah, A.A., Sanson, L., Scambos, T., Schloss, I.R., Shiraishi, K., Siegert, M.J., Simões, J.C., Storey, B., Sparrow, M.D., Wall, D.H., Walsh, J.C., Wilson, G., Winther, J.G., Xavier, J.C., Yang, H., Sutherland, W.J., 2015. A roadmap for Antarctic and Southern Ocean science for the next two decades and beyond. *Antarctic Science.* 27, 3–18. doi:10.1017/S0954102014000674

Köppen, W., 1936. Das Geographische System der Klimate, *in:* Köppen, W., Geiger, R. (Eds.), *Handbuch der Klimatologie*, 3. Gebrüder Borntraeger, Berlin, pp. 1–44.

Kottek, M., Grieser, J., Beck, C., Rudolf, B., Rubel, F., 2006. World Map of the Köppen-Geiger climate classification updated. *Meteorologische Zeitschrift.* 15, 259–263. doi:10.1127/0941-2948/2006/0130

Kotzé, C., 2016. *Active layer dynamics at four borehole sites in Western Dronning Maud Land, Antarctica* (MSc*).* Rhodes University, Grahamstown, South Africa.

Kück, K.M., 1997. *Periglacial features in the vicinity of Tiffindell Ski Resort, North East Cape Drakensberg, South Africa, and their implications for the development of the resort* (MSc). Rhodes University, Grahamstown, South Africa.

Lee, J.E., Le Roux, P.C., Meiklejohn, K.I., Chown, S.L., 2013. Species distribution modelling in low-interaction environments: Insights from a terrestrial Antarctic system. *Austral Ecology.* 38, 279–288. doi:10.1111/j.1442-9993.2012.02401.x

Lewis, C.A., 1988. Periglacial features in southern Africa: an assessment. *Palaeoecology of Africa.* 19, 357–370.

Lewis, C.A., 1994. Protalus Ramparts and the Altitude of the Local Equilibrium Line during the Last Glacial Stage in Bokspruit, East Cape Drakensberg, South Africa. *Geografiska Annaler. Series A, Physical Geography*. 76, 37–48. doi:10.2307/521318

Lewis, C.A., 2005. Late Glacial and Holocene palaeoclimatology of the Drakensberg of the Eastern Cape, South Africa. Quaternary International, *Highlights of Quaternary research in southern Africa 129*, 33–48. doi:10.1016/j.quaint.2004.04.005

Lewis, C.A., 2008a. Periglacial features, *in:* Lewis, C.A. (Ed.), *Geomorphology of the Eastern Cape, South Africa*. NISC, Grahamstown, pp. 149–185.

Lewis, C.A., 2008b. Late Pleistocene and early Holocene foragers in southern Africa, *in:* Pearsall, D.M. (Ed.), *Encyclopedia of Archaeology*. Elsevier/Academic Press, San Diego, California, pp. 86–93.

Lewis, C.A., Hanvey, P.M., 1993. The remains of rock glaciers in Bottelnek, East Cape Drakensberg, South Africa. *Transactions of the Royal Society of South Africa.* 48, 265–289. doi:10.1080/00359199309520275

Lewis, C.A., Hydrological Research Unit (Rhodes University), Southern African Society for Quaternary Research, 1994. *Field guide to the quaternary glacial, periglacial and colluvial features of the East Cape Drakensberg*. Published on behalf of the Southern African Society for Quaternary Research by the Dept. of Geography, Rhodes University, Grahamstown.

Marshall, D.J., Crafford, J.E., Krynauw, J.R., Drummond, A.E., Newton, I.P., 1995. The biology, physico-chemistry and geology of a nunatak pond at Valterkulten, western Dronning Maud Land, Antarctica. *South African Journal of Antarctic Research.* 25, 9–16.

Nel, W., 2001. *A spatial inventory of glacial, periglacial and rapid mass movement forms on part of Marion Island: implications for Quaternary environmental change* (MSc). University of Pretoria, Pretoria, South Africa.

Rudolph, E.M., 2015. *Surface characteristics of rock glaciers in the Jutulsessen, Dronning Maud Land, Antarctica* (MSc). Rhodes University, Grahamstown, South Africa.

Strahler, A.N., 1989. *Elements of Physical Geography*, 4th ed. Wiley, New York.

Sumner, P.D., 2004. Geomorphic and Climatic Implications of Relict Openwork Block Accumulations Near Thabana-Ntlenyana, Lesotho. *Geografiska Annaler: Series A, Physical Geography*. 86, 289–302.

Sumner, P.D., de Villiers, S., 2002. On the Pleistocene palaeoenvironmental evidence from the Amatola screes. *South African Journal of Science.* 98, 598–601.

Sumner, P.D., Meiklejohn, K.I., 2004. On the development of autochthonous blockfields in the grey basalts of sub-Antarctic Marion Island. Polar Geography 28, 120–132. doi:10.1080/789610121

Sumner, P.D., Nel, W., Holness, S.D., Boelhouwers, J.C., 2002. Rock weathering characteristics as relative-age indicators for glacial and post-glacial landforms on Marion Island. *South African Geographical Journal.* 84, 153–157. doi:10.1080/03736245.2002.9713766

Walter, H., 1985. *Vegetation of the Earth and Ecological Systems of the Geo-Biosphere*. Springer Berlin Heidelberg, Berlin, Heidelberg.

Washburn, A.L., 1979. *Geocryology: A Survey of Periglacial Processes and Environments*. Edward Arnold, London.

Williams, T.A., Sweeney, D.J., Anderson, D.R. (Eds.), 2006. *Contemporary Business Statistics with Microsoft Excel*. South-Western College Pub, Cincinnati, Ohio.

# On High-Altitude and High-Latitude Frost Environments:

## Landform Database Literary References

BY

CHRISTEL D HANSEN

LANDSCAPE PROCESSES IN ANTARCTIC ECOSYSTEMS

RHODES UNIVERSITY

# Table of Contents

## Executive Summary

This document and provides the literary references for an ArcGIS Online Map that displays periglacial and (limited) glacial features and landforms observed for Marion Island, Dronning Maud Land (Antarctica), the Eastern Cape Drakensberg of South Africa, and the Elandsberg near Hogsback (South Africa). The content of the landforms and features is derived from an academic literature review and augmented with observations taken during field visits to the study sites. Where the exact location of landforms was not provided in the literature an approximate location was obtained using Google Earth ™. Caution should be exercised when using such data. The location of features observed in the field are accurate to 3m and recorded in WGS 84.

The ArcGIS Online map is best navigated with the use of bookmarks. Bookmarks have been created for:

- Home (full view extent);
- Eastern Cape (full view extent of all Eastern Cape recorded landforms and features);
- Elandsberg, Eastern Cape, South Africa;
- Tiffindell Ski Resort, Ben MacDhui, Eastern Cape, South Africa;
- Marion Island, Southern Ocean, South Africa;
- Western Dronning Maud Land, Antarctica; and
- Jutulsessen (central Dronning Maud Land), Antarctica.

The map and its contents form part of a PhD thesis *'On high-altitude and -latitude diurnal frost environments'*, which forms part of the National Research Foundation (NRF) of South Africa's-funded project Landscape Processes in Antarctic Ecosystems. All landform and feature data are the property of Landscape Processes in Antarctic Ecosystems and the NRF. Detailed disclaimers and copyright information, data ownership and distribution of data are available on the project's website.

## Disclaimer



The PhD thesis, of which this document and the accompanying ArcGIS Online Map form a part, falls under a research grant as part of the SANAP/NRF grant no. 80264: Landscape processes in Antarctic

Ecosystems. Any opinions expressed are those of the author and the NRF and SANAP do not accept any liability in regard thereto. This disclaimer is subject to change at any time with or without notice.

## Copyright



## Relevant Metadata

Author: Christel D Hansen (g11h7349@gmail.ru.ac.za)
Feature Description: periglacial, glacial and other relevant landforms and observations
Geographical Extent:

- Eastern Cape Drakensberg and the Elandsberg (Hogsback), South Africa
- Marion Island, Southern Ocean, South Africa
- Dronning Maud Land (Central and Western), Antarctica

Coordinate System: WGS 84
Time Frame: 2012-2015
Observational Accuracy: 3m (horizontal); 10m (vertical)
Literary Observational Accuracy: variable

# Literary References


Boelhouwers, J.C., 1991. Present-day periglacial activity in the Natal Drakensberg, Southern Africa: A Short Review. *Permafrost and Periglacial Processes* 2, 5–12. doi:10.1002/ppp.3430020104

Boelhouwers, J.C., 1994. Periglacial landforms at Giant's Castle, Natal Drakensberg, South Africa. *Permafrost and Periglacial Processes* 5, 129–136. doi:10.1002/ppp.3430050302

Boelhouwers, J.C., 2003. Sensitivity and responses to climate change in the Subantarctic periglacial environment, *in:* Phillips, M., Springman, S.M., Arenson, L.U. (Eds.), *Permafrost: Proceedings of the 8th International Conference on Permafrost*, Zurich, Switzerland, 21-25 July 2003. A.A. Balkema Publishers, Lisse [Netherlands]; Exton, PA.

Boelhouwers, J.C., 2004. New perspectives on autochthonous blockfield development. *Polar Geography* 28, 133–146.

Boelhouwers, J.C., Holness, S.D., Meiklejohn, K.I., Sumner, P.D., 2002. Observations on a blockstream in the vicinity of Sani Pass, Lesotho highlands, Southern Africa. *Permafrost and Periglacial Processes* 13, 251–257. doi:10.1002/ppp.428

Boelhouwers, J.C., Holness, S.D., Sumner, P.D., 2000. Geomorphological characteristics of small debris flows on Junior's Kop, Marion Island, maritime sub - Antarctic. *Earth Surface Processes and Landforms* 25, 341–352. doi:10.1002/(SICI)1096-9837(200004)25:4<341::AID-ESP58>3.0.CO;2-D

Boelhouwers, J.C., Holness, S.D., Sumner, P.D., 2003. The maritime Subantarctic: a distinct periglacial environment. *Geomorphology* 52, 39–55. doi:10.1016/S0169-555X(02)00247-7

Boelhouwers, J.C., Meiklejohn, K.I., Holness, S.D., Hedding, D.W., 2008. Geology, Geomorphology and Climate Change, *in: The Prince Edward Islands: Land-Sea Interactions in a Changing Ecosystem*. SUN MeDIA, Stellenbosch, pp. 65–96.

Borg, C.-J., 2017. *Identifying growth criteria and sediment movement mechanisms of needle ice using high-frequency environmental and visual monitoring* (PhD). Rhodes University, Grahamstown, South Africa.

Dallmann, W.K., Norsk polarinstitutt, Norwegian Antarctic Research Expedition, 1990. *Geology around the Norwegian Antarctic station "Troll", Jutulsessen, Dronning Maud Land*. Norsk Polarinstitutt, Oslo.

Grab, S.W., 1994. Thúfur in the Mohlesi Valley, Lesotho, Southern Africa. *Permafrost and Periglacial Processes* 5, 111–118. doi:10.1002/ppp.3430050205

Grab, S.W., 1997a. Thermal regime for a thufa apex and its adjoining depression, Mashai Valley, Lesotho. *Permafrost and Periglacial Processes* 8, 437–445. doi:10.1002/(SICI)1099-1530(199710/12)8:4<437::AID-PPP264>3.0.CO;2-O

Grab, S.W., 1997b. Annually re-forming miniature sorted patterned ground in the High Drakensberg, Southern Africa. *Earth Surface Processes and Landforms* 22, 733–745. doi:10.1002/(SICI)1096-9837(199708)22:8<733::AID-ESP764>3.0.CO;2-L

Grab, S.W., 1998. Non-sorted patterned ground in the High Drakensberg, Southern Africa: Some New Data. *The Geographical Journal* 164, 19–31. doi:10.2307/3060542

Grab, S.W., 1999. Block and debris deposits in the High Drakensberg, Lesotho, Southern Africa: Implications for high altitude slope processes. *Geografiska Annaler: Series A, Physical Geography* 81, 1–16. doi:10.1111/j.0435-3676.1999.00045.x

Grab, S.W., 2000. Stone-banked lobes and environmental implications, High Drakensberg, Southern Africa. *Permafrost and Periglacial Processes* 11, 177–187. doi:10.1002/1099-1530(200007/09)11:3<177::AID-PPP349>3.0.CO;2-R

Grab, S.W., 2001. Needle ice observations from the High Drakensberg, Lesotho. *Permafrost and Periglacial Processes* 12, 227–231. doi:10.1002/ppp.371

Grab, S.W., 2002. Turf exfoliation in the High Drakensberg, Southern Africa. *Geografiska Annaler: Series A, Physical Geography* 84, 39–50. doi:10.1111/j.0435-3676.2002.00160.x

Grab, S.W., 2005. Earth hummocks (thúfur): new insights to their thermal characteristics and development in eastern Lesotho, southern Africa. *Earth Surface Processes and Landforms* 30, 541–555. doi:10.1002/esp.1150

Hall, K.J., 1981. Observations on stone-banked lobes of Marion Island. *South African Journal of Science* 77, 129–131.

Hansen, C.D., 2014. *The characterisation of an openwork block deposit, Northern Buttress, Vesleskarvet, Dronning Maud Land, Antarctica* (MSc). Rhodes University, Grahamstown, South Africa.

Hansen, C.D., Loubser, M.J., Rudolph, E.M., 2016. Observations on frost mounds in the Jutulsessen, Antarctica, *in: Antarctic Permafrost, Periglacial Processes and Soil Development*. Presented at the XXXIV Scientific Committee on Antarctic Research Open Science Conference (SCAR OSC), Kuala Lumpur, Malaysia.

Hansen, C.D., Meiklejohn, K.I., Dwight, R.A., Scott, D.A., Rudolph, E.M., 2014. An investigation into morphology and dynamics of thermal contraction crack polygons found at Mimelia in the Jutulsessen, Antarctica, *in: Antarctic Permafrost, Periglacial, Snow, Firn and Ice-Free Environment*. Presented at the XXXIII Scientific Committee on Antarctic Research Open Science Conference (SCAR OSC).

Hansen, C.D., Meiklejohn, K.I., Nel, W., Loubser, M.J., van Der Merwe, B.J., 2013. Aspect-controlled Weathering Observed on a Blockfield in Dronning Maud Land, Antarctica. *Geografiska Annaler: Series A, Physical Geography* 95, 305–313.

Hanvey, P.M., Marker, M.E., 1992. Present-day periglacial microforms in the Lesotho Highlands: Implications for present and past climatic conditions. *Permafrost and Periglacial Processes* 3, 353–361. doi:10.1002/ppp.3430030409

Haussmann, N.S., Boelhouwers, J.C., McGeoch, M.A., 2009a. Fine scale variability in soil frost dynamics surrounding cushions of the dominant vascular plant species (Azorella selago) on sub-Antarctic Marion Island. *Geografiska Annaler: Series A, Physical Geography* 91, 257–268. doi:10.1111/j.1468-0459.2009.00368.x

Haussmann, N.S., McGeoch, M.A., Boelhouwers, J.C., 2009b. Interactions between a cushion plant (Azorella selago) and surface sediment transport on sub-Antarctic Marion Island. *Geomorphology* 107, 139–148. doi:10.1016/j.geomorph.2008.12.002

Hedding, D.W., 2006. *Geomorphology and geomorphological responses to climate change in the interior of sub-Antarctic Marion Island* (MSc). University of Pretoria, Pretoria, South Africa.

Hedding, D.W., 2008. Spatial inventory of landforms in the recently exposed central highland of sub-Antarctic Marion Island. *South African Geographical Journal* 90, 11–21. doi:10.1080/03736245.2008.9725307

Hedding, D.W., Meiklejohn, K.I., le Roux, J.J., Loubser, M., Davis, J.K., 2010. Some observations on the formation of an active pronival rampart at Grunehogna Peaks, Western Dronning Maud Land, Antarctica. P*ermafrost and Periglacial Processes* 21, 355–361. doi:10.1002/ppp.698

Hedding, D.W., Sumner, P.D., Holness, S.D., Meiklejohn, K.I., 2007. Formation of a pronival rampart on sub-Antarctic Marion Island. *Antarctic Science* 19. doi:10.1017/S0954102007000582

Holness, S.D., 2001a. *Periglacial slope processes, landforms and environment at Marion island, Maritime Subantarctic* (PhD). University of the Western Cape, Cape Town, South Africa.

Holness, S.D., 2001b. The orientation of sorted stripes in the maritime subantarctic, Marion Island. *Earth Surface Processes and Landforms* 26, 77–89. doi:10.1002/1096-9837(200101)26:1<77::AID-ESP161>3.0.CO;2-N

Holness, S.D., 2003a. Sorted circles in the maritime Subantarctic, Marion Island. *Earth Surface Processes and Landforms* 28, 337–347. doi:10.1002/esp.430

Holness, S.D., 2003b. The periglacial record of Holocene environmental change, subantarctic Marion Island. *Permafrost and Periglacial Processes* 14, 69–74. doi:10.1002/ppp.439

Holness, S.D., 2004. Sediment movement rates and processes on cinder cones in the maritime Subantarctic (Marion Island). *Earth Surface Processes and Landforms* 29, 91–103. doi:10.1002/esp.1015

Holness, S.D., Boelhouwers, J.C., 1998. Some observations on Holocene changes in periglacial activity at Long Ridge, Marion Island. Sout*h African Journal of Science* 94, 399–403.

Kück, K.M., 1997. *Periglacial features in the vicinity of Tiffindell Ski Resort, North East Cape Drakensberg, South Africa, and their implications for the development of the resort* (MSc). Rhodes University, Grahamstown, South Africa.

Lee, J.E., Le Roux, P.C., Meiklejohn, K.I., Chown, S.L., 2013. Species distribution modelling in low-interaction environments: Insights from a terrestrial Antarctic system. *Austral Ecology* 38, 279–288. doi:10.1111/j.1442-9993.2012.02401.x

Lewis, C.A., 1988. Periglacial features in southern Africa: an assessment. Pala*eoecology of Africa* 19, 357–370.

Lewis, C.A., 1994. Protalus Ramparts and the Altitude of the Local Equilibrium Line during the Last Glacial Stage in Bokspruit, East Cape Drakensberg, South Africa. *Geografiska Annaler. Series A, Physical Geography* 76, 37–48. doi:10.2307/521318

Lewis, C.A., 2005. Late Glacial and Holocene palaeoclimatology of the Drakensberg of the Eastern Cape, South Africa. *Quaternary International, Highlights of Quaternary research in southern Africa* 129, 33–48. doi:10.1016/j.quaint.2004.04.005

Lewis, C.A., 2008a. *Periglacial features*, *in:* Lewis, C.A. (Ed.), Geomorphology of the Eastern Cape, South Africa. NISC, Grahamstown, South Africa, pp. 149–185.

Lewis, C.A., 2008b. Late Pleistocene and early Holocene foragers in southern Africa, *in:* Pearsall, D.M. (Ed.), *Encyclopedia of Archaeology*. Elsevier/Academic Press, San Diego, California, pp. 86–93.

Lewis, C.A., Hanvey, P.M., 1993. The remains of rock glaciers in Bottelnek, East Cape Drakensberg, South Africa. *Transactions of the Royal Society of South Africa* 48, 265–289. doi:10.1080/00359199309520275

Lewis, C.A., Hydrological Research Unit (Rhodes University), Southern African Society for Quaternary Research, 1994. *Field guide to the quaternary glacial, periglacial and colluvial features of the East Cape Drakensberg*. Published on behalf of the Southern African Society for Quaternary Research by the Dept. of Geography, Rhodes University, Grahamstown, South Africa.

Marshall, D.J., Crafford, J.E., Krynauw, J.R., Drummond, A.E., Newton, I.P., 1995. The biology, physico-chemistry and geology of a nunatak pond at Valterkulten, western Dronning Maud Land, Antarctica. *South African Journal of Antarctic Research* 25, 9–16.

Nel, W., 2001. *A spatial inventory of glacial, periglacial and rapid mass movement forms on part of Marion Island: implications for Quaternary environmental change* (MSc). University of Pretoria, Pretoria, South Africa.

Rudolph, E.M., 2015. *Surface characteristics of rock glaciers in the Jutulsessen, Dronning Maud Land, Antarctica* (MSc). Rhodes University, Grahamstown, South Africa.

Sumner, P.D., 2004. Geomorphic and Climatic Implications of Relict Openwork Block Accumulations Near Thabana-Ntlenyana, Lesotho. *Geografiska Annaler: Series A, Physical Geography* 86, 289–302.

Sumner, P.D., de Villiers, S., 2002. On the Pleistocene palaeoenvironmental evidence from the Amatola screes. Sou*th African Journal of Science* 98, 598–601.

Sumner, P.D., Meiklejohn, K.I., 2004. On the development of autochthonous blockfields in the grey basalts of sub-Antarctic Marion Island. *Polar Geography* 28, 120–132. doi:10.1080/789610121

Sumner, P.D., Nel, W., Holness, S.D., Boelhouwers, J.C., 2002. Rock weathering characteristics as relative-age indicators for glacial and post-glacial landforms on Marion Island. *South African Geographical Journal* 84, 153–157. doi:10.1080/03736245.2002.9713766